7. ภาคผนวก

overproduction [1, 5, 7], PRL was likely to modulate the expression of other genes essential for osteoclastogenesis. In general, besides RANKL which interacts with its receptors RANK on the plasma membrane of pre-osteoclasts [6], a number of osteoblast-derived paracrine factors, such as macrophage colony-stimulating factors (MCSF), interleukin (IL)-1, IL-6, and tumor necrosis factor (TNF)-α, are essential for proliferation and activation of pre-osteoclasts [6, 8, 9]. In addition, an upregulation of cyclooxygenase (Cox)-2 in osteoblasts may lead to an overproduction of prostaglandin E2, which in turn enhanced the osteoclastic bone resorption [10], whereas inhibition of Cox-2 activity by celecoxib and indomethacin restricted the osteoclast formation in a dose-dependent manner [11].

Besides using cytokines as signals between osteoblasts and osteoclasts, in bone remodeling, these bone cells can communicate with each other through a direct cell–cell contact using the ephrin receptor (Eph)/ephrin system [12]. The tyrosine kinase receptor Eph and its ligand ephrin are transmembrane proteins, both of which can initiate the signaling cascades [12]. An interaction between ephrin type-B receptor 4 (EphB4) expressed in osteoblasts and ephrin-B2 in osteoclasts was reported to inhibit osteoclastogenesis, while stimulating osteoblastogenesis through a bidirectional signaling, thereby inducing the transition from bone resorption to formation [13]. Thus, EphB4 and ephrin-B2 were parts of a negative feedback loop that counterbalanced the osteoblast-derived osteoclastogenic factors. In addition, ephrin-B1 was also essential for normal skeletal development in both humans and rodents [14, 15]. Ephrin-B1 knockout mice exhibited several bone anomalies, such as rib mispairing and fusion of sternebrae [14].

Therefore, the objectives of this study were (i) to determine the mRNA expressions of genes related to the osteoblast-derived osteoclastogenic paracrine factors in rat osteoblast-like UMR106 cells directly exposed to PRL; and (ii) to investigate the direct effect of PRL on the mRNA expression of Eph/ephrin in osteoblast-like cells. Unlike the previous investigations that used the pathological PRL concentration of 1000 ng/ml (as in prolactinoma) [5], in this study, the authors used high physiological concentrations of PRL, i.e., 100, 200–300, and 400–500 ng/ml which were comparable to the average plasma levels in pregnancy, lactation, and suckling-induced PRL surge, respectively [2, 16]. Thus, the results were more closely related to what happened in lactating mothers.

Materials and methods

Cell culture

Rat osteoblast-like UMR106 cells (American Type Culture Collection [ATCC] no. CRL-1661) were propagated in six-well culture plates with Dulbecco's modified Eagle's medium (DMEM) (Sigma, St. Louis, MO, USA) supplemented with 10% fetal bovine serum (FBS) (PAA Laboratories, Pasching, Austria), and 100 U/ml penicillin–streptomycin (Gibco, Grand Island, NY, USA). Cells were incubated with 5% CO_2 at 37°C, and subcultured according to the ATCC's protocol. Despite being a rat osteosarcoma cell line, Partridge et al. [17] provided evidence that UMR106 cells were more similar to the differentiated rat osteoblasts than their osteosarcoma parent because they exhibited high alkaline phosphatase activity and were well responsive to parathyroid hormone. This cell type has been reported to express several markers of normal differentiated osteoblasts, e.g., type I collagen, osteocalcin, and osteopontin [18, 19]. Therefore, UMR106 cell line is an appropriate model for studying the PRL regulation of osteoblast gene expression.

Experimental design

Total RNA of confluent UMR106 cells were collected at 96 h after seeding in six-well plates to demonstrate the mRNA expression profile of short (-S) and long (-L) isoforms of PRLR, as well as the anti-osteoclastogenic factor, osteoprotegerin (OPG), and various osteoclastogenic factors, namely, RANKL, MCSF, monocyte chemoattractant protein (MCP)-1, Cox-2, TNF-α, IL-1, IL-6, EphB4, ephrin-B1, and ephrin-B2, by using conventional reverse transcription (RT)-PCR. To investigate the time-dependent effects of PRL on osteoblast mRNA expression, confluent UMR106 cells were incubated in 500 ng/ml PRL (purified from ovine pituitary gland; catalog no. L6520; Sigma) for 0, 12, 24, 48, and 72 h before determination of RANKL expression by quantitative real-time PCR (qRT-PCR). The optimal incubating time (i.e., 48 h) from the time-dependent study was used in the subsequent experiments. For the dose-dependent study, confluent UMR106 cells were incubated with normal medium (0 ng/ml PRL; control) or medium containing various concentrations of PRL, i.e., 100, 200, 300, 400, and 500 ng/ml, for 48 h before determining the expression levels of PRLR and osteoclastogenic modulators by qRT-PCR. The effects of PRL on osteoblast proliferation and viability were determined by 5-bromo-2′-deoxyuridine (BrdU) and 3-(4,5-dimethylthiazol-2-yl)-2,5-diphenyltetrazolium bromide (MTT) assays, respectively.

Cell proliferation assay

UMR106 cells were seeded in 96-well culture plates (3,000 cells/well). Culture media also contained 10 μM BrdU to allow BrdU molecules to be incorporated into the newly synthesized DNA of proliferating cells. After a 48-h incubation with various concentrations of PRL, cell

proliferation was determined by BrdU-based cell proliferation ELISA kit (catalog no. 11647229001; Roche, Mannheim, Germany) according to the manufacturer's instruction. The absorbance of each well was determined at 370 nm with a reference wavelength of 490 nm by a microplate reader (model 1420; Wallac, Turku, Finland). Experiments with seven independent samples per each PRL concentration ($n = 7$) were performed in triplicate.

Cell viability assay

UMR-106 cells were seeded in 96-well culture plates (3,000 cells/well). After a 48-h incubation with various concentrations of PRL, MTT (catalog no. M2128; Sigma) was pipetted into each well to obtain a final concentration of 1 mg/ml. Cells were subsequently incubated at 37°C for 3.5 h, after which the culture medium was discarded. Each well was then filled with 150 µl of MTT solvent (isopropanol containing 4 mM HCl and 0.1% v/v Nonidet P-40), and the plate was finally incubated in the dark for 15 min. In living cells, yellow MTT was enzymatically reduced to purple formazan dye in the mitochondria. The absorbance of each well was determined at 590 nm with a reference wavelength of 620 nm by a microplate reader (model 1420; Wallac). Experiments with seven independent samples per each PRL concentration ($n = 7$) were performed in triplicate.

Total RNA preparation

The total RNA samples were prepared from UMR106 cells using TRIzol reagent (Invitrogen, Carlsbad, CA, USA) according to the manufacturer's instruction. Purity of the total RNA was evaluated by NanoDrop-2000c spectrophotometer (Thermo Scientific, Waltham, MA, USA) reading at 260 and 280 nm, the ratio of which was in the range of 1.8–2.0. One microgram of total RNA was reverse-transcribed with iScript cDNA synthesis kit (Bio-rad, Hercules, CA, USA) to cDNA by a conventional thermal cycler (model MyCycler; Bio-rad). Rat β-actin served as a control gene to check the consistency of the reverse transcription (percent coefficient of variation <5%).

Quantitative real-time PCR (qRT-PCR)

Primers used in this study are shown in Table 1. All the studied genes were first determined by conventional RT-PCR, as previously described [18, 20]. Conventional RT-PCR was performed using GoTaq Green Master Mix (Promega, Madison, WI, USA) and a thermal cycler (model MyCycler; Bio-rad). qRT-PCR and melting curve analyses were operated by Bio-rad MiniOpticon with iQ SYBR Green SuperMix (Bio-rad), as previously described [18, 21]. PCR was performed for 40 cycles at 95°C for 60 s, 51–57°C annealing temperature (Table 1) for 30 s, and 72°C for 30 s. PCR products were also visualized on 2% agarose gel stained with 1 µg/ml ethidium bromide (Sigma) under UV transilluminator (Alpha Innotech, San Leandro, USA). PCR experiments were performed in triplicate with 12 independent samples for each experimental condition ($n = 12$).

Statistical analysis

Unless otherwise specified, the results are expressed as means ± SE, whereas the qRT-PCR data are presented as $\log_2$ means ± SE. Two-group comparisons were performed by Student's t-test. Multiple comparisons were performed by one-way analysis of variance (ANOVA), followed by Dunnett's post-test. The level of significance was $P < 0.05$. Data were analyzed by GraphPad Prism 5 for Windows (GraphPad Software, San Diego, CA, USA).

Results

Before the investigation of PRL effects on mRNA expressions of osteoblast-derived osteoclastogenic factors, the background expression profile of all the studied genes and PRLRs was determined in osteoblast-like UMR106 cells. As shown in Fig. 1a, untreated UMR106 cells strongly expressed OPG, RANKL, MCSF, MCP-1, Cox-2, TNF-α, IL-1, IL-6, EphB4, ephrin-B1 and ephrin-B2. They were also found to constitutively express both PRLR-S and PRLR-L (Fig. 1b), the former of which was of greater abundance by 207% (Fig. 1c), suggesting that UMR106 cells could natively respond to PRL. This was in contrast to the human osteoblast-like MG-63 and Saos-2 cells in which 1,25-dihydroxyvitamin D_3 was necessary to induce PRLR expression [22].

Since it was reported that PRL was a key mediator of maternal bone resorption in lactating rodents [1], and that in the calvaria, RANKL mRNA levels and the RANKL/OPG ratio were significantly increased before returning rapidly to the baseline after weaning [7], the PRL effect on RANKL/OPG expression in the present in vitro UMR106 model was first confirmed. After being exposed to 300 ng/ml PRL for 48 h, UMR106 cells markedly increased RANKL mRNA expression by ~2-fold (Fig. 1d), while OPG mRNA expression was not altered (Fig. 1e). The RANKL/OPG ratio was, therefore, significantly elevated by ~45% (Fig. 1f), consistent with that reported by Ardeshirpour et al. [7]. Thus, the present in vitro model could be used to represent the osteoblastic response to PRL in lactating animals.

Table 1 Primers used in the PCR experiments

Gene	Accession no.	Primer (forward/reverse)	Product length (bp)	Annealing temperature (°C)
Prolactin receptors				
PRLR-S	NM_012630	5′-TTCTACCACCATCGCAAC-3′	120	53
		5′-CTGATCTCGTTTGTCATTGAG-3′		
PRLR-L	NM_001034111	5′-TCAAGCAACCGCAGACTC-3′	107	53
		5′-CAGTTTAGCCAATCGTTCCA-3′		
Anti-osteoclastogenic factor				
OPG	NM_012870	5′-ATTGGCTGAGTGTTCTGGT-3′	140	53
		5′-CTGGTCTCTGTTTTGATGC-3′		
Osteoclastogenic factors				
RANKL	NM_057149	5′-TCGCTCTGTTCCTGTACT-3′	145	53
		5′-AGTGCTTCTGTGTCTTCG-3′		
MCSF	NM_023981	5′-ATCCAGGCAGAGACTGACAGA-3′	182	55
		5′-CGCAGTGTAGATGAACCATCC-3′		
MCP-1	NM_031530	5′-TGAGTCGGCTGGAGAACTA-3′	104	51
		5′-ATTGGGGTCAGCACAGAT-3′		
Cox-2	NM_017232	5′-TATCAGGTCATCGGTGGAGAG-3′	161	56
		5′-CGAAGCCAGATGGTAGCATAC-3′		
TNF-α	NM_012675	5′-GCGTGTTCATCCGTTCTCTA-3′	198	55
		5′-ACTACTTCAGCGTCTCGTGTGT-3′		
IL-1	NM_031512	5′-TCAAGCAGAGCACAGACCTGT-3′	197	56
		5′-TGAGAGACCTGACTTGGCAGA-3′		
IL-6	NM_012589	5′-GCAAGAGACTTCCAGCCAGT-3′	145	54
		5′-AGCCTCCGACTTGTGAAGTG-3′		
EphB4	NM_010144	5′-GTGTATGCCACGATACGCTT-3′	167	56
		5′-ACTGTGTCCACCTTGATGTAGG-3′		
Ephrin-B1	NM_017089	5′-GTCTCTCTCCTTACCTTCGGCA-3′	200	57
		5′-CCAAGCAGCCTCTTCCTCTT-3′		
Ephrin-B2	NM_001107328	5′-AACACTCTCCACAGCACACG-3′	134	56
		5′-TGGGCAGAAGACACTGTCTG-3′		
Housekeeping gene				
β-actin	NM_031144	5′-CAGAGCAAGAGAGGCATCCT-3′	185	56
		5′-GTCATCTTTTCACGGTTGGC-3′		

PRLR-S short isoform of prolactin receptor, *PRLR-L* long isoform of prolactin receptor, *OPG* osteoprotegerin, *RANKL* receptor activator of nuclear factor-κB ligand, *MCSF* macrophage colony-stimulating factor, *MCP-1* monocyte chemoattractant protein-1, *Cox-2* cyclooxygenase-2, *TNF-α*, tumor necrosis factor-α, *IL* interleukin, *EphB4* ephrin type-B receptor 4

To determine the optimal incubating time with PRL, confluent UMR106 cells were incubated with 500 ng/ml PRL for 0, 12, 24, 48, and 72 h. After 48 and 72 h of continuous PRL exposure, RANKL mRNA expression was upregulated by ~2-fold (Fig. 2a). Therefore, the 48-h incubating period was used in the subsequent experiments. Moreover, PRL concentrations used in this study (100–500 ng/ml) did not affect the mRNA expressions of the housekeeping gene β-actin (Fig. 2b) or PRLR-S and -L (Fig. 2c). A 48-h exposure to 100–500 ng/ml PRL affected neither osteoblast proliferation (Fig. 3a) nor viability (Fig. 3b).

The mRNA expressions of six osteoblast-derived osteoclastogenic factors, namely, MCSF, MCP-1, Cox-2, TNF-α, IL-1, and IL-6 were thereafter demonstrated in UMR106 cells exposed for 48 h to various PRL concentrations. As shown in Fig. 4, the mRNA levels of MCP-1, which served to recruit osteoclast progenitors [12, 23], were increased by ~2-fold after exposure to 200–500 ng/ml PRL. Cox-2 mRNA expression was also upregulated by ~3-fold in the presence of 300 ng/ml PRL. Only the higher physiological PRL concentration of 500 ng/ml upregulated TNF-α and IL-1 by ~3-fold and ~2-fold,

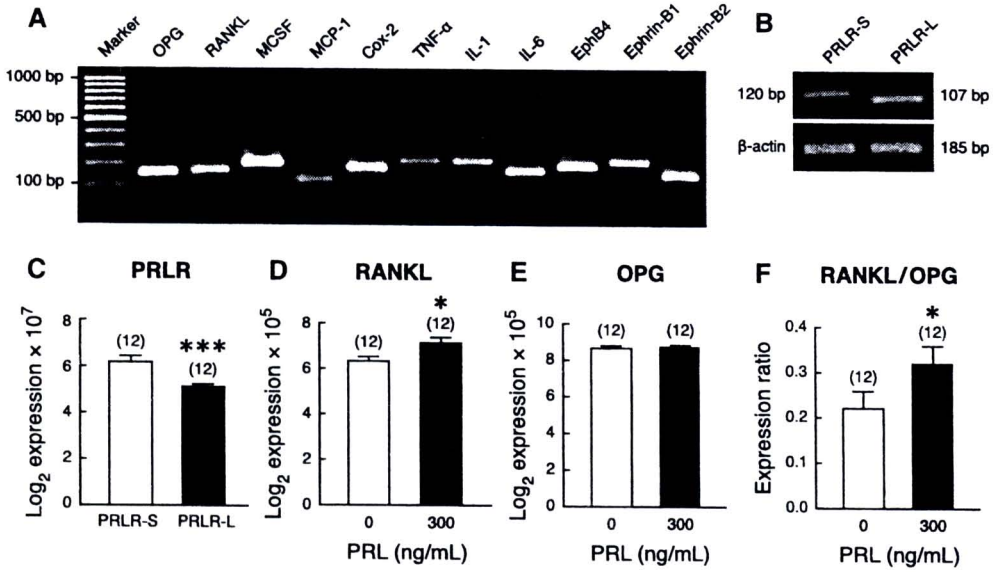

Fig. 1 **a** Representative electrophoretic bands of the osteoblast-derived osteoclast-regulating factors, namely *OPG* osteoprotegerin, *RANKL* receptor activator of nuclear factor-κB ligand, *MCSF* macrophage colony-stimulating factor, *MCP-1* monocyte chemoattractant protein-1, *Cox-2* cyclooxygenase-2, *TNF-α* tumor necrosis factor-α, *IL-1*, *IL-6*, *EphB4*, *ephrin-B1*, *and ephrin-B2* in UMR106 cells at 96 h after seeding. The culture medium was without PRL. Conventional PCR was performed for 40 cycles. **b** Representative electrophoretic bands of short (-S) and long (-L) isoforms of PRLR in UMR106 cells. Expression of β-actin, a housekeeping gene, was also presented along with the studied genes. **c** Expression of PRLR-S and PRLR-L in UMR106 cells at 96 h after seeding, as determined by qRT-PCR. $***P < 0.001$ compared with the PRLR-S expression level. **d–f** Expression of RANKL, OPG, and their expression ratio (RANKL/OPG) in UMR106 cells exposed for 48 h to 300 ng/ml PRL, a physiological concentration comparable to that observed in lactation. The mRNA expression of each gene was quantified in triplicate by qRT-PCR and normalized by β-actin expression. $*P < 0.05$ compared with the control group (0 ng/ml PRL). Numbers in parentheses represent the numbers of independent samples

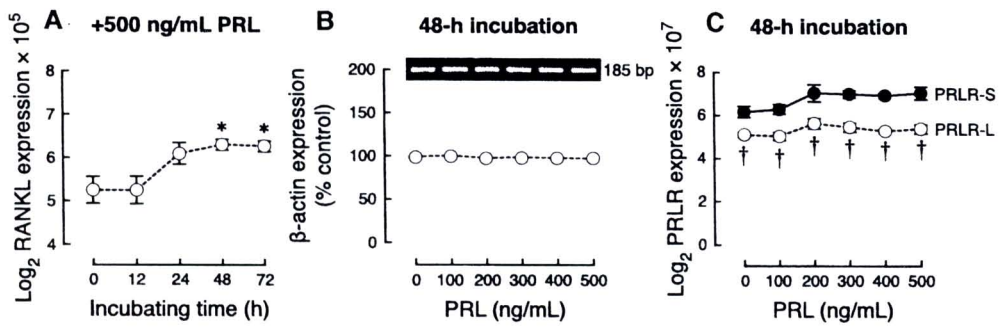

Fig. 2 **a** Expression of RANKL in UMR106 cells after direct exposure to 500 ng/ml PRL for 0 (control), 12, 24, 48, or 72 h. $*P < 0.05$ compared with the control group (one-way ANOVA). **b** Expression of β-actin, a housekeeping gene for normalization, in UMR106 cells directly exposed for 48 h to 0 (normal medium), 100, 200, 300, 400, or 500 ng/ml PRL. A representative electrophoretic image is also depicted. **c** Expression of short (-S) and long (-L) isoforms of PRLR in UMR106 cells exposed for 48 h to 0 (normal medium), 100, 200, 300, 400 or 500 ng/ml PRL. $^{\dagger}P < 0.001$ compared with the corresponding PRLR-S expression level (Student's *t*-test). The mRNA expression of each gene in 12 independent samples ($n = 12$ per group) was determined by qRT-PCR

respectively. In contrast, neither the MCSF nor the IL-6 mRNA expressions were affected by 100–500 ng/ml PRL.

Besides activating osteoclasts by the cytokine-mediated mechanism, osteoblasts also activate osteoclasts by a direct contact through Eph/ephrin interaction [12, 13]. As depicted in Fig. 5, only ephrin-B1 mRNA expression was significantly increased by ~2-fold after a 48-h exposure to 300 ng/ml PRL. The upregulation of ephrin-B1 and Cox-2 by 300 ng/ml, but not by lower or higher concentrations, could be considered as biphasic PRL responses as previously reported in other tissues, such as small intestine and Leydig cells [24, 25]. None of the PRL concentrations had any effect on the mRNA expression of EphB4 and ephrin-B2.

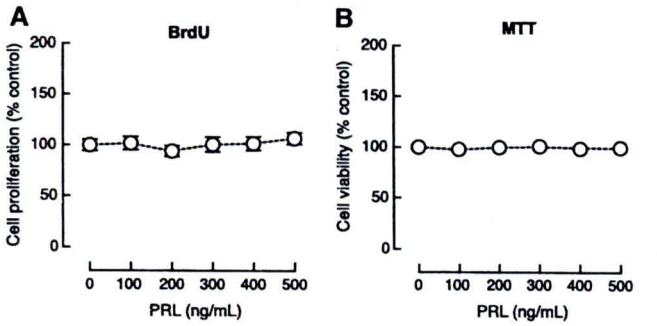

Fig. 3 **a** Proliferation and **b** viability of UMR106 cells after direct exposure for 48 h to 0 (normal medium; control), 100, 200, 300, 400, or 500 ng/ml PRL. Cell proliferation and viability in seven independent samples ($n = 7$ per group) were evaluated in triplicate by BrdU and MTT assays, respectively. The values of the control group (0 ng/ml PRL) were normalized to 100%

Discussion

The lactation-related skeletal changes, including rapid trabecular bone resorption and osteopenia [26, 27], were induced by the interplay between a number of hormones, such as PRL and parathyroid hormone-related peptide [1, 2, 28]. After binding to its receptors on osteoblasts, PRL was proposed to participate in the lactation-induced suppression of osteoblast functions, for example, by inhibiting alkaline phosphatase activity [4]. Moreover, PRL activated the osteoclast functions, as indicated by the increased active osteoclast surface and eroded surface in bone trabeculae [1]. Although little is known regarding the molecular mechanism of PRL action on bone resorption, its actions on the osteoclasts could only occur through the osteoblasts because osteoclasts did not express functional PRLR [4]. In General, osteoblasts recruit and activate osteoclasts by (i) upregulating RANKL and/or downregulating OPG, a decoy receptor of RANKL [6]; (ii) enhancing the productions of osteoclast-regulating factors, such as MCSF, IL-1, IL-6, TNF-α, MCP-1, and prostaglandin E2 (via Cox-2); and (iii) mediating osteoclast maturation through Eph/ephrin interaction [6, 8–10]. Herein, the evidence, for the first time, was provided in this study that osteoblasts could respond to high physiological levels of PRL by enhancing the mRNA expression of RANKL, MCP-1, Cox-2, TNF-α, IL-1, and ephrin-B1.

Previous investigations suggested that an increase in RANKL/OPG ratio, presumably under the regulation of PRL, was responsible for the enhanced osteoclastic bone resorption in lactating rodents [5, 7]. Consistent with that reported in the calvaria of lactating mice [7], the RANKL/OPG ratio in UMR106 cells was mainly increased by an upregulation of RANKL, but not by a downregulation of OPG. However, a higher pathological PRL concentration (1,000 ng/ml) could also downregulate OPG mRNA levels in osteoblasts, and chronic hyperprolactinemia in pituitary-grafted rats led to a reduction in serum OPG levels [5], thereby further enhancing the RANKL action. These findings also agreed with a report in humans that serum OPG levels in prolonged lactation were lower than that in near-term pregnancy [29]. It was apparent that the responses of osteoblasts to PRL in term of RANKL/OPG expressions were dependent on the age of the animals from which bone cells were derived. This was partly due to the

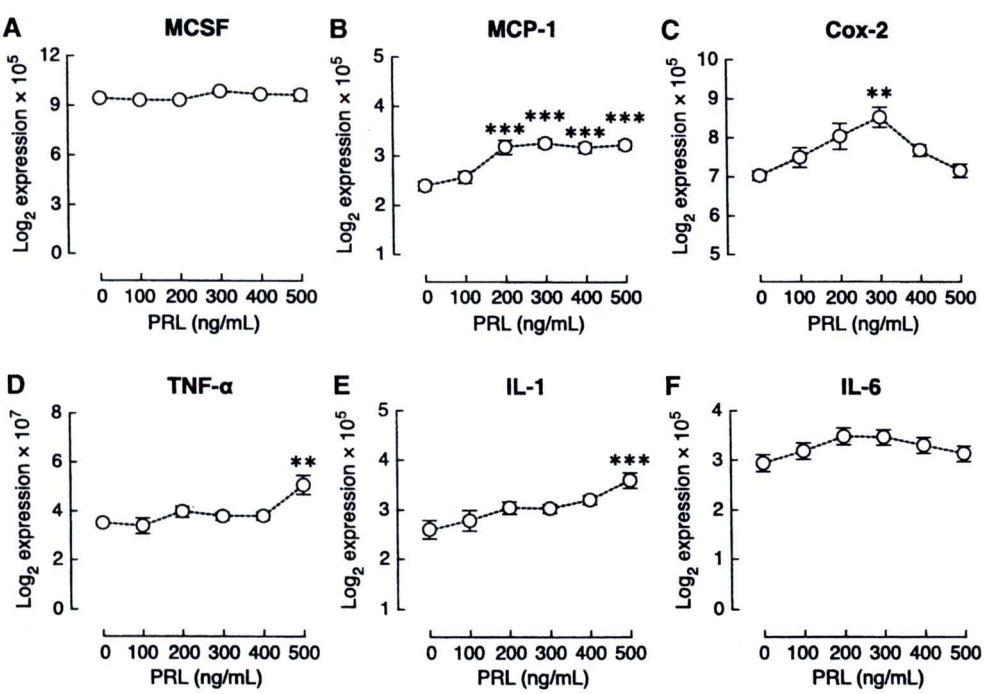

Fig. 4 Expression of **a** macrophage colony-stimulating factor (MCSF), **b** monocyte chemoattractant protein (MCP)-1, **c** cyclooxygenase (Cox)-2, **d** tumor necrosis factor (TNF)-α, **e** interleukin (IL)-1, **f** IL-6 in UMR106 cells directly exposed for 48 h to 0 (normal medium; control), 100, 200, 300, 400, or 500 ng/ml PRL. The mRNA expression of each gene in 12 independent samples ($n = 12$ per group) was determined by qRT-PCR, and was normalized to β-actin mRNA expression. $^{**}P < 0.01$, $^{***}P < 0.001$ compared with the control group (0 ng/ml PRL)

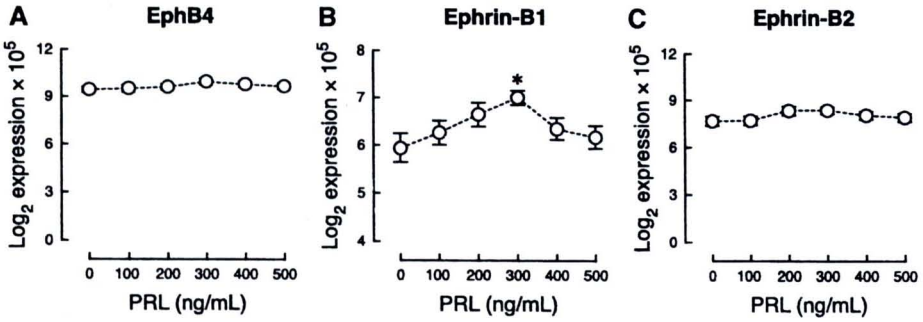

Fig. 5 Expression of **a** ephrin type-B receptor 4 (EphB4), **b** ephrin-B1, **c** ephrin-B2 in UMR106 cells directly exposed for 48 h to 0 (normal medium; control), 100, 200, 300, 400, or 500 ng/ml PRL. The mRNA expression of each gene in 12 independent samples ($n = 12$ per group) was determined by qRT-PCR, and was normalized to β-actin mRNA expression. $^*P < 0.05$ compared with the control group (0 ng/ml PRL)

age-dependent effect of PRL, which induced net bone gain in young growing individuals [30], but net bone loss in adults [31]. It was previously shown that human fetal osteoblast cells responded to PRL by decreasing the RANKL/OPG ratio [32], whereas primary osteoblasts derived from adolescent rats showed no change in the RANKL/OPG ratio [33]. Since the present PRL-induced increase in RANKL/OPG ratio agreed well with the high ratio observed in lactating mice [7], the rat osteoblast-like UMR106 cell line was an appropriate model for studying PRL effects.

Although the PRL-induced increase in RANKL/OPG ratio could explain osteoclast hyperactivity and trabecular erosion in lactating animals [5], this ratio alone could not fully explain the increase in osteoclast "number" during lactation because RANKL predominantly promoted the differentiation, but not proliferation, of osteoclast precursors [34]. It was, therefore, possible that other cytokines from osteoblasts and stromal cells, such as MCSF and MCP-1, contributed to the recruitment and proliferation as well as differentiation of osteoclast precursors [6, 12, 23]. In this study, despite having no effect on MCSF mRNA expression, 200–500 ng/ml PRL markedly upregulated the mRNA expression of the chemotactic cytokine MCP-1, which might in turn increase the number of osteoclast precursors in the vicinity of the resorptive area.

Other osteoblast-derived humoral factors, including TNF-α, IL-1, and prostaglandin E2 (produced by Cox-2), have been known to potentiate osteoclastogenesis and osteoclast activity [8, 10]. The release of prostaglandin E2 from osteoblasts as a result of upregulated Cox-2 was capable of enhancing the osteoclastic bone resorption [10, 11]. TNF-α also directly stimulated pre-osteoclast differentiation in vitro [9, 35–37]. In addition, TNF-α together with IL-1 helped in maintaining MCP-1 expression, which in turn facilitated the osteoclast recruitment, differentiation, and fusion [12, 23, 38]. Incidentally, the interactions among these factors could be complicated by the dose-specific responses of osteoblasts to PRL. For example, the upregulation of particular genes, such as TNF-α and IL-1, was observed only at a high PRL concentration of 500 ng/ml, implicating that the overexpression of TNF-α and IL-1 occurred only during suckling (when plasma PRL surge reached 500 ng/ml) to further stimulate the osteoclasts that had already been exposed to high RANKL levels induced by the baseline PRL concentration ($\sim$300 ng/ml) in lactating rats. Previous studies have provided corroborative evidence that the TNF-α-induced osteoclast differentiation in vitro was augmented in the presence of RANKL [37, 39], and the RANKL-primed osteoclasts did exist in ample number in maternal bone [7]. Indeed, the increased activity of osteoclasts might contribute considerably to the provision of a large quantity of calcium for milk production during suckling. It was apparent that intestinal calcium absorption and bone calcium release correlated with milk production [16, 27].

Besides inducing the mRNA expression of several osteoclastogenic factors, PRL also upregulated the expression of ephrin-B1, suggesting that PRL facilitated osteoblast-osteoclast communication through a direct cell–cell contact. Under normal conditions, a direct binding of EphB4 localized on the plasma membrane of osteoblasts to its ligand type-B ephrin (particularly ephrin-B2) on osteoclasts is known to stimulate osteoblastic bone formation, while inhibiting osteoclastic bone resorption [12, 40]. On the other hand, a direct interaction between ephrin-B1 on osteoblasts and EphB1 on monocytes or osteoclast precursors might have a role in the regulation of osteoclastogenesis [41, 42]. It was, therefore, possible that PRL enhanced bone resorption, in part, through the potentiation of EphB1/ephrin-B1 signaling, rather than the suppression of EphB4/ephrin-B2 signaling. However, the physiological significance of EphB1/ephrin-B1 interaction in bone resorption remains elusive, and further experiment is required to demonstrate an in vivo osteoblast-osteoclast contact in maternal bone.

Similar to Cox-2 mRNA expression, the PRL effect on ephrin-B1 expression was observed only in the presence of

300 ng/ml PRL, with lower or higher concentrations having no significant effects. Such biphasic and/or dose-specific responses to PRL were previously reported in several tissues and cells, e.g., small intestine, Leydig cells, mammary cells, and adrenocortical carcinoma cells [24, 25, 43, 44]. The exact explanation for this phenomenon is currently unknown but is generally explained by the increased amount of non-functional PRL–PRLR complex at high PRL concentrations. Normally, binding of one PRL molecule with two PRLRs induces dimerization of PRLRs, which in turn activates the downstream signaling cascade. At very high PRL concentrations, PRL binds to PRLR as a non-functional 1:1 PRL–PRLR complex rather than the functional 1:2 complex [45, 46], resulting in reduced downstream PRL signal transduction. The presence of different PRLR isoforms in the same cell type further added to the complexity to PRL signaling. Similar to the endothelial cells and hepatocytes [47–49], primary rat osteoblasts [5] and UMR106 cells (Fig. 1c) predominantly expressed more PRLR-S than PRLR-L, although PRL actions in several other tissues, such as intestine and mammary glands, were mainly mediated by PRLR-L [2, 45]. Little is known regarding the physiological significance of PRLR-S function, but the presence of PRLR-S was able to rescue mammopoiesis in $PRLR^{+/-}$ mice, and induced a specific response to PRL [47, 50, 51]. It was also possible that the observed PRL actions in UMR106 cells were mediated by PRLR-S.

In addition to the PRL-induced activation of osteoclasts through osteoblasts, PRL also suppressed the osteoblastic functions, e.g., osteocalcin expression and alkaline phosphatase activity [4, 52]. Although a 48-h exposure to 100–500 ng/ml PRL had no effect on the osteoblast proliferation (Fig. 3a) or cell viability (Fig. 3b), prolonged exposure to 100 ng/ml PRL for 5–21 days did inhibit osteoblast proliferation in vitro, but did not induce apoptosis of osteoblasts [52]. However, the long-term effects of PRL on osteoblast proliferation and functions might not be of physiological significance since bone surface covered by differentiated osteoblasts was not increased in 8–14 days of lactation [1].

In conclusion, besides RANKL, we provided corroborative evidence that high physiological PRL concentrations were capable of upregulating several other osteoblast-derived osteoclastogenic mediators, namely MCP-1, Cox-2, TNF-α, IL-1, and ephrin-B1, in UMR106 cells without affecting cell proliferation and viability. These mediators have been known to recruit osteoclast precursors to the resorptive area, and/or to induce proliferation, differentiation, and activation of osteoclasts [6, 8–10, 12]. Although further investigation is required to demonstrate the PRL-induced changes in protein expression levels as well as the related physiological significance in vivo and underlying molecular mechanisms, the findings of this study introduced, for the first time, the possible contributions of other osteoclastogenic mediators besides RANKL, which might help us explain the PRL-induced osteoclastic bone resorption in lactating mothers. Moreover, it was shown that UMR106 cell line that constitutively expressed PRLR was probably the most suitable in vitro model for studying PRL effects on osteoblasts since a high physiological PRL concentration (300 ng/ml), comparable to the plasma levels in lactation, increased the RANKL/OPG ratio by principally upregulating RANKL mRNA expression, agreeing with the pattern observed in lactating mice [7].

Acknowledgments The authors thank Amporn Nuntapornsak and Wacharaporn Tiyasatkulkovit for their excellent technical assistance. This research was supported by grants from the Faculty of Science, Mahidol University (SCY52-02 and SCR53-06 to N. Charoenphandhu), the Faculty of Allied Health Sciences, Burapha University (to K. Wongdee), and Thailand Research Fund (RSA5180001 to N. Charoenphandhu).

Conflict of interest None.

References

1. Suntornsaratoon P, Wongdee K, Goswami S, Krishnamra N, Charoenphandhu N (2010) Bone modeling in bromocriptine-treated pregnant and lactating rats: possible osteoregulatory role of prolactin in lactation. Am J Physiol Endocrinol Metab 299:E426–E436. doi:10.1152/ajpendo.00134.2010
2. Charoenphandhu N, Wongdee K, Krishnamra N (2010) Is prolactin the cardinal calciotropic maternal hormone? Trends Endocrinol Metab 21:395–401. doi:10.1016/j.tem.2010.02.002
3. Clément-Lacroix P, Ormandy C, Lepescheux L, Ammann P, Damotte D, Goffin V, Bouchard B, Amling M, Gaillard-Kelly M, Binart N, Baron R, Kelly PA (1999) Osteoblasts are a new target for prolactin: analysis of bone formation in prolactin receptor knockout mice. Endocrinology 140:96–105. doi:10.1210/en.140.1.96
4. Coss D, Yang L, Kuo CB, Xu X, Luben RA, Walker AM (2000) Effects of prolactin on osteoblast alkaline phosphatase and bone formation in the developing rat. Am J Physiol Endocrinol Metab 279:E1216–E1225
5. Seriwatanachai D, Thongchote K, Charoenphandhu N, Pandaranandaka J, Tudpor K, Teerapornpuntakit J, Suthiphongchai T, Krishnamra N (2008) Prolactin directly enhances bone turnover by raising osteoblast-expressed receptor activator of nuclear factor κB ligand/osteoprotegerin ratio. Bone 42:535–546. doi:10.1016/j.bone.2007.11.008
6. Teitelbaum SL (2000) Bone resorption by osteoclasts. Science 289:1504–1508. doi:10.1126/science.289.5484.1504
7. Ardeshirpour L, Dann P, Adams DJ, Nelson T, VanHouten J, Horowitz MC, Wysolmerski JJ (2007) Weaning triggers a decrease in receptor activator of nuclear factor-κB ligand expression, widespread osteoclast apoptosis, and rapid recovery of bone mass after lactation in mice. Endocrinology 148:3875–3886. doi:10.1210/en.2006-1467
8. Ragab AA, Nalepka JL, Bi Y, Greenfield EM (2002) Cytokines synergistically induce osteoclast differentiation: support by

immortalized or normal calvarial cells. Am J Physiol Cell Physiol 283:C679–C687. doi:10.1152/ajpcell.00421.2001
9. Kwan Tat S, Padrines M, Théoleyre S, Heymann D, Fortun Y (2004) IL-6, RANKL, TNF-alpha/IL-1: interrelations in bone resorption pathophysiology. Cytokine Growth Factor Rev 15:49–60. doi:10.1016/j.cytogfr.2003.10.005
10. Han SY, Lee NK, Kim KH, Jang IW, Yim M, Kim JH, Lee WJ, Lee SY (2005) Transcriptional induction of cyclooxygenase-2 in osteoclast precursors is involved in RANKL-induced osteoclastogenesis. Blood 106:1240–1245. doi:10.1182/blood-2004-12-4975
11. Kawashima M, Fujikawa Y, Itonaga I, Takita C, Tsumura H (2009) The effect of selective cyclooxygenase-2 inhibitor on human osteoclast precursors to influence osteoclastogenesis in vitro. Mod Rheumatol 19:192–198. doi:10.1007/s10165-008-0149-6
12. Matsuo K, Irie N (2008) Osteoclast–osteoblast communication. Arch Biochem Biophys 473:201–209. doi:10.1016/j.abb.2008.03.027
13. Mundy GR, Elefteriou F (2006) Boning up on ephrin signaling. Cell 126:441–443. doi:10.1016/j.cell.2006.07.015
14. Compagni A, Logan M, Klein R, Adams RH (2003) Control of skeletal patterning by EphrinB1–EphB interactions. Dev Cell 5:217–230. doi:10.1016/S1534-5807(03)00198-9
15. Twigg SR, Kan R, Babbs C, Bochukova EG, Robertson SP, Wall SA, Morriss-Kay GM, Wilkie AO (2004) Mutations of ephrin-B1 (EFNB1), a marker of tissue boundary formation, cause craniofrontonasal syndrome. Proc Natl Acad Sci USA 101:8652–8657. doi:10.1073/pnas.0402819101
16. Charoenphandhu N, Nakkrasae LI, Kraidith K, Teerapornpuntakit J, Thongchote K, Thongon N, Krishnamra N (2009) Two-step stimulation of intestinal Ca^{2+} absorption during lactation by long-term prolactin exposure and suckling-induced prolactin surge. Am J Physiol Endocrinol Metab 297:E609–E619. doi:10.1152/ajpendo.00347.2009
17. Partridge NC, Alcorn D, Michelangeli VP, Ryan G, Martin TJ (1983) Morphological and biochemical characterization of four clonal osteogenic sarcoma cell lines of rat origin. Cancer Res 43:4308–4314
18. Nuntapornsak A, Wongdee K, Thongbunchoo J, Krishnamra N, Charoenphandhu N (2010) Changes in the mRNA expression of osteoblast-related genes in response to β_3-adrenergic agonist in UMR106 cells. Cell Biochem Funct 28:45–51. doi:10.1002/cbf.1617
19. Li J, Jiang L, Liao G, Chen G, Liu Y, Wang J, Zheng Y, Luo S, Zhao Z (2009) Centrifugal forces within usually-used magnitude elicited a transitory and reversible change in proliferation and gene expression of osteoblastic cells UMR-106. Mol Biol Rep 36:299–305. doi:10.1007/s11033-007-9179-y
20. Wongdee K, Riengrojpitak S, Krishnamra N, Charoenphandhu N (2010) Claudin expression in the bone-lining cells of female rats exposed to long-standing acidemia. Exp Mol Pathol 88:305–310. doi:10.1016/j.yexmp.2009.12.005
21. Wongdee K, Teerapornpuntakit J, Riengrojpitak S, Krishnamra N, Charoenphandhu N (2009) Gene expression profile of duodenal epithelial cells in response to chronic metabolic acidosis. Mol Cell Biochem 321:173–188. doi:10.1007/s11010-008-9931-1
22. Bataille-Simoneau N, Gerland K, Chappard D, Basle MF, Mercier L (1996) Expression of prolactin receptors in human osteosarcoma cells. Biochem Biophys Res Commun 229:323–328. doi:10.1006/bbrc.1996.1800
23. Graves DT, Jiang Y, Valente AJ (1999) The expression of monocyte chemoattractant protein-1 and other chemokines by osteoblasts. Front Biosci 4:D571–D580
24. Jantarajit W, Thongon N, Pandaranandaka J, Teerapornpuntakit J, Krishnamra N, Charoenphandhu N (2007) Prolactin-stimulated transepithelial calcium transport in duodenum and Caco-2 monolayer are mediated by the phosphoinositide 3-kinase pathway. Am J Physiol Endocrinol Metab 293:E372–E384. doi:10.1152/ajpendo.00142.2007
25. Manna PR, El-Hefnawy T, Kero J, Huhtaniemi IT (2001) Biphasic action of prolactin in the regulation of murine Leydig tumor cell functions. Endocrinology 142:308–318. doi:10.1210/en.142.1.308
26. Bowman BM, Miller SC (2001) Skeletal adaptations during mammalian reproduction. J Musculoskelet Neuronal Interact 1:347–355
27. Kovacs CS (2005) Calcium and bone metabolism during pregnancy and lactation. J Mammary Gland Biol Neoplasia 10:105–118. doi:10.1007/s10911-005-5394-0
28. VanHouten JN, Wysolmerski JJ (2003) Low estrogen and high parathyroid hormone-related peptide levels contribute to accelerated bone resorption and bone loss in lactating mice. Endocrinology 144:5521–5529. doi:10.1210/en.2003-0892
29. Naylor KE, Rogers A, Fraser RB, Hall V, Eastell R, Blumsohn A (2003) Serum osteoprotegerin as a determinant of bone metabolism in a longitudinal study of human pregnancy and lactation. J Clin Endocrinol Metab 88:5361–5365. doi:10.1210/jc.2003-030486
30. Krishnamra N, Seemoung J (1996) Effects of acute and long-term administration of prolactin on bone ^{45}Ca uptake, calcium deposit, and calcium resorption in weaned, young, and mature rats. Can J Physiol Pharmacol 74:1157–1165
31. Thongchote K, Charoenphandhu N, Krishnamra N (2008) High physiological prolactin induced by pituitary transplantation decreases BMD and BMC in the femoral metaphysis, but not in the diaphysis of adult female rats. J Physiol Sci 58:39–45. doi:10.2170/physiolsci.RP015007
32. Seriwatanachai D, Charoenphandhu N, Suthiphongchai T, Krishnamra N (2008) Prolactin decreases the expression ratio of receptor activator of nuclear factor κB ligand/osteoprotegerin in human fetal osteoblast cells. Cell Biol Int 32:1126–1135. doi:10.1016/j.cellbi.2008.04.026
33. Charoenphandhu N, Teerapornpuntakit J, Methawasin M, Wongdee K, Thongchote K, Krishnamra N (2008) Prolactin decreases expression of Runx2, osteoprotegerin, and RANKL in primary osteoblasts derived from tibiae of adult female rats. Can J Physiol Pharmacol 86:240–248. doi:10.1139/y08-037
34. Pacifici R (2008) Mechanisms of estrogen action in bone. In: Bilezikian JP, Raisz LG, Martin TJ (eds) Principles of bone biology, 3rd edn. Academic Press, San Diego, pp 921–934
35. Kobayashi K, Takahashi N, Jimi E, Udagawa N, Takami M, Kotake S, Nakagawa N, Kinosaki M, Yamaguchi K, Shima N, Yasuda H, Morinaga T, Higashio K, Martin TJ, Suda T (2000) Tumor necrosis factor α stimulates osteoclast differentiation by a mechanism independent of the ODF/RANKL-RANK interaction. J Exp Med 191:275–286
36. Azuma Y, Kaji K, Katogi R, Takeshita S, Kudo A (2000) Tumor necrosis factor-α induces differentiation of and bone resorption by osteoclasts. J Biol Chem 275:4858–4864. doi:10.1074/jbc.275.7.4858
37. Lam J, Takeshita S, Barker JE, Kanagawa O, Ross FP, Teitelbaum SL (2000) TNF-α induces osteoclastogenesis by direct stimulation of macrophages exposed to permissive levels of RANK ligand. J Clin Invest 106:1481–1488. doi:10.1172/JCI11176
38. Li X, Qin L, Bergenstock M, Bevelock LM, Novack DV, Partridge NC (2007) Parathyroid hormone stimulates osteoblastic expression of MCP-1 to recruit and increase the fusion of

pre/osteoclasts. J Biol Chem 282:33098–33106. doi:10.1074/jbc.M611781200
39. Kim JH, Jin HM, Kim K, Song I, Youn BU, Matsuo K, Kim N (2009) The mechanism of osteoclast differentiation induced by IL-1. J Immunol 183:1862–1870. doi:10.4049/jimmunol.0803007
40. Edwards CM, Mundy GR (2008) Eph receptors and ephrin signaling pathways: a role in bone homeostasis. Int J Med Sci 5:263–272
41. Kitamura T, Kabuyama Y, Kamataki A, Homma MK, Kobayashi H, Aota S, Kikuchi S, Homma Y (2008) Enhancement of lymphocyte migration and cytokine production by ephrinB1 system in rheumatoid arthritis. Am J Physiol Cell Physiol 294:C189–C196. doi:10.1152/ajpcell.00314.2007
42. Yu G, Luo H, Wu Y, Wu J (2004) EphrinB1 is essential in T-cell-T-cell co-operation during T-cell activation. J Biol Chem 279:55531–55539. doi:10.1074/jbc.M410814200
43. Döll F, Pfeilschifter J, Huwiler A (2007) Prolactin upregulates sphingosine kinase-1 expression and activity in the human breast cancer cell line MCF7 and triggers enhanced proliferation and migration. Endocr Relat Cancer 14:325–335. doi:10.1677/ERC-06-0050
44. Jaroenporn S, Furuta C, Nagaoka K, Watanabe G, Taya K (2008) Comparative effects of prolactin versus ACTH, estradiol, progesterone, testosterone, and dihydrotestosterone on cortisol release and proliferation of the adrenocortical carcinoma cell line H295R. Endocrine 33:205–209. doi:10.1007/s12020-008-9075-9
45. Binart N, Bachelot A, Bouilly J (2010) Impact of prolactin receptor isoforms on reproduction. Trends Endocrinol Metab 21:362–368. doi:10.1016/j.tem.2010.01.008
46. Fuh G, Colosi P, Wood WI, Wells JA (1993) Mechanism-based design of prolactin receptor antagonists. J Biol Chem 268: 5376–5381
47. Jahn GA, Daniel N, Jolivet G, Belair L, Bole-Feysot C, Kelly PA, Djiane J (1997) In vivo study of prolactin (PRL) intracellular signalling during lactogenesis in the rat: JAK/STAT pathway is activated by PRL in the mammary gland but not in the liver. Biol Reprod 57:894–900. doi:10.1095/biolreprod57.4.894
48. Nagano M, Kelly PA (1994) Tissue distribution and regulation of rat prolactin receptor gene expression. Quantitative analysis by polymerase chain reaction. J Biol Chem 269:13337–13345
49. Ricken AM, Traenkner A, Merkwitz C, Hummitzsch K, Grosche J, Spanel-Borowski K (2007) The short prolactin receptor predominates in endothelial cells of micro- and macrovascular origin. J Vasc Res 44:19–30. doi:10.1159/000097892
50. Binart N, Imbert-Bolloré P, Baran N, Viglietta C, Kelly PA (2003) A short form of the prolactin (PRL) receptor is able to rescue mammopoiesis in heterozygous PRL receptor mice. Mol Endocrinol 17:1066–1074. doi:10.1210/me.2002-0181
51. Gadd SL, Clevenger CV (2006) Ligand-independent dimerization of the human prolactin receptor isoforms: functional implications. Mol Endocrinol 20:2734–2746. doi:10.1210/me.2006-0114
52. Seriwatanachai D, Krishnamra N, van Leeuwen JP (2009) Evidence for direct effects of prolactin on human osteoblasts: inhibition of cell growth and mineralization. J Cell Biochem 107: 677–685. doi:10.1002/jcb.22161

Histochem Cell Biol (2010) 134:483–491
DOI 10.1007/s00418-010-0745-3

Possible chondroregulatory role of prolactin on the tibial growth plate of lactating rats

Panan Suntornsaratoon · Kannikar Wongdee · Nateetip Krishnamra · Narattaphol Charoenphandhu

Accepted: 16 September 2010 / Published online: 2 October 2010

Abstract Besides calcium accretion in the cortical envelope, a marked increase in the length of long bone was observed in pregnant and lactating rats, and thus the growth plate change was anticipated. Since several bone changes, such as massive trabecular bone resorption in late lactation, were found to be prolactin (PRL)-dependent, PRL may also be responsible for the maternal bone elongation. Herein, we investigated the growth plate change and possible chondroregulatory roles of PRL in the tibiae of rats at mid-pregnancy until 15 days postweaning. We found that the tibial length of lactating rats was increased and was inversely correlated with the total growth plate height, as well as the heights of proliferating zone (PZ) and hypertrophic zone (HZ), but not the resting zone (RZ). Chondrocytes in all zones expressed PRL receptors as visualized by immunohistochemistry, suggesting that the growth plate cartilage was a target of PRL action. Further investigations in lactating rats treated with an inhibitor of pituitary PRL release, bromocriptine, with or without PRL supplement, revealed the PRL-induced decreases in total growth plate height and HZ height from early to late lactation. However, decreases in RZ and PZ heights were observed only in late and mid-lactation, respectively. Thus, this was the first report on the chondroregulatory action of PRL on the growth plate of long bone in lactating rats. The results provided better understanding of the maternal bone adaptation during lactation.

Keywords Cartilage · Chondrocytes · Goldner's trichrome · Hyperprolactinemia · Immunohistochemistry · Prolactin receptor

P. Suntornsaratoon · K. Wongdee · N. Krishnamra · N. Charoenphandhu
Consortium for Calcium and Bone Research (COCAB), Faculty of Science, Mahidol University, Rama VI Road, Bangkok 10400, Thailand

P. Suntornsaratoon · N. Krishnamra · N. Charoenphandhu (✉)
Department of Physiology, Faculty of Science, Mahidol University, Rama VI Road, Bangkok 10400, Thailand
e-mail: naratt@narattsys.com

K. Wongdee
Faculty of Allied Health Sciences, Burapha University, Chonburi 20131, Thailand

Introduction

During pregnancy and lactation, the microstructure of maternal bone is markedly changed to meet mineral demand for fetal skeletal development and milk production (Bowman and Miller 2001; Charoenphandhu et al. 2010). Specifically, pregnancy induces bone calcium accretion in the cortical and trabecular parts of the long bone as a reserved pool for later use, whereas lactation induces progressive trabecular bone loss (Charoenphandhu et al. 2010; Suntornsaratoon et al. 2010a, b). Although maternal osteopenia in humans is usually asymptomatic and reversible, some individuals may experience severe pathological bone loss, known as pregnancy/lactation-induced osteoporosis with low-back pain, loss of height, fragility fracture, and non-traumatic vertebral compression (Ofluoglu and Ofluoglu 2008). Besides cortical and trabecular bone changes, femoral bone length in rats was also increased during pregnancy and appeared to continue through late lactation, presumably to further expand the calcium reserve pool, and to maintain bone strength (Suntornsaratoon et al. 2010a, b). Such increased bone

length probably results from the pregnancy- and/or lactation-induced endochondral bone growth, which is the principal mechanism for elongation of long bones, especially femora, tibiae, and humeri (Bowman and Miller 2001; Rauch 2005). This process might also help replenish the metaphyseal spongiosa that is markedly resorbed during lactation (Rauch 2005; Suntornsaratoon et al. 2010a).

Generally, endochondral bone growth initiates at the growth plate cartilage with a sequence of chondrocyte proliferation, differentiation, hypertrophy, and apoptosis, thereby permitting vascular invasion and entrance of osteoprogenitor cells to replace degenerated chondrocytes with calcified bone matrix (Gartner and Hiatt 2001; Olsen 2006; Rauch 2005). In tibiae and femora, the growth plate cartilage is organized into three zones, namely resting zone (RZ), proliferating zone (PZ) and hypertrophic zone (HZ) (Rauch 2005). Van Buul-Offers and colleagues (1984) reported that longitudinal bone growth in rodents was closely associated with the heights of the growth plate zones, and an increase in tibial length showed negative correlations with the heights of RZ and PZ. Therefore, changes in the growth plate zones were anticipated in pregnant and lactating rats with the increased bone length.

Complex maternal bone changes are tightly regulated by a number of humoral factors, such as osteoprotegerin, insulin-like growth factor (IGF)-1, and parathyroid hormone-related peptide (PTHrP) (Hong et al. 2005; Kovacs 2005; O'Brien et al. 2006). Moreover, a recent investigation in rats revealed that prolactin (PRL) released from the pituitary gland during pregnancy (plasma levels ~100–200 ng/mL) and lactation (up to ~650 ng/mL; normal levels ~7–10 ng/mL) was also an important regulator of bone metabolism during these reproductive periods (Seriwatanachai et al. 2008; Suntornsaratoon et al. 2010a). After binding to PRL receptors (PRLR) on osteoblasts, PRL induced trabecular bone resorption and calcium release through the synthesis of an osteoblast-derived osteoclastogenic factor, namely receptor activator of nuclear factor-κB ligand (Seriwatanachai et al. 2008). Besides the osteoblasts, chondrocytes isolated from the rat articular cartilage were also found to express functional PRLR, which could prevent apoptosis of this cell type in vitro (Zermeño et al. 2006). Nevertheless, whether the growth plate changes during pregnancy and lactation were also PRL-dependent remained unknown.

Therefore, the objectives of the present study were (1) to demonstrate that growth plate chondrocytes expressed PRLR proteins, (2) to investigate changes in the growth plate zones during pregnancy and lactation, and (3) to provide evidence that growth plate changes in these reproductive periods were dependent on PRL.

Materials and methods

Animals

Non-mated (nulliparous) and pregnant Sprague-Dawley rats were obtained from the National Laboratory Animal Centre, Salaya, Nakhon Pathom, Thailand. They were housed in standard stainless steel cages under 12-h light/dark cycle for at least 7 days prior to the experiments and were fed standard chow and distilled water ad libitum. The room temperature was 25 ± 2°C with average illuminance of 200 lux and relative humidity of ~50–60%. This study has been approved by the Animal Care and Use Committee of the Faculty of Science, Mahidol University, Thailand.

Experimental design

The present experimental design was based on the previous experiment by Suntornsaratoon et al. (2010a, b) and used a new collection of bone specimens. In brief, the tibial growth plate changes were investigated in different reproductive phases, i.e., mid-pregnancy (day 14 of pregnancy; P14), late pregnancy (day 21; P21), early lactation (day 8 of lactation; L8), mid-lactation (day 14; L14), late lactation (day 21; L21) and day 15 postweaning (PW), as well as in the age-matched nulliparous controls. The ages of P14, P21, L8, L14, L21, and PW rats were 10, 11, 12, 13, 14, and 16 weeks, respectively. After delivery, the litter size was adjusted to 8 pups/dam for all lactating groups. In some experiments, dams were daily injected for 7 days prior to the experiment with 4 mg/kg bromocriptine s.c. (Bromo) (Sigma, St. Louis, MO, USA), or Bromo + PRL s.c. (purified from ovine pituitary gland; catalog no. L6520; Sigma). PRL doses for pregnant and lactating rats were 0.4 and 0.6 mg/kg/day, respectively, as reported previously (Charoenphandhu et al. 2009). This regimen of Bromo administration was found to successfully abolish hyperprolactinemia in maternal rats (Charoenphandhu et al. 2009). Finally, maternal rats were killed on the aforementioned designated time. Their tibiae and femora were removed and measured for total length.

Histomorphometric measurement of growth plate height

After being removed from maternal rats, tibiae were cleaned off adhering connective tissue and bone marrow. Tibial length was measured by a vernier caliper. Each specimen was then dehydrated serially in 70, 95, and 100% *v/v* ethanol for 3, 3, and 2 days, respectively, as described previously (Assapun et al. 2009). Dehydrated bone was embedded in methyl methacrylate resin at 42°C for 48 h. The resin-embedded bone was cut longitudinally into 7-μm sections by

a microtome equipped with a tungsten carbide blade (model RM2255; Leica, Nussloch, Germany). Bone sections were then mounted on microscope slides, deplastinated, dehydrated, and processed for the Goldner's trichrome staining (van't Hof et al. 2003). Growth plate height was measured under a light microscope (model BX51TRF; Olympus, Tokyo, Japan) with the computer-assisted Motic Images Plus 2.0 (Motic Instruments Inc., Richmond, Canada).

Histomorphometric measurement of growth plate zones (i.e., RZ, PZ and HZ) was previously described by Yakar and colleagues (2002). In brief, all measurements were performed within the central two-thirds of growth plate section. The height of each zone was determined by using the following criteria: (1) PZ contains three or more cells aligned with the long axis of the bone and each cell was not greater than 10 μm in height, (2) HZ is measured from the end of PZ to the border of primary spongiosa (i.e., at the site of vascular invasion), and (3) RZ is the subtraction of PZ and HZ heights from the total growth plate height.

Immunohistochemical localization of PRLR

Tibiae were dissected from lactating (L8) rats. After removal of adhering tissue and bone marrow, they were fixed overnight at 4°C in 0.1 M phosphate-buffered saline (PBS) containing 4% *w/v* paraformaldehyde. Decalcification was performed by immersing bone specimens in 15% *w/v* ethylenediaminetetraacetic acid (EDTA; Sigma) for 3 weeks (Wongdee et al. 2010). Decalcifying solution was changed every 3 days. After being embedded in paraffin, the specimens were cut longitudinally into 7-μm sections which were later incubated at 37°C for 30 min in antigen retrieval solution (0.01 mg/mL proteinase K, 50 mM Tris–HCl pH 8.0 and 5 mM EDTA). Thereafter, the sections were incubated for 1 h with 3% H_2O_2 to inhibit endogenous peroxidase activity. Non-specific bindings were blocked by 2-h incubation with 4% bovine serum albumin, 10% normal goat serum, and 0.7% Tween-20 in PBS. The sections were then incubated at 4°C overnight with 1:50 rabbit polyclonal primary antibody against PRLR (catalog no. sc-30225; Santa Cruz Biotechnology, CA, USA). After being washed with 0.7% Tween-20 in PBS, the sections were incubated for 1 h at room temperature with 1:500 biotinylated goat anti-rabbit IgG (catalog no. 656140; Zymed, South San Francisco, CA, USA), followed by 1-h incubation with streptavidin-conjugated horseradish peroxidase solution (Zymed) and 3,3′-diaminobenzidine chromogen (Pierce, Rockford, IL, USA). As for the negative control, the sections were incubated with 0.7% Tween-20 in PBS in the absence of PRLR primary antibody. Finally, the sections were counterstained with hematoxylin (Sigma), and examined under a light microscope and Image Pro Plus 5 (Media Cybernetics, Bethesda, MD, USA).

Statistical analysis

Unless otherwise specified, the results are expressed as means ± SE. Two sets of data were compared by the unpaired Student's *t*-test. One-way analysis of variance (ANOVA) with Newman–Keuls multiple comparison test was used for multiple sets of data. The level of significance for all statistical tests was $P < 0.05$. Data were analyzed by GraphPad Prism 4.0 for Mac OS X (GraphPad Software Inc., San Diego, CA, USA).

Results

Correlations between the heights of growth plate zones and tibial length

Consistent with the previous report (Suntornsaratoon et al. 2010a), the tibial and femoral lengths of maternal rats were significantly increased by ~2 and ~3%, respectively, at late lactation (L21) when compared with the age-matched controls (Fig. 1). Correlation plots indicated that the tibial length of L21 rats was negatively correlated with the total growth plate height, as well as PZ and HZ heights (Fig. 2). However, there was no correlation between the tibial length and RZ height (Fig. 2b).

Expression of PRLR in growth plate

Prior to investigation of possible PRL effect on growth plate, PRLR protein expression in the growth plate was first demonstrated by immunohistochemistry in decalcified tibial sections. As shown in Fig. 3, positive brownish signals of PRLR were localized in chondrocytes in all three zones of tibial growth plate cartilage from L21 lactating rats.

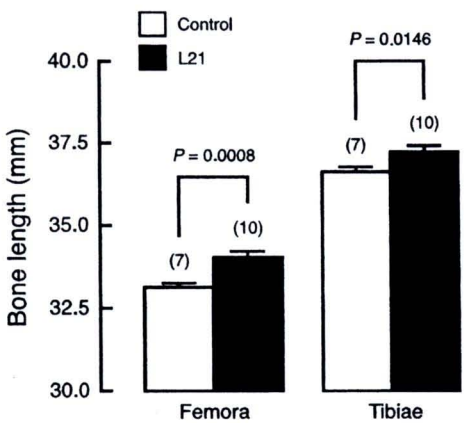

Fig. 1 Femoral and tibial lengths of L21 and age-matched control rats. *Numbers* in parentheses represent the numbers of experimental animals. *P*-values (unpaired Student's *t*-test) are presented above the corresponding *bars*

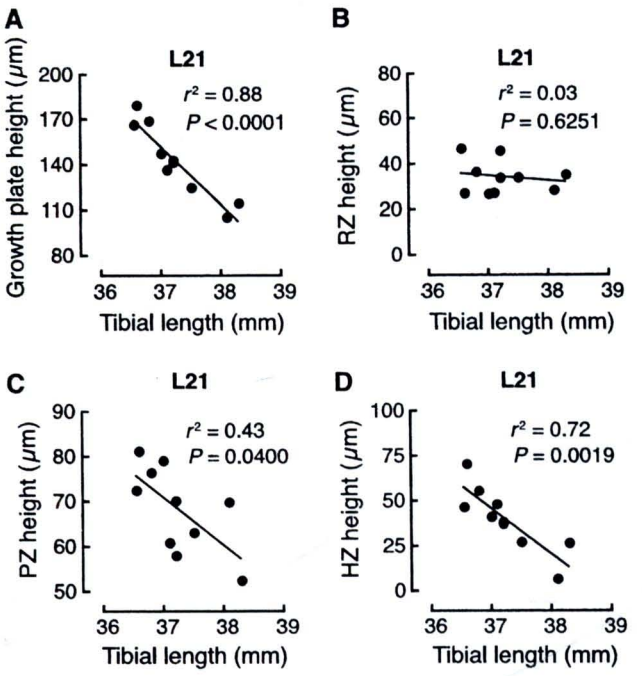

Fig. 2 Graphs of the lengths versus the heights of **a** growth plate, **b** resting zone (RZ), **c** proliferating zone (PZ), and **d** hypertrophic zone (HZ) in tibiae obtained from L21 rats. *P*-values, coefficients of determination (r^2), and regression lines are presented. The tibial length of L21 rats showed negative correlations with the heights of growth plate, PZ and HZ ($P < 0.05$), but showed no correlation with RZ height ($P > 0.05$)

However, in RZ, PZ and upper 2/3 of HZ, PRLR proteins were abundant in the cytoplasm, whereas they were localized at the cell periphery, presumably on the plasma membrane, in hypertrophic chondrocytes near primary spongiosa (lower 1/3 of HZ; Fig. 3f). PRLR proteins were also expressed in osteoblasts covering bone trabeculae (visualized at 1,000×; data not shown), but not in the embedded osteocytes. Similar pattern of PRLR protein expression was observed in the tibial growth plate cartilage of non-pregnant rats (Fig. 4).

Changes in growth plate height during pregnancy and lactation

Microscopic examination of tibial growth plate in different reproductive phases was performed in Goldner's trichrome-stained undecalcified sections. The total growth plate height of proximal tibia was initially decreased at late pregnancy (P21) by ~22%, when compared with the corresponding age-matched controls (Fig. 5). Thereafter, it was progressively decreased to the lowest point (~70% of the control value) in late lactation (L21), and was partially restored postweaning. Representative photomicrographs of the growth plate in L21 rats are also presented (Fig. 6). Inhibition of pituitary PRL secretion by Bromo completely prevented the reduction in growth plate heights in L14 and L21 rats (Figs. 5, 6). Bromo also partially restored the decreased growth plate height in L8 rats, but did not alter that in P21 rats (Fig. 5). Moreover, exogenous PRL supplement to Bromo-treated lactating rats reduced the growth plate heights to the values observed in lactation (Figs. 5, 6). The results suggested that the growth plate change during lactation was dependent on PRL.

Changes in the heights of growth plate zones during pregnancy and lactation

Histomorphometric analysis of Goldner's trichrome-stained tibial sections further revealed that the heights of all growth plate zones were markedly changed during pregnancy and lactation but within different timeframe. Although the RZ height (Fig. 7a) was significantly decreased only at late lactation (L21), the heights of PZ (Fig. 7b) and HZ (Fig. 7c) were dramatically reduced, especially from late pregnancy (P21) to mid-lactation (L14). A decrease in HZ height persisted until late lactation (L21). Fifteen days after weaning, PZ and HZ heights were still significantly lower than those of the controls.

Further investigations in Bromo- and Bromo + PRL-treated rats revealed that the pregnancy-induced changes in growth plate zones were independent of pituitary PRL (Fig. 7). On the other hand, the lactation-induced decreases in RZ and PZ heights in late and mid-lactation, respectively, were found to be PRL-dependent (Fig. 7a–b). Moreover, PRL was responsible for the reduction in HZ height throughout the lactating period (Fig. 7c). Our results therefore suggested the chondroregulatory action of PRL in maternal long bone during lactation.

Discussion

Whether PRL plays a role in the regulation of growth plate cartilage during pregnancy and lactation has not been known. Here, we provided, for the first time, suggestive evidence on the chondroregulatory action of PRL in the tibial growth plate, especially in lactating rats. Normally, PRL is one of the maternal calciotropic hormones, which helps supply sufficient calcium for the developing fetuses and milk production, in part, by increasing intestinal calcium absorption and enhancing bone resorption (Ajibade et al. 2010; Charoenphandhu et al. 2010). In order to supply adequate calcium from maternal bone for milk production, calcium accumulation in cortical envelope and continuing trabecular formation are requisite throughout the reproductive periods, particularly in pregnancy and early lactation (Bowman and Miller 2001; Miller et al. 1986; Suntornsaratoon et al. 2010a, b). Thereafter, in late

Fig. 3 a–f Immunohistochemical localization of PRLR proteins in paraffin-embedded decalcified tibial sections from lactating rats (L8; $n = 4$) at 100× (*bars*, 200 μm), 200× (*bars*, 100 μm), and 400× (*bars*, 50 μm) magnifications. The immuno-stained (+Anti-PRLR) and corresponding negative control (−Anti-PRLR) sections were incubated in the presence and absence of anti-PRLR antibody, respectively. Images of negative control do not show immunoreactive signal. The positive *brownish* signals are observed in chondrocytes in all three zones of the epiphyseal plate (*Ep*), i.e., resting zone (*RZ*), proliferating zone (*PZ*) and hypertrophic zone (*HZ*). Positive signals are also localized in osteoblasts in the primary spongiosa (*Sn*), but not in osteocytes embedded in mineralized matrix (*Md*) of bone trabeculae (*arrows*)

lactation, both cortical envelope and metaphyseal trabeculae are resorbed to release the stockpiled calcium under a concerted regulation of several hormones, such as PRL and PTHrP (Charoenphandhu et al. 2010; Kovacs 2005). Since bone resorption usually exceeds bone formation during lactation, osteopenia does occur in nursing mothers; however, bone loss is gradually reversed postweaning (Charoenphandhu et al. 2010; Kovacs 2005).

Elongation of the maternal bone during the reproductive periods is not uncommon in rodents (Dengler-Crish and Catania 2009). In primiparous mole rats, the lumbar vertebral length was markedly increased during pregnancy, and this lengthening was dampened after delivery (Dengler-Crish and Catania 2009). Our previous study in rats also demonstrated that, in addition to the increased bone length, the cortical envelope of long bone was also thickened during pregnancy, presumably to help maintain bone strength and/or prevent fracture during the lactation-induced massive trabecular bone loss (Suntornsaratoon et al. 2010a). This increase in bone length in lactating rats was previously shown to be dependent on PRL (Suntornsaratoon et al. 2010a). Moreover, as shown in the present study, the tibial length was negatively correlated with the total growth plate height, PZ height, and HZ heights, similar to that reported previously in mice (van Buul-Offers et al. 1984), thereby supporting the hypothesis that the increased length of maternal long bone resulted from the adaptive changes in the growth plate cartilage, and particularly from the accelerated endochondral ossification.

Data from the Bromo-treated P21 rats (Fig. 7b–c) indicated that the pregnancy-induced changes in growth plate zones were independent of pituitary PRL because PRL supplement was unable to restore the zone heights. It is currently not known why Bromo, a dopaminergic agonist, slightly but significantly diminished the change in HZ height in P21 rats (Fig. 7c). However, the direct Bromo effect on growth plate cartilage could not be excluded despite lack of reports on dopaminergic D2 receptor expression in growth plate cartilage of pregnant rats. A previous report using radioligand binding assays in human articular cartilage suggested that, under certain conditions

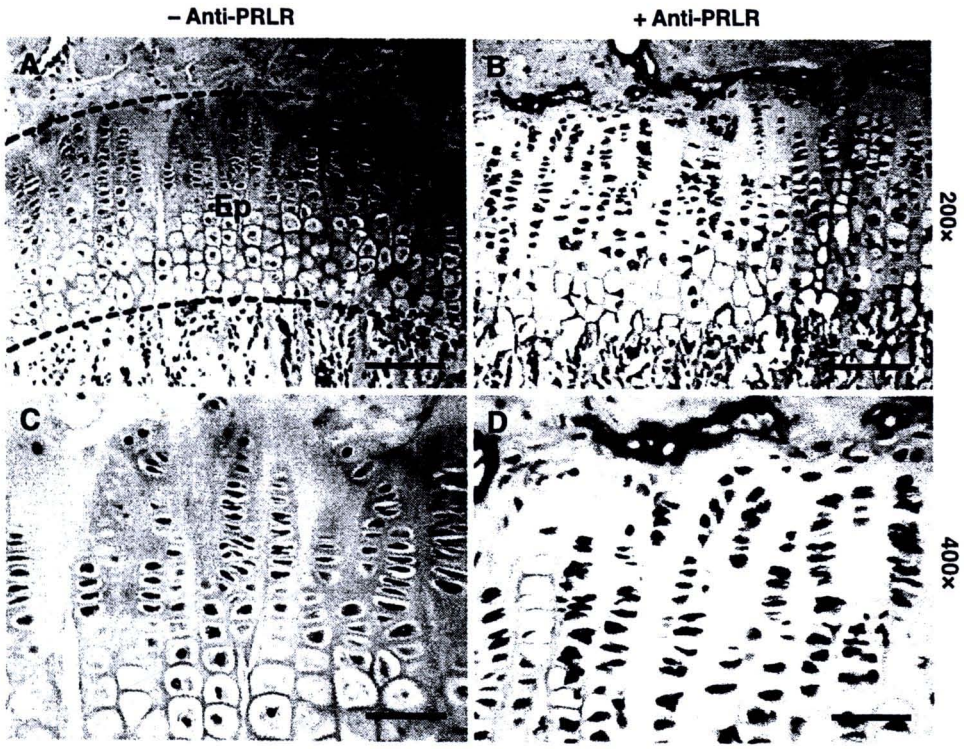

Fig. 4 a–d Immunohistochemical localization of PRLR proteins in paraffin-embedded decalcified tibial sections from non-pregnant rats (normal rats; $n = 5$) at 200× (*bars*, 100 μm) and 400× (*bars*, 50 μm) magnifications. The immuno-stained (+Anti-PRLR) and corresponding negative control (−Anti-PRLR) sections were incubated in the presence and absence of anti-PRLR antibody, respectively. Images of negative control sections do not show immunoreactive signal. The positive *brownish* signals are observed in chondrocytes in all three zones of the epiphyseal plate (*Ep*)

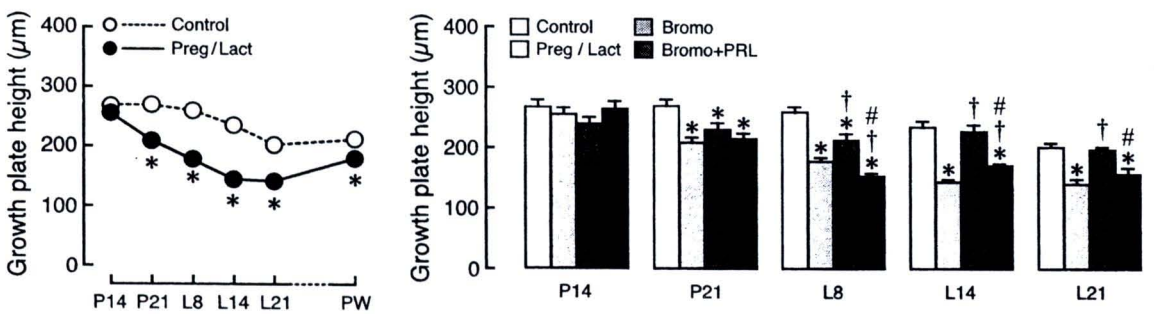

Fig. 5 Growth plate height of tibiae obtained from pregnant (P14 and P21), lactating (L8, L14 and L21), 15-day postweaning (PW), and aged-matched control rats. Some pregnant and lactating rats were administered for 7 days with 4 mg/kg/day bromocriptine s.c. (Bromo), or Bromo and PRL s.c. (Bromo + PRL). The PRL doses for pregnant and lactating rats were 0.4 and 0.6 mg/kg/day, respectively. All values in line graphs and bar graphs are presented as means ± SE ($n = 6$–10 rats per condition). $^{*}P < 0.05$ compared with age-matched control group. $^{\dagger}P < 0.05$ compared with the corresponding lactating group. $^{\#}P < 0.05$ compared with Bromo group

(e.g., osteoarthritis), chondrocytes might be responsive to dopamine agonist (Vignon et al. 1990).

On the other hand, the lactation-induced decreases in the total growth plate height as well as RZ, PZ, and HZ heights in different phases of lactation were found to be PRL-dependent (Fig. 7). Although decreases in the total height and HZ height observed throughout the entire lactating period were induced by PRL, the responses of the chondrocytes in RZ and PZ to PRL were less consistent (Fig. 7). Localization of PRLR proteins on the plasma membrane of hypertrophic chondrocytes (Fig. 3f) could partially explain why the PRL effects were clearly observed in HZ. It was also possible that PRL acted specifically on fully differentiated chondrocytes in HZ rather than on young proliferating and progenitor cells in PZ and RZ, respectively. The differential responsiveness to PRL was previously reported in human undifferentiated mesenchymal stem cells and their chondrocyte-like progeny expressing intermediate and long isoforms of PRLR, respectively (Ogueta et al. 2002), the latter of which was the functional PRLR isoform in several cell types, including mammary and intestinal epithelial cells (Binart et al. 2010; Thongon et al. 2008).

Although the underlying mechanism of PRL action on the growth plate is not known, the strong expression of

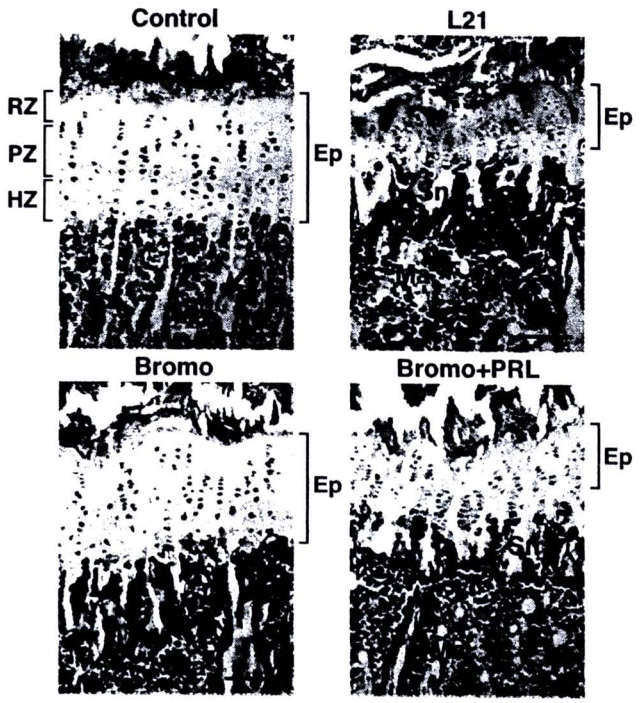

Fig. 6 Representative photomicrographs of Goldner's trichrome-stained tibial growth plates dissected from L21, Bromo-treated L21, Bromo + PRL-treated L21, and age-matched control rats. Primary spongiosa (*Sn*) and all three zones of epiphyseal plate (*Ep*), i.e., resting zone (*RZ*), proliferating zone (*PZ*) and hypertrophic zone (*HZ*) were identified. Mineralized trabeculae (*arrows*) and marrow cells (*Ma*) were stained *green* and *red*, respectively. *Bars*, 100 μm

PRLR in the growth plate chondrocytes of lactating rats suggested a direct action of PRL. Coss and co-workers (2000) also showed that PRLR was widely expressed in the growth plate chondrocytes in the digits of neonatal rats. Besides the growth plate chondrocytes, PRLR expression has been reported in articular chondrocytes from both humans and rats (Ogueta et al. 2002; Zermeño et al. 2006). In the articular chondrocytes in vitro, PRL has been found to inhibit apoptosis induced by serum starvation (Zermeño et al. 2006) and to increase type II collagen expression (Ogueta et al. 2002). Moreover, PRL could directly induce proliferation and chondrogenic differentiation of the human marrow-derived mesenchymal stem cells to mature chondrocytes (Ogueta et al. 2002). Although the chondrocytes in articular cartilages may have different functions from those in the growth plate since the articular chondrocytes do not proceed to hypertrophic differentiation, the aforementioned findings corroborated that PRL is a regulator of the growth of cartilage.

In addition to possible stimulatory effects of PRL on chondrogenesis (Ogueta et al. 2002; Zermeño et al. 2006), a previous study that showed the delay of calvarial ossification and a decrease in femoral mineral apposition rate in PRLR knockout mice also suggested a stimulatory action of PRL on osteogenesis (Clément-Lacroix et al. 1999). Since the growth plate height is normally maintained by keeping a precise balance between chondrogenesis and osteogenesis, the PRL-induced growth plate narrowing might be due to the enhanced turnover of chondrocyte replication and growth plate ossification, the latter of which probably occurred at the faster rate. Nevertheless, once bone trabeculae which serve as calcium storage pools are formed, later on, by as yet unknown mechanism, PRL appears to enhance bone resorption at the rate that matches the maternal requirement (Charoenphandhu et al. 2010).

In addition to PRL, other hormones, such as IGF-1, placental lactogen (PL) and PTHrP, released during pregnancy and lactation might participate in the present growth plate changes. Plasma levels of IGF-1 and PL were elevated in pregnant humans and rats (Freeman et al. 2000; O'Brien et al. 2006). Both systemic and local IGF-1 productions were known to be essential for chondrogenesis and endochondral ossification (Wang et al. 2006; Yakar et al. 2002). PL can bind to PRLR (Cohick et al. 1996), and thus can mimic the PRL effect on cartilage. In addition, growth plate changes during certain phases of lactation might be due to the circulating PTHrP from the mammary glands and its downstream Indian hedgehog signaling pathways (Goltzman 2010; Maeda et al. 2007; Olsen 2006). Nevertheless, further experiments are required to elucidate the interplay between these maternal hormones and their influence on the growth plate function.

However, the chondroregulatory actions of PRL should be apparent only in mammals with persistent growth plate cartilage. In adolescent humans, the accelerated endochondral ossification might be a compensatory mechanism which helped to maintain bone growth during lactation, despite having lactation-induced bone loss. We also further speculated that, in lactating mammals without growth plates, the PRL-induced bone loss became more pronounced, especially when the intestinal calcium absorption was restricted by inadequate calcium intake.

In conclusion, there was a decrease in the tibial growth plate height from late pregnancy to 15 days postweaning. Such a decrease in the total height in lactation showed a negative correlation with the tibial length, and was mainly due to a decrease in HZ height in a PRL-dependent manner. The presence of PRLR protein expression in growth plate chondrocytes further suggested that PRL exerted a direct action on the tibial growth plate cartilage. Although additional investigations are needed to demonstrate the underlying mechanism, the present results are helpful in understanding better the maternal bone adaptation during

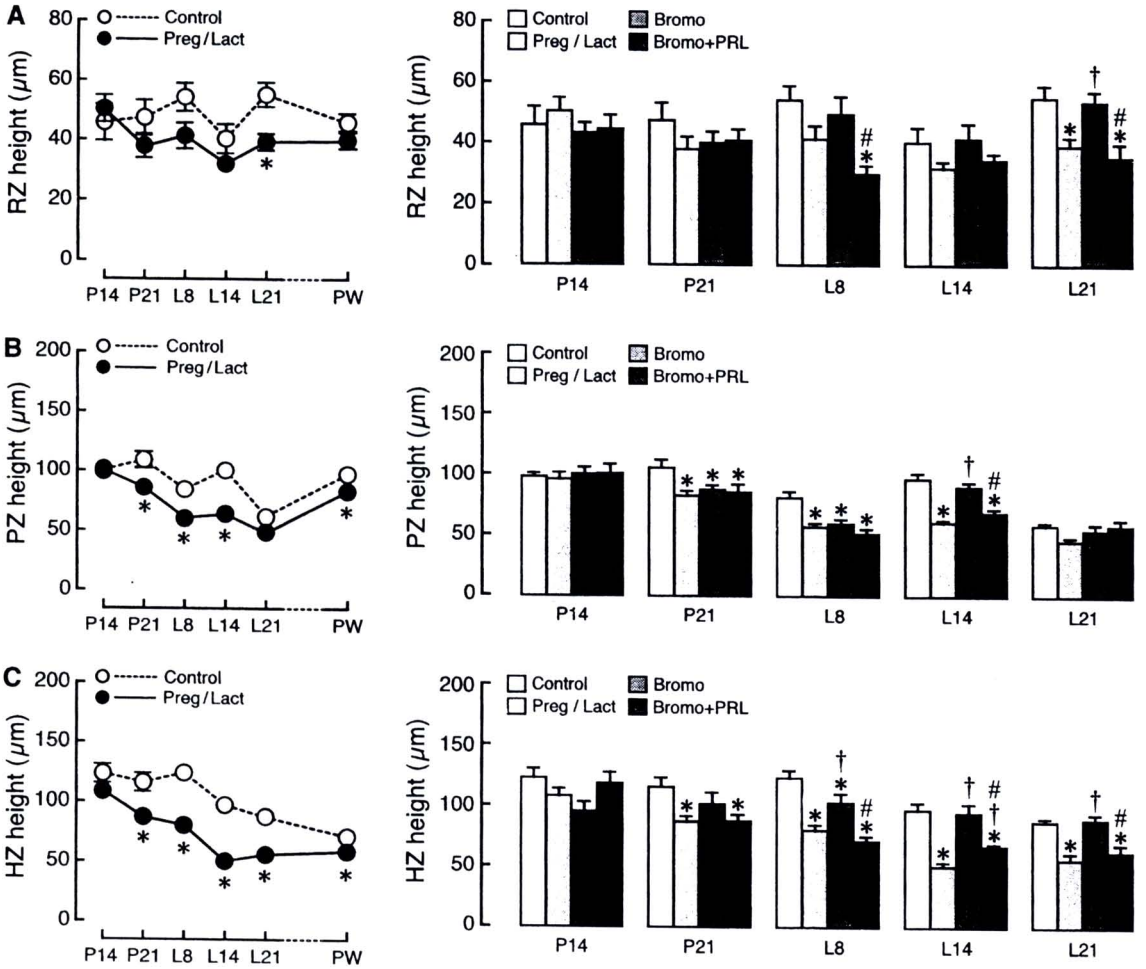

Fig. 7 The heights of **a** resting zone (RZ), **b** proliferating zone (PZ), and **c** hypertrophic zone (HZ) of tibial growth plate obtained from pregnant (P14 and P21), lactating (L8, L14 and L21), 15-day postweaning (PW), and age-matched control rats. Some pregnant and lactating rats were administered for 7 days with 4 mg/kg/day bromocriptine s.c. (Bromo), or Bromo and PRL s.c. (Bromo + PRL). The PRL doses for pregnant and lactating rats were 0.4 and 0.6 mg/kg/day, respectively. All values in *line graphs* and *bar graphs* are presented as means ± SE (n = 6–10 rats per condition). $^{*}P < 0.05$ compared with age-matched control group. $^{\dagger}P < 0.05$ compared with the corresponding lactating group. $^{\#}P < 0.05$ compared with Bromo group

lactation, and substantiate the chondroregulatory role of PRL in lactating rats.

Acknowledgments This research was supported by grants from the King Prajadhipok and Queen Rambhai Barni Memorial Foundation (to P. Suntornsaratoon), the Faculty of Graduate Studies, Mahidol University (to P. Suntornsaratoon), and the Thailand Research Fund (RSA5180001 to N. Charoenphandhu).

Conflict of interest The authors declare no conflicts of interest.

References

Ajibade DV, Dhawan P, Fechner AJ, Meyer MB, Pike JW, Christakos S (2010) Evidence for a role of prolactin in calcium homeostasis: regulation of intestinal transient receptor potential vanilloid type 6, intestinal calcium absorption, and the 25-hydroxyvitamin D_3 1α hydroxylase gene by prolactin. Endocrinology 151:2974–2984

Assapun J, Charoenphandhu N, Krishnamra N (2009) Early acceleration phase and late stationary phase of remodeling imbalance in long bones of male rats exposed to long-standing acidemia: a 10-month longitudinal study using bone histomorphometry. Calcif Tissue Int 85:1–9

Binart N, Bachelot A, Bouilly J (2010) Impact of prolactin receptor isoforms on reproduction. Trends Endocrinol Metab 21:362–368

Bowman BM, Miller SC (2001) Skeletal adaptations during mammalian reproduction. J Musculoskelet Neuronal Interact 1:347–355

Charoenphandhu N, Nakkrasae LI, Kraidith K, Teerapornpuntakit J, Thongchote K, Thongon N, Krishnamra N (2009) Two-step stimulation of intestinal Ca^{2+} absorption during lactation by long-term prolactin exposure and suckling-induced prolactin surge. Am J Physiol Endocrinol Metab 297:E609–E619

Charoenphandhu N, Wongdee K, Krishnamra N (2010) Is prolactin the cardinal calciotropic maternal hormone? Trends Endocrinol Metab 21:395–401

Clément-Lacroix P, Ormandy C, Lepescheux L, Ammann P, Damotte D, Goffin V, Bouchard B, Amling M, Gaillard-Kelly M, Binart

N, Baron R, Kelly PA (1999) Osteoblasts are a new target for prolactin: analysis of bone formation in prolactin receptor knockout mice. Endocrinology 140:96–105

Cohick CB, Dai G, Xu L, Deb S, Kamei T, Levan G, Szpirer C, Szpirer J, Kwok SC, Soares MJ (1996) Placental lactogen-I variant utilizes the prolactin receptor signaling pathway. Mol Cell Endocrinol 116:49–58

Coss D, Yang L, Kuo CB, Xu X, Luben RA, Walker AM (2000) Effects of prolactin on osteoblast alkaline phosphatase and bone formation in the developing rat. Am J Physiol Endocrinol Metab 279:E1216–E1225

Dengler-Crish CM, Catania KC (2009) Cessation of reproduction-related spine elongation after multiple breeding cycles in female naked mole-rats. Anat Rec (Hoboken) 292:131–137

Freeman ME, Kanyicska B, Lerant A, Nagy G (2000) Prolactin: structure, function, and regulation of secretion. Physiol Rev 80:1523–1631

Gartner LP, Hiatt JL (2001) Cartilage and bone. In: Gartner LP, Hiatt JL (eds) Color textbook of histology. Saunders, Philadelphia, pp 94–101

Goltzman D (2010) Emerging roles for calcium-regulating hormones beyond osteolysis. Trends Endocrinol Metab 21:512–518

Hong JS, Santolaya-Forgas J, Romero R, Espinoza J, Goncalves LF, Kim YM, Edwin S, Yoon BH, Nien JK, Hassan S, Mazor M (2005) Maternal plasma osteoprotegerin concentration in normal pregnancy. Am J Obstet Gynecol 193:1011–1015

Kovacs CS (2005) Calcium and bone metabolism during pregnancy and lactation. J Mammary Gland Biol Neoplasia 10:105–118

Maeda Y, Nakamura E, Nguyen MT, Suva LJ, Swain FL, Razzaque MS, Mackem S, Lanske B (2007) Indian hedgehog produced by postnatal chondrocytes is essential for maintaining a growth plate and trabecular bone. Proc Natl Acad Sci USA 104:6382–6387

Miller SC, Shupe JG, Redd EH, Miller MA, Omura TH (1986) Changes in bone mineral and bone formation rates during pregnancy and lactation in rats. Bone 7:283–287

O'Brien KO, Donangelo CM, Zapata CL, Abrams SA, Spencer EM, King JC (2006) Bone calcium turnover during pregnancy and lactation in women with low calcium diets is associated with calcium intake and circulating insulin-like growth factor 1 concentrations. Am J Clin Nutr 83:317–323

Ofluoglu O, Ofluoglu D (2008) A case report: pregnancy-induced severe osteoporosis with eight vertebral fractures. Rheumatol Int 29:197–201

Ogueta S, Muñoz J, Obregon E, Delgado-Baeza E, García-Ruiz JP (2002) Prolactin is a component of the human synovial liquid and modulates the growth and chondrogenic differentiation of bone marrow-derived mesenchymal stem cells. Mol Cell Endocrinol 190:51–63

Olsen BR (2006) Bone embryology. In: Favus MJ (ed) Primer on the metabolic bone diseases and disorders of mineral metabolism. American Society for Bone and Mineral Research, Washington, DC, pp 2–6

Rauch F (2005) Bone growth in length and width: the Yin and Yang of bone stability. J Musculoskelet Neuronal Interact 5:194–201

Seriwatanachai D, Thongchote K, Charoenphandhu N, Pandaranandaka J, Tudpor K, Teerapornpuntakit J, Suthiphongchai T, Krishnamra N (2008) Prolactin directly enhances bone turnover by raising osteoblast-expressed receptor activator of nuclear factor κB ligand/osteoprotegerin ratio. Bone 42:535–546

Suntornsaratoon P, Wongdee K, Goswami S, Krishnamra N, Charoenphandhu N (2010a) Bone modeling in bromocriptine-treated pregnant and lactating rats: possible osteoregulatory role of prolactin in lactation. Am J Physiol Endocrinol Metab 299:E426–E436

Suntornsaratoon P, Wongdee K, Krishnamra N, Charoenphandhu N (2010b) Femoral bone mineral density and bone mineral content in bromocriptine-treated pregnant and lactating rats. J Physiol Sci 60:1–8

Thongon N, Nakkrasae LI, Thongbunchoo J, Krishnamra N, Charoenphandhu N (2008) Prolactin stimulates transepithelial calcium transport and modulates paracellular permselectivity in Caco-2 monolayer: mediation by PKC and ROCK pathways. Am J Physiol Cell Physiol 294:C1158–C1168

van Buul-Offers S, Smeets T, Van den Brande JL (1984) Effects of growth hormone and thyroxine on the relation between tibial length and the histological appearance of the proximal tibial epiphysis in Snell dwarf mice. Growth 48:166–175

van't RJ, Clarkin CE, Armour KJ (2003) Studies of local bone remodeling: the calvarial injection assay. In: Helfrich MH, Ralston SH (eds) Bone research protocols. Humana Press, New Jersey, pp 345–351

Vignon E, Broquet P, Mathieu P, Louisot P, Richard M (1990) Histaminergic H1, serotoninergic, β-adrenergic and dopaminergic receptors in human osteoarthritic cartilage. Biochem Int 20:251–255

Wang Y, Nishida S, Sakata T, Elalieh HZ, Chang W, Halloran BP, Doty SB, Bikle DD (2006) Insulin-like growth factor-I is essential for embryonic bone development. Endocrinology 147:4753–4761

Wongdee K, Riengrojpitak S, Krishnamra N, Charoenphandhu N (2010) Claudin expression in the bone-lining cells of female rats exposed to long-standing acidemia. Exp Mol Pathol 88:305–310

Yakar S, Rosen CJ, Beamer WG, Ackert-Bicknell CL, Wu Y, Liu JL, Ooi GT, Setser J, Frystyk J, Boisclair YR, LeRoith D (2002) Circulating levels of IGF-1 directly regulate bone growth and density. J Clin Invest 110:771–781

Zermeño C, Guzmán-Morales J, Macotela Y, Nava G, López-Barrera F, Kouri JB, Lavalle C, de la Escalera GM, Clapp C (2006) Prolactin inhibits the apoptosis of chondrocytes induced by serum starvation. J Endocrinol 189:R1–R8

Am J Physiol Endocrinol Metab 299: E426–E436, 2010.
First published June 15, 2010; doi:10.1152/ajpendo.00134.2010.

Bone modeling in bromocriptine-treated pregnant and lactating rats: possible osteoregulatory role of prolactin in lactation

Panan Suntornsaratoon,[1,2] Kannikar Wongdee,[1,3] Suchandra Goswami,[1] Nateetip Krishnamra,[1,2] and Narattaphol Charoenphandhu[1,2]

[1]*Consortium for Calcium and Bone Research (COCAB),* [2]*Department of Physiology, Faculty of Science, Mahidol University, Bangkok; and* [3]*Faculty of Allied Health Sciences, Burapha University, Chonburi, Thailand*

Submitted 1 March 2010; accepted in final form 8 June 2010

Suntornsaratoon P, Wongdee K, Goswami S, Krishnamra N, Charoenphandhu N. Bone modeling in bromocriptine-treated pregnant and lactating rats: possible osteoregulatory role of prolactin in lactation. *Am J Physiol Endocrinol Metab* 299: E426–E436, 2010. First published June 15, 2010; doi:10.1152/ajpendo.00134.2010.— The lactogenic hormone prolactin (PRL) directly regulates osteoblast functions in vitro and modulates bone remodeling in nulliparous rats, but its osteoregulatory roles in pregnant and lactating rats with physiological hyperprolactinemia remained unclear. Herein, bone changes were investigated in rats treated with bromocriptine (Bromo), an inhibitor of pituitary PRL release, or Bromo+PRL at different reproductive phases, from mid-pregnancy to late lactation. PRL receptors were strongly expressed in osteoblasts lining bone trabeculae, indicating bone as a target of PRL actions. By using dual energy X-ray absorptiometry, we found a significant increase in bone mineral density in the femora and vertebrae of pregnant rats. Such pregnancy-induced bone gain was, however, PRL independent and may have resulted from the increased cortical thickness. Bone trabeculae were modestly changed during pregnancy as evaluated by bone histomorphometry. On the other hand, lactating rats, especially in late lactation, showed massive bone loss in bone trabeculae but not in cortical shells. Further study in Bromo- and Bromo+PRL-treated rats suggested that PRL contributed to decreases in trabecular bone volume and number and increases in trabecular separation and eroded surface, as well as a paradoxical increase in bone formation rate in late lactation. Uncoupling of trabecular bone formation and resorption was evident in lactating rats, with the latter being predominant. In conclusion, pregnancy mainly induced cortical bone gain, whereas lactation led to trabecular bone loss in both long bones and vertebrae. Although PRL was not responsible for the pregnancy-induced bone gain, it was an important regulator of bone modeling during lactation.

bone histomorphometry; hyperprolactinemia; ion chromatography; osteopenia; uncoupling

IN PREGNANT AND BREASTFEEDING WOMEN, massive calcium loss occurs for fetal development (~200–300 mg/day) and lactogenesis (~300–1,000 mg/day), respectively (4, 23, 36). A huge amount of calcium demand is accomplished, in part, by enhanced intestinal calcium absorption during these reproductive periods (9). Our recent studies in rats demonstrated that the lactogenic hormone prolactin (PRL), released from the anterior pituitary gland during pregnancy (~100–200 ng/ml) and lactation (~200–300 ng/ml), was the principal calciotropic maternal hormone, which was capable of stimulating calcium absorption in the small intestine and proximal large intestine (7, 21). Moreover, lactation-induced bone resorption provides additional calcium to match the increased calcium demand of the offspring, which in turn induces reversible osteopenia in mothers (20, 36).

In both humans and rodents, hormonal regulation of bone changes during pregnancy and lactation is not completely understood, but it is not directly regulated by the major calciotropic hormones, namely parathyroid hormone (PTH) and 1,25-dihydroxyvitamin D_3 [1,25$(OH)_2D_3$] (9, 30, 36). Other hormones with elevated plasma levels, such as PRL, PTH-related peptide (PTHrP), calcitonin, and insulin-like growth factor (IGF)-I, might contribute to the maternal bone changes, perhaps with each exerting action at different times and in a bone site-specific manner (4, 20). Among these hormones, PRL is of special interest, since its plasma levels are increased ~10-fold and ~20-fold in pregnant and lactating rats, respectively (6). In addition, primary osteoblasts cultured from rat bones were found to strongly express mRNAs and proteins of PRL receptors (PRLR), suggesting that bone could be another target tissue of PRL actions (40).

A recent investigation in nulliparous rats with hyperprolactinemia induced by pituitary transplantation showed that PRL could induce both bone formation and bone resorption, with the latter being predominant, thereby leading to net bone loss and osteopenia (40). $PRLR^{-/-}$ mice also manifested an impairment of bone growth and mineralization of bone matrix (11). Moreover, pathological hyperprolactinemia in nonpregnant patients with prolactinoma or chronic uses of antipsychotic drugs (i.e., dopaminergic antagonists) may lead to progressive osteopenia and osteoporosis (27, 42). Such bone loss in rodents was apparent mainly in the primarily trabecular site (e.g., vertebrae) or the trabecular parts of the long bone (e.g., metaphysis or secondary spongiosa) but was rarely observed in the cortex (8, 44). The PRL-related bone loss may result from direct actions of PRL on osteoblasts as well as indirectly from the PRL-induced hypoestrogenemia (8, 12, 27, 40).

Although pregnancy and lactation are considered a physiological hyperprolactinemic state (9), little is currently known regarding the effects of PRL on cortical and trabecular sites at different phases of the reproductive periods (e.g., early vs. late lactation). Generally, longitudinal studies of PRL actions on maternal bone metabolism are carried out in animals treated with bromocriptine (Bromo), an agonist of the PRL-inhibiting factor dopamine, which can inhibit pituitary PRL release by ~80–90% (3, 7, 35), in the presence or absence of exogenous PRL administration (43). The uses of $PRL^{-/-}$ or $PRLR^{-/-}$ mice are not possible due to infertility (2). Furthermore, disruption of PRL synthesis in the first week of pregnancy in rodents could lead to abortion (2). Thus, by using Bromo-treated lactating rats, the effect of PRL on the long bone could be demonstrated by densitometric analysis (43), but whether

Address for reprint requests and other correspondence: N. Charoenphandhu, Dept. of Physiology, Faculty of Science, Mahidol University, Rama VI Road, Bangkok 10400, Thailand (e-mail: naratt@narattsys.com).

microstructural changes in the cortices and trabeculae were different remained to be investigated. Nevertheless, the aforementioned findings in nulliparous rats (40, 44) suggested that PRL could have action on maternal bone, particularly in the trabeculae.

Therefore, the objectives of the present longitudinal study were *1*) to investigate macroscopic and microscopic bone changes by using dual energy X-ray absorptiometry (DEXA) and bone histomorphometry, respectively, in pregnant and lactating rats, from mid-pregnancy to day 15 postweaning, *2*) to reveal the possible roles of PRL in regulating maternal bone changes, and *3*) to demonstrate differential responses of maternal cortical and trabecular bones to PRL in different reproductive periods.

MATERIALS AND METHODS

Animals. Pregnant and age-matched nulliparous Sprague-Dawley rats (8 wk old) were obtained from the National Laboratory Animal Centre in Thailand. They were housed in the husbandry unit under a 12:12-h light-dark cycle (lights on at 0600) for at least 5 days prior to the experiments and were fed standard chow and distilled water ad libitum. The room had a temperature of 25 ± 2°C with average illuminance of 200 lux. This study was approved by the Animal Care and Use Committee of the Faculty of Science, Mahidol University. All animals were cared for in accordance with the principles and guidelines of the American Physiological Society's "Guiding Principles in the Care and Use of Animals."

Experimental design. Bone changes were investigated in different reproductive phases, i.e., mid-pregnancy (day 14, P14), late pregnancy (day 21, P21), early lactation (day 8, L8), mid-lactation (day 14, L14), late lactation (day 21, L21), and day 15 postweaning (PW). Since bone growth and calcium accretion are normally age dependent, we used age-matched nulliparous rats as a control group. Ages of P14, P21, L8, L14, L21, and PW rats were 10, 11, 12, 13, 14, and 16 wk old, respectively. Body weights of all rats were recorded weekly (Supplemental Fig. S1; supplemental materials are found in the online version of this paper at the Journal website). After delivery, litter size was adjusted to eight pups per dam for lactating groups, whereas in nonsuckling groups all pups were permanently separated from dams from birth. Such nonsuckling mothers were reported to have no hyperprolactinemia because the suckling-induced PRL surge was absent, and plasma PRL levels rapidly declined within 12 h after cessation of suckling (26, 34). In some experiments, dams were injected daily subcutaneously for 7 days with 4 mg/kg Bromo sc (Sigma, St. Louis, MO) or Bromo+PRL (purified from ovine pituitary gland; catalog no. L6520, Sigma) before being killed. PRL doses for pregnant and lactating rats were 0.4 and 0.6 mg/kg, respectively (7). These PRL regimens have been reported to completely restore the Bromo-induced decrease in the intestinal calcium absorption in pregnant and lactating rats (7). Finally, all rats in each pregnant (P14 and P21) or lactating (L8, L14, and L21) group were killed on the same day, between 0800 and 1000.

Preparation of bone samples. As previously described by Charoenphandhu et al. (8), femora (primarily cortical sites) and *L5* vertebrae (primarily trabecular sites) were cleaned and subjected to densitometric analysis. In some experiments, femoral length and dry and ash weights were recorded. Femora were dried in an oven at 80°C for 3 days and then ashed at 800°C overnight in a muffle furnace (model 48000; Thermolyne, Dubuque, IA). After bone ash was dissolved with 3.0 N HCl, the samples were diluted with a solution containing 0.38% wt/vol $SrCl_2$ and 0.9% vol/vol $HClO_4$ and were analyzed for total calcium and magnesium contents by atomic absorption spectrophotometry (for calcium only; model SpectrAA-300, Varian Techtron, Springvale, Australia) and ion chromatography (for calcium and magnesium).

Tibiae (primarily cortical sites) were also removed, cleaned, and fixed for PRLR expression study and histomorphometric analysis of their cortical and trabecular portions.

Immunohistochemical analysis of PRLR expression. Tibiae were dissected from P21 and L8 rats. After cleaning, they were fixed overnight in 0.1 M phosphate-buffered saline (PBS) containing 4% paraformaldehyde. Decalcification was later performed by immersing bone specimens in 15% wt/vol ethylenediaminetetraacetic acid (EDTA; Sigma) at 25°C for 3 wk. Decalcifying solution was replaced every 3 days. After being embedded in paraffin, bone specimens were cut longitudinally into 7-μm sections, which were later incubated at 37°C for 30 min in antigen retrieval solution (0.01 mg/ml proteinase K, 50 mM Tris·HCl, pH 8.0, and 5 mM EDTA). To inhibit background endogenous peroxidase activity, sections were incubated for 1 h with 10% H_2O_2. Nonspecific binding was blocked for 2 h by 4% bovine serum albumin, 10% normal goat serum, and 0.7% Tween-20 in PBS. Thereafter, sections were incubated at 4°C overnight with 1:50 rabbit polyclonal primary antibody against PRLR (catalog no. sc-30225; Santa Cruz Biotechnology, Santa Cruz, CA). After being washed with 0.7% Tween-20 in PBS, sections were incubated for 1 h at room temperature with 1:500 biotinylated goat anti-rabbit IgG (catalog no. 656140; Zymed, South San Francisco, CA) followed by incubation for 1 h with streptavidin-conjugated horseradish peroxidase solution (Zymed) and 3,3′-diaminobenzidine chromogen (Pierce, Rockford, IL). As for the negative control, sections were incubated with 0.7% Tween-20 in PBS in the absence of PRLR primary antibody. Sections were counterstained with hematoxylin and visualized under a light microscope (model BX51TRF; Olympus, Tokyo, Japan).

Measurement of bone calcium and magnesium contents by ion chromatography. A modular ion chromatographic system (Waters, Milford, MA) comprised a model-600 controller, model-600 pump, model-432 conductivity detector, and a cation column containing silica gel with sulfonic acid group (125 × 4 mm inner diameter, 5 μm particle size, model Nucleosil 5SA; Metrohm, Herisau, Switzerland). All components were connected through the Waters SAT/IN module to a Millennium 32 workstation, which performed system control, acquisition, and data analysis. The eluent for simultaneous separation of the divalent cations consisted of 4 mM tartaric acid, 0.5 mM citric acid, and 3 mM ethylenediamine in 5% vol/vol acetone and were degassed for 5 min before use. Eluent flow rates were adjusted at 1.5 ml/min, and the column was equilibrated in eluent for 45 min prior to sample charging. The analytic condition was optimized for isocratic elution using a 100-μl injection loop and total run time of 10 min. Calcium and magnesium were eluted at 5.9 and 7.0 min, respectively. Standard stock solutions were prepared by dissolving appropriate amounts of $CaCl_2$ or $MgCl_2$ in ultrapure Milli-Q water to obtain a final concentration of 1 M and kept at −20°C. Working standard solutions were prepared fresh by diluting the stock solutions to 10, 20, 50, 100, 150, and 200 μM with Milli-Q water (pH ~2.5–3.5 adjusted with 2 M HNO_3) for six-point calibration. The detection limit of both calcium and magnesium at a signal-to-noise ratio of 3:1 appeared to be ~0.02 and ~0.04 μM, respectively. The six-point calibrations for calcium and magnesium showed percent residual standard deviations of 0.9 and 0.5 and correlation coefficients of 0.9989 and 0.9993, respectively. A reproducibility test was performed by injecting standard solutions 10 times on the same day as well as on different days. The relative standard deviations of peak area of calcium and magnesium were varied by less than 0.5% and 3–5%, respectively, during intraday vs. interday tests.

For the analyses of bone calcium and magnesium contents, each bone sample was dissolved in 3 N HCl and diluted 100-fold with distilled water. Thereafter, all samples were filtered through 0.22-μm membranes prior to injection into the column. All samples were analyzed in duplicate and reported as millimoles per gram of dry weight of bone.

DEXA. Bone mineral density (BMD) and bone mineral content (BMC) were determined in the ex vivo whole femora and *L5* vertebrae by DEXA (model Lunar PIXImus2; GE Medical Systems, Madison, WI), operated with software version 2.10, as previously described (8). The system was calibrated daily with a standard material of known BMD and BMC of 0.0690 g/cm^2 and 0.697 g, respectively.

Bone histomorphometry. A tibia was cleaned of adhering tissues and bone marrow. Bone was then dehydrated in 70, 95, and 100% vol/vol ethanol for 3, 3, and 2 days, respectively. Dehydrated bone was embedded in methyl methacrylate resin at 42°C for 48 h. The resin-embedded tibia was cut longitudinally with a microtome equipped with a tungsten carbide blade (model RM2255; Leica, Nussloch, Germany) to obtain 7- and 12-μm-thick sections for the staining and unstaining histomorphometric techniques, respectively (16, 18). For the staining technique, longitudinal sections were mounted on standard microscope slides, deplastinated, dehydrated, and processed for Goldner's trichrome staining (45). The unstained slides were examined for the double lines of calcein labeling (10 mg/kg sc injected at 6-day interval, Sigma). Imaging analysis was performed under a fluorescent/light microscope using the computer-assisted Osteomeasure system (Osteometric, Atlanta, GA), operated with software version 4.1. The region of interest covered secondary spongiosa (the trabecular part of proximal tibia at 1–2 mm distal to the epiphysial plate), which was analyzed to obtain static and dynamic parameters from stained and unstained sections, respectively. Static parameters included trabecular bone volume normalized by tissue volume (BV/TV, %), trabecular number (Tb.N, mm^{-1}), trabecular separation (Tb.Sp, μm), trabecular thickness (Tb.Th, μm), osteoblast surface normalized by bone surface (Ob.S/BS, %), osteoclast surface (Oc.S/BS, %), and eroded surface (ES/BS, %). Dynamic parameters were double labeled surface (dLS/BS, %), mineralizing surface (MS/BS, %), mineral apposition rate (MAR, μm/day), and bone formation rate (BFR/BS, μm^3/μm^2/day). The nomenclature, symbols, and units complied with the report of the American Society for Bone and Mineral Research Nomenclature Committee (31).

For the cortical measurements, midfrontal tibial sections and mid-sagittal vertebral sections were used. Cortical thicknesses of tibiae were averaged from three points, i.e., at 2, 3, and 4 mm distal to the epiphysial plate, whereas those of *L5* vertebrae were averaged from the thickness at one-third and two-thirds of the length of the *L5* vertebral body. Cortical thicknesses were measured with Motic Images Plus 2.0 (Motic Instruments, Richmond, Canada).

Statistical analysis. Results are expressed as means ± SE. Two sets of data were compared with an unpaired Student's *t*-test. One-way analysis of variance with a Newman-Keuls multiple comparison test was used for multiple sets of data. The level of significance for all statistical tests was $P < 0.05$. Data were analyzed with GraphPad Prism 4.0 for Mac OS X (GraphPad Software, San Diego, CA).

RESULTS

Expression of PRLR proteins in bone. Prior to the investigation of the PRL effects on bone, the expression of PRLR proteins in bone was determined by immunohistochemical technique. As shown in Fig. 1, brownish signals of PRLR proteins were observed in flat osteoblasts lining bone trabeculae in the tibiae of nulliparous, pregnant (P21), and lactating (L8) rats. Several hematopoietic cells in bone marrow also showed positive PRLR signals, whereas no signal was observed in osteocytes embedded in bone trabeculae and cortices.

Densitometric analyses of femora and L5 vertebrae of pregnant and lactating rats. At a macroscopic level, bone densitometric analysis using DEXA in femora (a primarily cortical site) and *L5* vertebrae (a primarily trabecular site) demonstrated that BMD was markedly increased in mid- (P14) and late pregnancy (P21) but was decreased in late lactation (L21)

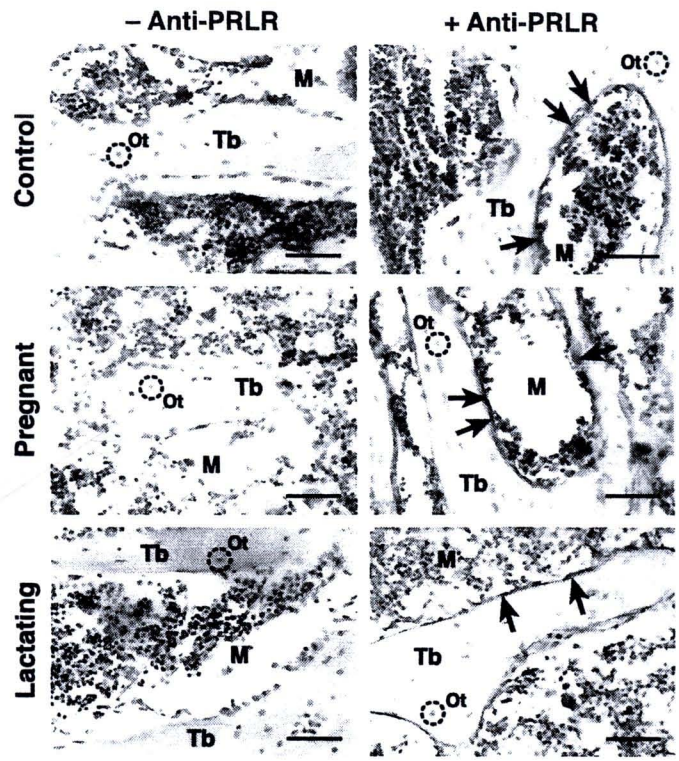

Fig. 1. Immunolocalization of prolactin receptor (PRLR) proteins in the tibiae of control (nulliparous), pregnant (P21), and lactating (L8) rats (n = 3–4 rats per group). Immunostained (+Anti-PRLR) and negative control (−Anti-PRLR) sections were incubated in the presence and absence of anti-PRLR antibody, respectively. Immunoreactive signals were observed in flat osteoblasts (arrows) lining bone trabeculae (Tb) and some leukocytes in bone marrow (M), but not in osteocytes (Ot). Bars, 50 μm.

compared with the age-matched controls (Fig. 2, *A* and *B*). In femora, an increase in BMD was maintained until early lactation (L8; Fig. 2*A*). Fifteen days after weaning, femoral BMD was restored, whereas vertebral BMD remained lower than the control level. Although whole bone BMC was also increased during pregnancy, BMC of L21 lactating rats was comparable to that of age-matched control rats (Fig. 2, *C* and *D*).

Neither exogenous PRL nor Bromo affected femoral and vertebral BMD during pregnancy (Fig. 2, *A* and *B*). On the other hand, Bromo restored femoral BMD but not vertebral BMD in L21 rats (Fig. 2, *A* and *B*). However, PRL administration did not decrease femoral BMD in Bromo-treated L21 rats (Fig. 2*A*). Interestingly, femoral BMDs in L8 and L21 nonsuckling rats were greater than that in age-matched control rats (Fig. 2*A*).

Femoral length, ash weight, and total contents of calcium and magnesium. Femoral length was significantly increased during pregnancy and lactation (Fig. 3*A*). Thereafter, the femoral elongation slowed down, as the femoral length of post-weaning rats was comparable to that of control rats (Fig. 3*A*). Femoral ash weight was increased only in pregnancy, but not in lactation, compared with age-matched control rats (Fig. 3*B*). Neither Bromo nor PRL altered femoral length and ash weight in pregnant rats. However, Bromo completely abolished the lactation-induced increase in femoral length. Exogenous PRL administration partially reversed the Bromo effect on femoral length in L21 rats (Fig. 3*A*).

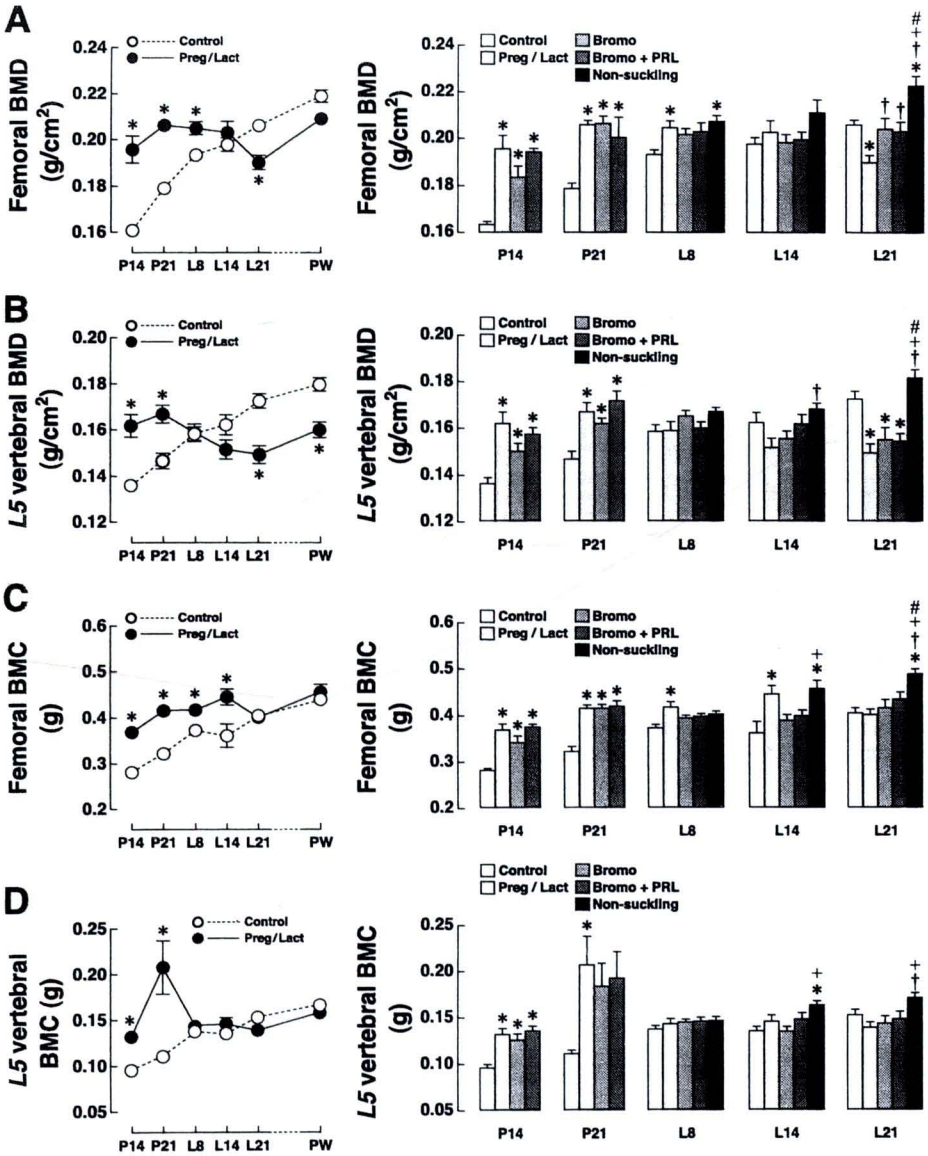

Fig. 2. Bone mineral density (BMD; *A* and *B*) and bone mineral content (BMC; *C* and *D*) of ex vivo femora (primarily cortical sites) and *L5* vertebrae (primarily trabecular sites) of age-matched control, pregnant (P14 and P21), lactating (L8, L14 and L21), and 15-day postweaning (PW) rats, as determined by DEXA. Some pregnant and lactating rats were administered bromocriptine (Bromo) for 7 days (4 $mg \cdot kg^{-1} \cdot day^{-1}$ sc) or Bromo plus PRL sc (Bromo+PRL). PRL doses for pregnant and lactating rats were 0.4 and 0.6 $mg \cdot kg^{-1} \cdot day^{-1}$, respectively. Some rats were permanently separated from their pups after parturition (nonsuckling). All values in line graphs and bar graphs are presented as means ± SE ($n = 7$–8 rats per each condition). *$P < 0.05$ vs. age-matched control group; †$P < 0.05$ vs. corresponding lactating group; +$P < 0.05$ vs. Bromo group; #$P < 0.05$ vs. Bromo+PRL group.

Since PRL was reported to inhibit in vitro matrix mineralization (39), we further investigated the total calcium and mineral contents normalized by the dry weight of the femora. Normally, bone dry weight includes dry weight of protein matrix and weight of minerals (e.g., calcium, magnesium, and phosphate). Therefore, if the studied conditions do not change the stoichiometry of mineralized bone matrix (i.e., relative quantities of minerals per weight of protein matrix), the total calcium and magnesium contents normalized by the dry weight should be constant. As demonstrated by ion chromatography, these parameters were not altered in pregnant and lactating rats and remained constant after Bromo or Bromo+PRL administration (Fig. 4). In addition, calcium content in bone ash was greater than magnesium content ~40-fold. A constant total calcium content normalized by dry femoral weight was also confirmed by atomic absorption spectrophotometry (Supplemental Fig. S2).

Cortical thicknesses of tibiae and L5 vertebrae. Goldner's trichrome staining of tibial and vertebral sections revealed that the thicknesses of tibial and vertebral cortical shells as well as of trabeculae were markedly increased during pregnancy (Figs. 5*A* and 6, *A* and *B*). The pregnancy-induced increase in cortical thickness was not dependent on PRL (data not shown). In L14 lactating rats, the thickness of tibial cortical shell, but not vertebral cortical shell, remained greater than that in the control groups (Figs. 5*B* and 6, *C* and *D*). In contrast, bone trabeculae in both tibiae and *L5* vertebrae became thinner during lactation (Fig. 5*B*).

Histomorphometry of trabecular microstructure in pregnant and lactating rats. Further investigation by bone histomorphometry in the trabecular portion of tibiae demonstrated that trabecular bone volume and trabecular number were not changed during pregnancy compared with the age-matched controls but were markedly decreased after mid-lactation, which lasted until day 15 postweaning (Fig. 7, *A* and *B*). Trabecular thickness was modestly altered during pregnancy and lactation with a significant increase only at day 15 postweaning (Fig. 7*C*). Trabecular separation was significantly increased after mid-lactation (Fig. 7*D*), consistent with a decrease in trabecular bone volume during the same period.

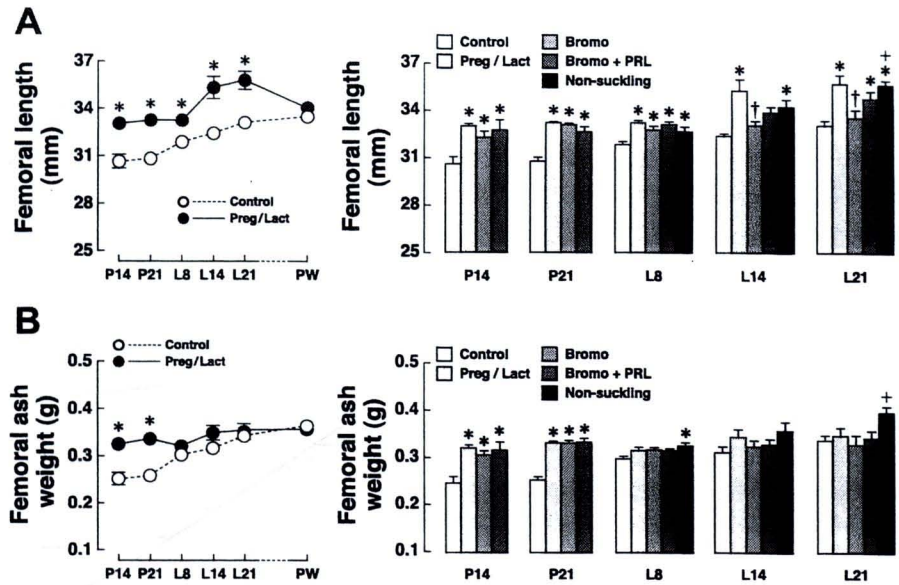

Fig. 3. Length (*A*) and ash weight (*B*) of femora dissected from age-matched control, pregnant (P14 and P21), lactating (L8, L14 and L21), and 15-day postweaning (PW) rats. Ash weight was determined after placing femora in a muffle furnace at 800°C overnight. Some pregnant and lactating rats were administered Bromo for 7 days (4 $mg \cdot kg^{-1} \cdot day^{-1}$ sc) or Bromo+PRL. PRL doses for pregnant and lactating rats were 0.4 and 0.6 $mg \cdot kg^{-1} \cdot day^{-1}$, respectively. Some rats were permanently separated from their pups after parturition (nonsuckling). All values in line graphs and bar graphs are presented as means ± SE ($n = 4–6$ rats per condition). $*P < 0.05$ vs. age-matched control group; $\dagger P < 0.05$ vs. the corresponding lactating group; $+P < 0.05$ vs. Bromo group.

Regarding bone formation-related parameters, although osteoblast surface was decreased during mid-pregnancy (Fig. 8*A*), double labeled surface, mineral apposition rate, and bone formation rate were significantly increased (Fig. 8, *B–D*) compared with the corresponding age-matched control groups. However, these parameters were relatively constant or modestly changed between late pregnancy and mid-lactation but were later drastically increased in late lactation and postweaning (Fig. 8, *A–D*). Mineralizing surface (Supplemental Fig. S3) was consistent with bone formation rate (Fig. 8*D*).

Interestingly, despite having net bone gain during pregnancy, as demonstrated by DEXA, osteoclast surface and eroded surface in tibial trabeculae had already increased from mid-pregnancy and lasted until late lactation (Fig. 9, *A* and *B*). These results suggested that trabecular bone formation and resorption were uncoupled during these reproductive periods, thereby leading to bone gain and bone loss in pregnant and lactating rats, respectively. In other words, "bone modeling" may be present, since bone formation was not proportionally coupled to bone resorption (13). Both osteoclast surface and eroded surface returned to the control values postweaning (Fig. 9, *A* and *B*).

Most histomorphometric parameters, with the exception of osteoblast surface, double labeled surface, and bone formation rate, were not altered in Bromo-treated or Bromo+PRL-treated pregnant rats (Figs. 7–9), suggesting that PRL did not have much influence on trabecular bone changes during pregnancy. On the other hand, during the lactation period, especially in late lactation, changes in several parameters related to both bone formation and resorption, e.g., bone volume, trabecular number, trabecular separation, osteoblast surface, double labeled surface, mineral apposition rate, bone formation rate, osteoclast surface, and eroded surface, were regulated by PRL (Figs. 7–9). Multinucleated or activated osteoclasts were more abundant in Bromo+PRL-treated L21 rats than in Bromo-treated L21 rats (data not shown). However, PRL-induced changes in these parameters showed different times of responses as reflected by nonuniform responses to exogenous

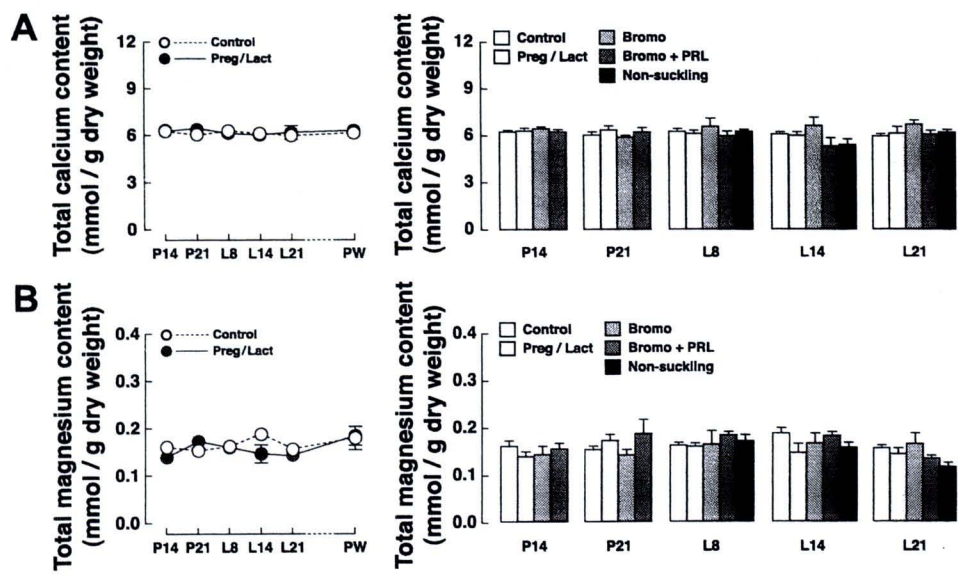

Fig. 4. Total calcium content (*A*) and total magnesium content (*B*) normalized by dry weight of femora obtained from age-matched control, pregnant (P14 and P21), lactating (L8, L14 and L21), and 15-day postweaning (PW) rats, as determined by ion chromatography. Some pregnant and lactating rats were administered Bromo 7 days (4 $mg \cdot kg^{-1} \cdot day^{-1}$ sc) for or Bromo+PRL. PRL doses for pregnant and lactating rats were 0.4 and 0.6 $mg \cdot kg^{-1} \cdot day^{-1}$, respectively. Some rats were permanently separated from their pups after parturition (nonsuckling). All values in line graphs and bar graphs are presented as means ± SE ($n = 4–6$ rats per condition).

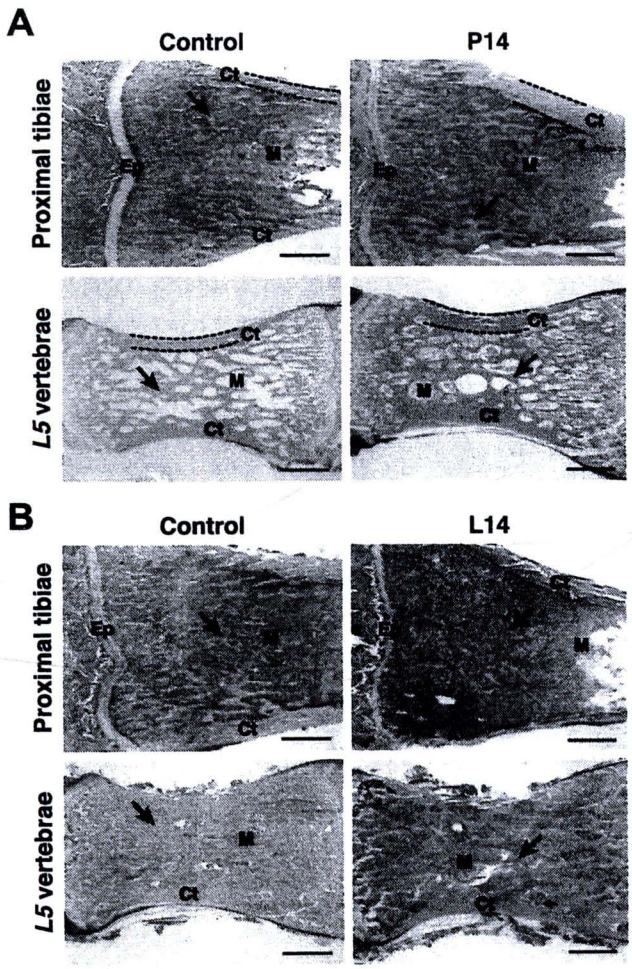

Fig. 5. Goldner's trichrome staining of tibiae (primarily cortical sites) and *L5* vertebrae (primarily trabecular sites) dissected from P14 (*A*) and L14 rats (*B*) and their corresponding age-matched controls (n = 3–4 rats per group). Cortical shell (Ct; bone tissue between dashed lines in *A*), epiphysial plate (Ep), bone trabeculae (arrows), and bone marrow (M) were identified. Mineralized bone matrix, erythrocytes, and cytoplasm were stained green, orange, and red, respectively. Bars, 1,000 μm.

PRL administration (Figs. 7–9). It is noteworthy that trabecular thickness in the rat tibiae was relatively constant from late pregnancy until late lactation, and also not responsive to both Bromo and PRL (Fig. 7*C*).

In nonsuckling rats, which had no hyperprolactinemia and the suckling-induced PRL surge (1, 34), most parameters with the exception of trabecular thickness were not much different from those of the age-matched control rats (Figs. 7–9).

DISCUSSION

How maternal bone adapts during pregnancy and lactation is crucial for growth, development, and calcium metabolism of the offspring. Herein, we provided evidence that bone changes during these periods were complex and time-dependent (pregnancy vs. lactation), and varied with sites of bone (femora/tibiae vs. vertebrae) as well as types of microstructure (cortical shells vs. trabeculae). Specifically, pregnancy predominantly induced femoral and vertebral bone gain in the cortical shells, whereas long-term lactation eventually led to trabecular bone loss. Lactation-induced trabecular bone loss, but not pregnancy-induced cortical bone gain, was found to be regulated by PRL. However, other hormones with elevated plasma levels, such as IGF-I and PTHrP, might also be responsible for bone changes during pregnancy and lactation, respectively (4, 28, 47).

In mid- and late pregnancy, the observed increases in femoral and vertebral BMD were due to an increase in cortical thickness, presumably by enhancing periosteal bone formation (4). Increased femoral bone length (or size), which probably results from pregnancy-enhanced endochondral bone growth (4), may also contribute to the increased femoral BMD in pregnant rats. Since bone size of pregnant rats was larger than that of their age-matched control rats, their whole bone BMC and ash weight were markedly increased during this period. However, the stoichiometry of calcium and magnesium in bone matrix remained unchanged. In contrast to the cortical parts, despite an increase in trabecular thickness in mid-pregnancy, changes in the trabecular microstructure in P14 and P21 rats were modest. Although P14 pregnant rats manifested the enhanced trabecular bone turnover, as indicated by the augmented bone formation and resorption, both processes were still coupled, and no change in trabecular bone volume was observed. These coupled processes in P14 rats could not be explained simply by osteoblast-induced bone formation, since osteoblast surface was indeed decreased in a PRL-dependent manner (Fig. 8*A*). It was hypothesized that surplus minerals supplied by the intestine might accelerate bone calcium acquisition (7, 9), as indicated by the twofold increase in the double labeled surface and mineral apposition rate in P14 rats (Fig. 8, *B* and *C*). On the other hand, uncoupling of trabecular bone formation and resorption, the latter of which being predominant, was evident in late pregnancy and continued throughout lactation. Therefore, the differential changes in cortical and trabecular structures (i.e., net bone gain and loss occurred at

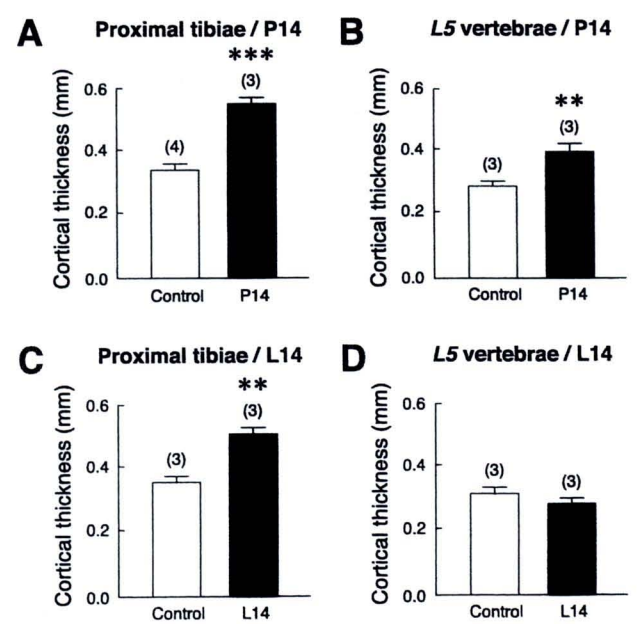

Fig. 6. Average thicknesses of cortical shells in proximal tibiae and *L5* vertebrae of P14 (*A–B*) and L14 (*C–D*) rats. $^{**}P < 0.01$, $^{***}P < 0.001$ vs. its respective control group. Nos. in parentheses represent nos. of experimental animals.

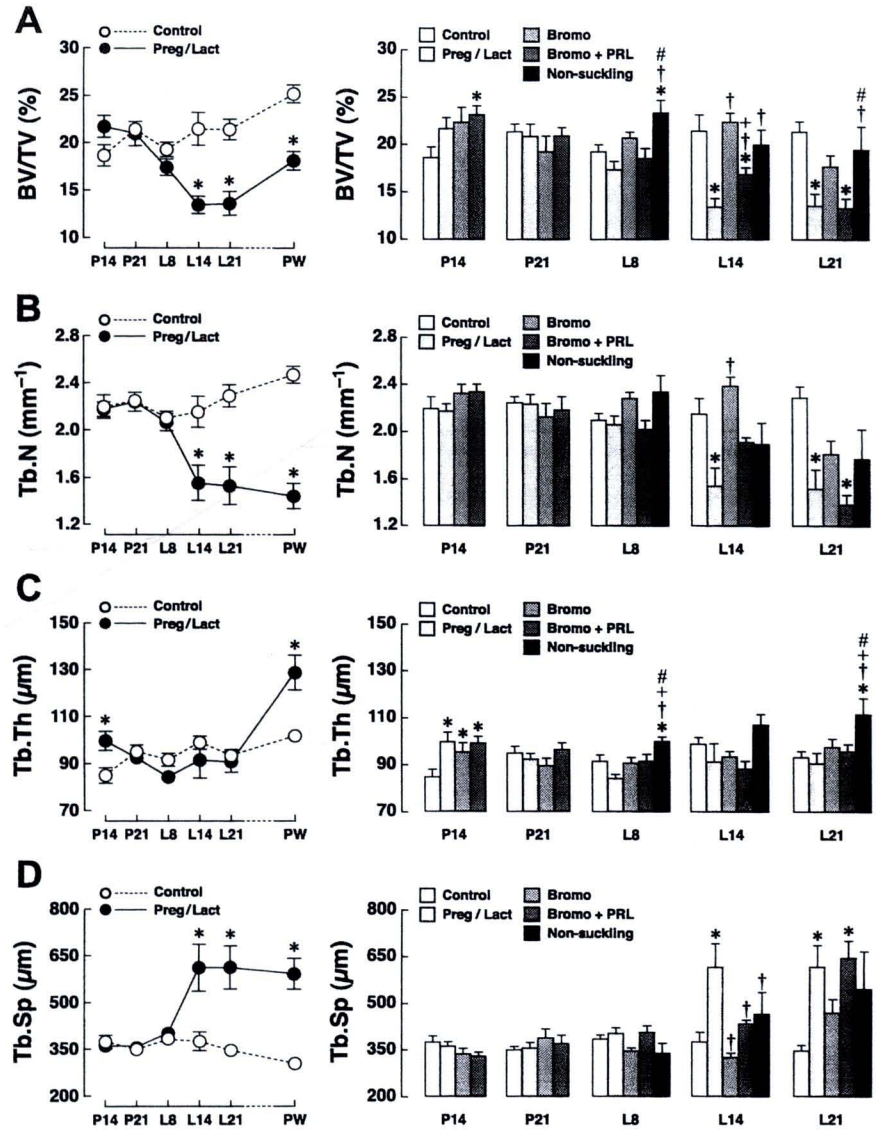

Fig. 7. *A*, trabecular bone volume normalized by tissue volume (BV/TV). *B*, trabecular number (Tb.N); *C*, trabecular thickness (Tb.Th); *D*, trabecular separation (Tb.Sp) of the trabecular portion (secondary spongiosa) of tibiae obtained from age-matched control, pregnant (P14 and P21), lactating (L8, L14 and L21), and 15-day postweaning (PW) rats, as determined by bone histomorphometry. Some pregnant and lactating rats were administered Bromo for 7 days (4 $mg \cdot kg^{-1} \cdot day^{-1}$ sc) or Bromo+PRL. PRL doses for pregnant and lactating rats were 0.4 and 0.6 $mg \cdot kg^{-1} \cdot day^{-1}$, respectively. Some rats were permanently separated from their pups after parturition (nonsuckling). All values in line graphs and bar graphs are presented as means ± SE (n = 7–8 rats per condition). *$P < 0.05$ vs. age-matched control group; †$P < 0.05$ vs. corresponding lactating group; +$P < 0.05$ vs. Bromo group; #$P < 0.05$ vs. Bromo+PRL group.

different parts of the same bone) indicated a process of bone modeling in this phase of the reproductive cycle (13).

It was postulated that pregnancy-induced bone gain was essential for the preparation of the maternal calcium pool during the last 5 days of pregnancy in rodents and the third trimester in humans for fetal skeletal mineralization and the upcoming lactogenesis (4). In addition, thickening of the cortical shells was important for maintaining bone shape and strength to compensate for the gradual increase in the trabecular separation during lactation (16). Such pregnancy-induced cortical adaptation was certainly under the regulation of hormone(s) other than PRL, such as progesterone and IGF-I (4, 17, 28). PRL might indirectly promote maternal bone gain through stimulation of intestinal calcium absorption to provide more calcium for mineralization (7). However, $1,25(OH)_2D_3$ and PTHrP might not participate directly in this bone gain, because bone mass was found to be increased in the vitamin D receptor knockout mice (17) and the plasma PTHrP levels were significantly increased in late pregnancy (20), after BMD had already been increased.

During lactation, progressive bone loss was evident, especially in the trabecular portions of both long bones and vertebrae. Since the trabecular surface was much greater than the exposed cortical surface (13), the lactation-induced bone loss occurred mainly in bone trabeculae rather than in cortical shells, thereby leading to a significant decrease in BMD in late lactation. Nevertheless, the endocortical surface of the rat tibiae showed greater erosion during lactation compared with the end of pregnancy (25). Previous investigations in humans also demonstrated that calcium lost during breastfeeding may cause a 10% loss of the total body skeletal mass (22, 37, 41). In rodents nursing around six to eight pups, bone mass could be decreased by ~30% in late lactation (5, 32, 47). Nevertheless, BMC and ash weight were not decreased, because bone size, as indicated by the femoral bone length, in lactating rat was actually larger than that of their age-matched controls. Similar to the pregnant rats, the stoichiometry of calcium and magnesium in bone matrix of lactating rats remained constant (Fig. 4), suggesting that the newly formed osteoid might be rapidly mineralized. It was possible that there was a sufficient amount

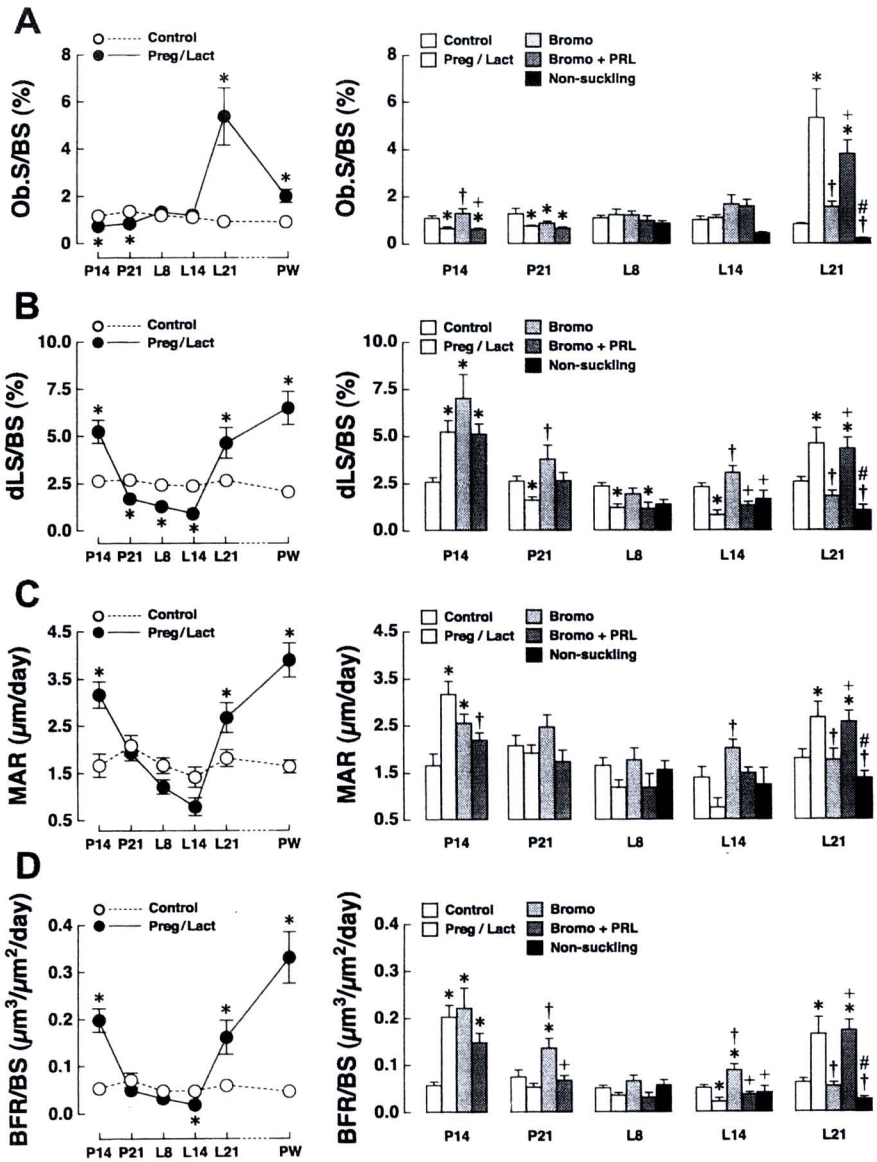

Fig. 8. Trabecular bone formation-related parameters: *A*, osteoblast surface normalized by trabecular bone surface (Ob.S/BS); *B*, double labeled surface (dLS/BS); *C*, mineral apposition rate (MAR); *D*, bone formation rate (BFR/BS) of the secondary spongiosa of tibiae obtained from age-matched control, pregnant (P14 and P21), lactating (L8, L14 and L21), and 15-day postweaning (PW) rats. Some pregnant and lactating rats were administered Bromo for 7 days (4 mg·kg^{-1}·day^{-1} sc) or Bromo+PRL. PRL doses for pregnant and lactating rats were 0.4 and 0.6 mg·kg^{-1}·day^{-1}, respectively. Some rats were permanently separated from their pups after parturition (nonsuckling). Ob.S/BS is a static histomorphometric parameter from the Goldner's trichrome-stained sections; dLS/BS, MAR, and BFR/BS are dynamic histomorphometric parameters from unstained sections. All values in line graphs and bar graphs are presented as means ± SE (n = 6–8 rats per condition). *$P < 0.05$ vs. age-matched control group; †$P < 0.05$ vs. corresponding pregnant or lactating groups; +$P < 0.05$ vs. Bromo group; #$P < 0.05$ vs. Bromo+PRL group.

of mineral supply for mineralization, perhaps from the intestine and kidney (9); otherwise, a decrease in normalized bone calcium content would be apparent as in dietary calcium deficiency with osteomalacia (15, 24, 33, 38).

It was evident that trabecular bone loss in lactating rats was induced by PRL, the plasma levels of which were ~200–300 ng/ml (normal levels ~7–10 ng/ml) and could further elevate up to ~600–800 ng/ml during suckling (1, 6, 7). The presence of PRLR in osteoblasts corroborated a direct effect of PRL on bone metabolism (12, 14, 40). Besides its direct action, PRL may indirectly induce bone resorption by suppressing ovarian estrogen synthesis (48). Furthermore, PRL may be responsible for calcium availability for bone mineralization, as it was the principal stimulator of intestinal calcium absorption in lactating rats (7, 9, 10).

Evidence that supported the PRL actions on bone in this study were based on the use of Bromo, which suppressed PRL release through stimulation of the pituitary D_2 dopaminergic receptors and in turn reduced circulating PRL levels by ~80–90% (3, 7, 35). Since osteoblasts did not express D_2 receptors (43), Bromo should not exert a direct action on this cell type. Although all histomorphometric parameters related to osteoblast functions and bone formation in L21 rats (e.g., osteoblast surface and bone formation rate) were completely inhibited by Bromo and restored by exogenous PRL supplement, changes in some other parameters seemed to be partially PRL dependent (e.g., osteoclast surface in L21 rats). It was possible that other hormones, such as PTHrP from the mammary glands, also contributed to the lactation-induced trabecular bone loss as reported previously (46). On the other hand, the PRL-induced bone changes were not clearly observed at the macroscopic level with DEXA, presumably because the gross changes in femoral BMD required prolonged duration of 2–7 wk of PRL exposure (40, 44).

Furthermore, the results in nonsuckling rats confirmed that the factor(s), either PRL or PTHrP, that induced trabecular bone loss during lactation was related to suckling. Normally, the plasma PRL levels decreased rapidly within 1–2 days after cessation of breastfeeding (26, 34). However, the significant increases in BMD and BMC in nonsuckling rats suggested that

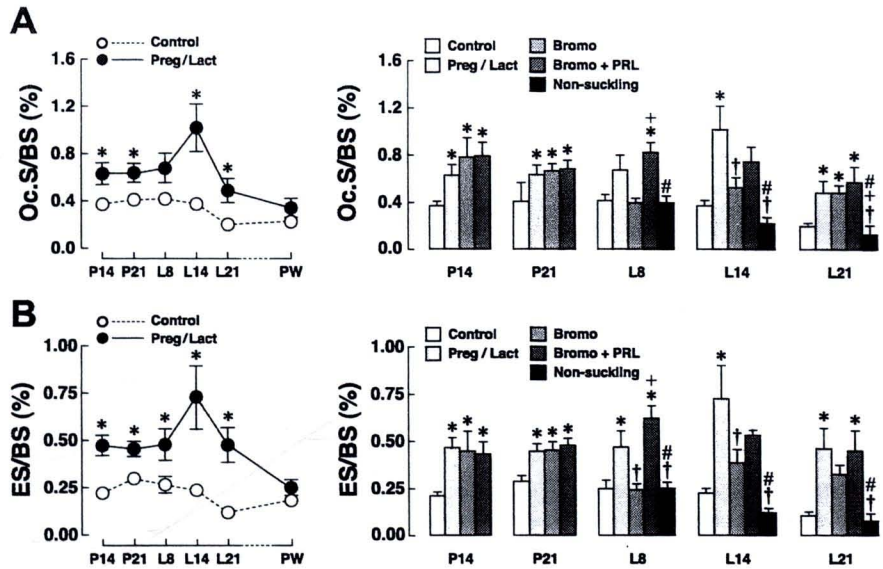

Fig. 9. Trabecular bone resorption-related parameters: osteoclast surface normalized by trabecular bone surface (Oc.S/BS; *A*), and eroded surface (ES/BS; *B*) of the secondary spongiosa of tibiae obtained from age-matched control, pregnant (P14 and P21), lactating (L8, L14 and L21), and 15-day postweaning (PW) rats. Some pregnant and lactating rats were administered Bromo for 7 days (4 $mg \cdot kg^{-1} \cdot day^{-1}$ sc) or Bromo+PRL. PRL doses for pregnant and lactating rats were 0.4 and 0.6 $mg \cdot kg^{-1} \cdot day^{-1}$, respectively. Some rats were permanently separated from their pups after parturition (nonsuckling). Both Oc.S/BS and ES/BS are static histomorphometric parameters from Goldner's trichrome-stained sections. All values in line graphs and bar graphs are presented as means ± SE (n = 6–8 rats per condition). $*P < 0.05$ vs. age-matched control group; $\dagger P < 0.05$ vs. corresponding lactating group; $+P < 0.05$ vs. Bromo group; $\#P < 0.05$ vs. Bromo+PRL group.

the absence of suckling pups and normal weaning might differentially affect bone metabolism, because BMD and BMC continued to increase in nonsuckling rats (Fig. 2), although their trabecular histomorphometric parameters showed similar modest changes (Figs. 7–9). It was, therefore, speculated that an endocrine factor that increased cortical bone growth during pregnancy remained active after parturition, perhaps due to the lack of antagonistic signals triggered by suckling.

Previous investigations concerning the direct effect of PRL on osteoblast-induced bone formation at the cellular and molecular levels agreed with the present histomorphometric findings. Specifically, PRL was found to downregulate *Runt*-related transcription factor-2, alkaline phosphatase, and osteocalcin (12, 40). Such direct PRL actions explained the PRL-induced decreases in osteoblast surface in tibial trabeculae of P14 rats and double labeled surface and bone formation rate of L14 rats. Interestingly, in L21 rats there were paradoxical increases in all bone formation-related parameters, which could be prevented by Bromo and restored by exogenous PRL administration (Fig. 8). The exact explanation of this paradox is not known, but it might be related to the PRL-enhanced intestinal calcium absorption (7, 19) and/or the calcitonin-induced renal calcium reabsorption (20), both of which could provide extra calcium for mineralization. Alternatively, extensive bone resorption in late lactation might lead to substantial release of the embedded growth factors, thus in turn stimulating bone formation (13).

Regarding PRL effects on bone resorption, a previous study using human osteoblasts showed that PRL upregulated the expression of receptor activator of nuclear factor-κB ligand (RANKL), while concurrently downregulating the osteoprotegerin (OPG) expression (40), thereby increasing the number of active osteoclasts and their activities. The PRL-induced increase in the RANKL/OPG ratio explained the present findings that osteoclast surface and eroded surface were markedly increased in mid- and late lactation. Besides PRL, mammary gland-derived PTHrP, which could directly stimulate osteoclasts, may also participate in maternal bone resorption, especially when its plasma levels were elevated from mid-pregnancy to late lactation (20, 46).

After weaning, BMD was restored by increasing trabecular bone formation (Fig. 8) and decreasing bone resorption (Fig. 9). BMD of the primarily cortical sites (e.g., femora) recovered faster than that of the trabecula-rich sites (e.g., *L5* vertebrae). It was apparent that the repair of trabecular microstructure in rats could not be accomplished within 15 days postweaning, but might require up to 20 wk of recovery (4). Similarly, in humans, bone mass could be restored after cessation of breast-feeding, although some mothers might develop the so-called pregnancy- and lactation-induced osteoporosis featuring bone pain, height loss, and fragility fracture (29).

In conclusion, we demonstrated herein that pregnancy increased bone mass predominantly in the cortical shells of both long bones and vertebrae, whereas lactation decreased bone mass predominantly in bone trabeculae. Thus, trabecular structures were an important source of calcium for lactogenesis. Interestingly, bone modeling was discernible during these reproductive periods as a result of increased bone length and uncoupling of bone formation and bone resorption. Although the pregnancy-induced cortical bone gain appeared to be PRL independent, PRL still contributed to maternal bone changes during pregnancy since it could decrease osteoblast surface in P14 rats. On the other hand, suppression of bone formation in mid-lactation and stimulation of bone resorption in mid- and late lactation were clearly PRL dependent and could be explained by the direct PRL actions on osteoblasts (39, 40). The present in vivo data, therefore, provided further information on a dynamic, time-dependent, site-specific adaptation of maternal bone, as well as differential osteoregulatory roles of PRL during pregnancy and lactation.

ACKNOWLEDGMENTS

We thank Jenjira Assapun, Kanogwun Thongchote, and Wasana Saengamnart for excellent technical assistance.

GRANTS

This research was supported by grants from the King Prajadhipok and Queen Rambhai Barni Memorial Foundation, the Faculty of Graduate Studies, Mahidol University, Academic Year 2008 (to P. Suntornsaratoon), the Mahidol University Postdoctoral Fellowship Program (to S. Goswami), and the Thailand Research Fund (RSA5180001 to N. Charoenphandhu).

DISCLOSURES

No conflicts of interest are reported by the authors.

REFERENCES

1. **Arbogast LA, Voogt JL.** Endogenous opioid peptides contribute to suckling-induced prolactin release by suppressing tyrosine hydroxylase activity and messenger ribonucleic acid levels in tuberoinfundibular dopaminergic neurons. *Endocrinology* 139: 2857–2862, 1998.
2. **Binart N, Bachelot A, Bouilly J.** Impact of prolactin receptor isoforms on reproduction. *Trends Endocrinol Metab* 21: 362–368, 2010.
3. **Bonomo IT, Lisboa PC, Passos MC, Alves SB, Reis AM, de Moura EG.** Prolactin inhibition at the end of lactation programs for a central hypothyroidism in adult rat. *J Endocrinol* 198: 331–337, 2008.
4. **Bowman BM, Miller SC.** Skeletal adaptations during mammalian reproduction. *J Musculoskelet Neuronal Interact* 1: 347–355, 2001.
5. **Brommage R, DeLuca HF.** Regulation of bone mineral loss during lactation. *Am J Physiol Endocrinol Metab* 248: E182–E187, 1985.
6. **Charoenphandhu N, Krishnamra N.** Prolactin is an important regulator of intestinal calcium transport. *Can J Physiol Pharmacol* 85: 569–581, 2007.
7. **Charoenphandhu N, Nakkrasae LI, Kraidith K, Teerapornpuntakit J, Thongchote K, Thongon N, Krishnamra N.** Two-step stimulation of intestinal Ca^{2+} absorption during lactation by long-term prolactin exposure and suckling-induced prolactin surge. *Am J Physiol Endocrinol Metab* 297: E609–E619, 2009.
8. **Charoenphandhu N, Tudpor K, Thongchote K, Saengamnart W, Puntheeranurak S, Krishnamra N.** High-calcium diet modulates effects of long-term prolactin exposure on the cortical bone calcium content in ovariectomized rats. *Am J Physiol Endocrinol Metab* 292: E443–E452, 2007.
9. **Charoenphandhu N, Wongdee K, Krishnamra N.** Is prolactin the cardinal calciotropic maternal hormone? *Trends Endocrinol Metab* 2010 Mar 19 [Epub ahead of print] PMID: 20304671.
10. **Charoenphandhu N, Wongdee K, Teerapornpuntakit J, Thongchote K, Krishnamra N.** Transcriptome responses of duodenal epithelial cells to prolactin in pituitary-grafted rats. *Mol Cell Endocrinol* 296: 41–52, 2008.
11. **Clément-Lacroix P, Ormandy C, Lepescheux L, Ammann P, Damotte D, Goffin V, Bouchard B, Amling M, Gaillard-Kelly M, Binart N, Baron R, Kelly PA.** Osteoblasts are a new target for prolactin: analysis of bone formation in prolactin receptor knockout mice. *Endocrinology* 140: 96–105, 1999.
12. **Coss D, Yang L, Kuo CB, Xu X, Luben RA, Walker AM.** Effects of prolactin on osteoblast alkaline phosphatase and bone formation in the developing rat. *Am J Physiol Endocrinol Metab* 279: E1216–E1225, 2000.
13. **Dempster DW.** Anatomy and functions of the adult skeleton. In: *Primer on the Metabolic Bone Diseases and Disorders of Mineral Metabolism*, edited by Favus MJ. Washington, DC: American Society for Bone and Mineral Research, 2006, p. 7–11.
14. **Deng C, Ueda E, Chen KE, Bula C, Norman AW, Luben RA, Walker AM.** Prolactin blocks nuclear translocation of VDR by regulating its interaction with BRCA1 in osteosarcoma cells. *Mol Endocrinol* 23: 226–236, 2009.
15. **Eklou-Kalonji E, Zerath E, Colin C, Lacroix C, Holy X, Denis I, Pointillart A.** Calcium-regulating hormones, bone mineral content, breaking load and trabecular remodeling are altered in growing pigs fed calcium-deficient diets. *J Nutr* 129: 188–193, 1999.
16. **Eriksen EF, Axelrod DW, Melsen F.** *Bone Histomorphometry*. New York: Raven, 1994, p. 33–50.
17. **Fudge NJ, Kovacs CS.** Pregnancy up-regulates intestinal calcium absorption and skeletal mineralization independently of the vitamin D receptor. *Endocrinology* 151: 886–895, 2010.
18. **Iwaniec UT, Wronski TJ, Turner RT.** Histological analysis of bone. *Methods Mol Biol* 447: 325–341, 2008.
19. **Jantarajit W, Thongon N, Pandaranandaka J, Teerapornpuntakit J, Krishnamra N, Charoenphandhu N.** Prolactin-stimulated transepithelial calcium transport in duodenum and Caco-2 monolayer are mediated by the phosphoinositide 3-kinase pathway. *Am J Physiol Endocrinol Metab* 293: E372–E384, 2007.
20. **Kovacs CS.** Calcium and bone metabolism during pregnancy and lactation. *J Mammary Gland Biol Neoplasia* 10: 105–118, 2005.
21. **Kraidith K, Jantarajit W, Teerapornpuntakit J, Nakkrasae LI, Krishnamra N, Charoenphandhu N.** Direct stimulation of the transcellular and paracellular calcium transport in the rat cecum by prolactin. *Pflügers Arch* 458: 993–1005, 2009.
22. **Laskey MA, Prentice A.** Bone mineral changes during and after lactation. *Obstet Gynecol* 94: 608–615, 1999.
23. **Laskey MA, Prentice A, Hanratty LA, Jarjou LM, Dibba B, Beavan SR, Cole TJ.** Bone changes after 3 mo of lactation: influence of calcium intake, breast-milk output, and vitamin D-receptor genotype. *Am J Clin Nutr* 67: 685–692, 1998.
24. **Marie PJ, Pettifor JM, Ross FP, Glorieux FH.** Histological osteomalacia due to dietary calcium deficiency in children. *N Engl J Med* 307: 584–588, 1982.
25. **Miller SC, Bowman BM.** Rapid improvements in cortical bone dynamics and structure after lactation in established breeder rats. *Anat Rec A Discov Mol Cell Evol Biol* 276: 143–149, 2004.
26. **Miller SC, Bowman BM.** Rapid inactivation and apoptosis of osteoclasts in the maternal skeleton during the bone remodeling reversal at the end of lactation. *Anat Rec (Hoboken)* 290: 65–73, 2007.
27. **Naliato EC, Farias ML, Braucks GR, Costa FS, Zylberberg D, Violante AH.** Prevalence of osteopenia in men with prolactinoma. *J Endocrinol Invest* 28: 12–17, 2005.
28. **O'Brien KO, Donangelo CM, Zapata CL, Abrams SA, Spencer EM, King JC.** Bone calcium turnover during pregnancy and lactation in women with low calcium diets is associated with calcium intake and circulating insulin-like growth factor 1 concentrations. *Am J Clin Nutr* 83: 317–323, 2006.
29. **Ofluoglu O, Ofluoglu D.** A case report: pregnancy-induced severe osteoporosis with eight vertebral fractures. *Rheumatol Int* 29: 197–201, 2008.
30. **Pahuja DN, DeLuca HF.** Stimulation of intestinal calcium transport and bone calcium mobilization by prolactin in vitamin D-deficient rats. *Science* 214: 1038–1039, 1981.
31. **Parfitt AM, Drezner MK, Glorieux FH, Kanis JA, Malluche H, Meunier PJ, Ott SM, Recker RR.** Bone histomorphometry: standardization of nomenclature, symbols, and units. Report of the ASBMR Histomorphometry Nomenclature Committee. *J Bone Miner Res* 2: 595–610, 1987.
32. **Peng TC, Garner SC, Kusy RP, Hirsch PF.** Effect of number of suckling pups and dietary calcium on bone mineral content and mechanical properties of femurs of lactating rats. *Bone Miner* 3: 293–304, 1988.
33. **Persson P, Gagnemo-Persson R, Håkanson R.** The effect of high or low dietary calcium on bone and calcium homeostasis in young male rats. *Calcif Tissue Int* 52: 460–464, 1993.
34. **Pi X, Voogt JL.** Effect of suckling on prolactin receptor immunoreactivity in the hypothalamus of the rat. *Neuroendocrinology* 71: 308–317, 2000.
35. **Piyabhan P, Krishnamra N, Limlomwongse L.** Changes in the regulation of calcium metabolism and bone calcium content during growth in the absence of endogenous prolactin and during hyperprolactinemia: a longitudinal study in male and female Wistar rats. *Can J Physiol Pharmacol* 78: 757–765, 2000.
36. **Prentice A.** Calcium in pregnancy and lactation. *Annu Rev Nutr* 20: 249–272, 2000.
37. **Ritchie LD, Fung EB, Halloran BP, Turnlund JR, Van Loan MD, Cann CE, King JC.** A longitudinal study of calcium homeostasis during human pregnancy and lactation and after resumption of menses. *Am J Clin Nutr* 67: 693–701, 1998.
38. **Salgueiro MJ, Torti H, Meseri E, Weill R, Orlandini J, Urriza R, Zubillaga M, Janjetic M, Barrado A, Boccio J.** Dietary zinc effects on zinc, calcium, and magnesium content in bones of growing rats. *Biol Trace Elem Res* 110: 73–78, 2006.
39. **Seriwatanachai D, Krishnamra N, van Leeuwen JP.** Evidence for direct effects of prolactin on human osteoblasts: inhibition of cell growth and mineralization. *J Cell Biochem* 107: 677–685, 2009.
40. **Seriwatanachai D, Thongchote K, Charoenphandhu N, Pandaranandaka J, Tudpor K, Teerapornpuntakit J, Suthiphongchai T, Krishnamra N.** Prolactin directly enhances bone turnover by raising osteoblast-expressed receptor activator of nuclear factor κB ligand/osteoprotegerin ratio. *Bone* 42: 535–546, 2008.
41. **Sowers M.** Pregnancy and lactation as risk factors for subsequent bone loss and osteoporosis. *J Bone Miner Res* 11: 1052–1060, 1996.
42. **Stubbs B.** Antipsychotic-induced hyperprolactinaemia in patients with schizophrenia: considerations in relation to bone mineral density. *J Psychiatr Ment Health Nurs* 16: 838–842, 2009.
43. **Suntornsaratoon P, Wongdee K, Krishnamra N, Charoenphandhu N.** Femoral bone mineral density and bone mineral content in bromocriptine-treated pregnant and lactating rats. *J Physiol Sci* 60: 1–8, 2010.

44. **Thongchote K, Charoenphandhu N, Krishnamra N.** High physiological prolactin induced by pituitary transplantation decreases BMD and BMC in the femoral metaphysis, but not in the diaphysis of adult female rats. *J Physiol Sci* 58: 39–45, 2008.
45. **van't Hof RJ, Clarkin CE, Armour KJ.** Studies of local bone remodeling: the calvarial injection assay. In: *Bone Research Protocols*, edited by Helfrich MH, Ralston SH. Totowa, NJ: Humana, 2003, p. 345–351.
46. **VanHouten JN, Dann P, Stewart AF, Watson CJ, Pollak M, Karaplis AC, Wysolmerski JJ.** Mammary-specific deletion of parathyroid hormone-related protein preserves bone mass during lactation. *J Clin Invest* 112: 1429–1436, 2003.
47. **VanHouten JN, Wysolmerski JJ.** Low estrogen and high parathyroid hormone-related peptide levels contribute to accelerated bone resorption and bone loss in lactating mice. *Endocrinology* 144: 5521–5529, 2003.
48. **Wang C, Chan V.** Divergent effects of prolactin on estrogen and progesterone production by granulosa cells of rat Graafian follicles. *Endocrinology* 110: 1085–1093, 1982.

Legends to supplemental figures

Supplemental Figure S1. Body weight of pregnant (P14 and P21), lactating (L8, L14 and L21) and age-matched control rats (n = 8–10 rats per group). * $P < 0.05$ compared with the corresponding age-matched control group.

Supplemental Figure S2. Total calcium content normalized by dry weight of femora obtained from age-matched control, pregnant (P14 and P21), lactating (L8, L14 and L21) and 15-day postweaning (PW) rats, as determined by atomic absorption spectrophotometer. Some pregnant and lactating rats were administered for 7 days with 4 mg/kg/day bromocriptine s.c. (Bromo), or Bromo plus PRL s.c. (Bromo+PRL). The PRL doses for pregnant and lactating rats were 0.4 and 0.6 mg/kg/day, respectively. Some rats were permanently separated from their pups after parturition (non-suckling). All values in line graphs and bar graphs are presented as means ± SE (n = 4–6 rats per condition).

Supplemental Figure S3. Mineralizing surface normalized by trabecular bone surface (MS/BS) of the secondary spongiosa of tibiae obtained from age-matched control, pregnant (P14 and P21), lactating (L8, L14 and L21) and 15-day postweaning (PW) rats. All values are presented as means ± SE (n = 7–8 rats per each condition). * $P < 0.05$ compared with age-matched control group.

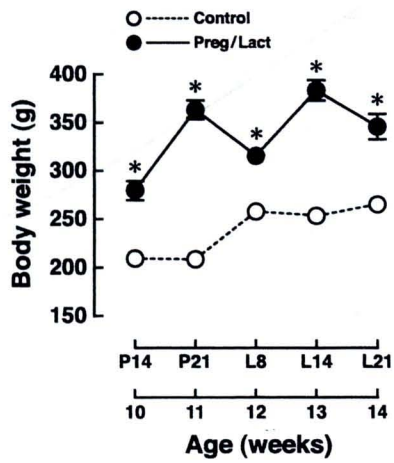

Supplemental Figure S1: Suntornsaratoon et al.

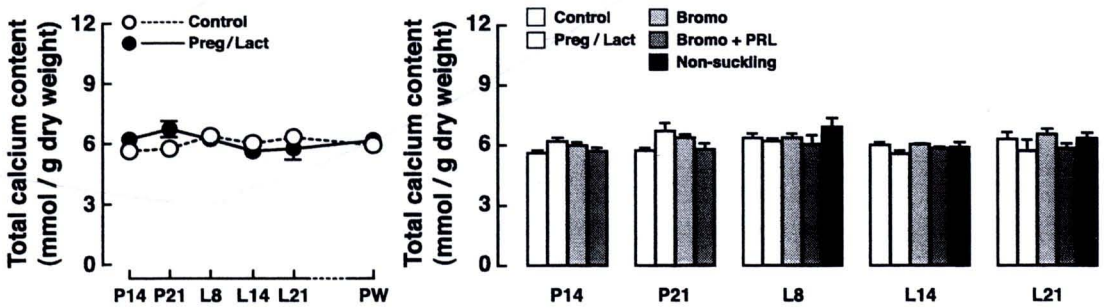

Supplemental Figure S2: Suntornsaratoon et al.

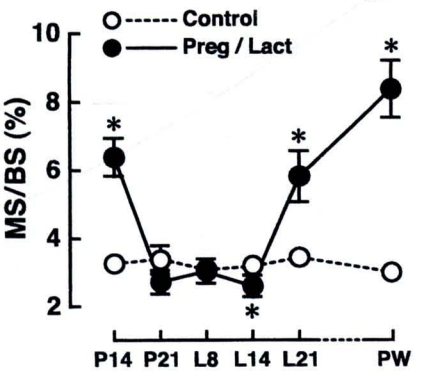

Supplemental Figure S3: Suntornsaratoon et al.

Cell PRESS

Is prolactin the cardinal calciotropic maternal hormone?

Narattaphol Charoenphandhu[1,2], Kannikar Wongdee[2,3] and Nateetip Krishnamra[1,2]

[1] Department of Physiology, Faculty of Science, Mahidol University, Bangkok 10400, Thailand
[2] Consortium for Calcium and Bone Research (COCAB), Faculty of Science, Mahidol University, Bangkok 10400, Thailand
[3] Faculty of Allied Health Sciences, Burapha University, Chonburi 20131, Thailand

To produce offspring, mothers require a large amount of calcium for fetal growth and milk production. Increased calcium demand leads to enhanced intestinal calcium absorption and stockpiling of bone calcium in pregnancy prior to demineralization in lactation. These coordinated events must be carefully organized by calciotropic hormone(s), but the classical hormones, namely 1,25-dihydroxyvitamin D_3, parathyroid hormone and calcitonin, do not appear to be responsible. Plasma prolactin (PRL) levels are elevated during pregnancy and, in view of the presence of PRL receptors in gut, bone and mammary glands, as well as recent evidence of the stimulatory effects of PRL on intestinal calcium transport, bone resorption and mammary calcium secretion, we postulate that PRL is the cardinal calciotropic hormone during pregnancy and lactation.

Stress on maternal calcium metabolism imposed by pregnancy and lactation

Women lose a huge amount of calcium, ~200–300 mg/day in the third trimester for fetal bone development and ~300–1000 mg/day during breastfeeding [1–3], and three maternal systems, namely intestine, bone and kidney (Figure 1), must work together in a highly coordinated manner under endocrine control to guarantee calcium adequacy for the developing fetus and newborn. Surprisingly, the principal calcium-regulating hormone in pregnancy and lactation remains a controversial issue. Several investigations have shown that neither bone mineral loss nor increased intestinal calcium absorption during these reproductive periods depend on ovarian or adrenal hormones [4]. Moreover, there is no strong correlation between maternal calcium demand and the major calcium-regulating hormones – 1,25-dihydroxyvitamin D_3 [$1,25(OH)_2D_3$], parathyroid hormone (PTH) and calcitonin [3,5,6]. In vitamin D receptor (VDR) knockout mice, expression of the transient receptor potential channel, subfamily V, member 6 (TRPV6), a calcium channel required for transcellular calcium absorption in the small intestine (Box 1), was still upregulated during pregnancy and lactation [7]. A recent study in pregnant VDR knockout mice confirmed that pregnancy stimulates duodenal calcium absorption in a VDR-independent manner [8]. Maternal calcium metabolism must therefore be regulated by some other hormone(s).

Evidence that supports calciotropic roles of PRL

Plasma levels of PRL, a 23 kDa polypeptide hormone secreted from the anterior pituitary gland, are strikingly elevated during pregnancy (75–100 ng/mL, compared to nonpregnant levels of 7–10 ng/mL) [5], to help maintain functional corpus luteum in pregnancy (for a review on PRL action, see Ref. [9]). To induce lactation, plasma PRL levels are elevated to 200–300 ng/mL, and transiently surge within 15 min of suckling to ~400–800 ng/mL, and these elevated levels last for 60–90 min [10]. Pregnancy and lactation are therefore considered to be physiological hyperprolactinemic states.

Why is PRL a strong candidate for the calcium-regulating hormone during these reproductive periods? In addition to its elevated plasma levels during pregnancy and lactation, PRL has been shown to have proto-osmoregulatory and hypercalcemic roles in fish, and increases branchial and intestinal calcium permeability while preventing excessive demineralization of bone and scale [11,12]. Indeed, on an evolutionary timescale, before PTH first appeared and fully functioned in amphibians, PRL and other PRL-like hormones (e.g. somatolactin) served as the major hypercalcemic hormones in fish [11]. Hypercalcemic activities of PRL are also evident in amphibians, reptiles and birds [11,13]. Although the lower vertebrates such as fishes and amphibians might have different modes of calcium homeostasis than mammals, this suggests a conserved role for PRL in calcium metabolism.

In mammals, PRL receptor (PRLR) expression in intestine, kidney and bone, the major calcium-handling organs, indicates a direct calciotropic action of PRL in these organs [14–16]. In fact, exogenous PRL administration stimulates intestinal calcium absorption in nonpregnant female rats [5] and increases intestinal calcium transport and bone calcium mobilization in vitamin D-deficient rats fed a low calcium diet [6]. PRLR knockout mice also manifest an impairment of bone development [17]. Moreover, in patients with PRL-producing tumors or pathological hyperprolactinemia induced by prolonged uses of antipsychotic drugs (e.g. risperidone and amisulpride, both of which antagonize the PRL-inhibiting factor dopamine), bone resorption is dramatically increased, resulting in low bone mass and overt osteoporosis [18,19].

Two-step stimulation of intestinal calcium absorption by PRL

PRL-stimulated maternal calcium absorption across the intestinal epithelium takes place by a two-step mechanism

Corresponding author: Charoenphandhu, N. (naratt@narattsys.com).

1043-2760/$ - see front matter doi:10.1016/j.tem.2010.02.002 Trends in Endocrinology and Metabolism 21 (2010) 395–401

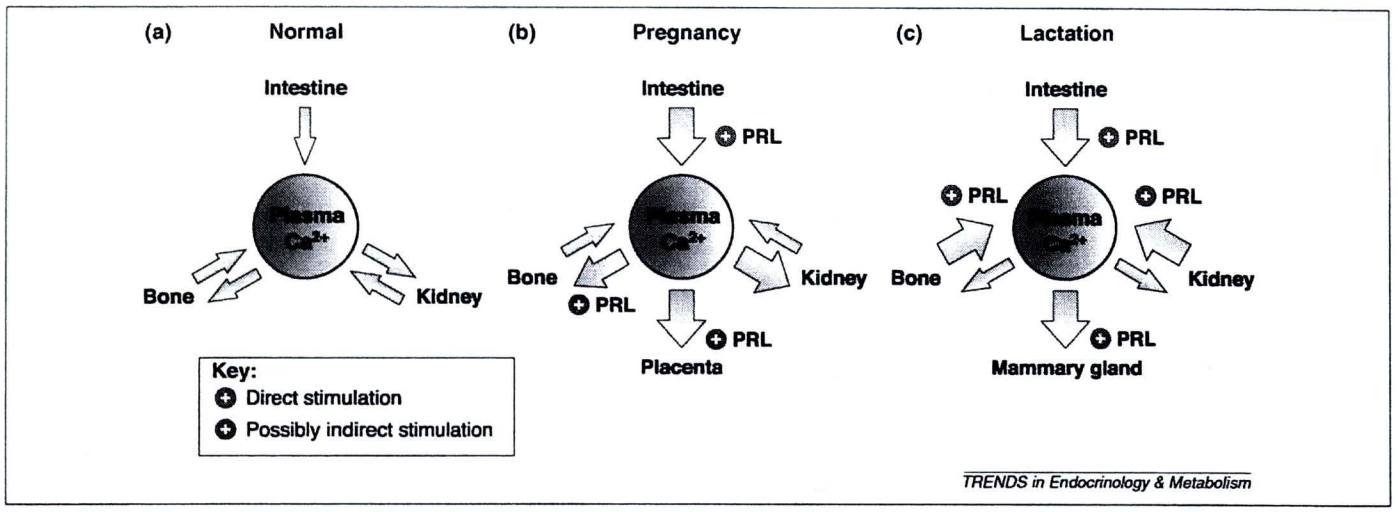

Figure 1. Hypothetical model for maternal total body calcium homeostasis as regulated by PRL. **(a)** Under normal conditions, bone formation and resorption are balanced, and renal calcium excretion is minimal. PRL acts as a coordinator to provide adequate calcium and to mobilize calcium for fetal bone development and milk production. **(b)** During pregnancy, PRL markedly enhances intestinal calcium absorption, that in turn indirectly increases maternal bone calcium accretion and placental calcium transfer [10,27]. If intestinal calcium absorption exceeds the body's requirement plus bone calcium accumulation, excess calcium will be excreted via the kidney, thereby leading to maternal hypercalciuria (also known as absorptive hypercalciuria) [29,33]. **(c)** In late lactation, PRL still enhances the intestinal calcium absorption to supply more calcium for milk production [10]. Adequate milk calcium supply is also achieved by PRL-enhanced renal calcium reabsorption and bone resorption, leading to maternal hypocalciuria and osteopenia, respectively [16,29,37]. Moreover, mammary calcium secretion has been found to be regulated by PRL [47].

(Figure 2) [10], similar to that which occurs in non-mated animals [6,14,20]. Specifically, sustained hyperprolactinemia of 75–100 ng/mL during pregnancy, or 200–300 ng/mL during lactation, induces a long-lasting adaptation in the intestinal absorptive cells to elevate the 'baseline calcium flux' by ~2-fold (Step-1), that is further increased (Step-2) by the transient PRL surge (400–800 ng/mL) ~15–90 min after suckling. Only Step-1 calcium absorption is dependent on *de novo* transcription of genes required for calcium absorption, for example those encoding TRPV6 and calbindin-D_{9k} (Box 1). However, the Step-2 calcium flux is well correlated with milk volume, and it is possible that the PRL surge during suckling serves as a signal to coordinate calcium mobilization from various sources to supply calcium for milk production [10]. Because inhibition of pituitary PRL secretion completely abolishes Step-1 and -2 calcium absorption [10], PRL might serve as a single salient factor for this maternal adaptation.

The duodenum and cecum are highly responsive to PRL [10,20]. Both transcellular and paracellular calcium transport in the duodenum are markedly stimulated by PRL during the reproductive periods [10]. Although the major driving force for paracellular intestinal calcium transport is the calcium concentration gradient, the tight junction acts as a barrier that restricts paracellular ion movement in a charge- and size-selective manner [21]. Paracellular permeability is thus regulated by tight junction proteins including occludin, ZO-1 and claudins [21]. PRL overcomes this barrier by lowering the transepithelial resistance and increasing calcium permeability, in part, by downregulating

Box 1. Redundancy in intestinal calcium transport

Calcium traverses the intestinal epithelium via paracellular and transcellular pathways, with the former being present in most intestinal segments and predominant in the presence of ~2–6 mM luminal calcium as found with a normal diet [50]. In the presence of 10 mM luminal calcium, for example after oral calcium supplementation, the paracellular calcium flux can be ~5 times as high as the transcellular flux [10,14]. However, transcellular calcium transport becomes more significant during low calcium intake or increased calcium demand, for example during pregnancy and lactation [10,24,50]. Nevertheless, the cellular and molecular mechanisms are still controversial and require further investigation.

Transcellular calcium transport in the intestine is a three-step active process, consisting of apical calcium uptake, cytoplasmic calcium translocation and basolateral calcium extrusion. The calcium channel TRPV6 and calbindin-D_{9k} were believed to be responsible for the apical uptake and facilitated diffusion across the cytoplasm, respectively. Thereafter, plasma membrane Ca^{2+}-ATPase-1b ($PMCA_{1b}$) and Na^+/Ca^{2+} exchanger-1 (NCX1) are responsible for ~85% and ~15% of calcium efflux, respectively [51]. Bianco and co-workers reported a 60% decrease in intestinal calcium absorption, growth retardation and low femoral bone mineral density in the TRPV6-null mice [52]. However, more recent investigations showed that TRPV6 knockout, calbindin-D_{9k} knockout, and TRPV6/calbindin-D_{9k} double knockout mice manifested normal serum calcium and $1,25(OH)_2D_3$-dependent active calcium transport [53]. Several alternative or compensatory mechanisms can partially explain these discrepancies. For example, calcium might enter intestinal epithelial cells via other channels, including voltage-dependent calcium channels (Ca_v), and especially when cells are slightly depolarized by apical sodium entry in the presence of high luminal glucose [sodium and glucose enter the cell together via the sodium-dependent glucose transporter (SGLT)-1] [48]. Cytoplasmic calcium translocation might also be accomplished by other calcium-binding proteins such as calmodulin and parvalbumin [25,51], or by vesicular transport or 'tunneling' through the endoplasmic reticulum [51].

It is reasonable to ask the question – why does the gut use so many transport mechanisms and transporters for calcium absorption? Because calcium is essential for many processes in the body and is obtained solely from the diet, such redundancy guarantees that calcium absorption is always sufficient and matches calcium demand. It is also possible that these various mechanisms of calcium absorption are differentially regulated by different hormones or conditions. For example, estrogen, endurance exercise and chronic metabolic acidosis can upregulate TRPV6 expression [7,51,54,55], whereas $Ca_v1.3$ is essential for glucose-stimulated calcium absorption [48].

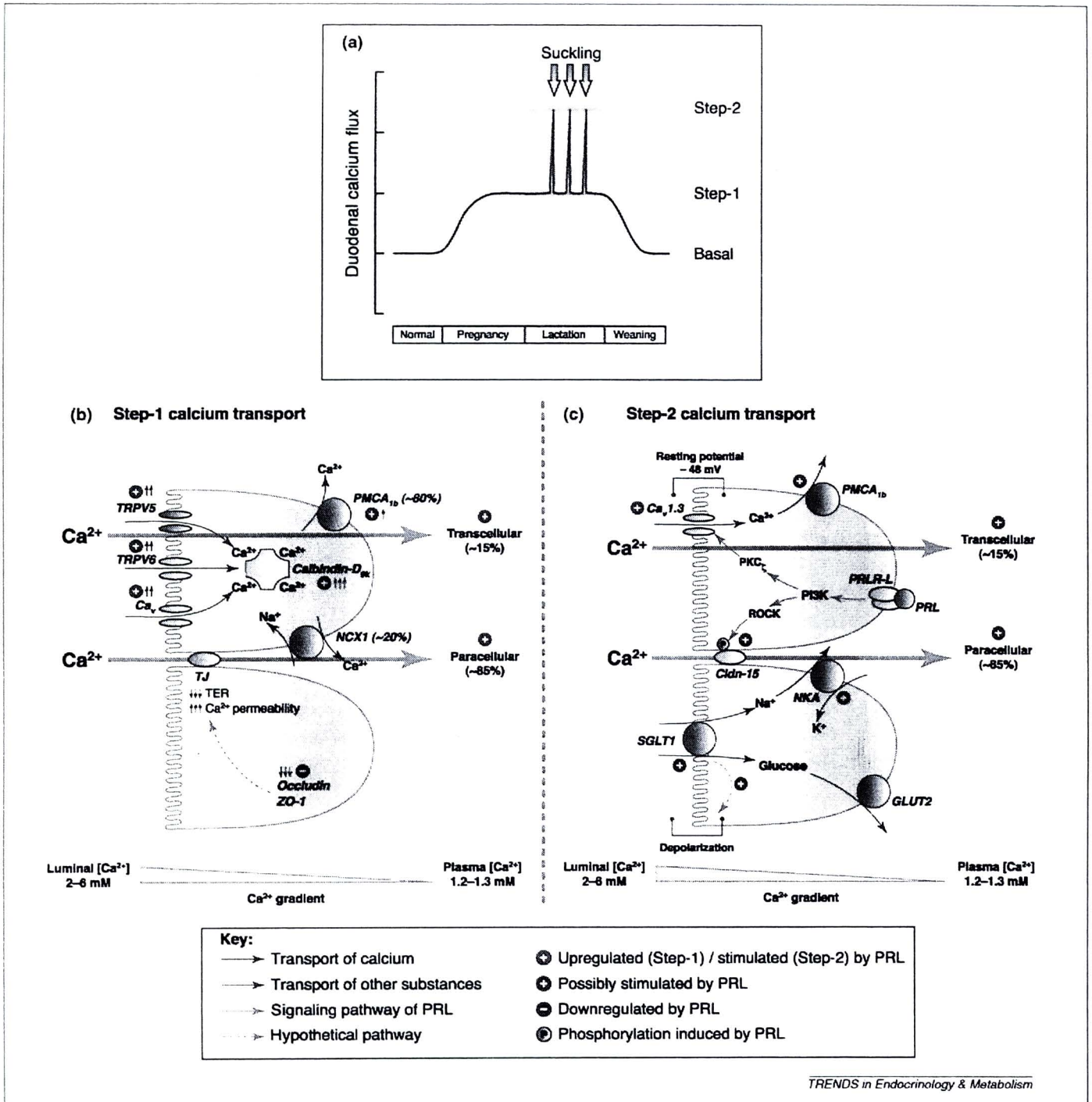

Figure 2. Hypothetical diagram of two-step stimulation of duodenal calcium absorption by PRL and its possible cellular mechanisms [10]. **(a)** Hyperprolactinemia during pregnancy and lactation elevates the 'basal calcium flux' to a new baseline (Step-1), whereas the suckling-induced PRL surge exerts a transient stimulatory effect on the calcium flux, that is further increased to the Step-2 level. This adaptation disappears after weaning. In the presence of a calcium gradient (i.e. luminal calcium > plasma free ionized calcium) and/or solvent drag, the PRL-enhanced paracellular calcium transport is predominant [14,23]. **(b)** The Step-1 calcium flux is achieved by PRL-induced upregulation of genes encoding proteins related to transcellular calcium transport (i.e. TRPV5, TRPV6, Ca_v, calbindin-D_{9k} and $PMCA_{1b}$), and downregulation of genes encoding tight junction (TJ) proteins (i.e. occludin and ZO-1) that are generally essential for the paracellular barrier functions as indicated by a high transepithelial resistance (TER) and restriction of paracellular ion permeability [10]. The degree of up- or downregulation is indicated by the number of small arrows. **(c)** Step-2 calcium transport through the transcellular pathway requires PRL-stimulated apical calcium entry via $Ca_v1.3$, and calcium extrusion via $PMCA_{1b}$, whereas transport through paracellular pathway involves PRL-induced phosphorylation of claudin (Cldn)-15 [10]. PRL signaling is mediated by several proteins, such as long isoform (-L) of PRLR, phosphoinositide 3-kinase (PI3K), Rho-associated kinase (ROCK) and protein kinase C (PKC)-ζ [14,20,22]. Glucose absorption via the sodium-dependent glucose transporter (SGLT)-1 and the glucose transporter (GLUT)-2 is also important for PRL action because sodium entry via SGLT1 can induce depolarization of the apical membrane, thereby activating $Ca_v1.3$ for transcellular calcium transport [48], whereas sodium extrusion via Na^+/K^+-ATPase (NKA) can increase the paracellular hyperosmotic gradient for solvent drag [5,23]. In addition, an increase in paracellular calcium transport induced by solvent drag also results from PRL-stimulated NKA activity [5].

occludin and ZO-1 (Figure 2), thereby leading to Step-1 paracellular calcium transport [10]. Step-2 paracellular calcium transport, on the other hand, is related to the PRL-induced serine phosphorylation of claudin-15 [10]. The downstream PRL signal transduction pathway is not completely understood, but appears to involve phosphoinositide 3-kinase (PI3K)- and Rho-associated kinase (ROCK)-related pathways, and not the classical Janus kinase-2 pathway [10,20,22].

Moreover, calcium also traverses the paracellular space of the proximal small intestine along with osmotic water flow – a process known as solvent drag-induced calcium transport [23]. Solvent drag is induced after sodium entering the cells via sodium-dependent glucose transporter (SGLT)-1, and exiting the cells via Na^+/K^+-ATPase, accumulates in the paracellular space as a standing hyperosmotic gradient (Figure 2) [5,23]. PRL stimulates this solvent drag-induced calcium transport by stimulating Na^+/K^+-ATPase activity [5].

Regarding transcellular calcium transport, PRL-induced upregulation of crucial transporter genes including those encoding TRPV5, TRPV6 and calbindin-D_{9k}, accomplishes Step-1 transcellular calcium transport [7,10,24]. A recent microarray study in duodenal epithelial cells suggested that PRL also upregulated other potential calcium transporters, for example the voltage-dependent L-type calcium channel (Ca_v) and parvalbumin [25], perhaps to ensure adequate intestinal calcium absorption during pregnancy and lactation. However, it remains to be investigated whether PRL directly upregulates these calcium transporter genes, or acts indirectly by stimulating renal and/or local $1,25(OH)_2D_3$ production [24].

In addition, acute PRL exposure directly activates the long isoform of PRLR and its downstream mediators, PI3K and protein kinase C-ζ, thereby leading to Step-2 transcellular calcium transport [10,22]. It appears likely that short isoforms of PRLR do not mediate PRL signaling in intestinal absorptive cells (for a review on PRLRs, see Ref. [9]). PRL-enhanced apical calcium uptake occurs very rapidly, within ~8–10 min after PRL exposure, and requires $Ca_v1.3$ [5,10,22] (Figure 2). We recently demonstrated that TRPV5 and TRPV6 were not involved because double knockdown of TRPV5 and TRPV6 did not abolish PRL-enhanced transcellular calcium transport [26]. Moreover, PRL also stimulates the basolateral calcium extrusion by increasing plasma membrane Ca^{2+}-ATPase-1b ($PMCA_{1b}$) activity [5]. It is noteworthy that the increased numbers of calcium transporter proteins (e.g. TRPV6 and calbindin-D_{9k}) induced by long-term PRL exposure (Step-1) might help to enhance Step-2 transcellular calcium absorption and/or increase the responsiveness of cells to acute PRL exposure during suckling [10].

Enhanced bone turnover and bone calcium release by PRL: friend or foe?

Pregnant mammals, including humans, sheep and rats, exhibit bone calcium accumulation in early and mid-pregnancy [1]. However, there is a slight decrease in maternal bone mineral density due to rapid fetal bone calcium accretion in the third trimester in humans, whereas maternal bone calcium accumulation in rats appears to continue until early lactation [1,27]. Activated osteoclast activity at both trabecular and cortical sites is already evident throughout pregnancy, presumably to prepare the maternal calcium pool for fetal transfer [1,28]. Regulation of maternal bone calcium accumulation is partially PRL-dependent [27,29] and might also be associated with increased plasma levels of progesterone, insulin-like growth factor-I and osteoprotegerin (OPG), the last of which counterbalances osteoclast-mediated bone resorption [1,30]. After delivery, bone resorption is markedly enhanced to release calcium for lactogenesis [3,31]. A ~10–30% reduction in bone mineral density (i.e. osteopenia) and a dramatic decline in bone strength that often accompany lactation sometimes lead to pregnancy and lactation-associated osteoporosis (PLO) featuring back pain, vertebral fracture, and height loss [3,32,33]. Decreased ovarian estrogen and increased mammary production of PTH-related peptide (PTHrP) – a hormone that induces osteoclast formation – can be responsible for maternal osteopenia [33], and PRL might act in concert to fine-tune maternal bone turnover or might even cause PLO.

PRL was previously thought to indirectly enhance bone resorption by suppressing ovarian production of estrogen that normally induces net bone gain [16,18]. However, osteoblasts strongly express PRLR, indicating a direct action of PRL on bone [16,34,35]. At the cellular level, PRL downregulates OPG while concurrently upregulating the receptor activator of nuclear factor-κB ligand (RANKL), a factor generally synthesized and/or released from osteoblasts to increase the number and activity of osteoclasts [16] (Figure 3). Although PRL can also increase osteoblast number *in vivo* [16], fully differentiated or functional osteoblasts could be decreased because PRL downregulates Runx2 (a transcription factor required for osteoblast differentiation), and two important differentiation markers, alkaline phosphatase and osteocalcin [16,34,36]. After weaning, bone mass is restored in both humans and rodents [1,33], coincidently with decreases in osteoblast-derived RANKL [31] and plasma levels of PRL and PTHrP [33]. The long-term effects of lactation-induced osteopenia on subsequent bone health is controversial, ranging from full recovery or minor deficits to a permanent decrease in bone mass [3,31–33,37]. Preexisting low bone mass prior to pregnancy might be a cause of incomplete recovery [38]. However, for the sake of maternal bone health, massive and/or permanent bone loss, if any, should be prevented [39].

Possible regulatory action of PRL on renal calcium handling

Renal calcium excretion is increased during pregnancy, but is decreased during lactation in both humans and rodents [29,33]. Pregnancy-induced hypercalciuria is caused by excess calcium absorption from the intestine (i.e. absorptive hypercalciuria; Figure 1) [33]. Moreover, elevated plasma calcitonin levels in pregnancy could contribute to maternal calciuresis [33].

PRLR expression was reported in renal tubular cells [15], suggesting the kidney as a probable target organ for PRL. As demonstrated by the calcium balance technique,

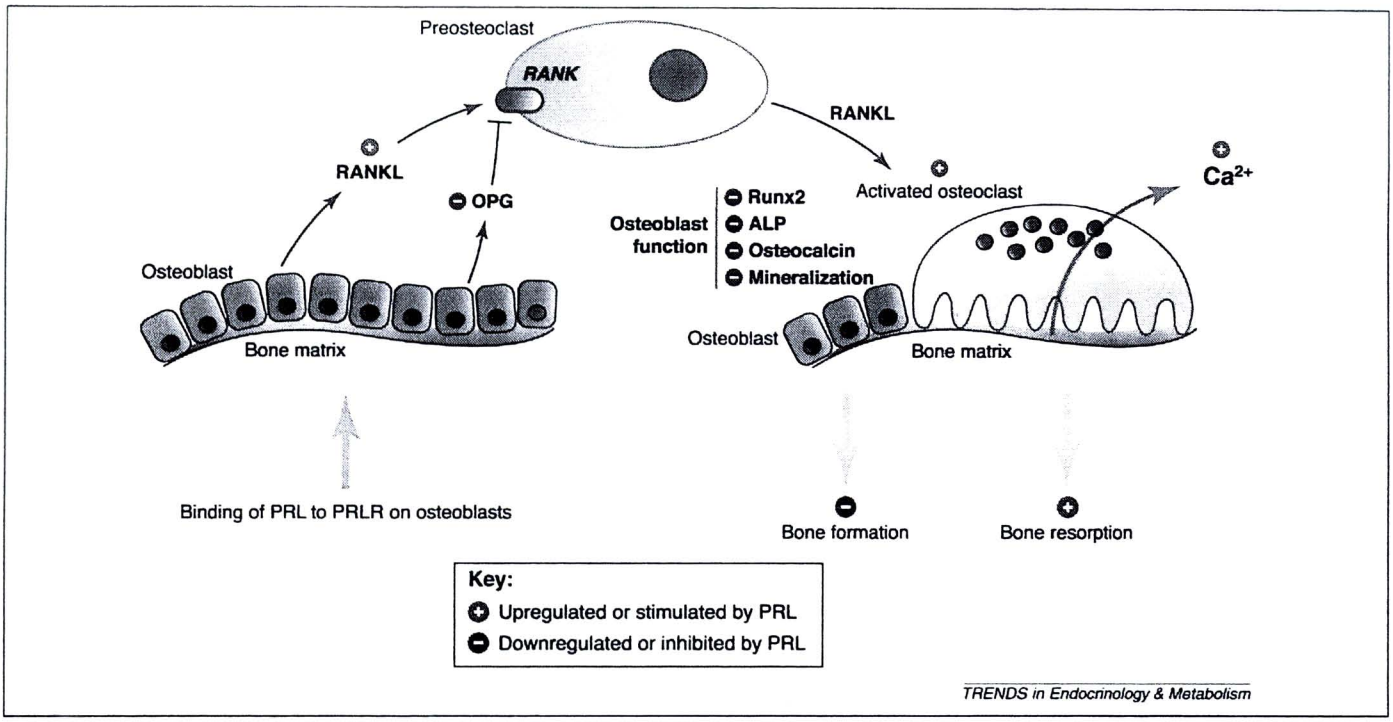

Figure 3. Possible mechanism of PRL-enhanced bone resorption in late lactation. PRL exerts a direct action on bone through osteoblasts because osteoclasts do not express PRLR [34]. Binding of PRL to PRLR on osteoblasts upregulates the expression of the receptor activator of nuclear factor-κB (RANK) ligand (RANKL), and downregulates osteoprotegerin (OPG), a decoy factor that blocks the RANKL–RANK interaction. After binding to its receptor RANK, RANKL induces osteoclastogenesis, activates osteoclasts, and maintains the survival of activated osteoclasts, thereby inducing bone demineralization to release more calcium into the plasma [16]. PRL also suppresses osteoblast functions by decreasing the expression of *Runt*-related transcription factor (Runx)-2, alkaline phosphatase (ALP) and osteocalcin, as well as the osteoblast-induced matrix mineralization [16,34,36]. The net result of PRL action on bone is therefore to stimulate bone resorption and inhibit bone formation.

PRL injection decreased renal calcium excretion in both non-mated and pregnant rats [29,40]. Although it was suggested that exogenous PRL enhanced renal calcium reabsorption [29,40], the role of endogenous PRL released during pregnancy and lactation remains uncertain because inhibition of pituitary PRL release by the dopaminergic agonist bromocriptine did not show a significant increase in renal calcium excretion [29]. Recent investigation showed that combined exposure to PRL and glucocorticoid directly modulates the barrier function of tight junctions in cultured renal epithelial monolayer, possibly by inducing redistribution of tight junction proteins occludin and ZO-1 [41]. Further *in vivo* investigations will be required to confirm a direct action of endogenous PRL on the renal tubular epithelium and on renal calcium handling in lactating animals.

Possible role of PRL in calcium transfer for fetal development and lactogenesis

Placental calcium transfer to the fetus and fetal bone mineralization largely take place in the third trimester in humans and the last five days of pregnancy in rats [42]. Several hormones including PTH and PTHrP are essential for placental calcium transfer in rodents [43]. Although the placenta is responsive to PRL and PRL-like factors [9], the physiological role of PRL in regulating placental calcium transport is currently not known. Nevertheless, it is possible that PRL contributes to calcium transfer across the placenta because it can increase calcium supply to the mother by stimulating intestinal calcium absorption [10].

After parturition, the mammary gland secretes up to 1000 mg/day of milk calcium, the concentration of which varies according to the stage of lactation (~5–8 mM) [1–3,44]. Because milk calcium is the sole calcium source for neonatal bone development and cellular metabolism, milk calcium secretion in mothers on a low calcium diet is maintained by the release of calcium from bone [2,44]. However, the hormone(s) responsible for controlling milk calcium secretion remains elusive.

Generally, transcellular calcium transport from plasma to the acinar lumen of the mammary gland consists of (i) calcium entry at the blood-facing plasma membrane, presumably via canonical transient receptor potential (TRPC) channels, (ii) uptake of cytoplasmic calcium into the Golgi apparatus by secretory pathway Ca^{2+}-ATPase system, and (iii) calcium extrusion via $PMCA_2$ and exocytosis [44,45]. In the Golgi apparatus and exocytotic vesicles, calcium binds to citrate, phosphate, and milk protein casein, the expression of which is enhanced by PRL [44,46]. Administration of exogenous PRL to lactating rats increases milk calcium concentration by ~10% [29]. Recently, PRL was reported to increase the expression of secretory pathway Ca^{2+}-ATPase-2 (SPCA2), and knockdown of SPCA2 abolished PRL-induced calcium uptake into the Golgi apparatus [47]. However, PRL did not alter TRPC channel mRNA expression levels [45]. Although the signaling pathway remains unknown, it is possible that the lactogenic hormone PRL directly regulates milk calcium secretion.

Possible directions for nutraceutical research and maternal health care

Because milk calcium is derived from both diet and bone in as yet unknown proportions, oral calcium supplementation should shift the proportion of milk calcium toward the

Box 2. Outstanding questions

- Does PRL enhance calcium uptake from the plasma into mammary epithelial cells? If so, what are the responsible calcium channels or transporters?
- Is PRL responsible for the maintenance of milk calcium concentration? What is the proportion of milk calcium content derived from diet versus bone?
- What is the exact role of PRL in renal calcium handling? Does PRL directly stimulate calcium reabsorption in the kidney?
- Does PRL directly enhance placental calcium transfer? How does maternal PRL contribute to skeletal development in the fetus?
- Can oral calcium supplementation prior to breastfeeding or PRL surge efficiently prevent maternal bone resorption, or even PLO and postmenopausal osteoporosis later in life, by supplying a larger proportion of calcium from the diet, thus reducing calcium mobilization from bone for milk production?

dietary source [10,39]. However, bone loss in breastfeeding mothers with relatively high calcium intake suggests that calcium supplementation alone is probably not enough to achieve this shift [1,37]. Because Step-2 calcium absorption is triggered by the suckling-induced PRL surge, to maximize the benefit of calcium supplementation we postulate that calcium should be administered orally at an appropriate time (e.g. 30–60 min) prior to breastfeeding in 3–4 divided doses/day (e.g. ~300–400 mg/dose; estimated from the recommended dietary intake of ~1200 mg/day). However, the effectiveness and potential long-term benefits of this regimen in humans remain to be validated.

Furthermore, certain nutrients such as glucose (and perhaps galactose, another substrate of SGLT1) can induce plasma membrane depolarization and increase Na^+/K^+-ATPase activity, thereby leading to $Ca_v1.3$ activation and solvent drag (Figure 2), respectively, both of which are important for PRL-stimulated duodenal calcium absorption [22,23,48]. Moreover, microflora can ferment prebiotics (non-digestible food ingredients) into acidic compounds, that then solubilize insoluble calcium complexes and promote calcium absorption [49], and especially in the cecum where PRL also markedly stimulates both transcellular and paracellular calcium transport [14,20]. It is therefore suggested that nutraceutical scientists might develop a calcium-rich product containing such additional ingredients as a supplement for breastfeeding mothers.

Concluding remarks

Several lines of evidence corroborate that PRL, with elevated plasma levels during mammalian reproductive periods, can be considered to be the cardinal calciotropic hormone that regulates maternal calcium homeostasis. PRL appears not only to provide more 'calcium input' during pregnancy and lactation, but also controls 'calcium output' via milk secretion (Figure 1). In other words, PRL acts as a coordinator to regulate and synchronize the calcium-regulating system to mobilize a sufficient amount of calcium for fetal development and lactogenesis. Calcium adequacy is achieved by PRL-enhanced intestinal calcium absorption, renal calcium reabsorption and bone resorption [6,10,14,27,29]. Although PRL is clearly a calcium regulating hormone, there are several questions that await further investigation (Box 2).

On the basis of findings that PRL stimulates intestinal calcium absorption in a two-step manner, it is suggested that oral calcium supplement for breastfeeding mothers should be given at appropriate times and doses to optimize calcium absorption. The development of a new calcium supplement that is well-absorbed in PRL-responsive intestinal segments including duodenum or cecum [14,20] should provide maximum benefit. Future holistic and integrative approaches in understanding physiological functions of PRL and maternal calcium homeostasis are important for preventing PLO and promoting fetomaternal bone health.

Acknowledgements

This work was supported by the Faculty of Science, Mahidol University, and the Thailand Research Fund.

References

1 Bowman, B.M. and Miller, S.C. (2001) Skeletal adaptations during mammalian reproduction. *J. Musculoskelet. Neuronal Interact.* 1, 347–355
2 Laskey, M.A. *et al.* (1998) Bone changes after 3 mo of lactation: influence of calcium intake, breast-milk output, and vitamin D-receptor genotype. *Am. J. Clin. Nutr.* 67, 685–692
3 Prentice, A. (2000) Calcium in pregnancy and lactation. *Annu. Rev. Nutr.* 20, 249–272
4 Brommage, R. and DeLuca, H.F. (1985) Regulation of bone mineral loss during lactation. *Am. J. Physiol. Endocrinol. Metab.* 248, E182–E187
5 Charoenphandhu, N. and Krishnamra, N. (2007) Prolactin is an important regulator of intestinal calcium transport. *Can. J. Physiol. Pharmacol.* 85, 569–581
6 Pahuja, D.N. and DeLuca, H.F. (1981) Stimulation of intestinal calcium transport and bone calcium mobilization by prolactin in vitamin D-deficient rats. *Science* 214, 1038–1039
7 Van Cromphaut, S.J. *et al.* (2003) Intestinal calcium transporter genes are upregulated by estrogens and the reproductive cycle through vitamin D receptor-independent mechanisms. *J. Bone Miner. Res.* 18, 1725–1736
8 Fudge, N.J. and Kovacs, C.S. (2010) Pregnancy up-regulates intestinal calcium absorption and skeletal mineralization independently of the vitamin D receptor. *Endocrinology* 151, 886–895
9 Soares, M.J. *et al.* (2007) The prolactin family: effectors of pregnancy-dependent adaptations. *Trends Endocrinol. Metab.* 18, 114–121
10 Charoenphandhu, N. *et al.* (2009) Two-step stimulation of intestinal Ca^{2+} absorption during lactation by long-term prolactin exposure and suckling-induced prolactin surge. *Am. J. Physiol. Endocrinol. Metab.* 297, E609–E619
11 Norris, D.O. (2007) Bioregulation of calcium and phosphate homeostasis, In *Vertebrate Endocrinology* (4th edn) (Norris, D.O., ed.), pp. 486–511, Elsevier
12 Takahashi, H. *et al.* (2008) Prolactin inhibits osteoclastic activity in the goldfish scale: a novel direct action of prolactin in teleosts. *Zoolog. Sci.* 25, 739–745
13 Srivastav, A.K. and Yadav, S. (2008) Prolactin effects on ultimobranchial and parathyroid glands in pigeon. *North-West J. Zool.* 4, 300–310
14 Jantarajit, W. *et al.* (2007) Prolactin-stimulated transepithelial calcium transport in duodenum and Caco-2 monolayer are mediated by the phosphoinositide 3-kinase pathway. *Am. J. Physiol. Endocrinol. Metab.* 293, E372–E384
15 Sakai, Y. *et al.* (1999) The prolactin gene is expressed in the mouse kidney. *Kidney Int.* 55, 833–840
16 Seriwatanachai, D. *et al.* (2008) Prolactin directly enhances bone turnover by raising osteoblast-expressed receptor activator of nuclear factor κB ligand/osteoprotegerin ratio. *Bone* 42, 535–546
17 Clément-Lacroix, P. *et al.* (1999) Osteoblasts are a new target for prolactin: analysis of bone formation in prolactin receptor knockout mice. *Endocrinology* 140, 96–105
18 Naliato, E.C. *et al.* (2005) Prevalence of osteopenia in men with prolactinoma. *J. Endocrinol. Invest.* 28, 12–17

19 Stubbs, B. (2009) Antipsychotic-induced hyperprolactinaemia in patients with schizophrenia: considerations in relation to bone mineral density. *J. Psychiatr. Ment. Health Nurs.* 16, 838–842

20 Kraidith, K. *et al.* (2009) Direct stimulation of the transcellular and paracellular calcium transport in the rat cecum by prolactin. *Pflügers Arch.* 458, 993–1005

21 Anderson, J.M. and Van Itallie, C.M. (2009) Physiology and function of the tight junction. *Cold Spring Harb. Perspect. Biol.* (doi:10.1101/cshperspect.a002584)

22 Thongon, N. *et al.* (2009) Enhancement of calcium transport in Caco-2 monolayer through PKC_{ζ}-dependent $Ca_v1.3$-mediated transcellular and rectifying paracellular pathways by prolactin. *Am. J. Physiol. Cell Physiol.* 296, C1373–C1382

23 Tanrattana, C. *et al.* (2004) Prolactin directly stimulated the solvent drag-induced calcium transport in the duodenum of female rats. *Biochim. Biophys. Acta* 1665, 81–91

24 Zhu, Y. *et al.* (1998) Pregnancy and lactation increase vitamin D-dependent intestinal membrane calcium adenosine triphosphatase and calcium binding protein messenger ribonucleic acid expression. *Endocrinology* 139, 3520–3524

25 Charoenphandhu, N. *et al.* (2008) Transcriptome responses of duodenal epithelial cells to prolactin in pituitary-grafted rats. *Mol. Cell Endocrinol.* 296, 41–52

26 Nakkrasae, L.I. *et al.* (2010) Transepithelial calcium transport in prolactin-exposed intestine-like Caco-2 monolayer after combinatorial knockdown of TRPV5, TRPV6 and $Ca_v1.3$. *J. Physiol. Sci.* 60, 9–17

27 Suntornsaratoon, P. *et al.* (2010) Femoral bone mineral density and bone mineral content in bromocriptine-treated pregnant and lactating rats. *J. Physiol. Sci.* 60, 1–8

28 Naylor, K.E. *et al.* (2000) The effect of pregnancy on bone density and bone turnover. *J. Bone Miner. Res.* 15, 129–137

29 Lotinun, S. *et al.* (1998) The study of a physiological significance of prolactin in the regulation of calcium metabolism during pregnancy and lactation in rats. *Can. J. Physiol. Pharmacol.* 76, 218–228

30 Hong, J.S. *et al.* (2005) Maternal plasma osteoprotegerin concentration in normal pregnancy. *Am. J. Obstet. Gynecol.* 193, 1011–1015

31 Ardeshirpour, L. *et al.* (2007) Weaning triggers a decrease in receptor activator of nuclear factor-κB ligand expression, widespread osteoclast apoptosis, and rapid recovery of bone mass after lactation in mice. *Endocrinology* 148, 3875–3886

32 Ofluoglu, O. and Ofluoglu, D. (2008) A case report: pregnancy-induced severe osteoporosis with eight vertebral fractures. *Rheumatol. Int.* 29, 197–201

33 Kovacs, C.S. (2005) Calcium and bone metabolism during pregnancy and lactation. *J. Mammary Gland Biol. Neoplasia* 10, 105–118

34 Coss, D. *et al.* (2000) Effects of prolactin on osteoblast alkaline phosphatase and bone formation in the developing rat. *Am. J. Physiol. Endocrinol. Metab.* 279, E1216–E1225

35 Deng, C. *et al.* (2009) Prolactin blocks nuclear translocation of VDR by regulating its interaction with BRCA1 in osteosarcoma cells. *Mol. Endocrinol.* 23, 226–236

36 Seriwatanachai, D. *et al.* (2009) Evidence for direct effects of prolactin on human osteoblasts: inhibition of cell growth and mineralization. *J. Cell Biochem.* 107, 677–685

37 Chan, S.M. *et al.* (2005) Bone mineral density and calcium metabolism of Hong Kong Chinese postpartum women – a 1-y longitudinal study. *Eur. J. Clin. Nutr.* 59, 868–876

38 Tanriover, M.D. *et al.* (2009) Pregnancy- and lactation-associated osteoporosis with severe vertebral deformities: can strontium ranelate be a new alternative for the treatment? *Spine J.* 9, e20–e24

39 Thomas, M. and Weisman, S.M. (2006) Calcium supplementation during pregnancy and lactation: effects on the mother and the fetus. *Am. J. Obstet. Gynecol.* 194, 937–945

40 Piyabhan, P. *et al.* (2000) Changes in the regulation of calcium metabolism and bone calcium content during growth in the absence of endogenous prolactin and during hyperprolactinemia: a longitudinal study in male and female Wistar rats. *Can. J. Physiol. Pharmacol.* 78, 757–765

41 Peixoto, E.B.M.I. and Collares-Buzato, C.B. (2006) Modulation of the epithelial barrier by dexamethasone and prolactin in cultured Madin–Darby canine kidney (MDCK) cells. *Cell Biol. Int.* 30, 101–113

42 Kovacs, C.S. (2006) Skeletal physiology: fetus and neonate, In *Primer on the Metabolic Bone Diseases and Disorders of Mineral Metabolism* (6th edn) (Favus, M.J., ed.), pp. 50–55, American Society for Bone and Mineral Research

43 Simmonds, C.S. *et al.* (2010) Parathyroid hormone regulates fetal–placental mineral homeostasis. *J. Bone Miner. Res.* doi:10.1359/jbmr.090825. (in press)

44 Neville, M.C. (2005) Calcium secretion into milk. *J. Mammary Gland Biol. Neoplasia* 10, 119–128

45 Anantamongkol, U. *et al.* (2010) Transcriptome analysis of mammary tissues reveals complex patterns of transporter gene expression during pregnancy and lactation. *Cell Biol. Int.* 34, 67–74

46 Stiening, C.M. *et al.* (2008) The effects of endocrine and mechanical stimulation on stage I lactogenesis in bovine mammary epithelial cells. *J. Dairy Sci.* 91, 1053–1066

47 Anantamongkol, U. *et al.* (2007) Regulation of Ca^{2+} mobilization by prolactin in mammary gland cells: possible role of secretory pathway Ca^{2+}-ATPase type 2. *Biochem. Biophys. Res. Commun.* 352, 537–542

48 Mace, O.J. *et al.* (2007) Calcium absorption by $Ca_v1.3$ induces terminal web myosin II phosphorylation and apical GLUT2 insertion in rat intestine. *J. Physiol.* 580, 605–616

49 Tenorio, M.D. *et al.* (2010) Soybean whey enhances mineral balance and caecal fermentation in rats. *Eur. J. Nutr.* doi:10.1007/s00394-009-0060-8. (in press)

50 Wasserman, R.H. (2004) Vitamin D and the dual processes of intestinal calcium absorption. *J. Nutr.* 134, 3137–3139

51 Khanal, R.C. and Nemere, I. (2008) Regulation of intestinal calcium transport. *Annu. Rev. Nutr.* 28, 179–196

52 Bianco, S.D. *et al.* (2007) Marked disturbance of calcium homeostasis in mice with targeted disruption of the Trpv6 calcium channel gene. *J. Bone Miner. Res.* 22, 274–285

53 Benn, B.S. *et al.* (2008) Active intestinal calcium transport in the absence of transient receptor potential vanilloid type 6 and calbindin-D_{9k}. *Endocrinology* 149, 3196–3205

54 Teerapornpuntakit, J. *et al.* (2009) Endurance swimming stimulates transepithelial calcium transport and alters the expression of genes related to calcium absorption in the intestine of rats. *Am. J. Physiol. Endocrinol. Metab.* 296, E775–E786

55 Charoenphandhu, N. *et al.* (2006) Chronic metabolic acidosis stimulated transcellular and solvent drag-induced calcium transport in the duodenum of female rats. *Am. J. Physiol. Gastrointest. Liver Physiol.* 291, G446–G455

Experimental and Molecular Pathology xxx (2010) xxx–xxx

Contents lists available at ScienceDirect

Experimental and Molecular Pathology

journal homepage: www.elsevier.com/locate/yexmp

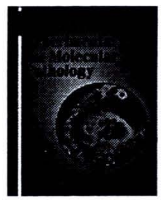

Claudin expression in the bone-lining cells of female rats exposed to long-standing acidemia

Kannikar Wongdee [a,b,c], Suda Riengrojpitak [b], Nateetip Krishnamra [a,d], Narattaphol Charoenphandhu [a,d,*]

[a] Consortium for Calcium and Bone Research (COCAB), Faculty of Science, Mahidol University, Bangkok, Thailand
[b] Department of Pathobiology, Faculty of Science, Mahidol University, Bangkok, Thailand
[c] Faculty of Allied Health Sciences, Burapha University, Chonburi, Thailand
[d] Department of Physiology, Faculty of Science, Mahidol University, Bangkok, Thailand

ARTICLE INFO

Article history:
Received 13 October 2009
and in revised form 9 December 2009
Available online xxxx

Keywords:
Acidosis
Bone membrane
Claudin
Immunohistochemistry
Osteoblasts
Tight junction

ABSTRACT

Besides enhancing osteoclast-mediated bone resorption, chronic metabolic acidosis (CMA) induces mineral efflux across the epithelial-like bone membrane formed by bone-lining cells (inactive osteoblasts), possibly via the paracellular pathway. However, there was a compensatory mechanism that restricted bone loss in the late phase of CMA, and changes in the expression of claudins, which are tight junction proteins known to regulate epithelial barrier function, were therefore anticipated in bone-lining cells. Herein, primary rat osteoblasts were found to express several transcripts of claudins, i.e., claudin-5, -11, -14, -15 and -16. Their protein expressions in bone-lining cells were demonstrated by immunohistochemistry in decalcified tibial sections. After exposure to CMA induced by oral administration of 1.5% NH_4Cl for 21 days, expression of claudin-14, which normally seals the paracellular space and restricts ion movement, was increased, whereas that of claudin-15 and -16 which form pores for ion transport were decreased. Expressions of claudin-5 and -11 were not changed by CMA. In conclusion, the bone-lining cells of rats exposed to CMA for 21 days upregulated an ion-restrictive claudin (i.e., claudin-14), while downregulating ion-permeable claudins (i.e., claudin-15 and -16). These cellular responses might be parts of a compensatory mechanism accounting for deceleration of bone loss in late CMA.

Introduction

Chronic metabolic acidosis (CMA) is a common acid-base disturbance caused by a reduction in capacity of the kidney to synthesize ammonia and excrete H^+ (e.g., chronic renal failure), continuous loss of HCO_3^- (e.g., distal renal tubular acidosis), or accumulation of acidic substances. A number of studies showed that CMA affects bone metabolism by inducing physicochemical dissolution of bone minerals, suppressing osteoblast-mediated bone formation, and enhancing osteoclast-mediated bone resorption, thereby resulting in massive bone loss, hypercalciuria, nephrocalcinosis and negative calcium balance (Bushinsky and Lechleider, 1987; Dominguez and Raisz, 1979; Kraut et al., 1986; Krieger et al., 1992). However, our recent longitudinal study in rats exposed to CMA for 10 months suggested the existence of an unknown compensatory mechanism that decelerated bone loss and maintained bone mass during CMA (Assapun et al., 2009).

Bone calcium is present in the form of hydroxyapatite crystal, as well as free ions dissolved in the bone extracellular fluid (BECF), which is an intraosseous fluid compartment with different ion compositions from plasma (e.g., high K^+ concentration in BECF) (Green and Kleeman, 1991; Rubinacci et al., 2000). BECF is separated from the plasma by a "functional" epithelial-like bone membrane created by bone-lining cells (inactive osteoblasts), and its ion compositions were reported to be controlled by bone-lining cells (Bushinsky et al., 1989; Parfitt 1989; Soares et al., 1992; Trumbore et al., 1980). In acidosis, calcium is released from BECF by transporting across the bone membrane, presumably via the paracellular pathway (Bushinsky and Frick, 2000; Bushinsky, 2001; Marenzana et al., 2005). Besides calcium, the effluxes of other bone minerals, such as sodium, potassium and phosphate may also help buffer acid during CMA (Bergstrom and Wallace, 1954; Green and Kleeman, 1991).

In normal epithelia, the presence of tight junction is crucial for the fine-tuning of paracellular permeability, the maintenance of epithelial integrity, and the formation of paracellular barrier (Furuse and Tsukita, 2006; Tsukita et al., 2001). Since tight junctions are also present in osteoblasts (Hatakeyama et al., 2008; Prêle et al., 2003; Soares et al., 1992; Weinger and Holtrop, 1974; Wongdee et al., 2008), several investigations have suggested that bone-lining cells might regulate the paracellular ion exchange between the two fluid compartments, i.e., plasma and BECF, in an epithelial-like manner (Bushinsky et al., 1989; Hatakeyama et al., 2008; Rubinacci et al., 2000; Trumbore et al., 1980). However, it was still not known how ions were transported across the tight junction in CMA.

Abbreviations: BECF, bone extracellular fluid; CMA, chronic metabolic acidosis.

* Corresponding author. Department of Physiology, Faculty of Science, Mahidol University, Rama 6 Road, Bangkok 10400, Thailand. Fax: +66 2 354 7154.
E-mail address: naratt@narattsys.com (N. Charoenphandhu).

0014-4800/$ – see front matter © 2009 Elsevier Inc. All rights reserved.
doi:10.1016/j.yexmp.2009.12.005

In general, regulation of tight junction permeability for the paracellular transport of ions and small molecules across normal epithelia requires tight junction proteins of the claudin family, which consists of 24 members. Although claudins are predominantly localized in the tight junction, some claudins (e.g., claudin-3 and -7) can be found in other parts of the plasma membrane (Charoenphandhu et al., 2007; Holmes et al., 2006). Several investigators provided evidence that claudins could be divided into 2 subtypes, i.e., ion-restrictive and ion-permeable claudins (for review Anderson and Van Itallie, 2009). For example, claudin-5, -11 and -14 were demonstrated to seal the paracellular space and restrict paracellular ion movement (Ben-Yosef et al., 2003; Gow et al., 1999; Nitta et al., 2003), while claudin-15 and -16 assembled into a row of channel-like pores for paracellular ion transport (Tsukita et al., 2001; Van Itallie and Anderson, 2006). Interestingly, osteoblasts and bone-lining cells were also reported to express claudins, and their expressions were controlled by various humoral mediators, e.g., insulin-like growth factor I (Hatakeyama et al., 2008; Prêle et al., 2003; Wongdee et al., 2008). Since it was recently shown that long-term exposure to CMA eventually induced a compensatory response to limit bone mineral loss (Assapun et al., 2009), we hypothesized that expression of ion-restrictive claudins may be upregulated, whereas that of ion-permeable claudins were downregulated in the bone-lining cells of rats exposed to long-standing acidemia.

Materials and methods

Animals

Female Sprague–Dawley rats (8-week-old, weighing 180–220 g) were obtained from the National Animal Centre, Salaya, Thailand. They were housed in the laboratory animal husbandry unit under 12:12-h light–dark cycle, and fed regular chows (Perfect Companion, Bangkok, Thailand), and distilled water *ad libitum*. Room temperature was maintained at 20–25 °C, and relative humidity was 50–60%. After acclimatization for 7 days, the rats were randomly divided into two groups, i.e., age-matched control ($n=6$) and CMA groups ($n=4$). In CMA group, rats were provided *ad libitum* for 21 days with water containing 1.5% w/v NH_4Cl (Sigma, St Louis, MO, USA) to induce an acid-loading acidemia. Food and water intake were recorded daily. This study has been approved by the Institutional Animal Care and Use Committee (IACUC) of the Faculty of Science, Mahidol University, Bangkok, Thailand.

Arterial blood gas analysis

Heparinized arterial blood sample (5 mL) was collected from the left ventricle. Blood gas analysis of plasma pH, partial pressure of O_2 and CO_2, and HCO_3^- concentration was performed to confirm the success of CMA induction by using an automated analyzer (model Ultra C; Nova Biomedical, Walthame, MA, USA).

Primary osteoblast culture

Under 50 mg/kg thiopental sodium i.p. anesthesia, tibiae were removed from a 9-week-old rat by sterile surgical technique, as previously described (Charoenphandhu et al., 2008; Wongdee et al., 2008). After the connective tissues and marrow cells were removed, bones were cut into small dice, and cultured in a 25-cm^2 T-flask (Corning, NY, USA) with DMEM supplemented with 15% fetal bovine serum, 100 U/mL penicillin-streptomycin, and 100 μg/mL ascorbate-2-phosphate (Sigma). Cells were incubated at 37 °C with 5% CO_2. Osteoblasts proliferated and migrated from the bone dice into culture medium within 3 days. The medium was changed every 3 days. Six flasks of confluent cells from the same rat were pooled together for total RNA preparation. Five rats ($n=5$) were used in PCR studies.

Total RNA preparation and PCR

The total RNA samples were prepared from primary osteoblasts by using TRIzol reagent (Invitrogen, Carlsbad, CA, USA). Total RNA was then treated with RQ1 RNase-free DNase (Promega, Madison, WI, USA) and subsequently purified by RNeasy mini kit (Qiagen, Valencia, CA, USA) according to the manufacturer's instructions. Purity of the total RNA was determined by the ratio of absorbance readings at 260 and 280 nm, the ratio of which was in the range of 1.8–2.0. One microgram of total RNA was reverse-transcribed with iScript cDNA Synthesis kit (Bio-Rad, Hercules, CA, USA) to cDNA by a Bio-Rad MyCycler. Rat glyceraldehyde-3-phosphate dehydrogenase (GAPDH) served as a control gene to check the consistency of the reverse transcription. Primers used in the PCR studies are shown in Table 1. Conventional PCR was performed with GoTaq Green Master Mix (Promega) and Bio-Rad MyCycler. PCR products were collected at 36 cycles and visualized on 2% agarose gel stained with 1 μg/mL ethidium bromide (Sigma) under UV transilluminator (Alpha Innotech, San Leandro, USA). The important steps, including PCR amplification, cycle optimization and electrophoresis were performed in triplicate.

Bone preparation

As previously described by Wongdee et al. (2008), tibiae from normal and CMA rats were dissected, washed with 0.9% w/v NaCl and fixed at 4 °C overnight in 4% paraformaldehyde in 0.1 M phosphate buffered saline (PBS). Thereafter, they were washed with cold PBS pH 7.4 and decalcified in 20% w/v ethylenediaminetetraacetic acid (EDTA; Sigma) at 4 °C for 3 weeks. Decalcifying solution was replaced every 3 days. The success of decalcification was confirmed by dual-energy X-ray absorptiometry (model Lunar PIXImus2; GE Medical Systems, Madison, WI, USA). Finally, decalcified bones were embedded in paraffin, and cut into 7-μm sections by a microtome.

Immunohistochemistry

After deparaffinization in xylene and graded ethanol, sections were incubated at 37 °C for 30 min in antigen retrieval solution (0.01 mg/mL proteinase K, 50 mM Tris–HCl pH 7.5 and 5 mM EDTA). They were then incubated in 3% H_2O_2 for 1 h to reduce the endogenous peroxidase activity. Non-specific binding was blocked by incubating sections in 4% bovine serum albumin (BSA) in 0.1 M PBS for 2 h. After blocking, sections were incubated overnight at 4 °C with 1:200 anti-claudin-5, -11, -15, -16 (Santa Cruz Biotechnology, CA, USA), or -14 antibodies (Abcam, Cambridge, MA, USA). The sections were later washed with 0.1 M PBS, incubated for 1 h with biotinylated goat anti-rabbit antibody (Zymed, South San Francisco, CA, USA), and finally incubated for 1 h at room temperature with streptavidin-

Table 1
Rattus norvegicus oligonucleotide sequences used in the PCR experiments.

Gene	Accession no.	Primer (forward/reverse)	Product length (bp)
Claudin-5	NM_031701	5′-CGCTTGTGGCACTCTTTGT-3′ 5′-ACTCCCGGACTACGATGTTG-3′	168
Claudin-11	NM_053457	5′-ATTGGCATCATCGTCACAAC-3′ 5′-ATGTCCACCAGGGGCTTG-3′	158
Claudin-14	NM_001013429	5′-CTGTACCTGGGCTTCATC-3′ 5′-CACACATAGTCATTCAACCTG-3′	230
Claudin-15	XM_222085	5′-GCTGTGCCACCGACTCCC-3′ 5′-CAGAGCCCAGTTCATACTTG-3′	330
Claudin-16	NM_131905	5′-ATCTTCTTCAGTACGCTGCC-3′ 5′-CGATGAGTAATACGGTCCC-3′	372
GAPDH	NM_017008	5′-AGTCTACTGGCGTCTTCAC-3′ 5′-TCATATTTCTCGTGGTTCAC-3′	133

GAPDH, glyceraldehyde-3-phosphate dehydrogenase.

Please cite this article as: Wongdee, K., et al., Claudin expression in the bone-lining cells of female rats exposed to long-standing acidemia, Exp. Mol. Pathol. (2010), doi:10.1016/j.yexmp.2009.12.005

conjugated horseradish peroxidase (HRP) solution (Zymed). As for claudin-16, the donkey anti-goat HRP-IgG antibody (Santa Cruz) was used instead of biotinylated antibody/streptavidin-HRP solution. Immunohistochemical reaction was developed with a chromogenic peroxidase substrate 3,3′-diaminobenzidine (DAB; Pierce, Rockford, IL, USA). The negative control sections were obtained by incubating the sections from the control or CMA rats in the absence of primary antibody. Sections were counterstained with hematoxylin and examined under a light microscope (model BX51TRF; Olympus, Tokyo, Japan) and Image-Pro Plus 5 (Media Cybernetics, Bethesda, MD, USA).

Measurement of signal intensity

Densitometric determination of immunohistochemical signals was modified from the method of Lehr et al. (1999). Selection of DAB-positive signals (brownish color) was performed with Adobe Photoshop 9 (Adobe System, San Jose, CA, USA) by filtering the specific color shade (in red-green-blue [RGB] mode) and color intensity in the regions of interest (ROI). The RGB color range was red = 142, green = 103 and blue = 65, and the fuzziness value was adjusted to 75%. All pixels with DAB-positive color on the ROI were automatically highlighted by the software. Pixel counting was performed by the Histogram command, which showed the numbers of the total and DAB-positive pixels in the ROI. Relative signal intensity was normalized to the negative control signals (i.e., signals from the negative control sections). The relative signal intensity was calculated as followed,

$$\text{Relative intensity} = (\text{Positive pixels}/\text{Total pixels})_{\text{Age-matched control or CMA}} / (\text{Positive pixels}/\text{Total pixels})_{\text{Negative control}}$$

Statistical analysis

The results are expressed as means ± SE. Comparisons between CMA and control groups were determined by unpaired Student's *t*-test. The level of significance for all statistical tests was $p<0.05$. Data were analyzed by GraphPad Prism 5.0 for Windows (GraphPad Software, San Diego, CA, USA).

Results

CMA was induced by continuous acid-loading with 1.5% NH_4Cl given in drinking water for 21 days. Plasma pH of CMA rats was significantly lower than that of control rats, i.e., 7.27 ± 0.02 ($n=4$) vs. 7.37 ± 0.04 ($n=6$, $p<0.05$), respectively, with a decrease in plasma HCO_3^- concentration. Daily water intake was not less than 60 mL/day, suggesting that consumption of NH_4Cl-containing water in CMA rats was sufficient to induce sustained acidemia throughout the experimental period. The present blood gas profile represented a normal metabolic response to CMA, consistent with that reported previously by Charoenphandhu et al. (2007).

Prior to immunohistochemical localization of claudins, PCR experiments were performed to demonstrate that primary osteoblasts derived from the tibiae of adult female rats expressed claudins. As shown in Fig. 1, primary rat osteoblasts strongly expressed claudin-5, -11, -14, -15 and -16 transcripts. Immunohistochemical analysis in tibial sections also confirmed that claudin-5, -11, -14, -15 and -16 proteins were expressed in the bone-lining cells (inactive or flat osteoblasts), but not in osteocytes or marrow cells (Figs. 2A–J). Morphology and localization of the present bone-lining cells were consistent with those described previously (Weinger and Holtrop, 1974). After exposure to long-standing acidemia, bone-lining cells upregulated claudin-14 expression by 1.62-fold, while downregulating expression of claudin-15 and -16 by 2.87- and 6.15-fold, respectively (Figs. 2 and 3). However, the expressions of claudin-5 and -11 were not changed by CMA (Figs. 2 and 3).

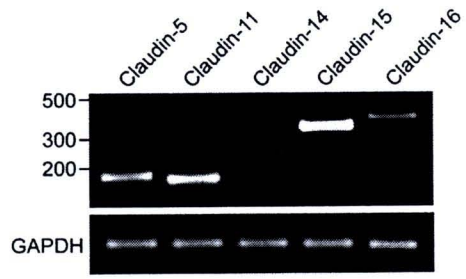

Fig. 1. Representative electrophoretic bands of claudin-5, -11, -14, -15 and -16 in primary rat osteoblasts ($n=5$). Expression of GAPDH, a housekeeping gene, is presented along with the studied genes. Numbers on the left indicate the base pairs of PCR products.

Discussion

During CMA, a number of compensatory responses are initiated to alleviate acidemia and negative calcium balance, e.g., increased intestinal calcium and phosphate absorption, and enhanced renal H^+ excretion and HCO_3^- reabsorption (Rose and Post, 2001). Bone also participates in the neutralization of H^+ by liberating calcium and other minerals, e.g., sodium, potassium, carbonate and phosphate, from BECF across bone membrane into the plasma (Bergstrom and Wallace, 1954; Bushinsky et al., 2003; Green and Kleeman, 1991; Rose and Post, 2001), leading to reduced bone mineral content. This compartmentalization (i.e., BECF and plasma) is achieved by a layer of bone-lining cells (Parfitt 1989; Soares et al., 1992). In addition, CMA also induced more calcium efflux from bone by enhancing the osteoclast-mediated bone resorption (Assapun et al., 2009). However, recent evidence showed that prolonged exposure to CMA appeared to induce a compensatory response in bone to restrict bone loss (Assapun et al., 2009). Specifically, a marked decrease in bone mass was observed only in the early phase of CMA. Thereafter, the rate of bone loss was gradually decreased (Assapun et al., 2009). Nevertheless, the exact mechanism responsible for this observation was unknown. It has been suggested that calcium efflux from BECF to plasma occurred through the paracellular pathway (Marenzana et al., 2005), perhaps across the tight junction formed by osteoblasts and bone-lining cells (Soares et al., 1992; Weinger and Holtrop, 1974). Since the paracellular ion transport in normal epithelia could be regulated and restricted by certain tight junction proteins of the claudin family (Anderson and Van Itallie, 2009), the CMA-induced changes in claudin expression in bone-lining cells might be a part of the adaptive response of bone to minimize mineral loss. Indeed, the possibility of the CMA-induced upregulation of claudin expression in epithelial cells is not totally without suggestive evidence. Recently, 21-day CMA was found to increase the expression of claudin-2, -3, -6, -8, -11, -12, -14, -19 and -22 in the duodenal epithelial cells, which presumably contributed to the CMA-induced increase in the intestinal calcium absorption (Charoenphandhu et al., 2006 and 2007).

In the present study, we found that expression of claudin-14 was upregulated, while that of claudin-15 and -16 was downregulated in the bone-lining cells. The expression patterns of claudins generally vary among different epithelia or epithelial-like structure, i.e., they are the "fingerprint" of the epithelia. Most claudins increase the tightness of tight junction and create a barrier to restrict the paracellular ion transport (e.g., claudin-5, -11 and -14), whereas some claudins possess the ion-permeable property (e.g., claudin-15 and -16), which were essential in the formation of paracellular pores to facilitate ion movement (Tsukita et al., 2001; Anderson and Van Itallie, 2009).

Please cite this article as: Wongdee, K., et al., Claudin expression in the bone-lining cells of female rats exposed to long-standing acidemia, Exp. Mol. Pathol. (2010), doi:10.1016/j.yexmp.2009.12.005

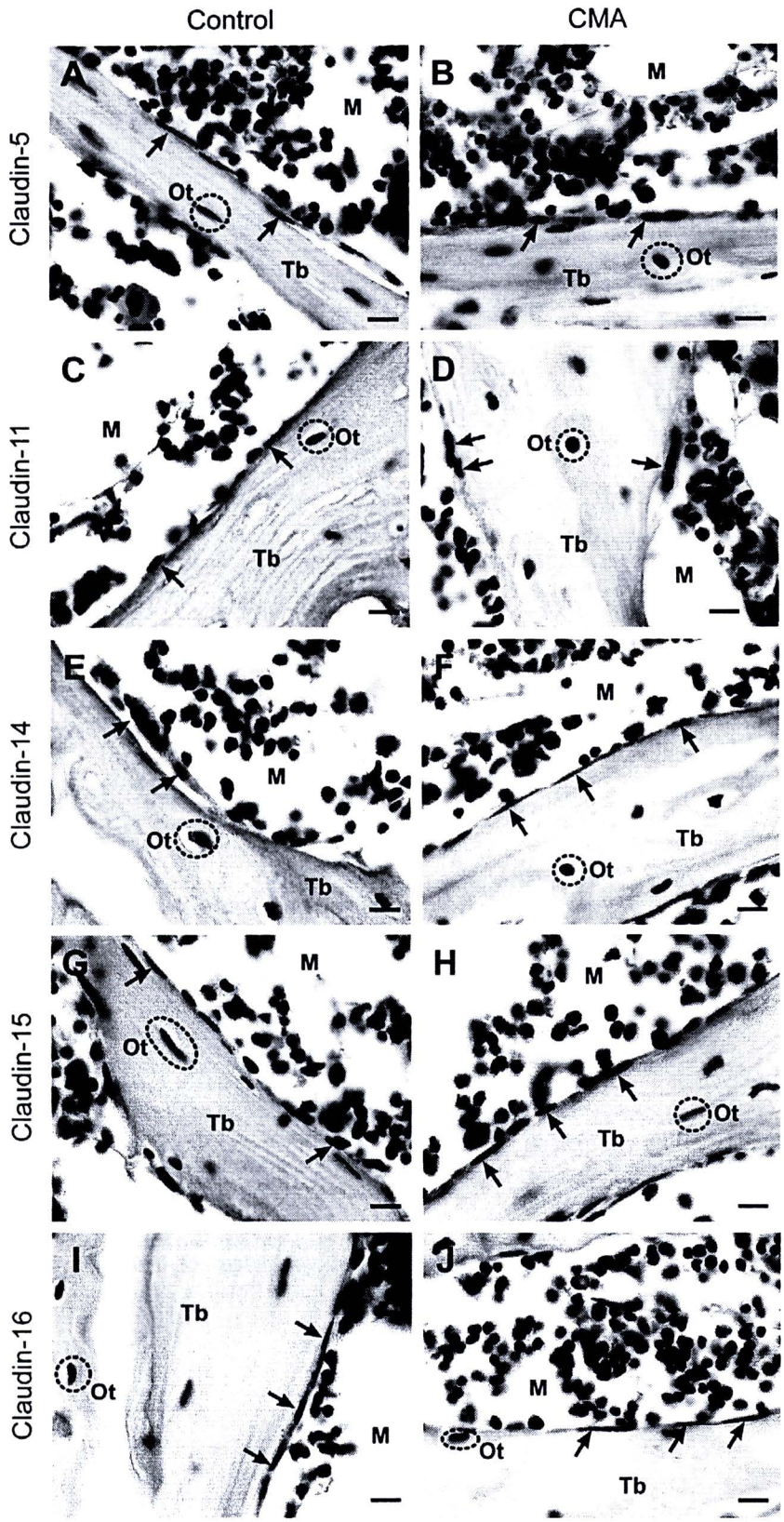

Fig. 2. (A–J) Immunohistochemical localization of claudin-5, -11, -14, -15 and -16 in paraffin-embedded decalcified tibial sections from control and CMA rats. The positive signals of claudins were seen in bone-lining cells (inactive osteoblasts; arrows), which covered bone trabeculae (Tb). No signal was detected in osteocytes (Ot) or bone marrow (M). Bars, 10 μm.

For instance, claudin-5 is expressed in endothelial cells for the maintenance of blood-brain barrier to protect the brain from circulating neurotoxic substances (Nitta et al., 2003). Similarly, claudin-11 is expressed in sertoli cells in the testis and forms the blood-testis barrier to prevent autoimmune responses against differentiated germ cells (Furuse and Tsukita, 2006). Nevertheless,

Please cite this article as: Wongdee, K., et al., Claudin expression in the bone-lining cells of female rats exposed to long-standing acidemia, Exp. Mol. Pathol. (2010), doi:10.1016/j.yexmp.2009.12.005

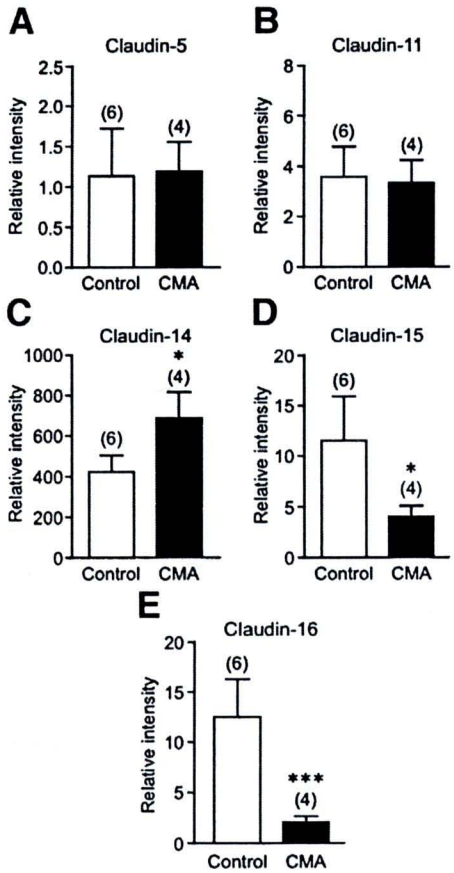

Fig. 3. (A–E) Relative signal intensity (arbitrary unit) of the expression of claudin-5, -11, -14, -15, and -16 in paraffin-embedded decalcified tibial sections from control and CMA rats. The intensities of the negative control sections were normalized to 1. Numbers in parentheses represent the number of animals in each group. $*p<0.05$, and $***p<0.001$ compared with its respective control group.

expressions of claudin-5 and -11 in bone-lining cells were not changed by CMA.

Similar to claudin-5 and -11, claudin-14 also shows an ion-restrictive property. Under normal conditions, claudin-14 is expressed in several epithelia, e.g., the outer hair cells of the inner ear and intestinal epithelium of rodents (Ben-Yosef et al., 2003; Holmes et al., 2006; Charoenphandhu et al., 2007). In humans, mutations of claudin-14 may lead to deafness because its presence is essential for the maintenance of proper ion compositions of the endolymph and perilymph for sound transduction (Ben-Yosef et al., 2003). Overexpression of claudin-14 in Madin–Darby canine kidney-II monolayer led to an increase in the transepithelial resistance and a decrease in the paracellular cation permeability (Ben-Yosef et al., 2003). It was thus possible that upregulation of claudin-14 in bone-lining cells may enhance barrier function of the bone membrane to restrict mineral efflux from bone.

In contrast to claudin-14, claudin-15 and -16 have ion-permeable property, and can form the paracellular pores for cation transport (Van Itallie et al., 2003). Claudin-15 knockout mice manifested an enlargement of the proximal small intestine by ~2-fold with a decrease in the transepithelial ionic conductance (Tamura et al., 2008). Knockdown of claudin-15 also reduced cation permeability in the intestine-like Caco-2 monolayer (Charoenphandhu et al., 2009). Similarly, claudin-16 is involved in the regulation of the paracellular cation transport, especially calcium and magnesium reabsorption in the thick ascending limb of the loop of Henle (Simon et al., 1999). A strong evidence for the significance of claudin-16 is from its mutation that leads to a lethal inherited disease called familial hypomagnesemia with hypercalciuria and nephrocalcinosis. Since claudin-15 and -16 normally enhance the paracellular cation transport, downregulation of both claudins in the present study suggested that mineral efflux across the bone membrane was reduced.

In conclusion, the bone-lining cells responded to CMA by upregulating claudin-14 and downregulating claudin-15 and -16, which could partially explain the previous *in vivo* findings that, in prolonged exposure to CMA, further bone loss was prevented, and bone mineral content was maintained at a subnormal level thereafter (Assapun et al., 2009). However, future investigation is required to demonstrate the molecular mechanisms of the CMA-induced changes in claudin expression in bone-lining cells in relation with changes in the rate of mineral efflux across the bone membrane in CMA rats.

Conflict of interest statement

The authors declare no conflict of interest.

Acknowledgments

We thank Kukiat Tudpor and Jirawan Thongbunchoo for the excellent technical assistance. This research was supported by grants from the Strategic Consortia for Capacity Building of University Faculties and Staff, Commission on Higher Education, Thailand (to K.W.), and the Thailand Research Fund (to N.C. and N.K.).

References

Anderson, J.M., Van Itallie, C.M., 2009. Physiology and function of the tight junction. Cold Spring Harb. Perspect. Biol. 1 doi:10.1101/cshperspect.a002584.

Assapun, J., Charoenphandhu, N., Krishnamra, N., 2009. Early acceleration phase and late stationary phase of remodeling imbalance in long bones of male rats exposed to long-standing acidemia: a 10-month longitudinal study using bone histomorphometry. Calcif. Tissue Int. 85, 1–9.

Ben-Yosef, T., Belyantseva, I.A., Saunders, T.L., Hughes, E.D., Kawamoto, K., Van Itallie, C.M., Beyer, L.A., Halsey, K., Gardner, D.J., Wilcox, E.R., Rasmussen, J., Anderson, J.M., Dolan, D.F., Forge, A., Raphael, Y., Camper, S.A., Friedman, T.B., 2003. Claudin 14 knockout mice, a model for autosomal recessive deafness *DFNB29*, are deaf due to cochlear hair cell degeneration. Hum. Mol. Genet. 12, 2049–2061.

Bergstrom, W.H., Wallace, W.M., 1954. Bone as sodium and potassium reservoir. J. Clin. Invest. 33, 867–873.

Bushinsky, D.A., 2001. Acid–base imbalance and the skeleton. Eur. J. Nutr. 40, 238–244.

Bushinsky, D.A., Lechleider, R.J., 1987. Mechanism of proton-induced bone calcium release: calcium carbonate dissolution. Am. J. Physiol. Renal Physiol. 253, F998–F1005.

Bushinsky, D.A., Frick, K.K., 2000. The effects of acid on bone. Curr. Opin. Nephrol. Hypertens. 9, 369–379.

Bushinsky, D.A., Chabala, J.M., Levi-Setti, R., 1989. Ion microprobe analysis of mouse calvariae *in vitro*: evidence for a "bone membrane". Am. J. Physiol. Endocrinol. Metab. 256, E152–E158.

Bushinsky, D.A., Smith, S.B., Gavrilov, K.L., Gavrilov, L.F., Li, J., Levi-Setti, R., 2003. Chronic acidosis-induced alteration in bone bicarbonate and phosphate. Am. J. Physiol. Renal Physiol. 285, F532–F539.

Charoenphandhu, N., Tudpor, K., Pulsook, N., Krishnamra, N., 2006. Chronic metabolic acidosis stimulated transcellular and solvent drag-induced calcium transport in the duodenum of female rats. Am. J. Physiol. Gastrointest. Liver Physiol. 291, G446–G455.

Charoenphandhu, N., Wongdee, K., Tudpor, K., Pandaranandaka, J., Krishnamra, N., 2007. Chronic metabolic acidosis upregulated claudin mRNA expression in the duodenal enterocytes of female rats. Life Sci. 80, 1729–1737.

Charoenphandhu, N., Teerapornpuntakit, J., Methawasin, M., Wongdee, K., Thongchote, K., Krishnamra, N., 2008. Prolactin decreases expression of Runx2, osteoprotegerin, and RANKL in primary osteoblasts derived from tibiae of adult female rats. Can. J. Physiol. Pharmacol. 86, 240–248.

Charoenphandhu, N., Nakkrasae, L., Kraidith, K., Teerapornpuntakit, J., Thongchote, K., Thongon, N., Krishnamra, N., 2009. Two-step stimulation of intestinal Ca^{2+} absorption during lactation by long-term prolactin exposure and suckling-induced prolactin surge. Am. J. Physiol. Endocrinol. Metab. 297, E609–E619.

Dominguez, J.H., Raisz, L.G., 1979. Effects of changing hydrogen ion, carbonic acid, and bicarbonate concentrations on bone resorption *in vitro*. Calcif. Tissue Int. 29, 7–13.

Furuse, M., Tsukita, S., 2006. Claudins in occluding junctions of humans and flies. Trends Cell Biol. 16, 181–188.

Gow, A., Southwood, C.M., Li, J.S., Pariali, M., Riordan, G.P., Brodie, S.E., Danias, J., Bronstein, J.M., Kachar, B., Lazzarini, R.A., 1999. CNS myelin and sertoli cell tight junction strands are absent in *Osp/claudin-11* null mice. Cell 99, 649–659.

Green, J., Kleeman, C.R., 1991. Role of bone in regulation of systemic acid–base balance. Kidney Int. 39, 9–26.

Hatakeyama, N., Kojima, T., Iba, K., Murata, M., Thi, M.M., Spray, D.C., Osanai, M., Chiba, H., Ishiai, S., Yamashita, T., Sawada, N., 2008. IGF-1 regulates tight-junction protein

claudin-1 during differentiation of osteoblast-like MC3T3-E1 cells via a MAP-kinase pathway. Cell Tissue Res. 334, 243–254.

Holmes, J.L., Van Itallie, C.M., Rasmussen, J.E., Anderson, J.M., 2006. Claudin profiling in the mouse during postnatal intestinal development and along the gastrointestinal tract reveals complex expression patterns. Gene Expr. Patterns 6, 581–588.

Kraut, J.A., Mishler, D.R., Singer, F.R., Goodman, W.G., 1986. The effects of metabolic acidosis on bone formation and bone resorption in the rat. Kidney Int. 30, 694–700.

Krieger, N.S., Sessler, N.E., Bushinsky, D.A., 1992. Acidosis inhibits osteoblastic and stimulates osteoclastic activity *in vitro*. Am. J. Physiol. Renal Physiol. 262, F442–F448.

Lehr, H.A., van der Loos, C.M., Teeling, P., Gown, A.M., 1999. Complete chromogen separation and analysis in double immunohistochemical stains using Photoshop-based image analysis. J. Histochem. Cytochem. 47, 119–126.

Marenzana, M., Shipley, A.M., Squitiero, P., Kunkel, J.G., Rubinacci, A., 2005. Bone as an ion exchange organ: evidence for instantaneous cell-dependent calcium efflux from bone not due to resorption. Bone 37, 545–554.

Nitta, T., Hata, M., Gotoh, S., Seo, Y., Sasaki, H., Hashimoto, N., Furuse, M., Tsukita, S., 2003. Size-selective loosening of the blood–brain barrier in claudin-5-deficient mice. J. Cell Biol. 161, 653–660.

Parfitt, A.M., 1989. Plasma calcium control at quiescent bone surfaces: a new approach to the homeostatic function of bone lining cells. Bone 10, 87–88.

Prêle, C.M., Horton, M.A., Caterina, P., Stenbeck, G., 2003. Identification of the molecular mechanisms contributing to polarized trafficking in osteoblasts. Exp. Cell Res. 282, 24–34.

Rose, B.D., Post, T.W., 2001. Metabolic acidosis, In: Rose, B.D., Post, T.W. (Eds.), Clinical physiology of acid-base and electrolyte disorders, 5th ed. McGraw-Hill, Singapore, pp. 578–646.

Rubinacci, A., Benelli, F.D., Borgo, E., Villa, I., 2000. Bone as an ion exchange system: evidence for a pump-leak mechanism devoted to the maintenance of high bone K^+. Am. J. Physiol. Endocrinol. Metab. 278, E15–E24.

Simon, D.B., Lu, Y., Choate, K.A., Velazquez, H., Al-Sabban, E., Praga, M., Casari, G., Bettinelli, A., Colussi, G., Rodriguez-Soriano, J., McCredie, D., Milford, D., Sanjad, S., Lifton, R.P., 1999. Paracellin-1, a renal tight junction protein required for paracellular Mg^{2+} resorption. Science 285, 103–106.

Soares, A.M., Arana-Chavez, V.E., Reid, A.R., Katchburian, E., 1992. Lanthanum tracer and freeze-fracture studies suggest that compartmentalisation of early bone matrix may be related to initial mineralisation. J. Anat. 181, 345–356.

Tamura, A., Kitano, Y., Hata, M., Katsuno, T., Moriwaki, K., Sasaki, H., Hayashi, H., Suzuki, Y., Noda, T., Furuse, M., Tsukita, S., Tsukita, S., 2008. Megaintestine in claudin-15-deficient mice. Gastroenterology 134, 523–534.

Trumbore, D.C., Heideger, W.J., Beach, K.W., 1980. Electrical potential difference across bone membrane. Calcif. Tissue Int. 32, 159–168.

Tsukita, S., Furuse, M., Itoh, M., 2001. Multifunctional strands in tight junctions. Nat. Rev. Mol. Cell Biol. 2, 285–293.

Van Itallie, C.M., Anderson, J.M., 2006. Claudins and epithelial paracellular transport. Annu. Rev. Physiol. 68, 403–429.

Van Itallie, C.M., Fanning, A.S., Anderson, J.M., 2003. Reversal of charge selectivity in cation or anion-selective epithelial lines by expression of different claudins. Am. J. Physiol. Renal Physiol. 285, F1078–F1084.

Weinger, J.M., Holtrop, M.E., 1974. An ultrastructural study of bone cells: the occurrence of microtubules, microfilaments and tight junctions. Calcif. Tissue Res. 14, 15–29.

Wongdee, K., Pandaranandaka, J., Teerapornpuntakit, J., Tudpor, K., Thongbunchoo, J., Thongon, N., Jantarajit, W., Krishnamra, N., Charoenphandhu, N., 2008. Osteoblasts express claudins and tight junction-associated proteins. Histochem. Cell Biol. 130, 79–90.

Please cite this article as: Wongdee, K., et al., Claudin expression in the bone-lining cells of female rats exposed to long-standing acidemia, Exp. Mol. Pathol. (2010), doi:10.1016/j.yexmp.2009.12.005

J Physiol Sci (2010) 60:9–17
DOI 10.1007/s12576-009-0068-0

ORIGINAL PAPER

Transepithelial calcium transport in prolactin-exposed intestine-like Caco-2 monolayer after combinatorial knockdown of TRPV5, TRPV6 and $Ca_v1.3$

La-iad Nakkrasae · Narongrit Thongon · Jirawan Thongbunchoo · Nateetip Krishnamra · Narattaphol Charoenphandhu

Received: 13 August 2009 / Accepted: 7 October 2009 / Published online: 3 November 2009

Abstract The milk-producing hormone prolactin (PRL) increases the transcellular intestinal calcium absorption by enhancing apical calcium uptake through voltage-dependent L-type calcium channel (Ca_v) 1.3. However, the redundancy of apical calcium channels raised the possibility that $Ca_v1.3$ may operate with other channels, especially transient receptor potential vanilloid family calcium channels (TRPV) 5 or 6, in an interdependent manner. Herein, TRPV5 knockdown (KD), TRPV5/TRPV6, TRPV5/$Ca_v1.3$, and TRPV6/$Ca_v1.3$ double KD, and TRPV5/TRPV6/$Ca_v1.3$ triple KD Caco-2 monolayers were generated by transfecting cells with small interfering RNAs (siRNA). siRNAs downregulated only the target mRNAs, and did not induce compensatory upregulation of the remaining channels. After exposure to 600 ng/mL PRL, the transcellular calcium transport was increased by ~2-fold in scrambled siRNA-treated, TRPV5 KD and TRPV5/TRPV6 KD monolayers, but not in TRPV5/$Ca_v1.3$, TRPV6/$Ca_v1.3$ and TRPV5/TRPV6/$Ca_v1.3$ KD monolayers. The results suggested that $Ca_v1.3$ was the sole apical channel responsible for the PRL-stimulated transcellular calcium transport in intestine-like Caco-2 monolayer.

Keywords Calcium absorption · Small interfering RNA (siRNA) · Transcellular transport · Triple knockdown · Voltage-dependent calcium channel (Ca_v)

L. Nakkrasae · N. Thongon · J. Thongbunchoo · N. Krishnamra · N. Charoenphandhu
Consortium for Calcium and Bone Research (COCAB), Faculty of Science, Mahidol University, Bangkok, Thailand

L. Nakkrasae
Department of Biology, Faculty of Science, Khon Kaen University, Khon Kaen, Thailand

N. Thongon
Department of Medical Science, Faculty of Science, Burapha University, Chonburi, Thailand

N. Krishnamra · N. Charoenphandhu (✉)
Department of Physiology, Faculty of Science, Mahidol University, Rama VI Road, Bangkok 10400, Thailand
e-mail: naratt@narattsys.com

Introduction

Prolactin (PRL) has been shown to be a calcium-regulating hormone since it could stimulate transcellular calcium absorption in intestinal epithelium of rats as well as in intestine-like Caco-2 monolayers [1–4]. Transcellular calcium transport is crucial during high calcium demand, such as pregnancy, lactation, or inadequate calcium intake [5]. It is a three-step process consisting of (1) apical calcium entry via transient receptor potential vanilloid Ca^{2+} channels (TRPV) 5, TRPV6 and voltage-dependent L-type calcium channel (Ca_v) 1.3, (2) cytoplasmic diffusion in a calbindin-D_{9k}-bound form, and (3) basolateral extrusion via plasma membrane Ca^{2+}-ATPase (PMCA) and Na^+/Ca^{2+} exchanger (NCX) [6–9]. In general, $Ca_v1.3$ mediates intestinal calcium absorption under certain conditions, e.g., in the presence of depolarization state induced by glucose absorption [7, 8].

Recently, PRL was found to rapidly enhance transcellular calcium absorption in a non-genomic manner via $Ca_v1.3$, but not TRPV6 [9]. Pituitary-grafted rats with hyperprolactinemia also exhibited upregulation of L-type calcium channels [10]. However, the redundancy of apical calcium channels raised the possibility that the PRL-stimulated transcellular calcium transport may still require the presence of TRPV5 and/or TRPV6. Alternatively, one channel may be upregulated to compensate for the absence of the others. For example, TRPV5 knockout mice with

hypercalciuria responded to negative calcium balance by upregulating TRPV6 expression in the small intestine to increase calcium absorption [11]. Indeed, it was not known whether calcium entry through TRPV5 contributed to the PRL-stimulated calcium flux in the intestine. Since TRPV5 and TRPV6, known to share 75% homology at the amino acid level and exhibit a similar ion permeation sequence for divalent cations ($Ca^{2+} > Sr^{2+} \approx Ba^{2+} > Mn^{2+}$), were co-expressed in the intestinal epithelial cells [12, 13], it was necessary to investigate the participation of TRPV5 in the PRL-stimulated calcium transport. Furthermore, whether $Ca_v1.3$ is the sole calcium channel required for PRL action was still not known.

Therefore, the objectives of the present study were (1) to examine the involvement of TRPV5 in the PRL-stimulated calcium absorption in intestinal epithelial monolayer, (2) to investigate whether an absence of one calcium channel led to upregulation of the others, and (3) to provide evidence that $Ca_v1.3$ was the sole calcium channel which mediated the PRL-stimulated calcium transport. Human colorectal adenocarcinoma cell line, Caco-2 cells, were used in the present study as they are easy to manipulate genetically. Despite being derived from the colon and having relatively low basal calcium flux compared to the small intestine [14], confluent Caco-2 monolayer has been widely used in the studies of drugs or hormones that enhance calcium absorption since it possesses characteristics of the small intestine, including the presence of the brush border, expression of sucrase-isomaltase enzymes, and expression of the transcellular calcium transporters [15–17]. Moreover, Caco-2 monolayer also expresses functional PRL receptors and responds well to PRL by increasing transcellular calcium flux by ~2-fold, similar to that observed in the rat duodenum [14].

Materials and methods

Cell culture

Caco-2 cells (ATCC No. HTB-37) were grown in Dulbecco's modified Eagle medium (DMEM; Sigma, St. Louis, MO, USA) supplemented with 15% fetal bovine serum (FBS; Gibco, Grand Island, NY, USA), 1% L-glutamine (Gibco), 1% non-essential amino acid (Sigma), 100 U/mL penicillin/streptomycin (Sigma), and 0.25 μL/mL amphotericin B (Sigma). Cells were later propagated in 25-cm^2 T-flask (Corning, NY, USA) under a humidified atmosphere containing 5% CO_2 at 37°C, and subcultured as described in the ATCC protocol. Confluent Caco-2 monolayers were prepared by seeding cells (5.0×10^5 cells/cm^2) on a polyester Snapwell with 12 mm diameter and 0.4 μm pore size (Corning). Culture medium was changed daily after 48 h of seeding.

Small interfering RNA transfection

Small interfering RNA oligonucleotides targeted for human TRPV5, TRPV6, and $Ca_v1.3$ as well as scrambled sequences were designed by siRNA Target Designer (version 1.51; Promega, Madison, WI, USA), as shown in Table 1. All oligonucleotides were synthesized by T7 RiboMax Express RNAi System (Promega) according to the manufacturer's instruction. At day 12 after seeding of Caco-2 cells on a Snapwell, in vitro transfection was performed with 10 μg/mL polyethyleneimine (PEI) and 1 μmol/mL siRNA molecules to generate TRPV5 knockdown (KD), TRPV5/TRPV6, TRPV5/$Ca_v1.3$, TRPV6/$Ca_v1.3$ double KD, and TRPV5/TRPV6/$Ca_v1.3$ triple KD monolayers. At day 14 (i.e., 48 h after transfection), the Snapwell was mounted in an Ussing chamber with an exposed surface area of 1.13 cm^2 to measure the electrical parameters and calcium fluxes, as previously described [18]. Efficiency of siRNA was evaluated by quantitative real-time PCR (qRT-PCR). Recent investigations showed that conventional siRNA KD successfully abolished the functions of TRPV5 and TRPV6 channels, as determined by patch-clamp technique [19, 20]. This KD protocol was approved by the Institutional Biosafety Committee of the Mahidol University.

Quantitative real-time PCR and sequencing

Expression levels of TRPV5, TRPV6 and $Ca_v1.3$ were quantified by a real-time PCR (model MiniOpticon; Bio-Rad) as described previously [9]. Glyceraldehyde-3-phosphate dehydrogenase (GAPDH), a housekeeping gene, served as a control for normalization. Sense and antisense primers used for qRT-PCR are presented in Table 2. PCR reaction was performed with iQ SYBR Green SuperMix (Bio-Rad). Relative expression of TRPV5, TRPV6 or $Ca_v1.3$ over GAPDH was calculated from the threshold

Table 1 siRNA oligonucleotides used in KD study

Targets	siRNA oligonucleotides
TRPV5 siRNA	5′-GGCACUUGAAUCUUGGACU-3′
	5′-AAAGUCCAAGAUUCAAGUGCC-3′
TRPV6 siRNA	5′-GGGAAACACAGUGUUACAC-3′
	5′-GTGUAACACUGUGUUUCCC-3′
$Ca_v1.3$ siRNA	5′-GAGCACCUUUGACAAUUUC-3′
	5′-AAGAAAUUGUCAAAGGTGCUC-3′
Scramble siRNA	5′-GGCGCAAUAAAGCAAGACC-3′
	5′-AAGGUCUUGCUUUAUUGCCC-3′

TRPV5/6 Transient receptor potential vanilloid family Ca^{2+} channels 5/6, *$Ca_v1.3$* voltage-dependent L-type Ca^{2+} channel 1.3

Table 2 *Homo sapiens* oligonucleotide sequences used in the qRT-PCR experiments

Name	Accession no.	Primer (forward/reverse)	Product length (bp)
TRPV5	NM_019841	5′–CACTGTTATTGATGCACCTGC–3′	120
		5′–CCATCATGGCGATGAACA–3′	
TRPV6	AF365928	5′–TCTGACTGCGTGTTCTCAC–3′	144
		5′–ACATTCCTTGGCGTTCAT–3′	
$Ca_v1.3$	NM_000720	5′–TGATCCAAGTGGAGCAGTCA–3′	113
		5′–GTGTGAAAGTCCGGTAGGAGA–3′	
GAPDH	NM_002046	5′–CTGGTAAAGTGGATATTGTTG–3′	359
		5′–GAGGCTGTTGTCATACTTCTC–3′	

TRPV5/6 Transient receptor potential vanilloid family Ca^{2+} channels 5/6, *$Ca_v1.3$* voltage-dependent L-type Ca^{2+} channel 1.3, *GAPDH* glyceraldehyde-3-phosphate dehydrogenase

cycle (C_t) values by using $2^{\Delta Ct}$ method. Besides melting curve analysis, PCR products were also visualized on 1.5% agarose gel stained with 1.0 μg/mL ethidium bromide. After electrophoresis, PCR bands were extracted by HiYield Gel/PCR DNA Extraction kit (Real Biotech Corporation, Taipei, Taiwan), and were sequenced by ABI Prism 3100 Genetic Analyzer (Applied Biosystems, Foster City, CA, USA). qRT-PCR experiments were performed in triplicate.

Bathing solution for Ussing chamber technique

The bathing solution for Ussing chamber experiments contained (in mmol/L) 118 NaCl, 4.7 KCl, 1.1 $MgCl_2$, 1.25 $CaCl_2$, 23 $NaHCO_3$, 12 D-glucose and 2 mannitol (all purchased from Sigma). The solution was continuously gassed with humidified 5% CO_2 in 95% O_2, maintained at 37°C, pH 7.4, and had an osmolality of 290–293 mmol/kg water. Distilled water used in the present work had a resistance higher than 18.3 MΩ cm and a free ionized calcium concentration of <2.5 nmol/L.

Measurement of electrical parameters

Three electrical parameters, i.e., potential (voltage) difference (PD), short-circuit current (I_{sc}), and transepithelial resistance (TER), were determined as described previously [14]. In brief, a pair of Ag/AgCl electrodes connected to agar bridges (3.0 mol/L KCl per 4% agar) was located near each surface of the mounted Snapwell for measurement of PD. The other ends of the PD-sensing electrodes were connected to a pre-amplifier (model EVC-4000; World Precision Instruments, Sarasota, FL, USA). Another pair of Ag/AgCl electrodes connected in series to the EVC-4000 current-generating unit was placed at the end of each hemichamber to supply I_{sc}, which is external current to nullify PD. TER was calculated from Ohm's equation. Fluid resistance was automatically subtracted by the EVC-4000 system.

Calcium flux measurement

Calcium fluxes were determined by the method of Thongon et al. [9]. In brief, after a 20-min incubation in the Ussing chamber, the bathing solution was changed with a fresh one. The solution on one side contained ^{45}Ca (initial specific activity of 5 mCi/mL, final specific activity of ~450–500 mCi/mol; Amersham, Buckinghamshire, UK). Unidirectional flux of calcium ($J_{H\rightarrow C}$, nmol h^{-1} cm^{-2}) from the hot side (H) to the cold side (C) was calculated with Eqs. 1 and 2.

$$J_{H\rightarrow C} = R_{H\rightarrow C}/(S_H \times A) \quad (1)$$

$$S_H = C_H/C_T \quad (2)$$

where $R_{H\rightarrow C}$ is the rate of tracer appearance in the cold side (cpm/h), S_H the specific activity in the hot side (cpm/nmol), A the surface area of Snapwell (cm^2), C_H is a radioactivity in the hot side (cpm), and C_T is the total calcium in the hot side (nmol). ^{45}Ca radioactivity in counts per minute (cpm) was analyzed by liquid scintillation spectrophotometer (model Tri-Carb 3100; Packard, Meriden, CT, USA). Total calcium concentration in the hot side was determined by atomic absorption spectrophotometer (model SpectrAA-300; Varian Techtron, Springvale, Australia). In the absence of transepithelial calcium gradient, i.e., bathing solution in both hemichambers contained equal calcium concentration of 1.25 mmol/L, the measured calcium fluxes represented the transcellular active calcium transport [9, 14]. In some experiments, Caco-2 monolayer was exposed on the basolateral side to 600 ng/mL recombinant human PRL (rhPRL; purity >97%; catalog no. 682-PL; R&D Systems, Minneapolis, MN, USA), which is the maximal effective concentration reported by Jantarajit et al. [14].

Statistic analysis

Unless otherwise specified, results are expressed as mean ± SE. Multiple sets of data were compared by one-way analysis of variance (ANOVA) with Dunnett's

multiple comparison test. The level of significance for all statistical tests was $P < 0.05$. Data were analyzed by GraphPad Prism (version 4.0 for Mac OS X; GraphPad Software, San Diego, CA, USA).

Results

Expression of TRPV5, TRPV6 and $Ca_v1.3$ in TRPV5 KD monolayer

Since it was not known whether TRPV5 mediated the PRL-stimulated transcellular calcium transport, we generated TRPV5 KD monolayers to demonstrate the significance of TRPV5 for such PRL action. After being treated with PEI, scrambled siRNA, or TRPV5 siRNA, Caco-2 cells exhibited a stable expression of GAPDH (Fig. 1a), indicating that GAPDH could be used as a control transcript. mRNA expression of TRPV5, but not TRPV6 or $Ca_v1.3$, markedly decreased in TRPV5 KD cells by ~17-fold (Fig. 1b–e). The results suggested that TRPV5 siRNA was effective in suppressing TRPV5 expression without causing compensatory upregulation of TRPV6 and $Ca_v1.3$.

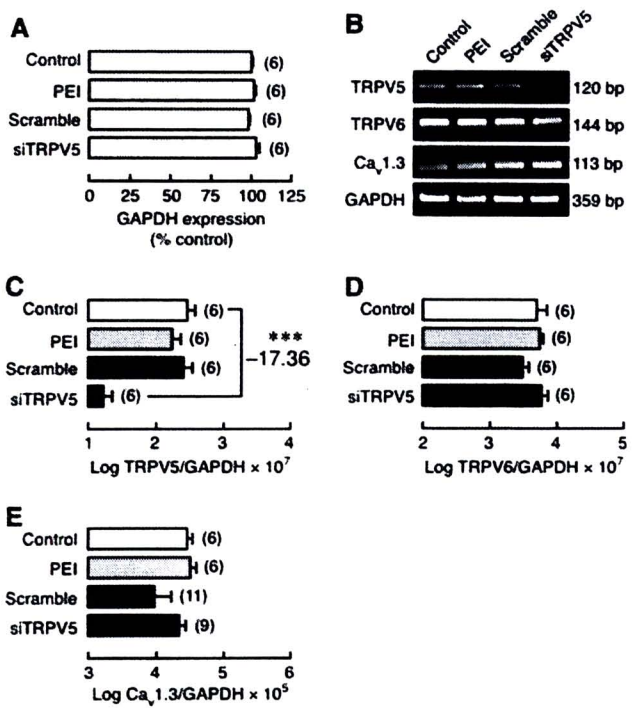

Fig. 1 **a** Expression of glyceraldehyde-3-phosphate dehydrogenase (*GAPDH*) mRNA in the control, PEI-treated, scrambled siRNA (*Scramble*)-transfected and TRPV5 siRNA (*siTRPV5*)-transfected Caco-2 monolayers. GAPDH expression of the control group was adjusted to 100%, while those of other groups were relative to the control group. **b** Representative electrophoretic bands of TRPV5, TRPV6 and $Ca_v1.3$ expression in the control, PEI, Scramble and siTRPV5 groups. **c–e** Expression of TRPV5, TRPV6 and $Ca_v1.3$ in TRPV5 KD Caco-2 monolayer as demonstrated by qRT-PCR. Expression levels were normalized by GAPDH expression. Values are presented as log mean ± SE. $***P < 0.001$ compared with the control group. Value of fold difference was also presented along with the *statistical symbol*. *Numbers* in *parentheses* represent the number of independent experiments. Each experiment was performed in triplicate

PRL-enhanced calcium transport in TRPV5 KD monolayer

After being exposed to 600 ng/mL rhPRL, both control and TRPV5 KD monolayers manifested an approximately twofold increase in the transcellular calcium transport (Fig. 2). The basal calcium transport was not affected by transfecting agent PEI, scrambled siRNA, or TRPV5 siRNA. The results, therefore, suggested that TRPV5 may not be required for the PRL-enhanced transcellular calcium transport.

Expression of TRPV5, TRPV6 and $Ca_v1.3$ in Caco-2 monolayers after combinatorial KD

To exclude the possibility that, in response to PRL, the remaining two channels were upregulated to compensate for the absence of the other channels after single KD of TRPV5, TRPV6, or $Ca_v1.3$, we generated Caco-2 monolayers with double KD of TRPV5/TRPV6, TRPV5/$Ca_v1.3$, or TRPV6/$Ca_v1.3$, or triple KD of TRPV5/TRPV6/$Ca_v1.3$. We first demonstrated that, in a control monolayer, exposure to 600 ng/mL rhPRL for 60 min did not alter TRPV5, TRPV6, and $Ca_v1.3$ expression (Fig. 3a). Moreover, GAPDH expression was stable in both double and triple

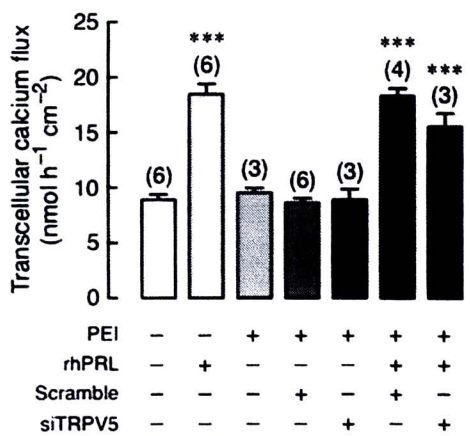

Fig. 2 Transcellular calcium transport in Caco-2 monolayer transfected with TRPV5 siRNA (*siTRPV5*) with or without 600 ng/mL rhPRL exposure. Scrambled siRNA was used as a negative control. Monolayer was bathed on both sides with 1.25 mmol/L calcium-containing solution. $***P < 0.001$ compared with the control group. *Numbers* in *parentheses* represent the number of independent experiments

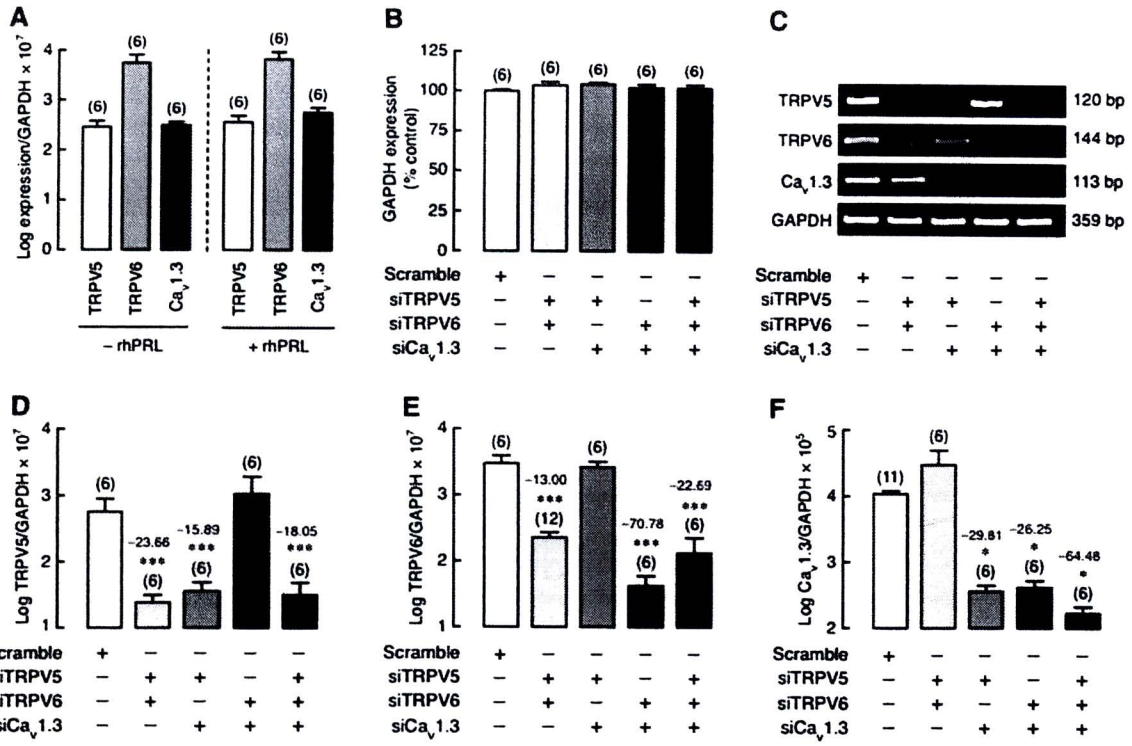

Fig. 3 **a** Expression of TRPV5, TRPV6, and $Ca_v1.3$ mRNA in Caco-2 monolayer directly exposed for 60 min to 600 ng/mL rhPRL. **b** GAPDH expression in TRPV5/TRPV6, TRPV5/$Ca_v1.3$, TRPV6/$Ca_v1.3$ double KD, and TRPV5/TRPV6/$Ca_v1.3$ triple KD monolayers. GAPDH expression in scrambled siRNA-treated group was adjusted to 100%. **c** Representative electrophoretic bands of TRPV5, TRPV6, and $Ca_v1.3$ mRNA expression in double and triple KD monolayers. **d–f** Expression of TRPV5, TRPV6, and $Ca_v1.3$ mRNA in double and triple KD Caco-2 monolayers as demonstrated by qRT-PCR. Expression levels were normalized by GAPDH expression. Data are presented as log mean ± SE. $*P < 0.05$, $***P < 0.001$ compared with the scrambled siRNA-treated group. Values of fold differences were also presented along with the *statistical symbols*. *Numbers* in *parentheses* represent the number of independent experiments. Each experiment was performed in triplicate. siTRPV5, siTRPV6, and si$Ca_v1.3$ mean siRNAs against TRPV5, TRPV6, and $Ca_v1.3$ mRNA, respectively

KD monolayers (Fig. 3b). TRPV5 mRNA expressions in TRPV5/TRPV6, TRPV5/$Ca_v1.3$, and triple KD monolayers were decreased by ~24-, ~16-, and ~18-fold, respectively, whereas no significant change was found in TRPV6/$Ca_v1.3$ KD monolayer (Fig. 3c, d). Similarly, TRPV6 and $Ca_v1.3$ mRNA expressions were downregulated only in the presence of their target siRNA molecules (Fig. 3c, e, f). These findings indicated that there was no compensatory expression of the remaining channel when mRNAs of the two channels were disrupted. In other words, the lack of expression of one channel could not be rescued by expression of the others.

PRL-enhanced calcium transport in Caco-2 monolayers after combinatorial KD of TRPV5, TRPV6 and $Ca_v1.3$

In TRPV5/TRPV6 double KD monolayer, 600 ng/mL rhPRL was able to stimulate the transcellular calcium transport, similar to that observed in the control and PEI-treated monolayers (Fig. 4). However, in TRPV5/$Ca_v1.3$, TRPV6/$Ca_v1.3$ double KD, and triple KD monolayers, the PRL-stimulated transcellular calcium transport was completely abolished (Fig. 4). Such combinatorial KD had no effect on the basal calcium transport, PD, I_{sc}, or the PRL-induced decrease in TER (Figs. 4, 5), the latter of which indirectly represented an increase in the paracellular permeability by PRL [9, 18, 21]. The results corroborated that $Ca_v1.3$ was the sole calcium channels required for the PRL-stimulated transcellular calcium transport across the intestinal epithelium.

Discussion

A significant amount of maternal calcium (~200–400 mg/day) is lost during pregnancy and lactation for fetal growth and milk production, thus resulting in severe negative calcium balance and osteopenia [22]. In lactation, PRL is not only an important hormone for lactogenesis but also for the regulation of overall calcium metabolism in pregnancy and lactation, in part, by stimulating renal calcium reabsorption and transcellular calcium absorption in the small

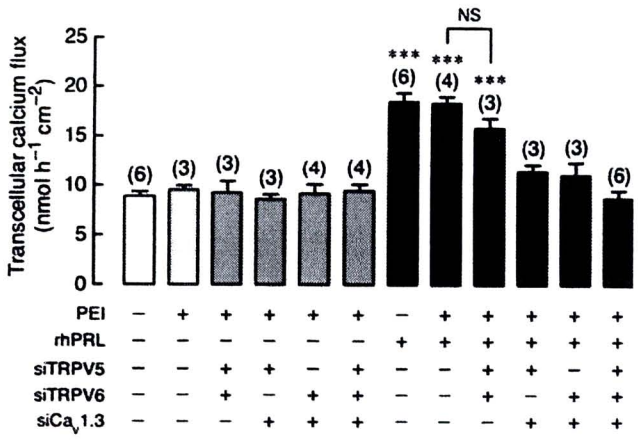

Fig. 4 Transcellular calcium transport in TRPV5/TRPV6, TRPV5/$Ca_v1.3$, TRPV6/$Ca_v1.3$ double KD, and TRPV5/TRPV6/$Ca_v1.3$ triple KD monolayers directly exposed to 600 ng/mL rhPRL. PEI was a transfecting agent. Monolayer was bathed on both sides with 1.25 mmol/L calcium-containing solution. $***P < 0.001$ compared with the scrambled siRNA-treated group (negative control). *Numbers* in *parentheses* represent the number of independent Snapwells. siTRPV5, siTRPV6, and si$Ca_v1.3$ mean siRNAs against TRPV5, TRPV6, and $Ca_v1.3$ mRNA, respectively. *NS* Not significant

intestine, thereby ameliorating stress on calcium metabolism [2, 5]. Previous investigations in duodenal epithelial cells showed that PRL enhanced the transcellular calcium transport by increasing the apical (brush-border) calcium uptake [23]. The present study further demonstrated that $Ca_v1.3$ was the sole apical calcium channel for the PRL-stimulated transcellular calcium transport in Caco-2 monolayer, which is an accepted model for calcium absorption study [9, 15].

Three calcium channels, namely TRPV5, TRPV6, and $Ca_v1.3$, were co-expressed on the apical membrane of duodenal, jejunal, and colonic epithelial cells [24, 25]. For the past decade, TRPV6 has been postulated to be the principal calcium channel for apical calcium entry in the small intestine, whereas TRPV5, with its expression being much lower than that of TRPV6 in both duodenum [26] and Caco-2 cells (Fig. 3a), was thought to play a minor role. However, physiological significance of TRPV6 became doubtful when TRPV6 null mice were found to be normocalcemic and responded to $1,25(OH)_2D_3$ by increasing transcellular calcium transport, similar to that observed in the wild-type mice [27, 28]. Moreover, Morgan and co-workers [8] suggested that TRPV5 and TRPV6 could not have been involved in the glucose-stimulated calcium absorption since both channels normally operated at negative membrane potentials below −90 mV (hyperpolarization), whereas postprandial glucose-rich luminal condition usually led to cell depolarization. Therefore, in the presence of luminal glucose, $Ca_v1.3$ must have been responsible for the intestinal calcium absorption [7, 8].

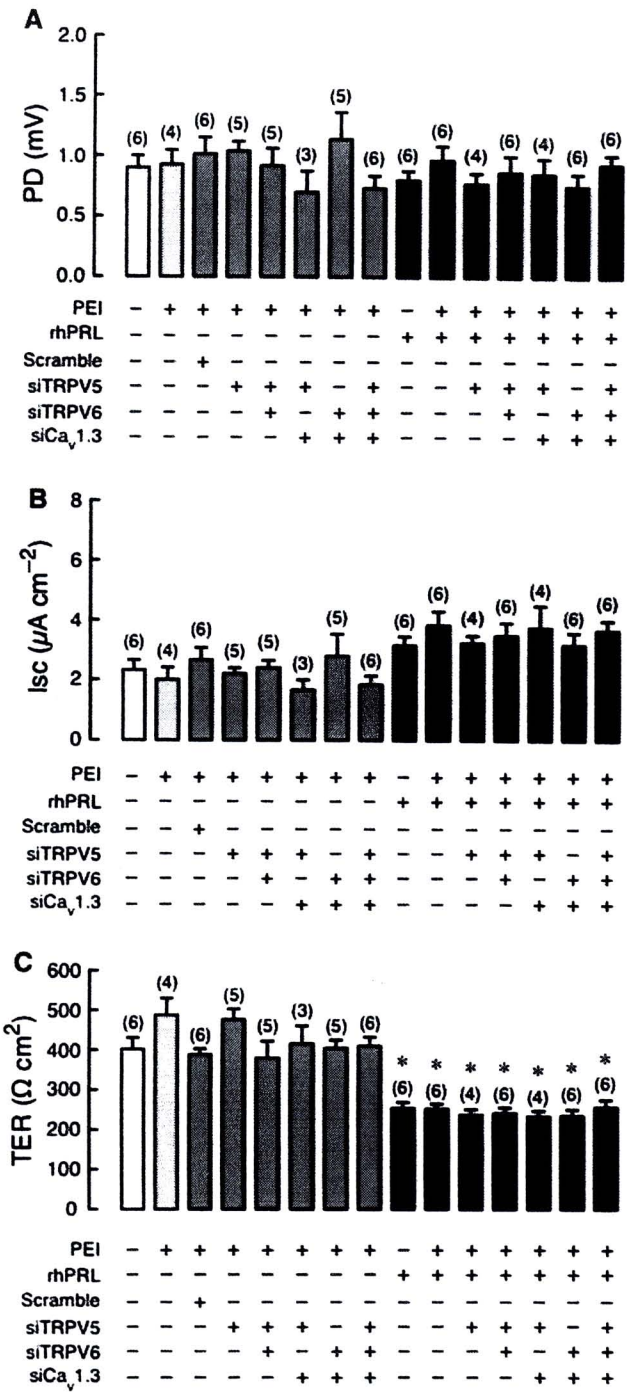

Fig. 5 **a** Transepithelial potential difference (*PD*), **b** short-circuit current (I_{sc}), and **c** transepithelial resistance (*TER*) in TRPV5 KD, TRPV5/TRPV6, TRPV5/$Ca_v1.3$, TRPV6/$Ca_v1.3$ double KD, and TRPV5/TRPV6/$Ca_v1.3$ triple KD monolayers directly exposed to 600 ng/mL rhPRL. PEI was a transfecting agent. The apical side had negative voltage with respect to the basolateral side. $*P < 0.05$ compared with the scrambled siRNA-treated group. *Numbers* in *parentheses* represent the number of independent Snapwells. siTRPV5, siTRPV6, and si$Ca_v1.3$ mean siRNAs against TRPV5, TRPV6, and $Ca_v1.3$ mRNA, respectively. The absence of changes in PRL actions in KD monolayers indicated that these calcium channels were not required for the PRL-induced increase in paracellular permeability

Nevertheless, intestinal TRPV5 and TRPV6 could be important for the enhancement of transcellular calcium transport in certain stimulating conditions, such as chronic metabolic acidosis, and long-term exposure to estrogen or $1,25(OH)_2D_3$ [26, 29–31]. Indeed, TRPV6 expression was markedly upregulated after $1,25(OH)_2D_3$ administration to vitamin D-deficient mice [32]. A number of hormones or local factors, such as parathyroid hormone, arginine vasopressin, prostaglandin E_2, and calcitonin, were also found to activate TRPV5 and/or TRPV6 by raising intracellular cAMP or cGMP levels [33]. It is possible that TRPV5, TRPV6, and $Ca_v1.3$ may differentially respond to various stimuli or extracellular environments. In other words, these channels have their own unique properties and can function independently of each other. Such a hypothesis was confirmed by the present findings that neither TRPV5 nor $Ca_v1.3$ was upregulated when TRPV6 expression was suppressed by siRNA. Nevertheless, other alternative mechanisms for apical calcium entry might exist, since TRPV5/TRPV6/$Ca_v1.3$ triple KD Caco-2 monolayer still exhibited transcellular calcium flux with a magnitude comparable to that of normal monolayer. Possible alternative pathways included the vesicular transport and voltage-dependent T-type calcium channels, the latter of which was reported to mediate the testosterone-stimulated calcium transport in renal tubular epithelium [34]. Alternatively, since siRNA-induced calcium channel KD did not totally suppress mRNA expression of target calcium channels (Fig. 3d–f), it was possible that a small number of calcium channels were sufficient to allow calcium entry under a non-stimulated condition. Feedback regulation of calcium influx could also explain the unaltered basal calcium transport after triple KD, which should lead to a decrease in the intracellular calcium concentration (Ca_i). Low Ca_i has been postulated to promote activities of TRPV5 and TRPV6 channels [35, 36], thereby leading to an increase in calcium influx.

Our previous investigation provided evidence that stimulatory effect of PRL on transepithelial calcium transport was abolished by $Ca_v1.3$ KD or L-type calcium channel blockers, nifedipine and verapamil, in the apical solution, but not in the basolateral solution [9]. $Ca_v1.3$ thus appeared to be responsible for apical calcium entry in PRL-exposed intestinal epithelium [9], but participation of TRPV5 and compensatory TRPV6 upregulation after $Ca_v1.3$ KD were still possible and were not excluded experimentally. Herein, we further elucidated that only $Ca_v1.3$ was involved in the PRL-stimulated transcellular calcium transport across the intestinal epithelium. Interdependent or interactive functions of TRPV5, TRPV6, and $Ca_v1.3$ in the presence of PRL could also be ruled out because enhanced transcellular calcium transport was still observed in TRPV5/TRPV6 double KD Caco-2 monolayer.

Molecular mechanism by which PRL stimulates intestinal calcium absorption is poorly understood. Recent studies in duodenal epithelium and Caco-2 monolayer substantiated pivotal roles of phosphoinositide 3-kinase (PI3K) and protein kinase C (PKC), especially PKC_ζ isozyme, in the intracellular PRL signaling [14]. Panspecific PKC inhibitor (GF109203X) was shown to diminish the PRL-accelerated apical calcium uptake [9]. Although $Ca_v1.3$ could be phosphorylated by several PKC isozymes, e.g., $PKC_{\beta II}$ [7], it is not known whether PRL-activated PKC directly phosphorylated $Ca_v1.3$. Since Na^+ and glucose uptake through sodium-dependent glucose transporter 1 (SGLT1) at the apical membrane is coupled with $Ca_v1.3$ opening, which requires cell depolarization induced by SGLT1-mediated Na^+ entry [8, 37], it is also possible that PRL indirectly activates $Ca_v1.3$ by acting through SGLT1, known to be expressed in Caco-2 cells [38].

Besides the transcellular calcium transport, PRL could also stimulate calcium transport across the paracellular route [5]. The observed decrease in TER by PRL in the present study confirmed an increase in paracellular permeability, which could facilitate the paracellular calcium transport [9, 18, 21]. Due to its non-saturable passive nature, paracellular calcium transport could become substantial after ingestion of calcium-rich meals, or in the presence of a transepithelial calcium gradient [6]. Moreover, the presence of PRL-induced decrease in TER in TRPV5/TRPV6/$Ca_v1.3$ KD monolayer suggested that the PRL-enhanced paracellular permeability did not involve the functions of these three calcium channels, although perijunctional cytoskeletal rearrangement, an initial step to increase paracellular permeability, may be controlled, in part, by apical calcium entry [37, 39].

In conclusion, we used siRNA-based combinatorial KD technique to elucidate that the apical calcium entry step in the PRL-stimulated transcellular calcium transport in the intestine-like Caco-2 monolayer occurred solely via $Ca_v1.3$. Although intestinal epithelial cells expressed several calcium channels, i.e., TRPV5, TRPV6, and $Ca_v1.3$, there was no redundancy in their functions, at least during PRL exposure, since the PRL-stimulated calcium transport was totally diminished after $Ca_v1.3$ siRNA transfection. The present results, therefore, provided corroborative evidence for better understanding of the cellular mechanism of PRL in intestinal epithelial cells, and could explain the mechanism by which PRL stimulated intestinal calcium absorption in pregnant and lactating animals.

Acknowledgments This research was supported by grants from the Mahidol University Postdoctoral Fellowship Program (to L. Nakkrasae), the Faculty of Science, Mahidol University (SCY52-02 and SCR52-01 to N. Charoenphandhu), the Commission on Higher Education, and the Thailand Research Fund (RSA5180001 to N. Charoenphandhu, and RTA5080008 to N. Krishnamra).

Conflict of interest statement The authors declare no conflict of interest.

References

1. Boass A, Lovdal JA, Toverud SU (1992) Pregnancy- and lactation-induced changes in active intestinal calcium transport in rats. Am J Physiol Gastrointest Liver Physiol 263:G127–G134
2. Charoenphandhu N, Nakkrasae LI, Kraidith K, Teerapornpuntakit J, Thongchote K, Thongon N, Krishnamra N (2009) Two-step stimulation of intestinal Ca^{2+} absorption during lactation by long-term prolactin exposure and suckling-induced prolactin surge. Am J Physiol Endocrinol Metab 297:E609–E619
3. Krishnamra N, Taweerathitam P (1995) Acute effect of prolactin on active calcium absorption in rats. Can J Physiol Pharmacol 73:1185–1189
4. Krishnamra N, Wirunrattanakij Y, Limlomwongse L (1998) Acute effects of prolactin on passive calcium absorption in the small intestine by in vivo perfusion technique. Can J Physiol Pharmacol 76:161–168
5. Charoenphandhu N, Krishnamra N (2007) Prolactin is an important regulator of intestinal calcium transport. Can J Physiol Pharmacol 85:569–581
6. Hoenderop JG, Nilius B, Bindels RJ (2005) Calcium absorption across epithelia. Physiol Rev 85:373–422
7. Morgan EL, Mace OJ, Affleck J, Kellett GL (2007) Apical GLUT2 and $Ca_v1.3$: regulation of rat intestinal glucose and calcium absorption. J Physiol 580:593–604
8. Morgan EL, Mace OJ, Helliwell PA, Affleck J, Kellett GL (2003) A role for $Ca_v1.3$ in rat intestinal calcium absorption. Biochem Biophys Res Commun 312:487–493
9. Thongon N, Nakkrasae LI, Thongbunchoo J, Krishnamra N, Charoenphandhu N (2009) Enhancement of calcium transport in Caco-2 monolayer through PKC_ζ-dependent $Ca_v1.3$-mediated transcellular and rectifying paracellular pathways by prolactin. Am J Physiol Cell Physiol 296:C1373–C1382
10. Charoenphandhu N, Wongdee K, Teerapornpuntakit J, Thongchote K, Krishnamra N (2008) Transcriptome responses of duodenal epithelial cells to prolactin in pituitary-grafted rats. Mol Cell Endocrinol 296:41–52
11. Hoenderop JG, van Leeuwen JP, van der Eerden BC, Kersten FF, van der Kemp AW, Merillat AM, Waarsing JH, Rossier BC, Vallon V, Hummler E, Bindels RJ (2003) Renal Ca^{2+} wasting, hyperabsorption, and reduced bone thickness in mice lacking TRPV5. J Clin Invest 112:1906–1914
12. Hoenderop JG, Hartog A, Stuiver M, Doucet A, Willems PH, Bindels RJ (2000) Localization of the epithelial Ca^{2+} channel in rabbit kidney and intestine. J Am Soc Nephrol 11:1171–1178
13. Zhuang L, Peng JB, Tou L, Takanaga H, Adam RM, Hediger MA, Freeman MR (2002) Calcium-selective ion channel, CaT1, is apically localized in gastrointestinal tract epithelia and is aberrantly expressed in human malignancies. Lab Invest 82:1755–1764
14. Jantarajit W, Thongon N, Pandaranandaka J, Teerapornpuntakit J, Krishnamra N, Charoenphandhu N (2007) Prolactin-stimulated transepithelial calcium transport in duodenum and Caco-2 monolayer are mediated by the phosphoinositide 3-kinase pathway. Am J Physiol Endocrinol Metab 293:E372–E384
15. Nakane M, Ma J, Rose AE, Osinski MA, Wu-Wong JR (2007) Differential effects of vitamin D analogs on calcium transport. J Steroid Biochem Mol Biol 103:84–89
16. Yee S (1997) In vitro permeability across Caco-2 cells (colonic) can predict in vivo (small intestinal) absorption in man—fact or myth. Pharm Res 14:763–766
17. Zweibaum A, Triadou N, Kedinger M, Augeron C, Robine-Leon S, Pinto M, Rousset M, Haffen K (1983) Sucrase-isomaltase: a marker of foetal and malignant epithelial cells of the human colon. Int J Cancer 32:407–412
18. Thongon N, Nakkrasae LI, Thongbunchoo J, Krishnamra N, Charoenphandhu N (2008) Prolactin stimulates transepithelial calcium transport and modulates paracellular permselectivity in Caco-2 monolayer: mediation by PKC and ROCK pathways. Am J Physiol Cell Physiol 294:C1158–C1168
19. Irnaten M, Blanchard-Gutton N, Harvey BJ (2008) Rapid effects of 17β-estradiol on epithelial TRPV6 Ca^{2+} channel in human T84 colonic cells. Cell Calcium 44:441–452
20. Irnaten M, Blanchard-Gutton N, Praetorius J, Harvey BJ (2009) Rapid effects of 17β-estradiol on TRPV5 epithelial Ca^{2+} channels in rat renal cells. Steroids 74:642–649
21. Greger R (1996) Epithelial transport. In: Greger R, Windhorst U (eds) Comprehensive human physiology: from cellular mechanisms to integration, 1st edn. Springer, Berlin, pp 1217–1232
22. Prentice A (2000) Calcium in pregnancy and lactation. Annu Rev Nutr 20:249–272
23. Charoenphandhu N, Limlomwongse L, Krishnamra N (2006) Prolactin directly enhanced Na^+/K^+- and Ca^{2+}-ATPase activities in the duodenum of female rats. Can J Physiol Pharmacol 84:555–563
24. Hoenderop JG, Vennekens R, Muller D, Prenen J, Droogmans G, Bindels RJ, Nilius B (2001) Function and expression of the epithelial Ca^{2+} channel family: comparison of mammalian ECaC1 and 2. J Physiol 537:747–761
25. Peng JB, Chen XZ, Berger UV, Weremowicz S, Morton CC, Vassilev PM, Brown EM, Hediger MA (2000) Human calcium transport protein CaT1. Biochem Biophys Res Commun 278:326–332
26. Van Cromphaut SJ, Dewerchin M, Hoenderop JG, Stockmans I, Van Herck E, Kato S, Bindels RJ, Collen D, Carmeliet P, Bouillon R, Carmeliet G (2001) Duodenal calcium absorption in vitamin D receptor-knockout mice: functional and molecular aspects. Proc Natl Acad Sci USA 98:13324–13329
27. Benn BS, Ajibade D, Porta A, Dhawan P, Hediger M, Peng JB, Jiang Y, Oh GT, Jeung EB, Lieben L, Bouillon R, Carmeliet G, Christakos S (2008) Active intestinal calcium transport in the absence of transient receptor potential vanilloid type 6 and calbindin-D_{9k}. Endocrinology 149:3196–3205
28. Kutuzova GD, Sundersingh F, Vaughan J, Tadi BP, Ansay SE, Christakos S, DeLuca HF (2008) TRPV6 is not required for 1α, 25-dihydroxyvitamin D_3-induced intestinal calcium absorption in vivo. Proc Natl Acad Sci USA 105:19655–19659
29. Charoenphandhu N, Tudpor K, Pulsook N, Krishnamra N (2006) Chronic metabolic acidosis stimulated transcellular and solvent drag-induced calcium transport in the duodenum of female rats. Am J Physiol Gastrointest Liver Physiol 291: G446–G455
30. Van Abel M, Hoenderop JG, Dardenne O, St Arnaud R, Van Os CH, Van Leeuwen HJ, Bindels RJ (2002) 1,25-dihydroxyvitamin D_3-independent stimulatory effect of estrogen on the expression of ECaC1 in the kidney. J Am Soc Nephrol 13:2102–2109
31. Weber K, Erben RG, Rump A, Adamski J (2001) Gene structure and regulation of the murine epithelial calcium channels ECaC1 and 2. Biochem Biophys Res Commun 289:1287–1294
32. Song Y, Peng X, Porta A, Takanaga H, Peng JB, Hediger MA, Fleet JC, Christakos S (2003) Calcium transporter 1 and epithelial calcium channel messenger ribonucleic acid are differentially regulated by 1,25 dihydroxyvitamin D_3 in the intestine and kidney of mice. Endocrinology 144:3885–3894
33. den Dekker E, Hoenderop JG, Nilius B, Bindels RJ (2003) The epithelial calcium channels, TRPV5 and TRPV6: from identification towards regulation. Cell Calcium 33:497–507

34. Couchourel D, Leclerc M, Filep J, Brunette MG (2004) Testosterone enhances calcium reabsorption by the kidney. Mol Cell Endocrinol 222:71–81
35. Lambers TT, Mahieu F, Oancea E, Hoofd L, de Lange F, Mensenkamp AR, Voets T, Nilius B, Clapham DE, Hoenderop JG, Bindels RJ (2006) Calbindin-D_{28K} dynamically controls TRPV5-mediated Ca^{2+} transport. EMBO J 25:2978–2988
36. Niemeyer BA, Bergs C, Wissenbach U, Flockerzi V, Trost C (2001) Competitive regulation of CaT-like-mediated Ca^{2+} entry by protein kinase C and calmodulin. Proc Natl Acad Sci USA 98:3600–3605
37. Mace OJ, Morgan EL, Affleck JA, Lister N, Kellett GL (2007) Calcium absorption by $Ca_v1.3$ induces terminal web myosin II phosphorylation and apical GLUT2 insertion in rat intestine. J Physiol 580:605–616
38. Mahraoui L, Rodolosse A, Barbat A, Dussaulx E, Zweibaum A, Rousset M, Brot-Laroche E (1994) Presence and differential expression of SGLT1, GLUT1, GLUT2, GLUT3 and GLUT5 hexose-transporter mRNAs in Caco-2 cell clones in relation to cell growth and glucose consumption. Biochem J 298(Pt 3): 629–633
39. Pérez M, Barber A, Ponz F (1997) Modulation of intestinal paracellular permeability by intracellular mediators and cytoskeleton. Can J Physiol Pharmacol 75:287–292

CELL BIOCHEMISTRY AND FUNCTION
Cell Biochem Funct 2010; **28**: 45–51.
Published online 13 October 2009 in Wiley InterScience
(www.interscience.wiley.com) **DOI**: 10.1002/cbf.1617

Changes in the mRNA expression of osteoblast-related genes in response to β_3-adrenergic agonist in UMR106 cells†

Amporn Nuntapornsak[1‡], Kannikar Wongdee[2,3‡], Jirawan Thongbunchoo[2], Nateetip Krishnamra[1,2] and Narattaphol Charoenphandhu[1,2*]

[1]*Department of Physiology, Faculty of Science, Mahidol University, Bangkok, Thailand*
[2]*Consortium for Calcium and Bone Research (COCAB), Faculty of Science, Mahidol University, Bangkok, Thailand*
[3]*Department of Medical Science, Faculty of Science, Burapha University, Chonburi, Thailand*

Activation of adrenergic receptors (AR) was demonstrated to result in either bone gain or bone loss depending on the activated AR subtypes and concentrations of agonists used. While β_2-AR agonist was extensively investigated as an osteopenic agent, effects of β_3-AR activation on osteoblasts were still elusive. Rat osteoblast-like UMR106 cells were herein found to express several AR subtypes, including β_3-AR. After exposure to a low-dose β_3-AR agonist BRL37344 (10 nmol L^{-1}), UMR106 cells downregulated the mRNA expression of transcription factors Runx2 and Dlx5, which are important for initiation of osteoblast differentiation. Low-dose BRL37344 also decreased the expression ratio of receptor activator of nuclear factor κB ligand (RANKL) over osteoprotegerin (OPG), suggesting the protective effect of β_3-AR agonist against bone resorption. Alkaline phosphatase expression was markedly decreased, whereas expressions of osteocalcin and osteopontin were increased by 100 nmol L^{-1} BRL37344, indicating that β_3-AR activation could accelerate the transition of matrix maturation stage to mineralization stage. In conclusion, β_3-AR activation in rat osteoblasts induced alteration in the expression of osteoblast-related transcription factor genes as well as genes required for bone formation and resorption. The present results also suggest that, besides β_2-AR, β_3-AR is another AR subtype responsible for the sympathetic nervous system-induced bone remodeling. Copyright © 2009 John Wiley & Sons, Ltd.

KEY WORDS — adrenergic receptor; alkaline phosphatase; bone remodeling; osteocalcin; osteoprotegerin; real-time PCR

INTRODUCTION

Besides humoral control, bone is regulated by an autonomic neural control via nerve fibers expressing catecholamine-synthesizing enzyme tyrosine hydroxylase and neuropeptide Y.[1] The sympathetic nervous system (SNS) has recently been demonstrated to play an important role in bone metabolism, in part, by suppressing osteoblast-induced bone formation and stimulating osteoclast differentiation and multinuclearity, thereby leading to bone loss.[2–6] Several studies indicated that β_2-adrenergic receptor (AR) in osteoblasts was responsible for SNS-induced bone loss through the upregulation of receptor activator of nuclear factor κB ligand (RANKL), a key osteoblast-derived mediator for osteoclastogenesis, and the downregulation of soluble decoy receptor osteoprotegerin (OPG), which could neutralize RANKL action.[2,7] Thus, chronic administration of a low-dose non-selective β-AR antagonist propranolol (0.1 mg kg^{-1}) could lead to significant bone gain. On the other hand, β_1-AR may mediate bone formation because administration of high-dose propranolol (20 mg kg^{-1}), which was believed to inhibit β_1-AR, did not increase bone mass.[8] Moreover, activation of α_1-AR in osteoblasts was reported to enhance osteoblast proliferation as well as the expression of RANKL and OPG.[7,9] It seemed that osteoblasts differentially responded to different AR subtype activation and concentrations of agonists or antagonists.[7–9]

In addition to β_2-AR and α_1-AR, β_3-adrenergic signaling may have a role in the bone remodeling process,[10] such as modulation of osteoblast differentiation, although the direct effect of β_3-AR on osteoblasts was not known. β_3-AR transcripts are primarily expressed in adipocytes, heart, skeletal muscles, the enteric nervous system, smooth muscle of the gastrointestinal tract and in the urogenital system.[11–14] It was reported that β_3-AR transcripts were not expressed in human osteoblasts and human osteosarcoma MG-63 cells as demonstrated by conventional RT-PCR.[7] However, β_3-AR transcripts were recently demonstrated in primary mouse osteoblasts by quantitative real-time PCR (qRT-PCR),[2] It was, therefore, possible that β_3-AR was expressed in a species-specific manner. Since activation of β_3-AR could accelerate the differentiation process in several cell types, such as adipocytes,[15] changes in the expression of osteoblast-related transcription factor genes, e.g., zinc finger

* Correspondence to: N. Charoenphandhu, M.D., Ph.D., Faculty of Science, Department of Physiology, Mahidol University, Rama VI Road, Bangkok 10400, Thailand. Tel & Fax: +66-2-354-7154.
E-mail: naratt@narattsys.com
†The authors declare no conflict of interest.
‡A.N. and K.W. contributed equally to this study.

Received 1 July 2009
Revised 22 August 2009
Accepted 27 August 2009

transcription factor AJ18, *runt*-related transcription factor (Runx) 2, osterix and distal-less homeobox (Dlx) 5, and genes related to osteoblast differentiation, e.g., RANKL, OPG, alkaline phosphatase, osteocalcin, and osteopontin were anticipated.

The objectives of the present study were (i) to investigate β_3-AR expression in rat osteoblast-like UMR106 cells and rat primary osteoblasts as well as distribution of β_3-AR in rat tissues, and (ii) to demonstrate the direct effects of β_3-AR stimulation on the expression of transcription factors, RANKL/OPG ratio, and genes associated with osteoblast differentiation.

MATERIALS AND METHODS

Animals

Female Sprague-Dawley rats (8-week-old, weighing 180–200 g) were obtained from the National Animal Centre, Thailand. They were housed in hanging stainless steel cages under 12:12-h light-dark cycle, and fed regular chow (Perfect Companion, Bangkok, Thailand). Room temperature was maintained at 20–25°C and relative humidity was 50–60%. This study has been approved by the Institutional Animal Care and Use Committee (IACUC) of the Faculty of Science, Mahidol University, Bangkok, Thailand.

Cell culture

Rat osteoblast-like UMR106 cells (American Type Culture Collection [ATCC] No. CRL-1661) were cultured in 100-mm petri dish with Dulbecco's modified Eagle's medium (DMEM) (Sigma, St. Louis, MO, USA) supplemented with 10% fetal bovine serum (FBS) (PAA, Pasching, Austria), and 100 U ml^{-1} penicillin-streptomycin (Gibco, Grand Island, NY, USA). Cells were incubated at 37°C with 5% CO_2 and subcultured according to the ATCC's protocol.

Primary osteoblast culture

Under 50 mg kg^{-1} thiopental sodium i.p. anesthesia, tibiae, and femora were removed from a rat by sterile surgical technique, as previously described.[16,17] After removing the connective tissues and marrow cells, bones were cut into small dice, and cultured in a 25-cm^2 T-flask (Corning, NY, USA) with DMEM supplemented with 15% FBS, 100 U ml^{-1} penicillin-streptomycin, and 100 μg ml^{-1} ascorbate-2-phosphate (Sigma). Cells were incubated at 37°C with 5% CO_2. Osteoblasts proliferated and migrated from the bone dice into culture medium within 3 days. The medium was changed every 3 days. Confluent cells from the same rat in six flasks were pooled together for total RNA preparation.

Cell proliferation assay

UMR106 cells were incubated in 96-well culture plate (3000 cells/well). After incubation with β_3-AR agonist for 48 h, cell proliferation was determined by 5-bromo-2′-deoxy-uridine (BrdU) labeling and detection kit III (catalog no. 11444611001, Roche, Mannheim, Germany) according to the manufacturer's instruction. The absorbance of each well was determined at 405 nm with a reference wavelength of 490 nm by a microplate reader (model 1420, Wallac, Turku, Finland). Experiments were performed in triplicate.

Total RNA preparation

The total RNA samples were prepared from UMR106 cells, primary osteoblasts, omental fat, whole brain, mucosal scrapings from duodenum and jejunum, liver, kidney, lung, and heart by using TRIzol reagent (Invitrogen, Carlsbad, CA, USA). They were then treated with RQ1 RNase-free DNase (Promega, Madison, WI, USA) and subsequently purified by RNeasy mini kit (Qiagen, Valencia, CA, USA) according to the manufacturer's instructions. Purity of the total RNA was determined by the ratio of absorbance readings at 260 and 280 nm, the ratio of which was in the range of 1.8–2.0. One microgram of total RNA was reverse-transcribed with iScript cDNA Synthesis kit (Bio-Rad, Hercules, CA, USA) to cDNA by a Bio-Rad MyCycler. Rat glyceraldehyde-3-phosphate dehydrogenase (GAPDH) served as a control gene to check the consistency of the reverse transcription.

Quantitative real-time PCR (qRT-PCR) and sequencing

Primers used in the present study are shown in Table 1. qRT-PCR and melting curve analyses were performed by Bio-Rad MiniOpticon with iQ SYBR Green SuperMix (Bio-Rad) as previously described.[16,17] Conventional PCR was performed with GoTaq Green Master Mix (Promega) and Bio-Rad MyCycler. PCR products were visualized on 2% agarose gel stained with 1 μg ml^{-1} ethidium bromide (Sigma) under UV transilluminator (Alpha Innotech, San Leandro, USA). After electrophoresis, all PCR products were extracted by HiYield Gel/PCR DNA Extraction kit (Real Biotech Corporation, Taipei, Taiwan), and were sequenced by ABI Prism 3100 Genetic Analyzer (Applied Biosystems, Foster City, CA, USA). PCR experiments were performed in triplicate.

Experimental protocol

UMR106 cells, primary osteoblasts, omental fat, whole brain, duodenal, and jejunal epithelial cells, liver, kidney, lung, and heart were first investigated for β_3-AR expression by using conventional RT-PCR. Other AR subtypes, including α_1, α_2, β_1, and β_2, were also studied in UMR106 cells. In some experiments, confluent UMR106 cells were incubated with normal medium (control, 0 nmol L^{-1} BRL37344) or medium containing various concentrations of 10, 100, and 1000 nmol L^{-1} BRL37344 (Sigma), a selective β_3-AR agonist, for 48 h prior to determination of osteoblast gene expression. Since it was reported that the half maximal effective concentrations (EC50) of BRL37344 for lipolysis in rat adipose tissues and relaxation of the rat distal colon were between 3.3–27.5 nmol L^{-1},[18] the lowest BRL37344 concentration used in the present study should fall within this range, i.e., 10 nmol L^{-1}. Expressions of AJ18, Runx2, osterix,

Table 1. *Rattus norvegicus* oligonucleotide sequences used in the PCR experiments

Gene	Accession no.	Primer (forward/reverse)	Product length (bp)
Adrenergic receptor (AR) genes			
α_{1b}-AR	NM_016991	5′-ATGAATCCCGATCTGGACAC-3′ 5′-CACGATGGCAAAGAGGATG-3′	183
α_{1d}-AR	NM_024483	5′-CGGGCCTTACTGTTTACACTG-3′ 5′-GGACAGTTTGCACAGTCTGAAC-3′	164
α_{2a}-AR	NM_012739	5′-TGCTCATGCTGTTCACCGT-3′ 5′-ACCAGTAGCCCATAACCTCGT-3′	174
α_{2b}-AR	NM_138505	5′-AGCAGTGGGACAACTTGGAA-3′ 5′-TGCAGATGGCTCTGAAGCA-3′	155
α_{2c}-AR	NM_138506	5′-TGGTGGGTTTCCTCATCGT-3′ 5′-GAAAAGGGCATGACCAGTGT-3′	154
β_1-AR	NM_012701	5′-CATCGTGCTGCTCATCGTA-3′ 5′-CACAGAAGAAGGAGCCGTACT-3′	194
β_2-AR	NM_012492	5′-AGCCACCTACGGTCTCTGAAT-3′ 5′-AAGTCGCTGTCATTCCCGT-3′	150
β_3-AR	NM_013108	5′-CCACCACCACCCTGCTTATTA-3′ 5′-TGGGAACACAGAACCTGGAGA-3′	145
Osteoblast-related genes			
AJ18	AF321874	5′-GTCCCTGGTATGTATCAC-3′ 5′-GAAGACTTTGGCTAAAAC-3′	133
Dlx5	NM_012943	5′-CTCTCTAGGACTGACGCAAAC-3′ 5′-GAGTTACACGCCATAGGGTC-3′	135
Osterix	AY177399	5′-GCCTACTTACCCGTCTGA-3′ 5′-CTCCAGTTGCCCACTATT-3′	139
Runx2	XM_001066909	5′-TAACGGTCTTCACAAATCCTC-3′ 5′-GGCGGTCAGAGAACAAACTA-3′	135
Alkaline phosphatase	NM_013059	5′-GCAGGATCGGAACGTCAAT-3′ 5′-ATGAGTTGGTAAGGCAGGGTC-3′	144
Osteocalcin	J04500	5′-CACAGGGAGGTGTGTGAG-3′ 5′-TGTGCCGTCCATACTTTC-3′	203
Osteopontin	NM_012881	5′-TTCACTGCCAGCACACAA-3′ 5′-TTTGACCTCAGTCCGTAAGC-3′	101
OPG	NM_012870	5′-ATTGGCTGAGTGTTCTGGT-3′ 5′-CTGGTCTCTGTTTTGATGC-3′	140
RANKL	NM_057149	5′-TCGCTCTGTTCCTGTACT-3′ 5′-AGTGCTTCTGTGTCTTCG-3′	145
Housekeeping gene			
GAPDH	NM_017008	5′-AGTCTACTGGCGTCTTCAC-3′ 5′-TCATATTTCTCGTGGTTCAC-3′	133

Dlx5, RANKL, OPG, alkaline phosphatase, osteocalcin, osteopontin were determined by qRT-PCR. The effect of β_3-agonist on cell proliferation was determined by BrdU cell proliferation assay.

Statistical analysis

The results are expressed as means ± SE or log means ± SE. Statistical analysis was performed by Mann–Whitney nonparametric test. The level of significance was $p < 0.05$. Data were analyzed by GraphPad Prism 5 (GraphPad Software, San Diego, CA, USA).

RESULTS

Expression of β_3-AR transcripts in UMR106 cells and rat tissues

As shown in Figure 1A, UMR106 cells strongly expressed several osteoblast differentiation markers, including AJ18, Runx2, osterix and Dlx5, indicating that UMR106 cells used in the present study were differentiated osteoblasts as reported previously.[16,17] These cells also expressed a number of AR subtypes, i.e., α_{1b}, α_{1d}, α_{2a}, α_{2b}, α_{2c}, β_1, β_2, and β_3 (Figure 1B). Expression of β_2-AR, which has

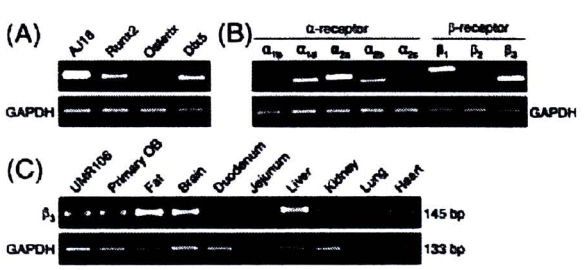

Figure 1. (A) Representative electrophoretic bands of osteoblast-related transcription factors AJ18, Runx2, osterix and Dlx5 in osteoblast-like UMR106 cells ($n = 5$). (B) Expression profile of adrenergic receptor (AR) subtypes in UMR106 cells ($n = 5$). (C) β_3-AR expression in UMR106 cells, primary osteoblasts (OB) and various tissues of normal rats, i.e., omental fat, brain, duodenal, and jejunal epithelial cells, liver, kidney, lung, and heart ($n = 5$ each). Expression of GAPDH, a housekeeping gene, was presented along with the studied genes. All PCR products were collected at 36 cycles

been thought to be the principal AR in osteoblasts, was much weaker than that of β_3-AR. Intense β_3-AR expression in UMR106 cells suggested that, in addition to β_2-AR,[2,7] β_3-AR mediated adrenergic signaling to modulate osteoblast functions. Moreover, β_3-AR was also found in primary rat osteoblasts as well as in adipose tissue, brain, duodenal, and jejunal epithelial cells, liver, kidney, lung, and heart (Figure 1C). Sequencing of PCR products confirmed the specificity of PCR reaction.

Effect of β_3-AR agonist on RANKL/OPG ratio

Since activation of SNS could alter bone remodeling, perhaps by changing the ratio of RANKL/OPG expression,[7] mRNA expressions of RANKL and OPG were determined in this study. Herein, we first demonstrated that 10–1000 nmol L^{-1} BRL37344, a selective β_3-AR agonist, did not affect GAPDH mRNA expression (data not shown) or cell proliferation (Figure 2). Expressions of all studied genes were thus normalized by GAPDH expression. Low-dose BRL37344 (10 nmol L^{-1}) significantly downregulated RANKL mRNA expression (Figure 3A) by 58%, without effect on OPG expression (Figure 3B), thereby leading to a decrease in RANKL/OPG ratio by 47% (Figure 3C). On the other hand, high-dose BRL37344 (1000 nmol L^{-1}) downregulated OPG expression (Figure 3B) by 31%, but had no effect on RANKL expression or RANKL/OPG ratio. A decrease in RANKL/OPG ratio by low-dose BRL37344 suggested a β_3-AR activation-induced suppression of bone resorption. Such BRL37344 actions were observed after 48 h, but not 24 h of incubation (data not shown).

Effects of β_3-AR agonist on osteoblast-related transcription factor expression

Four transcription factors, namely AJ18, Runx2, osterix and Dlx5 (Figures 1A and 4), are important for the initial step of osteoblast differentiation.[19,20] After 48 h exposure to low-dose BRL37344 (10 nmol L^{-1}), expressions of Runx2 (Figure 4B) and Dlx5 (Figure 4D), but not AJ18 (Figure 4A) and osterix (Figure 4C), were markedly decreased by 69% and 82%, respectively. In contrast, moderate-dose BRL37344 (100 nmol L^{-1}) significantly upregulated expressions of AJ18 (Figure 4A), osterix (Figure 4C) and Dlx5 (Figure 4D) by 6.26-, 5.96- and 2.11-fold, respectively. Although high-dose BRL37344 (1000 nmol L^{-1}) was without effect on the expression of AJ18, Runx2 and osterix, it could induce a 50% decrease in Dlx5 expression (Figure 4D). The results indicated that β_3-AR agonist modulated expression of these transcription factors in a complex dose-dependent manner.

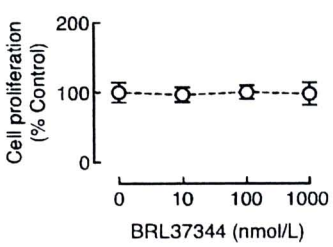

Figure 2. Proliferation of UMR106 cells after exposure for 48 h to 10, 100, and 1000 nmol L^{-1} BRL37344 ($n = 5$ per group). Cell proliferation was determined by 5-bromo-2′-deoxy-uridine (BrdU) labeling assay

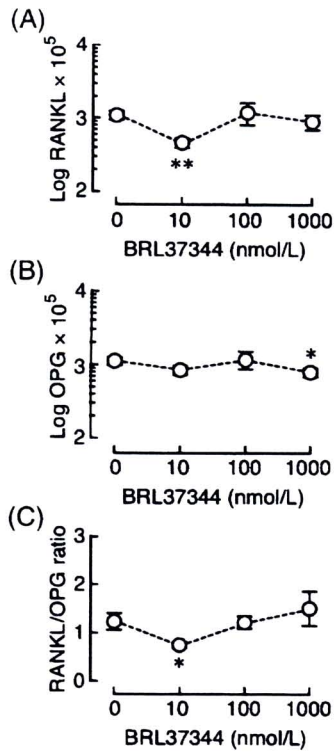

Figure 3. Expression of (A) RANKL, (B) OPG, and (C) RANKL/OPG ratio in UMR106 cells incubated for 48 h with 10, 100, and 1000 nmol L^{-1} BRL37344 ($n = 5$ per group). Expression of each studied gene was normalized by GAPDH mRNA expression. * $p < 0.05$, ** $p < 0.01$ compared with the control group (0 nmol L^{-1} BRL37344)

Effects of β_3-AR agonist on the mRNA expression of alkaline phosphatase, osteocalcin, and osteopontin

Under normal conditions, alkaline phosphatase is markedly expressed during the matrix maturation stage (early differentiation), while osteocalcin and osteopontin are expressed at the matrix mineralization stage (late differentiation).[21,22] After 48 h exposure to 10, 100, or 1000 nmol L^{-1} BRL37344, alkaline phosphatase expression was downregulated by 69%, 75% and 89%, respectively, in a dose-response manner (Figure 4E). However, 10 or 100 nmol L^{-1} BRL37344 upregulated osteocalcin expression by 65% and 311%, respectively (Figure 4F), while only 100 nmol L^{-1} BRL37344 induced a ~10-fold increase in osteopontin expression (Figure 4G). These results suggested that β_3-AR activation in rat osteoblasts might shift the differentiation stage from matrix maturation phase toward the matrix mineralization phase.

DOI: 10.1002/cbf

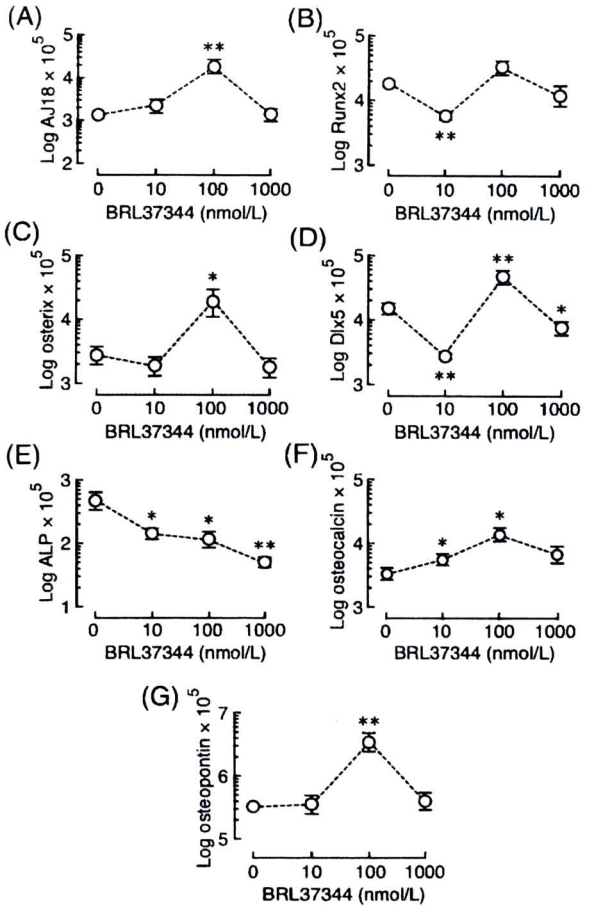

Figure 4. Expression of (A) AJ18, (B) Runx2, (C) osterix, (D) Dlx5, (E) alkaline phosphatase (ALP), (F) osteocalcin, and (G) osteopontin in UMR106 cells incubated for 48 h with 10, 100, and 1000 nmol L^{-1} BRL37344 ($n = 5$ per group). Expression of each studied gene was normalized by GAPDH mRNA expression. * $p < 0.05$, ** $p < 0.01$ compared with the control group (0 nmol L^{-1} BRL37344)

DISCUSSION

β-adrenergic system has recently been postulated to be a part of the SNS-mediated bone turnover.[2,10,23] β-AR is classified into three subtypes, namely β_1-AR, β_2-AR, and β_3-AR. β_2-AR appears to be upstream in the adrenergic signaling controlling bone remodeling.[2,7,23–25] However, the SNS-mediated bone turnover was also regulated through other AR subtypes, such as α_1-AR.[7,9] Herein, we provided further evidence that activation of β_3-AR could modulate expression of several genes related to osteoblast functions and bone remodeling in osteoblast-like UMR106 cells.

β_3-AR is a member of G-protein-coupled receptor family and is expressed in adipocytes, heart, skeletal muscles, bone marrow mesenchymal stem cells, enteric nervous system, smooth muscle of the gastrointestinal tract, and urogenital system.[11–14,25] By using conventional PCR, β_3-AR mRNA was found to be constitutively expressed in both UMR106 cells and rat primary osteoblasts, consistent with the previous report in mouse primary osteoblasts.[2] However, β_3-AR transcripts were not detected by conventional PCR in some human osteoblast-like cell lines, e.g., TE-85, SaOS-2, MG-63, and OHS-4.[26] It was possible that β_3-AR was expressed in human osteoblasts but at a relatively low level, which was not detected by the conventional PCR. Alternatively, β_3-AR expression may be restricted only to rodents.

Expressions of several osteoblast-related genes were altered by β_3-AR agonist. Alkaline phosphatase expression was downregulated in BRL37344-exposed osteoblasts. Although alkaline phosphatase is a generic marker of differentiated osteoblasts, its expression depends on the stage of osteoblast differentiation.[22] Osteoblast development generally proceeds through three distinct molecular events, i.e., cell proliferation, matrix maturation (early differentiation), and mineralization (late differentiation),[22,27,28] each of which requires different sets of stimulatory factors. Factors that enhance development in one stage may be inhibitory in the others. For example, fibroblast growth factor-8 which strongly stimulated osteoblast proliferation, was found to suppress osteoblast differentiation.[29] Normally, a decline in cell proliferation is accompanied by an increase in alkaline phosphatase, a marker of matrix maturation phase. In the last stage, mineralization was indicated by increases in osteocalcin and osteopontin expression.[21,22] Therefore, downregulation of alkaline phosphatase with upregulation of osteocalcin and osteopontin by 10–100 nmol L^{-1} BRL37344 suggested that β_3-AR activation accelerated the phase transition from matrix maturation to the mineralization stage of osteoblast differentiation.

Osteoblast differentiation was generally regulated by several osteoblast-specific transcription factors.[19,20] In the present study, β_3-AR activation altered the expressions of Runx2, Dlx5, AJ18, and osterix, all of which are important for commitment of osteoblast lineage.[19] Runx2 induces proliferation of the mesenchymal stem cells,[30,31] and initiates differentiation of those cells to pre-osteoblasts (early differentiation stage),[19,28] but it was also reported to inhibit the late differentiation stage.[30] Dlx5 is a bone-inducing transcription factor that acts as a transcriptional activator of Runx2 expression. Thus, a decrease in Runx2 expression (Figure 4B), which may have resulted from a low-dose β_3-AR agonist-induced downregulation of Dlx5 (Figure 4D), would lead to suppression of osteoblast differentiation. In contrast, both Dlx5 and AJ18 were upregulated by higher concentration of β_3-AR agonist (100 nmol L^{-1}). Since Runx2 expression can be suppressed by AJ18,[19,20] concurrent upregulation of AJ18 and Dlx5 resulted in no change in Runx2 expression. In addition, expression of osterix which induced osteoblast differentiation but inhibited proliferation,[32,33] was also upregulated by a moderate dose of β_3-AR agonist. Taken together, we speculated that β_3-AR activation triggered the transition of proliferating pre-osteoblasts to the early differentiation stage, and accelerated differentiation of immature osteoblasts into mature osteoblasts. The absence of change in osteoblast proliferation (Figure 2) agreed with our

DOI: 10.1002/cbf

hypothesis that β_3-AR activation predominantly affected osteoblast differentiation, and not proliferation.

Regarding bone remodeling regulators RANKL and OPG,[34] in contrast to β_2-AR which has been known to increase RANKL/OPG ratio,[2,7] β_3-AR activation by low-dose BRL37344 decreased the expression ratio of RANKL/OPG. Thus, β_3-AR activation may help prevent bone resorption and slow down bone turnover. However, it was not known as to why the high-dose β_3-AR agonist did not alter the RANKL/OPG ratio, but the results suggested that osteoblast responses to the β_3-AR agonist may be biphasic. Bonnet *et al.*[8] investigated the dose-dependent effects of β-blocker propranolol on trabecular and cortical bone of ovariectomized rats and found that, at low doses, propranolol exhibited a protective effect on trabecular and cortical bones, but such effect disappeared at higher doses. Hence, the biphasic action of AR agonists and antagonists may not be uncommon; however, the underlying mechanism remains to be investigated.

In conclusion, the present investigation provided evidence that rat osteoblast-like UMR106 cells and primary rat osteoblasts, known to be target cells of the SNS, strongly expressed β_3-AR. β_3-AR activation was likely to direct proliferating pre-osteoblasts toward the differentiation process since the β_3-AR agonist induced downregulation of Runx2, which was important for proliferation of osteoblast progenitors,[30,31] and upregulation of several osteoblast differentiation markers, e.g., osterix, osteocalcin, and osteopontin.[19,21,22] Furthermore, the low-dose β_3-AR agonist may have a protective effect against bone resorption as indicated by a decrease in the RANKL/OPG expression ratio. Although this study was performed at the transcriptional level, the findings suggested the significance of the β_3-AR system in the regulation of osteoblast function and bone remodeling. However, further investigations are required to demonstrate the molecular mechanisms of β_3-AR in osteoblasts as well as the effects of β_3-AR activation on bone metabolism *in vivo*.

ACKNOWLEDGEMENTS

The authors thank Dr. Jantarima Pandaranandaka for helpful discussion, and Kanogwun Thongchote for excellent technical assistance. This research was supported by grants from the Faculty of Science, Mahidol University (SCR52-01 to N. Charoenphandhu), the Commission on Higher Education, and the Thailand Research Fund (RTA5080008 to N. Krishnamra).

REFERENCES

1. Serre CM, Farlay D, Delmas PD, Chenu C. Evidence for a dense and intimate innervation of the bone tissue, including glutamate-containing fibers. *Bone* 1999; **25**: 623–629.
2. Aitken SJ, Landao-Bassonga E, Ralston SH, Idris AI. β_2-Adrenoreceptor ligands regulate osteoclast differentiation *in vitro* by direct and indirect mechanisms. *Arch Biochem Biophys* 2009; **482**: 96–103.
3. Elefteriou F. Regulation of bone remodeling by the central and peripheral nervous system. *Arch Biochem Biophys* 2008; **473**: 231–236.
4. Pierroz DD, Bouxsein ML, Rizzoli R, Ferrari SL. Combined treatment with a β-blocker and intermittent PTH improves bone mass and microarchitecture in ovariectomized mice. *Bone* 2006; **39**: 260–267.
5. Takeuchi T, Tsuboi T, Arai M, Togari A. Adrenergic stimulation of osteoclastogenesis mediated by expression of osteoclast differentiation factor in MC3T3-E1 osteoblast-like cells. *Biochem Pharmacol* 2001; **61**: 579–586.
6. Yirmiya R, Goshen I, Bajayo A, *et al.* Depression induces bone loss through stimulation of the sympathetic nervous system. *Proc Natl Acad Sci USA* 2006; **103**: 16876–16881.
7. Huang HH, Brennan TC, Muir MM, Mason RS. Functional α_1- and β_2-adrenergic receptors in human osteoblasts. *J Cell Physiol* 2009; **220**: 267–275.
8. Bonnet N, Laroche N, Vico L, Dolleans E, Benhamou CL, Courteix D. Dose effects of propranolol on cancellous and cortical bone in ovariectomized adult rats. *J Pharmacol Exp Ther* 2006; **318**: 1118–1127.
9. Nishiura T, Abe K. α_1-Adrenergic receptor stimulation induces the expression of receptor activator of nuclear factor κB ligand gene via protein kinase C and extracellular signal-regulated kinase pathways in MC3T3-E1 osteoblast-like cells. *Arch Oral Biol* 2007; **52**: 778–785.
10. Bouxsein ML, Devlin MJ, Glatt V, Dhillon H, Pierroz DD, Ferrari SL. Mice lacking β-adrenergic receptors have increased bone mass but are not protected from deleterious skeletal effects of ovariectomy. *Endocrinology* 2009; **150**: 144–152.
11. Berkowitz DE, Nardone NA, Smiley RM, *et al.* Distribution of β_3-adrenoceptor mRNA in human tissues. *Eur J Pharmacol* 1995; **289**: 223–228.
12. Cellek S, Thangiah R, Bassil AK, *et al.* Demonstration of functional neuronal β_3-adrenoceptors within the enteric nervous system. *Gastroenterology* 2007; **133**: 175–183.
13. Chamberlain PD, Jennings KH, Paul F, *et al.* The tissue distribution of the human β_3-adrenoceptor studied using a monoclonal antibody: direct evidence of the β_3-adrenoceptor in human adipose tissue, atrium and skeletal muscle. *Int J Obes Relat Metab Disord* 1999; **23**: 1057–1065.
14. Roberts SJ, Papaioannou M, Evans BA, Summers RJ. Functional and molecular evidence for β_1-, β_2- and β_3-adrenoceptors in human colon. *Br J Pharmacol* 1997; **120**: 1527–1535.
15. Dallner OS, Chernogubova E, Brolinson KA, Bengtsson T. β_3-adrenergic receptors stimulate glucose uptake in brown adipocytes by two mechanisms independently of glucose transporter 4 translocation. *Endocrinology* 2006; **147**: 5730–5739.
16. Charoenphandhu N, Teerapornpuntakit J, Methawasin M, Wongdee K, Thongchote K, Krishnamra N. Prolactin decreases expression of Runx2, osteoprotegerin, and RANKL in primary osteoblasts derived from tibiae of adult female rats. *Can J Physiol Pharmacol* 2008; **86**: 240–248.
17. Wongdee K, Pandaranandaka J, Teerapornpuntakit J, *et al.* Osteoblasts express claudins and tight junction associated proteins. *Histochem Cell Biol* 2008; **130**: 79–90.
18. Oriowo MA, Chapman H, Kirkham DM, Sennitt MV, Ruffolo RR Jr, Cawthorne MA. The selectivity *in vitro* of the stereoisomers of the β_3-adrenoceptor agonist BRL 37344. *J Pharmacol Exp Ther* 1996; **277**: 22–27.
19. Komori T. Regulation of osteoblast differentiation by transcription factors. *J Cell Biochem* 2006; **99**: 1233–1239.
20. Lee MH, Kim YJ, Yoon WJ, *et al.* Dlx5 specifically regulates Runx2 type II expression by binding to homeodomain-response elements in the *Runx2* distal promoter. *J Biol Chem* 2005; **280**: 35579–35587.
21. Jung C, Ou YC, Yeung F, Frierson HF Jr, Kao C. Osteocalcin is incompletely spliced in non-osseous tissues. *Gene* 2001; **271**: 143–150.
22. Owen TA, Aronow M, Shalhoub V, *et al.* Progressive development of the rat osteoblast phenotype in vitro: reciprocal relationships in expression of genes associated with osteoblast proliferation and differentiation during formation of the bone extracellular matrix. *J Cell Physiol* 1990; **143**: 420–430.
23. Bonnet N, Pierroz DD, Ferrari SL. Adrenergic control of bone remodeling and its implications for the treatment of osteoporosis. *J Musculoskelet Neuronal Interact* 2008; **8**: 94–104.

24. Bonnet N, Benhamou CL, Malaval L, *et al.* Low dose β-blocker prevents ovariectomy-induced bone loss in rats without affecting heart functions. *J Cell Physiol* 2008; **217**: 819–827.
25. Takahata Y, Takarada T, Iemata M, *et al.* Functional expression of β_2 adrenergic receptors responsible for protection against oxidative stress through promotion of glutathione synthesis after Nrf2 upregulation in undifferentiated mesenchymal C3H10T1/2 stem cells. *J Cell Physiol* 2009; **218**: 268–275.
26. Kellenberger S, Muller K, Richener H, Bilbe G. Formoterol and isoproterenol induce c-*fos* gene expression in osteoblast-like cells by activating β_2-adrenergic receptors. *Bone* 1998; **22**: 471–478.
27. Datta HK, Ng WF, Walker JA, Tuck SP, Varanasi SS. The cell biology of bone metabolism. *J Clin Pathol* 2008; **61**: 577–587.
28. Ducy P, Schinke T, Karsenty G. The osteoblast: a sophisticated fibroblast under central surveillance. *Science* 2000; **289**: 1501–1504.
29. Lin JM, Callon KE, Lin JS, *et al.* Actions of fibroblast growth factor-8 in bone cells in vitro. *Am J Physiol Endocrinol Metab* 2009; **297**: E142–E150.
30. Liu W, Toyosawa S, Furuichi T, *et al.* Overexpression of Cbfa1 in osteoblasts inhibits osteoblast maturation and causes osteopenia with multiple fractures. *J Cell Biol* 2001; **155**: 157–166.
31. Schroeder TM, Jensen ED, Westendorf JJ. Runx2: a master organizer of gene transcription in developing and maturing osteoblasts. *Birth Defects Res C Embryo Today* 2005; **75**: 213–225.
32. Cao Y, Zhou Z, de Crombrugghe B, *et al.* Osterix, a transcription factor for osteoblast differentiation, mediates antitumor activity in murine osteosarcoma. *Cancer Res* 2005; **65**: 1124–1128.
33. Nakashima K, Zhou X, Kunkel G, *et al.* The novel zinc finger-containing transcription factor osterix is required for osteoblast differentiation and bone formation. *Cell* 2002; **108**: 17–29.
34. Fazzalari NL, Kuliwaba JS, Atkins GJ, Forwood MR, Findlay DM. The ratio of messenger RNA levels of receptor activator of nuclear factor κB ligand to osteoprotegerin correlates with bone remodeling indices in normal human cancellous bone but not in osteoarthritis. *J Bone Miner Res* 2001; **16**: 1015–1027.

J Physiol Sci (2010) 60:1–8
DOI 10.1007/s12576-009-0059-1

ORIGINAL PAPER

Femoral bone mineral density and bone mineral content in bromocriptine-treated pregnant and lactating rats

Panan Suntornsaratoon · Kannikar Wongdee · Nateetip Krishnamra · Narattaphol Charoenphandhu

Received: 13 February 2009 / Accepted: 6 August 2009 / Published online: 17 September 2009

Abstract Since hyperprolactinemia was found to induce osteopenia in the metaphysis of long bone in non-mated female rats, pregnant and lactating rats with sustainedly high plasma prolactin (PRL) levels might also exhibit some changes in their long bones. We performed a longitudinal study in pregnant, lactating and post-weaning rats, using dual-energy X-ray absorptiometry to demonstrate site-specific changes (i.e., metaphysis vs. diaphysis) in femoral bone mineral density (BMD) and content (BMC). The results showed that femoral metaphyseal BMD and BMC were higher when compared to their age-matched controls during pregnancy, before decreasing in late lactation and post-weaning. On the other hand, femoral diaphyseal BMC increased during pregnancy, early lactating and mid-lactating periods without change during late lactation and post-weaning. After 7 days of bromocriptine administration which inhibited endogenous PRL secretion, the lactation-induced increases in BMC during early and mid-lactating periods were abolished. Moreover, a decrease in metaphyseal BMD during late lactation was restored to the control levels by bromocriptine. However, bromocriptine did not antagonize the pregnancy-induced increases in BMD and BMC. It could be concluded that the effect of PRL on bone was variable during the reproductive periods. While having no effect on femoral BMD and BMC during pregnancy, PRL was responsible for bone gain in early and mid-lactating periods, but induced bone loss during late lactating period.

Keywords Bone density · Dual-energy X-ray absorptiometry (DXA) · Femur · Lactation · Pregnancy

P. Suntornsaratoon · N. Krishnamra · N. Charoenphandhu (✉)
Department of Physiology, Faculty of Science,
Mahidol University, Rama VI Road,
Bangkok 10400, Thailand
e-mail: naratt@narattsys.com

K. Wongdee
Department of Medical Science, Faculty of Science,
Burapha University, Chonburi 20131, Thailand

P. Suntornsaratoon · K. Wongdee · N. Krishnamra · N. Charoenphandhu
Consortium for Calcium and Bone Research (COCAB),
Faculty of Science, Mahidol University, Rama VI Road,
Bangkok 10400, Thailand

Introduction

Previous investigations in non-mated female rats demonstrated that short-term exposure to high plasma prolactin (PRL) levels induced by 4 weeks of anterior pituitary transplantation (AP) led to net bone gain, while prolonged PRL exposure longer than 4 weeks gradually led to net bone loss [1, 2]. Such hyperprolactinemic effects appeared to be observed primarily at the trabecular sites, e.g., vertebrae and sternum, but not the cortical sites, e.g., tibiae and femora [3, 4]. However, by using dual-energy X-ray absorptiometric (DXA) analysis on specific regions of rat femur, we found that prolactin could decrease bone mineral density (BMD) and content (BMC) of the femoral metaphysis, which was predominantly trabecular bone, but not diaphysis which was predominantly cortical bone [5]. Thus, it was possible that elevated plasma PRL levels during pregnancy (~75–100 ng/mL) and lactation (~200–300 ng/mL), i.e., physiological hyperprolactinemia, could alter BMD and BMC of the long bone.

Reports on site-specific changes in BMD and BMC (metaphysis vs. diaphysis) of long bone during pregnancy and lactation in rats were controversial. Zeni and co-workers

[6] reported that in situ BMDs of the proximal and distal tibiae were not changed on the first day postpartum, but were decreased at the end of lactation. Similarly, single-photon absorptiometric analysis revealed greater lactation-induced bone loss in the femoral metaphysis than in the diaphysis [7]. However, densitometric changes at mid-pregnancy and mid-lactation, which have high rates of maternal calcium loss, were presently not known. Nishiwaki and co-workers [8] demonstrated decreases in BMDs in the distal femur, lumbar spine and caudal spine (i.e., trabecular sites) at week 2–3 of lactation, but changes in cortical BMDs were not studied. Thus, a complete longitudinal densitometric study was first performed to demonstrate changes in site-specific femoral BMD and BMC during these reproductive periods.

To investigate the effects of endogenous PRL on BMD and BMC during pregnancy and lactation, an inhibitor of pituitary PRL secretion, bromocriptine, was administered to the animals. Bromocriptine is a dopaminergic D2 receptor agonist which mimics the hypothalamic PRL-inhibitory factor dopamine, thereby suppressing PRL release from the pituitary lactotrophs [9, 10]. Since osteoblasts were found to directly respond to several monoamines, e.g., serotonergic and adrenergic agonists [11], expression of D2 receptors, which have two isoforms known as long and short isoforms, was also determined to exclude possible direct actions of bromocriptine on osteoblasts.

Materials and methods

Animals

Non-mated (nulliparous) and pregnant (primiparous) Sprague–Dawley rats (8-week-old, weighing 210–220 g), were obtained from the Animal Centre of Thailand, Salaya, Thailand. They were placed in hanging stainless steel cages, fed standard chow containing 1% w/w calcium and 4,000 IU/kg vitamin D (Perfect Companion, Bangkok, Thailand), and distilled water ad libitum under 12:12 h light:dark cycle. Room temperature was controlled at 23–25°C, and the relative humidity was about 50–60%. Body weight and food intake were recorded daily. After delivery, the litter size was adjusted to eight pups per dam. Animals were cared for in accordance with the "Guiding Principles for the Care and Use of Animals in the Field of Physiological Sciences". This study has been approved by the Institutional Animal Care and Use Committee (IACUC) of the Faculty of Science, Mahidol University.

Experimental design

Rats were divided into 6 groups, i.e., 14-day pregnancy (P14; mid-pregnancy), 21-day pregnancy (P21; late pregnancy), 8-day lactation (L8; early lactation), 14-day lactation (L14; mid-lactation), 21-day lactation (L21; late lactation), and 15-day post-weaning (PW), with ages of 10, 11, 12, 13, 14, and 16 weeks, respectively. In some experiments, prior to the removal of femora, pregnant and lactating rats were administered for 7 days with 4 mg/kg per day bromocriptine s.c., which have been known to diminish plasma PRL in pregnant and lactating rats [1, 9]. Thus, each group consisted of vehicle-treated mated (pregnant or lactating) rats, bromocriptine-treated mated rats, and vehicle-treated age-matched non-mated control rats. Bromocriptine (Sigma, St. Louis, MO, USA) was first dissolved in a mixture (vehicle) of tartaric acid, absolute ethanol, and normal saline, as described previously [12]. After the rats were killed, BMD and BMC of proximal metaphysis, distal metaphysis (trabecular sites), and diaphysis (cortical site) of the femur were determined.

Primary osteoblast culture

As described previously [13], tibiae were dissected from a 9-week-old non-mated female rat by sterile surgical technique. After removing the connective tissues and marrow cells, the bones were cut into small dice, and incubated on a shaker (60 cycles/min) for 2 h at 37°C in a 25-cm^2 T-flask (Corning, NY, USA) containing DMEM supplemented with 100 U/mL penicillin/streptomycin and 2 mg/mL collagenase (all purchased from Sigma). Thereafter, bone dice were washed with DMEM, and then cultured in DMEM supplemented with 15% FBS, 100 U/mL penicillin/streptomycin, 100 μg/mL ascorbate-2-phosphate, and 0.5 mM sodium pyruvate (Sigma) at 37°C with 5% CO_2. Osteoblasts proliferated and migrated from bone dice into the media within 3 days. Media were changed daily until day 20 for expression study. Rat osteoblast-like UMR-106 cells [American Type Culture Collection (ATCC) no. CRL-1661] were cultured as described by the ATCC's instruction.

Polymerase chain reaction (PCR) and sequencing

Total RNA was prepared from primary rat osteoblasts, UMR-106 cells, pituitary glands, gastrocnemius muscle (negative control), and brain (positive control) using TRIzol reagent (Invitrogen, Carlsbad, CA, USA), and purified with RNeasy Mini kit (Qiagen, Valencia, CA, USA). 1 μg of the total RNA was reverse-transcribed with oligo-dT_{20} primer and iScript kit (Bio-Rad, Hercules, CA, USA). Glyceraldehyde-3-phosphate dehydrogenase (GAPDH), a housekeeping gene, served as a control gene to check the consistency of reverse transcription. Conventional PCR was performed for 36 cycles with the GoTaq Green Master Mix (Promega, Madison, WI, USA) and Bio-rad

MyCycler. Oligonucleotide sequences used as primers were 5′-CAGTCGAGCTTTCAGAGCCAA-3′ and 5′-TCC ATTCTCCGCCTGTTCA-3′ for long isoform of rat D2 receptor (amplicon 129 bp), 5′-TATGGCTTGAAGAG CCGTG-3′ and 5′-TGTCTGCCTTCCCTTCTGA-3′ for short isoform of rat D2 receptor (amplicon 134 bp), and 5′-AGTCTACTGGCGTCTTCAC-3′ and 5′-TCATATTTC TCGTGGTTCAC-3′ for GAPDH (amplicon 133 bp). PCR products were visualized on a 1.5% agarose gel stained with 1.0 μg/mL ethidium bromide under a UV transilluminator (Alpha Innotech, San Leandro, CA, USA). After electrophoresis, PCR products were purified by the HiYield Gel/PCR DNA Extraction kit (Real Biotech Corporation, Taipei, Taiwan), and were sequenced by the ABI Prism 3100 Genetic Analyzer (Applied Biosystems, Foster City, CA, USA).

BMD and BMC measurements

Site-specific BMD and BMC were determined by the modified methods of Binkley et al. [14] and Thongchote et al. [5]. Femora of pregnant and lactating rats were removed and cleaned of adhesive tissue. Femoral BMD and BMC were assessed by a dual-energy X-ray absorptiometer (model Lunar PIXImus2; GE Medical Systems, Madison, WI, USA), operated with software version 2.10. The dual-energy supply was 80/35 kVp at 500 μA. The regions of interest (ROI) for femoral metaphysis included the proximal and distal 8 mm of the femur, whereas the ROI of femoral diaphysis included the middle part of the femur between its 8-mm ends. The machine was calibrated daily using a phantom provided by the manufacturer. The interassay coefficient of variation was less than 0.3%.

Statistical analysis

Results are expressed as mean ± SE. Two-group and multiple comparisons were performed by Student's t test and one-way ANOVA with Newman–Keuls post-test, respectively. The level of significance for all statistical tests was $P < 0.05$. Data were analyzed by GraphPad Prism 4.0 for Mac OS X (GraphPad Software, San Diego, CA, USA).

Results

Prior to investigating the effects of PRL on site-specific BMD and BMC of femora of pregnant and lactating rats, expression of dopaminergic D2 receptor was determined. As shown in Fig. 1, long isoform D2 receptor expression was observed only in pituitary gland and brain (positive control), but not in primary rat osteoblasts, osteoblast-like UMR-106 cells, or gastrocnemius muscle (negative control). Short isoform of D2 receptor mRNAs were not expressed in osteoblasts. Thus, the results indicated that bromocriptine had no direct action on osteoblasts.

Densitometric analysis in non-mated control rats showed that femoral BMD and BMC of both trabecular sites (proximal and distal metaphyses) and cortical site (diaphysis) increased with age (Figs. 2, 3). When compared to non-mated control, BMD of proximal femoral metaphysis in the P14, P21, and L8 groups were significantly higher, while that of the L21 and PW groups were lower (Fig. 2a). BMC of the proximal metaphysis was also higher during pregnancy (P14 and P21), early lactation (L8), and mid-lactation (L14), without any difference from control thereafter (Fig. 2b). Similarly, BMD of distal femoral metaphysis in the P14 and P21 groups were markedly elevated when compared to non-mated control, and became lower in the L21 and PW groups (Fig. 2c). BMC of distal femoral metaphysis was higher in the P14, P21, and L14 groups, and later became lower in the PW group (Fig. 2d). Neither BMD nor BMC of distal metaphysis in the L8 group was different from the control values. As for the cortical site, when compared to control, significantly higher BMD was found in the P14, P21, and L14 groups (Fig. 3a), while higher diaphyseal BMC was found in the P14, P21, L8, and L14 groups (Fig. 3b).

To demonstrate the effects of PRL on femoral BMD and BMC in pregnant and lactating rats, bromocriptine was administered for 7 days prior to removal of the femora. As shown in Fig. 4, suppression of PRL secretion had no effect on the pregnancy-induced increases in BMD and BMC in the P14 and P21 groups. On the other hand, during lactation, an absence of PRL abolished increases in metaphyseal and diaphyseal BMC, but not BMD, in the L8 and L14 groups (Fig. 5a–d). In the L21 group, absence of PRL secretion also prevented a decrease in BMD and restored it to the control levels (Fig. 5e), without effect on BMC (Fig. 5f).

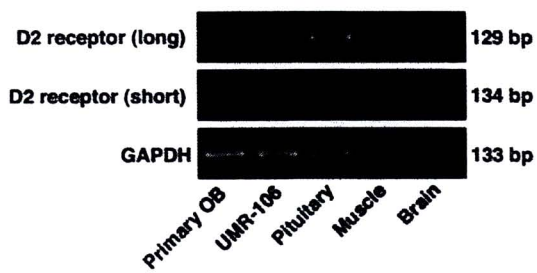

Fig. 1 Expression of long and short isoforms of subtype 2 dopamine (*D2*) receptor mRNAs in primary rat osteoblasts (*OB*), osteoblast-like UMR-106 cells, and pituitary gland. Gastrocnemius muscle and brain were used as negative and positive controls, respectively. Glyceraldehyde-3-phosphate dehydrogenase (*GAPDH*) is a housekeeping gene. This result was a representative of three independent repeats

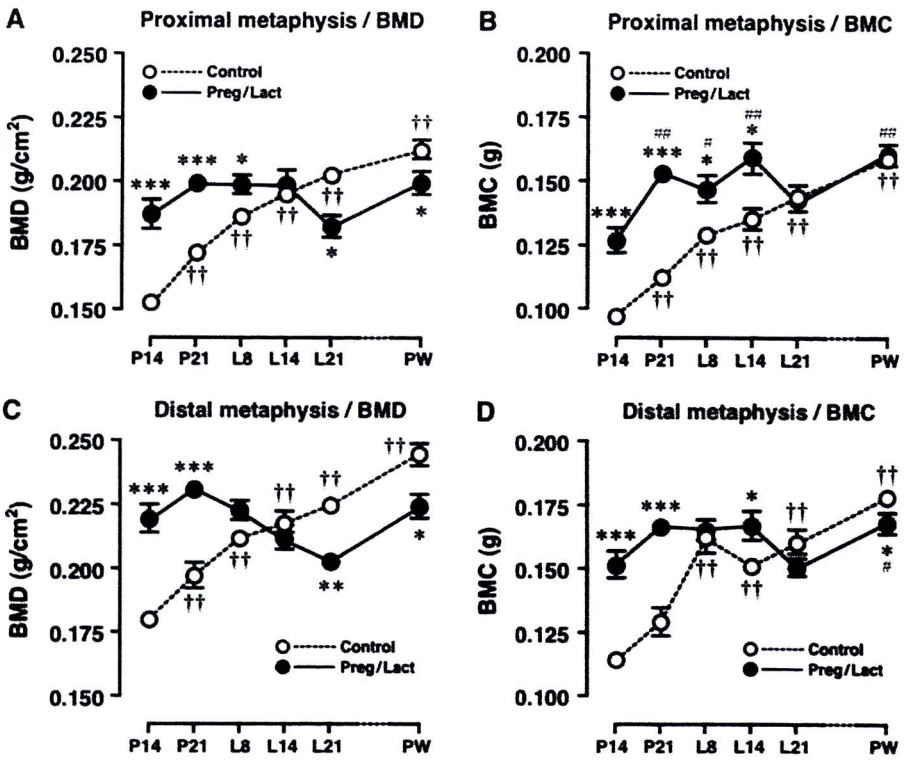

Fig. 2 BMD and BMC of **a–b** proximal and **c–d** distal femoral metaphyses in mated (pregnant, lactating, and post-weaning) and non-mated age-matched control rats ($n = 7$–9 per group). $^{*}P < 0.05$, $^{**}P < 0.01$, $^{***}P < 0.001$ compared with its respective age-matched control group. $^{\dagger\dagger}P < 0.01$ compared with age-matched control of P14 group. $^{\#}P < 0.05$, $^{\#\#}P < 0.01$ compared with the P14 group. *P14* and *P21* designate 14- and 21-day pregnant rats, while *L8*, *L14*, and *L21* designate 8-, 14-, and 21-day lactating rats, respectively. *PW* indicates 15-day post-weaning rats

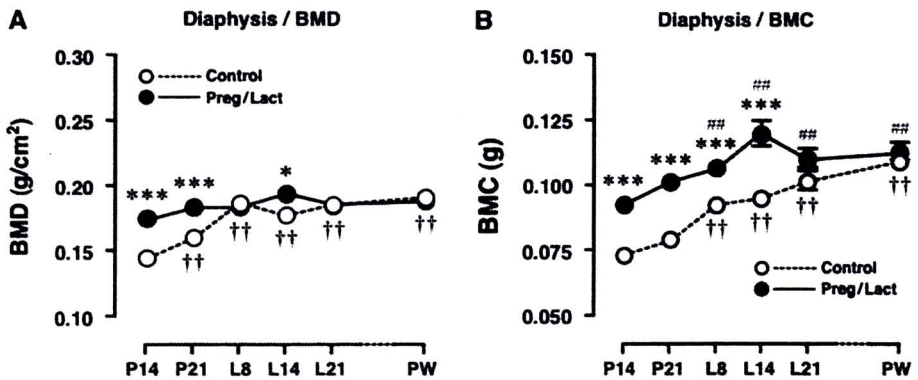

Fig. 3 **a** BMD and **b** BMC of femoral diaphyses in mated (pregnant, lactating, and post-weaning) and non-mated age-matched control rats ($n = 7$–9 per group). $^{*}P < 0.05$, $^{***}P < 0.001$ compared with its respective age-matched control group. $^{\dagger\dagger}P < 0.01$ compared with age-matched control of P14 group. $^{\#\#}P < 0.01$ compared with P14 group. *P14* and *P21* designate 14- and 21-day pregnant rats, while *L8*, *L14*, and *L21* designate 8-, 14-, and 21-day lactating rats, respectively. *PW* indicates 15-day post-weaning rats

Discussion

Little is currently known regarding the effects of hyperprolactinemia during pregnancy and lactation on the long bone. In the present study, we demonstrated that BMD and BMC of both trabecular and cortical parts of the rat femur were significantly increased during pregnancy until mid-lactation (L14). During late lactation (L21) and 15-day post-weaning, BMD of trabecular bone, but not cortical bone, was decreased. Furthermore, effects of PRL on bone during these reproductive periods were evaluated by administration of a selective D2 receptor agonist bromocriptine. The results suggested that PRL secreted from the pituitary gland was responsible for BMD and BMC changes during lactation, but not pregnancy. Daily administration of 4 mg/kg per day bromocriptine for 7 days was recently shown to decrease serum PRL of L7 rats by greater than 50% [15]. Moreover, in L7 rats with suckling, a single dose of bromocriptine injection markedly decrease serum PRL level from ~430 to ~100 ng/mL [15]. Since direct effect of bromocriptine on bone has never been reported, and osteoblasts did not express D2 receptor (Fig. 1), the bromocriptine effects observed in the present study

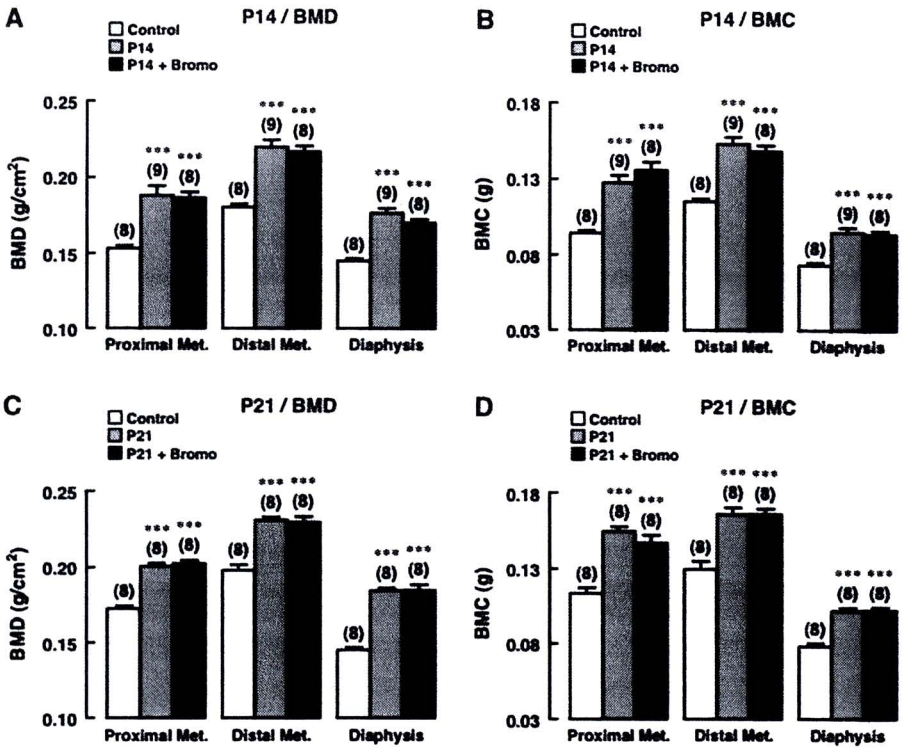

Fig. 4 BMD and BMC of proximal and distal femoral metaphyses (*Met.*) and femoral diaphyses in **a**,**b** 14-day pregnant rats (*P14*), and **c**,**d** 21-day pregnant rats (*P21*) treated with bromocriptine (*Bromo*). ***$P < 0.001$ compared with vehicle-treated age-matched control group. *Numbers in parentheses* represent the number of animals in each group

should occur through suppression of pituitary PRL release.

In general, fetal development during pregnancy leads to a massive drain on maternal calcium pool [16]. In humans, ~200–300 mg/day calcium was lost during the second and third trimester to maintain bone calcium accretion in the fetus [17]. However, changes in bone density during pregnancy remained controversial. Several investigators showed that there was no change in BMD in either pregnant women or rats [6, 16, 18]. In contrast, Gonen and coworkers [19] reported increased BMD of lumbar vertebrae, femur and tibia in pregnant rats, whereas others reported pregnancy-induced osteoporosis in humans [20, 21]. Such controversy could partly be due to the fact that an in situ densitometric measurement in living subjects is not sensitive enough to detect a slight change in bone density. Herein, by using ex vivo densitometric measurement, BMD and BMC of pregnant rats were found to increase at both femoral metaphysis and diaphysis. Despite the lack of evidence for the underlying mechanism, we speculated that the enhanced intestinal calcium absorption, in part, due to elevated serum PRL, placental lactogen and/or $1,25(OH)_2D_3$ levels, was responsible for supplying calcium both for fetuses, and for maternal trabecular and cortical bone calcium accretion [15, 22, 23], thereby leading to increases in ash weight, calcium content, and cross-sectional area of femur [1, 24]. Changes in the size and cross-sectional area of femur without proportional change in the total calcium content partially explained why BMC changes occurred in an absence of BMD change. Increased bone calcium content during pregnancy, as indicated by BMC (Figs. 2, 3), may also provide a reserved calcium pool for later use in milk production.

During lactation, an increase in BMC persisted until mid-lactation, presumably due to the lactation-induced increase in intestinal calcium absorption and renal calcium reabsorption [15, 16, 25]. PRL surge during suckling (~400–650 ng/mL) may further contribute to the elevated BMC, since short-term hyperprolactinemia of 2–4 weeks could increase bone calcium content in the rat femur, and further augment calcium absorption in the small intestine [1, 15, 26]. Besides metaphysis, PRL also had a positive effect on the femoral diaphysis of L8 and L14 rats, despite having no effect on the cortical sites in non-mated rats [4]. Although diaphyseal bone gain could be due to periosteal or endosteal bone formation, little is known regarding the direct effect of PRL on both processes in early lactation. We speculated that PRL did affect cortical bone but only in rats fed high-calcium diet [4], and perhaps in rats with enhanced intestinal calcium absorption. Bone histomorphometric study in hyperprolactinemic rats as well as in early lactating rats should reveal the effect of PRL on endosteal and periosteal calcium accretion.

When breastfeeding was prolonged, ongoing calcium loss in milk production eventually culminated in osteopenia in late lactation (L21), which was still detected at day 15 post-weaning. In exclusively breastfeeding women, calcium loss during this period can be as high as

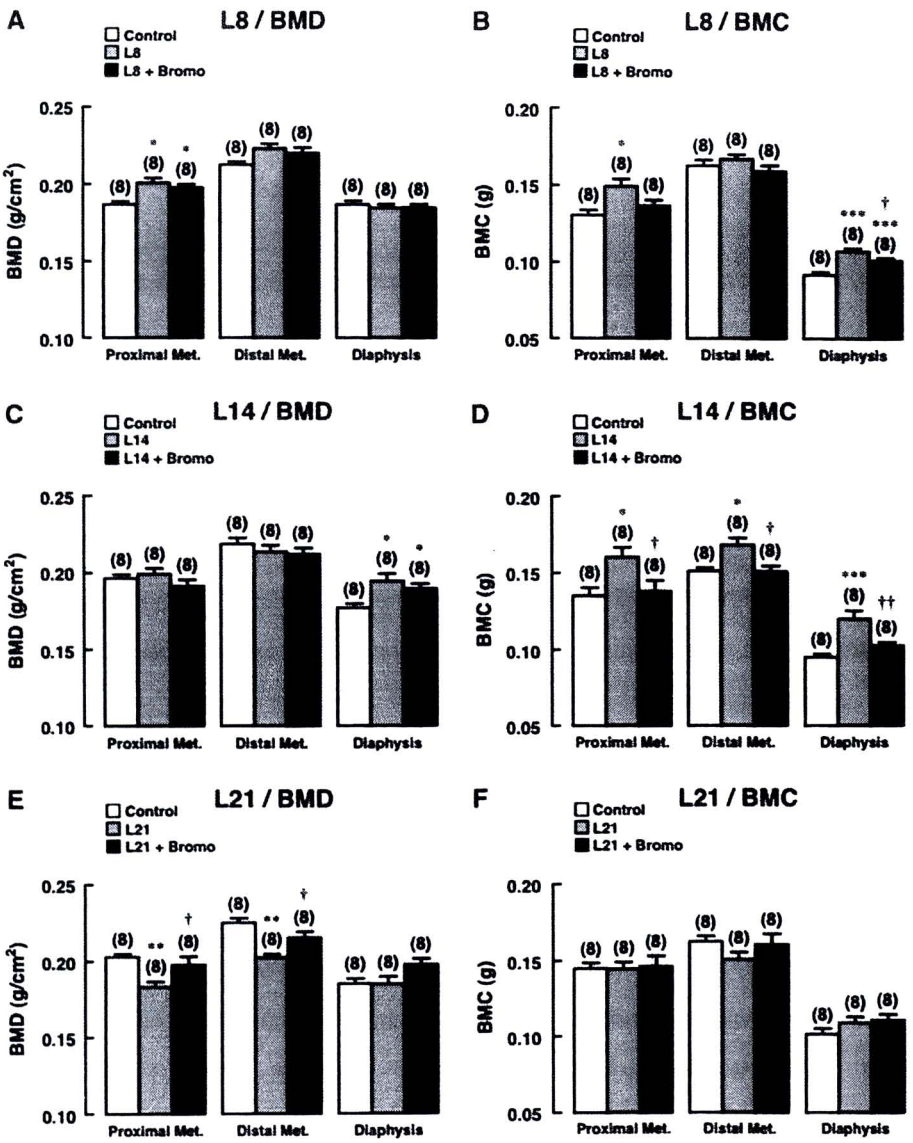

Fig. 5 BMD and BMC of proximal and distal femoral metaphyses (*Met.*) and femoral diaphyses in **a**,**b** 8-day lactating rats (*L8*), **c**,**d** 14-day lactating rats (*L14*), and **e**,**f** 21-day lactating rats (*L21*) treated with bromocriptine (*Bromo*). $^{*}P < 0.05$, $^{**}P < 0.01$, $^{***}P < 0.001$ compared with vehicle-treated age-matched control group. $^{\dagger}P < 0.05$, $^{\dagger\dagger}P < 0.01$ compared with its respective vehicle-treated lactating group. *Numbers in parentheses* represent the number of animals in each group

400 mg/day [17], while lactating rats lose 20–30% of their skeletal mass over 21 days of lactation [27, 28]. Interestingly, the observed bone loss only at trabecular site (metaphysis) was similar to that previously reported in rat vertebrae and distal femur [8]. Predominant bone loss in metaphyses may be due to the fact that the trabecular sites have more surface areas for bone resorption than the cortical sites. Several weeks after weaning, bone mass appeared to be completely restored to the normal level [16], presumably due to an increase in osteoclast apoptosis and decreased expression of osteoblast-derived bone resorption mediator, receptor activator of nuclear factor κB ligand (RANKL) [29].

A number of hormones act in concert to regulate bone resorption process during lactation. For example, parathyroid hormone-related protein (PTHrP) produced by the mammary gland is able to stimulate bone resorption and mobilize bone calcium for lactogenesis, whereas calcitonin helps to limit bone loss during lactation [16, 30]. In the present study, a decrease in metaphyseal BMD during late lactation was likely to be due to a lactogenic hormone PRL. Although PRL could induce a net bone gain in young growing rats or after short-term exposure in adults, chronic hyperprolactinemia longer than 5 weeks may lead to progressive trabecular osteopenia [2]. In non-mated female rats, chronic hyperprolactinemia markedly decreased trabecular bone volume and trabecular number, while enhancing bone turnover [2].

Since high plasma PRL levels suppressed ovarian estrogen synthesis [31–33], hyperprolactinemia-induced osteopenia was previously thought to be due to estrogen depletion. However, the presence of PRL receptors in primary rat osteoblasts and osteoblast-like MG-63 cells indicated direct PRL action on bone [2, 13]. At the

molecular level, PRL upregulated RANKL and downregulated osteoprotegerin (OPG) in osteoblasts, thereby enhancing osteoclastogenesis and osteoclast-mediated bone resorption [2]. PRL also suppressed alkaline phosphatase activity and osteocalcin expression, both of which were important for the osteoblast-mediated bone formation [2]. Although the aforementioned mechanism is able to explain metaphyseal bone loss in rat femur during late lactation, the molecular mechanism by which PRL increased bone mass during early and mid-lactation is currently unknown. In addition to the PRL-enhanced intestinal calcium absorption to supply more calcium for bone formation [23], it was possible that, during these reproductive periods, PRL may upregulate OPG rather than RANKL in osteoblasts of lactating rats, similar to that observed in human fetal osteoblasts [34], thus in turn reducing osteoclast proliferation.

In conclusion, from pregnancy to mid-lactation, BMD and BMC of both femoral metaphysis and diaphysis were increased. On the other hand, net bone loss was observed only in the femoral metaphysis during late lactation and day 15 post-weaning. Such bone changes during lactation, but not pregnancy, were found to be under the regulation of PRL. Interestingly, in contrast to non-mated rats in which PRL predominantly affected trabecular sites [3, 4], PRL induced net bone gain in both trabecular and cortical parts of femur of L8 and L14 rats, presumably to expand the calcium storage pool. Therefore, the present findings, together with the facts that PRL is able to stimulate intestinal calcium absorption and renal calcium reabsorption [1, 15, 23], suggested that PRL orchestrated total body calcium metabolism during lactation to guarantee an adequate calcium supply for milk production.

Acknowledgments We thank Kanogwun Thongchote, Jarinthorn Teerapornpuntakit, and Jirawan Thongbunchoo for the excellent technical assistance. This work was supported by the Thailand Research Fund (RSA5180001 to N. Charoenphandhu), the Faculty of Science, Mahidol University (SCR52-01 to N. Charoenphandhu), and the Faculty of Graduate Studies, Mahidol University, Academic Year 2008 (to P. Suntornsaratoon).

Conflict of interest statement The authors declare no conflicts of interest.

References

1. Piyabhan P, Krishnamra N, Limlomwongse L (2000) Changes in the regulation of calcium metabolism and bone calcium content during growth in the absence of endogenous prolactin and during hyperprolactinemia: a longitudinal study in male and female Wistar rats. Can J Physiol Pharmacol 78:757–765
2. Seriwatanachai D, Thongchote K, Charoenphandhu N, Pandaranandaka J, Tudpor K, Teerapornpuntakit J, Suthiphongchai T, Krishnamra N (2008) Prolactin directly enhances bone turnover by raising osteoblast-expressed receptor activator of nuclear factor κB ligand/osteoprotegerin ratio. Bone 42:535–546
3. Puntheeranurak S, Charoenphandhu N, Krishnamra N (2006) Enhanced trabecular-bone calcium deposition in female rats with a high physiological dose of prolactin diminishes after ovariectomy. Can J Physiol Pharmacol 84:993–1002
4. Charoenphandhu N, Tudpor K, Thongchote K, Saengamnart W, Puntheeranurak S, Krishnamra N (2007) High-calcium diet modulates effects of long-term prolactin exposure on the cortical bone calcium content in ovariectomized rats. Am J Physiol Endocrinol Metab 292:E443–E452
5. Thongchote K, Charoenphandhu N, Krishnamra N (2008) High physiological prolactin induced by pituitary transplantation decreases BMD and BMC in the femoral metaphysis, but not in the diaphysis of adult female rats. J Physiol Sci 58:39–45
6. Zeni SN, Di Gregorio S, Mautalen C (1999) Bone mass changes during pregnancy and lactation in the rat. Bone 25:681–685
7. Hagaman JR, Sanchez TV, Myers RC (1985) The effect of lactation on the mineral distribution profile of the rat femur by single photon absorptiometry. Bone 6:301–305
8. Nishiwaki M, Yasumizu T, Hoshi K, Ushijima H (1999) Effect of pregnancy, lactation and weaning on bone mineral density in rats as determined by dual-energy X-ray absorptiometry. Endocr J 46:711–716
9. Bonomo IT, Lisboa PC, Passos MC, Alves SB, Reis AM, de Moura EG (2008) Prolactin inhibition at the end of lactation programs for a central hypothyroidism in adult rat. J Endocrinol 198:331–337
10. Pi X, Voogt JL (2001) Mechanisms for suckling-induced changes in expression of prolactin receptor in the hypothalamus of the lactating rat. Brain Res 891:197–205
11. Elefteriou F (2008) Regulation of bone remodeling by the central and peripheral nervous system. Arch Biochem Biophys 473:231–236
12. Lux VA, Ramirez MI, Libertun C (1988) Natural and artificially induced ovulatory models related to lactation in the rat: role of prolactin. Proc Soc Exp Biol Med 188:301–307
13. Charoenphandhu N, Teerapornpuntakit J, Methawasin M, Wongdee K, Thongchote K, Krishnamra N (2008) Prolactin decreases expression of Runx2, osteoprotegerin, and RANKL in primary osteoblasts derived from tibiae of adult female rats. Can J Physiol Pharmacol 86:240–248
14. Binkley N, Dahl DB, Engelke J, Kawahara-Baccus T, Krueger D, Colman RJ (2003) Bone loss detection in rats using a mouse densitometer. J Bone Miner Res 18:370–375
15. Charoenphandhu N, Nakkrasae LI, Kraidith K, Teerapornpuntakit J, Thongchote K, Thongon N, Krishnamra N (2009) Two-step stimulation of intestinal Ca^{2+} absorption during lactation by long-term prolactin exposure and suckling-induced prolactin surge. Am J Physiol Endocrinol Metab 297:E609–E619
16. Kovacs CS, Kronenberg HM (2006) Skeletal physiology: pregnancy and lactation. In: Favus MJ (ed) Primer on the metabolic bone diseases and disorders of mineral metabolism, 6th edn. American Society for Bone and Mineral Research, Washington, DC, pp 63–68
17. Prentice A (2000) Calcium in pregnancy and lactation. Annu Rev Nutr 20:249–272
18. Ritchie LD, Fung EB, Halloran BP, Turnlund JR, Van Loan MD, Cann CE, King JC (1998) A longitudinal study of calcium homeostasis during human pregnancy and lactation and after resumption of menses. Am J Clin Nutr 67:693–701
19. Gonen E, Sahin I, Ozbek M, Kovalak E, Yologlu S, Ates Y (2005) Effects of pregnancy and lactation on bone mineral density, and their relation to the serum calcium, phosphorus, calcitonin and parathyroid hormone levels in rats. J Endocrinol Invest 28:322–326

20. Dunne F, Walters B, Marshall T, Heath DA (1993) Pregnancy associated osteoporosis. Clin Endocrinol 39:487–490
21. Smith R, Athanasou NA, Ostlere SJ, Vipond SE (1995) Pregnancy-associated osteoporosis. QJM 88:865–878
22. Fleet JC (2006) Molecular regulation of calcium metabolism. In: Weaver CM, Heaney RP (eds) Calcium in human health, 1st edn. Humana Press, New Jersey, pp 163–189
23. Jantarajit W, Thongon N, Pandaranandaka J, Teerapornpuntakit J, Krishnamra N, Charoenphandhu N (2007) Prolactin-stimulated transepithelial calcium transport in duodenum and Caco-2 monolayer are mediated by the phosphoinositide 3-kinase pathway. Am J Physiol Endocrinol Metab 293:E372–E384
24. Miller SC, Shupe JG, Redd EH, Miller MA, Omura TH (1986) Changes in bone mineral and bone formation rates during pregnancy and lactation in rats. Bone 7:283–287
25. Boass A, Lovdal JA, Toverud SU (1992) Pregnancy- and lactation-induced changes in active intestinal calcium transport in rat. Am J Physiol 263:G127–G134
26. Tudpor K, Charoenphandhu N, Saengamnart W, Krishnamra N (2005) Long-term prolactin exposure differentially stimulated the transcellular and solvent drag-induced calcium transport in the duodenum of ovariectomized rats. Exp Biol Med 230:836–844
27. Brommage R, DeLuca HF (1985) Regulation of bone mineral loss during lactation. Am J Physiol 248:E182–E187
28. Peng TC, Garner SC, Kusy RP, Hirsch PF (1988) Effect of number of suckling pups and dietary calcium on bone mineral content and mechanical properties of femurs of lactating rats. Bone Miner 3:293–304
29. Ardeshirpour L, Dann P, Adams DJ, Nelson T, VanHouten J, Horowitz MC, Wysolmerski JJ (2007) Weaning triggers a decrease in receptor activator of nuclear factor-κB ligand expression, widespread osteoclast apoptosis, and rapid recovery of bone mass after lactation in mice. Endocrinology 148:3875–3886
30. Woodrow JP, Sharpe CJ, Fudge NJ, Hoff AO, Gagel RF, Kovacs CS (2006) Calcitonin plays a critical role in regulating skeletal mineral metabolism during lactation. Endocrinology 147:4010–4021
31. Naliato EC, Farias ML, Braucks GR, Costa FS, Zylberberg D, Violante AH (2005) Prevalence of osteopenia in men with prolactinoma. J Endocrinol Invest 28:12–17
32. Schlechte JA (1995) Clinical impact of hyperprolactinaemia. Baillières Clin Endocrinol Metab 9:359–366
33. Wang C, Chan V (1982) Divergent effects of prolactin on estrogen and progesterone production by granulosa cells of rat Graafian follicles. Endocrinology 110:1085–1093
34. Seriwatanachai D, Charoenphandhu N, Suthiphongchai T, Krishnamra N (2008) Prolactin decreases the expression ratio of receptor activator of nuclear factor κB ligand/osteoprotegerin in human fetal osteoblast cells. Cell Biol Int 32:1126–1135

Am J Physiol Endocrinol Metab 297: E609–E619, 2009.
First published June 30, 2009; doi:10.1152/ajpendo.00347.2009.

Two-step stimulation of intestinal Ca^{2+} absorption during lactation by long-term prolactin exposure and suckling-induced prolactin surge

Narattaphol Charoenphandhu,[1,2] La-iad Nakkrasae,[1] Kamonshanok Kraidith,[2] Jarinthorn Teerapornpuntakit,[2] Kanogwun Thongchote,[2] Narongrit Thongon,[1,3] and Nateetip Krishnamra[1,2]

[1]*Consortium for Calcium and Bone Research;* [2]*Department of Physiology, Faculty of Science, Mahidol University, Bangkok; and* [3]*Department of Medical Science, Faculty of Science, Burapha University, Chonburi, Thailand*

Submitted 27 May 2009; accepted in final form 26 June 2009

Charoenphandhu N, Nakkrasae L, Kraidith K, Teerapornpuntakit J, Thongchote K, Thongon N, Krishnamra N. Two-step stimulation of intestinal Ca^{2+} absorption during lactation by long-term prolactin exposure and suckling-induced prolactin surge. *Am J Physiol Endocrinol Metab* 297: E609–E619, 2009. First published June 30, 2009; doi:10.1152/ajpendo.00347.2009.—During pregnancy and lactation, the enhanced intestinal Ca^{2+} absorption serves to provide Ca^{2+} for fetal development and lactogenesis; however, the responsible hormone and its mechanisms remain elusive. We elucidated herein that prolactin (PRL) markedly stimulated the transcellular and paracellular Ca^{2+} transport in the duodenum of pregnant and lactating rats as well as in Caco-2 monolayer in a two-step manner. Specifically, a long-term exposure to PRL in pregnancy and lactation induced an adaptation in duodenal cells at genomic levels by upregulating the expression of genes related to transcellular transport, e.g., TRPV5/6 and calbindin-D_{9k}, and the paracellular transport, e.g., claudin-3, thereby raising Ca^{2+} absorption rate to a new "baseline" (Step 1). During suckling, PRL surge further increased Ca^{2+} absorption to a higher level (Step 2) in a nongenomic manner to match Ca^{2+} loss in milk. PRL-enhanced apical Ca^{2+} uptake was responsible for the increased transcellular transport, whereas PRL-enhanced paracellular transport required claudin-15, which regulated epithelial cation selectivity and paracellular Ca^{2+} movement. Such nongenomic PRL actions were mediated by phosphoinositide 3-kinase, protein kinase C, and RhoA-associated coiled-coil-forming kinase pathways. In conclusion, two-step stimulation of intestinal Ca^{2+} absorption resulted from long-term PRL exposure, which upregulated Ca^{2+} transporter genes to elevate the transport baseline, and the suckling-induced transient PRL surge, which further increased Ca^{2+} transport to the maximal capacity. The present findings also suggested that Ca^{2+} supplementation at 15–30 min prior to breastfeeding may best benefit the lactating mother, since more Ca^{2+} could be absorbed as a result of the suckling-induced PRL surge.

calcium transport; lactating rats; pituitary transplantation; pregnancy; small interfering RNA

A TREMENDOUS AMOUNT of maternal Ca^{2+} (>200 mg/day) is lost during pregnancy and lactation for fetal growth and milk production, thereby leading to severe negative Ca^{2+} balance and progressive osteopenia in mothers (12, 29). Therefore, adequate oral Ca^{2+} intake is of critical importance for the maintenance of fetomaternal bone health (29, 30). How intestinal Ca^{2+} absorption is regulated during these reproductive periods is still elusive, but it is known to be $1,25(OH)_2D_3$ independent (16, 26). Our previous investigations in nulliparous rats and Caco-2 monolayer indicated that the lactogenic hormone prolactin (PRL) markedly enhanced the transepithelial Ca^{2+} transport through signaling pathways involving phosphoinositide 3-kinase (PI3K) as well as two serine/threonine kinases, namely protein kinase C (PKC) and RhoA-associated coiled-coil-forming kinase (ROCK) (20, 34, 35). Despite the markedly elevated plasma PRL levels during pregnancy (75–100 ng/ml), lactation (200–300 ng/ml), and suckling (400–650 ng/ml), i.e., >10 times the normal levels (7–10 ng/ml), physiological significances of the PRL-enhanced intestinal Ca^{2+} absorption in pregnancy and lactation have never been elucidated.

Generally, Ca^{2+} traverses the intestinal epithelium via transcellular and paracellular pathways (14). Transcellular active Ca^{2+} transport is a three-step metabolically energized process consisting of apical Ca^{2+} entry via the transient receptor potential vanilloid family Ca^{2+} channels (TRPV) 5/6 and L-type voltage-dependent Ca^{2+} channels (Ca_v), cytoplasmic Ca^{2+} translocation in a calbindin-D_{9k}-bound form, and basolateral Ca^{2+} extrusion via plasma membrane Ca^{2+}-ATPase ($PMCA_{1b}$) (18, 35). In contrast, the paracellular passive Ca^{2+} transport, which is dependent on the transepithelial Ca^{2+} gradient, does not occur when both sides of the epithelium contain equal Ca^{2+} concentration (14, 35) but may increase with a decrease in transepithelial resistance. Paracellular ion movement is normally regulated by the size- and charge-selective properties of the tight junction, which contains several charge-selective claudin proteins arranged in arrays of channel-like barriers (38). A number of claudins, such as claudin-2, -3, -8, -10, -12, and -15, were found to be cation selective (1, 15, 39, 40). Several mediators, e.g., PKA, PKC, PI3K, and ROCK, can modulate paracellular permselectivity in part via claudin phosphorylation (2, 11, 19, 31, 34).

Although PRL was reported to stimulate both transcellular and paracellular Ca^{2+} transport in ex vivo duodenal tissues (7), there was a disparity among results obtained from different models of PRL exposure. In the 4-wk anterior pituitary (AP)-grafted rats with sustained plasma PRL of 90–100 ng/ml comparable with the levels attained during pregnancy, the marked increase in duodenal Ca^{2+} transport was long lasting and was observed in PRL-free solution (36). In contrast, ex vivo duodenal tissue exhibited an abrupt increase in Ca^{2+} transport only when directly exposed to a much higher PRL concentration (>400 ng/ml) comparable with the levels of suckling-induced PRL surge (20). It is thus hypothesized that a modest hyperprolactinemia during pregnancy and lactation leads to a long-lasting adaptation in the intestinal absorptive cells to enhance Ca^{2+} absorption, whereas PRL surge after

Address for reprint requests and other correspondence: N. Charoenphandhu, Dept. of Physiology, Faculty of Science, Mahidol University, Rama VI Road, Bangkok 10400, Thailand (e-mail: naratt@narattsys.com).

intermittent suckling rapidly but transiently induces a further increase in Ca^{2+} absorption.

Therefore, the objectives of the present study were *1*) to elucidate the physiological significance of PRL in the regulation of intestinal Ca^{2+} absorption during pregnancy, lactation, and suckling and *2*) to demonstrate possible mechanisms and signaling pathways of the PRL-enhanced intestinal Ca^{2+} transport. Duodenum was used in this study because it is the efficient site for both transcellular and paracellular Ca^{2+} transport (18). In some experiments, human colorectal adenocarcinoma Caco-2 monolayer, a standard model for Ca^{2+} absorption study, was used since it can be genetically manipulated and has functional properties similar to the small intestinal cells (6, 44, 45).

MATERIALS AND METHODS

Animals. Pregnant and age-matched nulliparous Sprague-Dawley rats were obtained from the National Laboratory Animal Centre (Nakhon Pathom, Thailand). They were housed in the husbandry unit for ≥7 days prior to the experiments and were fed standard pellets and distilled water ad libitum. After delivery, the litter size was adjusted to 8 pups/dam. On the experimental day, pups were separated from the dam (−suckling) for 2 h before Ca^{2+} flux study. As for the suckling group (+suckling), pups were returned to the dam after 2-h separation, and suckling was allowed for 30 min before Ca^{2+} flux study. Milk volume was calculated from the weight of pups before and after suckling and milk density of 1.61 g/ml. In some experiments, dams were injected daily with bromocriptine and/or PRL subcutaneously (purified from ovine pituitary gland, catalog no. L6520; Sigma) for 7 days or given single injections 1 h prior to the experiment. This study was approved by the Animal Care and Use Committee of the Faculty of Science, Mahidol University.

Cell culture. Caco-2 cells (American Type Culture Collection no. HTB-37) were grown in Dulbecco's modified Eagle medium (Sigma) supplemented with 15% fetal bovine serum, 1% L-glutamine, 1% nonessential amino acid, 100 U/ml penicillin-streptomycin, and 0.25 μl/ml amphotericin B. Confluent Caco-2 monolayers were prepared by seeding cells (5×10^5 cells/cm^2) on polyester Snapwell with 12-mm diameter and 0.4-μm pore size (Corning). Culture medium was changed daily after 48 h of seeding. Monolayers were incubated at 37°C for 14 days in a humidified atmosphere containing 5% CO_2. To investigate PRL effects on Ca^{2+} transport, Caco-2 monolayer was exposed to 600 ng/ml recombinant human PRL (rhPRL; purity >97%, catalog no. 682-PL; R & D Systems), the most effective concentration reported by Jantarajit et al. (20).

Small interfering RNA transfection. Small interfering RNA (siRNA) oligonucleotides targeted for long isoform of human PRL receptor (PRLR-L; 5′-GGGCUAUAGCAUGGUGACCUU-3′ and 5′-GGUCACCAUGCUAUAGCCCUU-3′) and claudin-15 (5′-GCAAAUACGGCAGAAACGCUU-3′ and 5′-UUCGUUUAUGCCGUCUUUGCG-3′) were designed by siRNA Target Designer 1.51 and synthesized by T7 RiboMax Express RNAi System (Promega). Scramble siRNA (5′-GGCGCAAUAAAGCAAGACC-3′ and 5′-GGUCUUGCUUUAUUGCGCC-3′), which had no homology to any other genes, was used as a negative control. As described previously (35), Caco-2 cells were first plated on Snapwell at 5×10^5 cells/cm^2. On *day 12* after seeding, in vitro transfection was performed with 10 μg/ml polyethyleneimine (PEI) and 1 μmol/ml siRNA. On *day 14* (i.e., 48 h after transfection), siRNA-treated monolayers were used for the experiments. Efficiency of siRNA was evaluated by quantitative real-time PCR (qRT-PCR). The knockdown protocol was approved by the Institutional Biosafety Committee of Mahidol University.

AP transplantation. As described previously (10), two 10-wk-old donor rats were decapitated to collect the pituitary glands, which were immediately transplanted under the renal capsule of a recipient rat (i.e., 2 glands/rat). Sham operation consisted of exposure of the left kidney and a gentle touch of the renal fascia with forceps. Visual examination of the well-vascularized hypophyseal graft and immunohistochemical staining for PRL production were performed at the end

Table 1. *Oligonucleotide sequences used in PCR study*

Gene (Accession No.)	Primer	Product Length, bp
	Homo sapiens	
PRLR-S (AF416619)		145
Forward	5′-GGTGACCCCTTGATGTTG-3′	
Reverse	5′-TTCTGGTATATGCTCTTCAGC-3′	
PRLR-L (NM_000949)		100
Forward	5′-ACTTGCCTCTTTCTCCAG-3′	
Reverse	5′-TCCCTCAAGAATACTAAGCAG-3′	
Claudin-2 (NM_020384)		102
Forward	5′-CTCTTCAGGCGTAATGGA-3′	
Reverse	5′-CTTGGTGCTATGGTCTTTC-3′	
Claudin-3 (NM_001306)		121
Forward	5′-CTGCTCTGCTGCTCGTGT-3′	
Reverse	5′-TAGTCCTTGCGGTCGTAGC-3′	
Claudin-8 (NM_199328)		97
Forward	5′-TGGTGCTGATTGTTGGAGGAG-3′	
Reverse	5′-GTTGTGCGATGGGAAGGTATC-3′	
Claudin-10 (NM_182848)		179
Forward	5′-CTCTGGTGTCTGGTGTCG-3′	
Reverse	5′-GATAGTAAAATGCGGTCGG-3′	
Claudin-12 (NM_012129)		174
Forward	5′-GCCCATATACAATCTCTTAG-3′	
Reverse	5′-GTAAAGCCATACCTTACTTC-3′	
Claudin-15 (NM_014343)		90
Forward	5′-AAGTGGAGACGGACCTGAGC-3′	
Reverse	5′-GCGGCTAAGGAGGGTTGT-3′	
GAPDH (NM_002046)		359
Forward	5′-CTGGTAAAGTGGATATTGTTG-3′	
Reverse	5′-GAGGCTGTTGTCATACTTCTC-3′	
	Rattus norvegicus	
PRLR-S (NM_012630)		120
Forward	5′-TTCTACCACCATCGCAAC-3′	
Reverse	5′-CTGATCTCGTTTGTCATTGAG-3′	
PRLR-L (NM_001034111)		107
Forward	5′-TCAAGCAACCGCAGACTC-3′	
Reverse	5′-CAGTTTAGCCAATCGTTCCA-3′	
PRL (NM_012629)		171
Forward	5′-CAAACCTTCTGTTCTGCC-3′	
Reverse	5′-CACGATCTTGGACATACTG-3′	
TRPV5 (NM_053787)		163
Forward	5′-CTTACGGGTTGAACACCACCA-3′	
Reverse	5′-TTGCAGAACCACAGAGCCTCTA-3′	
TRPV6 (NM_053686)		80
Forward	5′-ATCCGCCGCTATGCAC-3′	
Reverse	5′-AGTTTTTCTGGTCACTGTTTTTGG-3′	
Calbindin-D_{9k} (X_16635)		174
Forward	5′-CCCGAAGAAATGAAGAGCATTTT-3′	
Reverse	5′-TTCTCCATCACCGTTCTTATCCA-3′	
$PMCA_{1b}$ (NM_053311)		109
Forward	5′-CGCCATCTTCTGCACAATT-3′	
Reverse	5′-CAGCCATTGTTCTATTGAAAGTTC-3′	
ZO-1 (XM_218747)		270
Forward	5′-GTATCCGATTGTTGTGTTCC-3′	
Reverse	5′-TCACTTGTAGCACCATCCGC-3′	
Occludin (NM_031329)		188
Forward	5′-CACGTTCGACCAATGC-3′	
Reverse	5′-CCCGTTCCATAGGCTC-3′	
Claudin-3 (NM_031700)		246
Forward	5′-GCACCCACCAAGATCCTCTA-3′	
Reverse	5′-AGGCTGTCTGTCCTCTTCCA-3′	
Claudin-15 (XM_222085)		330
Forward	5′-GCTGTGCCACCGACTCCC-3′	
Reverse	5′-CAGAGCCCAGTTCATACTTG-3′	
GAPDH (NM_017008)		133
Forward	5′-AGTCTACTGGCGTCTTCAC-3′	
Reverse	5′-TCATATTTCTCGTGGTTCAC-3′	

PRLR-S and -L, short and long isoforms, respectively, of prolactin receptor; PRL, prolactin; TRPV5 and -6, transient receptor potential vanilloid family Ca^{2+} channels 5 and 6, respectively; $PMCA_{1b}$, plasma membrane Ca^{2+}-ATPase isoform 1b.

of the experiments to confirm successful AP transplantation (10). At 4 wk after transplantation, plasma PRL levels are known to increase to 90–100 ng/ml (28).

Surgery and tissue collection. A median laparotomy was performed under 50 mg/kg ip pentobarbitone sodium (Abbott) anesthesia. Duodenal segment was removed and cut longitudinally to expose the mucosa. Duodenal segment was then mounted in a modified Ussing chamber to measure Ca^{2+} fluxes, as described previously (20). The tissue was incubated for 20 min in the chamber before the 60-min experiment. For mRNA and protein expression studies, epithelial cells were collected by scraping the mucosal surface with an ice-cold glass slide (10). Arterial blood (5 ml) was also collected by cardiac puncture.

Determination of serum PRL. Serum PRL concentrations were determined by rat PRL enzyme immunoassay kit (catalog no. A05101; SPI Bio, Massy Cedex, France) according to the manufacturer's instruction. The sensitivity of the assay was 0.4 ng/ml, and the intra- and interassay coefficients of variation were 10 and 15%, respectively.

RNA isolation, PCR, and sequencing. By using TRIzol reagent (Invitrogen), total RNA was prepared according to the method of Charoenphandhu et al. (10). One microgram of total RNA was reverse-transcribed with oligo$(dT)_{20}$ primer and iScript kit (Bio-Rad). Glyceraldehyde-3-phosphate dehydrogenase (GAPDH), a housekeeping gene, served as a control gene to check the consistency of reverse transcription. Primers are presented in Table 1 (9, 20, 34). Amplification reaction using conventional thermal cycler was performed with GoTaq Green Master Mix (Promega), whereas qRT-PCR using real-time PCR (model MiniOpticon; Bio-Rad) was performed with iQ SYBR Green SuperMix (Bio-Rad) according to the manufacturers' instructions. Relative expression was calculated from the threshold cycle (C_T) values by using the $2^{-\Delta\Delta C_T}$ method, and twofold change was considered significant (10). PCR products were also visualized on a 1.5% agarose gel stained with 1.0 μg/ml ethidium bromide under a UV transilluminator (Alpha Innotech). After electrophoresis, PCR products were extracted by HiYield Gel/PCR DNA Extraction kit (Real Biotech, Taipei, Taiwan) and were sequenced by ABI Prism 3100 Genetic Analyzer (Applied Biosystems). qRT-PCR experiments were performed in triplicate.

Immunoprecipitation. Cell lysate was sonicated and incubated at 4°C for 20 min. Thereafter, lysate was incubated for 2 h at 4°C on a rocking platform with 1:1,000 rabbit polyclonal antibodies against claudin-2, -3, -8, -10, -12, or -15 (Santa Cruz Biotechnology). The mixture was then incubated at 4°C for 2 h with EZview Red protein-A affinity gel (Sigma). Beads were washed three times and resuspended in 50 μl of buffer containing 20% glycerol, 10% SDS, 1% bromophenol blue, 4% 2-mercaptoethanol, and 0.5 mol/l Tris·HCl, pH 6.8. Eluted proteins were subjected to Western blot analysis.

Western blot analysis. As described previously (20), 100-μg proteins were separated by SDS-PAGE and transferred to a nitrocellulose membrane (Amersham) by electroblotting. Membranes were blocked at 25°C for 4 h with 5% nonfat milk and were probed overnight at 4°C with 1:1,000 rabbit polyclonal antibodies (Santa Cruz Biotechnology) raised against the conserved extracellular domain of PRLR, claudins, or phosphorylated amino acid residues (i.e., phosphorylated serine, thyrosine, and threonine). Membranes were also reprobed with 1:5,000 anti-β-actin monoclonal or 1:1,000 anti-claudin polyclonal antibodies (Santa Cruz Biotechnology). After 2-h incubation at 25°C with 1:2,000 secondary antibodies (Santa Cruz Biotechnology), blots were visualized by enhanced chemiluminescence kit (Amersham).

Confocal laser-scanning microscopy. Caco-2 cells were plated on coverslips in six-well culture plates (10^5 cells/cm^2) and maintained for 12 days. On *day 12*, cells were transfected with claudin-15 siRNA. After 48-h incubation, the monolayer was fixed with 100% ethanol for 20 min at −20°C. After blocking nonspecific bindings, cells were then incubated overnight at 4°C with 1:20 rabbit anti-occludin or claudin-15 polyclonal antibodies (Santa Cruz Biotechnology). They were later rinsed with phosphate-buffered saline (PBS) with Tween-20, pH 7.4, prior to 3-h incubation with 1:300 Alexa fluor 488-conjugated secondary antibody (Molecular Probes) at room temperature. For negative controls, cells were incubated with 3% bovine serum albumin in PBS instead of specific antibody. Images were captured with a FV1000 confocal laser-scanning microscope (Olympus).

Bathing solution for Ussing chamber study. The bathing solution, continuously gassed with humidified 5% CO_2 in 95% O_2, contained (in mmol/l) 118 NaCl, 4.7 KCl, 1.1 $MgCl_2$, 1.25 $CaCl_2$, 23 $NaHCO_3$,

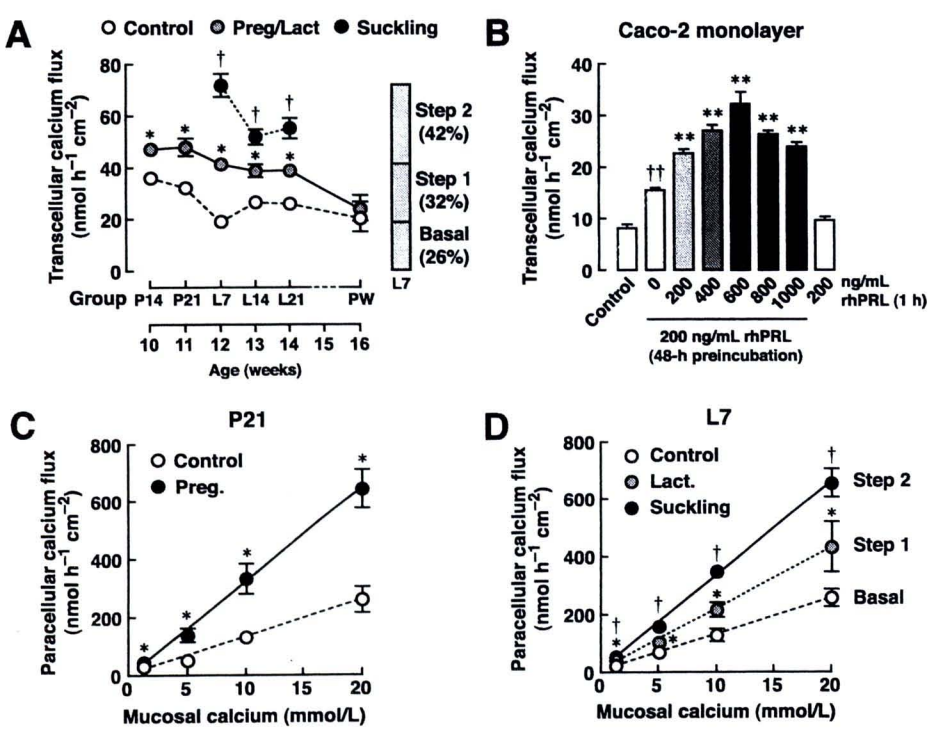

Fig. 1. *A*: transcellular Ca^{2+} transport in the duodenum of pregnant/lactating, suckling, and age-matched control rats (n = 5–9). Ca^{2+} flux was studied at midpregnancy (P14), late pregnancy (P21), early lactation (L7), midlactation (L14), late lactation (L21), and 15-day postweaning (PW). Two-step stimulation of the transcellular Ca^{2+} transport and the %contribution in L7 rats are depicted. $*P < 0.05$ compared with control group; $\dagger P < 0.05$ compared with corresponding lactating group. *B*: transcellular Ca^{2+} transport in 200 ng/ml recombinant human prolactin (rhPRL)-preincubated Caco-2 monolayer after acute exposure (1 h) to 200–1,000 ng/ml rhPRL (n = 3–6). Preincubation with 200 ng/ml rhPRL for 48 h was to represent long-term PRL effects in lactation, whereas acute PRL exposure was to mimic PRL surge during suckling. $\dagger\dagger P < 0.01$ compared with control group; $**P < 0.01$ compared with preincubated group without acute PRL treatment. *C* and *D*: paracellular Ca^{2+} transport in the duodenum of P21, L7, and L7 + suckling rats (n = 5–6/each Ca^{2+} concentration). Ca^{2+} flux was measured in the presence of transepithelial Ca^{2+} gradient (i.e., various mucosal Ca^{2+} concentrations). Two-step stimulation was demonstrated during lactation. $*P < 0.05$ compared with control group; $\dagger P < 0.05$ compared with corresponding lactating group.

12 D-glucose, and 2 mannitol (Sigma). The solution was maintained at 37°C, pH 7.4, and had an osmolality of 290–295 mmol/kg H_2O. In some experiments, PRL or inhibitors of gene transcription [RNA polymerase II inhibitor; 50 μmol/l 5,6-dichloro-1-β-D-ribobenzimidazole (DRB); Calbiochem], protein synthesis [70 μmol/l cycloheximide (CCH); Sigma], PI3K (75 μmol/l LY294002; Tocris), PKC (panspecific inhibitor; 1 μmol/l GF109203X; AG Scientific), or ROCK (1 μmol/l Y27632; Calbiochem) were added in the bathing solution.

Electrical measurement. Potential difference (PD), short-circuit current (Isc), and transepithelial resistance (TER) were determined as previously described (20). Briefly, a pair of Ag/AgCl electrodes connected to agar bridges (3.0 mol/l KCl per 4 g% agar) was located near each surface of the mounted tissue or Snapwell for measurement of PD. The other ends of the PD-sensing electrodes were connected to a preamplifier (model EVC-4000; World Precision Instruments) and finally to PowerLab 4/30 (AD Instruments). Another pair of Ag/AgCl electrodes was placed at the end of each hemichamber to supply Isc, which was also measured by a PowerLab 4/30 connected in series to EVC-4000 current-generating unit. TER and conductance were calculated by Ohm's equation.

Calcium flux measurement. Ca^{2+} flux was determined by the method of Charoenphandhu et al. (9). Briefly, after 20-min incubation, Ussing chamber was filled with fresh bathing solution. One side was $^{45}CaCl_2$-containing bathing solution (initial amount of 5 mCi/ml, final specific activity of ~450–500 mCi/mol; Amersham). ^{45}Ca radioactivity was analyzed by a liquid scintillation spectrophotometer (model Tri-Carb 3100; Packard Instruments). Total Ca^{2+} concentration of the bathing solution was analyzed by an atomic absorption spectrophotometer (model SpectrAA-300; Varian Techtron, Springvale, Australia). Ca^{2+} fluxes in the absence of Ca^{2+} concentration gradient (i.e., bathing solution in both hemichambers contained equal Ca^{2+} concentration) represented the active Ca^{2+} transport. The Ca^{2+} gradient-dependent paracellular passive fluxes were measured by determining Ca^{2+} fluxes in the presence of varying apical Ca^{2+} concentrations (9).

Permeability measurement. Permeability of sodium (P_{Na}) and chloride (P_{Cl}), which were indicative of charge selectivity, were measured by the dilution potential technique (34). In brief, duodenal epithelium or Caco-2 monolayer was equilibrated for 20 min in normal bathing solution containing 145 mmol/l NaCl before the apical solution was substituted with 72.5 mmol/l NaCl. Osmolality was maintained by an

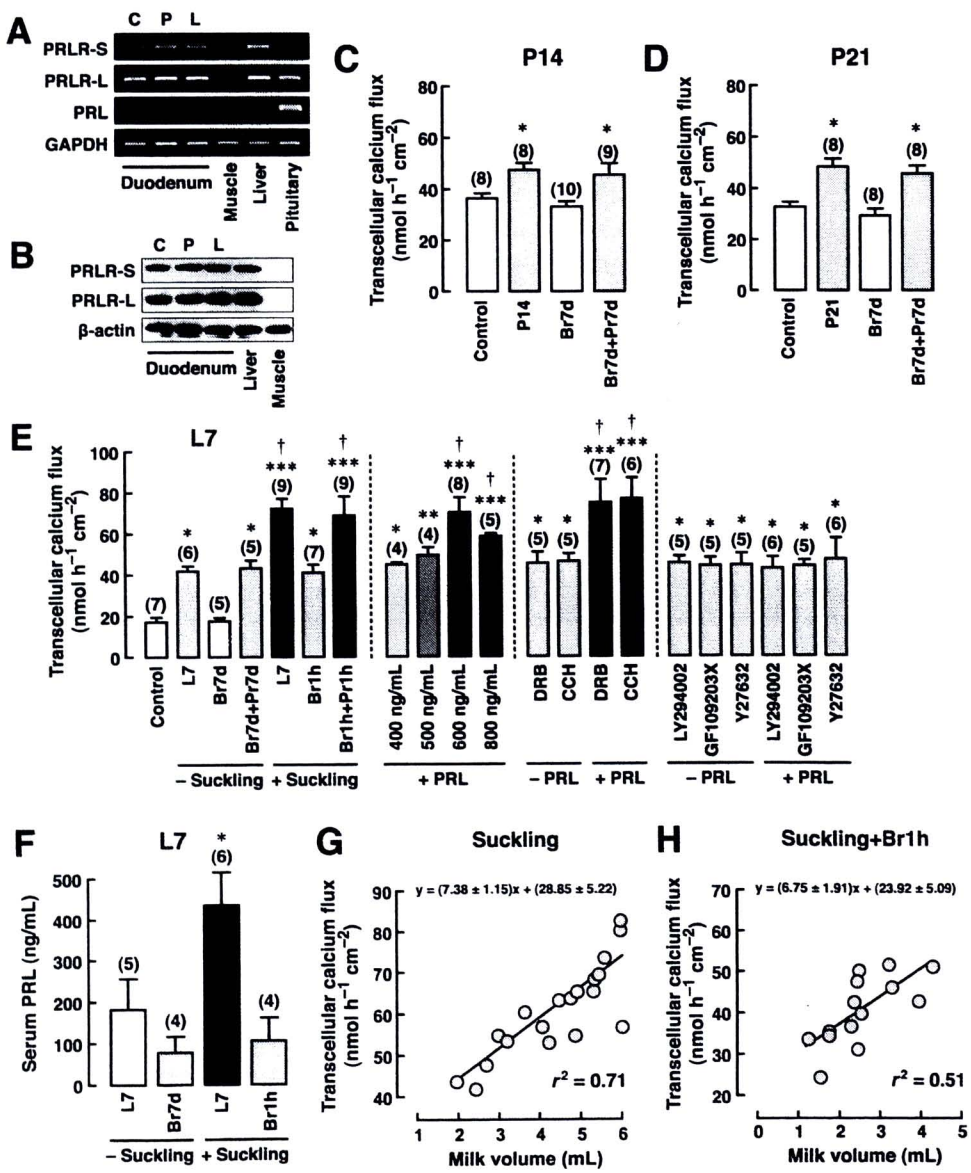

Fig. 2. Representative images of mRNA (n = 3; *A*) and protein expression (n = 3; *B*) of short (PRLR-S) and long (PRLR-L) isoforms of PRL receptors (PRLR) and PRL (mRNA only) in the duodenum of nonmated control (C), pregnant (P), and lactating (L) rats. GAPDH was a housekeeping gene for PCR study, whereas β-actin was a housekeeping gene for Western blot analysis. Liver and muscle served as positive and negative controls, respectively, for PRLR expression. Pituitary gland was a positive control for PRL expression. *C* and *D*: transcellular Ca^{2+} transport in P14 and P21 rats administered with bromocriptine (Br7d) with or without PRL supplementation (Pr7d) for 7 days. $^*P < 0.05$ compared with control group. Numbers of animals are shown in parentheses. *E*: transcellular Ca^{2+} transport in L7 rats with (+suckling) or without suckling (−suckling). Bromocriptine injection 1 h (Br1h) prior to Ca^{2+} flux study was to abolish the suckling-induced PRL surge, which was mimicked by concurrent PRL supplementation (Pr1h). In some experiments, duodenal tissues of L7 rats (−suckling) were acutely exposed to 400–800 ng/ml PRL in the bathing solution, which resembled acute exposure during PRL surge. To demonstrate PRL-signaling pathways, PRL and inhibitors of gene transcription [50 μmol/l 5,6-dichloro-1-β-D-ribobenzimidazole (DRB)], protein biosynthesis [70 μmol/l cycloheximide (CCH)], phosphoinositide 3-kinase (PI3K; 75 μmol/l LY-294002), PKC (1 μmol/l GF-109203X), or RhoA-associated coiled-coil-forming kinase (ROCK; 1 μmol/l Y-27632) were added in the solution. $^*P < 0.05$, $^{**}P < 0.01$, and $^{***}P < 0.001$ compared with nonmated control group (Basal Ca^{2+} flux). †$P < 0.05$ compared with L7 −suckling (Step 1 Ca^{2+} flux). *F*: serum PRL levels in L7 rats. PRL surge was determined at 30 min postsuckling. $^*P < 0.05$ compared with L7 −suckling group. *G* and *H*: correlation between Ca^{2+} fluxes and milk volume in suckling rats. Data were pooled from L7, L14, and L21 rats with (total animals = 14) or without (total animals = 19) Br1h administration.

equivalent amount of mannitol. Changes in the PD before and after fluid replacement (i.e., dilution potential) were recorded every 10 s until stable. P_{Na}/P_{Cl} was calculated from the dilution potential by using the Goldman-Hodgkin-Katz equation, whereas P_{Na} and P_{Cl} were calculated from the transepithelial conductance and P_{Na}/P_{Cl} by using Kimizuka-Koketsu equations (34). Permeability of Ca^{2+} (P_{Ca}) was calculated from the paracellular Ca^{2+} flux and the difference between apical and basolateral Ca^{2+} concentrations, as described previously (34).

^{45}Ca uptake study. Caco-2 cells were seeded on Snapwells for 12 days. On *day 12*, in vitro transfection was performed with 10 μg/ml PEI and 1 nmol/ml claudin-15 siRNA. Control cells were treated only with PEI. After 48-h incubation, the monolayer was exposed to 600 ng/ml rhPRL for 1 h and then bathed on the apical side with bathing solution containing 16,000 counts·min^{-1}·100 μl^{-1} $^{45}CaCl_2$ for 2 min before harvesting. ^{45}Ca radioactivity was analyzed by liquid scintillation spectrophotometer.

Statistical analysis. Results are expressed as means ± SE. Two sets of data were compared using the unpaired Student *t*-test. One-way analysis of variance with Dunnett's multiple comparison test was used for multiple sets of data. Linear regression with slope analysis was performed for correlation study. The level of significance was $P < 0.05$. Data were analyzed by GraphPad Prism 4.0 (GraphPad Software, San Diego, CA).

RESULTS

Two-step stimulation of duodenal Ca^{2+} absorption during pregnancy and lactation. Transepithelial Ca^{2+} transport was investigated in primiparous rats at different reproductive phases, i.e., midpregnancy (*day 14*; P14), late pregnancy (*day 21*; P21), early lactation (*day 7*; L7), midlactation (*day 14*; L14), late lactation (*day 21*; L21), and 15-day postweaning (PW), as well as in their age-matched nulliparous controls. Lactating rats were separated from pups for 2 h prior to Ca^{2+} flux study. As demonstrated by Ussing chamber technique (Fig. 1*A*), the transcellular Ca^{2+} transport was increased significantly in pregnancy and lactation, but not PW, to a new "baseline" level (Step 1). Thirty-minute suckling further increased the transcellular Ca^{2+} transport to a new level above the elevated baseline (Step 2). In L7 rats, Step 1 and Step 2 Ca^{2+} fluxes contributed ~32 and ~42%, respectively, to the total transcellular Ca^{2+} flux (Fig. 1*A*). Similarly, Caco-2 monolayer preincubated with 200 ng/ml rhPRL (dissolved in culture medium) for 48 h to represent long-term PRL exposure later exhibited 90% increase in the transcellular Ca^{2+} transport, although bathing solution in Ussing chamber contained no rhPRL (Fig. 1*B*). Acute exposure of preincubated Caco-2 monolayer to 200–1,000 ng/ml rhPRL (dissolved in bathing solution) further enhanced the transcellular Ca^{2+} transport in a dose-response manner. However, without 48-h preincubation, 200 ng/ml rhPRL in bathing solution was unable to stimulate Ca^{2+} transport (Fig. 1*B*).

The paracellular Ca^{2+} transport was also enhanced in P21 rats (Fig. 1*C*). Furthermore, consistent with the transcellular

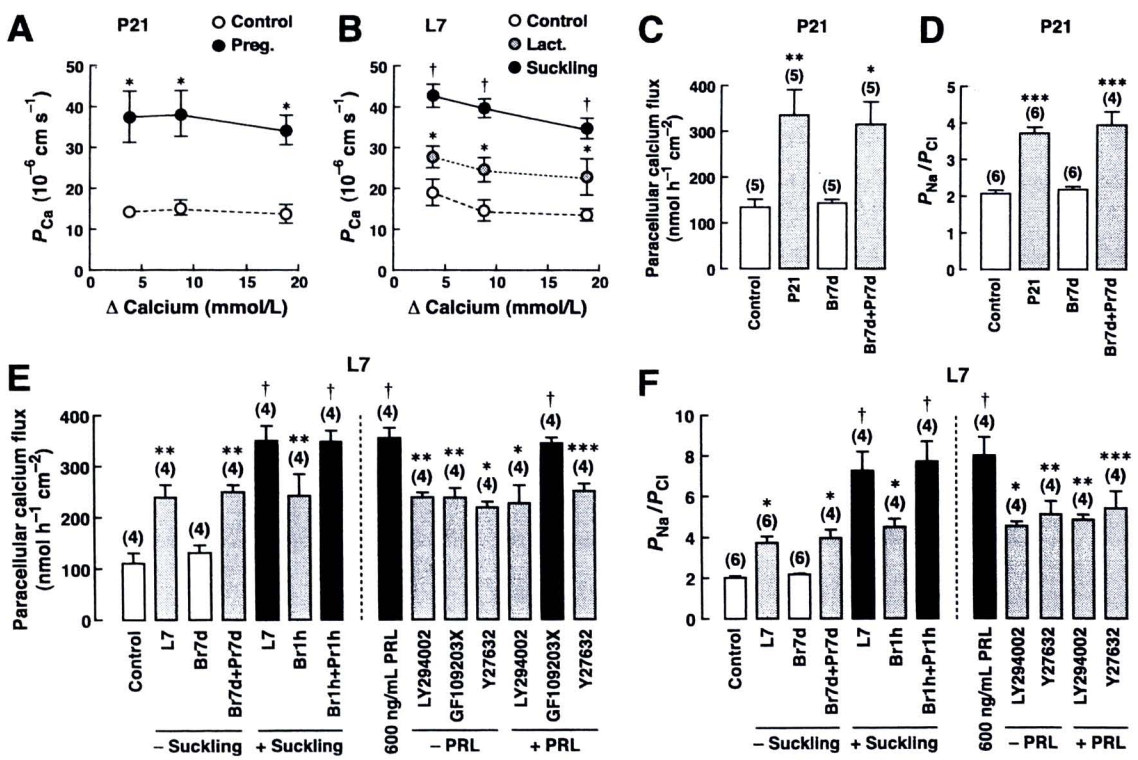

Fig. 3. *A* and *B*: permeability of Ca^{2+} (P_{Ca}) in the duodenum of pregnant, lactating, and suckling rats (n = 5–6/each Ca^{2+} concentration) plotted against Ca^{2+} concentration differences between apical and basolateral compartments (Δcalcium). *C*: paracellular Ca^{2+} fluxes measured in the presence of 10 mmol/l apical Ca^{2+} in the duodenum of P21 rats. *D*: permeability of sodium/chloride (P_{Na}/P_{Cl}) as an indicator of charge selectivity in the duodenum of P21 rats. *E* and *F*: paracellular duodenal Ca^{2+} transport and P_{Na}/P_{Cl} in L7 rats with or without suckling. In some experiments, L7 rats were administered with Br7d or Br1h to suppress chronic PRL secretion and suckling-induced PRL surge, respectively. PRL signalings were investigated by exposing 600 ng/ml PRL-treated L7 duodenal tissues to various inhibitors. $*P < 0.05$, $**P < 0.01$, and $***P < 0.001$ compared with control group (Basal). $\dagger P < 0.05$ compared with L7 −suckling (Step 1). Numbers in parentheses represent the number of rats.

transport, the two-step stimulation of the paracellular Ca^{2+} transport was similarly observed in L7 rats (Fig. 1*D*).

PRL as a regulator of transcellular Ca^{2+} transport during pregnancy and lactation. To find out whether PRL was the key regulator of the two-step increase in Ca^{2+} transport in lactating animals, the presence of PRLR was first investigated in the duodenal epithelial cells of P21, L7, and control rats. By using conventional PCR (Fig. 2*A*) and Western blot analysis (Fig. 2*B*), short (PRLR-S) and long (PRLR-L) isoforms of PRLR were identified, confirming the duodenum as a target of PRL. Figure 2*A* also shows that duodenal cells did not express endogenous PRL; i.e., the observed PRL effects were due to circulating PRL.

In P14 and P21 rats, 7-day administration of 4 $mg \cdot kg^{-1} \cdot day^{-1}$ sc bromocriptine (Br7d), an inhibitor of pituitary PRL secretion, completely abolished the pregnancy-enhanced transcellular Ca^{2+} transport (Step 1), whereas exogenous PRL supplementation [0.6 $mg \cdot kg^{-1} \cdot day^{-1}$ sc for 7 days (Pr7d)] totally reversed the bromocriptine effects (Fig. 2, *C* and *D*). Inhibition of Step 1 Ca^{2+} transport by Br7d was also observed in L7 (Fig. 2*E*), L14, and L21 rats (data not shown). Interestingly, in L7 rats with suckling, a single dose of 4 mg/kg bromocriptine administered 1 h before suckling (Br1h) completely abolished PRL surge (Fig. 2*F*) as well as the Step 2 transcellular Ca^{2+} transport (Fig. 2*E*), which was restored by a single dose of PRL [0.6 mg/kg sc (Pr1h)]. In addition, there was a strong correlation between the volume of milk ingested by pups and Ca^{2+} absorption during suckling (Fig. 2*G*). Such correlation became less significant after Br1h administration (Fig. 2*H*), suggesting that PRL surge may be the signal to match Ca^{2+} absorption with Ca^{2+} loss in milk.

The enhanced Ca^{2+} transport by the suckling-induced PRL surge could be mimicked in vitro by incubating an ex vivo duodenal tissue from L7 rats in bathing solution containing 600 and 800 but not 400 and 500 ng/ml PRL (Fig. 2*E*). The acute stimulatory effect of 600 ng/ml PRL was not abolished by inhibitors of gene transcription (50 μmol/l DRB) or protein biosynthesis (70 μmol/l cycloheximide) (Fig. 2*E*) but was completely abolished by inhibitors of PI3K (75 μmol/l LY-294002), PKC (1 μmol/l GF-109203X), and ROCK (1 μmol/l Y-27632). The present findings suggested that the acute stimulatory effect of PRL surge on the transcellular Ca^{2+} transport (Step 2) in lactating rats was mediated by nongenomic signaling pathways involving PI3K, PKC, and ROCK.

PRL as a regulator of paracellular Ca^{2+} transport during pregnancy and lactation. In addition to transcellular Ca^{2+} transport, pregnancy and lactation increased paracellular Ca^{2+} permeability (P_{Ca}; Fig. 3, *A* and *B*), whereas it decreased the TER (Supplemental Fig. S1, *A* and *B*; Supplemental Material for this article is available at the *AJP-Endocrinology and Metabolism* web site) of the duodenal epithelium. Suckling further increased P_{Ca} above the baseline level in lactation (Fig. 3*B*). The findings that decreases in TER that accompanied the increased Ca^{2+} transport were abolished by Br7d and then restored by Pr7d (Supplemental Fig. S1, *A* and *B*) strongly suggested that PRL was responsible for these responses. Further studies in P21 rats demonstrated that long-term PRL exposure markedly stimulated the gradient-dependent paracellular passive Ca^{2+} flux (Fig. 3*C*) in part by increasing the cation selectivity of the paracellular space, as indicated by the permeability ratio of sodium/chloride (P_{Na}/P_{Cl}) (Fig. 3*D*). The PRL-induced increase in P_{Na}/P_{Cl} in pregnancy resulted from an increase in P_{Na}, without a change in P_{Cl} (Supplemental Fig. S1, *C* and *D*).

Long-term PRL exposure during lactation also stimulated the paracellular Ca^{2+} transport (Fig. 3*E*) and increased P_{Na}/P_{Cl} (Fig. 3*F*) by raising P_{Na} (Supplemental Fig. S1*E*), without affecting P_{Cl} (Supplemental Fig. S1*F*). Suckling-induced PRL surge further increased the paracellular Ca^{2+} flux, P_{Na}/P_{Cl}, and P_{Na} above the baseline levels in lactation. Acute effects of direct exposure to 600 ng/ml PRL, which mimicked the suckling-induced PRL surge, were totally diminished by inhibitors of PI3K and ROCK, but not by PKC inhibitor (Fig. 3, *E* and *F*, and Supplemental Fig. S1, *E* and *F*). These findings corroborated that the acute effects of PRL surge on the paracellular Ca^{2+} transport (Step 2) and charge selectivity in lactating rats were mediated by nongenomic PI3K and ROCK pathways.

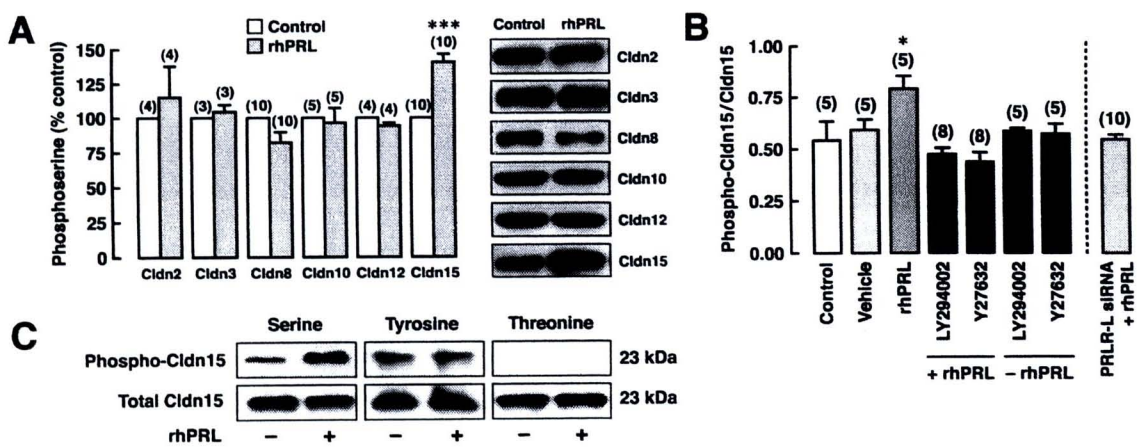

Fig. 4. *A*: phosphorylated claudin (Cldn)-2, -3, -8, -10, -12, and -15 at serine residues in 600 ng/ml rhPRL-treated Caco-2 monolayers, as demonstrated by immunoprecipitation. Representative electrophoretic images were also depicted. ***$P < 0.001$ compared with its respective control. Numbers in parentheses represent the number of independent monolayers. *B*: serine-phosphorylated Cldn-15 levels normalized with total claudin-15 in 600 ng/ml rhPRL-treated native and PRLR-L knockdown Caco-2 monolayers. In some experiments, 75 μmol/l LY-294002 or 1 μmol/l Y-27632 was added in the medium to demonstrate PRL-signaling pathways. *$P < 0.05$ compared with control group. *C*: representative bands of phosphorylated Cldn-15 at serine and tyrosine residues in rhPRL-treated Caco-2 monolayers ($n = 5$), as demonstrated by immunoprecipitation. Cldn-15 did not exhibit threonine phosphorylation.

Claudin-15 was essential for the PRL-stimulated paracellular Ca^{2+} transport. Since PRL augmented the paracellular Ca^{2+} transport by altering the charge selectivity of duodenal epithelium, it was possible that PRL may have changed the properties of certain charge-selective proteins of the claudin family. Generally, alterations of claudin functions are regulated by phosphorylation (11, 19). Therefore, we determined the amount of phosphorylated claudins in 600 ng/ml rhPRL-exposed Caco-2 monolayer by immunoprecipitation technique. The results showed that PRL induced serine phosphorylation of claudin-15 but not claudin-2, -3, -8, -10, or -12 (Fig. 4*A*). Serine phosphorylation of claudin-15 was prevented by PI3K and ROCK inhibitors as well as PRLR-L knockdown using siRNA (Fig. 4*B*). PRL was without effect on tyrosine or threonine phosphorylation of claudin-15 (Fig. 4*C*). PRLR-L siRNA did not interfere with PRLR-S or claudin-15 expression (Fig. 5*A*).

To verify the involvement of claudin-15 in the PRL-stimulated paracellular Ca^{2+} transport, Caco-2 monolayer was subjected to claudin-15 siRNA transfection. Claudin-15 knockdown markedly reduced mRNA expression, protein expression, and membrane localization of claudin-15 (Fig. 5, *B–F*), as demonstrated by qRT-PCR, Western blot analysis, and confocal laser-scanning microscopic techniques, respectively. Claudin-15 siRNA did not alter the expression of claudin-2, -3, -8, -10, -12, or occludin (Fig. 5, *C–F*). Scrambled siRNA and transfecting agent (10 μg/ml PEI) had no effect on claudin-15 expression (Fig. 5*B*). Ussing chamber study of normal Caco-2 monolayer showed that 600 ng/ml rhPRL markedly increased the paracellular Ca^{2+} transport (Fig. 6*A*) and P_{Ca} (Fig. 6*B*), whereas it decreased TER (Fig. 6*C*), similar to what was observed in the duodenum of lactating rats. This PRL-enhanced paracellular Ca^{2+} transport could be explained by a large increase in cation selectivity (P_{Na}/P_{Cl} and P_{Na}) and a slight decrease in P_{Cl} (Fig. 6*D* and Supplemental Fig. S2, *A* and *B*). Moreover, PRL effects on the paracellular Ca^{2+} flux, P_{Ca}, TER, P_{Na}/P_{Cl}, and P_{Na} were diminished after claudin-15 knockdown (Fig. 6, *A–D*, and Supplemental Fig. S2*A*). Since

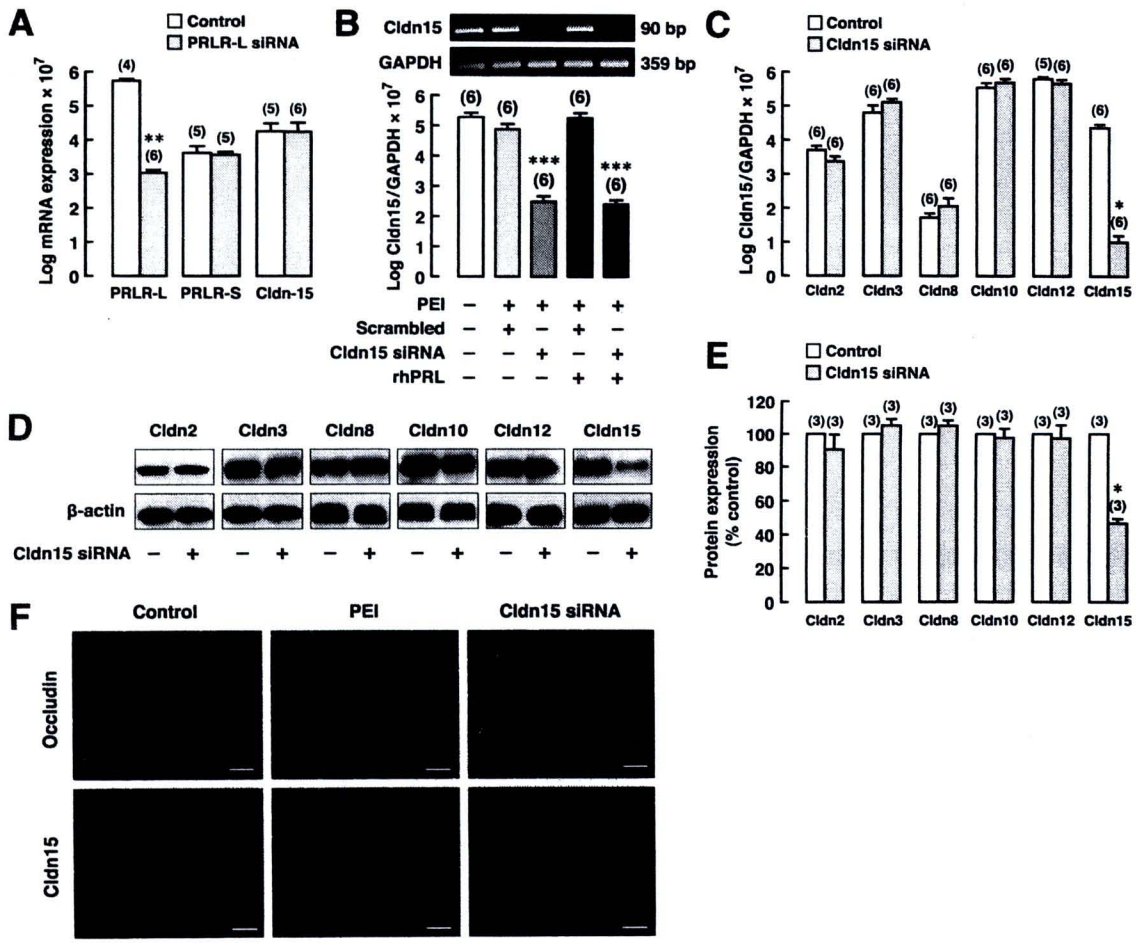

Fig. 5. *A*: expression of PRLR-L, PRLR-S, and Cldn-15 in PRLR-L knockdown Caco-2 cells, as demonstrated by quantitative real-time PCR (qRT-PCR). $^{**}P < 0.01$, small interfering RNA (siRNA) vs. control [polyethyleneimine (PEI) treated]. Numbers in parentheses represent the number of independent samples. *B*: Cldn-15 expression normalized by GAPDH expression in Cldn-15 siRNA-treated Caco-2 monolayers. Some monolayers were also exposed to 600 ng/ml rhPRL for 1 h before qRT-PCR study. Representative electrophoretic bands of Cldn-15 from conventional PCR were also illustrated along with those of GAPDH (36 cycles). $^{***}P < 0.001$ compared with control (open bar). *C–E*: mRNA and protein expression of Cldn-2, -3, -8, -10, -12, and -15, as demonstrated by qRT-PCR and Western blot analysis, respectively, in Cldn-15 siRNA-treated Caco-2 monolayers. Cldn protein expression was normalized by β-actin expression. $^{*}P < 0.05$ compared with corresponding control. *F*: localization of tight junction protein occludin and Cldn-15 in control (no treatment), PEI-treated, and Cldn-15 siRNA-treated Caco-2 monolayers, as demonstrated by confocal laser-scanning microscopic technique. Cldn-15 fluorescent signals were detected on the lateral membrane of control and PEI-treated monolayers but not in Cldn-15 siRNA-treated monolayer. Cldn-15 knockdown had no effect on occludin localization. Scale bars, 10 μm.

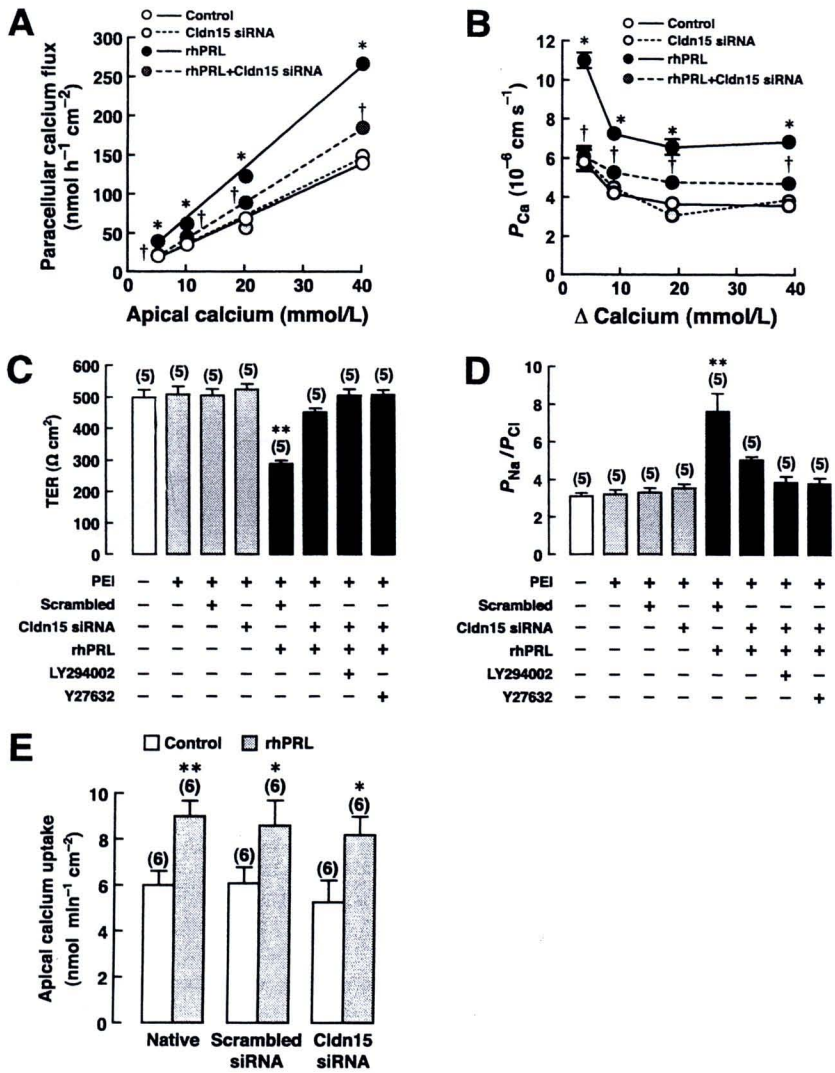

Fig. 6. *A* and *B*: paracellular Ca^{2+} transport and P_{Ca} in native and Cldn-15 knockdown Caco-2 monolayers directly exposed to 600 ng/ml rhPRL (n = 5/each Ca^{2+} concentration). *$P < 0.05$ rhPRL vs. control; †$P < 0.05$, rhPRL vs. rhPRL + Cldn-15 siRNA. *C* and *D*: transepithelial resistance (TER) and P_{Na}/P_{Cl} of native and Cldn-15 knockdown Caco-2 monolayers directly exposed to rhPRL or rhPRL plus inhibitors. **$P < 0.01$, rhPRL vs. control (open bar). *E*: ^{45}Ca uptake at 2 min in native (PEI-treated) and Cldn-15 knockdown Caco-2 monolayers directly exposed to rhPRL. *$P < 0.05$ and **$P < 0.01$ compared with its respective control group. Numbers in parentheses represent the number of independent experiments.

PI3K and ROCK inhibitors did not further increase TER (Fig. 6*C*) or further decrease P_{Na}/P_{Cl} and P_{Na} (Fig. 6*D* and Supplemental Fig. S2*A*), the cation-selective claudin-15 might be a target of both mediators.

PRL stimulated apical Ca^{2+} uptake. To determine the effect of PRL on Ca^{2+} entry, which is the first step of the transcellular Ca^{2+} transport, ^{45}Ca uptake study was performed in Caco-2 monolayer. Two minutes after ^{45}Ca-containing medium was added to the apical compartment, the PRL-stimulated Ca^{2+} uptake of comparable rates was observed in both native and claudin-15 knockdown Caco-2 monolayers (Fig. 6*E*), suggesting that acute PRL exposure stimulated the transcellular Ca^{2+} transport by enhancing apical Ca^{2+} uptake.

Long-term PRL exposure altered the expression of genes related to Ca^{2+} transport and permselectivity. Besides nongenomic actions induced by transient PRL surge during suckling, chronic PRL exposure during pregnancy and lactation may induce long-lasting adaptations to enhance Ca^{2+} absorption, e.g., upregulation of certain Ca^{2+} transporter genes. Thus, the Step 1 Ca^{2+} transport was completely diminished by Br7d but not by Br1h (Fig. 2*E*). This hypothesis was confirmed by using nulliparous rats transplanted with two extra AP glands under the renal fascia. In the absence of hypothalamic inhibition, the AP grafts continuously released PRL but not other AP hormones that, in contrast, required hypothalamic stimulation. The AP-grafted rats were hyperprolactinemic with reported plasma PRL levels of ~90–100 ng/ml, comparable with the levels attained during pregnancy (28). PRL synthesis in AP grafts was confirmed by immunohistochemistry (Fig. 7, *A* and *B*).

Four weeks after AP transplantation, hyperprolactinemia led to upregulation of several genes involved in Ca^{2+} transport, i.e., TRPV5, TRPV6, calbindin-D_{9k}, and claudin-3 (9, 18), whereas the tight junction genes ZO-1 and occludin were downregulated (Fig. 7*C*).

DISCUSSION

The question of what factor enhances the intestinal Ca^{2+} absorption to mitigate negative Ca^{2+} balance and optimize fetomaternal Ca^{2+} homeostasis in pregnancy and lactation has remained enigmatic for decades. In humans, mothers lose ~200–300 and ~300–400 mg of Ca^{2+} each day during pregnancy and lactation, respectively, thereby leading to an ~10% decrease in total bone mass (29). Rodents with a litter of 8–10 pups may lose up to 20% of their skeletal mass in milk

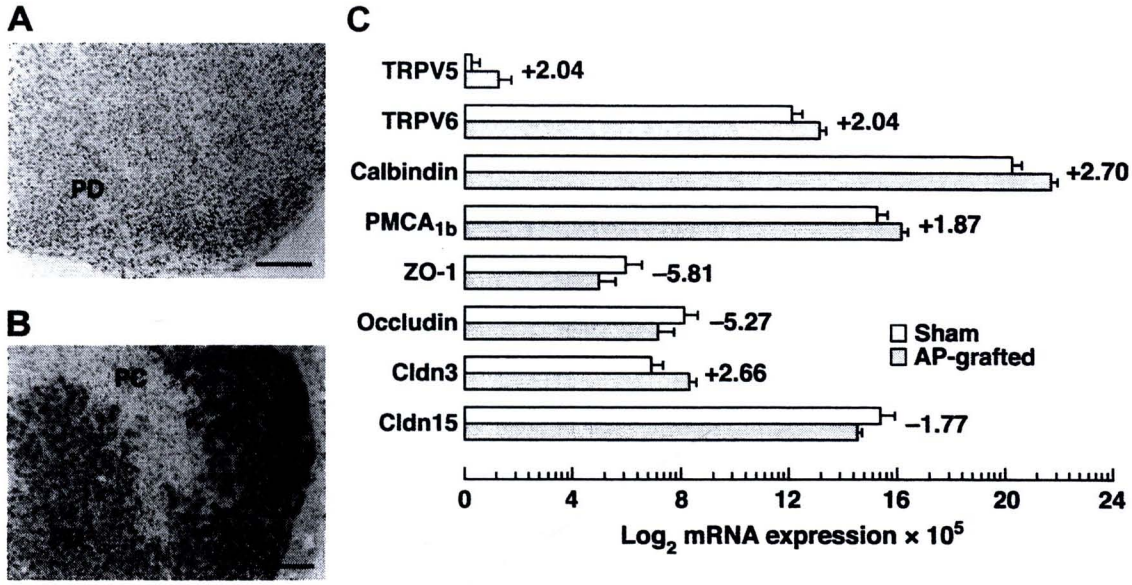

Fig. 7. Representative photomicrographic images of a pituitary graft dissected from a 4-wk anterior pituitary (AP) rat (n = 10). *A*: control image for PRL immunohistochemical analysis; i.e., the 4-μm paraffin-embedded section was incubated with secondary antibody in the absence of anti-PRL primary antibody. Active signs of microvascular endothelial damage and lymphoid proliferation were not seen, suggesting no graft rejection and allograft vasculopathy. *B*: immunohistochemical staining of an implanted pituitary gland with anti-PRL antibody. The pars distalis (PD) is strongly labeled with brownish products of peroxidase, whereas the perirenal connective tissues (PC) do not show PRL immunoreactivity. Scale bars, 100 μm. *C*: expression of genes related to Ca^{2+} transport and paracellular permeability in duodenal epithelial cells of 4-wk hyperprolactinemic AP-grafted rats (n = 7–10) vs. age-matched sham rats (n = 7–10), as demonstrated by qRT-PCR (log_2 means ± SE × 10^5). Fold change value of each gene is presented on its respective columns. + and −, upregulation and downregulation, respectively. TRPV5 and -6, transient receptor potential vanilloid family Ca^{2+} channels 5 and 6, respectively; $PMCA_{1b}$, $plasma_{1b}$ Ca^{2+} ATPase isoform 1b.

production (27). With such high Ca^{2+} loss, it is surprising that intestinal Ca^{2+} absorption during pregnancy and lactation is $1,25(OH)_2D_3$ independent and does not correlate with the levels of other Ca^{2+}-regulating hormones, namely parathyroid hormone (PTH), PTH-related peptide, calcitonin, and estrogen (14, 29). Herein, we elucidated for the first time that PRL is a novel Ca^{2+}-regulating hormone that induces a two-step stimulation of Ca^{2+} absorption during pregnancy, lactation, and suckling. Therefore, PRL is essentially a regulator of Ca^{2+} balance by controlling both input (i.e., provision of Ca^{2+}) and output (i.e., lactogenesis) of Ca^{2+} in these reproductive phases.

Long-term PRL exposure over a period of several days led to an adaptive elevation of the basal intestinal Ca^{2+} transport to a new baseline (Step 1). This adaptation occurred at genomic levels through alteration of gene expression and was abolished by Br7d but not Br1h. In suckling rats (+suckling), Br1h could only decrease Step 2 Ca^{2+} transport to Step 1 level without further decreasing Step 1 Ca^{2+} transport (Fig. 2*E*). van Cromphaut et al. (37) previously showed that upregulation of TRPV6, calbindin-D_{9k}, and $PMCA_{1b}$ could account for the enhanced transcellular Ca^{2+} absorption in the duodenum of pregnant and lactating mice. Similarly, the present findings showed PRL-induced upregulation of TRPV5, TRPV6, and calbindin-D_{9k} in the duodenal cells of AP-grafted rats, which was consistent with an earlier report of a 25% upregulation of duodenal calbindin-D_{9k} by 9-day administration of PRL (5). Moreover, our previous genome-wide study in the rat duodenum by microarray indicated the PRL-induced increases in the expression of other Ca^{2+} transporter genes, namely Ca_v and parvalbumin, which may also contribute to the enhanced transcellular Ca^{2+} absorption (4, 10). Upregulation of these Ca^{2+} transporter genes, i.e., TRPV5, TRPV6, and Ca_v for apical Ca^{2+} uptake or calbindin-D_{9k} and parvalbumin for cytoplasmic diffusion, stressed the importance of adequate Ca^{2+} supply for fetal development and lactogenesis. Such redundancy also explains why TRPV6/calbindin-D_{9k} double-knockout mice were normocalcemic and still exhibited transcellular active Ca^{2+} absorption (3).

The Step 1 enhancement of the paracellular Ca^{2+} absorption appeared to involve the PRL-induced downregulation of occludin and ZO-1, both of which are important for the tight junction assembly, size-selective paracellular permeability, and maintenance of transepithelial resistance (13, 41). A decrease in transepithelial resistance after long-term PRL exposure in P21 and L7 rats (Supplemental Fig. S1, *A* and *B*) suggested possible enlargement of paracellular pores for passage of small solutes. In addition to the size selectivity, long-term PRL exposure also altered the charge selectivity of the paracellular barriers to favor cations over anions (i.e., an increase in P_{Na}/P_{Cl}; Fig. 3, *D* and *F*), which was consistent with the PRL-induced upregulation of cation-selective tight junction gene claudin-3. Previous investigations provided evidence that duodenal claudin-3 expression was $1,25(OH)_2D_3$ dependent (23), and its upregulation was associated with conditions of increased intestinal Ca^{2+} absorption, e.g., chronic metabolic acidosis (9). Although PRL augmented both transcellular and paracellular components of Step 1 Ca^{2+} absorption, the latter may be of greater physiological significance since, under normal luminal Ca^{2+} concentration of ~2–6 mmol/l (42), the paracellular Ca^{2+} flux was about three times greater than the transcellular flux (i.e., ~150 vs. ~50 $nmol \cdot h^{-1} \cdot cm^{-2}$). Nevertheless, transcellular active Ca^{2+} transport may become significant in low dietary Ca^{2+} intake condition.

The present results (Fig. 2), together with previous findings by Tudpor et al. (36), suggested that chronic PRL effects on the intestinal Ca^{2+} absorption (Step 1) were seen at plasma PRL concentrations ~100–200 ng/ml, as in pregnancy and lactation. In contrast, the acute stimulatory effect on Ca^{2+} absorption required ~400 ng/ml PRL, as attained during the suckling-induced PRL surge (Fig. 2*F*). This acute effect, which was superimposed on chronic PRL action, was responsible for the Step 2 transcellular and paracellular Ca^{2+} transport and could also be mimicked in vitro in Caco-2 monolayer (Fig. 1*B*) and in 600–800 ng/ml PRL-exposed duodenum of L7 rats (Fig. 2*E*). Moreover, the significant correlation between the suckling-enhanced transcellular Ca^{2+} flux and milk volume was suggestive of the orchestrating role of PRL in matching Ca^{2+} absorption to Ca^{2+} loss in milk.

Regarding the mechanisms of acute PRL action, it has been reported that PRL stimulated PMCA activity in purified basolateral membrane of the rat duodenum, thereby enhancing Ca^{2+} extrusion (8). Moreover, consistent with the previous report (35), the Step 2 transcellular Ca^{2+} transport also resulted from the PRL-enhanced apical Ca^{2+} entry, particularly via $Ca_v1.3$. However, further in vivo investigation is required to confirm that the mechanisms by which PRL enhanced apical Ca^{2+} entry in the Step 1 and Step 2 transcellular Ca^{2+} transport were different, i.e., TRPV5/6 for Step 1 and $Ca_v1.3$ for Step 2. On the other hand, the Step 2 paracellular Ca^{2+} transport was likely to be dependent on phosphorylation of certain charge-selective claudins. Ikari et al. (19) revealed that serine phosphorylation of the kidney-specific claudin-16 by protein kinase A was crucial for Mg^{2+} reabsorption in the thick ascending limb of the loop of Henle. Although a number of claudins, e.g., claudin-3, -8, and -10, were cation selective (1, 39, 40), and some, e.g., claudin-2 and -12, were required for the $1,25(OH)_2D_3$-stimulated Ca^{2+} absorption (15), only claudin-15 was essential for the PRL-induced increases in the paracellular Ca^{2+} transport, cation selectivity, and Ca^{2+} permeability as well as the decrease in transepithelial resistance (Fig. 6, *A–D*). Since claudin-15 possesses several negatively charged amino acids on the first extracellular loop for cation permeability (39), it was not surprising to find that P_{Na}, but not P_{Cl}, was markedly increased by PRL. The significance of claudin-15 was demonstrated recently in claudin-15-knockout mice that exhibited a decrease in the paracellular ion permeability and enlargement of the small intestine (33). Since claudin-15 mRNA was not upregulated in the long-term PRL-exposed duodenal epithelial cells, claudin-15 may be important only for the Step 2 paracellular Ca^{2+} transport or nongenomic PRL action. Alternatively, long-term exposure to PRL may increase protein expression and/or activity of claudin-15 without an increase in claudin-15 mRNA expression.

Since we found previously that PRLR-L knockdown diminished the transcellular Ca^{2+} transport in Caco-2 monolayer (34), and PRLR-L knockdown in this study completely abolished the PRL-induced claudin-15 phosphorylation, it was likely that the PRL-enhanced Ca^{2+} absorption was mediated by PRLR-L despite the fact that both PRLR-L and -S were expressed in duodenal epithelial cells of pregnant and lactating rats and in Caco-2 monolayer. This was consistent with the PRL-induced increases in lactogenesis and electrolyte transport in mammary epithelial cells (25). Although PRL actions in Step 1 Ca^{2+} absorption involved de novo gene transcription and those in Step 2 were, in contrast, nongenomic, their signal transduction should be quite similar since the signals presumably originated from the same receptor isoform. Step 2 transcellular Ca^{2+} absorption was mediated by PI3K, PKC, and ROCK, whereas claudin-15 phosphorylation and paracellular Ca^{2+} transport were dependent only on PI3K and ROCK, similar to that in the duodenum of nulliparous rat (20). However, PI3K, PKC, and ROCK are closely associated since both PKC and ROCK are downstream from PI3K (17). The ROCK-related pathway of PRL signaling was also reported in endothelial cells (24), whereas the PKC pathway mediated PRL actions in adrenocortical cells (21) and cholangiocytes (32). In the small intestine, PKC activation is known to be important for both apical Ca^{2+} entry and basolateral Ca^{2+} extrusion (22), presumably via phosphorylation of TRPV6 and PMCA, respectively. Interestingly, PRL signaling in the small intestine was independent of Janus kinase 2, an important mediator of PRL in mammary epithelial cells (43).

In conclusion, we elucidated the complexity of PRL-induced stimulation of intestinal Ca^{2+} absorption in pregnancy and lactation and demonstrated a two-step stimulation in suckling. Long-term PRL exposure led to adaptations of intestinal cells at genomic levels to upregulate several Ca^{2+} transport genes, thereby raising the "baseline" Ca^{2+} absorption (Step 1). During suckling, transient PRL surge further increased Ca^{2+} absorption (Step 2) within 30 min to the maximal capacity, which apparently matched Ca^{2+} loss in milk. The PRL-stimulated Step 2 Ca^{2+} transport occurred via both transcellular and paracellular pathways in a PI3K/PKC/ROCK-dependent manner in part by increasing apical Ca^{2+} uptake and claudin-15 phosphorylation, respectively. Thus, the present findings provide significant fundamental knowledge for physiological, nutraceutical, and medical scientists to gain more insight into Ca^{2+} homeostasis in the reproductive periods and for further development of Ca^{2+}-fortified diet to help alleviate negative Ca^{2+} balance. The finding that suckling-induced PRL surge considerably increases the efficiency of intestinal Ca^{2+} absorption may provide direction for health policy. For example, Ca^{2+} supplementation at 15–30 min prior to breastfeeding may best benefit fetal and maternal Ca^{2+} metabolism while reducing the incidence of pregnancy-induced osteoporosis.

ACKNOWLEDGMENTS

We thank Dr. Kannikar Wongdee and Jirawan Thongbunchoo for excellent technical assistance.

GRANTS

This research was supported by grants from the Mahidol University Postdoctoral Fellowship Program (to L. Nakkrasae), the Faculty of Science, Mahidol University (SCY52-02 and SCR52-01 to N. Charoenphandhu), the Royal Golden Jubilee Ph.D Program (PHD/0042/2551 to J. Teerapornpuntakit), and the Thailand Research Fund (RSA5180001 to N. Charoenphandhu).

REFERENCES

1. **Angelow S, Kim KJ, Yu AS.** Claudin-8 modulates paracellular permeability to acidic and basic ions in MDCK II cells. *J Physiol* 571: 15–26, 2006.
2. **Banan A, Zhang LJ, Shaikh M, Fields JZ, Choudhary S, Forsyth CB, Farhadi A, Keshavarzian A.** theta Isoform of protein kinase C alters barrier function in intestinal epithelium through modulation of distinct claudin isotypes: a novel mechanism for regulation of permeability. *J Pharmacol Exp Ther* 313: 962–982, 2005.

3. **Benn BS, Ajibade D, Porta A, Dhawan P, Hediger M, Peng JB, Jiang Y, Oh GT, Jeung EB, Lieben L, Bouillon R, Carmeliet G, Christakos S.** Active intestinal calcium transport in the absence of transient receptor potential vanilloid type 6 and calbindin-D_{9k}. *Endocrinology* 149: 3196–3205, 2008.
4. **Bindels RJ, Timmermans JA, Hartog A, Coers W, van Os CH.** Calbindin-D_{9k} and parvalbumin are exclusively located along basolateral membranes in rat distal nephron. *J Am Soc Nephrol* 2: 1122–1129, 1991.
5. **Bruns ME, Vollmer SS, Bruns DE, Overpeck JG.** Human growth hormone increases intestinal vitamin D-dependent calcium-binding protein in hypophysectomized rats. *Endocrinology* 113: 1387–1392, 1983.
6. **Carr G, Haslam IS, Simmons NL.** Voltage dependence of transepithelial guanidine permeation across Caco-2 epithelia allows determination of the paracellular flux component. *Pharm Res* 23: 540–548, 2006.
7. **Charoenphandhu N, Krishnamra N.** Prolactin is an important regulator of intestinal calcium transport. *Can J Physiol Pharmacol* 85: 569–581, 2007.
8. **Charoenphandhu N, Limlomwongse L, Krishnamra N.** Prolactin directly enhanced Na^+/K^+- and Ca^{2+}-ATPase activities in the duodenum of female rats. *Can J Physiol Pharmacol* 84: 555–563, 2006.
9. **Charoenphandhu N, Tudpor K, Pulsook N, Krishnamra N.** Chronic metabolic acidosis stimulated transcellular and solvent drag-induced calcium transport in the duodenum of female rats. *Am J Physiol Gastrointest Liver Physiol* 291: G446–G455, 2006.
10. **Charoenphandhu N, Wongdee K, Teerapornpuntakit J, Thongchote K, Krishnamra N.** Transcriptome responses of duodenal epithelial cells to prolactin in pituitary-grafted rats. *Mol Cell Endocrinol* 296: 41–52, 2008.
11. **D'Souza T, Indig FE, Morin PJ.** Phosphorylation of claudin-4 by PKC_ε regulates tight junction barrier function in ovarian cancer cells. *Exp Cell Res* 313: 3364–3375, 2007.
12. **Dunne F, Walters B, Marshall T, Heath DA.** Pregnancy associated osteoporosis. *Clin Endocrinol (Oxf)* 39: 487–490, 1993.
13. **Fischer S, Wobben M, Marti HH, Renz D, Schaper W.** Hypoxia-induced hyperpermeability in brain microvessel endothelial cells involves VEGF-mediated changes in the expression of zonula occludens-1. *Microvasc Res* 63: 70–80, 2002.
14. **Fleet JC.** Molecular regulation of calcium metabolism. In: *Calcium in Human Health*, edited by Weaver CM and Heaney RP. Totowa, NJ: Humana, 2006, p. 163–189.
15. **Fujita H, Sugimoto K, Inatomi S, Maeda T, Osanai M, Uchiyama Y, Yamamoto Y, Wada T, Kojima T, Yokozaki H, Yamashita T, Kato S, Sawada N, Chiba H.** Tight junction proteins claudin-2 and -12 are critical for vitamin D-dependent Ca^{2+} absorption between enterocytes. *Mol Biol Cell* 19: 1912–1921, 2008.
16. **Halloran BP, DeLuca HF.** Calcium transport in small intestine during pregnancy and lactation. *Am J Physiol Endocrinol Metab* 239: E64–E68, 1980.
17. **Hirsch E, Costa C, Ciraolo E.** Phosphoinositide 3-kinases as a common platform for multi-hormone signaling. *J Endocrinol* 194: 243–256, 2007.
18. **Hoenderop JG, Nilius B, Bindels RJ.** Calcium absorption across epithelia. *Physiol Rev* 85: 373–422, 2005.
19. **Ikari A, Ito M, Okude C, Sawada H, Harada H, Degawa M, Sakai H, Takahashi T, Sugatani J, Miwa M.** Claudin-16 is directly phosphorylated by protein kinase A independently of a vasodilator-stimulated phosphoprotein-mediated pathway. *J Cell Physiol* 214: 221–229, 2008.
20. **Jantarajit W, Thongon N, Pandaranandaka J, Teerapornpuntakit J, Krishnamra N, Charoenphandhu N.** Prolactin-stimulated transepithelial calcium transport in duodenum and Caco-2 monolayer are mediated by the phosphoinositide 3-kinase pathway. *Am J Physiol Endocrinol Metab* 293: E372–E384, 2007.
21. **Kaminska B, Ciereszko RE, Opalka M, Dusza L.** Prolactin signaling in porcine adrenocortical cells: involvement of protein kinases. *Domest Anim Endocrinol* 23: 475–491, 2002.
22. **Khanal RC, Nemere I.** Endocrine regulation of calcium transport in epithelia. *Clin Exp Pharmacol Physiol* 35: 1277–1287, 2008.
23. **Kutuzova GD, DeLuca HF.** Gene expression profiles in rat intestine identify pathways for 1,25-dihydroxyvitamin D_3 stimulated calcium absorption and clarify its immunomodulatory properties. *Arch Biochem Biophys* 432: 152–166, 2004.
24. **Lee SH, Kunz J, Lin SH, Yu-Lee LY.** 16-kDa prolactin inhibits endothelial cell migration by down-regulating the Ras-Tiam1-Rac1-Pak1 signaling pathway. *Cancer Res* 67: 11045–11053, 2007.
25. **Neville MC, Morton J.** Physiology and endocrine changes underlying human lactogenesis II. *J Nutr* 131: 3005S–3008S, 2001.
26. **Pahuja DN, DeLuca HF.** Stimulation of intestinal calcium transport and bone calcium mobilization by prolactin in vitamin D-deficient rats. *Science* 214: 1038–1039, 1981.
27. **Peng TC, Garner SC, Kusy RP, Hirsch PF.** Effect of number of suckling pups and dietary calcium on bone mineral content and mechanical properties of femurs of lactating rats. *Bone Miner* 3: 293–304, 1988.
28. **Piyabhan P, Krishnamra N, Limlomwongse L.** Changes in the regulation of calcium metabolism and bone calcium content during growth in the absence of endogenous prolactin and during hyperprolactinemia: a longitudinal study in male and female Wistar rats. *Can J Physiol Pharmacol* 78: 757–765, 2000.
29. **Prentice A.** Calcium in pregnancy and lactation. *Annu Rev Nutr* 20: 249–272, 2000.
30. **Sabour H, Hossein-Nezhad A, Maghbooli Z, Madani F, Mir E, Larijani B.** Relationship between pregnancy outcomes and maternal vitamin D and calcium intake: A cross-sectional study. *Gynecol Endocrinol* 22: 585–589, 2006.
31. **Stamatovic SM, Dimitrijevic OB, Keep RF, Andjelkovic AV.** Protein kinase C_α-RhoA cross-talk in CCL2-induced alterations in brain endothelial permeability. *J Biol Chem* 281: 8379–8388, 2006.
32. **Taffetani S, Glaser S, Francis H, DeMorrow S, Ueno Y, Alvaro D, Marucci L, Marzioni M, Fava G, Venter J, Vaculin S, Vaculin B, Lam IP, Lee VH, Gaudio E, Carpino G, Benedetti A, Alpini G.** Prolactin stimulates the proliferation of normal female cholangiocytes by differential regulation of Ca^{2+}-dependent PKC isoforms. *BMC Physiol* 7: 6, 2007.
33. **Tamura A, Kitano Y, Hata M, Katsuno T, Moriwaki K, Sasaki H, Hayashi H, Suzuki Y, Noda T, Furuse M, Tsukita S.** Megaintestine in claudin-15-deficient mice. *Gastroenterology* 134: 523–534, 2008.
34. **Thongon N, Nakkrasae LI, Thongbunchoo J, Krishnamra N, Charoenphandhu N.** Prolactin stimulates transepithelial calcium transport and modulates paracellular permselectivity in Caco-2 monolayer: mediation by PKC and ROCK pathways. *Am J Physiol Cell Physiol* 294: C1158–C1168, 2008.
35. **Thongon N, Nakkrasae LI, Thongbunchoo J, Krishnamra N, Charoenphandhu N.** Enhancement of calcium transport in Caco-2 monolayer through PKCζ-dependent $Ca_v1.3$-mediated transcellular and rectifying paracellular pathways by prolactin. *Am J Physiol Cell Physiol* 296: C1373–C1382, 2009.
36. **Tudpor K, Charoenphandhu N, Saengamnart W, Krishnamra N.** Long-term prolactin exposure differentially stimulated the transcellular and solvent drag-induced calcium transport in the duodenum of ovariectomized rats. *Exp Biol Med (Maywood)* 230: 836–844, 2005.
37. **van Cromphaut SJ, Rummens K, Stockmans I, van Herck E, Dijcks FA, Ederveen AG, Carmeliet P, Verhaeghe J, Bouillon R, Carmeliet G.** Intestinal calcium transporter genes are upregulated by estrogens and the reproductive cycle through vitamin D receptor-independent mechanisms. *J Bone Miner Res* 18: 1725–1736, 2003.
38. **Van Itallie CM, Anderson JM.** Claudins and epithelial paracellular transport. *Annu Rev Physiol* 68: 403–429, 2006.
39. **Van Itallie CM, Fanning AS, Anderson JM.** Reversal of charge selectivity in cation or anion-selective epithelial lines by expression of different claudins. *Am J Physiol Renal Physiol* 285: F1078–F1084, 2003.
40. **Van Itallie CM, Rogan S, Yu A, Vidal LS, Holmes J, Anderson JM.** Two splice variants of claudin-10 in the kidney create paracellular pores with different ion selectivities. *Am J Physiol Renal Physiol* 291: F1288–F1299, 2006.
41. **Wang W, Dentler WL, Borchardt RT.** VEGF increases BMEC monolayer permeability by affecting occludin expression and tight junction assembly. *Am J Physiol Heart Circ Physiol* 280: H434–H440, 2001.
42. **Wasserman RH.** Vitamin D and the dual processes of intestinal calcium absorption. *J Nutr* 134: 3137–3139, 2004.
43. **Xie J, LeBaron MJ, Nevalainen MT, Rui H.** Role of tyrosine kinase Jak2 in prolactin-induced differentiation and growth of mammary epithelial cells. *J Biol Chem* 277: 14020–14030, 2002.
44. **Yee S.** In vitro permeability across Caco-2 cells (colonic) can predict in vivo (small intestinal) absorption in man—fact or myth. *Pharm Res* 14: 763–766, 1997.
45. **Zweibaum A, Triadou N, Kedinger M, Augeron C, Robine-Leon S, Pinto M, Rousset M, Haffen K.** Sucrase-isomaltase: a marker of foetal and malignant epithelial cells of the human colon. *Int J Cancer* 32: 407–412, 1983.

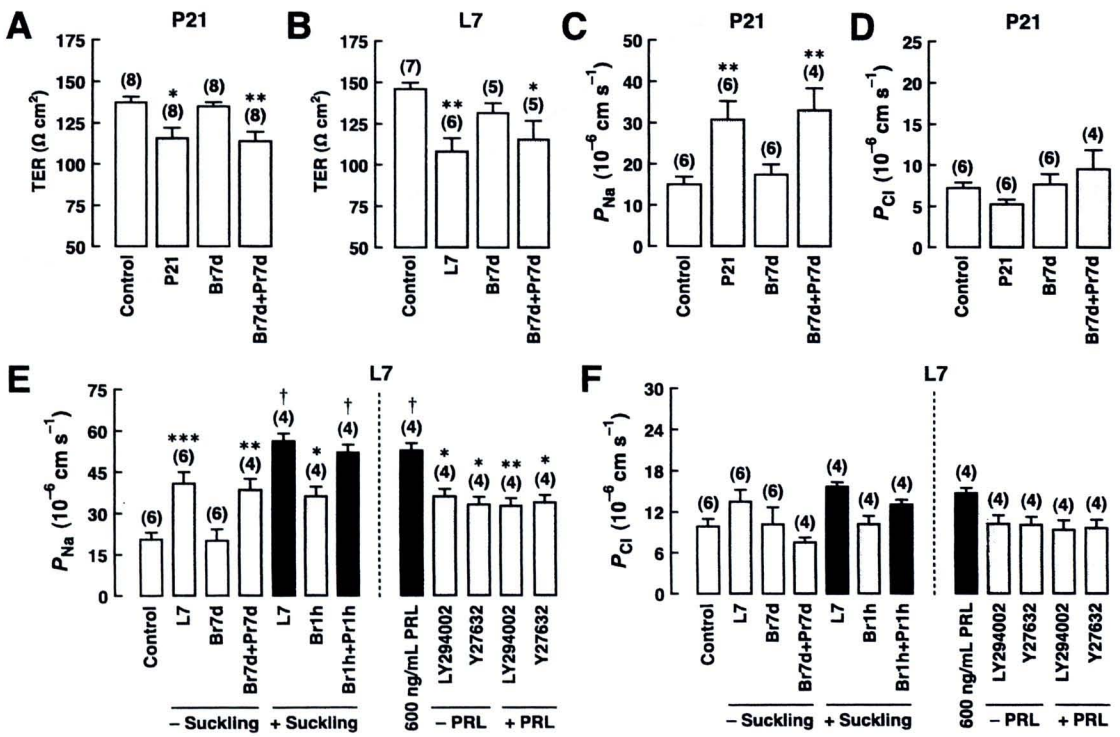

Figure S1: Charoenphandhu et al.

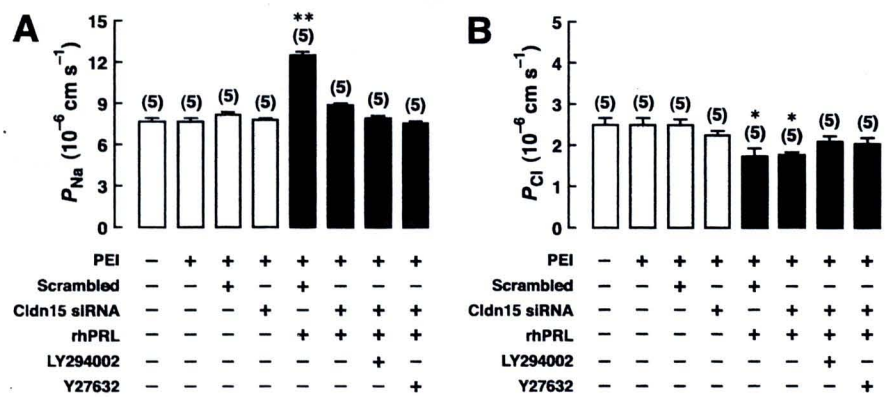

Figure S2: Charoenphandhu et al.

Legends to supplemental figures

Figure S1. (*A–B*) Transepithelial resistance (TER) in the duodenum of P21 and L7 rats. (*C–F*) P_{Na} and P_{Cl} in the duodenum of P21, L7 and suckling rats. Rats were administered with Br7d or Br1h to suppress chronic PRL secretion (with or without Pr7d supplementation) and suckling-induced PRL surge (with or without Pr1h supplementation), respectively. PRL signalings were investigated by exposing 600 ng/mL PRL-treated L7 duodenal tissues to various inhibitors. * $P < 0.05$, ** $P < 0.01$, *** $P < 0.001$ compared with control group. † $P < 0.05$ compared with L7 without suckling. Numbers in parentheses represent the number of rats.

Figure S2. (*A–B*) P_{Na} and P_{Cl} in claudin-15 siRNA-treated Caco-2 monolayers directly exposed to 600 ng/mL rhPRL. In some experiments, claudin-15 knockdown monolayers were also incubated with rhPRL plus 75 μmol/L LY294002 or 1 μmol/L Y27632. * $P < 0.05$, ** $P < 0.01$ compared with control (white column). Numbers in parentheses represent the number of independent Snapwells.

Pflugers Arch - Eur J Physiol (2009) 458:993–1005
DOI 10.1007/s00424-009-0679-6

TRANSPORT PHYSIOLOGY

Direct stimulation of the transcellular and paracellular calcium transport in the rat cecum by prolactin

Kamonshanok Kraidith · Walailuk Jantarajit · Jarinthorn Teerapornpuntakit · La-iad Nakkrasae · Nateetip Krishnamra · Narattaphol Charoenphandhu

Received: 12 January 2009 / Revised: 5 April 2009 / Accepted: 28 April 2009 / Published online: 17 May 2009

Abstract Prolactin (PRL) is reported to stimulate calcium absorption in the rat's small intestine. However, little is known regarding its effects on the cecum, a part of the large intestine with the highest rate of intestinal calcium transport. We demonstrated herein by quantitative real-time polymerase chain reaction and Western blot analysis that the cecum could be a target organ of PRL since cecal epithelial cells strongly expressed PRL receptors. In Ussing chamber experiments, PRL enhanced the transcellular cecal calcium absorption in a biphasic dose–response manner. PRL also increased the paracellular calcium permeability and passive calcium transport in the cecum, which could be explained by the PRL-induced decrease in transepithelial resistance and increase in cation selectivity of the cecal epithelium. PRL actions in the cecum were abolished by inhibitors of phosphoinositide 3-kinase (PI3K), protein kinase C (PKC), and RhoA-associated coiled-coil forming kinase (ROCK), but not inhibitors of gene transcription and protein biosynthesis. In conclusion, PRL directly enhanced the transcellular and paracellular calcium transport in the rat cecum through the nongenomic signaling pathways involving PI3K, PKC, and ROCK.

Keywords Calcium absorption · Dilution potential · Paracellular transport · Prolactin receptor · Transcellular transport · Ussing chamber

Introduction

During pregnancy and lactation, prolactin (PRL) serves as a calcium-regulating hormone which markedly stimulates intestinal calcium absorption to help alleviate negative calcium balance due to massive calcium loss for fetal growth and milk production [5]. The PRL-enhanced calcium absorption has been intensively investigated in the small intestine [6, 25], especially in the duodenum, where the transcellular active calcium transport is prominent [11, 29]. However, the effects of PRL on the large intestine as well as its mechanisms were largely unknown.

It is widely known that, in monogastric herbivores, rats and humans, the cecum is for absorption of fluids and salts and is the site for luminal microfloral production of short-chain fatty acids, folate, and vitamin K [16, 32, 33]. Studies on the intestinal calcium absorption demonstrated that, besides the duodenum, the proximal part of the large intestine, particularly the cecum, is another important site for the transcellular active calcium transport [40]. Moreover, experiments in rats showed that when compared to other intestinal segments, cecum has the highest rate of calcium transport [28, 39]. Under normal conditions, it was suggested that the cecal epithelium absorbs a significant amount of free calcium which is released during microbial fermentation of the cecal contents through production of short-chain fatty acids and other acidic molecules, such as lactic acid, butyric acid, and

Electronic supplementary material The online version of this article (doi:10.1007/s00424-009-0679-6) contains supplementary material, which is available to authorized users.

K. Kraidith · N. Krishnamra · N. Charoenphandhu (✉)
Department of Physiology, Faculty of Science,
Mahidol University,
Rama VI Road,
Bangkok 10400, Thailand
e-mail: naratt@narattsys.com

W. Jantarajit · J. Teerapornpuntakit · L.-i. Nakkrasae · N. Krishnamra · N. Charoenphandhu
Consortium for Calcium and Bone Research (COCAB),
Faculty of Science, Mahidol University,
Bangkok, Thailand

succinic acid, as well as calcium released from the degradation of dietary fiber [10, 36]. Accumulation of free calcium in the cecal lumen may also be enough to increase the paracellular passive calcium transport [28]. Since PRL plays an important role in supplying additional calcium to the body, we postulated that it may increase the cecal calcium absorption via both transcellular and paracellular routes as seen in the small intestine [5].

Generally, the transcellular calcium transport is a three-step metabolically energized process, consisting of the apical uptake via the transient receptor potential vanilloid family calcium channel 5 and 6 (TRPV5/6) and L-type calcium channel $Ca_v1.3$, cytoplasmic translocation in a calbindin-D_{9k}-bound form, and the basolateral extrusion via the plasma membrane Ca^{2+}-ATPase 1b ($PMCA_{1b}$) and Na^+/Ca^{2+} exchanger 1 (NCX1) [20, 30, 49]. In contrast, the paracellular passive calcium transport is dependent on the transepithelial calcium gradient and is absent when both sides of the epithelium have equal calcium concentration [29]. Paracellular calcium movement is regulated by the tight junction, which contains several charge-selective proteins, particularly claudin-2, claudin-3, and claudin-12, arranged in the arrays of channel-like paracellular pores [14, 30]. Besides, the integrity of the tight junction is regulated by tight junction proteins, such as zonula occludens-1 (ZO-1) and occludin [50].

It is apparent that the paracellular calcium transport is predominant in the small intestine [10, 29]. However, when calcium demand is markedly increased, such as during pregnancy and lactation, contribution from the transcellular transport component to the total calcium absorption becomes more significant, in part, as a result of the stimulatory action of PRL [3, 5]. Recently, we demonstrated in the duodenum and Caco-2 monolayer that PRL enhanced both transcellular active and paracellular passive calcium transport through the phosphoinositide 3-kinase (PI3K), protein kinase C (PKC), and RhoA-associated coiled-coil forming kinase (ROCK) pathways [25, 48, 49]. However, PRL signaling in the large intestine, including the cecum, had never been investigated.

Therefore, the objectives of the present study were (a) to demonstrate that the cecum was a target organ of PRL, (b) to investigate the effects of PRL on the cecal calcium transport, and (c) to investigate the mechanisms of the PRL-enhanced calcium absorption in the cecum.

Materials and methods

Animals

Female Sprague–Dawley rats (8 weeks old, weighing 180–200 g) were obtained from the National Laboratory Animal Centre, Thailand. They were placed in hanging stainless steel cages, fed with standard pellets containing 1% wt/wt calcium and 100 IU vitamin D per 100 g of diet (Perfect Companion, Bangkok, Thailand), and provided with distilled water ad libitum under 12:12 h light/dark cycle. The room had temperature of 20–25°C, humidity of 50–60%, and average illuminance of 150–200 lux in the daytime. Body weight and food intake were recorded daily. This study has been approved by the Institutional Animal Care and Use Committee of the Faculty of Science, Mahidol University, Bangkok, Thailand.

Tissue preparation

After 7-day acclimatization, the rat was anesthetized by administering 50 mg/kg sodium pentobarbitone i.p. (Abbott, North Chicago, IL, USA). Thereafter, median laparotomy was performed. Duodenum (10 cm), proximal and distal jejunum (10 cm each), ileum (8 cm), cecum (4 cm), and proximal and distal colon (8 cm each) were removed and cut longitudinally to expose the mucosa. In the calcium transport experiments, the muscularis proper was stripped off before the tissue was mounted in a modified Ussing chamber as described previously [25]. The tissue was incubated for 20 min in the chamber before the 60-min experiment was carried out. As for the mRNA and protein expression studies, epithelial cells were collected by scraping the mucosal surface with an ice-cold glass slide [8].

Total RNA preparation and cDNA synthesis

Total RNA was extracted from mucosal scrapings by using TRIzol reagent (Invitrogen, Carlsbad, CA, USA) and purified with RNeasy Mini kit (Qiagen, Valencia, CA, USA). Purity and integrity of RNA were determined by 260/280 nm absorbance and denaturing agarose gel electrophoresis, respectively [8]. One microgram of the total RNA was then reverse-transcribed to cDNA with the oligo-dT_{20} primer and the iScript kit (Bio-Rad, Hercules, CA, USA). Glyceraldehyde-3-phosphate dehydrogenase (GAPDH), a housekeeping gene, served as a control gene to check the consistency of the reverse transcription.

Quantitative real-time PCR and sequencing

Primers used in this study were shown in Table 1. Quantitative real-time polymerase chain reaction (qRT-PCR) and melting curve analysis were performed by the Bio-rad MiniOpticon with the iQ SYBR Green SuperMix (Bio-rad) as previously described [8]. Relative expression of PRL receptor (PRLR) over GAPDH was calculated from the threshold cycle (C_t) values by using $2^{-\Delta C_t}$ method. The

Table 1 *Rattus norvegicus* oligonucleotide sequences used in qRT-PCR experiments

Name	Accession no.	Primer (forward/reverse)	Product length (bp)
Prolactin receptors			
PRLR-S	NM_012630	5′-TTCTACCACCATCGCAAC-3′ 5′-CTGATCTCGTTTGTCATTGAG-3′	120
PRLR-L	NM_001034111	5′-TCAAGCAACCGCAGACTC-3′ 5′-CAGTTTAGCCAATCGTTCCA-3′	107
Transcellular genes			
TRPV5	NM_053787	5′-CTTACGGGTTGAACACCACCA-3′ 5′-TTGCAGAACCACAGAGCCTCTA-3′	163
TRPV6	NM_053686	5′-ATCCGCCGCTATGCAC-3′ 5′-AGTTTTTCTGGTCACTGTTTTTGG-3′	80
$Ca_v1.3$	NM_017298	5′-TCAGCGTCAGTGTGTGGAATA-3′ 5′-CGAAAGGCGAGGAGTTCAC-3′	110
Calbindin-D_{9k}	X_16635	5′-CCCGAAGAAATGAAGAGCATTTT-3′ 5′-TTCTCCATCACCGTTCTTATCCA-3′	174
$PMCA_{1b}$	NM_053311	5′-CGCCATCTTCTGCACAATT-3′ 5′-CAGCCATTGTTCTATTGAAAGTTC-3′	109
NCX1	NM_019268	5′-GTTGTGTTCGCTTGGGTTGC-3′ 5′-CGTGGGAGTTGACTACTTTC-3′	163
Paracellular genes			
Claudin-2	NM_001106846	5′-GCTGCTGAGGGTAGAATGA-3′ 5′-GCTCGCTTGATAAGTGTCC-3′	107
Claudin-3	NM_031700	5′-GCACCCACCAAGATCCTCTA-3′ 5′-AGGCTGTCTGTCCTCTTCCA-3′	246
Claudin-12	XM_001067932	5′-CCTTCAAGTCTTCGGTGCC-3′ 5′-CAGGAGGATGGGAGTACAG-3′	312
ZO-1	XM_218747	5′-GTATCCGATTGTTGTGTTCC-3′ 5′-TCACTTGTAGCACCATCCGC-3′	270
Occludin	NM_031329	5′-CACGTTCGACCAATGC-3′ 5′-CCCGTTCCATAGGCTC-3′	188
Housekeeping gene			
GAPDH	NM_017008	5′-AGTCTACTGGCGTCTTCAC-3′ 5′-TCATATTTCTCGTGGTTCAC-3′	133

PRLR-S short isoform of prolactin receptor, *PRLR-L* long isoform of prolactin receptor, *TRPV5* transient receptor potential vanilloid family Ca^{2+} channel 5, *TRPV6* transient receptor potential vanilloid family Ca^{2+} channel 6, *$Ca_v1.3$* voltage-dependent L-type Ca^{2+} channel 1.3, *$PMCA_{1b}$* plasma membrane Ca^{2+}-ATPase isoform 1b, *NCX1* Na^+/Ca^{2+} exchanger 1, *ZO-1* zonula occludens-1, *GAPDH* glyceraldehyde-3-phosphate dehydrogenase

PCR products were also visualized on a 1.5% agarose gel stained with 1.0 μg/mL ethidium bromide under a UV transilluminator (Alpha Innotech, San Leandro, CA, USA). After electrophoresis, all PCR products were purified from a gel by the HiYield Gel/PCR DNA Extraction kit (Real Biotech Corporation, Taipei, Taiwan) and sequenced by the ABI Prism 3100 Genetic Analyzer (Applied Biosystems, Foster City, CA, USA).

Western blot analysis

As previously described [25], scraped mucosal cells were lysed in lysis buffer (0.5 mmol/L Tris pH 7.5, 1.5 mol/L NaCl, 10% NP-40, 5% DOC, 10 mmol/L Na ethylenediaminetetraacetic acid, 1 mmol/L phenylmethylsulfonyl fluoride, 1 μg/mL leupeptin, 1 μg/mL aprotinin, 1 μg/mL pepstatin A; all purchased from Sigma, St. Louis, MO, USA). Lysates were sonicated at 4°C and centrifuged at 20,000×*g* for 10 min. One hundred micrograms proteins were separated by sodium dodecyl sulfate polyacrylamide gel electrophoresis and transferred to a nitrocellulose membrane (Amersham, Buckinghamshire, UK) by electroblotting. Membranes were blocked at 25°C for 4 h with 5% nonfat milk and were probed overnight at 4°C with 1:500 rabbit antirat PRLR polyclonal antibodies (catalog no. sc-30225; Santa Cruz Biotechnology, Santa Cruz, CA, USA) raised against the conserved extracellular domain. Membranes were later reprobed with 1:5,000 mouse antirat β-actin monoclonal antibodies (catalog no. sc-47778; Santa Cruz). After 2-h incubation at 25°C with 1:20,000 goat antirabbit (catalog no. sc-2004) or antimouse (catalog no. sc-2005) secondary antibodies (Santa Cruz), blots were visualized by enhanced chemiluminescence kit (Amersham).

Bathing solution for Ussing chamber study

The bathing solution continuously gassed with humidified 5% CO_2 in 95% O_2, contained (in mmol/L) 118 NaCl, 4.7 KCl, 1.1 $MgCl_2$, 1.25 $CaCl_2$, 23 $NaHCO_3$, 12 D-glucose, and 2 mannitol (all purchased from Sigma). The solution

was maintained at 37°C, pH 7.4, and had an osmolality of 290–293 mmol kg^{-1} water as measured by a freezing point-based osmometer (model 3320; Advanced Instruments, Norwood, MA, USA).

Measurement of epithelial electrical parameters

Three electrical parameters, i.e., potential difference (PD), short-circuit current (Isc), and transepithelial resistance (TER), were determined according to the method of Charoenphandhu et al. [6]. In brief, a pair of Ag/AgCl electrodes connected to agar bridges was placed near each surface of the mounted tissue for PD measurement. The other ends of the PD-sensing electrodes were connected to the EVC-4000 pre-amplifier (World Precision Instruments, Sarasota, FL, USA) and finally to a PowerLab 4/30 operated with the software Chart 5.2.2 for Mac OS X (ADInstruments, Colorado Springs, CO, USA). Another pair of Ag/AgCl electrodes was placed at the end of each hemichamber to supply external current, which was also measured by a PowerLab 4/30 connected in series to the EVC-4000 current-generating unit. TER and conductance (G; G=1/TER) were calculated by Ohm's equation. Fluid resistance was automatically subtracted by the EVC-4000 system. In some experiments, Isc was continuously applied to nullify PD, i.e., the experiments were performed under short-circuit condition. Unless otherwise specified, the experiments were normally performed under open-circuit condition since the absence of PD did not significantly affect calcium flux (Supplemental Figure S1). In other words, the voltage-dependent calcium transport in the cecum could be considered negligible, similar to that observed in the duodenum [6].

Measurement of calcium flux

Transepithelial calcium flux was determined by the method of Charoenphandhu et al. [6]. In brief, after 20-min incubation, Ussing chamber was filled on one side with $^{45}CaCl_2$-containing bathing solution (specific activity of 500 mCi/mol; Amersham). Unidirectional flux ($J_{H\rightarrow C}$) from the hot side (H) to the cold side (C) was calculated with Eqs. 1 and 2.

$$J_{H\rightarrow C} = R_{H\rightarrow C}/(S_H \times A) \quad (1)$$

$$S_H = C_H/C_T \quad (2)$$

where $R_{H\rightarrow C}$ was the rate of tracer appearance in the cold side (counts per minute per hour), S_H was the specific activity in the hot side (counts per minute per nanomole) and did not vary with time (a constant value), A was the surface area of the tissue (0.69 cm^2), C_H was the radioactivity in the hot side (counts per minute), and C_T was the total calcium in the hot side (nanomole). Radioactivity of ^{45}Ca in counts per minute was analyzed by liquid scintillation spectrophotometry (model Tri-Carb 3100; Packard Instruments, Meriden, CT, USA). Total calcium concentration in the hot side was determined by atomic absorption spectrophotometry (model SpectrAA-300; Varian Techtron, Springvale, Australia).

Calcium fluxes in the absence of transepithelial calcium gradient, i.e., bathing solution in both hemichambers containing equal calcium concentration, represented the active calcium transport [6]. The calcium gradient-dependent paracellular passive fluxes were measured by determining the calcium fluxes in the presence of varying apical calcium concentrations [48], i.e., 1.25, 2.5, 5, 10, and 20 mmol/L (n=4 per each concentration).

Unless otherwise specified, the measured calcium fluxes represented calcium transport in mucosa-to-serosa direction. The serosa-to-mucosa calcium flux in the cecum was relatively small and had no significant influence on the net calcium transport (Supplemental Figure S2). In addition, PRL did not enhance calcium transport in serosa-to-mucosa direction (Supplemental Figure S2).

Determination of the epithelial permeability and Na^+/Cl^- selectivity

Permeability of sodium (P_{Na}) and chloride (P_{Cl}) which are indicative of the epithelial charge selectivity were measured by the dilution potential technique [21, 26]. The mounted cecum was equilibrated for 20 min in bathing solution containing 145 mmol/L NaCl before the apical solution was replaced with 72.5 mmol/L NaCl-containing solution. Osmolality of the solution was maintained by an equivalent amount of mannitol. Changes in the electrical parameters before and after fluid replacement were continuously recorded by PowerLab 4/30 until stable. The ion permeability ratio (P_{Na}/P_{Cl}) was calculated from the dilution potential (V_δ) using the modified Goldman–Hodgkin–Katz equation (Eq. 3).

$$\rho = (\phi - e^{\nu})/(\phi e^{\nu} - 1) \quad (3)$$

where ρ=P_{Na}/P_{Cl}; ϕ=C_b/C_a; ν=FV_δ/RT; P_{Na} was the absolute permeability of sodium; P_{Cl} was the absolute permeability of chloride; C_a was the mucosal NaCl concentration; C_b was the serosal NaCl concentration; and R, T, and F had their conventional meanings.

Thereafter, P_{Na} and P_{Cl} were calculated from the conductance (G) and P_{Na}/P_{Cl} using Kimizuka–Koketsu equations [31], as follows:

$$P_{Na} = \frac{GRT}{C_a F^2} \times \frac{\rho}{1+\rho} \quad (4)$$

$$P_{Cl} = P_{Na}/\rho \quad (5)$$

The paracellular calcium permeability (P_{Ca}) was calculated from Eq. 6 [48].

$$P_{Ca} = J_{Ca}/\Delta C \tag{6}$$

where J_{Ca} was the paracellular passive calcium flux and ΔC was the difference between the apical and basolateral calcium concentrations.

Experimental protocol

To demonstrate the effects of PRL on calcium transport, electrical parameters, and epithelial permeability, the mounted cecal tissue was directly exposed on the serosal side to 200, 400, 600, 800, or 1,000 ng/mL PRL (catalog no. L6520; Sigma) during the 80-min experiment. In some experiments, the most efficient dose of PRL (i.e., 800 ng/mL) plus RNA polymerase II inhibitor (50 μmol/L 5,6-dichloro-1-β-D-ribofuranosylbenzimidazole (DRB); Calbiochem, San Diego, CA, USA), protein synthesis inhibitor (70 μmol/L cycloheximide (CCH); Sigma), Janus kinase (JAK) 2 inhibitor (50 μmol/L AG490; Calbiochem), PI3K inhibitors (75 μmol/L LY294002 or 200 nmol/L wortmannin; Tocris Bioscience, Bristol, UK), pan-specific PKC inhibitor (1 μmol/L GF109203X; A.G. Scientific, San Diego, CA, USA), selective ROCK inhibitor (1 μmol/L Y27632; Calbiochem), or myristoylated protein kinase A inhibitor 14–22 amide (10 μmol/L PKAI 14–22; Calbiochem) were added to the serosal solution to identify possible PRL signaling pathways. Wortmannin was more potent but less specific than LY294002 [18, 23]. PKAI 14–22 was first dissolved in distilled water, while other inhibitors were dissolved in DMSO (Sigma). Concentration of dimethyl sulfoxide (DMSO) in the bathing solution was 0.3% vol/vol, which did not affect the viability of cells [6]. To verify that PRL was able to stimulate the transcellular calcium transport, the cecal tissue was directly exposed to inhibitors of apical calcium uptake (50 μmol/L ruthenium red; Sigma) or calmodulin-dependent PMCA (100 μmol/L trifluoperazine; TFP; Sigma). Polyclonal antibody against PRLR (1 μg/mL; catalog no. sc-30225; Santa Cruz) was directly

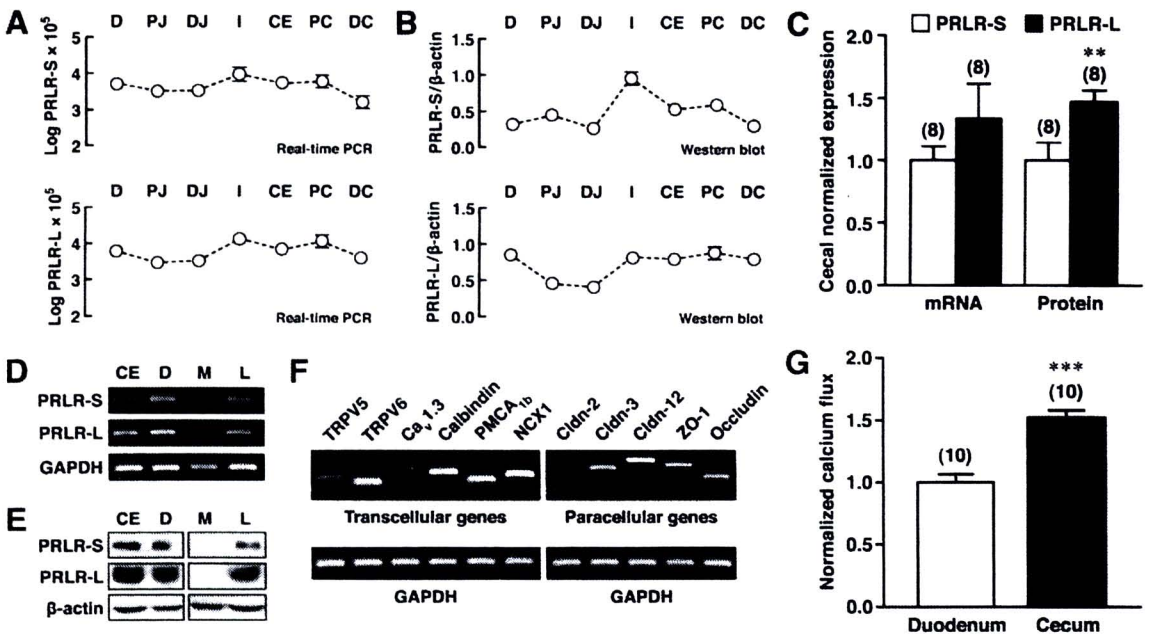

Fig. 1 **a**, **b** Expression of short (-S) and long (-L) isoforms of PRLRs in the duodenum (*D*), proximal (*PJ*) and distal jejunum (*DJ*), ileum (*I*), cecum (*CE*), and proximal (*PC*) and distal colon (*DC*) as demonstrated by qRT-PCR (**a**; $n=8$ per segment) and Western blot analysis (**b**; $n=8$ per segment). qRT-PCR data expressed as log means ± SE were normalized by GAPDH expression, while PRLR protein expression was normalized by β-actin expression. **c** Normalized expression of PRLR-S and PRLR-L in the cecum of female rats. PRLR-L expression appears as fold difference from PRLR-S expression, while setting PRLR-S expression as 1. $^{**}p<0.01$ PRLR-S expression vs. PRLR-L expression. **d** Representative electrophoretic bands of PRLR-S and PRLR-L mRNAs in duodenum (*D*) and cecum (*CE*). Gastrocnemius muscle (*M*) and liver (*L*) were used as negative and positive controls, respectively. **e** Representative bands of PRLR-S and PRLR-L proteins in duodenum (*D*) and cecum (*CE*). Gastrocnemius muscle (*M*) and liver (*L*) were negative and positive controls, respectively. **f** Electrophoretic bands of genes related to the transcellular and paracellular calcium transport in the cecum ($n=10$). GAPDH was used as a housekeeping gene. **g** Normalized transepithelial calcium fluxes in the duodenum and cecum as determined by Ussing chamber technique. Calcium concentration on both sides was 1.25 mmol/L. $^{***}p<0.001$ cecal flux vs. duodenal flux. *Numbers in parentheses* (**c** and **g**) represent the number of experimental animals

added in bathing solution to confirm that PRLR mediated PRL actions.

Statistical analysis

Results are expressed as means ± standard error (SE). Two sets of data were compared by using the unpaired Student's *t* test. Multiple comparisons were performed by one-way analysis of variance with Dunnett's multiple comparison test. Linear regression was used to demonstrate the relationships between mucosal calcium and paracellular calcium flux, and mucosal calcium and TER. The level of significance for all statistical tests was $p<0.05$. All data were analyzed by GraphPad Prism 4.0 for Mac OS X (GraphPad Software, San Diego, CA, USA).

Results

Cecal epithelial cells expressed PRLRs and essential calcium transporters

As shown in Fig. 1a, b, both short (-S) and long (-L) isoforms of PRLR mRNAs and proteins were expressed in the duodenum, proximal and distal jejunum, ileum, cecum, and proximal and distal colon of rats. In the cecum (Fig. 1c–e), PRLR-L was more abundant than PRLR-S. Although calcium absorption has been demonstrated in cecum [28], the expression of calcium transport genes has not been completely investigated in cecal epithelial cells. Therefore, we used PCR to show that cecal cells strongly expressed all essential genes required for the transcellular calcium transport, i.e., TRPV5, TRPV6, $Ca_v1.3$, calbindin-D_{9k}, $PMCA_{1b}$, and NCX1, and for the paracellular calcium transport, i.e., claudin-2, claudin-3, claudin-12, ZO-1, and occludin (Fig. 1f). Thus, the results suggested that the cecal epithelium of female rats could absorb calcium via both transcellular and paracellular pathways. Calcium transport in the cecum may be of importance since the cecal calcium flux was ~1.5-fold higher than that in the duodenum even in the absence of calcium concentration gradient (Fig. 1g).

PRL stimulated the cecal calcium transport in a biphasic dose–response manner

Dose–response study demonstrated that high physiological concentrations of PRL of 600 and 800 ng/mL, which were comparable to the levels observed during suckling in lactating rats [1], markedly enhanced the transcellular calcium transport by ~1.5- and ~2-fold, respectively, while 200 and 400 ng/mL PRL were without effects (Fig. 2a). Interestingly, the pathological concentration of 1,000 ng/mL, as seen in prolactinomas, only slightly increased calcium transport in the cecum (Fig. 2a). Since such PRL effect was not observed in the presence of apical calcium uptake inhibitor (50 μmol/L ruthenium red) or basolateral calcium extrusion inhibitor (100 μmol/L trifluoperazine), the PRL-stimulated calcium transport in this experiment was confirmed to occur via the transcellular pathway (Fig. 2b). The fact that the PRL-enhanced cecal calcium transport occurred rapidly within 60 min after exposure and was not abolished by inhibitors of gene transcription (50 μmol/L DRB) or protein biosynthesis (70 μmol/L cycloheximide; Fig. 2b), suggesting that the stimulatory actions of PRL was exerted via the nongenomic signaling pathways. Direct exposure to DRB and cycloheximide alone did not affect the basal rate of the transcellular

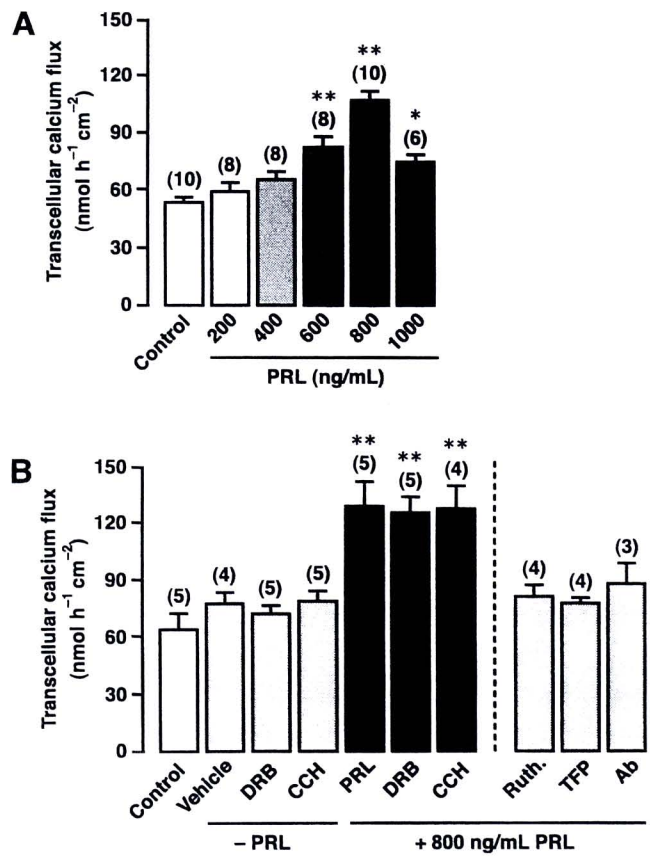

Fig. 2 **a** Dose-dependent effect of PRL on the transcellular calcium transport in the cecum. **b** Transcellular calcium transport in the cecum directly exposed to inhibitors of RNA polymerase II (50 μmol/L DRB), protein synthesis (70 μmol/L CCH), apical calcium uptake (50 μmol/L ruthenium red (*Ruth.*); apical side), basolateral calcium extrusion (100 μmol/L trifluoperazine (*TFP*); basolateral side), or 1 μg/mL PRLR antibody (*Ab*; basolateral side) with (+*PRL*) and without (−*PRL*) 800 ng/mL PRL (maximal effective concentration). DMSO was a vehicle for preparation of DRB and CCH. *Numbers in parentheses* represent the number of animals. *$p<0.05$, **$p<0.01$ compared with its respective control group

Table 2 Effects of PRL on epithelial electrical parameters

Condition	Number	Electrical parameters		
		PD (mV)	Isc (μAcm^{-2})	TER ($\Omega\ cm^2$)
Control	7	5.43±0.67	55.23±4.15	102.90±11.53
PRL				
200 ng/mL	5	3.67±0.39	52.20±5.50	71.90±3.39
400 ng/mL	4	4.22±0.69	55.21±6.29	79.02±11.04
600 ng/mL	4	3.97±0.72	57.37±8.06	68.23±5.93*
800 ng/mL	8	4.26±0.18	59.52±1.22	69.41±3.27*
1,000 ng/mL	5	4.02±0.56	58.84±9.52	69.91±2.65*

Values are means ± SE. Cecum was directly exposed to 200, 400, 600, 800, or 1,000 ng/mL PRL. Mounted tissue was bathed on both sides with 1.25 mmol/L calcium-containing solution. The mucosal side was negative with respect to the serosal side. The experiments were performed under open-circuit condition interrupted by measuring the short-circuit current

*$p<0.05$ compared with the control group

calcium transport (Fig. 2b). PRL-stimulated calcium transport was absent when the cecum was continuously exposed to 1 μg/mL PRLR antibody, indicating that PRLR mediated PRL actions in this intestinal segment (Fig. 2b). Moreover, the decrease in TER by 600, 800, and 1,000 ng/mL PRL (Table 2) suggested the PRL-induced increase in paracellular permeability. Since 800 ng/mL was the maximal effective concentration of PRL for stimulation of calcium transport, this concentration was used in the subsequent experiments.

The PRL-enhanced transcellular calcium transport in cecum was mediated by PI3K, PKC, and ROCK signaling pathways

Previous investigations showed that PRL signaling in mammary epithelium was mediated by JAK2, whereas that in the duodenum and Caco-2 monolayer was mediated by PI3K, PKC, and ROCK [25, 48]. Moreover, an increase in intestinal calcium absorption via the transcellular route was also reported to be protein kinase A (PKA)-dependent [9, 30]. Herein, we found that the PRL-enhanced transcellular calcium transport in cecum was completely abolished by inhibitors of PI3K (75 μmol/L LY294002 and 200 nmol/L wortmannin), PKC (1 μmol/L GF109203X), and ROCK (1 μmol/L Y27632), but not inhibitors of JAK2 (50 μmol/L AG490) and PKA (10 μmol/L PKAI 14–22; Fig. 3). Exposure to inhibitors alone did not affect the calcium flux. The data, therefore, indicated that PRL exerted its stimulatory actions on the cecal calcium transport via the PI3K, PKC, and ROCK signaling pathways.

PRL increased the paracellular calcium transport and calcium permeability in cecum via PI3K and ROCK pathways

Paracellular calcium transport and calcium permeability were evaluated in the presence of the transepithelial calcium gradient. Under normal conditions (Fig. 4a–d), the paracellular cecal calcium transport increased linearly with the mucosal calcium concentration ($r^2=0.86$). After exposure to PRL (Fig. 4a–d), the paracellular calcium

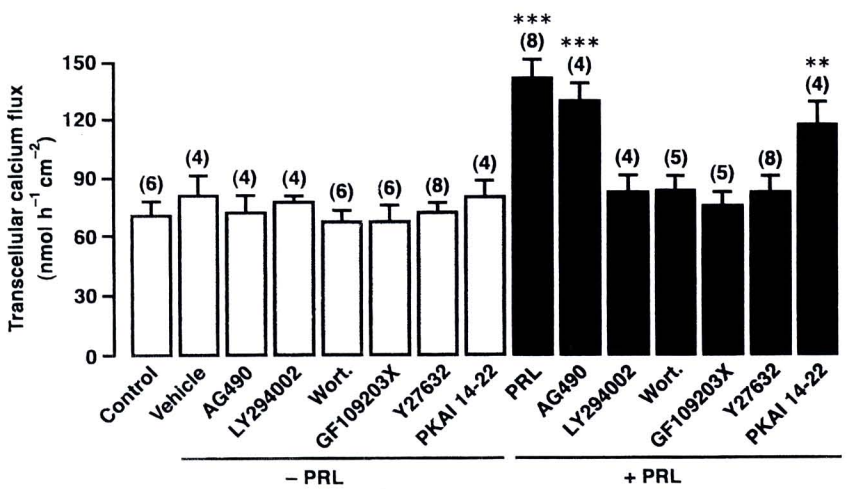

Fig. 3 Transcellular calcium transport in the cecum exposed to JAK2 inhibitor (50 μmol/L AG490), PI3K inhibitors (75 μmol/L LY294002 and 200 nmol/L wortmannin), PKC inhibitor (1 μmol/L GF109203X), ROCK inhibitor (1 μmol/L Y27632), or myristoylated PKA inhibitor 14–22 amide (10 μmol/L PKAI 14–22) with (+*PRL*) and without (−*PRL*) 800 ng/mL PRL. PKAI 14–22 was dissolved in water, whereas other inhibitors were dissolved in DMSO (vehicle). All experiments were performed under open-circuit condition. *Numbers in parentheses* represent the number of animals. **$p<0.01$, ***$p<0.001$ compared with the control group

fluxes were markedly enhanced, and the correlation between mucosal calcium concentrations and calcium fluxes still showed linearity (r^2=0.93). The slopes of the regression lines were significantly increased by 2.4-fold, i.e., from the control value of 63.06±5.95 to 152.62± 9.67 cm h^{-1} (p<0.001). PRL also increased calcium permeability of the cecal epithelium as demonstrated in Fig. 4e–h. The PRL-induced increases in the paracellular calcium transport and calcium permeability in the cecum were totally abolished by inhibitors of PI3K (Fig. 4a, e) and ROCK (Fig. 4c, g), but not by PKC inhibitor (Fig. 4b, f) or JAK2 inhibitor (Fig. 4d, h).

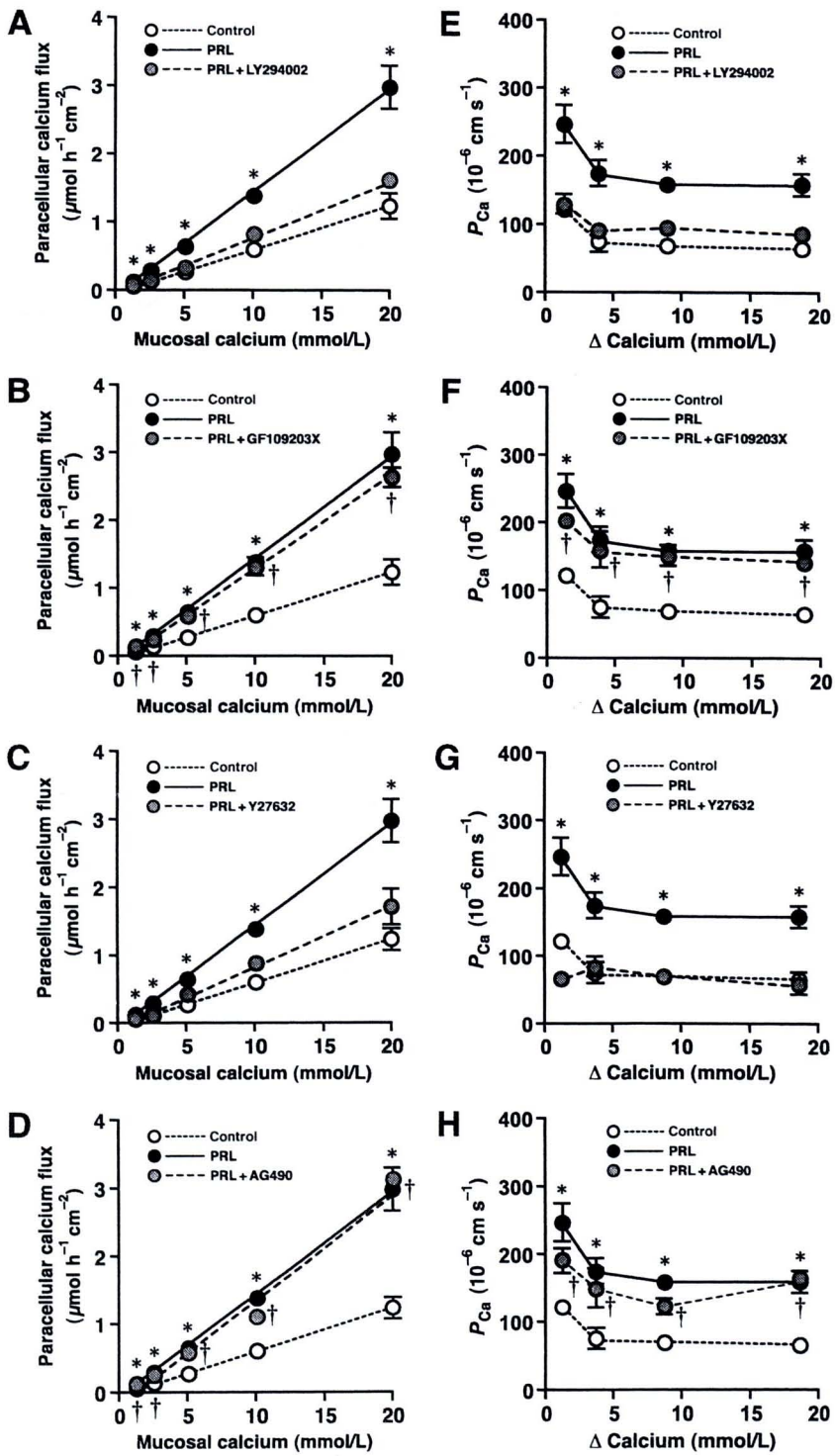

Fig. 4 **a–d** Paracellular calcium transport and **e–h** calcium permeability (P_{Ca}) in the cecum directly exposed to 800 ng/mL PRL in the presence and absence of PI3K inhibitor (75 μmol/L LY294002), PKC inhibitor (1 μmol/L GF109203X), ROCK inhibitor (1 μmol/L Y27632), or JAK2 inhibitor (50 μmol/L AG490). The mucosal side was bathed with solution containing various calcium concentrations, i.e., 1.25, 2.5, 5, 10, or 20 mmol/L (n=4 per each concentration; total 120 setups used), whereas the serosal solution had calcium concentration of 1.25 mmol/L. The same values of the control and PRL-treated groups are presented in **a–d** and **e–h** with those of the inhibitor-treated groups for clear comparisons. All experiments were performed under open-circuit condition. *p<0.001 PRL vs. control. †p<0.001 PRL+inhibitor vs. control

As seen in Fig. 5, TER values of normal cecal epithelia were linearly increased with mucosal calcium concentration (r^2=0.99) as a result of the calcium-induced conductance block of the paracellular pores, similar to that reported previously [47]. Hence, Isc but not PD was gradually decreased when mucosal calcium concentration was increased (data not shown). In 800 ng/mL PRL-treated cecal epithelia, although the relationship between mucosal calcium and TER still showed linearity (r^2=0.99), PRL markedly reduced TER, and the slopes were reduced from the control value of 119.59±3.03 to 71.01±1.77 kΩ cm^2 L mmol^{-1} (p<0.001). Such PRL effects on TER were abolished by PI3K inhibitor (Fig. 5a) and ROCK inhibitor (Fig. 5c), but not by PKC inhibitor (Fig. 5b) or JAK2 inhibitor (Fig. 5d). Inhibitors alone and vehicle (DMSO) had no effect on TER (data not shown).

PRL altered Na^+/Cl^--selective property of the cecal epithelium

Since the paracellular calcium transport and epithelial calcium permeability could be increased by altering the charge-selective property of cecal epithelium, we determined the absolute permeability to sodium (P_{Na}) and chloride (P_{Cl}) as well as the P_{Na}/P_{Cl} ratio, all of which are indicative of the paracellular charge selectivity [21, 47]. Under normal conditions (Fig. 6), the cecal epithelium exhibited a cation selectivity with P_{Na} being greater than P_{Cl} (p<0.001), and P_{Na}/P_{Cl} was ~2.0. After exposure to 800 ng/mL PRL, P_{Na} was markedly increased by ~2.6-fold (Fig. 6a) without any change in P_{Cl} (Fig. 6b), thereby raising P_{Na}/P_{Cl} (Fig. 6c). The increases in P_{Na} and P_{Na}/P_{Cl}, similar to the increase in paracellular calcium transport, were diminished by PI3K and ROCK inhibitors, but not by PKC inhibitor (Fig. 6a, c). Inhibitors alone were without effects. The results, therefore, suggested that PRL enhanced the paracellular cecal calcium transport by increasing the epithelial cation selectivity through PI3K and ROCK pathways.

Discussion

In the present study, we demonstrated, for the first time, that PRL stimulated the transcellular and paracellular calcium transport in rat cecum. The presence of PRLRs in cecal epithelial cells and the ability of PRLR antibody to block PRL-stimulated calcium transport confirmed direct action of PRL on this intestinal segment. It was evident that the PRL-enhanced transcellular cecal calcium transport was dependent on PI3K, PKC, and ROCK, while the enhanced paracellular calcium transport required PI3K and ROCK, but not PKC. Such PRL signalings were nongenomic, since they were observed within 60 min after PRL exposure, and were not abolished by inhibitors of gene transcription (DRB) or protein biosynthesis (cycloheximide).

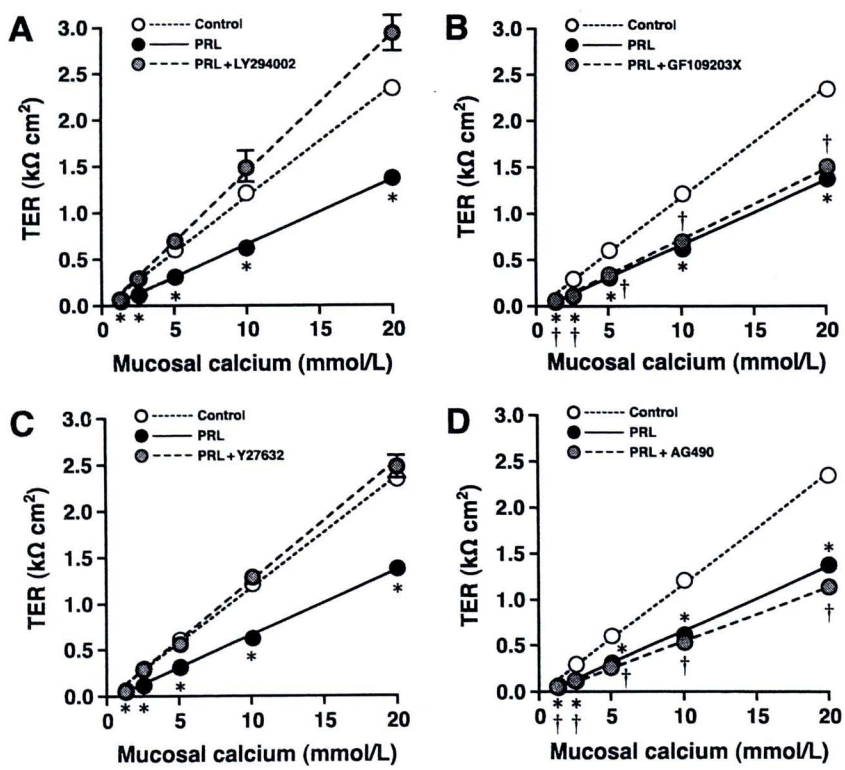

Fig. 5 Effect of 800 ng/mL PRL on the relationship between mucosal calcium concentration and transepithelial resistance (*TER*) of cecal epithelium (n=4 per each concentration) incubated with **a** PI3K inhibitor (75 μmol/L LY294002), **b** PKC inhibitor (1 μmol/L GF109203X), **c** ROCK inhibitor (1 μmol/L Y27632), or **d** JAK2 inhibitor (50 μmol/L AG490). The same control and PRL data are presented in **a**–**d** with those of the inhibitor-treated groups for clear comparisons. *p<0.001 PRL vs. control. †p<0.001 PRL+inhibitor vs. control

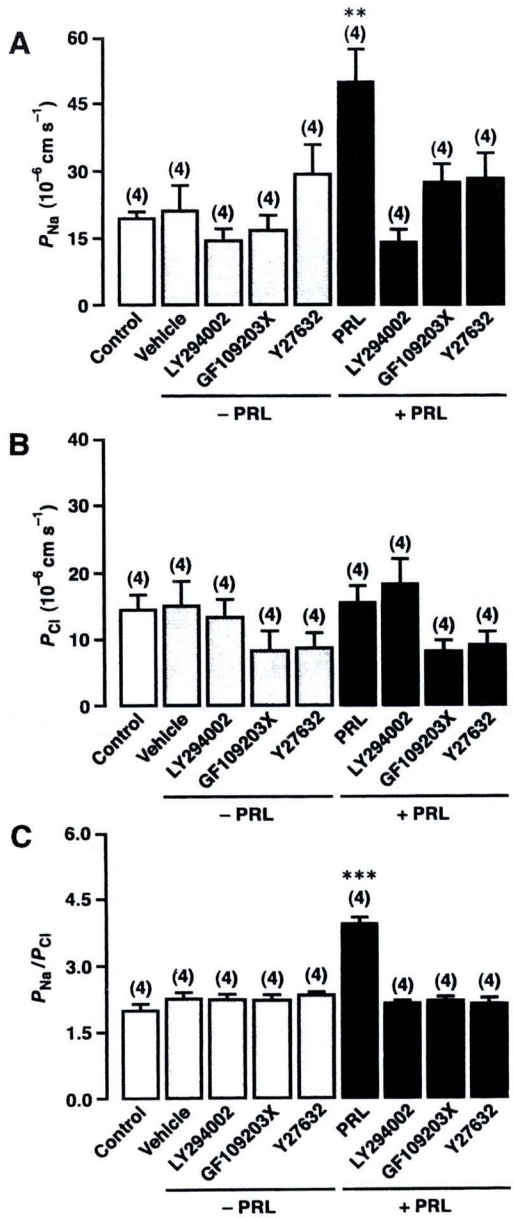

Fig. 6 **a** P_{Na}, **b** P_{Cl}, and **c** P_{Na}/P_{Cl} of the cecal epithelia exposed to PI3K inhibitor (75 μmol/L LY294002), PKC inhibitor (1 μmol/L GF109203X), or ROCK inhibitor (1 μmol/L Y27632) with (+*PRL*) and without (−*PRL*) 800 ng/mL PRL. DMSO was used as vehicle for inhibitor preparation. *Numbers in parentheses* represent the number of animals. $^{**}p<0.01$, $^{***}p<0.001$ compared with the control group

Although most recent investigations have focused on calcium transport in the small intestine, the proximal large intestine, particularly the cecum, is a highly efficient site for calcium absorption [39]. Karbach and Feldmeier reported that the rat cecum, as compared to other intestinal segments, had the highest rate of calcium absorption [28]. The present calcium flux study confirmed that the cecal calcium transport was greater than that in the duodenum by ~1.5-fold. Besides, the cecum which strongly expresses transcellular calcium transporters (Fig. 1f) is another site with sizable transcellular calcium absorption [28]. In some mammals, e.g., mole rats, the transcellular active calcium transport exclusively occurs in the proximal large intestine [41].

Physiological significance of the cecum in an overall calcium absorption was questionable because calcium may be present in the cecal lumen as a water-insoluble complex with indigestible luminal content [12]. Cecectomy also did not affect the fractional calcium absorption in 1,25 $(OH)_2D_3$-repleted rats [4]. However, other studies showed that microbial fermentation in the cecum could liberate calcium from the indigestible fibers [10, 51]. Moreover, short-chain fatty acid as well as small organic acids, e.g., propionic acid, succinic acid, and lactic acid, produced during fermentation decreased the luminal pH, which in turn released calcium from the complexes [10, 36, 38]. Cecal calcium absorption becomes salient when hindgut fermentors, such as humans and rats, ingest naturally occurring resistant starch (e.g., oatmeal and pearl barley), a fermentable carbohydrate that benefits healthy individuals as well as diabetic patients [44, 51].

The aforementioned evidence also collectively suggests that the cecum has a high capacity to supply additional calcium to the body when needed, for examples, in pregnancy and lactation [42]. Coincidentally, PRL is a hormone with markedly elevated levels during these periods, and we have previously shown that it was an important hormone to enhance calcium absorption, especially in the duodenum and proximal jejunum [5]. However, PRL was without effect on calcium transport in the distal large intestine although it could regulate water absorption and inhibit the calcium-dependent Cl^- and K^+ secretion in the colon [34, 43]. In the present study, the cecum, which expressed essential genes for the transcellular and paracellular calcium transport, responded to PRL by increasing calcium fluxes via both transcellular and paracellular pathways, similar to that seen in the duodenum [25]. Calcium fluxes observed in the 800 ng/mL PRL-treated cecum was greater than that in the duodenum exposed to the same PRL concentration by 2-fold, i.e., ~120 nmol h^{-1} cm^{-2} in the cecum compared to ~60 nmol h^{-1} cm^{-2} reported in the duodenum [25]. In the presence of ~5–20 mmol/L transepithelial calcium gradient, this PRL concentration markedly increased the amount of calcium transported by cecal epithelium from a nanomole range to micromole range. These information collectively strengthened the physiological significance of the cecal calcium absorption during hyperprolactinemic states, such as in lactating animals.

Nevertheless, nothing was known pertaining the detailed mechanisms by which PRL enhanced cecal calcium transport. The PRL-stimulated transcellular calcium absorption in the duodenum was explained by increases in the brush-border calcium uptake and PMCA activity [7]. In the

cecum, the PRL effect was also abolished by inhibitors of apical calcium uptake (ruthenium red) or basolateral calcium extrusion (trifluoperazine). Regarding the cecal paracellular calcium transport, the PRL-induced increase in calcium movement through the paracellular space was explained by a decrease in TER (Fig. 5) as well as an increase in the epithelial cation selectivity, as indicated by the increased P_{Na} and P_{Na}/P_{Cl} (Fig. 6), similar to that observed in Caco-2 monolayer [48]. The P_{Na}/P_{Cl} value of the control groups, which increased from the mobility ratio of Na^+ and Cl^- of ~0.6 in free solution to ~2.0 [17], also suggested that, under normal conditions, the cecal epithelium naturally prefers paracellular movement of cations more than anions. Generally, tight junction proteins of the claudin family undergo polymerization to form charge-selective paracellular pores [15]. Thus, the epithelial charge selectivity is determined by the fixed negative or positive charges on the extracellular loops of claudins which impede the movement of ions with the opposite charge [50]. Claudin-2, claudin-3, and claudin-12, which are also expressed in cecal epithelial cells, have been suggested to regulate the paracellular calcium transport [14, 35]. Our recent preliminary study in Caco-2 monolayer showed that an increase in cation selectivity observed after the PRL-induced claudin phosphorylation could increase the paracellular calcium movement (Nakkrasae et al. 2009, unpublished observation). However, further experiment is required to demonstrate that the PRL-induced increases in paracellular cecal calcium transport and cation selectivity are directly mediated by claudin phosphorylation.

PRL signaling pathways in the intestinal epithelial cells have been studied in the duodenum and Caco-2 intestinal-like cells [25, 48], while that in the cecum was unknown. Since cecal epithelial cells predominantly expressed PRLR-L, it was likely that PRL exerted its functions through PRLR-L, similar to that reported in Caco-2 cells [48]. In contrast, as PRLR-S lacks the cytoplasmic tails required to activate the intracellular downstream pathways, PRLR-S may act as the dominant-negative molecules to silence or reduce PRL actions [2]. Interestingly, the typical biphasic response to PRL was also demonstrated in the cecum, i.e., in contrast to the lower effective doses (600 and 800 ng/mL), 1,000 ng/mL PRL only slightly increased calcium transport. This phenomenon has been explained by inability of PRLRs to form functional dimers. At extremely high PRL concentrations, most available PRLRs were occupied as nonfunctional 1:1 complexes instead of 1:2 functional complexes needed to induce signal transduction [13, 22].

The principal PRL signaling pathways found in the cecum, i.e., PI3K, PKC, and ROCK, were consistent with those reported in duodenal epithelial cells and Caco-2 monolayer [25, 48]. Although JAK2 usually mediates PRL signals in several tissues, e.g., mammary epithelium [24], and several factors, e.g., $1,25(OH)_2D_3$, could increase calcium uptake through PKA [30], the PRL effects herein appeared to be independent of both JAK2 and PKA. Generally, PI3K is the most upstream enzyme of several kinase targets, including PKC and ROCK known to modulate the transepithelial calcium transport and paracellular permeability [19, 27, 37, 46]. In the cecum, PKC was likely to be more important in the transcellular calcium transport than the paracellular transport, presumably by its ability to augment the basolateral calcium efflux [30]. In contrast, ROCK was essential for both transport mechanisms. It was noteworthy that activation of ROCK is commonly required to increase paracellular permeability or decrease TER in several epithelia, e.g., brain endothelium, renal proximal tubule, and human colonic epithelial monolayer [27, 45, 46]. Hence, PRL might use this common pathway to decrease TER, and increase cation selectivity and paracellular calcium permeability, thereby enhancing the paracellular calcium transport.

Finally, it could be concluded that the rat cecum was a target tissue of PRL, in which it directly stimulated the transcellular and paracellular calcium transport via the non-genomic signaling pathways. The downstream pathways for PRL signaling involved PI3K, ROCK, and PKC, the last of which mainly mediated the signal for the PRL-enhanced transcellular calcium transport. The present investigation, therefore, elaborated possible physiological roles of PRL in the cecum and provided more complete understanding of the effects of PRL on calcium homeostasis. Since the rate of cecal calcium absorption is subjected to effects of certain dietary components, e.g., resistant carbohydrates, we speculate that such nutraceuticals could be useful for enhancement of calcium absorption during lactation, when the plasma PRL surge is in the range of ~650–800 ng/mL [1].

Acknowledgments This work was supported by the Thailand Research Fund (RSA5180001 to N. Charoenphandhu) and the Mahidol University Postdoctoral Fellowship Program (to L.-i. Nakkrasae).

Conflict of interest The authors have no conflict of interest.

References

1. Arbogast LA, Voogt JL (1998) Endogenous opioid peptides contribute to suckling-induced prolactin release by suppressing tyrosine hydroxylase activity and messenger ribonucleic acid levels in tuberoinfundibular dopaminergic neurons. Endocrinology 139:2857–2862
2. Berlanga JJ, Garcia-Ruiz JP, Perrot-Applanat M, Kelly PA, Edery M (1997) The short form of the prolactin (PRL) receptor silences PRL induction of the β-casein gene promoter. Mol Endocrinol 11:1449–1457
3. Boass A, Lovdal JA, Toverud SU (1992) Pregnancy- and lactation-induced changes in active intestinal calcium transport in rats. Am J Physiol Gastrointest Liver Physiol 263:G127–G134

4. Brommage R, Binacua C, Carrie AL (1995) The cecum does not participate in the stimulation of intestinal calcium absorption by calcitriol. J Steroid Biochem Mol Biol 54:71–73
5. Charoenphandhu N, Krishnamra N (2007) Prolactin is an important regulator of intestinal calcium transport. Can J Physiol Pharmacol 85:569–581
6. Charoenphandhu N, Limlomwongse L, Krishnamra N (2001) Prolactin directly stimulates transcellular active calcium transport in the duodenum of female rats. Can J Physiol Pharmacol 79:430–438
7. Charoenphandhu N, Limlomwongse L, Krishnamra N (2006) Prolactin directly enhanced Na^+/K^+- and Ca^{2+}-ATPase activities in the duodenum of female rats. Can J Physiol Pharmacol 84:555–563
8. Charoenphandhu N, Wongdee K, Teerapornpuntakit J, Thongchote K, Krishnamra N (2008) Transcriptome responses of duodenal epithelial cells to prolactin in pituitary-grafted rats. Mol Cell Endocrinol 296:41–52
9. de Boland AR, Norman A (1990) Evidence for involvement of protein kinase C and cyclic adenosine 3′, 5′ monophosphate-dependent protein kinase in the 1, 25-dihydroxyvitamin D_3-mediated rapid stimulation of intestinal calcium transport, (transcaltachia). Endocrinology 127:39–45
10. Duflos C, Bellaton C, Pansu D, Bronner F (1995) Calcium solubility, intestinal sojourn time and paracellular permeability codetermine passive calcium absorption in rats. J Nutr 125:2348–2355
11. Favus MJ (1985) Factors that influence absorption and secretion of calcium in the small intestine and colon. Am J Physiol 248: G147–G157
12. Favus MJ, Pak C (2001) Evidence for absorption of ionic calcium and soluble calcium complexes by the duodenum and cecum in the rat. Am J Ther 8:425–431
13. Fuh G, Colosi P, Wood WI, Wells JA (1993) Mechanism-based design of prolactin receptor antagonists. J Biol Chem 268:5376–5381
14. Fujita H, Sugimoto K, Inatomi S, Maeda T, Osanai M, Uchiyama Y, Yamamoto Y, Wada T, Kojima T, Yokozaki H, Yamashita T, Kato S, Sawada N, Chiba H (2008) Tight junction proteins claudin-2 and -12 are critical for vitamin D-dependent Ca^{2+} absorption between enterocytes. Mol Biol Cell 19:1912–1921
15. Furuse M, Tsukita S (2006) Claudins in occluding junctions of humans and flies. Trends Cell Biol 16:181–188
16. Garcia J, Carabano R, Perez-Alba L, de Blas JC (2000) Effect of fiber source on cecal fermentation and nitrogen recycled through cecotrophy in rabbits. J Anim Sci 78:638–646
17. Greger R (1996) Epithelial transport. In: Greger R, Windhorst U (eds) Comprehensive human physiology: from cellular mechanisms to integration. Springer, Berlin, pp 1217–1232
18. Hawkins PT, Anderson KE, Davidson K, Stephens LR (2006) Signalling through class I PI3Ks in mammalian cells. Biochem Soc Trans 34:647–662
19. Hirsch E, Costa C, Ciraolo E (2007) Phosphoinositide 3-kinases as a common platform for multi-hormone signaling. J Endocrinol 194:243–256
20. Hoenderop JG, Nilius B, Bindels RJ (2005) Calcium absorption across epithelia. Physiol Rev 85:373–422
21. Hou J, Paul DL, Goodenough DA (2005) Paracellin-1 and the modulation of ion selectivity of tight junctions. J Cell Sci 118:5109–5118
22. Ilondo MM, Damholt AB, Cunningham BA, Wells JA, de Meyts P, Shymko RM (1994) Receptor dimerization determines the effects of growth hormone in primary rat adipocytes and cultured human IM-9 lymphocytes. Endocrinology 134:2397–2403
23. Imaizumi MO, Sakurai T, Nakamura S, Nakanishi S, Matsuda Y, Muramatsu S, Nonomura Y, Kumakura K (1992) Inhibition of Ca^{2+}-dependent catecholamine release by myosin light chain kinase inhibitor, wortmannin, in adrenal chromaffin cells. Biochem Biophys Res Commun 185:1016–1021
24. Jahn GA, Daniel N, Jolivet G, Belair L, Bole-Feysot C, Kelly PA, Djiane J (1997) In vivo study of prolactin (PRL) intracellular signalling during lactogenesis in the rat: JAK/STAT pathway is activated by PRL in the mammary gland but not in the liver. Biol Reprod 57:894–900
25. Jantarajit W, Thongon N, Pandaranandaka J, Teerapornpuntakit J, Krishnamra N, Charoenphandhu N (2007) Prolactin-stimulated transepithelial calcium transport in duodenum and Caco-2 monolayer are mediated by the phosphoinositide 3-kinase pathway. Am J Physiol Endocrinol Metab 293:E372–E384
26. Kahle KT, Macgregor GG, Wilson FH, Van Hoek AN, Brown D, Ardito T, Kashgarian M, Giebisch G, Hebert SC, Boulpaep EL, Lifton RP (2004) Paracellular Cl^- permeability is regulated by WNK4 kinase: insight into normal physiology and hypertension. Proc Natl Acad Sci USA 101:14877–14882
27. Kapus A, Szászi K (2006) Coupling between apical and paracellular transport processes. Biochem Cell Biol 84:870–880
28. Karbach U, Feldmeier H (1993) The cecum is the site with the highest calcium absorption in rat intestine. Dig Dis Sci 38:1815–1824
29. Khanal RC, Nemere I (2008) Regulation of intestinal calcium transport. Annu Rev Nutr 28:179–196
30. Khanal RC, Nemere I (2008) Endocrine regulation of calcium transport in epithelia. Clin Exp Pharmacol Physiol 35:1277–1287
31. Kimizuka H, Koketsu K (1964) Ion transport through cell membrane. J Theor Biol 6:290–305
32. Kornberg A, Daft FS, Sebrell WH (1944) Mechanism of production of vitamin K deficiency in rats by sulfonamides. J Biol Chem 155:193–200
33. Krause LJ, Forsberg CW, O'Connor DL (1996) Feeding human milk to rats increases *Bifidobacterium* in the cecum and colon which correlates with enhanced folate status. J Nutr 126:1505–1511
34. Krishnamra N, Ousingsawat J, Limlomwongse L (2001) Study of acute pharmacologic effects of prolactin on calcium and water transport in the rat colon by an in vivo perfusion technique. Can J Physiol Pharmacol 79:415–421
35. Kutuzova GD, DeLuca HF (2004) Gene expression profiles in rat intestine identify pathways for 1, 25-dihydroxyvitamin D_3 stimulated calcium absorption and clarify its immunomodulatory properties. Arch Biochem Biophys 432:152–166
36. Levrat MA, Remesy C, Demigne C (1991) High propionic acid fermentations and mineral accumulation in the cecum of rats adapted to different levels of inulin. J Nutr 121:1730–1737
37. Little D, Dean RA, Young KM, McKane SA, Martin LD, Jones SL, Blikslager AT (2003) PI3K signaling is required for prostaglandin-induced mucosal recovery in ischemia-injured porcine ileum. Am J Physiol Gastrointest Liver Physiol 284: G46–G56
38. Mineo H, Amano M, Minaminida K, Chiji H, Shigematsu N, Tomita F, Hara H (2006) Two-week feeding of difructose anhydride III enhances calcium absorptive activity with epithelial cell proliferation in isolated rat cecal mucosa. Nutrition 22:312–320
39. Nellans HN, Goldsmith RS (1981) Transepithelial calcium transport by rat cecum: high-efficiency absorptive site. Am J Physiol 240:G424–G431
40. Nellans HN, Goldsmith RS (1983) Mucosal calcium uptake by rat cecum: identity with transcellular calcium absorption. Am J Physiol 244:G618–G622
41. Pitcher T, Buffenstein R (1995) Intestinal calcium transport in mole-rats (*Cryptomys damarensis* and *Heterocephalus glaber*) is independent of both genomic and non-genomic vitamin D mediation. Exp Physiol 80:597–608
42. Prentice A (2000) Calcium in pregnancy and lactation. Annu Rev Nutr 20:249–272

43. Puntheeranurak S, Schreiber R, Spitzner M, Ousingsawat J, Krishnamra N, Kunzelmann K (2007) Control of ion transport in mouse proximal and distal colon by prolactin. Cell Physiol Biochem 19:77–88
44. Robertson MD, Bickerton AS, Dennis AL, Vidal H, Frayn KN (2005) Insulin-sensitizing effects of dietary resistant starch and effects on skeletal muscle and adipose tissue metabolism. Am J Clin Nutr 82:559–567
45. Samarin SN, Ivanov AI, Flatau G, Parkos CA, Nusrat A (2007) Rho/Rho-associated kinase-II signaling mediates disassembly of epithelial apical junctions. Mol Biol Cell 18:3429–3439
46. Stamatovic SM, Dimitrijevic OB, Keep RF, Andjelkovic AV (2006) Protein kinase Cα-RhoA cross-talk in CCL2-induced alterations in brain endothelial permeability. J Biol Chem 281:8379–8388
47. Tang VW, Goodenough DA (2003) Paracellular ion channel at the tight junction. Biophys J 84:1660–1673
48. Thongon N, Nakkrasae LI, Thongbunchoo J, Krishnamra N, Charoenphandhu N (2008) Prolactin stimulates transepithelial calcium transport and modulates paracellular permselectivity in Caco-2 monolayer: mediation by PKC and ROCK pathways. Am J Physiol Cell Physiol 294:C1158–C1168
49. Thongon N, Nakkrasae LI, Thongbunchoo J, Krishnamra N, Charoenphandhu N (2009) Enhancement of calcium transport in Caco-2 monolayer through PKC_{ζ}-dependent $Ca_v1.3$-mediated transcellular and rectifying paracellular pathways by prolactin. Am J Physiol Cell Physiol (in press). doi: 10.1152/ajpcell.00053.2009
50. Van Itallie CM, Anderson JM (2006) Claudins and epithelial paracellular transport. Annu Rev Physiol 68:403–429
51. Younes H, Demigne C, Remesy C (1996) Acidic fermentation in the caecum increases absorption of calcium and magnesium in the large intestine of the rat. Br J Nutr 75:301–314

Electronic supplementary material

Below is the link to the electronic supplementary material.

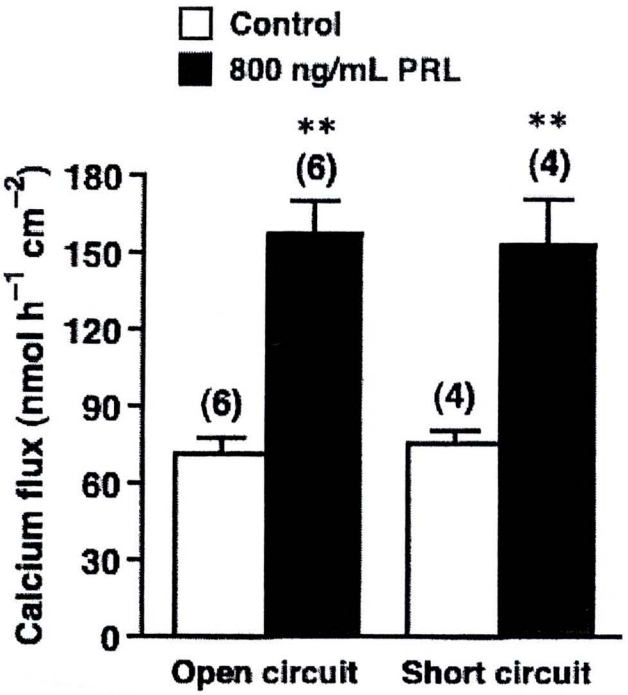

Supplemental Figure S1: Kraidith et al.

Supplemental Figure S1 Transepithelial calcium flux in 800 ng/mL PRL-exposed cecal tissues under open- and short-circuit conditions. The tissue was bathed on both sides with 1.25 mmol/L Ca^{2+}-containing solution. Numbers in parentheses represent the number of animals. $^{**}p < 0.01$ compared with its respective control group (GIF 15 kb)

High resolution image file (EPS 390 kb)

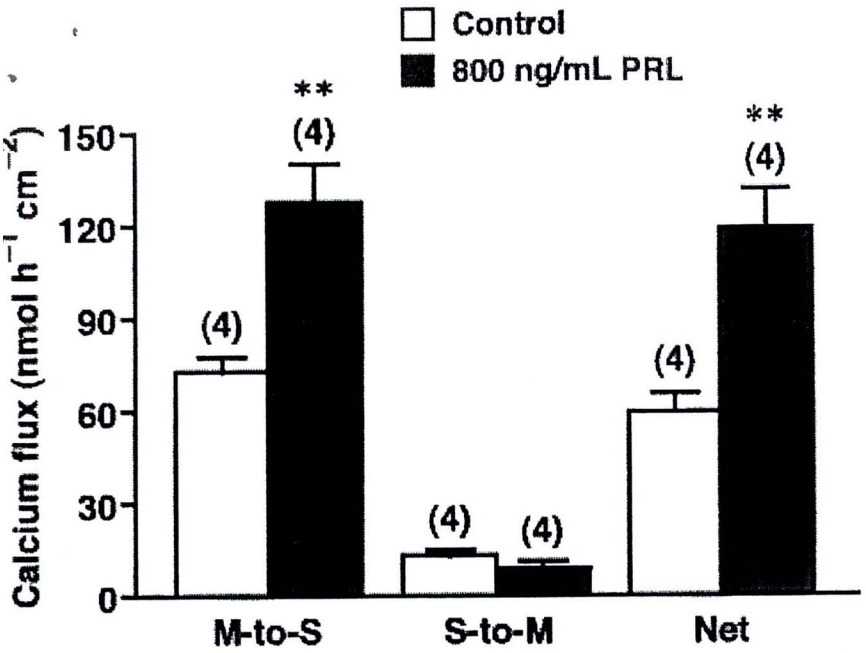

Supplemental Figure S2: Kraidith et al.

Supplemental Figure S2 Mucosa (M)-to-serosa (S) and S-to-M calcium fluxes in 800 ng/mL PRL-exposed cecal tissues under short-circuit condition. The removed cecal tissue from a rat was divided into two pieces for M-to-S and S-to-M studies. Net calcium flux was calculated by subtracting S-to-M calcium flux from M-to-S calcium flux. Each tissue was bathed on both sides with 1.25 mmol/L Ca^{2+}-containing solution. Numbers in parentheses represent the number of animals. $^{**}p < 0.01$ compared with its respective control group (GIF 17 kb)

High resolution image file (EPS 383 kb)

Am J Physiol Cell Physiol 296: C1373–C1382, 2009.
First published April 1, 2009; doi:10.1152/ajpcell.00053.2009.

Enhancement of calcium transport in Caco-2 monolayer through PKC_ζ-dependent $Ca_v1.3$-mediated transcellular and rectifying paracellular pathways by prolactin

Narongrit Thongon,[1,2,3] La-iad Nakkrasae,[1] Jirawan Thongbunchoo,[1] Nateetip Krishnamra,[1,2] and Narattaphol Charoenphandhu[1,2]

[1]*Consortium for Calcium and Bone Research (COCAB) and* [2]*Department of Physiology, Faculty of Science, Mahidol University, Bangkok, Thailand; and* [3]*Department of Medical Science, Faculty of Science, Burapha University, Chonburi, Thailand*

Submitted 28 January 2009; accepted in final form 29 March 2009

Thongon N, Nakkrasae L, Thongbunchoo J, Krishnamra N, Charoenphandhu N. Enhancement of calcium transport in Caco-2 monolayer through PKC_ζ-dependent $Ca_v1.3$-mediated transcellular and rectifying paracellular pathways by prolactin. *Am J Physiol Cell Physiol* 296: C1373–C1382, 2009. First published April 1, 2009; doi:10.1152/ajpcell.00053.2009.—Previous investigations suggested that prolactin (PRL) stimulated the intestinal calcium absorption through phosphoinositide 3-kinase (PI3K), protein kinase C (PKC), and RhoA-associated coiled-coil forming kinase (ROCK) signaling pathways. However, little was known regarding its detailed mechanisms for the stimulation of transcellular and voltage-dependent paracellular calcium transport. By using Ussing chamber technique, we found that the PRL-induced increase in the transcellular calcium flux and decrease in transepithelial resistance of intestinal-like Caco-2 monolayer were not abolished by inhibitors of gene transcription and protein biosynthesis. The PRL-stimulated transcellular calcium transport was completely inhibited by the L-type calcium channel blockers (nifedipine and verapamil) and plasma membrane Ca^{2+}-ATPase (PMCA) inhibitor (trifluoperazine) as well as small interfering RNA targeting voltage-dependent L-type calcium channel $Ca_v1.3$, but not TRPV6 or calbindin-D_{9k}. As demonstrated by ^{45}Ca uptake study, PI3K and PKC, but not ROCK, were essential for the PRL-enhanced apical calcium entry. In addition, PRL was unable to enhance the transcellular calcium transport after PKC_ζ knockdown or exposure to inhibitors of PKC_ζ, but not of PKC_α, PKC_β, PKC_ε, PKC_μ, or protein kinase A. Voltage-clamping experiments further showed that PRL markedly stimulated the voltage-dependent calcium transport and removed the paracellular rectification. Such PRL effects on paracellular transport were completely abolished by inhibitors of PI3K (LY-294002) and ROCK (Y-27632). It could be concluded that the PRL-stimulated transcellular calcium transport in Caco-2 monolayer was mediated by $Ca_v1.3$ and PMCA, presumably through PI3K and PKC_ζ pathways, while the enhanced voltage-dependent calcium transport occurred through PI3K and ROCK pathways.

calcium uptake; protein kinase C; rectification; small interfering RNA; voltage-dependent calcium transport

PROLACTIN (PRL) IS A CRUCIAL calcium-regulating hormone in pregnant and lactating animals since it increases intestinal calcium absorption, renal calcium reabsorption, and bone turnover ultimately to supply more calcium for fetal growth and milk production (4, 5). In vivo studies in rats suggested that PRL could stimulate transcellular and paracellular calcium absorption in several intestinal segments, particularly in the duodenum and proximal jejunum in which PRL receptors (PRLR) are strongly expressed (20, 25, 26). Although direct stimulatory actions of PRL on intestinal calcium transport has been demonstrated, little is currently known regarding the detailed mechanisms of PRL in intestinal epithelial cells.

Under normal conditions, calcium predominantly traverses the intestinal epithelium via the paracellular pathway, especially after a calcium-enriched meal that favors the calcium gradient-dependent paracellular calcium transport, whereas the transcellular calcium transport becomes more significant during high calcium demand, such as pregnancy and lactation (5, 23). A number of calcium transport proteins are essential for the transcellular calcium transfer, namely, transient receptor potential vanilloid family calcium channel (TRPV)-6 and voltage-dependent L-type calcium channel $Ca_v1.3$ for the apical calcium entry, calcium-binding protein (CaBP) calbindin-D_{9k} for cytoplasmic translocation, and plasma membrane Ca^{2+}-ATPase (PMCA) isoform 1b and Na^+/Ca^{2+} exchanger (NCX)-1 for basolateral extrusion (18, 34, 35). It was apparent that, under the influence of various hormones and physiological conditions, different transport proteins may be recruited to augment calcium absorption. For example, L-type calcium channels were responsible for the enhanced transcellular calcium transport in response to parathyroid hormone-related peptide and luminal glucose (34, 51), while TRPV6 was required for the $1,25(OH)_2D_3$- and 17β-estradiol-stimulated calcium absorption (23, 46). Regarding the PRL-stimulated calcium transport, it was not known which transporter proteins were involved.

The paracellular calcium transport driven by an electrochemical gradient (i.e., calcium gradient and voltage difference), on the other hand, is regulated by several tight junctions proteins, e.g., claudin-2 and -12, which polymerize to form an array of channel-like paracellular pores (15, 43, 47). Thus, the paracellular channels appeared to exhibit charge and size selectivity, voltage response, and rectification similar to those found in typical ion channels (12, 30, 41, 43). Physiological significance of the voltage-dependent calcium transport in the small intestine is controversial, but it may be of greater importance when the transepithelial potential difference (PD) is increased by some nutrients, such as glucose, short-chain fatty acid, phenylalanine, cysteine, and proline (14, 40, 48). Recently, PRL has been shown to modify some properties of the paracellular channel, i.e., charge selectivity and calcium permeability, which led to an enhancement of the calcium gradient-dependent paracellular calcium transport (45). The effects of PRL on other paracellular properties, such as response to

Address for reprint requests and other correspondence: N. Charoenphandhu, Dept. of Physiology, Faculty of Science, Mahidol Univ., Rama VI Road, Bangkok 10400, Thailand (e-mail: naratt@narattsys.com).

voltage change and rectification, or the voltage-dependent calcium transport remained unknown. However, they could not be demonstrated in the presence of calcium gradient because high calcium concentration occluded the paracellular pores (known as the paracellular conductance block), which in turn altered the transepithelial resistance (TER) (43, 45). Such paracellular properties should be validated by a voltage-clamp study in an absence of calcium gradient.

In addition to the calcium transport mechanism, the signaling pathways of PRL were also elusive. In the rat duodenum and intestinal epithelium-like Caco-2 monolayer, phosphoinositide 3-kinase (PI3K) was required for PRL signaling (20, 45). Further investigations in Caco-2 cells suggested that the PRL-stimulated transcellular and gradient-dependent paracellular calcium transport relied on protein kinase C (PKC) and RhoA-associated coiled-coil forming kinase (ROCK) (45), but which PKC isozyme was involved was not known.

Therefore, the objectives of the present study were *1*) to identify the transcellular transporters and PKC isozyme that were essential for the PRL-stimulated transcellular calcium transport, *2*) to investigate the paracellular properties altered by PRL, and *3*) to demonstrate the effects of PRL on the voltage-dependent calcium transport as well as the responsible signaling pathways. The human colorectal adenocarcinoma Caco-2 cells were used in this study because they have functional similarities to the small intestinal cells, including the presence of brush border, expression of sucrase-isomaltase, and expression of the transcellular calcium transporters and charge-selective paracellular proteins, e.g., TRPV6, PMCA, claudin-1, -2, -3, and -5 (32, 37, 38, 50, 52). Caco-2 monolayer was also a standard model for calcium absorption study and was responsive to PRL (20, 45).

MATERIALS AND METHODS

Cell culture. Caco-2 intestinal cells [no. HTB-37, American Type Culture Collection (ATCC)] were grown in Dulbecco's modified Eagle's medium (Sigma, St. Louis, MO) supplemented with 15% fetal bovine serum (Gibco, Grand Island, NY), 1% L-glutamine (Gibco), 1% nonessential amino acid (Sigma), 100 U/ml penicillin/streptomycin (Sigma), and 0.25 μl/ml amphotericin B (Sigma). Cells were propagated in 75-cm^2 T flask (Corning, NY) under a humidified atmosphere containing 5% CO_2 at 37°C and were subcultured as described in the ATCC protocol. Confluent Caco-2 monolayers were prepared by seeding cells (5.0×10^5 cells/cm^2) on polyester Snapwell with 12-mm diameter and 0.4-μm pore size (Corning). Culture medium was changed daily after 48 h of seeding. On *day 14* after seeding, the Snapwell was mounted in a modified Ussing chamber with an exposed surface area of 1.13 cm^2 to measure the electrical parameters and calcium fluxes, as previously described (45). The monolayer was equilibrated for 20 min in the chamber before the 60-min experiment was performed.

Small interfering RNA transfection. Small interfering RNA (siRNA) oligonucleotides targeted for human TRPV6 (5′-GGGAAACACAGUGUUACAC-3′ and 5′-GTGUAACACUGUGUUUCCC-3′), $Ca_v1.3$ (5′-GAGCACCUUUGACAAUUUC-3′ and 5′-AAGAAAUUGUCAAAGGTGCUC-3′), calbindin-D_{9k} (5′-GAUGAUCUCUUUCAAGAAC-3′ and 5′-GUUCUUGAAAGAGAUCAUC-3′), and PKC_ζ (5′-GACGACAAGAACGAGGACG-3′ and 5′-CUGCUGUUCUUGCUCCUGCAA-3′) were designed by siRNA Target Designer (version 1.51; Promega, Madison, WI), and synthesized by T7 RiboMax Express RNAi System (Promega) according to the manufacturer's instruction. Scramble siRNA that had no homology to any other genes was used as a negative control. As previously described (45), Caco-2 cells were first plated on Snapwell at 5.0×10^5 cells/cm^2. At *day 12* after seeding, in vitro transfection was performed with 10 μg/ml polyethyleneimine and 1 μmol/ml siRNA molecules. At *day 14* (i.e., 48 h after transfection), transepithelial calcium flux was determined. Efficiency of siRNA was evaluated by quantitative real-time PCR (qRT-PCR). The knockdown protocol was approved by the Institutional Biosafety Committee (IBC) of Mahidol University.

mRNA isolation, quantitative real-time PCR, and sequencing. By using TRIzol reagent (Invitrogen, Carlsbad, CA), total RNA was prepared from Caco-2 cells, as previously described (45). One microgram of total RNA was reverse-transcribed with iScript kit (Bio-Rad, Hercules, CA). Glyceraldehyde-3-phosphate dehydrogenase (GAPDH), a housekeeping gene, served as a control gene to check the consistency of the reverse transcription. Sense and antisense primers used for qRT-PCR are presented in Table 1. The amplification reaction using real-time PCR (model MiniOpticon; Bio-Rad) was performed with iQ SYBR Green SuperMix (Bio-Rad). Relative expression of studied genes over GAPDH was calculated from the threshold cycle (C_t) values by using $2^{\Delta C_t}$ method. After qRT-PCR, the PCR products were also visualized on a 1.5% agarose gel stained with 1.0 μg/ml ethidium bromide. Thereafter, all PCR products were extracted by the HiYield Gel/PCR DNA Extraction kit (Real Biotech, Taipei, Taiwan) and were sequenced by the ABI Prism 3100 Genetic Analyzer (Applied Biosystems, Foster City, CA).

Bathing solution. The bathing solution for Ussing chamber experiments contained (in mmol/l) 118 NaCl, 4.7 KCl, 1.1 $MgCl_2$, 1.25 $CaCl_2$, 23 $NaHCO_3$, 12 D-glucose, and 2 mannitol (all purchased from Sigma). The solution, continuously gassed with humidified 5% CO_2 in 95% O_2, was maintained at 37°C, pH 7.4, and had an osmolality of 290–293 mmol/kg water as measured by a freezing point-based osmometer (model 3320; Advanced Instruments, Norwood, MA).

Table 1. *Homo sapiens oligonucleotide sequences used in the quantitative real-time PCR experiments*

Name	Accession No.	Primer (forward/reverse)	Product Length, bp
TRPV6	AF365928	5′-TCTGACTGCGTGTTCTCAC-3′ 5′-ACATTCCTTGGCGTTCAT-3′	144
$Ca_v1.3$	EU363339	5′-TGATCCAAGTGGAGCAGTCA-3′ 5′-GTGTGAAAGTCCGGTAGGAGA-3′	113
Calbindin-D_{9k}	L13220	5′-TCTCCTGAGGAACTGAAGAGG-3′ 5′-GGGAATTCAGCCTGAATCAA-3′	106
PKC_ζ	NM_002744	5′-TAATCAGAGTCATCGGGCG-3′ 5′-TCTGTCTGTACCCAGTCAA-3′	138
GAPDH	NM_002046	5′-CTGGTAAAGTGGATATTGTTG-3′ 5′-GAGGCTGTTGTCATACTTCTC-3′	359

TRPV6, transient receptor potential vanilloid family Ca^{2+} channel 6; $Ca_v1.3$, voltage-dependent L-type Ca^{2+} channel 1.3; PKC_ζ, ζ-isozyme of protein kinase C; GAPDH, glyceraldehyde-3-phosphate dehydrogenase.

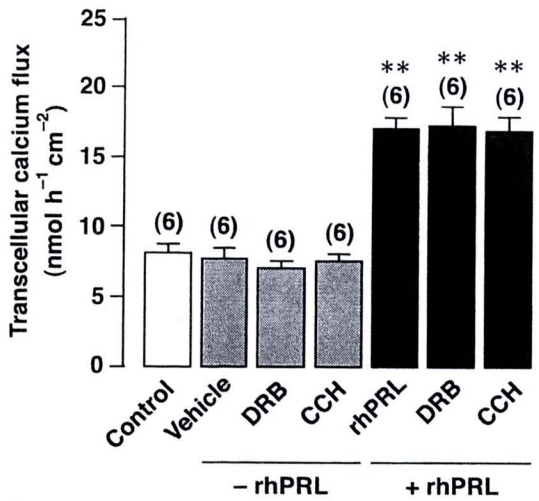

Fig. 1. Transcellular calcium transport in Caco-2 monolayers directly exposed to RNA polymerase II inhibitor [50 μmol/l 5,6-dichloro-1-β-D-ribobenzimidazole (DRB); inhibitor of gene transcription] or protein synthesis inhibitor (70 μmol/l cycloheximide; CCH) in the presence (+rhPRL) and absence (−rhPRL) of 600 ng/ml recombinant human prolactin (rhPRL). DMSO was used as vehicle for inhibitor preparation. Numbers in parentheses represent the number of independent Snapwells. $^{**}P < 0.01$ compared with the control group.

Distilled water used in the present work had a resistance >18.3 MΩ·cm and free-ionized calcium <2.5 nmol/l.

Measurement of electrical parameters. Electrical parameters, i.e., potential (voltage) difference (PD), short-circuit current (I_{sc}), and TER, were determined as described previously (7, 20). In brief, a pair of Ag/AgCl electrodes connected to agar bridges (3.0 mol/l KCl per 4 g% agar) was located near each surface of the mounted Snapwell for measurement of PD. The other ends of the PD-sensing electrodes were connected to a preamplifier (model EVC-4000; World Precision Instruments, Sarasota, FL). Another pair of Ag/AgCl electrodes connected in series to the EVC-4000 current-generating unit was placed at the end of each hemichamber to supply I_{sc} or external current for voltage clamping. TER was calculated from Ohm's equation. Fluid resistance was automatically subtracted by the EVC-4000 system.

Calcium flux measurement. Calcium fluxes were determined by modified method of Charoenphandhu et al. (7). After a 20-min incubation in Ussing chamber, the bathing solution was changed to a fresh one. The solution on one side contained ^{45}Ca (initial specific activity of 5 mCi/ml, final specific activity of ~450–500 mCi/mol; Amersham, Buckinghamshire, UK). Samples were collected from the chamber to calculate the unidirectional flux ($J_{H\rightarrow C}$) from the hot side (H) to the cold side (C), as follows:

$$J_{H\rightarrow C} = R_{H\rightarrow C}/(S_H \times A)$$

$$S_H = C_{45_{Ca}}/C_T$$

where $R_{H\rightarrow C}$ was the rate of tracer appearance in the cold side (cpm/h), S_H was the specific activity in the hot side (cpm/nmol), A was the surface area of Snapwell (cm^2), $C_{45_{Ca}}$ was a mean radioactivity in the hot side (cpm), and C_T was the total calcium in the hot side (nmol).

Radioactivity of ^{45}Ca in counts per minute (cpm) was analyzed by liquid scintillation spectrophotometer (model Tri-Carb 3100; Packard, Meriden, CT). Total calcium concentration in the hot side was determined by atomic absorption spectrophotometry (model SpectrAA-300; Varian Techtron, Springvale, Victoria, Australia). In the absence of transepithelial calcium gradient, i.e., bathing solution in both hemichambers contained equal calcium concentration of 1.25 mmol/l, the measured calcium fluxes represented the transcellular active calcium transport (45).

As for the experimental protocol, Caco-2 monolayer was directly incubated on the basolateral side for 60 min with 600 ng/ml recombinant human PRL (rhPRL) (purity >97%; catalog no. 682-PL; R&D Systems, Minneapolis, MN), which is the maximal effective concentration reported by Jantarajit et al. (20). In some experiments, the monolayers were also exposed to PKC activator [100 nmol/l phorbol-12-myristate-13-acetate (PMA), Calbiochem, San Diego, CA], or inhibitors for RNA polymerase II [50 μmol/l 5,6-dichloro-1-β-D-ribobenzimidazole (DRB), Calbiochem], protein biosynthesis (70 μmol/l cycloheximide, Sigma), L-type calcium channel (1, 5, or 10 μmol/l nifedipine, or 100 nmol/l verapamil; Sigma), calmodulin-dependent PMCA (100 μmol/l trifluoperazine, Sigma), $PKC_{\alpha/\beta}$ (5 μmol/l Gö-6976, Calbiochem), PKC_ζ (40 μmol/l myristoylated PKC_ζ pseudosubstrate peptide; Calbiochem), PKC_θ (30 μmol/l myristoylated PKC_θ pseudosubstrate peptide; Calbiochem), PKC_ε (4 μmol/l PKC_ε translocation inhibitor peptide; Calbiochem), or PKA (10 μmol/l myristoylated PKA inhibitor 14–22 amide; Calbiochem).

Voltage clamping. Calcium fluxes in clamped preparations represented the voltage-dependent calcium transport through the paracellular route (22). Transepithelial potential differences across the con-

Table 2. *Epithelial electrical parameters of Caco-2 monolayers*

Condition	n	Electrical Parameter		
		PD, mV	I_{sc}, μA/cm^2	TER, Ω·cm^2
Control	15	1.01±0.12	2.73±0.70	376.67±37.56
Vehicle	10	0.94±0.32	2.60±0.84	386.67±35.83
600 ng/ml rhPRL	15	0.88±0.19	3.47±0.92	253.22±28.01*
Inhibitors				
50 μmol/l DRB	12	1.03±0.28	2.50±0.67	418.75±82.28
70 μmol/l CCH	13	1.03±0.23	2.62±0.51	396.15±55.76
10 μmol/l Nifedipine	14	1.17±0.33	3.00±0.88	395.48±48.35
100 nmol/l Verapamil	10	0.95±0.22	2.50±0.53	381.67±46.78
100 μmol/l TFP	10	0.96±0.28	2.40±0.70	405.00±66.23
5 μmol/l Gö-6976	6	1.27±0.19	3.17±0.40	394.44±15.47
40 μmol/l myr-PKC_ζ	6	1.28±0.14	3.50±0.43	371.39±15.09
30 μmol/l myr-PKC_θ	6	1.08±0.12	2.67±0.33	430.56±23.34
4 μmol/l trans-PKC_ε	6	1.03±0.11	2.50±0.22	413.89±23.37
100 nmol/l PMA	4	1.08±0.13	2.25±0.25	408.33±49.30
10 μmol/l PKAI 14-22	4	1.00±0.12	2.50±0.58	408.35±48.11
600 ng/ml rhPRL$^+$				
50 μmol/l DRB	12	0.83±0.31	3.33±1.03	241.39±40.14*
70 μmol/l CCH	13	0.89±0.27	3.46±0.88	256.28±36.57*
10 μmol/l Nifedipine	14	0.77±0.22	3.14±0.77	243.45±29.63*
100 nmol/l Verapamil	10	0.92±0.40	3.67±1.37	245.83±34.86*
100 μmol/l TFP	10	0.87±0.16	3.50±0.55	248.61±35.13*
5 μmol/l Gö-6976	6	1.02±0.21	3.83±0.98	268.06±19.62*
40 μmol/l myr-PKC_ζ	6	1.00±0.19	4.50±0.89	225.00±06.80*
30 μmol/l myr-PKC_θ	6	1.13±0.20	4.33±0.71	259.80±08.52*
4 μmol/l trans-PKC_ε	6	0.93±0.19	3.50±1.05	276.94±49.89*
100 nmol/l PMA	4	1.00±0.21	4.00±0.82	250.00±10.21*
10 μmol/l PKAI 14-22	4	0.95±0.13	3.75±0.50	254.17±22.05*

Values are means ± SE. Caco-2 monolayer was exposed to recombinant human prolactin (rhPRL), RNA polymerase II inhibitor [5,6-dichloro-1-β-D-ribobenzimidazole (DRB)], protein synthesis inhibitor [cycloheximide (CCH)], L-type calcium channel blockers (nifedipine and verapamil), plasma membrane Ca^{2+}-ATPase (PMCA) inhibitor [trifluoperazine (TFP)], PKC inhibitors [Gö-6976 for $PKC_{\alpha/\beta}$, myristoylated (myr) pseudosubstrates for $PKC_{\zeta/\theta}$ and translocation (trans) inhibitor peptide for PKC_ε], PKC activator (PMA), myristoylated PKA inhibitor 14-22 amide (PKAI 14-22), or rhPRL plus inhibitors. DMSO (0.3% vol/vol) was used as vehicle for preparation of inhibitors. Mounted monolayer was bathed on both sides with 1.25 mmol/l calcium-containing solution. The apical side was negative with respect to the basolateral side. PD, potential difference; I_{sc}, short-circuit current; TER, transepithelial resistance. $^*P < 0.01$ compared with the control group.

trol and 600 ng/ml rhPRL-treated monolayers were clamped to −25, −10, −5, 0, +5, +10, or +25 mV (the serosal side was considered zero) during 60-min experiment by using EVC-4000 system. Transepithelial calcium fluxes in apical-to-basolateral (A-to-B) and basolateral-to-apical (B-to-A) directions were determined. Net calcium flux was a subtraction of B-to-A flux from A-to-B flux. In some experiments, Caco-2 monolayers (n = 5 per each voltage; total 280 Snapwells used) were exposed to 600 ng/ml rhPRL plus PI3K inhibitor (75 μmol/l LY-294002; Tocris Bioscience, Bristol, UK), panspecific PKC inhibitor (1 μmol/l GF-109203X; AG Scientific, San Diego, CA), or ROCK inhibitor (1 μmol/l Y-27632; Calbiochem).

Calcium uptake study. The calcium uptake protocol was modified from the method of Charoenphandhu et al. (6). In brief, Caco-2 cells (1.0×10^6 cells/cm^2) were propagated in 6-well plates for 3 days. Confluent Caco-2 cells were then incubated with 600 ng/ml rhPRL for 60 min until ^{45}Ca was added to obtain a final specific activity of ~500 mCi/mol. After exactly 1-, 3-, 6-, 9-, 12-, 20-, 30-, or 40-min exposure to ^{45}Ca (n = 5 per each time interval; total 225 setups used; cells for 0 min were not incubated with ^{45}Ca), cells were immediately washed in ice-cold ^{45}Ca-free solution to stop the physiological processes, placed in 5 mmol/l EGTA-containing solution to eliminate the adsorbed extracellular calcium, centrifuged at 550 g for 5 min, and finally lysed by 30% vol/vol Triton X-100. Radioactivity of ^{45}Ca in the homogenate was analyzed by a liquid scintillation spectrophotometer (Packard). Cellular protein was determined by bicinchoninic acid method using a commercial kit (Sigma). In some experiments, 600 ng/ml rhPRL-treated cells were also incubated with 75 μmol/l LY-294002, 1 μmol/l GF-109203X, or 1 μmol/l Y-27632.

Statistical analysis. Results are expressed as means ± SE. Two sets of data were compared using the unpaired Student's t-test. One-way analysis of variance with Dunnett's multiple-comparison test was used for multiple sets of data. The level of significance for all statistical tests was $P < 0.05$. The curves of calcium uptake vs. time and of calcium flux vs. voltage were obtained using one-phase association and second-order polynomial equations, respectively (36). Data were analyzed by GraphPad Prism 4.0 for Mac OS X (GraphPad Software, San Diego, CA).

RESULTS

PRL signaling in Caco-2 monolayer was nongenomic and protein synthesis independent. Calcium flux studies using Ussing chamber technique demonstrated that 600 ng/ml rhPRL significantly increased the transcellular calcium transport by ~2.13-fold (Fig. 1), while decreasing TER in Caco-2 monolayer (Table 2). PRL effects occurred within 60 min after treatment. Exposure to PRL plus inhibitors of de novo gene transcription (50 μmol/l DRB) or protein biosynthesis (70 μmol/l cycloheximide) had no effect on the transcellular calcium transport (Fig. 1). DRB or cycloheximide alone were without effect on the basal calcium transport (Fig. 1) and

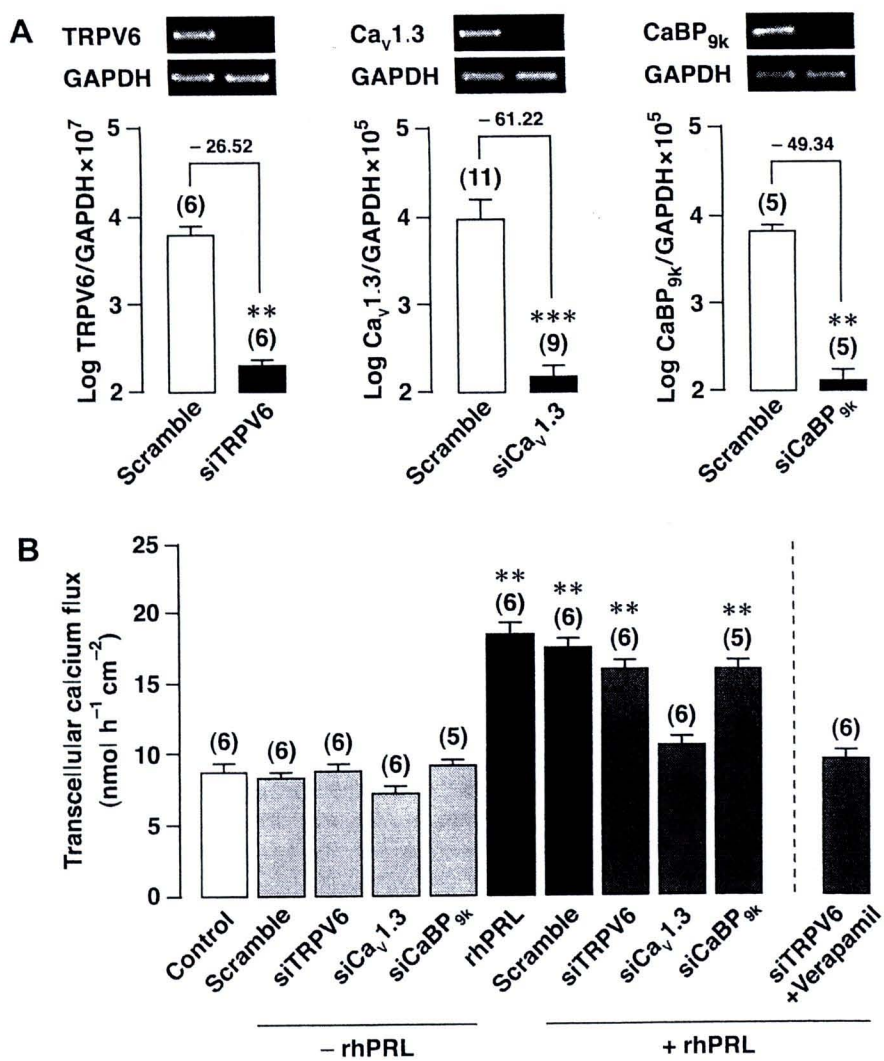

Fig. 2. *A*: expression of transient receptor potential vanilloid family calcium channel 6 (TRPV6), voltage-dependent L-type Ca^{2+} channel 1.3 ($Ca_v1.3$) and calbindin-D_{9k} ($CaBP_{9k}$) in Caco-2 cells transfected with scramble small interfering RNA (siRNA; negative control) or siRNA targeting (si) TRPV6, $Ca_v1.3$, or $CaBP_{9k}$ mRNAs. Quantitative real-time PCR (qRT-PCR) results are expressed as log means ± SE. Representative electrophoretic bands and fold differences between the expression in control and knockdown cells (conventional PCR, 36 cycles) are also presented along with qRT-PCR results. GAPDH was used for normalization. $^{**}P < 0.01$, $^{***}P < 0.001$ compared with scramble. *B*: transcellular calcium transport in TRPV6, $Ca_v1.3$, and $CaBP_{9k}$ knockdown Caco-2 monolayers with (+rhPRL) or without (−rhPRL) 600 ng/ml rhPRL in the basolateral solution. In some experiments, TRPV6 knockdown monolayers were exposed to 600 ng/ml rhPRL plus 100 nmol/l verapamil ($Ca_v1.3$ blocker; on the apical side). Control group denotes normal Caco-2 monolayers (without siRNA transfection). $^{**}P < 0.01$ compared with the control group. Numbers in parentheses represent the number of independent Snapwells.

Table 3. *Epithelial electrical parameters of knockdown Caco-2 monolayers*

Condition	n	Electrical Parameter		
		PD, mV	I_{sc}, μA/cm²	TER, Ω·cm²
Control	6	0.98±0.24	2.33±0.52	427.78±89.24
Scramble	6	0.88±0.54	2.17±1.17	409.72±66.34
siTRPV6	6	0.98±0.43	2.33±0.82	416.67±75.28
si$Ca_v1.3$	6	0.90±0.30	2.60±0.24	391.67±49.16
si$CaBP_{9k}$	5	1.10±0.23	3.17±0.75	351.38±35.13
siPKC_ζ	3	0.87±0.21	2.33±0.58	372.22±25.46
600 ng/ml rhPRL	6	0.84±0.11	3.17±0.98	248.89±27.22*
600 ng/ml rhPRL⁺				
Scramble	6	0.75±0.58	2.83±1.60	250.00±49.55*
siTRPV6	6	0.82±0.37	3.17±1.17	252.22±35.07*
si$Ca_v1.3$	6	0.93±0.62	3.67±1.86	243.06±33.51*
si$CaBP_{9k}$	5	1.00±0.28	4.17±1.17	242.22±34.10*
siTRPV6 + verapamil	6	0.87±0.27	3.83±0.98	225.28±31.10*
siPKC_ζ	3	0.80±0.30	3.33±0.58	236.11±60.28*

Values are means ± SE. Caco-2 cells were transfected with small interfering (si)RNAs targeting (si) TRPV6, $Ca_v1.3$, calbindin-D_{9k} ($CaBP_{9k}$), or PKC_ζ. Mounted monolayer was bathed on both sides with 1.25 mmol/l calcium-containing solution. The apical side was negative with respect to the basolateral side. In some experiments, TRPV6-knockdown monolayers were incubated with 100 nmol/l verapamil, which inhibited $Ca_v1.3$ activity. *$P < 0.01$ compared with the control group.

electrical parameters (Table 2). The effect of DRB were consistent with that reported previously (45). The data indicated that PRL exerted stimulatory effects on the transcellular calcium transport via nongenomic, protein synthesis-independent signaling pathways.

PRL increased transcellular calcium transport via L-type calcium channel $Ca_v1.3$ and PMCA. In the transcellular calcium transport, calcium has been reported to traverse the apical membrane through TRPV6 and $Ca_v1.3$ before binding to calbindin-D_{9k} for cytoplasmic translocation to the basolateral side (18, 31, 34). We therefore generated siRNA-transfected Caco-2 monolayers to verify the significance of each putative protein in the PRL-stimulated calcium transport. We show in Fig. 2 that knockdown of TRPV6, $Ca_v1.3$, and calbindin-D_{9k} markedly reduced mRNA expressions by 26.52-, 61.22-, and 49.34-fold, respectively, with no significant effect on the basal calcium transport or electrical parameters (Table 3). Interestingly, the PRL-enhanced calcium transport was completely abolished in $Ca_v1.3$ knockdown monolayer, and not in the TRPV6 and calbindin-D_{9k} knockdown monolayers (Fig. 2*B*). Exposure to 1, 5, and 10 μmol/l nifedipine, a classical L-type calcium channel blocker (dihydropyridine group), on the apical side, but not the basolateral side, diminished the PRL-stimulated transcellular calcium transport in a concentration-dependent manner (Fig. 3). Similar inhibition was observed after incubating Caco-2 monolayer on the apical side with another L-type calcium channel blocker, verapamil (phenylalkylamine group) (Fig. 3). The involvement of $Ca_v1.3$ in the calcium transport response to PRL was supported by the finding that 100 nmol/l verapamil could prevent the PRL-stimulated calcium transport in TRPV6 knockdown monolayer (Fig. 2*B*). The results, therefore, indicated that $Ca_v1.3$ at the apical membrane was required for calcium entry during the PRL-stimulated transcellular calcium transport. Basolateral calcium extrusion under PRL stimulation was likely to be mediated by PMCA rather than NCX1, since calcium flux was totally abolished by a calmodulin-dependent PMCA inhibitor trifluoperazine (Fig. 3).

PRL stimulated apical calcium uptake via the PKC signaling pathway. Although $Ca_v1.3$, a channel for calcium entry, was required for PRL actions, the effects of PRL on apical calcium uptake in Caco-2 cells as well as responsible signaling pathways were not known. Herein, the calcium uptake study showed that, under normal conditions, the relationship between calcium uptake and time complied with the one-phase association equation ($r^2 = 0.95$), and calcium accumulation in Caco-2 cells ascended to the maximal value (Y_{max}) of ~15 nmol/μg protein with a rate constant of ~0.15 min^{-1} (Fig. 4). Exposure to 600 ng/ml rhPRL did not change Y_{max} value. However, the rate constant that represented the rate of calcium uptake was increased in PRL-treated cells by approximately twofold (Fig. 4*D*).

To demonstrate the PRL signaling pathways for stimulation of apical calcium uptake, Caco-2 cells were incubated with inhibitors for PI3K, PKC, and ROCK, all of which have been reported to mediate PRL actions in intestinal epithelial cells (20, 45). The results showed that PI3K inhibitor (LY-294002) and panspecific PKC inhibitor (GF-109203X), but not ROCK

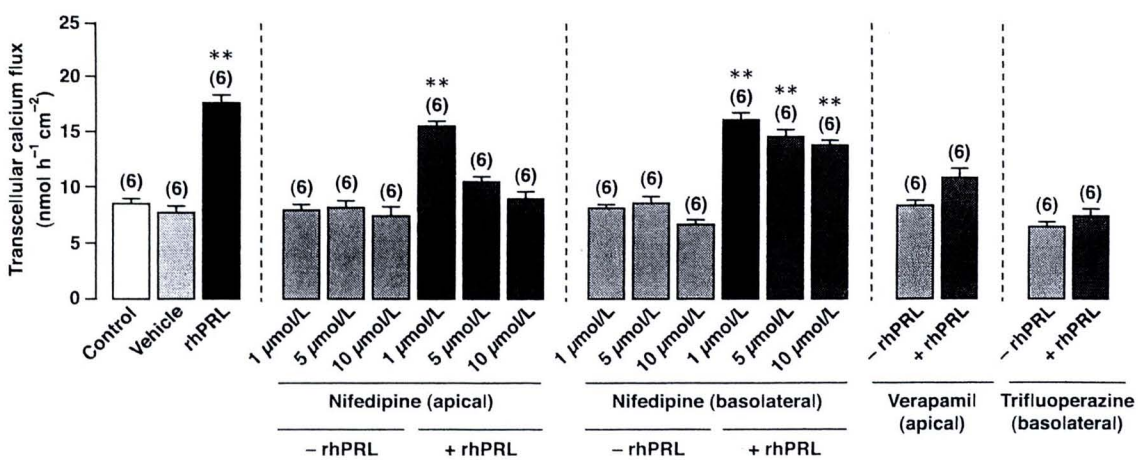

Fig. 3. Transcellular calcium transport in Caco-2 monolayers directly exposed on the apical side to L-type calcium channel blockers (1, 5, and 10 μmol/l nifedipine or 100 nmol/l verapamil), or on the basolateral side to various concentrations of nifedipine or plasma membrane Ca^{2+}-ATPase (PMCA) inhibitor (100 μmol/l trifluoperazine) in the presence (+rhPRL) and absence (−rhPRL) of 600 ng/ml rhPRL. DMSO was used as vehicle for inhibitor preparation. Numbers in parentheses represent the number of independent Snapwells. **$P < 0.01$ compared with the control group.

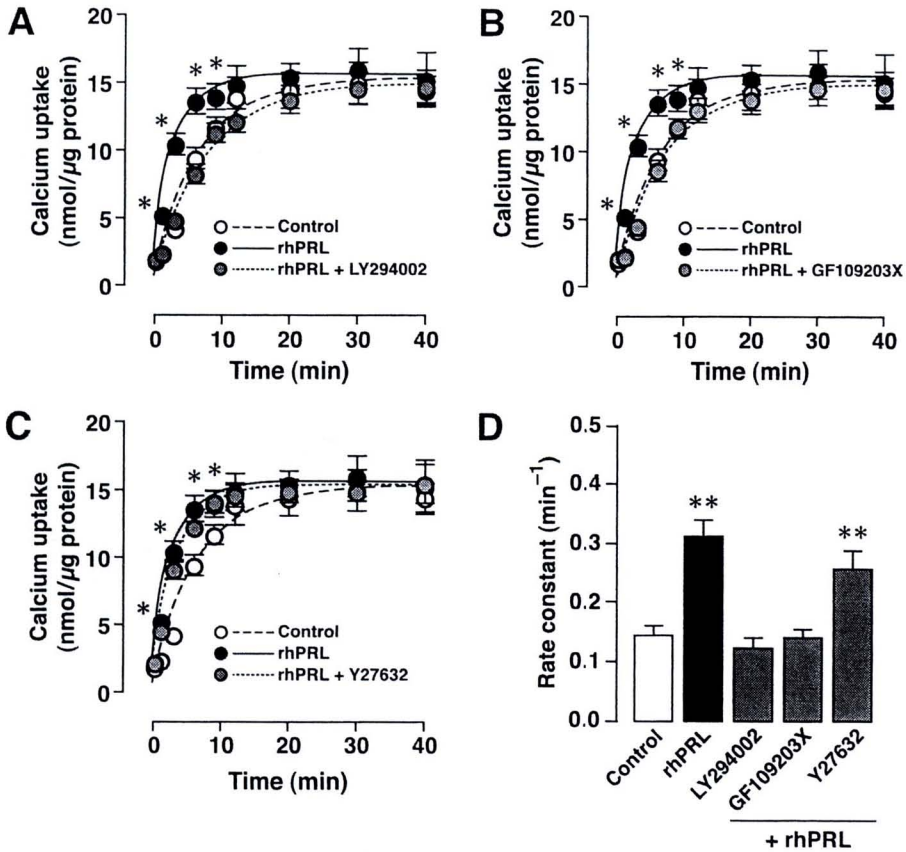

Fig. 4. Calcium uptake in Caco-2 cells ($n = 5$ per each time interval; total 225 Snapwells used) treated with 600 ng/ml rhPRL, or rhPRL plus phosphoinositide 3-kinase (PI3K) inhibitor (75 μmol/l LY-294002) (*A*), panspecific PKC inhibitor (1 μmol/l GF-109203X) (*B*), or RhoA-associated coiled-coil forming kinase (ROCK) inhibitor (1 μmol/l Y-27632) (*C*). Cells were incubated in ^{45}Ca-containing solution for 0, 1, 3, 6, 9, 12, 20, 30, or 40 min. Control and rhPRL data in *A* were reused in *B* and *C* for better comparison. $^*P < 0.01$ rhPRL vs. control. *D*: rate constant, which is indicative of the rate of calcium uptake, in Caco-2 cells exposed to rhPRL or rhPRL plus inhibitors. Data were obtained from the one-phase association curves in *A–C*. $^{**}P < 0.01$ compared with the control group.

inhibitor (Y-27632), could abolish the effect of PRL on calcium uptake (Fig. 4).

The effect of PRL on the transcellular calcium transport was mediated by PKC$_\zeta$. Since the calcium uptake study showed that PKC was required for the PRL-stimulated transcellular calcium transport, we proceeded to identify the responsible PKC isozyme by exposing Caco-2 monolayer to various PKC isozyme inhibitors in the presence or absence of 600 ng/ml rhPRL. We demonstrated that PKC inhibitors alone had no effect on the basal calcium transport (Fig. 5). PKC$_\zeta$ inhibitor, but not inhibitors of PKC$_{\alpha/\beta}$ (Gö-6976), PKC$_\theta$, or PKC$_\varepsilon$, abolished the PRL-enhanced transcellular calcium transport in Caco-2 monolayer (Fig. 5). Since a high concentration of Gö-6976 (5 μmol/l) used in the present study also inhibited PKC$_\mu$ (16), it was likely that PRL action did not involve PKC$_\mu$. A classical PKC activator, phorbol-12-myristate-13-acetate (PMA), which could not activate PKC$_\zeta$, also itself stimulated the transcellular calcium transport but with a smaller magnitude than PRL (Fig. 5). Exposure to 600 ng/ml rhPRL further increased calcium transport in PMA-treated monolayer (Fig. 5). Neither PKC inhibitors nor PMA had effect on the PRL-induced decrease in TER (Table 2).

Since a number of hormones, such as parathyroid hormone and $1,25(OH)_2D_3$, enhanced calcium transport through the

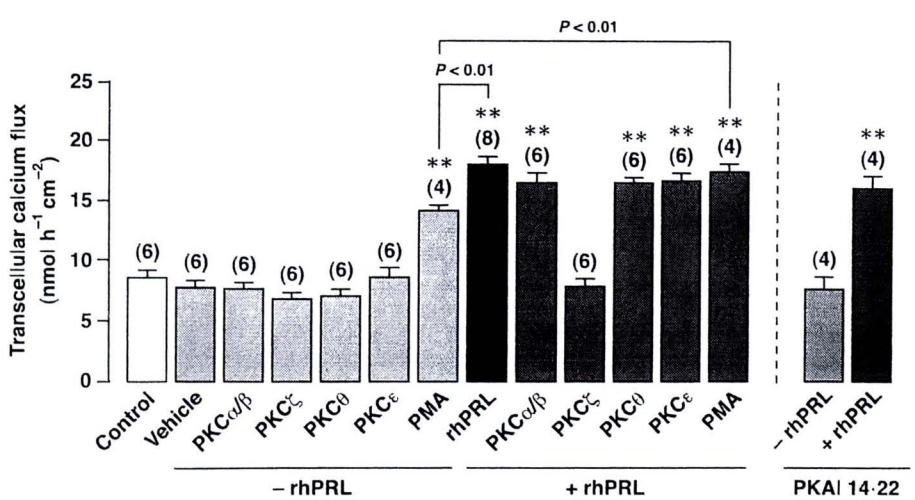

Fig. 5. Transcellular calcium transport in Caco-2 monolayers exposed to selective PKC$_{\alpha/\beta}$ inhibitor (5 μmol/l Gö-6976), 40 μmol/l myristoylated PKC$_\zeta$ pseudosubstrate peptide, 30 μmol/l myristoylated PKC$_\theta$ pseudosubstrate peptide, 4 μmol/l PKC$_\varepsilon$ translocation inhibitor peptide, PKC activator (100 nmol/l phorbol-12-myristate-13-acetate; PMA), or 10 μmol/l myristoylated PKA inhibitor 14-22 amide (PKAI 14-22), in the presence (+rhPRL) or absence (−rhPRL) of 600 ng/ml rhPRL. All cell-permeable inhibitor peptides were dissolved in water. Gö-6976 and PMA were dissolved in DMSO (vehicle). Numbers in parentheses represent the number of independent Snapwells. $^{**}P < 0.01$ compared with the control group.

transcellular route in a protein kinase A (PKA)-dependent manner (10, 11, 23), we examined a possibility of PKA-mediated PRL action. However, exposure to a cell-permeable PKA inhibitor, myristoylated PKA inhibitor 14-22 amide, did not prevent the PRL effect on the transcellular calcium transport (Fig. 5).

PKC_ζ knockdown abolished the PRL-stimulated transcellular calcium transport. To confirm that PRL exerted its actions through PKC_ζ, calcium fluxes were determined in PKC_ζ knockdown Caco-2 monolayer, which manifested a decrease in PKC_ζ mRNA expression by 68.86-fold (Fig. 6*A*). The results showed that 600 ng/ml rhPRL did not increase the transcellular calcium flux in PKC_ζ knockdown monolayer (Fig. 6*B*), while neither scramble siRNA nor PKC_ζ siRNA altered the basal calcium flux (Fig. 6*B*) or electrical parameters (Table 3). However, PKC_ζ knockdown had no effect on the PRL-induced decrease in TER (Table 3).

PRL enhanced the voltage-dependent paracellular calcium via ROCK pathway. In addition to the transcellular pathway, PRL has been reported to augment calcium movement through the paracellular space. However, effects of PRL on the voltage-dependent paracellular calcium transport were not known. Under normal conditions, the voltage-clamp study revealed that the apical-to-basolateral (A-to-B; Fig. 7*A*) calcium fluxes were dramatically increased with positive apical voltage (basolateral voltage was zero), whereas the increase in basolateral-to-apical (B-to-A; Fig. 7*B*) calcium fluxes with negative apical voltage was comparatively much smaller. Given an equal driving force (i.e., transepithelial voltage) of opposite signs, the presence of unidirectional calcium fluxes being larger in one direction than the other suggested that the paracellular space of Caco-2 monolayer possessed a property known as rectification. This phenomenon, therefore, resulted in a large net calcium flux (equivalent to electrical current) at apical voltage positive and a relatively small net calcium flux at voltage negative (Fig. 7, *C* and *F*).

PRL-treated Caco-2 monolayer exhibited significant increases in A-to-B and B-to-A calcium fluxes at the apical voltage ranges of 0 to +25 mV and −25 to −5 mV, respectively, thereby increasing the net calcium fluxes (Fig. 7*C*). Interestingly, after PRL exposure, the B-to-A calcium flux vs. voltage curve nearly became a mirror image of the A-to-B curve. In other words, paracellular space of PRL-treated Caco-2 monolayer no longer exhibited rectification. Such PRL effects on the voltage-dependent paracellular calcium transport were completely abolished by 75 μmol/l LY-294002 (Fig. 7, *A–C*) and 1 μmol/l Y-27632 (Fig. 7, *D–F*), which were PI3K and ROCK inhibitors, respectively.

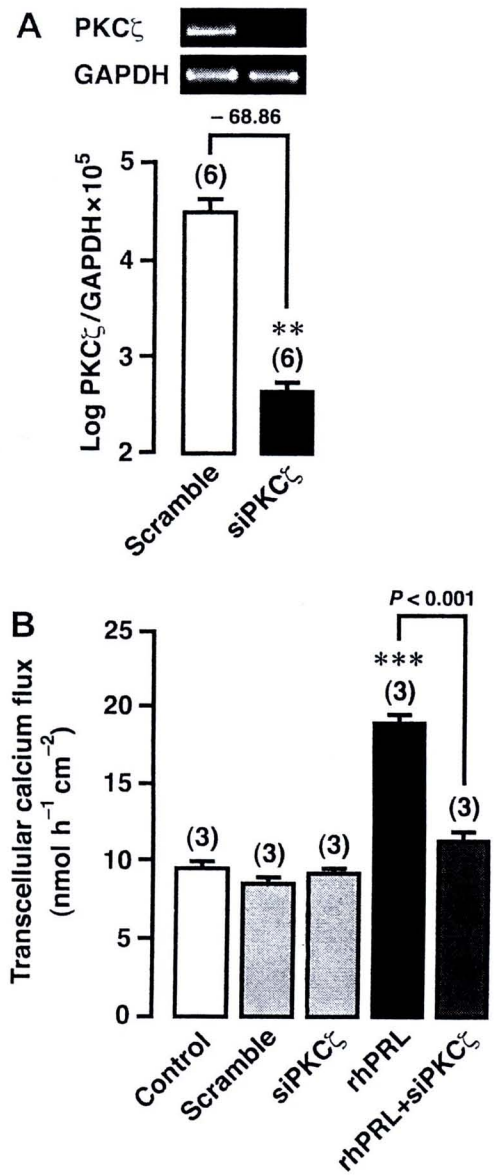

Fig. 6. *A*: expression of PKC_ζ in Caco-2 cells transfected with scramble siRNA (negative control) or siRNA targeting PKC_ζ. qRT-PCR results are expressed as log means ± SE. Representative electrophoretic bands and fold differences between the expression in control and knockdown cells (conventional PCR, 36 cycles) are also presented along with qRT-PCR results. GAPDH was used for normalization. $^{**}P < 0.01$ compared with scramble. *B*: transcellular calcium transport in PKC_ζ knockdown Caco-2 monolayers exposed to 600 ng/ml rhPRL. The control group denotes normal Caco-2 monolayers (without siRNA transfection). $^{***}P < 0.001$ rhPRL vs. rhPRL + $siPKC_\zeta$. Numbers in parentheses represent the number of independent Snapwells.

DISCUSSION

Although the cellular mechanism of PRL action was still not fully understood, a twofold increase in the intestinal calcium absorption both in vivo and in vitro induced by PRL suggested a significant role of this hormone as a regulator of calcium homeostasis in conditions of high circulating PRL levels, such as in pregnancy and lactation (5). In the present study, we provided further information on the cellular mechanism of PRL as well as the possible signaling pathways. Acting via PI3K and PKC_ζ, PRL enhanced the transcellular active calcium transport by increasing calcium entry through $Ca_v1.3$ and the basolateral calcium extrusion by PMCA. PRL also stimulated the voltage-dependent paracellular calcium transport through PI3K and ROCK.

The theoretical concept of the transcellular calcium transport in the intestine was recently challenged by the findings that calbindin-D_{9k} knockout and TRPV6/calbindin-D_{9k} double-knockout mice were normocalcemic and still exhibited active calcium absorption (1, 2, 27). We also found in this study that the rapid nongenomic effects of PRL on the transcellular active calcium transport in Caco-2 monolayer did not require the

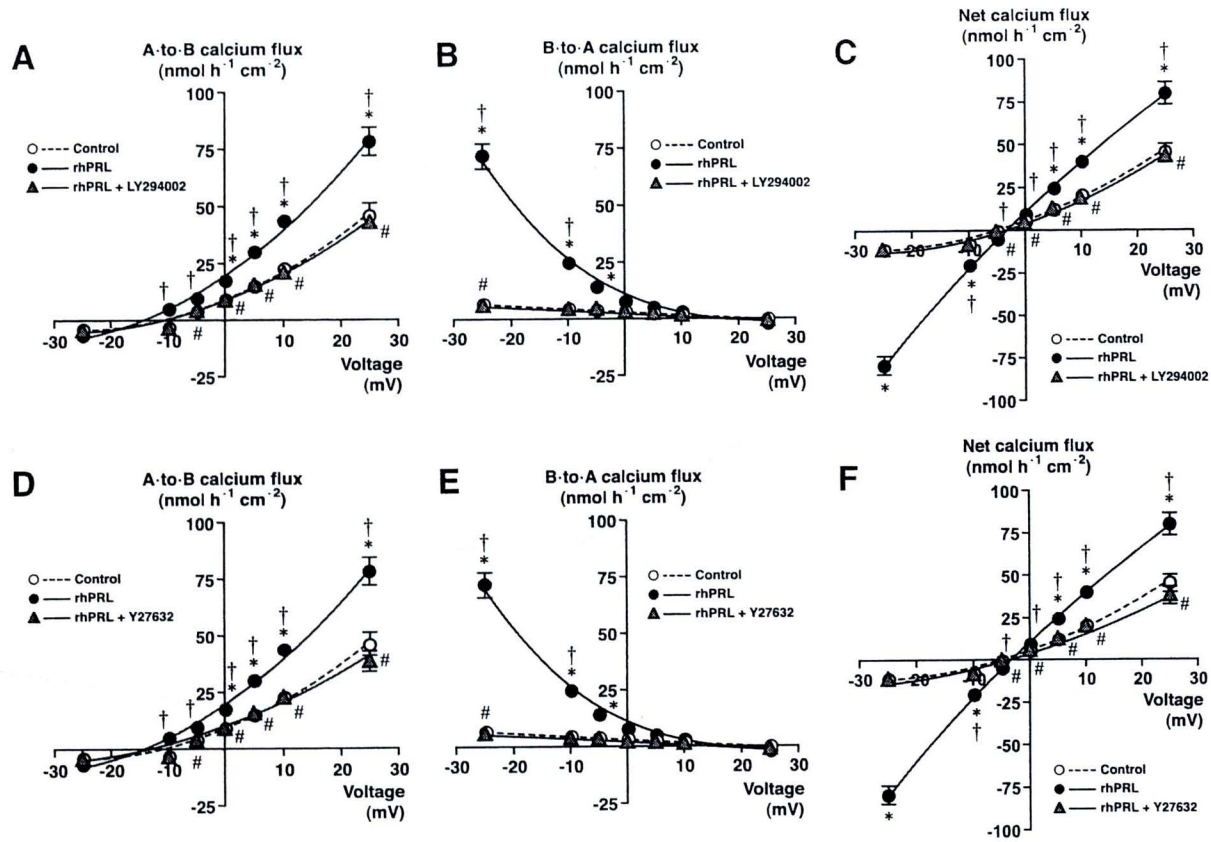

Fig. 7. Effects of PI3K inhibitor (75 μmol/l LY-294002) (*A–C*) and ROCK inhibitor (1 μmol/l Y-27632) (*D–F*) on the PRL-enhanced voltage-dependent paracellular calcium transport across Caco-2 monolayer ($n = 5$ per each voltage point; total 280 Snapwells used). The apical voltage was clamped to −25, −10, −5, 0, +5, +10, or +25 mV, with the basolateral side being a reference. Calcium fluxes in the apical-to-basolateral (A-to-B) (*A* and *D*) and basolateral-to-apical (B-to-A) (*B* and *E*) directions as well as net calcium fluxes (*C* and *F*) are presented. By using paired Snapwells, the net calcium flux was a subtraction of B-to-A flux from A-to-B flux. The mounted Snapwell was bathed on both sides with 1.25 mmol/l Ca^{2+}-containing solution. $^*P < 0.01$ rhPRL vs. control. †$P < 0.01$, value of the rhPRL-treated group vs. value of the rhPRL-treated group at −25 mV (for A-to-B and net flux) or +25 mV (for B-to-A). #$P < 0.01$ value of the control group vs. value of the control group at −25 mV (for A-to-B and net flux) or +25 mV (for B-to-A). Values of the control and rhPRL-treated groups in *D*, *E*, and *F* are from those in *A*, *B*, and *C*, respectively.

presence of TRPV6 or calbindin-D_{9k}, although both transport proteins may contribute to the responses to other hormones, such as genomic $1,25(OH)_2D_3$, 17β-estradiol, and glucocorticoids (19, 46). It appeared that redundancy in the mechanisms underlying calcium absorption may involve other calcium channel(s), such as L-type and T-type calcium channels, which could provide alternative route for apical calcium entry (9). Supporting evidence was provided by recent reports that dihydropyridine (nifedipine)- and phenylalkylamine (verapamil)-sensitive L-type calcium channel $Ca_v1.3$ could mediate calcium entry for the transcellular calcium absorption, especially during ingestion of high-calcium diet (31, 34). Nifedipine and verapamil also inhibited the stimulatory effects of parathyroid hormone-related peptide, nongenomic $1,25(OH)_2D_3$, and luminal glucose on intestinal calcium absorption (10, 34, 51). Our previous microarray study has identified several L-type calcium channels upregulated in the duodenal epithelial cells of the pituitary-grafted hyperprolactinemic rats (8). Here, the absence of PRL effect on calcium transport after $Ca_v1.3$ knockdown or nifedipine/verapamil exposure strongly suggested a physiological role of $Ca_v1.3$ during PRL stimulation.

Similar to the apical calcium entry, the cytoplasmic calcium translocation across the intestinal epithelial cells may be mediated by other calcium-binding proteins (CaBP) besides calbindin-D_{9k}, e.g., calmodulin and parvalbumin, as well as vesicular calcium transport (3, 13). Interestingly, the duodenal epithelial cells of hyperprolactinemic rats were found to manifest a ~17-fold increase in parvalbumin mRNA expression as demonstrated by microarray (8), but its physiological significance in calcium transport remains to be investigated. Regarding the basolateral calcium extrusion, ~80–85% of calcium efflux normally occurs through PMCA, whereas the remaining is performed by NCX1 (18, 49). PRL was previously found to increase PMCA activity in purified basolateral membrane vesicles from the duodenum (6); therefore, PMCA was likely to mediate the PRL-enhanced calcium transport.

As for the paracellular pathway, the present results together with that reported by Thongon et al. (45) suggest that PRL augmented the paracellular calcium absorption in a concentration- and voltage-dependent manner. In the study of passive calcium absorption, PRL was found to alter the charge-selective property of tight junction without changing the pore size, thereby increasing calcium permeability and calcium flux through the paracellular route (44, 45). Our present investigation (Fig. 7) further suggests that the paracellular pores for calcium transport are rectifiers. In other words, the paracellular pores can conduct much larger A-to-B calcium flux at apical voltages positive than B-to-A calcium flux at apical voltage

negative even in an absence of the transepithelial calcium gradient, rendering the degree of rectification $J_{i,+25}/J_{o,-25} = 46.23/6.95 \approx 7$ (where J represents calcium flux in $nmol \cdot h^{-1} \cdot cm^{-2}$ at +25 mV or −25 mV; i and o denote A-to-B and B-to-A, respectively). The paracellular rectification could be explained by a model of a channel (or pore) with an energy barrier that impedes calcium movement in a B-to-A direction (for review see Ref. 41). Although the exact paracellular structures acting as the energy barrier have never been identified, we speculated that they might be tight junction proteins, claudins, which had their charge-selective extracellular loops protruding into the paracellular space (47). Several claudins, such as claudin-2, -3, and -12, are known to be involved in the intestinal calcium absorption (7, 15).

After exposure to PRL, the voltage-dependent calcium transport in both A-to-B and B-to-A directions were markedly increased, and the degree of rectification was reduced to ~1, suggesting that an energy barrier or cation-selective barriers of the paracellular pores were removed by PRL. Changes in the paracellular barrier properties could have resulted from the PRL-induced claudin phosphorylation (L. Nakkrasae and N. Charoenphandhu, unpublished observation, 2009). PRL-enhanced voltage-dependent paracellular calcium transport may be of physiological importance, presumably when the intestinal absorptive cells were exposed to nutrients that could alter the transepithelial potential difference, e.g., glucose, short-chain fatty acid, and neutral amino acids (14, 40, 48). Although the modulation of potential difference could also facilitate calcium transport via the transcellular pathway (11), the transcellular calcium transport was much smaller in magnitude when compared with the paracellular calcium transport, particularly in Caco-2 monolayer (7, 45). However, there was a disparity regarding the magnitude of paracellular calcium flux between different models. For example, in perfused intestinal loop, nifedipine inhibited calcium absorption in the presence of 10 mmol/l luminal calcium with similar extent to 1.25 mmol/l calcium, suggesting that the majority of calcium flux in this model was Ca_v mediated rather than diffusive paracellular (35).

The action of PRL on calcium absorption involved the signaling molecules PI3K, PKC, and ROCK (20, 45). PI3K was likely to be the most upstream mediator, which transmitted PRL signals to PKC and ROCK for the transcellular and paracellular calcium transport, respectively (17, 21, 29, 45). In some cells, e.g., L6 muscle cells, PKC_ζ is a key molecule within the PI3K signal cascade (39). PKC is a large family of serine/threonine kinases, consisting of ~12 members (33). Some PKC isozymes, e.g., PKC_α, PKC_β, and PKC_θ, but not PKC_ζ, are activated by diacylglycerol (DAG), rendering them sensitive to DAG analog phorbol ester (i.e., PMA) (33). Several investigators provided evidence that activities of the transcellular calcium transport proteins TRPV6, $Ca_v1.3$, and PMCA could be modulated by PKA and/or PKC, especially $PKC_{\beta II}$ (23, 24, 34). However, PKA and phorbol-sensitive PKCs (e.g., PKC_α, PKC_β, and PKC_θ) were not involved in PRL signaling, since PRL actions were blocked only by an inhibitor or siRNA of PKC_ζ, which is a phorbol-insensitive isozyme (33). The presence of the additive effect of PRL in PMA-treated monolayer also suggested that PRL signaled through another signaling pathway that was not phorbol-sensitive PKCs. The absence of PRL-PMA synergism or truly additive effect, on the other hand, probably indicated that PKC_ζ and phorbol-sensitive PKCs shared some target proteins.

In addition to the calcium gradient-dependent calcium transport, PRL exerted its stimulatory effects on the voltage-dependent calcium transport via ROCK pathway. PRL was previously reported to use the Rho-associated pathway in endothelial cells (28), in which a GTP-bound RhoA activated the serine/threonine kinase ROCK. In T84 colonic adenocarcinoma cell monolayer, the presence of Rho/ROCK activities was essential for a decrease in TER and disassembly of apical junctional complex triggered by extracellular calcium depletion (42). However, it is currently unknown as to why the PRL-induced decrease in TER, which was closely related to the increased paracellular permeability, was not abolished by LY-294002 and Y-27632. It was possible that PRL may have other signaling molecules for modulation of paracellular properties. PKC_ζ might be not involved in the PRL-enhanced calcium transport via the paracellular pathway because PKC_ζ inhibitor was without effect on the PRL-induced decrease in TER.

In conclusion, we demonstrated that PRL stimulated the transcellular active calcium transport via $Ca_v1.3$ and PMCA, but not TRPV6, calbindin-D_{9k}, or NCX1. Such PRL action was mediated by PI3K and phorbol-insensitive PKC_ζ in a nongenomic manner. Moreover, PRL removed the paracellular rectification and enhanced the voltage-dependent paracellular calcium transport via the PI3K and ROCK pathways. The present findings provide more detailed information on the cellular mechanisms of PRL in the intestinal epithelial cells, which could be used to explain how PRL enhances calcium absorption in pregnant and lactating animals.

GRANTS

This research was supported by grants from the Royal Golden Jubilee (RGJ) Program (PHD48K0063 to N. Thongon) and the Faculty of Science, Burapha University (to N. Thongon), the Mahidol University Postdoctoral Fellowship Program (to L. Nakkrasae), the Commission on Higher Education, and the Thailand Research Fund (RSA5180001 to N. Charoenphandhu, and RTA5080008 to N. Krishnamra).

REFERENCES

1. **Akhter S, Kutuzova GD, Christakos S, DeLuca HF.** Calbindin D_{9k} is not required for 1,25-dihydroxyvitamin D_3-mediated Ca^{2+} absorption in small intestine. *Arch Biochem Biophys* 460: 227–232, 2007.
2. **Benn BS, Ajibade D, Porta A, Dhawan P, Hediger M, Peng JB, Jiang Y, Oh GT, Jeung EB, Lieben L, Bouillon R, Carmeliet G, Christakos S.** Active intestinal calcium transport in the absence of transient receptor potential vanilloid type 6 and calbindin-D_{9k}. *Endocrinology* 149: 3196–3205, 2008.
3. **Bindels RJ, Timmermans JA, Hartog A, Coers W, van Os CH.** Calbindin-D_{9k} and parvalbumin are exclusively located along basolateral membranes in rat distal nephron. *J Am Soc Nephrol* 2: 1122–1129, 1991.
4. **Boass A, Lovdal JA, Toverud SU.** Pregnancy- and lactation-induced changes in active intestinal calcium transport in rats. *Am J Physiol Gastrointest Liver Physiol* 263: G127–G134, 1992.
5. **Charoenphandhu N, Krishnamra N.** Prolactin is an important regulator of intestinal calcium transport. *Can J Physiol Pharmacol* 85: 569–581, 2007.
6. **Charoenphandhu N, Limlomwongse L, Krishnamra N.** Prolactin directly enhanced Na^+/K^+- and Ca^{2+}-ATPase activities in the duodenum of female rats. *Can J Physiol Pharmacol* 84: 555–563, 2006.
7. **Charoenphandhu N, Tudpor K, Pulsook N, Krishnamra N.** Chronic metabolic acidosis stimulated transcellular and solvent drag-induced calcium transport in the duodenum of female rats. *Am J Physiol Gastrointest Liver Physiol* 291: G446–G455, 2006.
8. **Charoenphandhu N, Wongdee K, Teerapornpuntakit J, Thongchote K, Krishnamra N.** Transcriptome responses of duodenal epithelial cells

to prolactin in pituitary-grafted rats. *Mol Cell Endocrinol* 296: 41–52, 2008.

9. **Couchourel D, Leclerc M, Filep J, Brunette MG.** Testosterone enhances calcium reabsorption by the kidney. *Mol Cell Endocrinol* 222: 71–81, 2004.
10. **De Boland AR, Norman A.** Evidence for involvement of protein kinase C and cyclic adenosine 3′,5′ monophosphate-dependent protein kinase in the 1,25-dihydroxy-vitamin D_3-mediated rapid stimulation of intestinal calcium transport (transcaltachia). *Endocrinology* 127: 39–45, 1990.
11. **De Boland AR, Norman AW.** Influx of extracellular calcium mediates 1,25-dihydroxyvitamin D_3-dependent transcaltachia (the rapid stimulation of duodenal Ca^{2+} transport). *Endocrinology* 127: 2475–2480, 1990.
12. **Eisenman G, Horn R.** Ionic selectivity revisited: the role of kinetic and equilibrium processes in ion permeation through channels. *J Membr Biol* 76: 197–225, 1983.
13. **Feher JJ, Fullmer CS, Fritzsch GK.** Comparison of the enhanced steady-state diffusion of calcium by calbindin-D_{9K} and calmodulin: possible importance in intestinal calcium absorption. *Cell Calcium* 10: 189–203, 1989.
14. **Ferrante PL, Freeman DE, Whitlock RH, Kronfeld DS.** Effect of D-glucose on in vitro short-circuit current in neonatal calf jejunum and rabbit ileum. *Am J Vet Res* 49: 715–719, 1988.
15. **Fujita H, Sugimoto K, Inatomi S, Maeda T, Osanai M, Uchiyama Y, Yamamoto Y, Wada T, Kojima T, Yokozaki H, Yamashita T, Kato S, Sawada N, Chiba H.** Tight junction proteins claudin-2 and -12 are critical for vitamin D-dependent Ca^{2+} absorption between enterocytes. *Mol Biol Cell* 19: 1912–1921, 2008.
16. **Hill KJ, Webber AC, Hill SJ.** A role of protein kinase Cμ in signalling from the human adenosine A_1 receptor to the nucleus. *Br J Pharmacol* 139: 721–732, 2003.
17. **Hirsch E, Costa C, Ciraolo E.** Phosphoinositide 3-kinases as a common platform for multi-hormone signaling. *J Endocrinol* 194: 243–256, 2007.
18. **Hoenderop JG, Nilius B, Bindels RJ.** Calcium absorption across epithelia. *Physiol Rev* 85: 373–422, 2005.
19. **Huybers S, Naber TH, Bindels RJ, Hoenderop JG.** Prednisolone-induced Ca^{2+} malabsorption is caused by diminished expression of the epithelial Ca^{2+} channel TRPV6. *Am J Physiol Gastrointest Liver Physiol* 292: G92–G97, 2007.
20. **Jantarajit W, Thongon N, Pandaranandaka J, Teerapornpuntakit J, Krishnamra N, Charoenphandhu N.** Prolactin-stimulated transepithelial calcium transport in duodenum and Caco-2 monolayer are mediated by the phosphoinositide 3-kinase pathway. *Am J Physiol Endocrinol Metab* 293: E372–E384, 2007.
21. **Kapus A, Szászi K.** Coupling between apical and paracellular transport processes. *Biochem Cell Biol* 84: 870–880, 2006.
22. **Karbach U, Feldmeier H.** The cecum is the site with the highest calcium absorption in rat intestine. *Dig Dis Sci* 38: 1815–1824, 1993.
23. **Khanal RC, Nemere I.** Endocrine regulation of calcium transport in epithelia. *Clin Exp Pharmacol Physiol* 35: 1277–1287, 2008.
24. **Khanal RC, Nemere I.** Regulation of intestinal calcium transport. *Annu Rev Nutr* 28: 179–196, 2008.
25. **Krishnamra N, Taweerathitam P.** Acute effect of prolactin on active calcium absorption in rats. *Can J Physiol Pharmacol* 73: 1185–1189, 1995.
26. **Krishnamra N, Wirunrattanakij Y, Limlomwongse L.** Acute effects of prolactin on passive calcium absorption in the small intestine by in vivo perfusion technique. *Can J Physiol Pharmacol* 76: 161–168, 1998.
27. **Lee GS, Lee KY, Choi KC, Ryu YH, Paik SG, Oh GT, Jeung EB.** Phenotype of a calbindin-D_{9k} gene knockout is compensated for by the induction of other calcium transporter genes in a mouse model. *J Bone Miner Res* 22: 1968–1978, 2007.
28. **Lee SH, Kunz J, Lin SH, Yu-Lee LY.** 16-kDa prolactin inhibits endothelial cell migration by down-regulating the Ras-Tiam1-Rac1-Pak1 signaling pathway. *Cancer Res* 67: 11045–11053, 2007.
29. **Little D, Dean RA, Young KM, McKane SA, Martin LD, Jones SL, Blikslager AT.** PI3K signaling is required for prostaglandin-induced mucosal recovery in ischemia-injured porcine ileum. *Am J Physiol Gastrointest Liver Physiol* 284: G46–G56, 2003.
30. **Lu Z.** Mechanism of rectification in inward-rectifier K^+ channels. *Annu Rev Physiol* 66: 103–129, 2004.
31. **Mace OJ, Morgan EL, Affleck JA, Lister N, Kellett GL.** Calcium absorption by $Ca_v1.3$ induces terminal web myosin II phosphorylation and apical GLUT2 insertion in rat intestine. *J Physiol* 580: 605–616, 2007.
32. **McLaughlin J, Padfield PJ, Burt JP, O'Neill CA.** Ochratoxin A increases permeability through tight junctions by removal of specific claudin isoforms. *Am J Physiol Cell Physiol* 287: C1412–C1417, 2004.
33. **Mellor H, Parker PJ.** The extended protein kinase C superfamily. *Biochem J* 332: 281–292, 1998.
34. **Morgan EL, Mace OJ, Affleck J, Kellett GL.** Apical GLUT2 and $Ca_v1.3$: regulation of rat intestinal glucose and calcium absorption. *J Physiol* 580: 593–604, 2007.
35. **Morgan EL, Mace OJ, Helliwell PA, Affleck J, Kellett GL.** A role for $Ca_v1.3$ in rat intestinal calcium absorption. *Biochem Biophys Res Commun* 312: 487–493, 2003.
36. **Motulsky H, Christopoulos A.** *Fitting Models to Biological Data Using Linear and Nonlinear Regression: A Practical Guide to Curve Fitting.* New York, NY: Oxford Univ. Press, 2004, p. 312–321.
37. **Murphy EF, Hooiveld GJ, Muller M, Calogero RA, Cashman KD.** Conjugated linoleic acid alters global gene expression in human intestinal-like Caco-2 cells in an isomer-specific manner. *J Nutr* 137: 2359–2365, 2007.
38. **Nakane M, Ma J, Rose AE, Osinski MA, Wu-Wong JR.** Differential effects of vitamin D analogs on calcium transport. *J Steroid Biochem Mol Biol* 103: 84–89, 2007.
39. **Powell DJ, Hajduch E, Kular G, Hundal HS.** Ceramide disables 3-phosphoinositide binding to the pleckstrin homology domain of protein kinase B (PKB)/Akt by a PKC_ζ-dependent mechanism. *Mol Cell Biol* 23: 7794–7808, 2003.
40. **Rexhepaj R, Artunc F, Metzger M, Skutella T, Lang F.** PI3-kinase-dependent electrogenic intestinal transport of glucose and amino acids. *Pflügers Arch* 453: 863–870, 2007.
41. **Sabah NH.** Rectification in biological membranes. *IEEE Eng Med Biol Mag* 19: 106–113, 2000.
42. **Samarin SN, Ivanov AI, Flatau G, Parkos CA, Nusrat A.** Rho/Rho-associated kinase-II signaling mediates disassembly of epithelial apical junctions. *Mol Biol Cell* 18: 3429–3439, 2007.
43. **Tang VW, Goodenough DA.** Paracellular ion channel at the tight junction. *Biophys J* 84: 1660–1673, 2003.
44. **Tanrattana C, Charoenphandhu N, Limlomwongse L, Krishnamra N.** Prolactin directly stimulated the solvent drag-induced calcium transport in the duodenum of female rats. *Biochim Biophys Acta* 1665: 81–91, 2004.
45. **Thongon N, Nakkrasae LI, Thongbunchoo J, Krishnamra N, Charoenphandhu N.** Prolactin stimulates transepithelial calcium transport and modulates paracellular permselectivity in Caco-2 monolayer: mediation by PKC and ROCK pathways. *Am J Physiol Cell Physiol* 294: C1158–C1168, 2008.
46. **Van Abel M, Hoenderop JG, van der Kemp AW, van Leeuwen JP, Bindels RJ.** Regulation of the epithelial Ca^{2+} channels in small intestine as studied by quantitative mRNA detection. *Am J Physiol Gastrointest Liver Physiol* 285: G78–G85, 2003.
47. **Van Itallie CM, Anderson JM.** Claudins and epithelial paracellular transport. *Annu Rev Physiol* 68: 403–429, 2006.
48. **Wall MJ, Declusin RJ, Soergel KH, Baker RD.** The effect of short chain fatty acids on transmural electrical potential across rat small intestine in vivo. *Biochim Biophys Acta* 433: 654–661, 1976.
49. **Wasserman RH, Chandler JS, Meyer SA, Smith CA, Brindak ME, Fullmer CS, Penniston JT, Kumar R.** Intestinal calcium transport and calcium extrusion processes at the basolateral membrane. *J Nutr* 122: 662–671, 1992.
50. **Yee S.** In vitro permeability across Caco-2 cells (colonic) can predict in vivo (small intestinal) absorption in man - fact or myth. *Pharm Res* 14: 763–766, 1997.
51. **Zhou LX, Nemere I, Norman AW.** A parathyroid-related peptide induces transcaltachia (the rapid, hormonal stimulation of intestinal Ca^{2+} transport). *Biochem Biophys Res Commun* 186: 69–73, 1992.
52. **Zweibaum A, Triadou N, Kedinger M, Augeron C, Robine-Leon S, Pinto M, Rousset M, Haffen K.** Sucrase-isomaltase: a marker of foetal and malignant epithelial cells of the human colon. *Int J Cancer* 32: 407–412, 1983.

ARTICLE

Journal of Cellular Biochemistry 107:677–685 (2009)

Journal of Cellular Biochemistry

Evidence for Direct Effects of Prolactin on Human Osteoblasts: Inhibition of Cell Growth and Mineralization

Dutmanee Seriwatanachai,[1,2] Nateetip Krishnamra,[1] and J.P.T.M. van Leeuwen[2]*

[1]Faculty of Science, Department of Physiology, Mahidol University, Rama VI Road, Bangkok 10400, Thailand

[2]Department of Internal Medicine, Erasmus Medical Center, Rotterdam, The Netherlands

ABSTRACT

Hyperprolactinemia is one of the risk factor of decrease in bone mass which has been believed to be mediated by hypogonadism. However, the presence of prolactin receptor in human osteosarcoma cell line and primary bone cell culture from mouse calvariae supported the hypothesis of a direct prolactin (PRL) action on bone cells. Therefore, the aim of this study was to investigate the role of PRL and its signal transduction pathway in the regulation of bone metabolism via osteoblast differentiation. Human pre-osteoblasts (SV-HFO) that differentiate in a 3-week period from proliferating pre-osteoblasts (days 2–7) to extracellular matrix producing cells (days 7–14) which is eventually mineralized (days 14–21) were used. Concentration of PRL mimicked a lactating period (100 ng/ml) was used to incubate SV-HFO for 21 days in osteogenic medium. Human prolactin receptor mRNA and protein are expressed in SV-HFO. PRL significantly decreased osteoblast number (DNA content) which was due to a decrease in proliferation. PRL increased osteogenic markers, RUNX2 and ALP in early stage of osteoblast differentiation while decreasing it later suggesting a bi-directional effect. Calcium measurement and Alizarin red staining showed a reduction of mineralization by PRL while having neither an effect on osteoblast activity nor RANKL/OPG mRNA ratio. We also demonstrated that PRL action on mineralization was not via PI-3 kinase pathway. The present study provides evidence of a direct effect of prolactin on osteoblast differentiation and in vitro mineralization. J. Cell. Biochem. 107: 677–685, 2009. © 2009 Wiley-Liss, Inc.

KEY WORDS: HYPERPROLACTINEMIA; OSTEOBLAST DIFFERENTIATION; BONE FORMATION; RANKL/OPG

A number of causes have been implicated to physiological and pathological hyperprolactinemia. Pregnancy and lactation produced physiologically high concentration of prolactin (PRL) of ~75–100 and ~200–300 ng/ml [Ritchie et al., 1998; Prentice, 2000], anterior pituitary tumor [Schlechte et al., 1983; Greenspan et al., 1986; Klibanski and Greenspan, 1986] or use of antipsychotic drug in schizophrenia patients elevates prolactin (PRL) levels by dopaminergic inhibition [Naidoo et al., 2003]. Hyperprolactinemia-induced osteoporosis is, so far, believed to be mediated by hypogonadism. However, in hyperprolactinemic women with normal estrogen levels, net bone loss still occurred, but its severity was significantly less than that in hyperprolactinemia without estrogen. PRL is a peptide hormone produced by the lactotrope cells in the anterior pituitary gland and is primarily associated with lactation. We previously found in the in vivo studies that PRL has a significant effect on bone remodeling in lactating rat, stimulating recruitment of calcium for fetal development and breast feeding [Lotinun et al., 1998; Lotinun et al., 2003]. The prolactin receptor (PRLR) knockout mice were shown to have a significant effect on fetal skeletal development suggesting a role for PRL signaling to maintain a normal fetal bone development [Clement-Lacroix et al., 1999]. In addition, the expression PRL receptor (PRLR) in osteoblasts as assessed by PCR and immunohistochemistry suggested a direct effect of PRL on bone remodeling [Bataille-Simoneau et al., 1996; Coss et al., 2000; Seriwatanachai et al., 2008a,b]. However, it is yet not clear whether bone is directly regulated by PRL. The skeletal effects observed in the lactating rats and PRLR knockout mice may still be due to the presence of other hormones in lactating stage and other changes in the PRLR knockout mice. Nevertheless, the expression of PRLR in human fetal osteoblast (hFOB 1.19), osteoblast-like cell, MG-63 and Saos-2 and rat osteoblast suggested a direct effect of PRL on osteoblasts [Bataille-Simoneau et al., 1996; Coss et al., 2000; Seriwatanachai et al., 2008a,b]. There are only few studies focusing on the direct short-term effects of PRL

The authors declare no conflict of interest.

Grant sponsor: Royal Golden Jubilee Program; Grant sponsor: Thailand Research Fund.

*Correspondence to: Prof. Dr. J.P.T.M. van Leeuwen, Department of Internal Medicine, Room Ee585c, Erasmus Medical Center's Gravendijkwal 230, 3015 CE Rotterdam, The Netherlands. E-mail: j.vanleeuwen@erasmusmc.nl

Received 12 February 2009; Accepted 5 March 2009 • DOI 10.1002/jcb.22161 • © 2009 Wiley-Liss, Inc.

Published online 13 April 2009 in Wiley InterScience (www.interscience.wiley.com).

on osteoblast [Coss et al., 2000; Seriwatanachai et al., 2008a,b]. None of them has studied the putative role of human PRL on human osteoblast differentiation and bone formation.

The aim of this study was to assess the impact of PRL and PRL signaling, on human osteoblast differentiation related to bone formation. The expression of PRLR and the effect of PRL on osteoblast activity and matrix mineralization were measured together with studies on PRL signal transduction pathway.

MATERIALS AND METHODS

CELL CULTURE

SV-HFO are human pre-osteoblast [van Driel et al., 2004; Eijken et al., 2006] were cultured in α-MEM (GIBCO, Paisley, UK) supplemented with 20 mM HEPES, pH 7.5, streptomycin/penicillin, 1.8 mM $CaCl_2$ (Sigma, St. Louis, MO) and heat-inactivated FCS (GIBCO, Paisley, UK) at 37°C and 5% CO_2 in a humidified atmosphere. Cells were seeded in a density of 5×10^3 vital cells/cm^3 and pre-cultured for 1 week in the presence of 10% FCS. During this pre-culture, SV-HFO cells remained in an undifferentiated stage. After preculture, cells were seeded in density of 10×10^3 vital cells/cm^2 in osteogenic medium consisting of 2% charcoal-treated FCS supplemented with 10 mM β-glycerophosphate (Sigma) and dexamethasone (Sigma).

Recombinant human PRL (R&D Systems, Inc., Minneapolis, MN) was reconstituted in BSA and HCl following the manufacturer's instruction before being diluted in α-MEM. Medium freshly supplemented with and without PRL was replaced every 2–3 days. For biochemical analysis, medium was collected and stored at −20°C and cells were scraped from the culture dish in PBS containing 0.1% Triton X-100 and stored at −80°C. Cell lysates were sonicated on ice in a sonifier cell disrupter for 2×15 s before analysis.

IMMUNOCYTOCHEMISTRY

To verify and localize the PRLR proteins in osteoblasts, SV-HFO cells were seeded on cover slips in density of 10×10^3 vital cells/cm^2 and incubated with osteogenic medium for 5 and 12 days. Unattached cells were then removed by washing with PBS pH 7.4 twice. The cover slips were removed from the incubator and were fixed with 4% of paraformaldehyde for 10 min at room temperature. Cells were then washed three times with PBS, and permeabilized with 0.15% Triton-X100 in PBS for 5 min at room temperature. Then cells were washed twice with PBS, and nonspecific proteins were blocked with 10% BSA for 30 min at room temperature. Samples were then incubated with the 1:300 diluted rabbit polyclonal anti-PRLR (Santa Cruz, CA) primary antibody for 1 h at room temperature. Cells were further incubated with 1:200 diluted Alexa Fluor 488 conjugated anti-rabbit IgG antibody as a secondary antibody for 1 h at room temperature. Cells were then stained with nuclear DAPI stain for 2 min. Anti-PRLR was digitally captured by using inverted fluorescence microscopy (Bio-Rad MRC1024 MP scanning system mounted on a Nikon Eclipse TE300 fluorescence microscope).

DNA CONTENT

For DNA measurements, 100 μl SV-HFO cell lysates were treated with 200 μl heparin (8 IU/ml in PBS) and 100 μl ribonuclease A (50 μg/ml in PBS) for 30 min at 37°C. This was followed by adding 100 μl ethidium bromide solution (25 μg/ml in PBS). Samples were analyzed on the Wallac 1420 victor2 (Perkin-Elmer, Wellesley, MA) using an extinction filter of 340 nm and an emission filter of 590 nm. For standards, calf thymus DNA (Sigma) was used.

ALKALINE PHOSPHATASE (ALP) ACTIVITY

ALP activity was assayed by determining the release of *p*-nitrophenol from *p*-nitrophenylphosphate (20 mM in 1 M diethanolamine buffer supplemented with 1 mM $MgCl_2$ at pH 9.8) in the SV-HFO cell lysates for 10 min at 37°C. The reaction was stopped by adding 0.06 M NaOH. Absorption was measured at 405 nm. Results were adjusted for DNA content of the cell lysates.

MINERALIZATION

For quantification of the mineral content cell lysates were incubated overnight in 0.24 M HCl at 4°C. Calcium content was colorimetrically determined colorimetrically with a calcium assay kit (Sigma) according to the manufacturer's description. Results were adjusted for DNA content of the cell lysates. For Alizarin Red S staining cell cultures were fixed for 60 min with 70% ethanol on ice. After fixation, cells were washed twice with PBS and stained for 10 min with an anthraquinone derivative, Alizarin Red S solution.

APOPTOSIS ASSAY

Apoptosis was measured through the binding of annexin V and uptake of propidium iodide (PI) by flow cytometry using a Apoptest-FITC kit (Nexins research, Kattendijke, The Netherlands). For analysis 10,000 osteoblasts were counted using a FACScalibur (Becton Dickinson). Percentage total apoptotic cells was calculated by counting apoptotic (annexin V or PI stained) cells.

PROLIFERATION ASSAY

Osteoblast proliferation was examined by using a colorimetric BrdU cell proliferation enzyme-linked immunosorbent assay kit (No. 1 647 229, Roche, Mannheim, Germany). SV-HFO cells were seeded into 96-well plates, in osteogenic medium with and without 100 ng/ml PRL. 100 μM BrdU labeling solution was added to each well giving a final concentration of 10 μM. After 24 h incubation and removal of the culture medium the cells were fixed and DNA was denaturated. Subsequently, the anti-BrdU-peroxidase conjugate was added which binds to the incorporated in newly synthesized DNA. The immune complexes were detected by subsequent reaction with tetramethylbenzidine as substrate for 10 min. The reaction was stopped by addition of 200 μl 1 M H_2SO_4 to each well, and the reaction product was quantified by measuring the absorbance at 450 nm with reference to 690 nm using the Wallac 1420 victor2 (Perkin-Elmer, Wellesley, MA) [Gratzner, 1982].

QUANTIFICATION OF mRNA EXPRESSION

Total RNA was isolated using RNA-Bee solution (Tel-Test, Friendwood, TX) according to the manufacturer's protocol. To remove calcium (derived from extracellular matrix), RNA was precipitated by overnight incubation with 4 M LiCl and 50 mM EDTA at −20°C. After precipitation and centrifugation for 30 min at 14,000 rpm and 4°C, the RNA pellet was washed four times with 70% EtOH and dissolved in H_2O. The total amount of RNA was quantified using the RiboGreen RNA Quantitation Kit (Molecular Probes, Eugene, OR). One microgram total RNA was reverse transcribed into cDNA using 0.2 μg oligo(dT)18 and 0.2 μg random hexamer primers and a cDNA synthesis kit (MBI Fermentas, St. Leon-Rot, Germany).

Quantitative real-time PCR (QPCR) was carried out using an ABI 7700 sequence detection system (Applied Biosystems, Foster City, CA). Reactions were performed in 25 μl volumes using a qPCR core kit (Eurogentec, Seraing, Belgium). Reaction mixes contained 20 ng cDNA, 5 mM $MgCl_2$, 200 μM dNTPs, and 0.025 U/μl Hot GoldStar enzyme. Primer and probe sets were designed, using the Primer Express software (version 1.5; Applied Biosystems), amplicons overlapped at least one exon boundary. Cycling conditions were 50°C for 2 min, 95°C for 10 min, followed by 40 cycles of 95°C for 15 s and 60°C for 1 min. The relative gene expression was calculated by the comparative Ct method of which Ct sample is normalized to endogenous house keeping gene, GAPDH, according to the calculation; relative Ct value $= 2^{-[\text{delta}]Ct_{SAMPLE}-[\text{delta}]Ct_{GAPDH}}$

STATISTICS

Data are presented as mean ± SEM and are derived of at least two independent experiments each consisting of at least three cultures. Differences between groups were analyzed by the Student's *t*-test.

RESULTS

EXPRESSION OF HUMAN PROLACTIN RECEPTOR (hPRLR)

hPRLR expression and PRL effects were studied in detail using the SV-HFO osteoblast differentiation model. This human pre-osteoblast model produces an extracellular matrix during culture, which eventually is mineralized in 2–3 weeks time period [Chiba et al., 1993; Eijken et al., 2006], as shown in Figure 1. hPRLR mRNA was found to be expressed in human osteoblasts and the expression remained constant during differentiation (Fig. 2). Incubation with PRL did not significantly change the hPRLR mRNA expression significantly at the various days albeit that at all days tested hPRLR mRNA expression appeared to be lower than in untreated cultures. Also at protein level, the hPRLR was demonstrated in human osteoblasts (Fig. 3).

EFFECTS OF PROLIFERATION AND APOPTOSIS

PRL treatment decreased total cell number as reflected by a decrease in the total amount DNA during osteoblast differentiation (Fig. 4A). The decrease in DNA only became apparent after 7 days of culture. For total protein we found a similar pattern after PRL treatment as observed for total DNA with a reduction from day 7 of culture onwards (data not shown). The reduction in cell number can be due

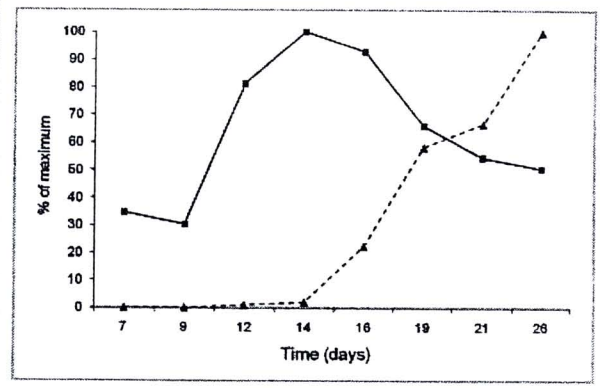

Fig. 1. Temporal pattern of alkaline phosphatase activity (solid line) and mineralization (dashed line) during differentiation of SV-HFO pre-osteoblasts induced by osteogenic medium.

to an increase in apoptosis and/or an inhibition of cell proliferation. PRL did not affect apoptosis of human osteoblasts (Fig. 4B) but inhibited cell proliferation (Fig. 4C).

EFFECTS ON HUMAN OSTEOBLAST DIFFERENTIATION

To investigate the role of PRL on osteoblast differentiation, we analyzed the expression of known osteoblast marker genes and the effect of on ALP activity. PRL significantly increased Runx2 at early differentiation, day 5 while decreasing it at the late osteoblast differentiation, day 21 (Fig. 5A). This pattern is similar to that of ALP mRNA expression as shown in Figure 5B. PRL increased collagen type Ia mRNA expression at d5 but did not affect it later on during differentiation (Fig. 5C). ALP activity showed a peak around days 10–12 of culture and in this period the ALP activity in the PRL condition was significantly higher at day 12 while it did not reach significantly at day 10 (Fig. 5D).

PRL EFFECTS ON MINERALIZATION

Next we examined the direct effect of PRL on osteoblast mineralization using Alizarin Red staining at day 14 and day 21.

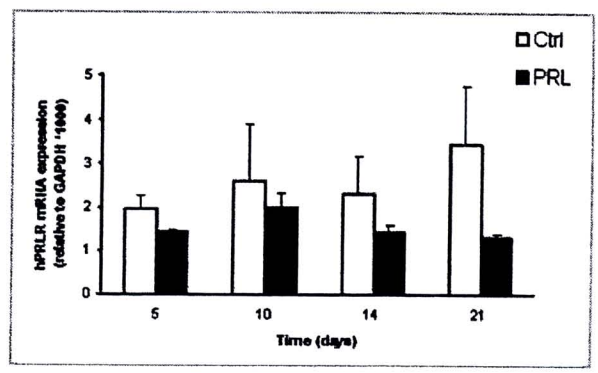

Fig. 2. Expression of hPRLR mRNA (QPCR) during human osteoblast differentiation in control condition (open bars) and after treatment with 100 ng/ml PRL (solid bars).

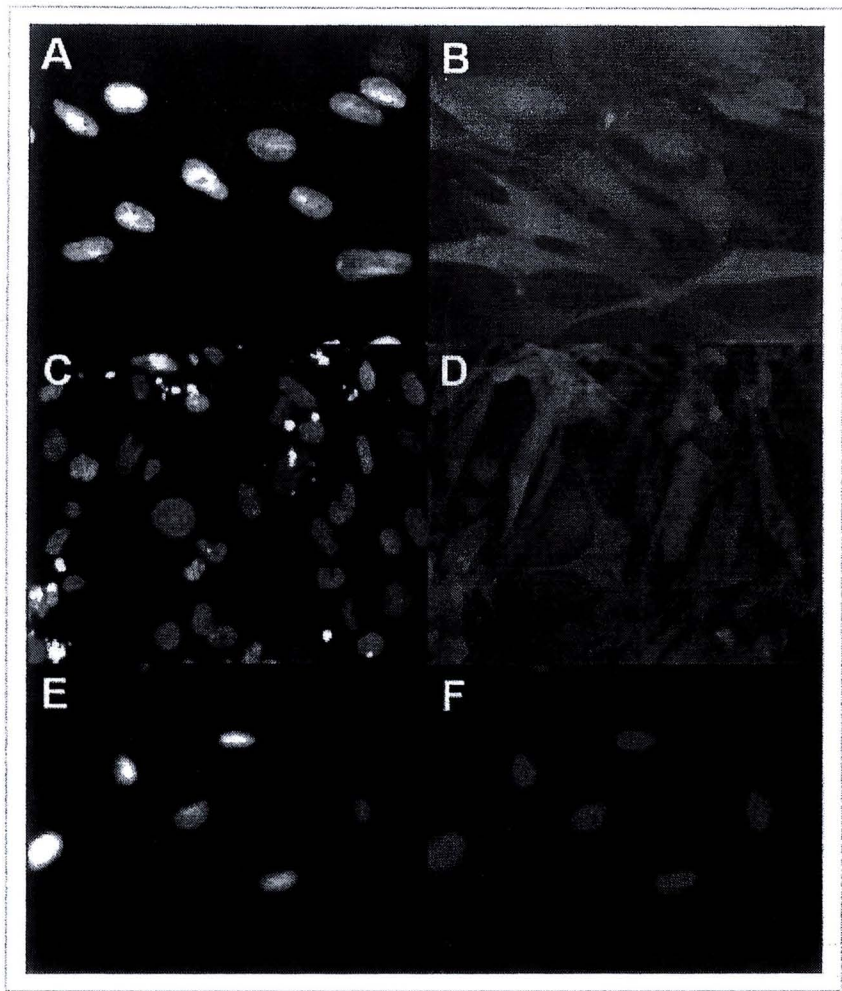

Fig. 3. Immunofluorescent analysis of hPRLR protein expression in SV-HFO cells exposed for 5 days (A,B) and 12 days (C,D) to osteogenic medium (n = 3). A,C,E: DAPI nuclear staining, (B,D,F) double staining with DAPI (blue) and hPRLR antibody conjugated with ALEXA (green). Cells were incubated in the absence (anti-hPRLR) of primary antibody against hPRLR proteins (E,F). Experiments were performed in triplicate, magnification 400×.

We found that PRL visibly reduced the alizarin red staining at day 14 and day 21 (Fig. 6A). In contrast to the control condition, total Ca^{2+} was not yet detectable at d14 in PRL treated group, and at day 21 of culture it was significantly decreased in the PRL condition (Fig. 6B). After correcting the total Ca^{2+} with DNA, it did not change the PRL effect and significance (Fig. 6C).

EFFECTS OF PRL ON RANKL AND OPG EXPRESSION

To elucidate the action of PRL on osteoclastogenesis function of osteoblast, we measured the expression of RANKL and its decoy receptor, OPG. We could not find a significant change in their expression as well as the bone resorption indicator, RANKL/OPG ratio, in PRL-treated group in any given days (Fig. 7A–C).

PI3 KINASE AND PRL ACTION

PI3 kinase pathway is one of the recent pathways reported to be involved in PRL action in many kinds of cells [al Sakkaf et al., 1996; Hugl and Merger, 2007; Jantarajit et al., 2007; Seriwatanachai et al., 2008b]. Our previous report [Seriwatanachai et al., 2008b] also suggested that the shortterm action of PRL on the reduction of osteoblastic ALP activity is via PI-3 kinase activity. We tested the effect of PI3 kinase inhibition by LY294002 in various phases (d0–3, d4–7, and d11–14) during osteoblast differentiation. In general these studies showed that treatment with PRL reduced total DNA (Fig. 8A–C). In none of the phases inhibition of PI-3 kinase alone did effect total DNA level nor did it inhibit the PRL effect (Fig. 8A–C). When LY294002 was added together with PRL at days 11–14 the reduction in DNA was even stronger (Fig. 8C). We confirmed the inhibitory effect of PRL on mineralization (Fig. 8D–F). Inhibition of PI-3 kinase activity in control condition suppressed the mineralization only when added at the early differentiating stage (d0–3 and d4–7) but not when added at the onset of mineralization (d11–14) (Fig. 8D–F). PI-3 kinase inhibition did not block the PRL effect on mineralization, in contrast, when added in the early phases it even augmented the inhibition by PRL (Fig. 8D,E).

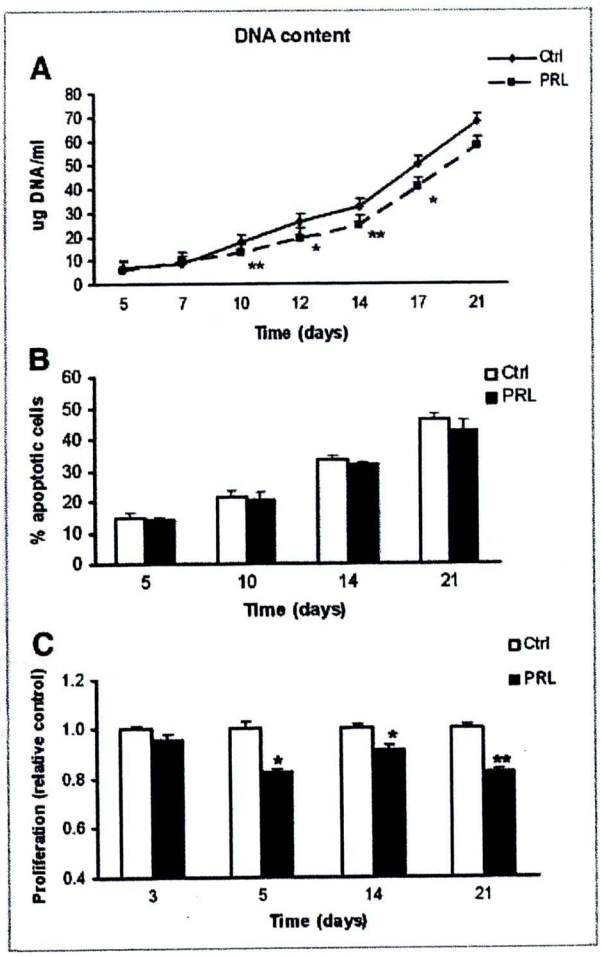

Fig. 4. Effect of PRL treatment on total cell number as reflected by (A) total DNA content, (B) apoptosis, and (C) proliferation. Data shown are mean of two independent cultures performed in triplicate. $^{*}P < 0.05$, and $^{**}P < 0.01$ compared with their respective values of control group.

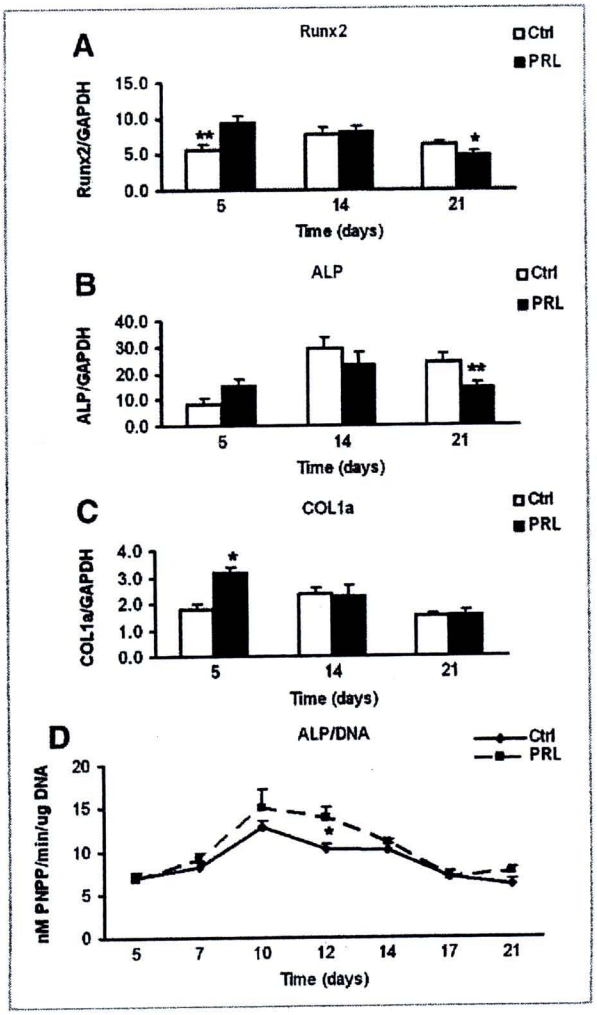

Fig. 5. Effect of PRL on osteoblast differentiation as presented by RUNX2 (A) ALP (B), collagen Type Ia; COL Ia (C) mRNAs expression and ALP/DNA (D). Data shown are mean of two independent cultures performed in triplicate. $^{*}P < 0.05$, and $^{**}P < 0.01$ compared with their respective values of control group.

DISCUSSION

The current study demonstrates for the first time direct effects PRL on human osteoblast differentiation. PRL treatment had a bi-directional effect on osteoblast differentiation and bone formation. PRL reduces human osteoblast proliferation while accelerating its differentiation. However, this acceleration is not accompanied by an enhanced mineralization. Apparently, the accelerated differentiation did not lead to a condition favorable for mineralization. An explanation for this yet elusive but the decrease in total protein may be linked to an insignificant matrix protein production.

Recently, an increased understanding has been acquired with respect to the therapeutic treatment of hyperprolactinemic patients. However, the role of prolactin in the regulation of bone remodeling and the associated bone loss remains largely unclear. Of note was our previous demonstration that PRL receptor is expressed in human fetal osteoblast (hFOB 1.19), osteoblast-like cell (MG-63) and primary rat osteoblast derived from mesenchymal stem cells [Seriwatanachai et al., 2008a,b]. Also other evidence provided osteoblast as a new target of PRL. Deformed skeletal development in PRL receptor knock out pup suggesting an importance role of PRL for maintaining fetal bone development [Clement-Lacroix et al., 1999]. However, so far no data were available on direct effects of PRL on human fetal osteoblast differentiation. We demonstrated hPRLR expression at all stages during differentiation of the human pre-osteoblast cell line, SV-HFO. This model produces an extracellular matrix during culture which eventually is mineralized in 2–3 weeks time period [Chiba et al., 1993; Eijken et al., 2006] therefore, it is suitable for studying PRL effect on human osteoblast differentiation and in vitro bone formation. We presented that in vitro administration of PRL result in a reduction of osteoblast growth. The observation that in PRL-treated osteoblast shows a declinement of osteoblast number as represented by DNA content in a time-dependent manner (Fig. 4A). This finding suggested

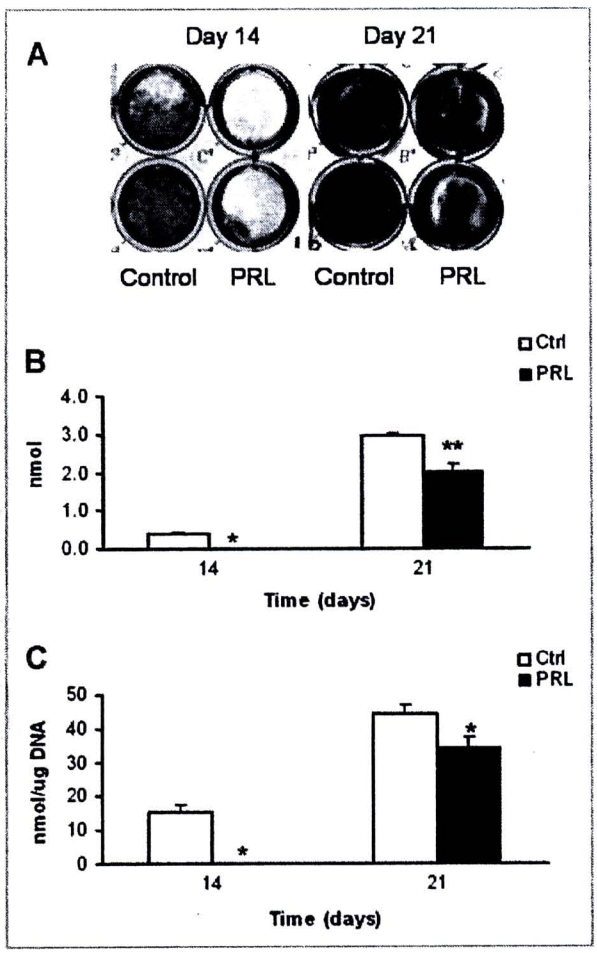

Fig. 6. The effect of PRL on mineralization as presented by mineral Alizarin Red staining (A), total Ca^{+2} (B), and Ca^{+2}/DNA (C). Data shown are mean of two independent cultures performed in triplicate. $^{*}P < 0.05$, and $^{**}P < 0.01$ compared with their respective values of control group. [Color figure can be viewed in the online issue, which is available at www.interscience.wiley.com.]

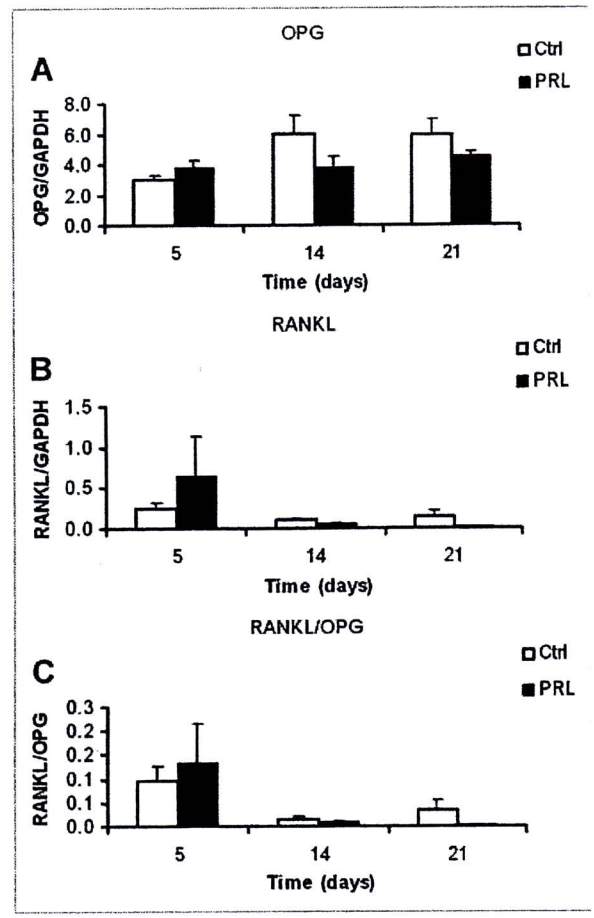

Fig. 7. The effect of 100 ng/ml PRL on the bone resorption-associated parameters which are mRNA expressions of OPG (A) RANKL (B) and the ratios of RANKL/OPG mRNA (C). SV-HFO was exposed to a osteogenic medium (open bar) or with PRL (close bar) for 5, 14, and 21 days. Data shown are mean of two independent cultures performed in triplicate.

that the downregulation of osteoblast quantity is enhanced by PRL action. Therefore, in the next part of the study, we checked whether the reduction of osteoblast quantity regarding the effect of PRL on osteoblast number also could be indirectly manifested through an induction of spontaneous apoptosis or reduction of its proliferation. Indeed, PRL-treated osteoblasts were found reduced proliferation at early phase of osteoblast differentiation, without enhancing a number of apoptosis in PRL treated group. Interestingly, in the present experiment of which tested between vehicle and PRL treated group, and previous observation has found that PRL has no effect on osteoblast-like cell and rat osteoblast proliferation, however, in shortterm PRL administration and in non-osteogenic medium [Coss et al., 2000; Seriwatanachai et al., 2008a,b]. Thus it could simply suggest that change in osteoblast proliferation in bone development influenced by PRL was occurred only in osteogenic medium and in prolonged administration of PRL.

Extensive collagen degradation during a tissue-turnover processes in variety of biological and physiological provides a dynamic cellular activity including proliferation [Hotary et al., 2003; Mott and Werb, 2004; Chun et al., 2006]. Recently, a combined deficiencies in uPARAP/Endo180, a cellular collagen receptor, and MT1-MMP, a principal mesenchymal cell collagenase, mice found to have a severe effect on bone formation and that caused by a proliferative failure and poor survival of bone- and cartilage-forming cells suggesting a necessary of collagen degradation for osteoblast proliferation [Wagenaar-Miller et al., 2007]. In fact, we observed a augmented collagen type I mRNA expression as affected by PRL at early stage of differentiation (d5) which could considerably propose that it could inhibit the early osteoblast proliferation resulting in a certain reduction in DNA accumulating content along culturing period.

The central regulator of bone formation is the Runx2 (also known as Cbfa1/AML3). This transcription factor is required for osteoblastic fate determination, and mediated the complex pathways required for bone formation and turnover [Lian and Stein, 2003; Lian et al., 2004]. We showed that RUNX2 and ALP mRNA were reduced in PRL-treated group in late differentiation suggesting a decrease in

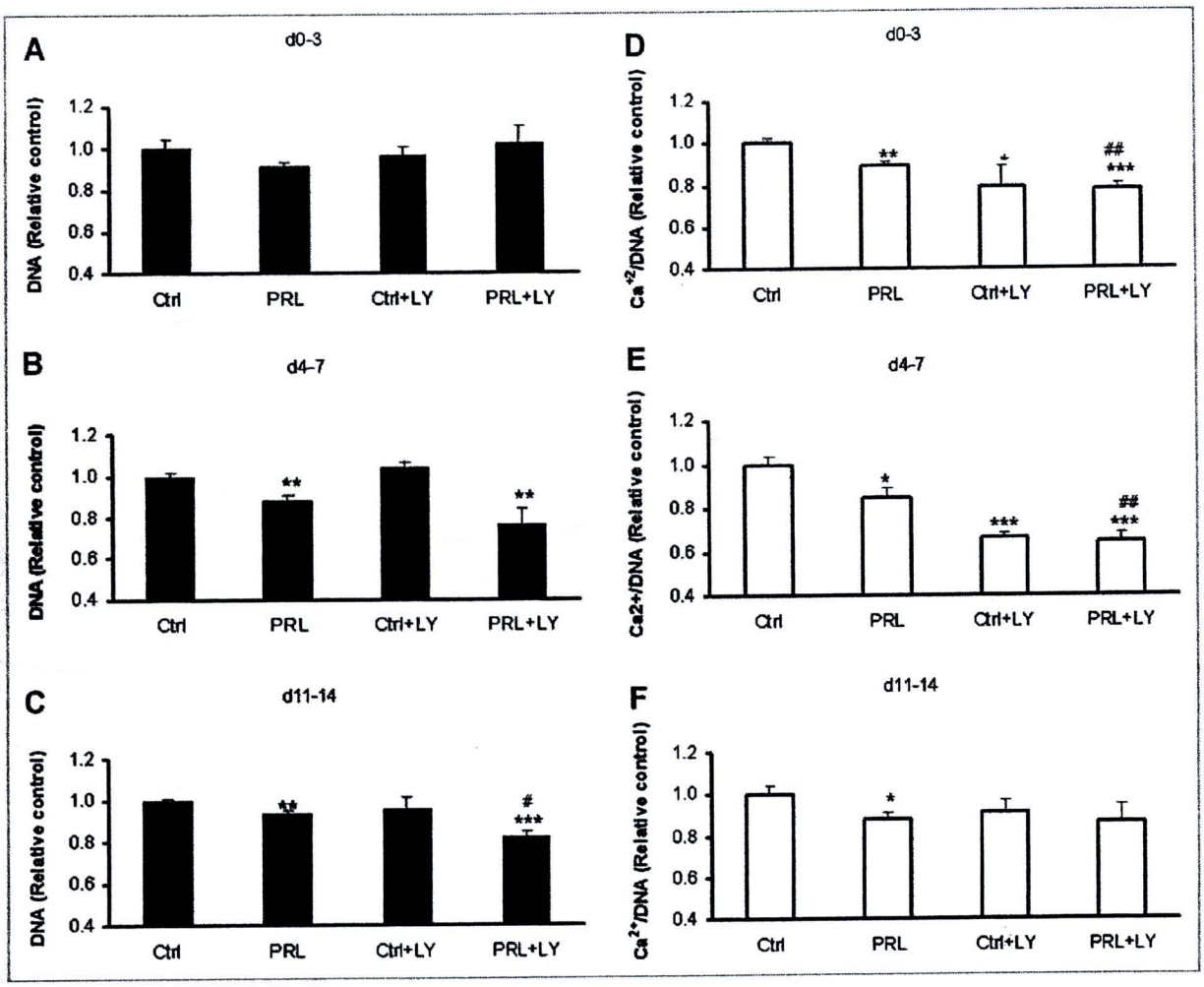

Fig. 8. The combined action of PRL and PI-3 kinase inhibitor (LY294002) on DNA (A–C) and Ca^{2+}/DNA (D–F). LY294002 was added into osteogenic medium with and without PRL at d0–3 (A,D), d4–7 (B,E), and d11–14 (C,F). All plates were harvested at d14 to determine DNA content and Ca^{2+}/DNA. $^{*}P < 0.05$, $^{**}P < 0.01$, and $^{***}P < 0.001$ compared with control group, $^{\#}P < 0.05$ and $^{\#\#}P < 0.01$, compared with PRL group. Data shown are mean of two independent cultures performed in triplicate.

pre-osteoblast differentiation and bone formation. Albeit this should be investigated more detail as RUNX2 has been shown to exert a complex role in osteoblast differentiation, crucial for osteoblast differentiation in early stages but inhibitory in later stages [Liu et al., 2001; Maruyama et al., 2007]. A number of experiments also observed the reduction of osteocalcin, ALP mRNA effected by PRL [Coss et al., 2000; Seriwatanachai et al., 2008b], consistent with our present finding. ALP activity remained unchanged which is possibly due to a reduction of DNA and protein content. Regardless of the reduction of total protein, we similarly found a decrease in its total activity (data not shown), indeed, we showed a significant reduction of ALP mRNA expression. Interestingly, RUNX2 and ALP mRNA expression was found to be enhanced in PRL-treated group at early stage of differentiation (d5). This observation is consistent with the recent report that shortterm PRL administration increases osteocalcin mRNA, a marker of late osteoblast differentiation, while reducing RANKL/OPG ratio in human osteoblast derived from fetal bone tissue favors osteoblast differentiation and bone formation [Seriwatanachai et al., 2008a]. This contradictory finding implies a bi-directional effect of PRL regarding to the stage of osteoblast differentiation. However, the different incubation period, PRL level and medium condition should be also taken into account.

The next step of experiment was concerned about the role of PRL on mineralization since some evidence found a contradictory action according to different model and technical approaches. We observed a decrease in Ca^{2+} content by biochemical assay, and as shown by Alizarin Red staining, which is truly resulted from a reduction of Ca^{2+} content, not secondary to the decrease in DNA content as it is proved by the reduction of Ca^{2+}/DNA content. Indeed, a reduction of bone ossification and mineralizing rate in PRL receptor knockout murine embryo and 8-week-old mouse [Clement-Lacroix et al., 1999] supports a significance role of PRL in fetal and adult bone mineralization.

Up to date, they have been stated of knowledge concerning signal transduction of the PRLR. Nb2 cells are some of the favored models with which to study PRL actions, as shown that PRL induces a rapid tyrosine phosphorylation of IRS-1 and of the 85-kDa subunit of the phosphatidyl-inositol (PI)-3 kinase [al Sakkaf et al., 1996; Berlanga et al., 1997]. Both PI-3 kinase and IRS-1 appear to associate with the

PRLR in a PRL-dependent manner. It has been proposed that a proliferative effect of PRL activation of PI-3 kinase might be mediated by Fyn in Nb2 cells [al Sakkaf et al., 1997] and beta-cell line [Hugl and Merger, 2007]. We previously demonstrated that a certain concentration of PI3 kinase inhibition reverses PRL reduced ALP activity without effecting cell survival in MG-63 and hFOB suggesting PI3 kinase is one of potential PRL pathways in human osteoblast [Seriwatanachai et al., 2008a]. However, the present study found that shortterm administration of PI3 kinase inhibitor did not reverse the inhibitory action of PRL on DNA and Ca^{2+} content suggesting PI3 kinase involved in bone mineralization and osteoblast number is independent to PRL action. Noted, the induction of apoptotis according to the inhibition of PI-3 kinase was ruled out by optimizing the concentration of LY294002, and was not shown to decrease DNA content. However we found that the combination of PRL and PI3 kinase inhibitor constantly induced a decreased in DNA content in d4–7 and d11–14 but not d0–3 confirming the action of PRL on DNA content is not via PI3 kinase pathway. Moreover, data from Ca^{2+} content demonstrated that shortterm PI3 kinase inhibition at proliferative not mineralizing stage is sufficient for inhibiting the mineralization where as the osteoblast number remains unchanged. This time specific manner can also be found in glucocorticoid (dexamethasone) action of which is capable to decrease bone mineralization once cell have not entered to osteoblast differentiation pathway [Eijken et al., 2006].

The results also demonstrated unchanged in OPG, a decoy receptor of RANKL, and RANKL mRNA expression in osteoblast at entire stage of differentiation leading to non-significance RANKL/OPG ratio. Unlikely, the results from osteosarcoma showed that PRL increases RANKL/OPG ratio after administrating PRL in nondexamethasone medium for shortterm incubation. It, however, suggested the cell type specificity and differentiation dependence. Besides, a number of in vivo studies reported the diverse effect of PRL on bone remodeling in which depends on age of animal, weight bearing and connective structure [Krishnamra and Cheeveewattana, 1994; Krishnamra and Seemoung, 1996; Krishnamra et al., 1997]. The combined dimerization of PRL receptor isoforms through its action on bone development and osteoblast differentiation also is not ruled out. Indeed, evidences show that PRL receptor may be crossly combined among isoforms in which gives variety biological effects in a number of kinds of cell [Perrot-Applanat et al., 1997; Qazi et al., 2006]. In conclusion, despite the issues discussed above, the observations of the present study demonstrate that a prolonged incubation of PRL can have an inhibitory effect on osteoblast number, mineralization and differentiation as altered by a reduction of bone precursor marker.

ACKNOWLEDGMENTS

This research was supported by grants from the Royal Golden Jubilee Program (to D.S.) and the Thailand Research Fund (TRF).

REFERENCES

al Sakkaf KA, Dobson PR, Brown BL, 1996. Activation of phosphatidylinositol 3-kinase by prolactin in Nb2 cells. Biochem Biophys Res Commun 221:779–784.

al Sakkaf KA, Dobson PR, Brown BL. 1997. Prolactin induced tyrosine phosphorylation of p59fyn may mediate phosphatidylinositol 3-kinase activation in Nb2 cells. J Mol Endocrinol 19:347–350.

Bataille-Simoneau N, Gerland K, Chappard D, Basle MF, Mercier L. 1996. Expression of prolactin receptors in human osteosarcoma cells. Biochem Biophys Res Commun 229:323–328.

Berlanga JJ, Gualillo O, Buteau H, Applanat M, Kelly PA, Edery M. 1997. Prolactin activates tyrosyl phosphorylation of insulin receptor substrate 1 and phosphatidylinositol-3-OH kinase. J Biol Chem 272:2050–2052.

Chiba H, Sawada N, Ono T, Ishii S, Mori M. 1993. Establishment and characterization of a simian virus 40-immortalized osteoblastic cell line from normal human bone. Jpn J Cancer Res 84:290–297.

Chun TH, Hotary KB, Sabeh F, Saltiel AR, Allen ED, Weiss SJ. 2006. A pericellular collagenase directs the 3-dimensional development of white adipose tissue. Cell 125:577–591.

Clement-Lacroix P, Ormandy C, Lepescheux L, Ammann P, Damotte D, Goffin V, Bouchard B, Amling M, Gaillard-Kelly M, Binart N, Baron R, Kelly PA. 1999. Osteoblasts are a new target for prolactin: Analysis of bone formation in prolactin receptor knockout mice. Endocrinology 140:96–105.

Coss D, Yang L, Kuo CB, Xu X, Luben RA, Walker AM. 2000. Effects of prolactin on osteoblast alkaline phosphatase and bone formation in the developing rat. Am J Physiol Endocrinol Metab 279:E1216–E1225.

Eijken M, Koedam M, van Driel M, Buurman CJ, Pols HA, van Leeuwen JP. 2006. The essential role of glucocorticoids for proper human osteoblast differentiation and matrix mineralization. Mol Cell Endocrinol 248: 87–93.

Gratzner HG. 1982. Monoclonal antibody to 5-bromo- and 5-iododeoxyuridine: A new reagent for detection of DNA replication. Science 218:474–475.

Greenspan SL, Neer RM, Ridgway EC, Klibanski A. 1986. Osteoporosis in men with hyperprolactinemic hypogonadism. Ann Intern Med 104:777–782.

Hotary KB, Allen ED, Brooks PC, Datta NS, Long MW, Weiss SJ. 2003. Membrane type I matrix metalloproteinase usurps tumor growth control imposed by the three-dimensional extracellular matrix. Cell 114: 33–45.

Hugl SR, Merger M. 2007. Prolactin stimulates proliferation of the glucose-dependent beta-cell line INS-1 via different IRS-proteins. JOP 8:739–752.

Jantarajit W, Thongon N, Pandaranandaka J, Teerapornpuntakit J, Krishnamra N, Charoenphandhu N. 2007. Prolactin-stimulated transepithelial calcium transport in duodenum and Caco-2 monolayer are mediated by the phosphoinositide 3-kinase pathway. Am J Physiol Endocrinol Metab 293:E372–E384.

Klibanski A, Greenspan SL. 1986. Increase in bone mass after treatment of hyperprolactinemic amenorrhea. N Engl J Med 315:542–546.

Krishnamra N, Cheeveewattana V. 1994. Studies of acute effect of prolactin on distribution of absorbed calcium and long-term effect on calcium balance in weaned, young, and sexually mature rats. Can J Physiol Pharmacol 72:1521–1527.

Krishnamra N, Seemoung J. 1996. Effects of acute and long-term administration of prolactin on bone 45Ca uptake, calcium deposit, and calcium resorption in weaned, young, and mature rats. Can J Physiol Pharmacol 74:1157–1165.

Krishnamra N, Seemoung J, Limlomwongse L. 1997. Acute effect of prolactin on bone 45Ca accumulation in rats. Endocr J 44:257–264.

Lian JB, Stein GS. 2003. Runx2/Cbfa1: A multifunctional regulator of bone formation. Curr Pharm Des 9:2677–2685.

Lian JB, Javed A, Zaidi SK, Lengner C, Montecino M, van Wijnen AJ, Stein JL, Stein GS. 2004. Regulatory controls for osteoblast growth and differentiation: Role of Runx/Cbfa/AML factors. Crit Rev Eukaryot Gene Expr 14: 1–41.

Liu W, Toyosawa S, Furuichi T, Kanatani N, Yoshida C, Liu Y, Himeno M, Narai S, Yamaguchi A, Komori T. 2001. Overexpression of Cbfa1 in osteoblasts inhibits osteoblast maturation and causes osteopenia with multiple fractures. J Cell Biol 155:157–166.

Lotinun S, Limlomwongse L, Krishnamra N. 1998. The study of a physiological significance of prolactin in the regulation of calcium metabolism during pregnancy and lactation in rats. Can J Physiol Pharmacol 76:218–228.

Lotinun S, Limlomwongse L, Sirikulchayanonta V, Krishnamra N. 2003. Bone calcium turnover, formation, and resorption in bromocriptine- and prolactin-treated lactating rats. Endocrine 20:163–170.

Maruyama Z, Yoshida CA, Furuichi T, Amizuka N, Ito M, Fukuyama R, Miyazaki T, Kitaura H, Nakamura K, Fujita T, Kanatani N, Moriishi T, Yamana K, Liu W, Kawaguchi H, Nakamura K, Komori T. 2007. Runx2 determines bone maturity and turnover rate in postnatal bone development and is involved in bone loss in estrogen deficiency. Dev Dyn 236:1876–1890.

Mott JD, Werb Z. 2004. Regulation of matrix biology by matrix metalloproteinases. Curr Opin Cell Biol 16:558–564.

Naidoo U, Goff DC, Klibanski A. 2003. Hyperprolactinemia and bone mineral density: The potential impact of antipsychotic agents. Psychoneuroendocrinology 28(Suppl 2):97–108.

Perrot-Applanat M, Gualillo O, Pezet A, Vincent V, Edery M, Kelly PA. 1997. Dominant negative and cooperative effects of mutant forms of prolactin receptor. Mol Endocrinol 11:1020–1032.

Prentice A. 2000. Maternal calcium metabolism and bone mineral status. Am J Clin Nutr 71:1312S–1316S.

Qazi AM, Tsai-Morris CH, Dufau ML. 2006. Ligand-independent homo- and heterodimerization of human prolactin receptor variants: Inhibitory action of the short forms by heterodimerization. Mol Endocrinol 20:1912–1923.

Ritchie LD, Fung EB, Halloran BP, Turnlund JR, Van Loan MD, Cann CE, King JC. 1998. A longitudinal study of calcium homeostasis during human pregnancy and lactation and after resumption of menses. Am J Clin Nutr 67:693–701.

Schlechte JA, Sherman B, Martin R. 1983. Bone density in amenorrheic women with and without hyperprolactinemia. J Clin Endocrinol Metab 56: 1120–1123.

Seriwatanachai D, Charoenphandhu N, Suthiphongchai T, Krishnamra N. 2008a. Prolactin decreases the expression ratio of receptor activator of nuclear factor kappaB ligand/osteoprotegerin in human fetal osteoblast cells. Cell Biol Int 32(9): 1126–1135.

Seriwatanachai D, Thongchote K, Charoenphandhu N, Pandaranandaka J, Tudpor K, Teerapornpuntakit J, Suthiphongchai T, Krishnamra N. 2008b. Prolactin directly enhances bone turnover by raising osteoblast-expressed receptor activator of nuclear factor kappaB ligand/osteoprotegerin ratio. Bone 42:535–546.

van Driel M, Pols HA, van Leeuwen JP. 2004. Osteoblast differentiation and control by vitamin D and vitamin D metabolites. Curr Pharm Des 10:2535–2555.

Wagenaar-Miller RA, Engelholm LH, Gavard J, Yamada SS, Gutkind JS, Behrendt N, Bugge TH, Holmbeck K. 2007. Complementary roles of intracellular and pericellular collagen degradation pathways in vivo. Mol Cell Biol 27:6309–6322.

Molecular and Cellular Endocrinology 296 (2008) 41–52

Contents lists available at ScienceDirect

Molecular and Cellular Endocrinology

journal homepage: www.elsevier.com/locate/mce

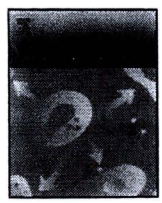

Transcriptome responses of duodenal epithelial cells to prolactin in pituitary-grafted rats

Narattaphol Charoenphandhu[a,b,*], Kannikar Wongdee[a,c], Jarinthorn Teerapornpuntakit[a], Kanogwun Thongchote[a], Nateetip Krishnamra[a,b]

[a] Consortium for Calcium and Bone Research, Faculty of Science, Mahidol University, Bangkok, Thailand
[b] Department of Physiology, Faculty of Science, Mahidol University, Bangkok, Thailand
[c] Department of Pathobiology, Faculty of Science, Mahidol University, Bangkok, Thailand

ARTICLE INFO

Article history:
Received 5 June 2008
Received in revised form
19 September 2008
Accepted 22 September 2008

Keywords:
Duodenum
Gene ontology
Hyperprolactinemia
Microarray
Pituitary transplantation
Real-time PCR

ABSTRACT

Chronic prolactin (PRL) exposure can affect several functions of duodenal epithelia, especially those associated with fluid and electrolyte transport. However, little is known regarding its molecular mechanism. To identify PRL-regulated genes, microarray analysis was performed on RNA samples from duodenal epithelial cells of anterior pituitary (AP)-grafted hyperprolactinemic rats. Herein, we identified 321 transcripts upregulated and 241 transcripts downregulated after 4 weeks of AP transplantation. Results from real-time PCR analyses of 15 selected genes were consistent with the microarray results. Gene ontology analysis demonstrated pleiotropic effects of PRL on several cellular processes, including cellular metabolic process, cell communication and cell adhesion. Interestingly, 17 upregulated transcripts and 12 downregulated transcripts are involved in the transport of ions and nutrients, e.g., Ca^{2+}, Na^+, K^+, Cl^- and glucose, thus agreeing with the established action of PRL on electrolyte homeostasis. The present results provided fundamental information for further investigations on mechanism of PRL actions in the intestine.

1. Introduction

Prolactin (PRL) is one of the most versatile hormones with respect to its array of actions in vertebrates. The more than 300 PRL actions can be classified into 5 categories, i.e., water and electrolyte balance, growth and development, brain and behavior, reproduction, and immunoregulation (Bole-Feysot et al., 1998). PRL receptors (PRLR) are widely expressed in tissues from all 3 germ layers including the digestive tract where PRL exerts 3 major actions, i.e., ion and nutrient absorption, epithelial cell proliferation, and gastrointestinal motility (Charoenphandhu and Krishnamra, 2007; Bujanover et al., 2002; Chen et al., 1997). Most effects of PRL on the intestinal epithelial cells are genomic and are dependent on de novo gene transcription (Bole-Feysot et al., 1998). However, little is known regarding the PRL-regulated intestinal genes.

Salient actions of PRL on the intestinal epithelial cells are related to ion transport. Duodenum appears to be the most responsive intestinal segment to PRL (Charoenphandhu and Krishnamra, 2007). In pregnant and lactation rats, PRL acts as a Ca^{2+}-regulating hormone that enhances the duodenal Ca^{2+} absorption, thus mitigating massive Ca^{2+} loss from bone for fetal growth and galactopoiesis (Charoenphandhu and Krishnamra, 2007; Boass et al., 1992). Long-term exposure to hyperprolactinemia induced by 4-week anterior pituitary (AP) transplantation was found to increase the transcellular Ca^{2+} transport in rat duodenum by ~2-fold (Tudpor et al., 2005). The direct stimulatory action of PRL on Ca^{2+} absorption has been confirmed by investigations using ex vivo duodenal tissue and the intestinal epithelium-like Caco-2 monolayer (Jantarajit et al., 2007; Thongon et al., 2008). In addition to Ca^{2+}, exposure to PRL for 2 days also increased the intestinal transport of water, Na^+, K^+ and Cl^- as well as nutrient molecules, such as glucose and neutral amino acids (e.g., glycine and proline) (Mainoya, 1975a,d). Thus, we hypothesized that a number of duodenal transporter genes involved in ion and nutrient transport may be upregulated in response to long-term hyperprolactinemia.

Besides the transport activities, growth and maturation of the intestinal mucosa is influenced by PRL. In the jejunum of 2-week-old rats, PRL induced proliferation of epithelial cells and ~3-fold increases in maltase and alkaline phosphatase activities (Bujanover et al., 2002). PRL also led to mucosal hypertrophy in pregnant and lactating rats (Mainoya, 1978). Moreover, an increase in the plasma PRL level was reported to stimulate proliferation of the colonic epithelial cells, and could be an unfavorable prognostic

* Corresponding author at: Department of Physiology, Faculty of Science, Mahidol University, Rama VI Road, Bangkok 10400, Thailand. Tel.: +66 2 354 7154; fax: +66 2 354 7154.
E-mail address: naratt@narattsys.com (N. Charoenphandhu).

0303-7207/$ – see front matter © 2008 Elsevier Ireland Ltd. All rights reserved.
doi:10.1016/j.mce.2008.09.025

factor in patients with colonic carcinoma (Bhatavdekar et al., 1995). Regarding PRL effect on the cellular metabolism, PRL increased the activities of UDP-glucuronosyltransferase and glutathione S-transferase in the jejunal epithelial cells of lactating rats (Luquita et al., 1999). Therefore, PRL appeared to exert a variety of actions beyond the scope of ion or nutrient transport, and considerable genomic response of the intestinal epithelial cells to long-term PRL exposure, which could be determined by a genome-wide expression study, was anticipated.

To avoid chronic stress from daily handling and PRL injection, hyperprolactinemia in the present study was induced by AP transplantation. Within 15 days after transplanting two extra AP glands from donors under the renal capsule of the recipient, continuous secretion of PRL from the AP allografts in the absence of the hypothalamic dopaminergic inhibition resulted in a sustained increase in the plasma PRL level (Charoenphandhu et al., 2007; Adler et al., 1989). Four weeks after transplantation, the plasma PRL levels are known to be maintained within the range of 90–100 ng/mL (Piyabhan et al., 2000), which are comparable to the levels attained during pregnancy in humans and rats (Boass et al., 1992). Other AP hormones were not secreted from the grafts due to the absence of their respective trophic factors from the hypothalamus.

The principal objective of this study was to analyze the profile of PRL-regulated genes in the duodenal epithelial cells by using microarray and quantitative real-time PCR (qRT-PCR) techniques. Prior to the profile study, expression of PRLR was determined to show that the duodenal tissue was a target of PRL, and whether hyperprolactinemia induced the downregulation of PRLR. The Illumina's high-performance BeadArray™ technology was used in our microarray study because it has been reported to exhibit high selectivity and sensitivity in gene expression profiling as a result of the high redundancy of each probe built in the bead array (Kuhn et al., 2004; Yan et al., 2008).

2. Materials and methods

2.1. Animals

Eighteen female Sprague–Dawley rats (10-week-old, weighing 200–220 g), were obtained from the National Laboratory Animal Centre, Thailand. They were individually placed in hanging stainless steel cages, fed standard pellets (Perfect Companion, Bangkok, Thailand) and distilled water ad libitum under 12/12 h light/dark cycle. Room temperature was controlled at 23–25 °C, and the relative humidity was about 50–60%. After 7-day acclimatization period, rats were randomly divided into two groups, i.e., sham-operated ($n = 6$) and AP-grafted groups ($n = 4$). Eight rats acted as donors for AP transplantation. This study has been approved by the Institutional Animal Care and Use Committee of the Faculty of Science, Mahidol University, Bangkok, Thailand.

2.2. Anterior pituitary (AP) transplantation

The procedure was modified from the methods of Adler et al. (1989) and Charoenphandhu et al. (2007). In brief, a 1.0 cm paracostal incision was made to expose the left renal capsule of the recipient rat. Two 10-week-old donors were then decapitated to collect the pituitary glands which were immediately inserted into the prepared renal capsule of the recipient rat (i.e., 2 glands/rat) and finally covered with the renal fascia. Muscle and skin were sutured with sterile silk 3/0, and cleaned with 70% ethanol and povidone-iodine. Wound dressing was performed daily. Sham operation consisted of exposure of the left kidney and a gentle touch of the renal fascia with forceps. Visual examination of the well-vascularized hypophyseal graft and immunohistochemical staining for PRL production were performed at the end of the experiments to confirm successful AP transplantation (Charoenphandhu et al., 2007). At 4 weeks after transplantation, plasma PRL levels have been known to increase to 90–100 ng/mL, which are comparable to the levels during pregnancy (Boass et al., 1992).

2.3. Tissue preparation

A median laparotomy was performed under 50 mg/kg sodium pentobarbitone i.p. (Abbott, North Chicago, IL, USA) anesthesia. The hypophyseal grafts were gently dissected from the perirenal tissue for immunohistochemical analysis. The duodenal segment (10 cm) was removed and cut longitudinally along the radix mesenterii to expose the mucosa. Duodenal epithelial cells were collected by scraping the mucosal surface with an ice-cold glass slide, and homogenized at 4 °C with a glass-Teflon Potter-Elvehjem tissue grinder (Wheaton, Millville, NJ, USA) as previously described (Jantarajit et al., 2007). Gene expression profile of each duodenal sample was analyzed separately by microarray.

2.4. Immunohistochemistry for PRL production

Imaging technique was performed to evaluate the viability of AP grafts (e.g., no sign of inflammation or graft rejection) as well as PRL production. Paraffin-embedded 4.0-μm sections were used to detect PRL production in the hypophyseal grafts. After blocking endogenous peroxidase activity and non-specific background with 3% H_2O_2 and 3% horse serum (Sigma, St. Louis, MO, USA), respectively, the sections were incubated for 60 min with 1:300 PRL polyclonal antibody (Dako, Carpinteria, CA, USA) prior to 10-min incubation with biotin-conjugated anti-rabbit secondary antibody and peroxidase-conjugated streptavidin (Dako). The chromogenic reaction was carried out with 3,3′-diaminobenzidine (Dako) to produce a brownish product. The slides were finally counterstained with hematoxylin (Sigma) for 5 min. The normal pituitary gland and perirenal fat pad were used as positive and negative controls, respectively. Hematoxylin–eosin (H&E) staining was also performed to identify structures of the graft. Images were acquired under light microscope (model BX51 TRF; Olympus, Tokyo, Japan).

2.5. Total RNA and cDNA preparation

By using TRIzol reagent (Invitrogen, Carlsbad, CA, USA), the total RNA was prepared from duodenal epithelial cells, as previously described (Thongon et al., 2008). The total RNA was treated with RQ1 DNase (Promega, Madison, WI, USA), and later purified with RNeasy Mini kit (Qiagen, Valencia, CA, USA). Purity of the total RNA was determined by the ratio of absorbance readings at 260 and 280 nm, the ratio of which fell in the range of 1.8–2.0. Integrity of RNA was analyzed by denaturing agarose gel electrophoresis with the 28S rRNA band appearing approximately twice as intense as the 18S rRNA band. Purified total RNA samples were later used for both microarray and qRT-PCR studies. As for qRT-PCR, 1 μg total RNA was reverse-transcribed with the oligo-dT_{15} primer and the iScript kit (Bio-rad, Hercules, CA, USA) to cDNA by a thermal cycler (model MyCycler; Bio-rad). Glyceraldehyde-3-phosphate dehydrogenase (GAPDH), a housekeeping gene, served as a control gene to check the consistency of the reverse transcription (percent coefficient of variation <10%, $n = 10$).

2.6. Microarray

Illumina TotalPrep RNA amplification/in vitro transcription kit (catalog no. IL1791; Ambion, Austin, TX, USA) was used to amplify and generate biotinylated cRNA from 500 ng total RNA for hybridization with Illumina BeadChip array. After purification, biotinylated cRNA was quantified with NanoDrop 1000 spectrophotometer (Thermo Scientific, Waltham, MA, USA). 750 ng of biotinylated cRNA from each duodenal sample was separately hybridized on the RatRef-12 Expression BeadChip (binary manifest file version V1_0_R0_11222119_A; Illumina, San Diego, CA, USA). Each RatRef-12 BeadChip is constructed with BeadArray™ technology, and contains 12 whole-genome gene expression arrays, thus allowing 12 independent samples to be hybridized to a single chip. Each array, which can probe 21,910 genes, consists of 22,523 oligonucleotide probes (50-base gene-specific sequence and 29-base address sequence per probe) selected primarily from the National Center for Biotechnology Information (NCBI) Reference Sequence (RefSeq) database (release 16; http://www.ncbi.nlm.nih.gov/RefSeq). After incubation at 58 °C for 20 h, the BeadChip was washed, blocked and incubated at room temperature with streptavidin-Cy3-containing solution (Illumina) according to the manufacturer's instruction. Fluorescent signals were scanned with BeadStation 500GX Genetic Analysis System (Illumina). Image registration and data extraction were automated with BeadStudio 3.1.3 (Illumina).

2.7. Quantitative real-time PCR (qRT-PCR) and sequencing

Primers used in the present study were designed by OLIGO 6 (Molecular Biology Insights, Cascade, CO, USA) and Primer Validator 1.4 (Naratt Software, Bangkok, Thailand), as shown in Table 1. qRT-PCR and melting curve analyses were performed by Bio-rad MiniOpticon with the iQ SYBR Green SuperMix (Bio-rad) as previously described (Thongon et al., 2008). Gene expression levels were normalized to GAPDH expression. The PCR products were also visualized on 1.5% agarose gel stained with 1.0 μg/mL ethidium bromide under a UV transilluminator (Alpha Innotech, San Leandro, CA, USA). After electrophoresis, all PCR products were extracted by the HiYield Gel/PCR DNA Extraction kit (Real Biotech Corporation, Taipei, Taiwan), and were sequenced by the ABI Prism 3100 Genetic Analyzer (Applied Biosystems, Foster City, CA, USA). qRT-PCR experiments were performed in triplicate.

Table 1
Rattus norvegicus oligonucleotide sequences used in qRT-PCR experiments.

Gene	Accession no.	Primer (forward/reverse)	Product length (bp)
Prolactin receptor			
Short isoform	NM_012630	5′-TTCTACCACCATCGCAAC-3′; 5′-CTGATCTCGTTTGTCATTGAG-3′	120
Long isoform	NM_001034111	5′-TCAAGCAACCGCAGACTC-3′; 5′-CAGTTTAGCCAATCGTTCCA-3′	107
Cell adhesion (GO:0007155)			
Ceacam10	NM_173339	5′-TCTCCTTTGATTGCTCTTCCT-3′; 5′-CTCTGGGGTTCACGAGTG-3′	75
Cellular component organization and biogenesis (GO:0016043)			
Syngr1	NM_019166	5′-TCGGCTCCATTGTGAATGAG-3′; 5′-CTTTCTTGCGGTCCTTGACA-3′	192
Cellular developmental process (GO:0048869)			
Epim	NM_012748	5′-TCCGTAGATTACGTGGAGCA-3′; 5′-AGGACAGCAATGACAGCCA-3′	119
Cellular metabolic process (GO:0044237)			
Cpz	NM_031766	5′-GGATGCGGCCTATAACCAT-3′; 5′-TCCAGGAGAAAGTGCAGCA-3′	114
Kynu	NM_053902	5′-GAGGAGTCGTCTGTGACAAG-3′; 5′-GCAGTAAGCAGTCTGATGAAC-3′	106
Sardh	NM_053664	5′-TTGCTAGGAATCTCCCAGGA-3′; 5′-TGGAACACTCTTCTCAGTGGTG-3′	194
Developmental process (GO:0032502)			
Dbn1	NM_031024	5′-ACCTGTCTGCTTCTCTACCCA-3′; 5′-CTAAGCTACAATCTGGTCTGGG-3′	160
Metabolism (GO:0008152)			
Pon1	NM_032077	5′-TTGAATGAGAAGGAGCCAGC-3′; 5′-TAAACACCTCCACGGTGGA-3′	166
Regulation of biological process (GO:0050789)			
CD40lg	NM_053353	5′-TGGAAAATGGGAGACAACT-3′; 5′-CAGAGGCTGACGATGAAT-3′	118
Gkn1	NM_198972	5′-GACAGCAATGTAGACGGAAGT-3′; 5′-TTTTCATAGTCCCAGAGGC-3′	119
Inhba	NM_017128	5′-GAATGAACTCATGGAGCAGACC-3′; 5′-TGCTGAAACAGACGGATGGT-3′	195
Syn2	NM_019159	5′-GTAATGGCATTGCAGTAGGTCC-3′; 5′-AACATGCCGTCAGCACTGAG-3′	181
Transport (GO:0006810)			
Cacnb1	NM_017346	5′-AGGACTTCCTGCACATCAAGG-3′; 5′-TTGTCACCTGACTTGCTGGAG-3′	175
Clcnkb	NM_173103	5′-CTCCACATTCACCTCTCCC-3′; 5′-GCAGCAGACAACCCTAGAAG-3′	104
Slc22a17	NM_177421	5′-GTCGTGGGATTGTACTGCTGA-3′; 5′-CATCAGGTAGACACCAAGGTCA-3′	146
Housekeeping gene			
GAPDH	NM_017008	5′-AGTCTACTGGCGTCTTCAC-3′; 5′-TCATATTTCTCGTGGTTCAC-3′	133

GAPDH, glyceraldehyde-3-phosphate dehydrogenase; full names of other genes are presented in Tables 2 and 3. Gene ontology (GO) identifiers are presented in parentheses.

2.8. Data analysis

Unless otherwise specified, differential gene expression of microarray and qRT-PCR were considered statistically significant when there was a 2-fold or greater difference in expression between the sham-operated and AP-grafted groups (Sigala et al., 2008). Microarray data were analyzed by BeadStudio Gene Expression Module 3.2.6 and Genome Viewer 3.2.7 (Illumina). The Illumina's Cubic-Spline normalization algorithm was applied to adjust sample signals to minimize the effects of variation arising from non-biological factors. False discovery checks were performed with the "compute false discovery rate" function of the BeadStudio. Comparison between two groups of samples (sham-operated vs. AP-grafted) was done with the *t*-test differential expression algorithm. $P < 0.05$ was used as the criterion for statistical significance. Gene Ontology (GO) analysis for characterizing the biological properties of gene products was performed according to the GO Consortium's instruction at the GO website (http://www.geneontology.org). The used GO search engines were AmiGO (http://amigo.geneontology.org), High-Throughput GoMiner (http://discover.nci.nih.gov/gominer), and Ensembl (http://www.ensembl.org). Gene symbol and full name of gene can be searched from the Rat Genome Database (http://rgd.mcw.edu). The qRT-PCR results compared by using $2^{-\Delta\Delta C_T}$ method (Livak and Schmittgen, 2001) are expressed as $\log_2$ means ± S.E. Graphics were performed with GraphPad Prism 5 (GraphPad Software, San Diego, CA, USA).

3. Results

3.1. Immunohistochemical analysis showed PRL production in the hypophyseal allograft

At 4 weeks after AP transplantation, the two implanted glands were removed from the perirenal connective tissues, and were analyzed for their viability and function histologically and immunohistochemically. The excised grafts were highly vascularized reddish-gray tissue with an average diameter of 1.5–2.5 mm ($n = 4$). H&E staining demonstrated a group of cells of varying size, arranged in irregular cords and clusters (Fig. 1A), agreeing with the histological morphology of normal pituitary gland. Numerous thin-walled sinusoidal networks with richly fenestrated endothelia were seen between the clusters of cells. Immunohistochemical analysis revealed the presence of PRL inside the pars distalis of the implanted glands (Fig. 1B and C), similar to that seen in normal pituitary gland (Fig. 1D). The adjacent fat tissues, fascia, and pars intermedia (negative control) did not show PRL immunoreactivity. Active signs of microvascular endothelial damage and lymphoid proliferation were not seen, suggesting the absence of graft rejection and allograft vasculopathy. The results corroborated that the AP-grafted rats possessed two healthy ectopic pituitary glands which actively produced extra PRL.

3.2. Chronic PRL exposure downregulated PRLR in the duodenal epithelial cells

PRLR mRNA expression was demonstrated by PCR. Since chronic exposure to PRL did not change GAPDH expression (Fig. 2A), mRNA expression levels were first normalized by GAPDH expression. In the present study, both short (-S) and long (-L) isoforms of PRLRs were strongly expressed in the duodenal epithelial cells (Fig. 2B), suggesting that these cells could be target of PRL action. The electrophoretic bands obtained were of expected sizes (Fig. 2B), and amplicon sequencing confirmed qRT-PCR findings. Since prolonged exposure to a high level of PRL could downregulate its receptor (Bowen et al., 2000; Swaminathan et al., 2008), a study of PRLR expression after AP transplantation was performed. qRT-PCR demonstrated (Fig. 2C) that the duodenal epithelial cells from AP-grafted rats showed a decrease in PRLR-L expression by −2.146-fold ($P < 0.05$). In contrast, the expression levels of PRLR-S in both sham-operated and AP-grafted rats were comparable.

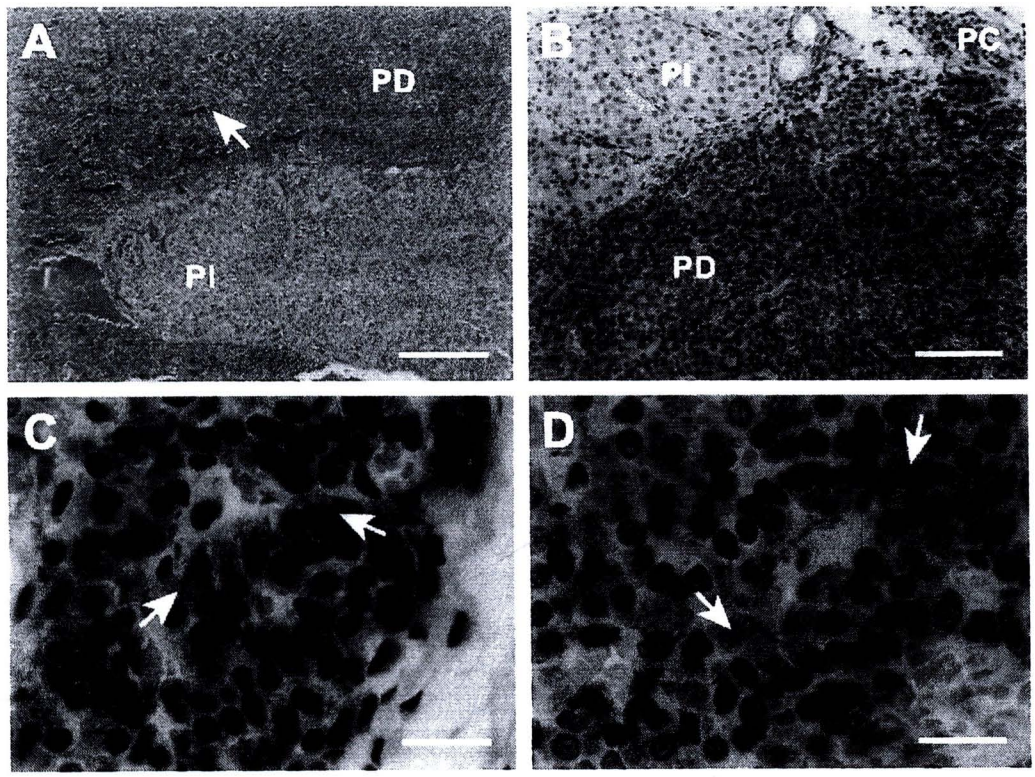

Fig. 1. Representative data of the immunohistochemical analysis for PRL production ($n=4$–6). (A) Hematoxylin–eosin (H&E) staining of the pars distalis (PD) and pars intermedia (PI) of a hypophyseal allograft dissected from a 4-week AP-grafted rat. The arrow indicates a thin-walled sinusoid filled with numerous erythrocytes. Scale bar, 200 μm. (B) Immunohistochemical staining of an implanted pituitary gland with anti-PRL antibody. The PD is strongly labelled with brownish products of peroxidase, whereas the PI used as a negative control is not stained. The perirenal connective tissues (PC) do not show PRL immunoreactivity. Scale bar, 100 μm. (C) PRL-producing cells (arrows) in a hypophyseal allograft. Scale bar, 20 μm. (D) PRL-producing cells (arrows) in a normal pituitary gland, which is used as a positive control. This gland was dissected from the pituitary fossa of a sham-operated rat. Scale bar, 20 μm.

3.3. Microarray study revealed transcriptome responses of the duodenal epithelial cells after 4 weeks of AP transplantation

Among the 21,910 genes, the microarray analysis detected a total of 321 genes upregulated by more than 2-fold (287 known genes and 34 unknown genes) and 241 genes downregulated by lower than −2-fold (210 known genes and 31 unknown genes) in the duodenal epithelial cells of AP-grafted rats (Fig. 3A and B, and Supplemental Tables S1 and S2). All known genes which were upregulated by more than 10-fold or downregulated by less than −10-fold are listed in order of fold change in Tables 2 and 3, respectively. As shown in Fig. 3, analysis of the distribution of fold changes demonstrated that one half of the PRL-altered genes were increased in the range of 2- to 4-fold (156 known genes and 25 unknown genes), or were decreased in the range of −2 to −4-fold (111 known genes and 18 unknown genes). There were 8 upregulated genes, i.e., Kynu, Clcnkb, Kcnab2, Rup2, Clstn2, Prlpd, Sardh and Epim, and 4 downregulated genes, i.e., Apoa2, S100a9, Mfap4 and Grik3, the expression levels of which were changed by a factor of 100 or higher (Tables 2 and 3).

Furthermore, we searched the GO and Ensembl databases to obtain functional classification of each PRL-altered gene. Only the genes changed by more than 10-fold or less than −10-fold were categorized into 14 major GO groups, each with unique GO identifier, as depicted in Fig. 4A. There were a total of 49 annotated genes in the upregulated set, and 37 annotated genes in the downregulated set (Table 4). The upregulated genes (Fig. 4B) were predominantly involved in the molecular function (11 genes, 20.75% of >10-fold upregulated genes), cellular metabolic process (10 genes, 18.87%), regulation of biological process (7 genes, 13.21%), transport (5 genes, 9.43%) and cellular component (4 genes, 7.55%). Within the downregulated group (Fig. 4C), the majority of genes were involved in the regulation of biological process (8 genes, 20% of <−10-fold downregulated genes), cell communication (7 genes, 17.50%) and molecular function (6 genes, 15%).

Since the effects of PRL on ion and nutrient transport have been well established in the intestine, especially in the duodenum (Charoenphandhu and Krishnamra, 2007; Mainoya, 1975a,b), we further analyzed all upregulated and downregulated genes in the transport category (GO identifier 0006810). The results showed that PRL changed the expression of several genes involved in the transport of Ca^{2+}, Na^+, K^+, Cl^-, H^+, Zn^{2+}, Cu^{2+}, HCO_3^-, phosphate, glucose, neutral amino acid, organic cation, and organic anion (Tables 5 and 6). Interestingly, the majority of the PRL-altered transporter genes were involved in K^+ transport (Fig. 5A and B), i.e., 5 upregulated transcripts (29.41% of upregulated transcripts in the transport category) and 3 downregulated transcripts (25%). PRL also altered the expression of two genes which are subunits of Na^+/K^+-ATPase, a known target protein of PRL (Laborde et al., 1992; Charoenphandhu et al., 2006), i.e., Atp1a2 and Atp1a3 by 2.023- and −7.244-fold (Tables 5 and 6), respectively.

Moreover, PRL increased the expression of several duodenal genes reported to be involved in ion and nutrient transport in the intestine and/or the total body water and electrolyte homeostasis, such as Klk7, Avp, Npb, Kng1, Ren1, Trpc2, Npy2r, Nppc and Gcgr (Supplemental Table S1), while decreasing the expression of others, such as Npy1r, Npy5r, Chrm1, P2ry12, Galr3, Hrh2, Npr2 and Drd3 (Supplemental Table S2). PRL also upregulated Pthr1 encoding parathyroid hormone receptor 1 by 2.015-fold, and downregulated Calca encoding calcitonin/calcitonin-related polypeptide

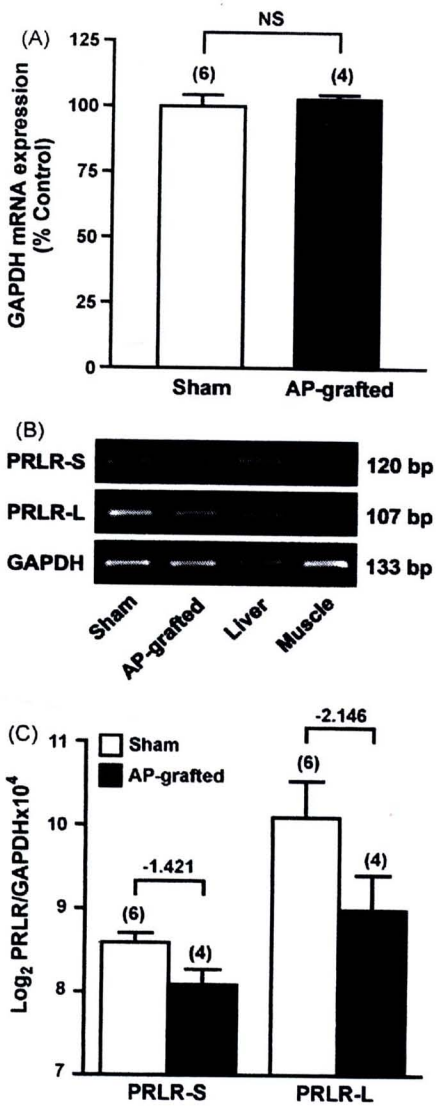

Fig. 2. (A) Expression of GAPDH, the housekeeping gene used for normalization in the qRT-PCR study, in the duodenal epithelial cells of sham-operated (Sham) and AP-grafted rats. Results were obtained from qRT-PCR and expressed as means ± S.E. NS, not significant. (B) Representative electrophoretic bands of short (-S) and long (-L) isoforms of PRLR in the duodenal epithelial cells of Sham and AP-grafted rats. Liver and gastrocnemius muscle from a Sham rat were used as positive and negative controls, respectively. Data were obtained from conventional RT-PCR at 36 cycles. (C) Expression of PRLR-S and -L in the duodenal epithelial cells of Sham and AP-grafted rats as determined by qRT-PCR. GAPDH is a housekeeping gene used for normalization. Results are expressed as $\log_2$ means ± S.E. Fold changes of PRLR-S and PRLR-L expression are presented above their respective columns. Numbers in parentheses represent the number of animals.

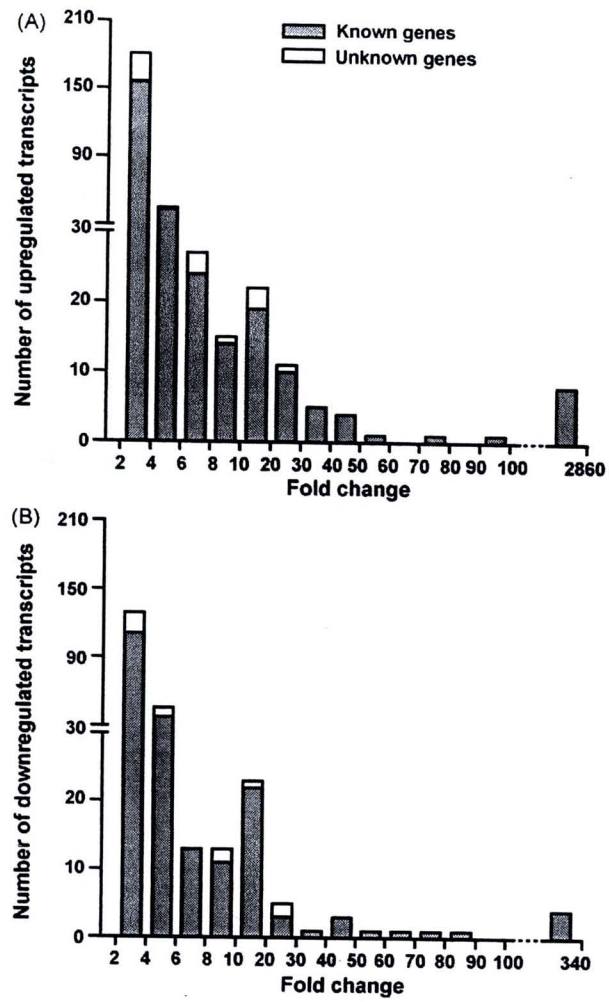

Fig. 3. Distribution of fold changes of genes upregulated (A) and downregulated (B) in the duodenal epithelial cells of AP-grafted rats as determined by microarray. This data set includes transcripts with expression levels changed by more than 2-fold or less than −2-fold.

α by −2.300-fold, both of which have been known to regulate intestinal Ca^{2+} transport and/or Ca^{2+} homeostasis.

Finally, we used qRT-PCR to verify changes in gene expression demonstrated by microarray. We selected genes to be tested by qRT-PCR according to their biological functions, i.e., 1–3 genes per each category (Table 1). As shown in Fig. 6, the qRT-PCR results of 15 studied transcripts were all consistent with the microarray results in response to hyperprolactinemia.

4. Discussion

In the present study, we demonstrated, for the first time, the transcriptome responses of the duodenal epithelial cells to hyperprolactinemia using the highly sensitive Illumina microarray. There was a good quantitative correlation between the fold changes determined by microarray and qRT-PCR. The present results supported the hypothesis that PRL could exert its actions on the duodenal epithelium in a genomic manner. Gene ontology analysis also suggested pleiotropic actions of PRL on a number of cellular processes, especially the transport function, thus confirming the previous studies both in vitro at the tissue level and in vivo that PRL regulated the body electrolyte homeostasis by controlling the rates of intestinal ion transport. Although the samples were collected by scraping and may contain other mucosal cells, e.g., goblet cells, there has been no report on the effect of PRL on other mucosal cell types. It was, therefore, implicated that our results represented the expression profile of the duodenal absorptive cells.

The presence of PRLR in the duodenal epithelial cells indicated that these cells could be direct targets of PRL actions. Our results were consistent with several previous investigations which showed PRLR expression in the duodenum at both transcriptional and translational levels (Jantarajit et al., 2007). However, nothing is known pertaining duodenal PRLR expression under either physiological (e.g., pregnancy and lactation) or pathological (e.g., prolactinoma) hyperprolactinemia. As demonstrated by our qRT-PCR, chronic exposure to PRL could downregulate duodenal PRLR, similar to that typically seen in other cells, such as luteal cells and human

Table 2
Known genes upregulated in the duodenal epithelial cells of AP-grafted rats.

Gene name	Gene symbol	Accession no.	Fold change
Kynureninase (L-kynurenine hydrolase)	Kynu	NM_053902	2859.417
Chloride channel Kb	Clcnkb	NM_173103	397.970
Potassium voltage-gated channel, shaker-related subfamily, beta member 2	Kcnab2	NM_017304	213.821
Urinary protein 2	Rup2	NM_001034950	147.546
Calsyntenin 2	Clstn2	NM_134377	136.802
Prolactin-like protein D	Prlpd	NM_022537	134.864
Sarcosine dehydrogenase	Sardh	NM_053664	123.675
Epimorphin	Epim	NM_012748	100.643
Pyrimidinergic receptor P2Y, G-protein coupled, 6	P2ry6	NM_057124	93.969
Carboxypeptidase Z	Cpz	NM_031766	75.040
Solute carrier family 38, member 5	Slc38a5	NM_138854	52.576
Toll-like receptor 4	Tlr4	NM_019178	46.702
Cholinergic receptor, muscarinic 2	Chrm2	NM_031016	42.014
Paraoxonase 1	Pon1	NM_032077	41.760
Fatty acid binding protein 3	Fabp3	NM_024162	40.893
Insulin 2	Ins2	NM_019130	39.318
Protease, serine, 2	Prss2	NM_012729	39.121
CEA-related cell adhesion molecule 10	Ceacam10	NM_173339	34.794
Kallikrein 7	Klk7	NM_012593	33.569
Mitogen-activated protein kinase 15	Mapk15	NM_173331	32.832
Drebrin 1	Dbn1	NM_031024	28.679
Synapsin II, transcript variant 2	Syn2	NM_019159	28.674
Pregnancy upregulated non-ubiquitously expressed CaM kinase	Pnck	NM_017275	27.032
Synaptogyrin 1	Syngr1	NM_019166	27.020
GTP binding protein 3	Gtpbp3	NM_001011919	25.783
Sex hormone binding globulin	Shbg	NM_012650	22.897
Nuclear factor of activated T-cells, cytoplasmic, calcineurin-dependent 2 interacting protein	Nfatc2ip	NM_001007692	22.859
Syncollin	Sycn	NM_139086	22.518
Formin binding protein 1	Fnbp1	NM_138914	22.349
Unc-5 homolog A (*C. elegans*)	Unc5a	NM_022206	21.680
Parvalbumin	Pvalb	NM_022499	17.373
Zinc finger protein 382	Znf382	NM_144749	16.306
Hemochromatosis type 2 (juvenile) homolog (human)	Hfe2	NM_001012080	16.123
FSH primary response 1	Fshprh1	NM_012955	15.476
GATA binding protein 3	Gata3	NM_133293	15.366
Sodium channel, voltage-gated, type I, alpha	Scn1a	NM_030875	14.246
MAD homolog 9 (*Drosophila*)	Smad9	NM_138872	14.104
Growth arrest specific 8	Gas8	NM_001039030	13.856
Calcium channel, voltage-dependent, beta 1 subunit	Cacnb1	NM_017346	12.633
CD40 ligand	Cd40lg	NM_053353	12.457
Zona pellucida glycoprotein 4	Zp4	NM_172330	12.451
Insulin 1	Ins1	NM_019129	12.398
Protamine 3	Prm3	NM_001002855	12.356
Outer dense fiber of sperm tails 4	Odf4	NM_001007670	11.871
FYVE, RhoGEF and PH domain containing 1	Fgd1	NM_001037546	11.434
Mitochondrial hepatocellular carcinoma-downregulated carrier protein	Hdmcp	NM_001001509	11.245
Calpain 6	Capn6	NM_031808	10.646
Calpain 3	Capn3	NM_017117	10.388
SH3-domain GRB2-like 3	Sh3gl3	NM_031238	10.101

Results are expressed as fold difference in signal intensity. This data set includes mRNAs whose levels changed by more than 10-fold in response to hyperprolactinemia. The complete list of the upregulated transcripts (more than 2-fold) is presented as supplemental data (Table S1).

embryo kidney 293T cells (Bowen et al., 2000; Swaminathan et al., 2008). However, despite the downregulation of PRLR, the duodenum appeared to be responsive to PRL since the stimulatory effect of PRLR on the transepithelial Ca^{2+} absorption in the duodenum of AP-grafted rats was still detectable (Tudpor et al., 2005). Moreover, similar to the results in luteal cells (Bowen et al., 2000), chronic PRL exposure predominantly downregulated PRLR-L, but not PRLR-S. The exact explanation of the differential PRLR isoform expression is not fully understood. Generally, PRLR-S and -L are expressed as cell surface receptors, and both isoforms possess comparable binding affinities (Bole-Feysot et al., 1998). It is suggested that PRL exerts its actions through PRLR-L, whereas PRLR-S does not mediate the transcriptional activation (Lesueur et al., 1991), or may even block the signal transduction of PRLR-L (Hu et al., 2001). Nevertheless, overexpression of PRLR-S completely rescued mammopoiesis in the heterozygous PRLR ($PRLR^{+/-}$) mice (Binart et al., 2003), indicating possible role of PRLR-S in the mammary gland in vivo. In the intestine, known direct PRL actions are presumably mediated by PRLR-L, especially those involved in water, electrolyte and nutrient absorption (Thongon et al., 2008). The absence of change in the duodenal PRLR-S expression after AP transplantation suggested that PRL exerted its actions predominantly via PRLR-L.

Microarray analysis revealed several PRL-regulated genes in the transport category. Functions of PRL as an osmoregulatory and calciotropic hormone are conserved throughout the evolution from fishes to mammals (Sakamoto and McCormick, 2006; Charoenphandhu and Krishnamra, 2007; Norris, 2007). In rats, PRL has long been known to stimulate Ca^{2+}, Na^+ and Cl^- transport in the duodenum (Tudpor et al., 2005; Mainoya, 1975d), and its Ca^{2+}-regulating action becomes more significant during pregnancy and lactation (Boass et al., 1992). Herein, we found that PRL altered the expression of Na^+/K^+-ATPase α polypeptides Atp1a2 and Atp1a3, which are subunits of Na^+/K^+-ATPase essential for the transcellular Na^+ transport and the solvent drag-induced paracellular transport

Table 3
Known genes downregulated in the duodenal epithelial cells of AP-grafted rats.

Gene name	Gene symbol	Accession no.	Fold change
Apolipoprotein A-II	Apoa2	NM_013112	−333.239
S100 calcium binding protein A9 (calgranulin B)	S100a9	NM_053587	−184.269
Microfibrillar-associated protein 4	Mfap4	NM_001034124	−132.304
Glutamate receptor, ionotropic, kainate 3	Grik3	NM_181373	−103.219
Kinesin 13B	Kif13B	NM_213626	−81.392
Inhibin beta-A	Inhba	NM_017128	−75.430
Phosphate cytidylyltransferase 1, choline, beta isoform	Pcyt1b	NM_173151	−69.764
Kringle containing transmembrane protein 1	Kremen1	NM_053649	−55.434
Dyslexia susceptibility 1 candidate 1 homolog (human)	Dyx1c1	NM_001007010	−44.282
Potassium inwardly rectifying channel, subfamily J, member 16	Kcnj16	NM_053314	−43.750
Mast cell protease 8	Mcpt8	NM_021598	−43.715
Connector enhancer of kinase suppressor of Ras 2	Cnksr2	NM_021686	−36.672
Ataxin 1	Atxn1	NM_012726	−24.906
Olfactory receptor 1078	Olr1078	NM_207597	−21.566
Dynein, axonemal, light intermediate polypeptide 1	Dnali1	NM_001031647	−21.532
Patched homolog 1 (*Drosophila*)	Ptch1	NM_053566	−19.512
T-complex protein 11 (mouse)	Tcp11	NM_001007695	−19.249
Sterol O-acyltransferase 1	Soat1	NM_031118	−19.244
Neurogenic differentiation 3	Neurod3	NM_019207	−18.431
Src-related kinase lacking C-terminal regulatory tyrosine and N-terminal myristylation sites	Srms	NM_001011961	−16.639
p21 (CDKN1A)-activated kinase 3	Pak3	NM_019210	−15.416
Taste receptor, type 2, member 10	Tas2r10	NM_023995	−14.844
PR-Vbeta1	VCS-beta1	NM_001017497	−14.458
Vomeronasal 1 receptor, B9	V1rb9	NM_173297	−13.607
CNDP dipeptidase 2 (metallopeptidase M20 family)	Cndp2	NM_001010920	−13.014
Solute carrier family 9, member 4	Slc9a4	NM_173098	−12.871
Succinate receptor 1	Sucnr1	NM_001001518	−12.769
Ly49 inhibitory receptor 5	Ly49i5	NM_001009501	−12.573
Tumor necrosis factor receptor superfamily, member 8	Tnfrsf8	NM_019135	−12.454
Surfactant associated protein D	Sftpd	NM_012878	−12.059
Gamma-aminobutyric acid (GABA-A) receptor, subunit alpha 4	Gabra4	NM_080587	−12.047
Profilin 2	Pfn2	NM_030873	−11.924
Prostaglandin D receptor	Ptgdr	NM_022241	−11.867
Erythrocyte protein band 4.1-like 1, transcript variant 2	Epb4.1l1	NM_021681	−11.439
G protein-coupled receptor 44	Gpr44	NM_001012070	−11.342
Trace-amine-associated receptor 7e	Taar7e	NM_175590	−10.730
Inter-alpha trypsin inhibitor, heavy chain 3	Itih3	NM_017351	−10.660

Results are expressed as fold difference in signal intensity. This data set includes mRNAs whose levels changed by less than −10-fold in response to hyperprolactinemia. The complete list of the downregulated transcripts (lower than −2-fold) is presented as supplemental data (Table S2).

of ions and nutrients (Charoenphandhu et al., 2006; Tanrattana et al., 2004). Na^+/K^+-ATPase is a principal target protein of PRL in several tissues of vertebrates, e.g., branchial epithelium of marine teleost (Pickford et al., 1970), ascending limb and distal convoluted tubule of rat kidneys (Laborde et al., 1992), and duodenal epithelium of rats (Charoenphandhu et al., 2006). Furthermore, PRL changed the expression of the voltage-dependent Ca^{2+} channel (Ca_V) subunits. Since the transepithelial Ca^{2+} flux exhibited a good correlation with L-type Ca_V activity and the L-type Ca_V blocker verapamil could block intestinal Ca^{2+} absorption (Morgan et al., 2007; Pento and Johnson, 1983), the altered Ca_V expression could explain the PRL-enhanced transepithelial calcium transport. In addition to Ca^{2+}, Na^+ and Cl^-, some investigators demonstrated a stimulatory effect of PRL on the intestinal transport of K^+, glucose and neutral amino acids (Mainoya, 1975a,b,c). The effect of PRL on K^+ transport is indeed predominant in the colon where it inhibits the Ca^{2+}-dependent K^+ secretion (Puntheeranurak et al., 2007). Physiological significance of the PRL-regulated K^+ transport in the rat duodenum is currently not known, but it may be essential for maternal K^+ homeostasis since the expression of eight K^+-related genes were altered by PRL. Furthermore, the PRL-induced downregulation of Zn^{2+} transporter Slc30a3 supported the previous finding reported by Travaglini and co-workers (1991) that hyperprolactinemia from prolactinoma led to a decrease in serum Zn^{2+} levels, which could be normalized by administration of bromocriptine, an inhibitor of pituitary PRL secretion. As for the intestinal transport of Cu^{2+}, HCO_3^-, phosphate, organic cations and organic anions, the effect of PRL on their transporters have never been demonstrated functionally either in vitro or in vivo, although the expression of the related genes were altered quite significantly by PRL.

Moreover, PRL also upregulated several genes known to regulate the intestinal ion transport and/or total body fluid and electrolyte homeostasis, e.g., kallikrein 7 (Klk7), arginine vasopressin (Avp), neuropeptide B (Npb), kininogen 1 (Kng1), renin 1 (Ren1), transient receptor potential cation channel (Trpc2), neuropeptide Y receptors (Npy1r, Npy2r and Npy5r), natriuretic peptide precursor type C (Nppc), glucagon receptor (Gcgr), muscarinic cholinergic receptor 1 (Chrm1), purinergic receptors (P2rx2 and P2ry12), galanin receptor 3 (Galr3), histamine receptor H2 (Hrh2), natriuretic peptide receptor 2 (Npr2) and dopamine receptor D3 (Drd3) (Antunes-Rodrigues et al., 2004; Cox, 2007; Hirota and McKay, 2006; Kinoshita et al., 2006; Margolius et al., 1985; Norris, 2007; Schultheiss et al., 2006; Walling et al., 1977; Zhang et al., 2007). Avp encoding arginine vasopressin not only plays a major role in osmoregulation, but also increases the duodenal motility (Li et al., 2007a). Thus, Avp upregulation could partially explain the PRL-induced increase in the gastrointestinal emptying time during lactation (Chen et al., 1997). Regarding Klk7 as a member of the kallikrein-kinin system, products of this system were found to stimulate Na^+ transport across the basolateral membrane of the intestinal absorptive cells (Moriwaki and Fujimori, 1979). Some natriuretic peptide-related genes, e.g., natriuretic peptide precursor type C (Nppc) and natriuretic peptide receptor 2 (Npr2), as well as renin-angiotensin system-related genes, e.g., renin (Ren1), are widely accepted as regulators of water

Table 4
Identification of PRL-altered transcripts in each gene ontology category.

Upregulated transcripts		Downregulated transcripts	
GO:000815 Biological process		GO:000815 Biological process	
GO:0007155 Cell adhesion		GO:0007155 Cell adhesion	
Ceacam10	(34.794)	Mfap4	(−132.304)
GO:0007154 Cell communication		GO:0007154 Cell communication	
Clstn2	(136.802)	Grik3	(−103.219)
Chrm2	(42.014)	Cnksr2	(−36.672)
Fshprh1	(15.476)	Olr1078	(−21.566)
		Pak3	(−15.416)
		Sucnr1	(−12.769)
		Gabra4	(−12.047)
		Taar7e	(−10.730)
GO:0016043 Cellular component organization and biogenesis		GO:0016043 Cellular component organization and biogenesis	
Syngr1	(27.020)	Kif13B	(−81.392)
Hdmcp	(11.245)		
GO:0048869 Cellular developmental process			
Epim	(100.643)		
GO:0044237 Cellular metabolic process		GO:0044237 Cellular metabolic process	
Carbohydrate metabolism		Lipid metabolism	
Ins2	(39.318)	Apoa2	(−333.239)
Ins1	(12.398)	Pcyt1b	(−69.764)
Lipid metabolism		Soat1	(−19.244)
Fabp3	(40.893)	Amine metabolism	
Nucleic acid metabolism		Itih3	(−10.660)
Gtpbp3	(25.783)		
Protein metabolism			
Kynu	(2859.417)		
Sardh	(123.675)		
Cpz	(75.040)		
Mapk15	(32.832)		
Pnck	(27.032)		
Capn3	(10.388)		
GO:0032502 Developmental process		GO:0032502 Developmental process	
Dbn1	(28.679)	Kremen1	(−55.434)
		Sftpd	(−12.059)
		Ptgdr	(−11.867)
GO:0008152 Metabolism			
Pon1	(41.760)		
GO:0050789 Regulation of biological process		GO:0050789 Regulation of biological process	
Syn2	(28.674)	S100a9	(−184.269)
Nfatc2ip	(22.859)	Inhba	(−75.430)
Sycn	(22.518)	Atxn1	(−24.906)
Znf382	(16.306)	Ptch1	(−19.512)
Smad9	(14.104)	Neurod3	(−18.431)
Cd40lg	(12.457)	Tnfrsf8	(−12.454)
Fgd1	(11.434)	Pfn2	(−11.924)
		Gpr44	(−11.342)
GO:0042221 Response to chemical stimulus			
Prss2	(39.121)		
GO:0006950 Response to stress			
Tlr4	(46.702)		
GO:0005575 Cellular component		GO:0005575 Cellular component	
Hfe2	(16.123)	Mcpt8	(−43.715)
Gas8	(13.856)	Dnali1	(−21.532)
Prm3	(12.356)	VCS-beta1	(−14.458)
Odf4	(11.871)		
GO:0003674 Molecular function		GO:0003674 Molecular function	
Calcium ion binding		Protein binding	
Pvalb	(17.373)	Epb4.1l1	(−11.439)
Protein binding		Peptidase activity	
Shbg	(22.897)	Cndp2	(−13.014)
Fnbp1	(22.349)	Receptor activity	
Zp4	(12.451)	Tcp11	(−19.249)
Sh3gl3	(10.101)	Tas2r10	(−14.844)
Hormone activity		V1rb9	(−13.607)
Prlpd	(134.864)	Ly49i5	(−12.573)
Peptidase activity			
Klk7	(33.569)		
Capn6	(10.646)		
Receptor activity			
P2ry6	(93.969)		
Unc5a	(21.680)		
Transcription factor activity			
Gata3	(15.366)		
Unknown		Unknown	

Table 4 (*Continued*)

Upregulated transcripts		Downregulated transcripts	
Rup2	(147.546)	Dyx1c1	(−44.282)
MGC108778	(23.930)	RN.13478	(−22.425)
LOC363483	(19.150)	LOC312102	(−20.541)
LOC497899	(18.844)	Srms	(−16.639)
RN.37544	(17.404)	RN.3886	(−12.456)

Numbers in parentheses represent fold changes of corresponding transcripts. Each category is accompanied by a unique GO identifier supplied by the GO search engines. Within each category, transcripts are listed in order of fold change. This data set includes mRNAs with the expression levels changed by more than 10-fold or less than −10-fold in response to hyperprolactinemia.

Table 5
PRL-upregulated transcripts in the transport category (GO:0006810).

Gene name	Gene symbol	Accession no.	Fold change
Calcium transport			
Calcium channel, voltage-dependent, beta 1 subunit	Cacnb1	NM_017346	12.633
Calcium channel, voltage-dependent, T type, alpha 1H subunit	Cacna1h	NM_153814	8.392
Calcium channel, voltage-dependent, T type, alpha 1G subunit	Cacna1g	NM_031601	7.017
Phosphate transport			
Solute carrier family 17 (sodium-dependent inorganic phosphate cotransporter), member 7	Slc17a7	NM_053859	3.582
Sodium transport			
Sodium channel, voltage-gated, type I, alpha	Scn1a	NM_030875	14.246
Amiloride-sensitive cation channel 3	Accn3	NM_173135	2.084
ATPase, Na^+/K^+ transporting, alpha 2 polypeptide	Atp1a2	NM_012505	2.023
Chloride transport			
Chloride channel Kb	Clcnkb	NM_173103	397.970
Potassium transport			
Potassium voltage-gated channel, shaker-related subfamily, beta member 2	Kcnab2	NM_017304	213.821
Potassium voltage-gated channel, Isk-related subfamily, member 1	Kcne1	NM_012973	5.314
Potassium inwardly rectifying channel, subfamily J, member 5	Kcnj5	NM_017297	2.547
Potassium voltage-gated channel, subfamily H (eag-related), member 2	Kcnh2	NM_053949	2.209
Potassium voltage-gated channel, subfamily Q, member 3	Kcnq3	NM_031597	2.049
Bicarbonate transport			
Solute carrier family 4, sodium bicarbonate cotransporter, member 9	Slc4a9	NM_152938	2.353
Copper transport			
ATPase, Cu^{2+} transporting, beta polypeptide	Atp7b	NM_012511	4.160
Organic cation transport			
Solute carrier family 22 (organic cation transporter), member 17	Slc22a17	NM_177421	2.646
Neutral amino acid transport			
Solute carrier family 38, member 5	Slc38a5	NM_138854	52.576

Results are expressed as fold difference in signal intensity. This data set includes mRNAs with the expression levels changed by more than 2-fold in response to hyperprolactinemia.

Table 6
PRL-downregulated transcripts in the transport category (GO:0006810).

Gene name	Gene symbol	Accession no.	Fold change
Calcium transport			
Calcium channel, voltage-dependent, L type, alpha 1E subunit	Cacna1e	NM_019294	−2.424
Sodium transport			
Solute carrier family 9, member 4	Slc9a4	NM_173098	−12.871
ATPase, Na^+/K^+ transporting, alpha 3 polypeptide	Atp1a3	NM_012506	−7.244
Potassium transport			
Potassium inwardly rectifying channel, subfamily J, member 16	Kcnj16	NM_053314	−43.750
Potassium voltage-gated channel, subfamily H (eag-related), member 1	Kcnh1	NM_031742	−2.297
Potassium voltage-gated channel, subfamily G, member 3, transcript variant 1	Kcng3	NM_133426	−2.061
Hydrogen ion transport			
ATPase, H^+ transporting, V0 subunit D, isoform 2	Atp6v0d2	NM_001011972	−4.735
ATPase, H^+ transporting, V1 subunit G isoform 2	Atp6v1g2	NM_212490	−3.151
Zinc transport			
Solute carrier family 30 (zinc transporter), member 3	Slc30a3	NM_001013243	−2.737
Organic anion transport			
Solute carrier organic anion transporter family, member 6c1	Slco6c1	NM_173338	−2.767
Kidney specific organic anion transporter	Slc21a4	NM_030837	−2.473
Glucose transport			
Solute carrier family 2 (facilitated glucose transporter), member 4	Slc2a4	NM_012751	−2.137

Results are expressed as fold difference in signal intensity. This data set includes mRNAs with the expression levels changed by lower than −2-fold in response to hyperprolactinemia.

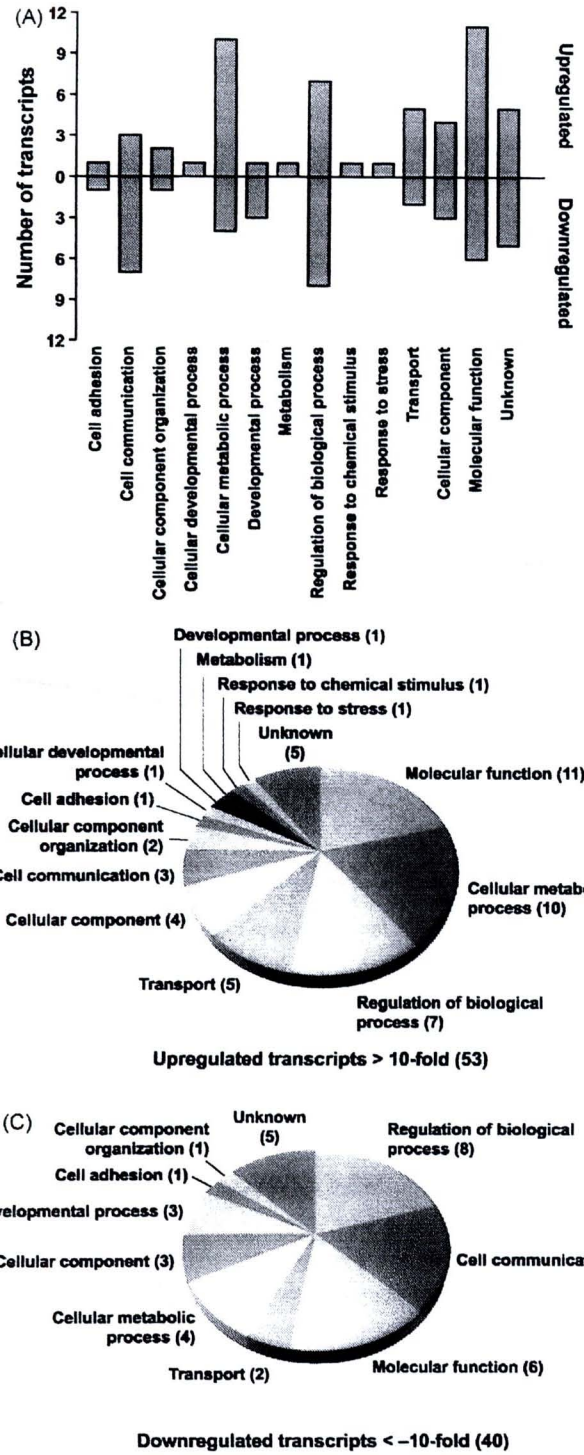

Fig. 4. (A) Distribution of genes in each gene ontology category. Columns above the abscissa represent transcripts that were upregulated at 4 weeks after AP transplantation, whereas columns below the abscissa represent downregulated transcripts. All transcripts were functionally classified according to known cellular functions by using GO search engines. (B) A pie chart shows proportional distribution of upregulated genes in each gene ontology category. (C) A pie chart shows proportional distribution of downregulated genes in each category. Numbers in parentheses represent the number of upregulated or downregulated transcripts. This data set includes transcripts whose levels changed by more than 10-fold or less than −10-fold.

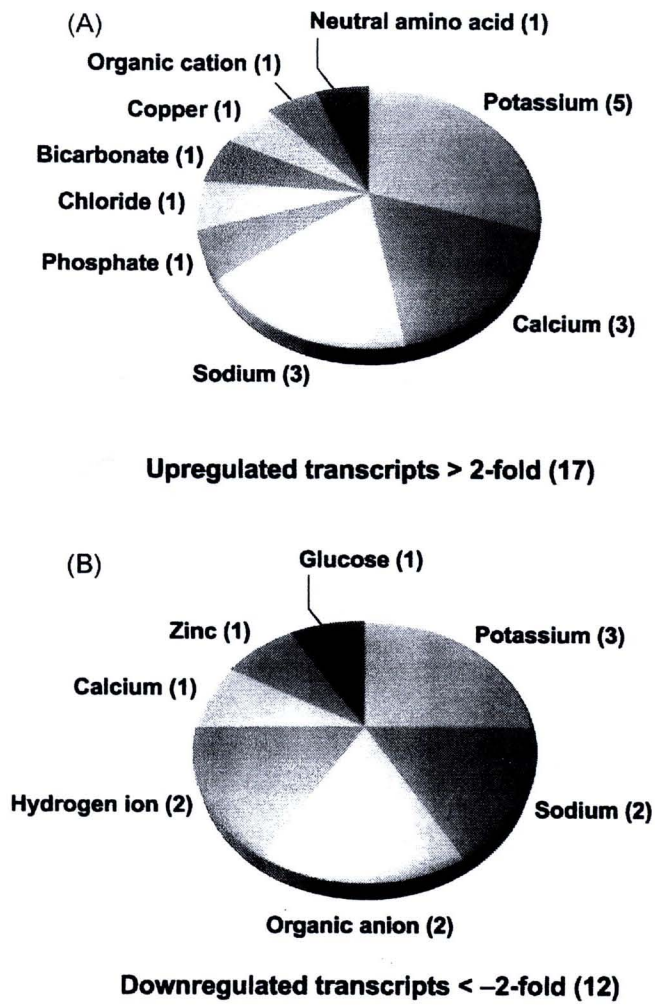

Fig. 5. Pie charts show proportional distributions of upregulated (A) and downregulated (B) genes in the transport category (GO:0006810). The transcripts were functionally classified according to the transported ions or substances. Numbers in parentheses represent the number of upregulated or downregulated transcripts. This data set includes transcripts with expression levels changed by more than 2-fold or less than −2-fold.

and Na^+ balance (Antunes-Rodrigues et al., 2004), whereas the muscarinic cholinergic receptors (Chrm) and neuropeptide Y receptors (e.g., Npy1r, Npy2r and Npy5r) are capable of modulating intestinal fluid secretion (Cox, 2007; Hirota and McKay, 2006). Downregulation of galanin receptor 3 (Galr3) possibly affected the intestinal transport activity, since galanin could increase the active Na^+ and Cl^- absorption in the rabbit ileum (Homaidan et al., 1994).

Of interest is the finding of the PRL-induced upregulation of Pthr1 encoding parathyroid hormone receptor 1 and the downregulation of Calca encoding calcitonin/calcitonin-related polypeptide α, a hypocalcemic hormone. Although the actions of both proteins on the duodenal epithelium have never been reported, we postulate that such actions might be part of the indirect mechanism by which PRL regulates the duodenal Ca^{2+} absorption and/or Ca^{2+} balance. Nemere and Norman (1986) previously reported that parathyroid hormone 1–34, which could bind to Pthr1, significantly stimulated Ca^{2+} transport in the perfused, isolated duodenal loops.

Besides the genes related to electrolyte homeostasis, PRL also altered a number of genes in other categories, including cell adhesion, cell communication, cellular developmental process, and cellular metabolic process, as shown in Table 4. Although most PRL-altered genes are of unknown functions in the intestine,

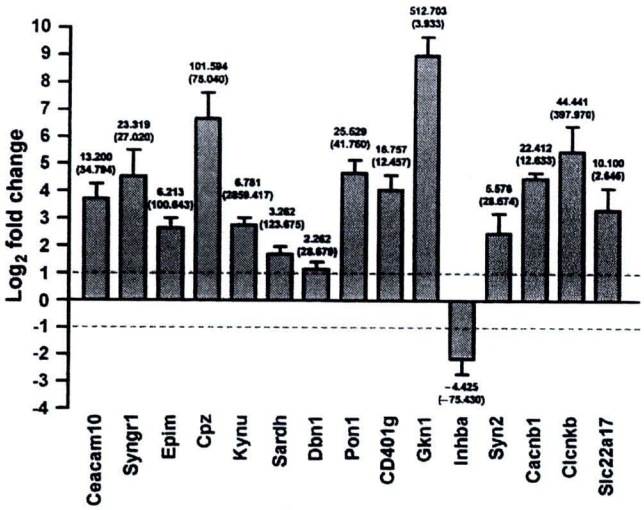

Fig. 6. Fold changes in the expression levels of 15 transcripts selected from various GO categories in the duodenal epithelial cells of AP-grafted rats ($n=4$) vs. sham-operated rats ($n=6$). Gene expression was normalized by GAPDH. Twofold upregulation or downregulation are indicated by the two dashed lines. Fold change value of each gene from qRT-PCR is presented on its respective column. Corresponding microarray data are given in parentheses. Full names of genes are shown in Tables 2 and 3.

alteration of some transcripts, such as epimorphin (Epim), zinc finger protein 382 (Znf382), kringle-containing transmembrane protein 1 (Kremen1), purinergic receptor (P2rx2), and insulin (Ins1 and Ins2), might explain PRL actions on the intestinal cell proliferation and maturation (Coutinho-Silva et al., 2005; Gebelein et al., 1998; Iizuka et al., 2007; Ménard et al., 1999). Mainoya (1978) demonstrated that, during pregnancy and lactation, the intestinal weight of rats was markedly increased, and such effect could be abolished by bromocriptine. Hence, the lactation-induced intestinal hypertrophy could be attributed to the proliferative effect of PRL. In contrast, Muller and Dowling (1981) could not detect intestinal hypertrophy in hyperprolactinemic rats with serum PRL of 870 ng/mL. This discrepancy could be due to the typical biphasic action of PRL, in which excess PRL molecules bind to PRLRs as non-functional 1:1 PRL-PRLR complex instead of a functional 1:2 complex (Fuh et al., 1993). To induce intestinal hypertrophy, we speculate that PRL may do so by increasing the expression of a morphogenic protein epimorphin (Epim) or purinergic receptor P2X (P2rx2), both of which have been reported to enhance survival of intestinal epithelial cells (Iizuka et al., 2007; Coutinho-Silva et al., 2005). Alternatively, PRL may induce production of certain local growth factors, such as insulin (Ins1 and Ins2), which can stimulate proliferation of jejunal epithelial cells (Ménard et al., 1999). Other upregulated transcripts in the regulation of biological process and molecular function categories, e.g., mothers against decapentaplegic homolog 9 (Smad9), also appear to be essential for growth and development of the intestinal epithelium.

PRL is also involved in the biotransformation of certain exogenous and endogenous compounds, e.g., *p*-nitrophenol and androgenic steroids (Luquita et al., 1999). Since the intestinal epithelia are normally exposed to drugs and toxic substances, an elevated plasma PRL in lactating animals may help neutralize these chemicals at the absorptive sites, thereby reducing the amount of their toxic metabolites in milk. It is possible that the upregulation of UDP-glucuronosyltransferase (Udpgtr2) gene of the cellular metabolic process category (Supplemental Tables S1) could be important for the PRL-regulated phase II biotransformation of drugs and steroid hormones during lactation. Luquita and co-workers (1999) demonstrated that 1–3 mg/kg/day) PRL administration over 4 days increased UDP-glucuronosyltransferase activity in the jejunum of ovariectomized rats. Consistent with a previous report on a high activity of an antioxidative protein paraoxonase in lactating animals (Turk et al., 2005), paraoxonase (Pon1) expression was increased in our microarray study by ~41-fold (Table 2). In addition, other genes, e.g., nuclear factor of activated T-cells, cytoplasmic, calcineurin-dependent 2 interacting protein (Nfatc2ip) and GATA binding protein 3 (Gata3), may also function in the modulation of the immunoprotective or barrier function of the intestinal epithelium (Li et al., 2007b; Kiwamoto et al., 2006).

In summary, the present study demonstrated that PRL altered the expression of a number of genes related to fluid and electrolyte homeostasis (especially for Ca^{2+}, Na^+, K^+ and Cl^- transport) and cell proliferation, both of which are well-established functions of PRL in the intestine. However, the precise functions of these PRL-regulated genes in the duodenal epithelial cells as well as the association between PRL and the functions of those genes are currently unknown. Our results thus provide direction for further investigations into the mechanism of PRL actions in the intestine during pregnancy and lactation.

Conflict of interest

None.

Acknowledgments

This research was supported by grants from the Commission on Higher Education, and the Thailand Research Fund (RSA5180001 to N. Charoenphandhu and RTA5080008 to N. Krishnamra).

Appendix A. Supplementary data

Supplementary data associated with this article can be found, in the online version, at doi:10.1016/j.mce.2008.09.025.

References

Adler, R.A., Farrell, M.E., Krieg, R.J., Deiss, W.P., 1989. Hypogonadism does not mediate urinary calcium loss in pituitary-grafted rats. Metabolism 38, 805–809.
Antunes-Rodrigues, J., de Castro, M., Elias, L.L., Valenca, M.M., McCann, S.M., 2004. Neuroendocrine control of body fluid metabolism. Physiol. Rev. 84, 169–208.
Bhatavdekar, J.M., Patel, D.D., Shah, N.G., Karelia, N.H., Vora, H.H., Ghosh, N., Suthar, T.P., Balar, D.B., 1995. Prognostic value of insulin-like growth factor-1 receptors in patients with colon/rectal cancer: correlation with plasma prolactin. Eur. J. Surg. Oncol. 21, 23–26.
Binart, N., Imbert-Bolloré, P., Baran, N., Viglietta, C., Kelly, P.A., 2003. A short form of the prolactin (PRL) receptor is able to rescue mammopoiesis in heterozygous PRL receptor mice. Mol. Endocrinol. 17, 1066–1074.
Boass, A., Lovdal, J.A., Toverud, S.U., 1992. Pregnancy- and lactation-induced changes in active intestinal calcium transport in rat. Am. J. Physiol. 263, G127–G134.
Bole-Feysot, C., Goffin, V., Edery, M., Binart, N., Kelly, P.A., 1998. Prolactin (PRL) and its receptor: actions, signal transduction pathways and phenotypes observed in PRL receptor knockout mice. Endocr. Rev. 19, 225–268.
Bowen, J.M., Telleria, C.M., Towns, R., Keyes, P.L., 2000. Downregulation of long-form prolactin receptor mRNA during prolactin-induced luteal regression. Eur. J. Endocrinol. 143, 285–292.
Bujanover, Y., Wollman, Y., Reif, S., Golander, A., 2002. A possible role of prolactin on growth and maturation of the gut during development in the rat. J. Pediatr. Endocrinol. Metab. 15, 789–794.
Charoenphandhu, N., Krishnamra, N., 2007. Prolactin is an important regulator of intestinal calcium transport. Can. J. Physiol. Pharmacol. 85, 569–581.
Charoenphandhu, N., Limlomwongse, L., Krishnamra, N., 2006. Prolactin directly enhanced Na^+/K^+- and Ca^{2+}-ATPase activities in the duodenum of female rats. Can. J. Physiol. Pharmacol. 84, 555–563.
Charoenphandhu, N., Tudpor, K., Thongchote, K., Saengamnart, W., Puntheeranurak, S., Krishnamra, N., 2007. High-calcium diet modulates effects of long-term prolactin exposure on the cortical bone calcium content in ovariectomized rats. Am. J. Physiol. Endocrinol. Metab. 292, E443–E452.
Chen, T.S., Doong, M.L., Wang, S.W., Tsai, S.C., Lu, C.C., Shih, H.C., Chen, Y.H., Chang, F.Y., Lee, S.D., Wang, P.S., 1997. Gastric emptying and gastrointestinal transit during lactation in rats. Am. J. Physiol. 272, G626–G631.

Coutinho-Silva, R., Stahl, L., Cheung, K.K., de Campos, N.E., de Oliveira Souza, C., Ojcius, D.M., Burnstock, G., 2005. P2X and P2Y purinergic receptors on human intestinal epithelial carcinoma cells: effects of extracellular nucleotides on apoptosis and cell proliferation. Am. J. Physiol. Gastrointest. Liver Physiol. 288, G1024–G1035.

Cox, H.M., 2007. Neuropeptide Y receptors; antisecretory control of intestinal epithelial function. Auton. Neurosci. 133, 76–85.

Fuh, G., Colosi, P., Wood, W.I., Wells, J.A., 1993. Mechanism-based design of prolactin receptor antagonists. J. Biol. Chem. 268, 5376–5381.

Gebelein, B., Fernandez-Zapico, M., Imoto, M., Urrutia, R., 1998. KRAB-independent suppression of neoplastic cell growth by the novel zinc finger transcription factor KS1. J. Clin. Invest. 102, 1911–1919.

Hirota, C.L., McKay, D.M., 2006. Cholinergic regulation of epithelial ion transport in the mammalian intestine. Br. J. Pharmacol. 149, 463–479.

Homaidan, F.R., Tang, S.H., Donowitz, M., Sharp, G.W., 1994. Effects of galanin on short circuit current and electrolyte transport in rabbit ileum. Peptides 15, 1431–1436.

Hu, Z.Z., Meng, J., Dufau, M.L., 2001. Isolation and characterization of two novel forms of the human prolactin receptor generated by alternative splicing of a newly identified exon 11. J. Biol. Chem. 276, 41086–41094.

Iizuka, M., Sasaki, K., Hirai, Y., Shindo, K., Konno, S., Itou, H., Ohshima, S., Horie, Y., Watanabe, S., 2007. Morphogenic protein epimorphin protects intestinal epithelial cells from oxidative stress by the activation of EGF receptor and MEK/ERK, PI3 kinase/Akt signals. Am. J. Physiol. Gastrointest. Liver Physiol. 292, G39–G52.

Jantarajit, W., Thongon, N., Pandaranandaka, J., Teerapornpuntakit, J., Krishnamra, N., Charoenphandhu, N., 2007. Prolactin-stimulated transepithelial calcium transport in duodenum and Caco-2 monolayer are mediated by the phosphoinositide 3-kinase pathway. Am. J. Physiol. Endocrinol. Metab. 293, E372–E384.

Kinoshita, N., Takahashi, T., Tada, S., Shinozuka, K., Mizuno, N., Takahashi, K., 2006. Activation of P2Y receptor enhances high-molecular compound absorption from rat ileum. J. Pharm. Pharmacol. 58, 195–200.

Kiwamoto, T., Ishii, Y., Morishima, Y., Yoh, K., Maeda, A., Ishizaki, K., Iizuka, T., Hegab, A.E., Matsuno, Y., Homma, S., Nomura, A., Sakamoto, T., Takahashi, S., Sekizawa, K., 2006. Transcription factors T-bet and GATA-3 regulate development of airway remodeling. Am. J. Respir. Crit. Care Med. 174, 142–151.

Kuhn, K., Baker, S.C., Chudin, E., Lieu, M.H., Oeser, S., Bennett, H., Rigault, P., Barker, D., McDaniel, T.K., Chee, M.S., 2004. A novel, high-performance random array platform for quantitative gene expression profiling. Genome Res. 14, 2347–2356.

Laborde, K., Bussieres, L., Dechaux, M., Shahedi, M., Sachs, C., 1992. Effects of prolactin on Na^+/K^+-ATPase activity in the nephron during maturation in the rat. Pediatr. Res. 31, 207–210.

Lesueur, L., Edery, M., Ali, S., Paly, J., Kelly, P.A., Djiane, J., 1991. Comparison of long and short forms of the prolactin receptor on prolactin-induced milk protein gene transcription. Proc. Natl. Acad. Sci. U.S.A. 88, 824–828.

Li, L., Kong, X., Liu, H., Liu, C., 2007a. Systemic oxytocin and vasopressin excite gastrointestinal motility through oxytocin receptor in rabbits. Neurogastroenterol. Motil. 19, 839–844.

Li, S.Z., McDill, B.W., Kovach, P.A., Ding, L., Go, W.Y., Ho, S.N., Chen, F., 2007b. Calcineurin-NFATc signaling pathway regulates AQP2 expression in response to calcium signals and osmotic stress. Am. J. Physiol. Cell Physiol. 292, C1606–C1616.

Livak, K.J., Schmittgen, T.D., 2001. Analysis of relative gene expression data using real-time quantitative PCR and the $2^{-\Delta\Delta C_T}$ method. Methods 25, 402–408.

Luquita, M.G., Catania, V.A., Sánchez Pozzi, E.J., Vore, M., Veggi, L.M., Pellegrino, J.M., Mottino, A.D., 1999. Induction of phase II biotransformation reactions in rat jejunum during lactation. Possible involvement of prolactin. Biochim. Biophys. Acta 1472, 82–92.

Mainoya, J.R., 1975a. Effect of prolactin on sugar and amino acid transport by the rat jejunum. J. Exp. Zool. 192, 149–154.

Mainoya, J.R., 1975b. Further studies on the action of prolactin on fluid and ion absorption by the rat jejunum. Endocrinology 96, 1158–1164.

Mainoya, J.R., 1975c. Analysis of the role of endogenous prolactin on fluid and sodium chloride absorption by the rat jejunum. J. Endocrinol. 67, 343–349.

Mainoya, J.R., 1975d. Effects of bovine growth hormone, human placental lactogen and ovine prolactin on intestinal fluid and ion transport in the rat. Endocrinology 96, 1165–1170.

Mainoya, J.R., 1978. Possible influence of prolactin on intestinal hypertrophy in pregnant and lactating rats. Experientia 34, 1230–1231.

Margolius, H.S., Halushka, P.V., Chao, J., Miller, D.H., Cuthbert, A.W., Spayne, J.A., 1985. Studies of the kallikrein-kinin system and prostaglandins in epithelial ion transport. Soc. Gen. Physiol. Ser. 39, 121–133.

Ménard, D., Corriveau, L., Beaulieu, J.F., 1999. Insulin modulates cellular proliferation in developing human jejunum and colon. Biol. Neonate 75, 143–151.

Morgan, E.L., Mace, O.J., Affleck, J., Kellett, G.L., 2007. Apical GLUT2 and $Ca_V1.3$: regulation of rat intestinal glucose and calcium absorption. J. Physiol. 580, 593–604.

Moriwaki, C., Fujimori, H., 1979. Effect of kallikrein-kinin system on ion transport across rat small intestine. Adv. Exp. Med. Biol. 120A, 461–471.

Muller, E., Dowling, R.H., 1981. Prolactin and the small intestine. Effect of hyperprolactinaemia on mucosal structure in the rat. Gut 22, 558–565.

Nemere, I., Norman, A.W., 1986. Parathyroid hormone stimulates calcium transport in perfused duodena from normal chicks: comparison with the rapid (transcaltachic) effect of 1,25-dihydroxyvitamin D_3. Endocrinology 119, 1406–1408.

Norris, D.O., 2007. Bioregulation of calcium and phosphate homeostasis. In: Norris, D.O. (Ed.), Vertebrate Endocrinology. Elsevier, San Diego, pp. 486–511.

Pento, J.T., Johnson, M.E., 1983. The influence of verapamil on calcium transport and uptake in segments of rat intestine. Pharmacology 27, 343–349.

Pickford, G.E., Griffith, R.W., Torretti, J., Hendlez, E., Epstein, F.H., 1970. Branchial reduction and renal stimulation of Na^+, K^+-ATPase by prolactin in hypophysectomized killifish in fresh water. Nature 228, 378–379.

Piyabhan, P., Krishnamra, N., Limlomwongse, L., 2000. Changes in the regulation of calcium metabolism and bone calcium content during growth in the absence of endogenous prolactin and during hyperprolactinemia: a longitudinal study in male and female Wistar rats. Can. J. Physiol. Pharmacol. 78, 757–765.

Puntheeranurak, S., Schreiber, R., Spitzner, M., Ousingsawat, J., Krishnamra, N., Kunzelmann, K., 2007. Control of ion transport in mouse proximal and distal colon by prolactin. Cell. Physiol. Biochem. 19, 77–88.

Sakamoto, T., McCormick, S.D., 2006. Prolactin and growth hormone in fish osmoregulation. Gen. Comp. Endocrinol. 147, 24–30.

Schultheiss, G., Hennig, B., Schunack, W., Prinz, G., Diener, M., 2006. Histamine-induced ion secretion across rat distal colon: involvement of histamine H1 and H2 receptors. Eur. J. Pharmacol. 546, 161–170.

Sigala, S., Bodei, S., Missale, C., Zani, D., Simeone, C., Cunico, S.C., Spano, P.F., 2008. Gene expression profile of prostate cancer cell lines: effect of nerve growth factor treatment. Mol. Cell. Endocrinol. 284, 11–20.

Swaminathan, G., Varghese, B., Thangavel, C., Carbone, C.J., Plotnikov, A., Kumar, K.G., Jablonski, E.M., Clevenger, C.V., Goffin, V., Deng, L., Frank, S.J., Fuchs, S.Y., 2008. Prolactin stimulates ubiquitination, initial internalization, and degradation of its receptor via catalytic activation of Janus kinase 2. J. Endocrinol. 196, R1–R7.

Tanrattana, C., Charoenphandhu, N., Limlomwongse, L., Krishnamra, N., 2004. Prolactin directly stimulated the solvent drag-induced calcium transport in the duodenum of female rats. Biochim. Biophys. Acta 1665, 81–91.

Thongon, N., Nakkrasae, L.I., Thongbunchoo, J., Krishnamra, N., Charoenphandhu, N., 2008. Prolactin stimulates transepithelial calcium transport and modulates paracellular permselectivity in Caco-2 monolayer: mediation by PKC and ROCK pathways. Am. J. Physiol. Cell Physiol. 294, C1158–C1168.

Travaglini, P., Mocchegiani, E., De Min, C., Re, T., Fabris, N., Faglia, G., 1991. Zinc and bromocriptine long-term administration in patients with prolactinomas: effects on prolactin and thymulin circulating levels. Int. J. Neurosci. 59, 119–125.

Tudpor, K., Charoenphandhu, N., Saengamnart, W., Krishnamra, N., 2005. Long-term prolactin exposure differentially stimulated the transcellular and solvent drag-induced calcium transport in the duodenum of ovariectomized rats. Exp. Biol. Med. (Maywood) 230, 836–844.

Turk, R., Juretić, D., Geres, D., Turk, N., Rekić, B., Simeon-Rudolf, V., Robić, M., Svetina, A., 2005. Serum paraoxonase activity in dairy cows during pregnancy. Res. Vet. Sci. 79, 15–18.

Walling, M.W., Brasitus, T.A., Kimberg, D.V., 1977. Effects of calcitonin and substance P on the transport of Ca, Na and Cl across rat ileum in vitro. Gastroenterology 73, 89–94.

Yan, J., Barnes, B.M., Kohl, F., Marr, T.G., 2008. Modulation of gene expression in hibernating arctic ground squirrels. Physiol. Genomics 32, 170–181.

Zhang, G.H., Zhu, J.X., Xue, H., Fan, J., Chen, X., Tsang, L.L., Chung, Y.W., Xing, Y., Chan, H.C., 2007. Dopamine stimulates Cl^- absorption coupled with HCO_3^- secretion in rat late distal colon. Eur. J. Pharmacol. 570, 188–195.

ELSEVIER

Cell Biology International 32 (2008) 1126–1135

Cell Biology International

www.elsevier.com/locate/cellbi

Prolactin decreases the expression ratio of receptor activator of nuclear factor κB ligand/osteoprotegerin in human fetal osteoblast cells

Dutmanee Seriwatanachai [a], Narattaphol Charoenphandhu [a,c,*], Tuangporn Suthiphongchai [b,c], Nateetip Krishnamra [a,c,*]

[a] *Department of Physiology, Faculty of Science, Mahidol University, Rama VI Road, Bangkok 10400, Thailand*
[b] *Department of Biochemistry, Faculty of Science, Mahidol University, Rama VI Road, Bangkok 10400, Thailand*
[c] *Consortium for Calcium and Bone Research, Faculty of Science, Mahidol University, Rama VI Road, Bangkok 10400, Thailand*

Received 18 December 2007; revised 28 March 2008; accepted 30 April 2008

Abstract

Prolactin (PRL) enhanced bone remodeling leading to net bone loss in adult and net bone gain in young animals. Studies in PRL-exposed osteoblasts derived from adult humans revealed an increase in the expression ratio of receptor activator of nuclear factor κB ligand (RANKL) and osteoprotegerin (OPG), thus supporting the previous finding of PRL-induced bone loss in adults. This study thus investigated the effects of PRL on the osteoblast functions and the RANKL/OPG ratio in human fetal osteoblast (hFOB) cells which strongly expressed PRL receptors. After 48 h incubation, PRL increased osteocalcin expression, but had no effect on cell proliferation. However, the alkaline phosphatase activity was decreased in a dose–response manner within 24 h. The effect of PRL on alkaline phosphatase was abolished by LY294002, a phosphoinositide 3-kinase (PI3K) inhibitor. PRL also decreased the RANKL/OPG ratio by downregulating RANKL and upregulating OPG expression, implicating a reduction in the osteoblast signal for osteoclastic bone resorption. It could be concluded that, unlike the osteoblasts derived from adult humans, PRL-exposed hFOB cells exhibited indices suggestive of bone gain, which could explain the in vivo findings in young rats. The signal transduction of PRL in osteoblasts involved the PI3K pathway.

Keywords: Alkaline phosphatase; hFOB; OPG; Osteocalcin; PI3K; Prolactin receptor; RANKL

1. Introduction

Pregnant and lactating mammals use prolactin (PRL) as a calcium-regulating hormone to stimulate intestinal calcium absorption and mobilize calcium from bone for fetal development and milk production (Charoenphandhu and Krishnamra, 2007; Lotinun et al., 1998; Thongon et al., 2008). However, PRL action on calcium metabolism was also reported in non-pregnant/lactating rats, in which PRL induced a positive calcium balance by directly stimulating the intestinal calcium absorption and renal calcium reabsorption (Jantarajit et al., 2007; Piyabhan et al., 2000). Interestingly, young rats were more responsive to PRL than adult and aging rats (Krishnamra et al., 1993; Krishnamra and Seemoung, 1996).

Studies of the in vivo effects of PRL on bone are generally complicated by chronic estrogen deficiency caused by PRL-induced hypogonadism (Wang and Chan, 1982; Wang et al., 1980). However, osteoblasts have been known to express PRL receptors (PRLR), which indicated that bone cells are direct targets of PRL (Coss et al., 2000). Our in vivo studies using bone histomorphometry in adult rats showed that PRL exerted an estrogen-independent action by enhancing bone turnover with a greater effect on bone resorption (Seriwatanachai et al., 2008). At the cellular level, PRL directly decreased osteocalcin expression and alkaline phosphatase activity in an osteoblast cell line (MG-63) derived from an adult human,

* Corresponding authors. Department of Physiology, Faculty of Science, Mahidol University, Rama VI Road, Bangkok 10400, Thailand. Tel./fax: +66 2354 7154.

E-mail addresses: naratt@narattsys.com (N. Charoenphandhu), scnks@mahidol.ac.th (N. Krishnamra).

1065-6995/$ - see front matter © 2008 International Federation for Cell Biology. Published by Elsevier Ltd. All rights reserved.
doi:10.1016/j.cellbi.2008.04.026

thus supporting the in vivo findings of PRL-induced bone loss (Seriwatanachai et al., 2008). Interestingly, the effects of PRL on bone varied with age. In contrast to adult rats (more than 8 weeks old), PRL stimulated calcium deposition and induced net bone gain in femur, tibia and sternum of 3-week-old young rats (Krishnamra and Seemoung, 1996). We therefore hypothesized that, unlike its action in MG-63 osteoblasts derived from adult humans, PRL may increase the cellular activities of osteoblasts derived from young humans leading to bone formation. Although the expression of PRLR in human fetal osteoblast (hFOB) cell lines had not been reported, we herein used differentiated hFOB cells, which had minimal chromosome aberration and exhibited the matrix-producing properties of normal differentiated osteoblasts (Harris et al., 1995; Subramaniam et al., 2002), in the investigation of PRL actions. In addition, undifferentiated hFOB cells have recently been shown to possess multilineage differentiation potential (Yen et al., 2007), suggesting that they retained the characteristics of fetal cells.

Bone turnover is a coupled process of the osteoblastic bone formation and osteoclastic bone resorption. Since osteoclasts did not express PRLR (Coss et al., 2000; Kelly et al., 2001), enhanced bone resorption in hyperprolactinemic rats could be due to changes in the osteoblast-expressed mediators, the receptor activator of nuclear factor κB ligand (RANKL) and osteoprotegerin (OPG). Binding of RANKL to its receptors on osteoclasts stimulated bone resorption, whereas binding to its decoy receptors, OPG, decreased bone resorption (Kostenuik, 2005). Thus, the RANKL/OPG ratio determined osteoclast activity, bone resorption as well as bone turnover (Abdallah et al., 2005; Grimaud et al., 2003; Kostenuik, 2005). Our recent findings of the PRL-induced increase in the RANKL/OPG ratio in MG-63 cells and decrease in the OPG expression in primary osteoblasts from adult rats supported the in vivo report of net bone loss in adult hyperprolactinemic rats (Seriwatanachai et al., 2008). Hence, it was possible that hFOB cells may respond to PRL by decreasing the RANKL/OPG expression ratio.

Nothing is known regarding PRL signaling in osteoblasts. The putative signaling pathway of PRL in mammary epithelia was the Janus kinase (JAK2) pathway (Bole-Feysot et al., 1998), whereas the phosphoinositide 3-kinase (PI3K) pathway was reported in non-mammary tissues, e.g., liver, duodenum, colon, pancreatic islets, and Nb2 lymphoma cells (Amaral et al., 2004; Bishop et al., 2006; Jantarajit et al., 2007; Puntheeranurak et al., 2007; Yamauchi et al., 1998). We recently demonstrated that the PRL-stimulated transepithelial calcium transport in the duodenum was via the PI3K, and not the JAK2 pathway (Jantarajit et al., 2007). Therefore, signal transduction of PRL in osteoblasts may also occur via the PI3K.

The objectives of the present study were (i) to demonstrate the expression of PRLR in hFOB cells; (ii) to study the effect of PRL on functions of hFOB cells, including cell proliferation, osteocalcin expression, and alkaline phosphatase activity; (iii) to show whether there was a change in the expression ratio of RANKL/OPG in PRL-exposed hFOB cells; and (iv) to investigate whether PRL signaling in hFOB cells involved the PI3K pathway.

2. Materials and methods

2.1. Cell culture

Human fetal osteoblast 1.19 (hFOB) cells (ATCC No. CRL-11372), an immortalized cell line, were propagated in DMEM/F-12 media, supplemented with 10% fetal bovine serum (FBS), 100 U/mL penicillin/streptomycin, and 0.25 μL/mL amphotericin B (Sigma, St. Louis, MO, USA). Cells were cultured in 75-cm^2 T-flasks at 37 °C in a 5% CO_2 in air humidified incubator. Culture medium was changed every 2 days, and the cultures were split 1:10 when cells had reached 80% confluence. Cells were counted using a hemocytometer and trypan blue dye exclusion.

Osteoblast-like MG-63 cells (ATCC No. CRL-1427; a kind gift from Dr Suttatip Kamolmatyakul, Prince of Songkla University, Thailand), derived from human osteosarcoma, were cultured in 75-cm^2 T-flasks with α-MEM supplemented with 10% FBS, 100 U/mL penicillin/streptomycin, and 0.25 μL/mL amphotericin B (Sigma). To induce maximal expression of PRLR, 1 μM dexamethasone and 0.1 μM 1,25-$(OH)_2D_3$ (Sigma) were also added to the medium, as previously described (Bataille-Simoneau et al., 1996). Cells were incubated at 37 °C with 5% CO_2, and subcultured according to the ATCC's protocol.

2.2. Immunofluorescent analysis

hFOB cells were cultured on a coverslip at 10^5 cells/coverslip in the presence of 0.2% FBS for 16 h. Cells were fixed for 10 min with 3% paraformaldehyde and 2% sucrose at 25 °C, washed 3 times with PBS, and permeabilized for 5 min with 0.5% Triton X-100 in PBS at 25 °C. Non-specific sites were blocked with 10% FBS for 30 min at room temperature. Samples were then incubated overnight at 4 °C with 1:300 rabbit polyclonal anti-PRLR primary antibody (Santa Cruz Biotechnology, Santa Cruz, CA, USA), and finally with 1:200 Alexa Fluor 488-conjugated goat anti-rabbit secondary antibody (Molecular Probes, Eugene, OR, USA). Images were captured with an inverted fluorescent microscope (model Eclipse TE2000-U; Nikon, Tokyo, Japan).

2.3. Cell proliferation assay

hFOB cells were inoculated in a 96-well culture plate (5000 cells/well). After 48 h incubation with 1, 10, 100, 1000 ng/mL PRL, the culture medium was replaced by a medium containing 10% 3-(4,5-dimethylthiazol-2-yl)-2,5-diphenyltetrazolium bromide (MTT) (Sigma). After 3 h incubation with MTT at 37 °C, the absorbance of each well was determined at 540 nm by a microplate reader (model Multiscan EX; Thermo Labsystems, Cergy-Pontoise, France), as described previously (Mosmann, 1983). The absorbance of control cells was considered to be 100%. The relative proliferation of PRL-exposed cells was presented as a percent of control. Each sample was an average of 6 replications, and the relative proliferation of each n was averaged from 3 independent samples (triplicate).

2.4. Alkaline phosphatase activity assay

MG-63 or hFOB cells were cultured in 6-well culture plates (10^5 cells/well). Alkaline phosphatase activity was determined by the conversion of *p*-nitrophenyl phosphate to *p*-nitrophenol, as previously described (Coss et al., 2000). In brief, cells were washed twice with PBS pH 7.4, and incubated for 1 h with 2 mL solution containing (in mM) 100 Na_2CO_3, 10 $MgCl_2$, 20 *p*-nitrophenyl phosphate (Sigma), pH 10.3. Thereafter, 1 mL of 5 M NaOH was added. Color development was quantified immediately at 410 nm.

2.5. Preparation of total RNA and RT-PCR

As previously described (Charoenphandhu et al., 2007; Seriwatanachai et al., 2008), the total RNA of hFOB cells was prepared by using the RNeasy mini kit (Qiagen, Valencia, CA, USA). Two micrograms of the total RNA were reverse-transcribed with the oligo-dT_{20} primer and SuperScript III kit (Invitrogen, Carlsbad, CA, USA) to cDNA by a thermal cycler (model Minicycler; MJ Research, Watertown, MA, USA). Sense and antisense primers for PRLR, osteocalcin, RANKL, OPG, and glyceraldehyde-3-phosphate dehydrogenase (GAPDH) are shown in Table 1. GAPDH served as a control gene to check the consistency of the reverse transcription and to normalize values between samples. After amplification with Taq polymerase (Qiagen), the PCR products were visualized on a 1% agarose gel stained with 1.0 μg/mL ethidium bromide under a trans-UV system (model Quantity One 2000; BioRad, Hercules, CA, USA). The cycle-band intensity curve was plotted for each gene to obtain an optimal PCR cycle which fell in the exponential phase. For a semi-quantitative analysis, the expression of a studied gene in the control group was considered to be 100%, while that in the experimental group was calculated as a percent change relative to the value of the control group.

2.6. Western blot analysis

hFOB cells were lysed in a lysis buffer (150 mM Tris–HCl pH 7.4, 150 mM NaCl, 0.1% SDS, 1% Triton X-100, 1% Nonidet P-40, protease inhibitor, 1 M NaF, 1 M β-glycerophosphate, 0.5 M Na_3VO_4, 1 M DTT, 1% sodium deoxycholate, and 5 mM EDTA) (Sigma). After 30 min incubation at 4 °C, lysates were sonicated and centrifuged at 12,000 × *g* for 10 min at 4 °C, and heated for 5 min at 95 °C before being loaded on a gel. Proteins (100 μg/well) were separated by sodium dodecylsulfate polyacrylamide gel electrophoresis (SDS-PAGE), and subsequently transferred to a nitrocellulose membrane (Amersham, Buckinghamshire, UK) by electroblotting. Non-specific binding sites on the membrane were blocked for 1 h at room temperature by 5% skim milk in TBS containing 0.1% Tween-20. Membranes were probed overnight at 4 °C with 1:2000 rabbit polyclonal anti-RANKL or anti-OPG primary antibodies (Santa Cruz), and re-probed with 1:5000 mouse anti-β-actin antibody (Santa Cruz). After 1 h incubation at 25 °C with 1:2000 goat anti-rabbit or anti-mouse secondary antibodies (Santa Cruz), blots were visualized using the enhanced chemiluminescence (ECL Plus) kit (Amersham). Expression of each protein in the control group was considered as 100%.

2.7. Experimental protocols

Protocol 1

The objective of this protocol was to determine the expression of PRLR in hFOB cells. Normally, osteoblasts constitutively express PRLR; however, some osteoblastic cell lines, e.g., MG-63 cells, require mediators such as vitamin D or dexamethasone for PRLR expression (Bataille-Simoneau et al., 1996). Therefore, hFOB cells were cultured in the presence of 0.2% and 10% fetal bovine serum (FBS; controls), 0.1 μM 1,25-$(OH)_2D_3$ (Vit D) (Sigma), 1 μM dexamethasone (DEX) (Sigma), or a combination of Vit D and DEX. Expression of PRLR transcripts was determined by RT-PCR, and expression of PRLR proteins was demonstrated by immunofluorescent imaging.

Protocol 2

To investigate the direct effects of PRL on osteoblast functions, hFOB cells were incubated in normal media (control) or medium containing 1, 10, 100 or 1000 ng/mL recombinant human PRL (rhPRL) (purity >97% as determined by SDS-PAGE; R&D Systems, Minneapolis, MN, USA) at 37 °C for

Table 1
Homo sapiens oligonucleotide sequences used in the PCR experiment

Gene	Reference or accession no.	Primer (forward/reverse)	Product length (bp)	Cycle
PRLR	[a]	5′-AAATGTGGCATCTGCAACCGTTTTCAC-3′ 5′-GCACTTGCTTGATGTTGCAGTGAAGTT-3′	1790	30
OC	[a]	5′-GGCCAGGCAGGTGCGAAGC-3′ 5′-GCCAGGCCAGCAGAGCGACAC-3′	271	30
RANKL	[a]	5′-GCCAGTGGGAGATGTTAG-3′ 5′-TTAGCTGCAAGTTTTCCC-3′	486	33
OPG	[a]	5′-GCTAACCTCACCTTCGAG-3′ 5′-TGATTGGACCTGGTTACC-3′	324	22
GAPDH[b]	NM_002046	5′-CACCCACTCCTCCACCTTTG-3′ 5′-CCACCACCCTGTTGCTGTAG-3′	110	20

PRLR, prolactin receptor; OC, osteocalcin; RANKL, receptor activator of nuclear factor κB ligand; OPG, osteoprotegerin; GAPDH, glyceraldehyde-3-phosphate dehydrogenase.

[a] Seriwatanachai et al., 2008.

[b] Custom-design primer.

0, 0.5, 3, 6, 12, 24 and 48 h prior to determination of alkaline phosphatase activity. The maximal suppression of alkaline phosphatase activity by PRL was seen at 48 h similar to that reported previously by Seriwatanachai et al. (2008). Therefore, the 48 h incubation period was used to demonstrate the effects of PRL on osteoblast proliferation and functions, including osteocalcin mRNA expression and RANKL/OPG mRNA and protein expression. Expression of mRNAs and proteins was determined in triplicate by RT-PCR and Western blot analysis, respectively.

Protocol 3

Since one of the signaling pathways of PRL was the PI3K pathway (Jantarajit et al., 2007; Puntheeranurak et al., 2007), this protocol aimed to demonstrate whether PRL affected osteoblast activity via this pathway. hFOB or MG-63 cells were incubated at 37 °C for 48 h with normal media (control) or media containing 0.3% dimethyl sulfoxide (DMSO; vehicle; Sigma), 100 nM LY294002 (PI3K inhibitor; Sigma), 100 ng/mL rhPRL, or 100 ng/mL rhPRL plus 100 nM LY294002. Finally, the alkaline phosphatase activity was determined.

2.8. Statistical analysis

Results are expressed as mean ± SEM. Multiple comparisons were performed by one-way analysis of variance (ANOVA) with Newman–Keuls post-test. The level of significance for all statistical tests was $P < 0.05$. Data were analyzed by GraphPad Prism 4.0 for Mac OS X (GraphPad Software, San Diego, CA, USA).

3. Results

3.1. hFOB cells expressed mRNAs and proteins of PRLR

Our RT-PCR study revealed a constitutive expression of PRLR in hFOB cells under the control condition (Fig. 1A). In contrast to the previous report on MG-63 cells (Seriwatanachai et al., 2008), the expression of PRLR in hFOB cells was not altered by 1,25-$(OH)_2D_3$, dexamethasone or the combination of both. Both agents were known to upregulate PRLR in other osteoblast cell lines, e.g., MG-63 and Saos-2 cells (Bataille-Simoneau et al., 1996). Immunofluorescent analysis confirmed that hFOB cells strongly expressed PRLR proteins (Fig. 1B). These findings indicated that this fetal osteoblast cell line served as a target of PRL.

3.2. PRL upregulated osteocalcin expression in hFOB cells

Since PRL stimulates bone growth and bone calcium deposition in young animals, we studied osteoblast functions that were associated with bone formation. We found that PRL had no effect on hFOB cell proliferation (Fig. 2A). However, 100 and 1000 ng/mL rhPRL increased the expression of osteocalcin mRNA from the control level (100.00 ± 5.74%) to 155.27 ± 13.02% ($n = 5$, $P < 0.05$) and 174.73 ± 12.08 ($n = 5$, $P < 0.01$), respectively. The results implied the stimulatory effect of PRL on osteoblastic functions in fetal osteoblasts.

3.3. PRL decreased alkaline phosphatase activity in hFOB cells

In contrast to the osteocalcin expression, the activity of alkaline phosphatase was decreased by 100 and 1000 ng/mL rhPRL to 83.31 ± 2.97% ($n = 5$, $P < 0.05$) and 77.70 ± 5.07% ($n = 5$, $P < 0.01$), respectively (Fig. 3A). A time-dependent study showed a significant decrease in alkaline phosphatase activity at 24 h after exposure to 1000 ng/mL rhPRL (Fig. 3B).

3.4. PRL decreased the expression ratio of RANKL/OPG in hFOB cells

Effects of rhPRL exposure on the markers of osteoblast-mediated activation of bone resorption are presented in Fig. 4. The expression ratio of RANKL and OPG, both of which were

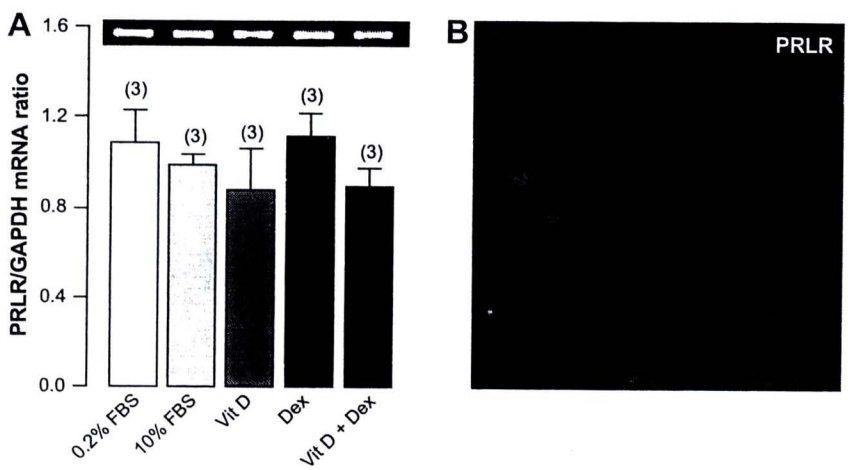

Fig. 1. (A) Expression of PRLR transcripts in hFOB cells exposed for 48 h to 0.2% and 10% fetal bovine serum (FBS, control), 0.1 μM 1,25-$(OH)_2D_3$ (Vit D), 1 μM dexamethasone (DEX), or a combination of Vit D and DEX (Vit D + DEX). A representative electrophoretic image of PRLR is also demonstrated. Numbers in parentheses are numbers of independent flasks. (B) A representative immunofluorescent image showing PRLR protein expression in hFOB cells ($n = 5$), magnification ×400.

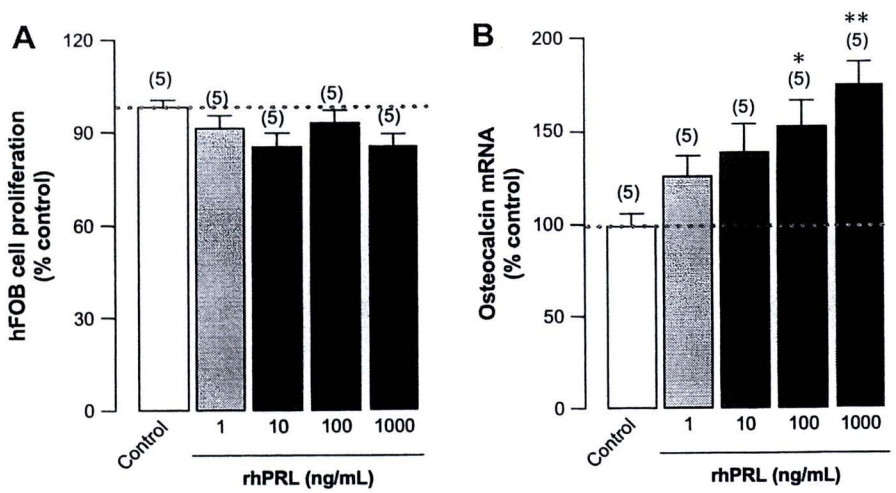

Fig. 2. Dose-dependent changes in (A) cell proliferation and (B) osteocalcin mRNA expression in hFOB cells incubated for 48 h with 1, 10, 100 or 1000 ng/mL rhPRL. Values of the control groups were normalized to 100%. $^{*}P < 0.05$, $^{**}P < 0.01$ compared with the control group. Numbers in parentheses are numbers of independent flasks. Experiments were performed in triplicate.

synthesized by osteoblasts, represented bone resorption (Kostenuik, 2005). Expression of RANKL transcripts were decreased by 10, 100 and 1000 ng/mL rhPRL to 76.56 ± 4.97% ($n = 3, P < 0.05$), 76.81 ± 3.96% ($n = 3, P < 0.05$) and 57.58 ± 7.73% ($n = 3, P < 0.01$) of the control level, respectively, while RANKL protein was decreased by 100 and 1000 ng/mL rhPRL to 71.53 ± 2.79% ($n = 7, P < 0.01$) and 64.78 ± 6.46% ($n = 7, P < 0.01$). Although PRL did not change the expression of OPG transcripts, 100 and 1000 ng/mL rhPRL upregulated expression of OPG protein to 122.96 ± 5.42% ($n = 5, P < 0.05$) and 140.12 ± 7.53% ($n = 5, P < 0.001$), respectively. Therefore, the ratios of RANKL/OPG mRNAs in hFOB cells were significantly decreased by 24, 21 and 43% after 48 h exposure to 10, 100 and 1000 ng/mL rhPRL, respectively, while the ratios of RANKL/OPG proteins were decreased by 41% and 56% after 100 and 1000 ng/mL rhPRL exposure. The decreased RANKL/OPG ratio implicated a suppression of the osteoclast-mediated bone resorption by PRL.

3.5. PRL-mediated decreases in alkaline phosphatase activity in hFOB and MG-63 cells were completely blocked by a PI3K inhibitor

Because the PI3K pathway was one of the signaling pathways of PRL, we investigated whether PRL used this pathway in osteoblasts (i.e., hFOB and MG-63 cells). We found that LY294002, a specific PI3K inhibitor, at concentrations ranging from 10 nM to 1 μM did not affect the viability or the proliferation rate of hFOB and MG-63 cells (Fig. 5A,B). Exposure to 100 ng/mL rhPRL decreased alkaline phosphatase activity in both hFOB and MG-63 cells; however, this PRL action was completely abolished by 100 nM LY294002 (Fig. 5C,D). DMSO, a vehicle for LY294002 preparation, and 100 nM LY294002 alone had no effect on the alkaline phosphatase activity in both cell lines. The results suggested that PRL decreased the osteoblastic alkaline phosphatase activity via the PI3K pathway.

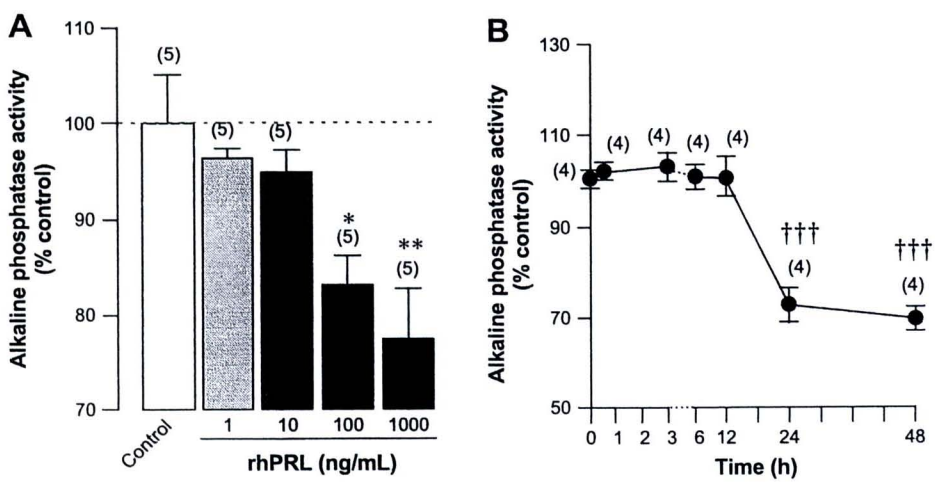

Fig. 3. Dose-dependent changes in alkaline phosphatase activity (A) in hFOB cells incubated for 48 h with 1, 10, 100 or 1000 ng/mL rhPRL. Values of the control groups were normalized to 100%. $^{*}P < 0.05$, $^{**}P < 0.01$ compared with the control group. (B) Time-dependent changes in alkaline phosphatase activity in hFOB cells exposed to 1000 ng/mL rhPRL. The value at 0 h was normalized to 100%. $^{\dagger\dagger\dagger}P < 0.001$ compared with the values at 0 h. Numbers in parentheses are numbers of independent flasks. Experiments were performed in triplicate.

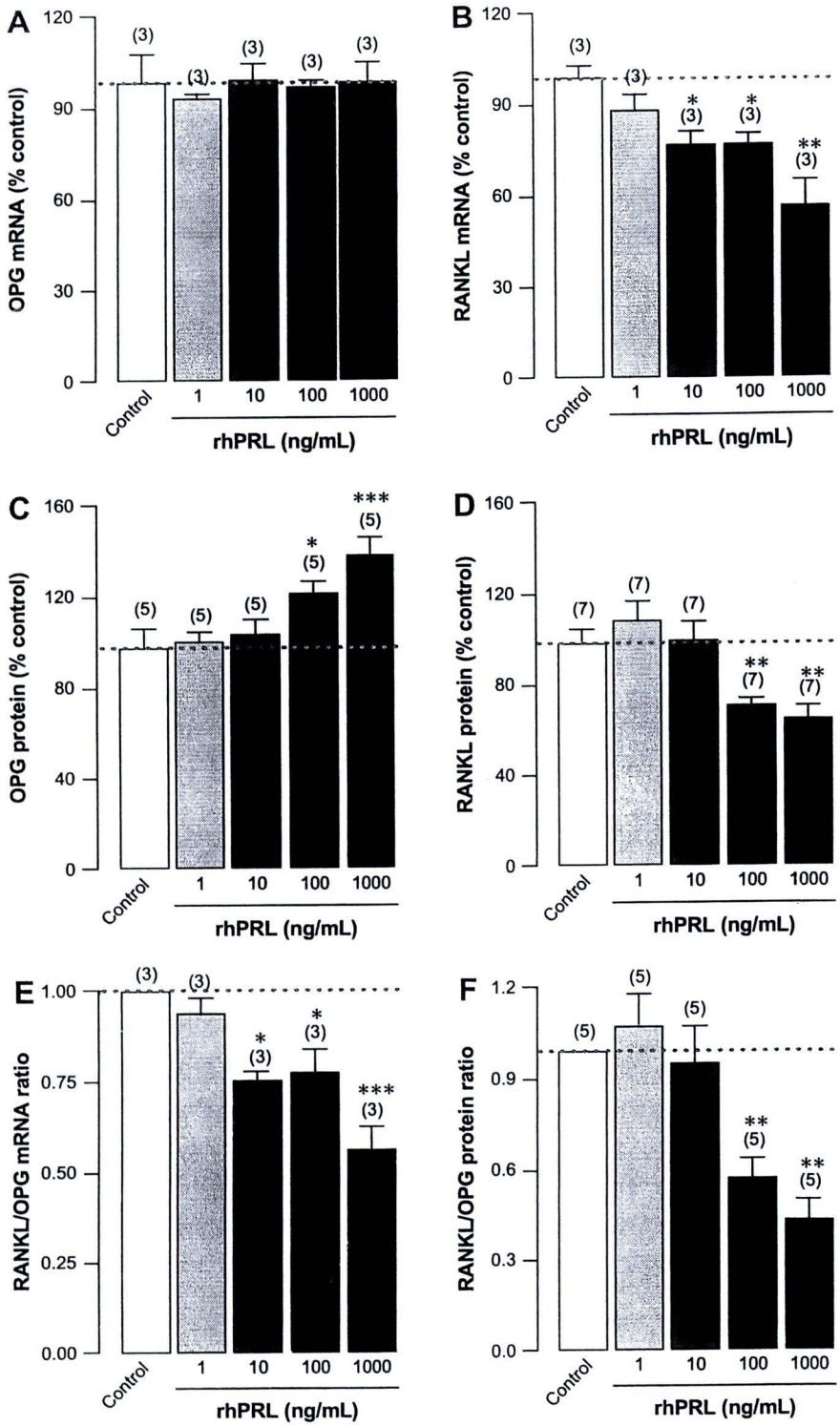

Fig. 4. Dose-dependent changes in the mRNA expressions of OPG (A) and RANKL (B), protein expressions of OPG (C) and RANKL (D), and the ratios of RANKL/OPG mRNA (E) and protein (F) expressions in hFOB cells incubated for 48 h with 1, 10, 100 or 1000 ng/mL rhPRL. Values of the control groups were normalized to 100%. $*P < 0.05$, $**P < 0.01$, $***P < 0.001$ compared with the control group. Numbers in parentheses are numbers of independent flasks. Experiments were performed in triplicate.

4. Discussion

In adult animals, high bone turnover is a characteristic of both physiological and pathological hyperprolactinemia (Krishnamra et al., 1997; Lotinun et al., 2003; Meaney et al., 2004). Generally, high bone turnover accelerates bone loss, especially when the resorption cavities are incompletely replaced. However, under certain conditions, such as during growth hormone administration, the increased bone turnover shifts the balance between bone formation and resorption

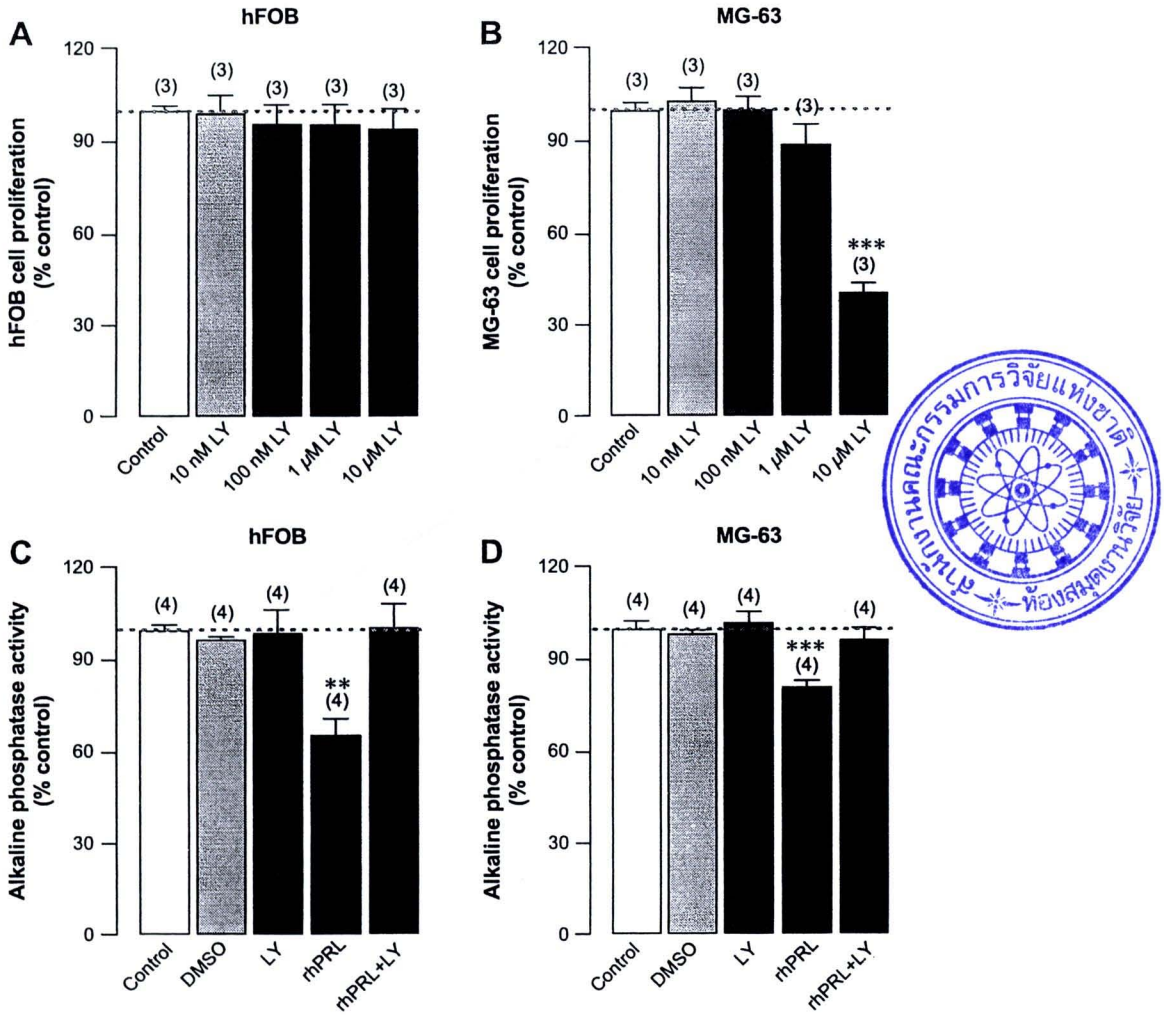

Fig. 5. (A,B) Proliferation of hFOB and MG-63 cells after incubation for 48 h with 10 nM, 100 nM, 1 μM or 10 μM LY294002 (LY, PI3K inhibitor). (C,D) Alkaline phosphatase activity in hFOB and MG-63 cells incubated for 48 h in normal culture media (control) or media containing 0.3% DMSO (vehicle), 100 nM LY294002, 100 ng/mL rhPRL, or 100 ng/mL rhPRL plus 100 nM LY294002. Values of the control groups were normalized to 100%. $^{**}P < 0.01$, $^{***}P < 0.001$ compared with the control group. Numbers in parentheses are numbers of independent flasks. Experiments were performed in triplicate.

toward net bone calcium deposition (Parfitt, 1991). Although high physiological PRL of ~75–100 ng/mL during pregnancy did not produce a significant bone loss, transient osteopenia was reported after 3 months of lactation when plasma PRL ranged between 200 and 350 ng/mL (Prentice, 2000; Ritchie et al., 1998). Furthermore, high PRL levels (up to ~1000 ng/mL) found in several pathological conditions, e.g., prolactinomas or prolonged antipsychotic drug use, induced massive bone loss and overt osteopenia (Biller et al., 1992; Crosignani, 2006; Meaney et al., 2004). Thus, PRL exposure in adult animals and humans, depending on the PRL concentrations, could lead to bone loss. On the other hand, by using the in vivo ^{45}Ca kinetic study, Krishnamra and Seemoung (1996) reported that young rats responded differently to PRL, i.e., by enhancing bone gain instead of bone loss despite the presence of high bone turnover. Moreover, PRL administration in 3-week-old weaned rats resulted in a dose-dependent increase in the calcium content of femur, tibia and vertebrae (Krishnamra and Seemoung, 1996). The present investigation showed an increase in osteocalcin expression and a decrease in the RANKL/OPG ratio in hFOB cells which indicated that PRL-exposed osteoblasts derived from immature animals could potentially induce bone gain.

Indeed, the in vivo osteopenic action of PRL had long been explained by estrogen deficiency due to PRL-induced hypogonadism (Meaney et al., 2004; Wang et al., 1980). However, the PRLR knockout mice manifested a 60% decrease in the rate of bone formation (Clément-Lacroix et al., 1999), and PRL-exposed rats exhibited high bone turnover with different histomorphometric patterns from those seen in ovariectomized (Ovx) rats, i.e., higher mineral apposition rate and bone formation rate (Seriwatanachai et al., 2008). It is possible that PRL could also exert a direct estrogen-independent action on bone cells. The finding of PRLR in osteoblasts also supported this hypothesis. Although the levels of PRLR transcript in MG-63 cells were significantly elevated in the presence of 1,25-$(OH)_2D_3$ and dexamethasone (Bataille-Simoneau et al., 1996), the expression of PRLR mRNAs and proteins in hFOB cells similar to that in the primary rat osteoblasts (Seriwatanachai et al., 2008) was constitutive and independent of both hormones.

We further investigated the effect of PRL on hFOB cell functions and found that PRL stimulated osteocalcin expression in hFOB cells without affecting cell proliferation. This effect of PRL agreed with the recent report on neonatal osteoblasts (Seriwatanachai et al., 2008), and was also consistent with the action of other hormones, such as leptin which enhanced osteoblast differentiation but not proliferation (Thomas et al., 1999). On the other hand, MG-63 cells derived from adult humans showed a decrease in osteocalcin expression after a 48-h PRL exposure (Seriwatanachai et al., 2008). The PRL-induced increase in the activity of hFOB cells supported our hypothesis that PRL could increase bone formation in osteoblasts derived from young animals.

Similar to the primary neonatal rat osteoblasts (Coss et al., 2000) and MG-63 cells (Seriwatanachai et al., 2008), PRL-exposed hFOB cells manifested a decrease in alkaline phosphatase activity. Although alkaline phosphatase is a classical marker of bone formation (Stein et al., 1996), its expression depends on the developmental stage of osteoblasts (Owen et al., 1990). Normally, osteoblasts have roles in all 3 steps of bone formation, i.e., cell proliferation, extracellular matrix maturation, and mineralization (Owen et al., 1990). Responses of osteoblast proliferation, gene expression and enzyme activities to various humoral factors depend on the stage of development of the cells. For example, transforming growth factor β and its downstream protein Smad3 inhibited osteoblast proliferation, but enhanced alkaline phosphatase activity, mineralization, and expression of bone matrix proteins (Sowa et al., 2002). Generally, alkaline phosphatase expression is increased immediately after cessation of cell proliferation, while the expression of osteocalcin, which is important for the formation of hydroxyapatite crystal lattices (Hoang et al., 2003), is increased later during matrix maturation near the onset of mineralization (Owen et al., 1990). Therefore, a disparate relationship between osteocalcin expression and alkaline phosphatase activity could be observed during the development of osteoblasts.

Since PRL enhanced osteocalcin expression in the matrix maturation step (Fig. 2B) without affecting the in vitro mineralization of primary rat osteoblasts (Charoenphandhu et al., 2008), it appeared that PRL increased bone calcium deposition in young rats by downregulating RANKL and upregulating OPG, thereby decreasing the RANKL/OPG ratio. Similar to PRL, growth hormone which increases bone turnover and bone gain (Brixen et al., 2000; Landin-Wilhelmsen et al., 2003; Schlemmer et al., 1991) also stimulates OPG synthesis in hFOB cells (Mrak et al., 2007). In contrast, MG-63 cells responded to 48-h PRL exposure by increasing the RANKL/OPG ratio (Seriwatanachai et al., 2008). An increase in this ratio has been associated with osteopenic conditions, such as hyperparathyroidism and aging (Cao et al., 2003; Stilgren et al., 2004). In the transgenic mice, overexpression of RANKL increased the cortical porosity, whereas overexpression of OPG prevented bone loss and improved cortical bone strength (Kostenuik, 2005; Mizuno et al., 2002). The ~50% decrease in RANKL/OPG ratio in the present study implied that PRL could potentially suppress bone resorption, thus supporting the earlier report of greater calcium deposition in bones of PRL-treated young rats (Krishnamra and Seemoung, 1996).

Although the direct actions of PRL in osteoblasts have been demonstrated, nothing was known regarding its signaling pathway. PRL binding to PRLRs triggers dimerization of PRLRs and activation of the downstream signals (Bole-Feysot et al., 1998). In the mammary epithelia, PRL-PRLR complex used the JAK2 signaling pathway in the stimulation of milk production (Bole-Feysot et al., 1998). However, in other tissues, such as liver and calcium-transporting epithelia, e.g., duodenum and colon, mitogen-activated protein kinase (MAPK) and PI3K pathways have been reported (Amaral et al., 2004; Yamauchi et al., 1998). We recently showed that PRL directly stimulated duodenal calcium absorption (Jantarajit et al., 2007), and inhibited colonic Ca^{2+}-dependent Cl^- and K^+ secretion via the PI3K pathway (Puntheeranurak et al., 2007). By using a potent inhibitor of PI3K (LY294002), the present study showed that the suppressive effect of PRL on alkaline phosphatase activity in hFOB cells was completely abolished. Therefore, the PI3K pathway could be one of the signaling pathways of PRL in osteoblasts. The detailed signaling cascade, however, remains to be investigated.

It can be concluded that hFOB cells strongly and constitutively express PRLR. PRL directly increases osteocalcin mRNA expression, and decreases the RANKL/OPG ratio in these cells, indicating the stimulation of bone formation and suppression of bone resorption, respectively. PRL also decreases alkaline phosphatase activity, in part, via the PI3K signaling pathway. Our in vitro study supported the previous in vivo findings that, unlike mature rats, PRL enhances bone calcium deposition and bone gain in young rats.

Acknowledgements

We thank Dr Sinee Disthabanchong from the Faculty of Medicine, Ramathibodi Hospital, Mahidol University, for her technical guidance and helpful comments. We thank Dr Suttatip Kamolmatyakul from the Prince of Songkla University, Thailand, for a kind gift of MG-63 cells. This research was supported by grants from the Royal Golden Jubilee Program (to DS), the Thailand Research Fund (TRF) and the National Center for Genetic Engineering and Biotechnology (BIOTEC).

References

Abdallah BM, Stilgren LS, Nissen N, Kassem M, Jorgensen HR, Abrahamsen B. Increased RANKL/OPG mRNA ratio in iliac bone biopsies from women with hip fractures. Calcif Tissue Int 2005;76:90–7.

Amaral ME, Cunha DA, Anhê GF, Ueno M, Carneiro EM, Velloso LA, et al. Participation of prolactin receptors and phosphatidylinositol 3-kinase and MAP kinase pathways in the increase in pancreatic islet mass and sensitivity to glucose during pregnancy. J Endocrinol 2004;183:469–76.

Bataille-Simoneau N, Gerland K, Chappard D, Basle MF, Mercier L. Expression of prolactin receptors in human osteosarcoma cells. Biochem Biophys Res Commun 1996;229:323–8.

Biller BM, Baum HB, Rosenthal DI, Saxe VC, Charpie PM, Klibanski A. Progressive trabecular osteopenia in women with hyperprolactinemic amenorrhea. J Clin Endocrinol Metab 1992;75:692–7.

Bishop JD, Nien WL, Dauphinee SM, Too CK. Prolactin activates mammalian target-of-rapamycin through phosphatidylinositol 3-kinase and stimulates phosphorylation of p70S6K and 4E-binding protein-1 in lymphoma cells. J Endocrinol 2006;190:307–12.

Bole-Feysot C, Goffin V, Edery M, Binart N, Kelly PA. Prolactin (PRL) and its receptor: actions, signal transduction pathways and phenotypes observed in PRL receptor knockout mice. Endocr Rev 1998;19:225–68.

Brixen K, Hansen TB, Hauge E, Vahl N, Jorgensen JO, Christiansen JS, et al. Growth hormone treatment in adults with adult-onset growth hormone deficiency increases iliac crest trabecular bone turnover: a 1-year, double-blind, randomized, placebo-controlled study. J Bone Miner Res 2000;15:293–300.

Cao J, Venton L, Sakata T, Halloran BP. Expression of RANKL and OPG correlates with age-related bone loss in male C57BL/6 mice. J Bone Miner Res 2003;18:270–7.

Charoenphandhu N, Krishnamra N. Prolactin is an important regulator of intestinal calcium transport. Can J Physiol Pharmacol 2007;85: 569–81.

Charoenphandhu N, Teerapornpuntakit J, Methawasin M, Wongdee K, Thongchote K, Krishnamra N. Prolactin decreases expression of Runx2, osteoprotegerin and RANKL in primary osteoblasts derived from tibiae of adult female rats. Can J Physiol Pharmacol 2008;86:240–8.

Charoenphandhu N, Wongdee K, Tudpor K, Pandaranandaka J, Krishnamra N. Chronic metabolic acidosis upregulated claudin mRNA expression in the duodenal enterocytes of female rats. Life Sci 2007;80:1729–37.

Clément-Lacroix P, Ormandy C, Lepescheux L, Ammann P, Damotte D, Goffin V, et al. Osteoblasts are a new target for prolactin: analysis of bone formation in prolactin receptor knockout mice. Endocrinology 1999;140: 96–105.

Coss D, Yang L, Kuo CB, Xu X, Luben RA, Walker AM. Effects of prolactin on osteoblast alkaline phosphatase and bone formation in the developing rat. Am J Physiol Endocrinol Metab 2000;279:E1216–25.

Crosignani PG. Current treatment issues in female hyperprolactinaemia. Eur J Obstet Gynecol Reprod Biol 2006;125:152–64.

Grimaud E, Soubigou L, Couillaud S, Coipeau P, Moreau A, Passuti N, et al. Receptor activator of nuclear factor κB ligand (RANKL)/osteoprotegerin (OPG) ratio is increased in severe osteolysis. Am J Pathol 2003;163: 2021–31.

Harris SA, Enger RJ, Riggs BL, Spelsberg TC. Development and characterization of a conditionally immortalized human fetal osteoblastic cell line. J Bone Miner Res 1995;10:178–86.

Hoang QQ, Sicheri F, Howard AJ, Yang DS. Bone recognition mechanism of porcine osteocalcin from crystal structure. Nature 2003;425:977–80.

Jantarajit W, Thongon N, Pandaranandaka J, Teerapornpuntakit J, Krishnamra N, Charoenphandhu N. Prolactin-stimulated transepithelial calcium transport in duodenum and Caco-2 monolayer are mediated by the phosphoinositide 3-kinase pathway. Am J Physiol Endocrinol Metab 2007;293:E372–84.

Kelly PA, Binart N, Freemark M, Lucas B, Goffin V, Bouchard B. Prolactin receptor signal transduction pathways and actions determined in prolactin receptor knockout mice. Biochem Soc Trans 2001;29:48–52.

Kostenuik PJ. Osteoprotegerin and RANKL regulate bone resorption, density, geometry and strength. Curr Opin Pharmacol 2005;5:618–25.

Krishnamra N, Lotinun S, Limlomwongse L. Acute effect and mechanism of action of prolactin on the in situ passive calcium absorption in rat. Bone Miner 1993;23:253–66.

Krishnamra N, Seemoung J. Effects of acute and long-term administration of prolactin on bone ^{45}Ca uptake, calcium deposit, and calcium resorption in weaned, young, and mature rats. Can J Physiol Pharmacol 1996;74: 1157–65.

Krishnamra N, Seemoung J, Limlomwongse L. Acute effect of prolactin on bone ^{45}Ca accumulation in rats. Endocr J 1997;44:257–64.

Landin-Wilhelmsen K, Nilsson A, Bosaeus I, Bengtsson BA. Growth hormone increases bone mineral content in postmenopausal osteoporosis: a randomized placebo-controlled trial. J Bone Miner Res 2003;18:393–405.

Lotinun S, Limlomwongse L, Krishnamra N. The study of a physiological significance of prolactin in the regulation of calcium metabolism during pregnancy and lactation in rats. Can J Physiol Pharmacol 1998;76:218–28.

Lotinun S, Limlomwongse L, Sirikulchayanonta V, Krishnamra N. Bone calcium turnover, formation, and resorption in bromocriptine- and prolactin-treated lactating rats. Endocrine 2003;20:163–70.

Meaney AM, Smith S, Howes OD, O'Brien M, Murray RM, O'Keane V. Effects of long-term prolactin-raising antipsychotic medication on bone mineral density in patients with schizophrenia. Br J Psychiatry 2004; 184:503–8.

Mizuno A, Kanno T, Hoshi M, Shibata O, Yano K, Fujise N, et al. Transgenic mice overexpressing soluble osteoclast differentiation factor (sODF) exhibit severe osteoporosis. J Bone Miner Metab 2002;20:337–44.

Mosmann T. Rapid colorimetric assay for cellular growth and survival: application to proliferation and cytotoxicity assays. J Immunol Methods 1983;65:55–63.

Mrak E, Villa I, Lanzi R, Losa M, Guidobono F, Rubinacci A. Growth hormone stimulates osteoprotegerin expression and secretion in human osteoblast-like cells. J Endocrinol 2007;192:639–45.

Owen TA, Aronow M, Shalhoub V, Barone LM, Wilming L, Tassinari MS, et al. Progressive development of the rat osteoblast phenotype in vitro: reciprocal relationships in expression of genes associated with osteoblast proliferation and differentiation during formation of the bone extracellular matrix. J Cell Physiol 1990;143:420–30.

Parfitt AM. Growth hormone and adult bone remodelling. Clin Endocrinol (Oxf) 1991;35:467–70.

Piyabhan P, Krishnamra N, Limlomwongse L. Changes in the regulation of calcium metabolism and bone calcium content during growth in the absence of endogenous prolactin and during hyperprolactinemia: a longitudinal study in male and female Wistar rats. Can J Physiol Pharmacol 2000; 78:757–65.

Prentice A. Calcium in pregnancy and lactation. Annu Rev Nutr 2000;20: 249–72.

Puntheeranurak S, Schreiber R, Spitzner M, Ousingsawat J, Krishnamra N, Kunzelmann K. Control of ion transport in mouse proximal and distal colon by prolactin. Cell Physiol Biochem 2007;19:77–88.

Ritchie LD, Fung EB, Halloran BP, Turnlund JR, Van Loan MD, Cann CE, et al. A longitudinal study of calcium homeostasis during human pregnancy and lactation and after resumption of menses. Am J Clin Nutr 1998;67:693–701.

Schlemmer A, Johansen JS, Pedersen SA, Jorgensen JO, Hassager C, Christiansen C. The effect of growth hormone (GH) therapy on urinary pyridinoline cross-links in GH-deficient adults. Clin Endocrinol (Oxf) 1991;35:471–6.

Seriwatanachai D, Thongchote K, Charoenphandhu N, Pandaranandaka J, Tudpor K, Teerapornpuntakit J, et al. Prolactin directly enhances bone turnover by raising osteoblast-expressed receptor activator of nuclear factor κB ligand/osteoprotegerin ratio. Bone 2008;42:535–46.

Sowa H, Kaji H, Yamaguchi T, Sugimoto T, Chihara K. Smad3 promotes alkaline phosphatase activity and mineralization of osteoblastic MC3T3-E1 cells. J Bone Miner Res 2002;17:1190–9.

Stein GS, Lian JB, Stein JL, Van Wijnen AJ, Montecino M. Transcriptional control of osteoblast growth and differentiation. Physiol Rev 1996;76: 593–629.

Stilgren LS, Rettmer E, Eriksen EF, Hegedus L, Beck-Nielsen H, Abrahamsen B. Skeletal changes in osteoprotegerin and receptor activator of nuclear factor-κB ligand mRNA levels in primary hyperparathyroidism: effect of parathyroidectomy and association with bone metabolism. Bone 2004;35:256–65.

Subramaniam M, Jalal SM, Rickard DJ, Harris SA, Bolander ME, Spelsberg TC. Further characterization of human fetal osteoblastic hFOB 1.19 and hFOB/ERα cells: bone formation in vivo and karyotype analysis using multicolor fluorescent in situ hybridization. J Cell Biochem 2002;87: 9–15.

Thomas T, Gori F, Khosla S, Jensen MD, Burguera B, Riggs BL. Leptin acts on human marrow stromal cells to enhance differentiation to osteoblasts and to inhibit differentiation to adipocytes. Endocrinology 1999;140: 1630–8.

Thongon N, Nakkrasae LI, Thongbunchoo J, Krishnamra N, Charoenphandhu N. Prolactin stimulates transepithelial calcium transport and modulates paracellular permselectivity in Caco-2 monolayer: Mediation by PKC and ROCK pathways. Am J Physiol Cell Physiol 2008;294:C1158–68.

Wang C, Chan V. Divergent effects of prolactin on estrogen and progesterone production by granulosa cells of rat Graafian follicles. Endocrinology 1982;110:1085–93.

Wang C, Hsueh AJ, Erickson GF. Prolactin inhibition of estrogen production by cultured rat granulosa cells. Mol Cell Endocrinol 1980;20:135–44.

Yamauchi T, Kaburagi Y, Ueki K, Tsuji Y, Stark GR, Kerr IM, et al. Growth hormone and prolactin stimulate tyrosine phosphorylation of insulin receptor substrate-1, -2, and -3, their association with p85 phosphatidylinositol 3-kinase (PI3-kinase), and concomitantly PI3-kinase activation via JAK2 kinase. J Biol Chem 1998;273:15719–26.

Yen ML, Chien CC, Chiu IM, Huang HI, Chen YC, Hu HI, et al. Multilineage differentiation and characterization of the human fetal osteoblastic 1.19 cell line: a possible in vitro model of human mesenchymal progenitors. Stem Cells 2007;25:125–31.

Histochem Cell Biol (2008) 130:79–90
DOI 10.1007/s00418-008-0419-6

ORIGINAL PAPER

Osteoblasts express claudins and tight junction-associated proteins

Kannikar Wongdee · Jantarima Pandaranandaka · Jarinthorn Teerapornpuntakit · Kukiat Tudpor · Jirawan Thongbunchoo · Narongrit Thongon · Walailak Jantarajit · Nateetip Krishnamra · Narattaphol Charoenphandhu

Accepted: 12 March 2008 / Published online: 26 March 2008

Abstract Osteoblasts were previously reported to form tight junctions, which may play an important role in the regulation of ion transport across the epithelial-like bone membrane. However, the evidence for the presence of tight junction-associated proteins in osteoblasts is lacking. We therefore studied the expression of tight junction-associated genes in primary rat osteoblasts and bone tissues. Quantitative real-time PCR showed that osteoblasts expressed ZO-1, -2, -3, cingulin, occludin, claudin-1 to -12, -14 to -20, -22 and -23. By using western blot analyses of selected claudins, expression of claudin-5, -11, -14 and -15, but not claudin-3, were identified in osteoblasts. A confocal immunofluorescent study in undecalcified tibial sections confirmed that claudin-16 was localized on the trabecular surface, normally covered by osteoblasts and bone-lining cells. In addition, immunohistochemical studies in decalcified tibial sections demonstrated the expression of claudin-5, -11, -14, -15 and -16 in bone-lining cells (inactive osteoblasts). Primary osteoblasts cultured in the Snapwell for 19–26 days were found to form a monolayer with measurable transepithelial resistance of ~110–180 Ωcm^2, confirming the presence of barrier functions of the tight junction. It was concluded that osteoblasts expressed several tight junction-associated proteins, which possibly regulated ion transport across the bone membrane.

Keywords Bone membrane · Claudin · Confocal microscope · Occludin · Real-time PCR

K. Wongdee · J. Pandaranandaka · K. Tudpor · J. Thongbunchoo · N. Krishnamra · N. Charoenphandhu
Consortium for Calcium and Bone Research (COCAB),
Faculty of Science, Mahidol University,
Rama VI Road, Bangkok 10400, Thailand

K. Wongdee
Department of Pathobiology, Faculty of Science,
Mahidol University, Rama VI Road, Bangkok 10400, Thailand

J. Teerapornpuntakit · N. Thongon · W. Jantarajit · N. Krishnamra · N. Charoenphandhu (✉)
Department of Physiology, Faculty of Science,
Mahidol University, Rama VI Road, Bangkok 10400, Thailand
e-mail: naratt@narattsys.com

J. Pandaranandaka
Faculty of Medicine, Thammasat University,
Pathumthani 12120, Thailand

Introduction

Besides the skeletal function, bone acts as an ion exchange system which maintains differential ion compositions, such as Ca^{2+} and K^+, between the two fluid compartments, i.e., plasma and bone extracellular fluid (BECF) (Armstrong and Singer 1965; Marenzana et al. 2005; Rubinacci et al. 2000). The Ca^{2+} efflux from BECF was important for a rapid or short-term correction of the plasma Ca^{2+} without the activation of bone remodeling, while high K^+ concentration in BECF may control bone mineralization (Bushinsky et al. 1997; Marenzana et al. 2005; Rubinacci et al. 2000). It was evident that, to maintain an ionic gradient, osteoblasts and bone-lining cells (inactive osteoblasts) formed a bone membrane to actively control the paracellular exchange of specific ions between the two fluid compartments in an epithelial-like manner (Bushinsky et al. 1989; Rubinacci et al. 2000; Trumbore et al. 1980). In typical epithelia, such processes require the presence of tight junctions which help restrict the paracellular ion movement and maintain membrane integrity, as indicated by the presence of transepithelial resistance (TER) (Furuse and Tsukita

2006; Greger 1996; Shu et al. 2006). Interestingly, several investigators reported that osteoblasts and osteocytes could form tight junctions both in vivo and in vitro (Weinger and Holtrop 1974; Prêle et al. 2003), suggesting a presence of bone membrane with its possible role in the regulation of ion compositions of the BECF.

The expression profiles of tight junction proteins in osteoblasts have never been studied. In simple epithelia lining the cavities and surfaces of structures such as intestinal epithelium and renal tubular epithelium, the tight junction consists of cytoplasmic proteins, e.g., zonula occludens (ZO)-1, -2, -3 and cingulin, and transmembrane proteins, e.g., occludin and claudin-1 to -24 (Furuse and Tsukita 2006). The cytoplasmic proteins are involved in the signaling pathways that alter the tight junction permeability and expression of tight junction-related genes (Guillemot and Citi 2006; Ikari et al. 2004). On the other hand, the transmembrane proteins, especially claudins, form a continuous network of cell–cell contacts that maintain cell adhesion and regulate paracellular transport of ions. Since claudins possess several charged amino acids on their extracellular loops, claudin-expressing epithelial cells manifest charge-, size- and/or ion-selective properties, and permit ion movement in a channel-like fashion (Furuse and Tsukita 2006; Van Itallie and Anderson 2006). Among the 24 claudins, claudin-16 is of particular interest because its functions are specifically related to the transepithelial Ca^{2+} and Mg^{2+} transport. Thus, we hypothesize that osteoblasts, which can form tight junctions and exhibit ion-selective paracellular transport, also express claudins and other tight junction-related genes.

The objectives of this study were (1) to demonstrate the expression patterns of tight junction-related genes in primary rat osteoblasts and bone tissues, and (2) to show that osteoblasts could form a monolayer that generated TER which was indicative of the barrier property of the tight junction. The epithelial-like monolayer of osteoblasts was obtained by seeding osteoblasts on a Snapwell, which is a compartmentalized permeable support. A standard method, namely Ussing chamber technique, allowed us to determine the TER (Greger 1996), which represents the ability of cells to restrict the paracellular ion movement across the monolayer, and is measurable only when tight junctions are formed.

Materials and methods

Animals

Female 8-week-old Sprague–Dawley rats weighing 180–200 g were obtained from the Animal Centre of Thailand. They were placed in hanging stainless steel cages, fed standard pellets (Perfect Companion, Bangkok, Thailand) and distilled water ad libitum under 12/12 h light/dark cycle. Room temperature was controlled at 23–25°C, and relative humidity was about 50–60%. This study has been approved by the Institutional Animal Care and Use Committee of the Faculty of Science, Mahidol University, Bangkok, Thailand.

Primary osteoblast culture

The culture technique was modified from the method of Bakker and Klein-Nulend (2003). Tibiae and femora were removed from a rat by sterile surgical technique. After removing the connective tissues and marrow cells, bones were cut into small dice, and cultured in a 25-cm^2 T flask (Corning, NY, USA) with DMEM supplemented with 15% FBS, 100 U/mL penicillin/streptomycin and 100 μg/mL ascorbate-2-phosphate (all purchased from Sigma, St Louis, MO, USA). Cells were incubated at 37°C with 5% CO_2, and subcultured every 3 days until day 9. The medium was changed daily. Confluent cells from the same rat in six flasks were pooled together for the total RNA preparation. Morphology and nine markers of osteoblast differentiation, i.e., expression of osteocalcin, osteopontin, *runt*-related transcription factor (Runx) 2, osterix, distal-less homeobox 5 (Dlx5), *msh* homeobox homolog 2 (Msx2), AJ18, osteoprotegerin (OPG), and receptor activator of nuclear factor κB ligand (RANKL), were carefully checked. Since morphology and viability of primary osteoblasts became altered after the fourth passage, we used only confluent cells from the first and second passages in this study.

As for the electrical measurements, a confluent osteoblast monolayer was prepared by seeding cells (2×10^5 cells/cm^2) on a polyester Snapwell (compartmentalized permeable support) with 12-mm diameter and 0.4-μm pore size (Corning). The medium was changed daily after 48 h of seeding. Monolayers were incubated at 37°C for 19, 21, 23 or 26 days in a humidified atmosphere containing 5% CO_2. Morphology of the monolayer was visualized by scanning electron microscopy.

Total RNA and cDNA preparation

By using TRIzol reagent (Invitrogen, Carlsbad, CA, USA), total RNA was prepared from calvarial homogenate, primary osteoblasts, kidney, duodenum and distal colon of rats, as previously described (Charoenphandhu et al. 2007). The total RNA was treated with RQ1 DNase (Promega, Madison, WI, USA), and later purified with RNeasy Mini kit (Qiagen, Valencia, CA, USA). Purity of the total RNA was determined by the ratio of absorbance readings at 260 and 280 nm, the ratio of which fell in the range of 1.8–2.0. Integrity of RNA was analyzed by denaturing agarose gel

electrophoresis with the 28S rRNA band appearing approximately twice as intense as the 18S rRNA band. A total of 1 μg of the total RNA was reverse-transcribed with the oligo-dT_{15} primer and the iScript kit (Bio-Rad, Hercules, CA, USA) to cDNA by a thermal cycler (model MyCycler; Bio-Rad). Glyceraldehyde-3-phosphate dehydrogenase (GAPDH), a housekeeping gene, served as a control gene to check the consistency of the reverse transcription (percent coefficient of variation <1%, $n = 30$).

Quantitative real-time PCR (qRT-PCR) and sequencing

Primers used in the present study were designed by OLIGO 6 (Molecular Biology Insights, Cascade, CO, USA) and Primer Validator 1.4 (Naratt Software, Bangkok, Thailand), as shown in Table 1. qRT-PCR was performed by Bio-rad MiniOpticon with the iQ SYBR Green SuperMix (Bio-rad). As for the absolute qRT-PCR of claudin-16, the LightCycler 480 System (Roche, Mannheim, Germany) with high-resolution melting curve analysis was used. The PCR products were also visualized on a 2% agarose gel stained with 1.0 μg/mL ethidium bromide under a UV transilluminator (Alpha Innotech, San Leandro, CA, USA). After electrophoresis, all PCR products were extracted by the HiYield Gel/PCR DNA Extraction kit (Real Biotech Corporation, Taipei, Taiwan), and were sequenced by the ABI Prism 3100 Genetic Analyzer (Applied Biosystems, Foster City, CA, USA). qRT-PCR experiments were performed in triplicate.

Plasmid construction

Claudin-16 from the rat kidneys was amplified by a thermal cycler (model MyCycler; Bio-Rad) with the GoTaq Green Master Mix (Promega). After amplicon sequencing, PCR fragments were cloned into the pGEM-T Easy vector (Promega) and introduced into *Escherichia coli* (JM109; Promega). Thereafter, cultured bacteria were harvested, and the plasmid was purified with the HiYield Plasmid kit (Real Biotech Corporation), sequenced and quantified by using a spectrophotometer at 260/280 nm (model UV-2550; Shimadzu, Kyoto, Japan). Cloned claudin-16 fragments were used to create a standard curve for absolute qRT-PCR of claudin-16.

Western blot analysis

Primary osteoblasts were lysed in lysis buffer (0.5 mM Tris pH 7.5, 1.5 M NaCl, 10% NP-40, 5% DOC, 10 mM Na EDTA, 1 mM PMSF, 1 μg/mL leupeptin, 1 μg/mL aprotinin, 1 μg/mL pepstatin A) (Sigma). After 20-min incubation at 4°C, lysates were sonicated, centrifuged at 12,000×g for 10 min, and then heated for 5 min at 95°C. Proteins were separated by SDS–PAGE, and transferred to a polyvinylidene fluoride membrane (Amersham, Buckinghamshire, UK) by electroblotting. After being blocked at 25°C for 4 h with 5% non-fat milk, membranes were probed overnight at 4°C with 1:500 anti-claudin-3, -5, -11, -14, -15 and -16 polyclonal antibodies (Santa Cruz Biotechnology, Santa Cruz, CA, USA). Membranes were later re-probed with 1:5,000 mouse anti-rat β-actin monoclonal antibodies (Santa Cruz). After 2-h incubation at 25°C with 1:20,000 secondary antibodies (Santa Cruz), blots were visualized by enhanced chemiluminescence (ECL Plus; Amersham). Band density was measured by FluorChem SP 4.1 (Alpha Innotech, San Leandro, CA, USA). β-actin was used for normalization.

Immunohistochemistry

Tibiae from five rats were dissected and fixed in 4% paraformaldehyde in 0.1 M PBS at 4°C overnight. They were then washed in cold PBS pH 7.4 and decalcified in 20% w/v EDTA at 4°C for 15 days. Decalcifying solution was replaced every 3 days. The success of decalcification was confirmed by dual-energy X-ray absorptiometry (model Lunar PIXImus2; GE Medical Systems, Madison, WI, USA) with X-ray energy of 80/35 kVp at 500 μA. Thereafter, decalcified bones were embedded in paraffin, and cut into 7-μm sections by a microtome. After deparaffinization in xylene and graded ethanol, sections were incubated at 37°C for 5 min in the antigen retrieval solution containing 0.01 mg/mL proteinase K, 50 mM Tris–HCl pH 7.5, 5 mM EDTA, and later incubated in 3% H_2O_2 for 30 min to reduce the endogenous peroxidase activity. Non-specific binding was blocked by incubating the sections with 4% BSA in 0.1 M PBS for 2 h. After blocking, the sections were incubated at 4°C overnight with 1:200 polyclonal antibodies against claudin-14, -15 or -16. Then, they were washed with 0.1 M PBS, incubated for 1 h with biotinylated goat anti-rabbit antibody (Zymed, South San Francisco, CA, USA), and finally incubated for 1 h at room temperature with streptavidin-conjugated horseradish peroxidase (Zymed). Color was developed with 3,3′-diaminobenzidine (Pierce, Rockford, IL, USA) as a chromogenic peroxidase substrate. Sections were eventually counterstained with hematoxylin and examined under a light microscope (Olympus, Tokyo, Japan) and Image-Pro Plus 5 (Media Cybernetics, Bethesda, MD, USA). Signal intensity was quantified by the method of Lehr et al. (1999).

Confocal laser-scanning microscopy

Immunofluorescent technique was described previously (Jantarajit et al. 2007). Tibiae from three rats were dehydrated with sequential ethanol (70, 95, and 100%), and

Table 1 *Rattus norvegicus* oligonucleotide sequences used in qRT-PCR experiments

Gene	Accession no.	Primer (forward/reverse)	Product length (bp)
Osteoblast-related proteins			
Osteocalcin	J04500	5′–CACAGGGAGGTGTGTGAG–3′ 5′–TGTGCCGTCCATACTTTC–3′	203
Osteopontin	NM_012881	5′–TTCACTGCCAGCACACAA–3′ 5′–TTTGACCTCAGTCCGTAAGC–3′	101
Runx2	XM_001066909	5′–TAACGGTCTTCACAAATCCTC–3′ 5′–GGCGGTCAGAGAACAAACTA–3′	135
Osterix	AY177399	5′–GCCTACTTACCCGTCTGA–3′ 5′–CTCCAGTTGCCCACTATT–3′	139
Dlx5	NM_012943	5′–CTCTCTAGGACTGACGCAAAC–3′ 5′–GAGTTACACGCCATAGGGTC–3′	135
Msx2	NM_012982	5′–TAGACCTGTGCTTCCCAT–3′ 5′–ACAAACATCCATCCTAGAGTG–3′	114
AJ18	AF321874	5′–GTCCCTGGTATGTATCAC–3′ 5′–GAAGACTTTGGCTAAAAC–3′	133
Osteoprotegerin	NM_012870	5′–ATTGGCTGAGTGTTCTGGT–3′ 5′–CTGGTCTCTGTTTTGATGC–3′	140
RANKL	NM_057149	5′–TCGCTCTGTTCCTGTACT–3′ 5′–AGTGCTTCTGTGTCTTCG–3′	145
Transmembrane tight junction proteins			
Cldn-1	NM_031699	5′–AGGTCTGGCGACATTAGTGG–3′ 5′–TGGTGTTGGGTAAGAGGTTG–3′	202
Cldn-2	XM_236535	5′–TCTGGATGGAGTGTGCGAC–3′ 5′–AGTGGCAAGAGGCTGGGC–3′	467
Cldn-3	NM_031700	5′–GCACCCACCAAGATCCTCTA–3′ 5′–AGGCTGTCTGTCCTCTTCCA–3′	246
Cldn-4	NM_001012022	5′–TGGATGAACTGCGTGGTGC–3′ 5′–CCCTACGACTGAGAGAAGC–3′	153
Cldn-5	NM_031701	5′–CGCTTGTGGCACTCTTTGT–3′ 5′–ACTCCCGGACTACGATGTTG–3′	168
Cldn-6	XM_001055688	5′–GGAGGGGCTATGGATGTC–3′ 5′–GCAGATGGGAATGAGGGT–3′	271
Cldn-7	NM_031702	5′–ACTACTGGGCTTTTCAATGGC–3′ 5′–CACCGAGTCGTACATTTTGC–3′	190
Cldn-8	NM_001037774	5′–GCTGGAATCATCTTCTTCAT–3′ 5′–CATCCACCAGCGGGTTGTAG–3′	100
Cldn-9	NM_001011889	5′–CTTCATTGGCAACAGCATCG–3′ 5′–CCTTGGCACCTTCGTCCTC–3′	242
Cldn-10	XM_001074876	5′–CATATTGTCAGGTCTGTGTTC3′ 5′–TGGGTGTTTTGTTGTTGTC–3′	200
Cldn-11	NM_053457	5′–ATTGGCATCATCGTCACAAC–3′ 5′–ATGTCCACCAGGGGCTTG–3′	158
Cldn-12	XM_001067932	5′–CCTTCAAGTCTTCGGTGCC–3′ 5′–CAGGAGGATGGGAGTACAG–3′	312
Cldn-14	NM_001013429	5′–CTGTACCTGGGCTTCATC–3′ 5′–CACACATAGTCATTCAACCTG–3′	230
Cldn-15	XM_222085	5′–GCTGTGCCACCGACTCCC–3′ 5′–CAGAGCCCAGTTCATACTTG–3′	330
Cldn-16	NM_131905	5′–ATCTTCTTCAGTACGCTGCC–3′ 5′–CGATGAGTAATACGGTCCC–3′	372
Cldn-17	XM_221711	5′–CTCCAGTGAGAGGGTCAAAG–3′ 5′–AGCAGCAGTATCCACAGAGC–3′	236
Cldn-18	NM_001014096	5′–CCGTTCAGACCAGGTACAC–3′ 5′–CTCCAGGCTTATAGGCAAC–3′	180

Table 1 continued

Gene	Accession no.	Primer (forward/reverse)	Product length (bp)
Cldn-19	NM_001008514	5′–TGCTGAAGGACCCATCTG–3′ 5′–TGTGCTTGCTGTGAGAACTG–3′	129
Cldn-20	XM_973727	5′–GCACTCTAAAATACTCCATTC–3′ 5′–TGAAGCAGACTCCTCCAGC–3′	186
Cldn-22	XM_001059255	5′–ATGGGCTTAGTCTTCCGAAC–3′ 5′–TGGATGACGCAGGATTTC–3′	170
Cldn-23	NM_001033062	5′–GTGGAACTACTTCGGGACTC–3′ 5′–CCCAGCACCAGACTGTAGC–3′	285
Occludin	NM_031329	5′–CACGTTCGACCAATGC–3′ 5′–CCCGTTCCATAGGCTC–3′	188
Cytoplasmic tight junction proteins			
ZO-1	XM_218747	5′–GTATCCGATTGTTGTGTTCC–3′ 5′–TCACTTGTAGCACCATCCGC–3′	270
ZO-2	NM_053773	5′–TCTGAAGGTGAACACACAA–3′ 5′–CCAGGATGTCTCTATACACG–3′	134
ZO-3	XM_001069839	5′–TGCTAATGAGACCGCTAAAG–3′ 5′–GACACTCCGTTGATCTGTAA–3′	169
Cingulin	XM_001059265	5′–ATCGGGAACTCCAGTCAAC–3′ 5′–TGACGGGAACGGCTAAAG–3′	121
Housekeeping gene			
GAPDH	NM_017008	5′–AGTCTACTGGCGTCTTCAC–3′ 5′–TCATATTTCTCGTGGTTCAC–3′	133

Runx runt-related transcription factor, *Dlx5* distal-less homeobox 5, *Msx2 msh* homeobox homolog 2, *RANKL* receptor activator of nuclear factor κB ligand, *Cldn* claudin, *ZO* zonula occludens, *GAPDH* glyceraldehyde-3-phosphate dehydrogenase

embedded in methyl methacrylate resin. The embedded tibiae were cut longitudinally at a thickness of 7 μm with a RM2255 microtome (Leica, Nussloch, Germany). After deplastination, the sections were incubated overnight at 4°C with 1:200 goat anti-claudin-16 antibody (Santa Cruz). Thereafter, they were incubated for 3 h at 20°C with 1:200 FITC-conjugated donkey anti-goat secondary antibody (green signal; Santa Cruz). Nuclei were stained with 1:1000 TO-PRO-3 (red signal; Molecular Probes, Eugene, OR, USA). Negative control was obtained by incubating a tissue section with a secondary antibody in the absence of a primary antibody. Samples were examined for fluorescent signals by using a FV1000 confocal microscope (Olympus).

As for the immunocytochemistry in primary osteoblasts, cells were plated on a coverslip in six-well culture discs (10^4 cells/cm^2), and maintained for 2 days before being fixed for 5 min in 3% paraformaldehyde and 2% sucrose. After blocking non-specific bindings, cells were incubated overnight at 4°C with 1:200 rabbit anti-claudin-5, -11, -14 and -15 polyclonal antibodies (Santa Cruz), and were later incubated with 1:200 Alexa Fluor 488-conjugated mouse anti-rabbit secondary antibody (green signal; Molecular Probes) at 20°C. Negative controls were incubated with an equivalent volume of PBS instead of the anti-claudin antibodies. Nuclei were stained with 1:500 TO-PRO-3 (red signal). Images were captured with a confocal microscope.

Scanning electron microscopy (SEM)

Primary osteoblasts were seeded on a Snapwell at a density of 2×10^5 cells/cm^2. After 21 days of culture, Snapwell-cultured osteoblasts were fixed with 2.5% glutaraldehyde in 0.1 M PBS pH 7.2 and 2.5 mM $MgCl_2$ for 2 h at 4°C. Samples were dehydrated in graded ethanols (50, 70, 80, 90, 95 and 100%) for 10 min each. The fixed samples were freeze-dried, coated with a thin layer of platinum and palladium, and examined under SEM (model S-2500; Hitachi, Tokyo, Japan).

Electrical measurements

Three electrical parameters, i.e., epithelial potential difference (PD), short-circuit current (Isc) and transepithelial resistance (TER), were determined by Ussing chamber technique as previously described (Jantarajit et al. 2007). This technique allowed us to determine whether tight junctions were formed. A Snapwell was mounted in the chamber for 40-min electrical measurements. The monolayer was bathed on both sides with buffer containing (in mM) 118 NaCl, 4.7 KCl, 1.1 $MgCl_2$, 1.25 $CaCl_2$, 23 $NaHCO_3$, 12 D-glucose and 2 mannitol (Sigma), and continuously gassed with humidified 5% CO_2 in 95% O_2. A pair of Ag/AgCl electrodes connected to agar bridges (3.0 M KCl per 4 g % agar) was located near each surface of the Snapwell for

measurement of PD. The other ends of the PD-sensing electrodes were connected to a pre-amplifier (model EVC-4000; World Precision Instruments, Sarasota, FL, USA), and finally to a PowerLab 4/30 operated with a software Chart 5.4 (ADInstruments, Colorado Springs, CO., USA). Another pair of Ag/AgCl electrodes was placed at the end of each chamber to supply Isc, which was also measured by a PowerLab 4/30 connected in series to the EVC-4000 current-generating unit. TER was calculated by the Ohm's equation.

Statistical analysis

Results are expressed as means ± SE. Multiple comparisons were performed by one-way analysis of variance (ANOVA) with the Dunnett post-test. Data were analyzed by GraphPad Prism 4 (GraphPad Software, San Diego, CA, USA).

Results

Prior to the investigation on the tight junction protein expression, we performed an experiment to confirm that the cultured cells obtained from tibiae and femora of rats were differentiated osteoblasts. As shown in Fig. 1, primary osteoblasts and cells in the rat calvaria strongly expressed all markers of osteoblast differentiation, i.e., osteocalcin, osteopontin, Runx2, osterix, Dlx5, Msx2, AJ18, OPG and RANKL (Kostenuik 2005; Owen et al. 1990; Zhang et al. 2006).

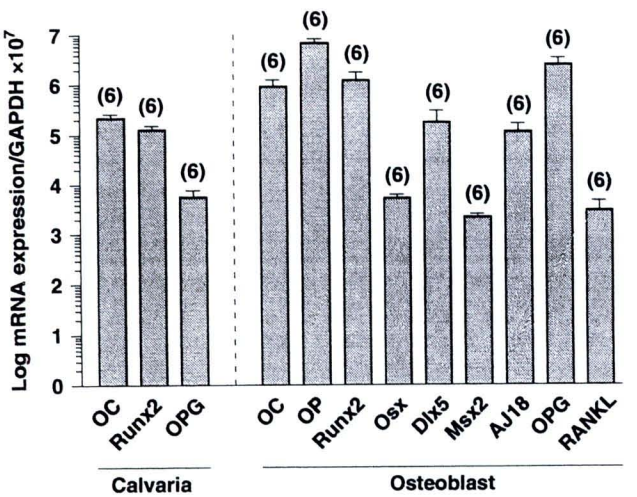

Fig. 1 Expression of the marker genes related to osteoblast differentiation, namely osteocalcin (*OC*), osteopontin (*OP*), Runx2, osterix (*Osx*), Dlx5, Msx2, AJ18, OPG and RANKL, in calvaria and primary osteoblasts. GAPDH is a housekeeping gene for normalization. *Numbers* in parentheses represent the number of animals in each group

In the investigation on the expression of tight junction genes, we used qRT-PCR to demonstrate the expression of the cytoplasmic tight junction genes, ZO-1, -2, -3 and cingulin, as well as the transmembrane tight junction gene, occludin in the calvarial homogenate (Fig. 2a) and primary rat osteoblasts (Fig. 2b). Moreover, as depicted in Fig. 3, both primary osteoblasts and calvarial cells exhibited mRNA expression of claudin-1 to -12, -14 to -20, -22 and -23. Expression of claudin-3, -5 and -8 in osteoblasts were very low. We did not study the expression of claudin-13, -21 and -24 as these genes have never been reported in rats (Charoenphandhu et al. 2007).

Although claudin-16 was previously known to be expressed exclusively in the thick ascending limb of the loop of Henle (Simon et al. 1999), it was also identified in primary osteoblasts (Fig. 3b). We further performed absolute qRT-PCR to compare the expression of claudin-16 in primary osteoblasts with those in the kidney (positive control) and calvaria as well as in other Ca^{2+}-transporting epithelia, i.e., duodenum and distal colon. The results confirmed that primary osteoblasts and all three tissues expressed claudin-16 mRNA, but the levels in the kidney were ~600 times higher than others ($P < 0.01$, Fig. 4a).

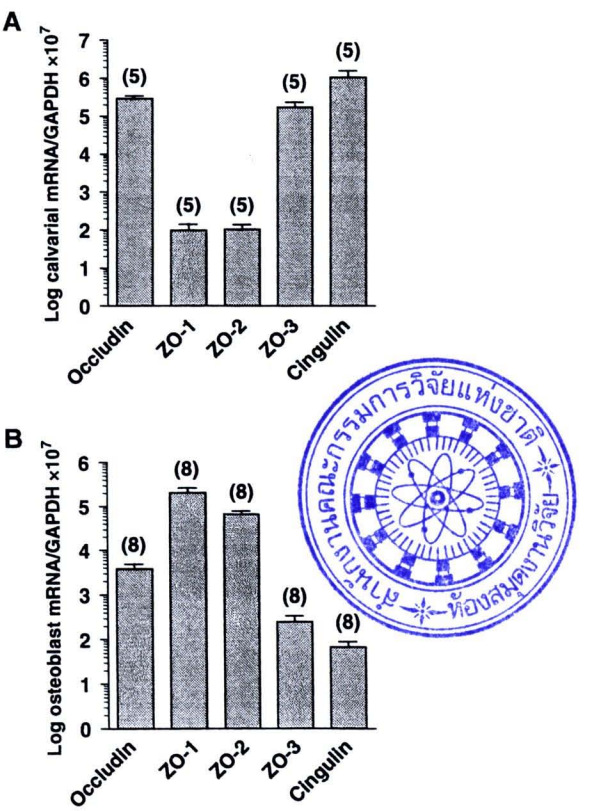

Fig. 2 Expression of genes of tight junction proteins, including occludin, ZO-1, -2, -3 and cingulin, in calvaria (**a**) and primary rat osteoblasts (**b**). GAPDH is a housekeeping gene for normalization. *Numbers* in parentheses represent the number of animals in each group

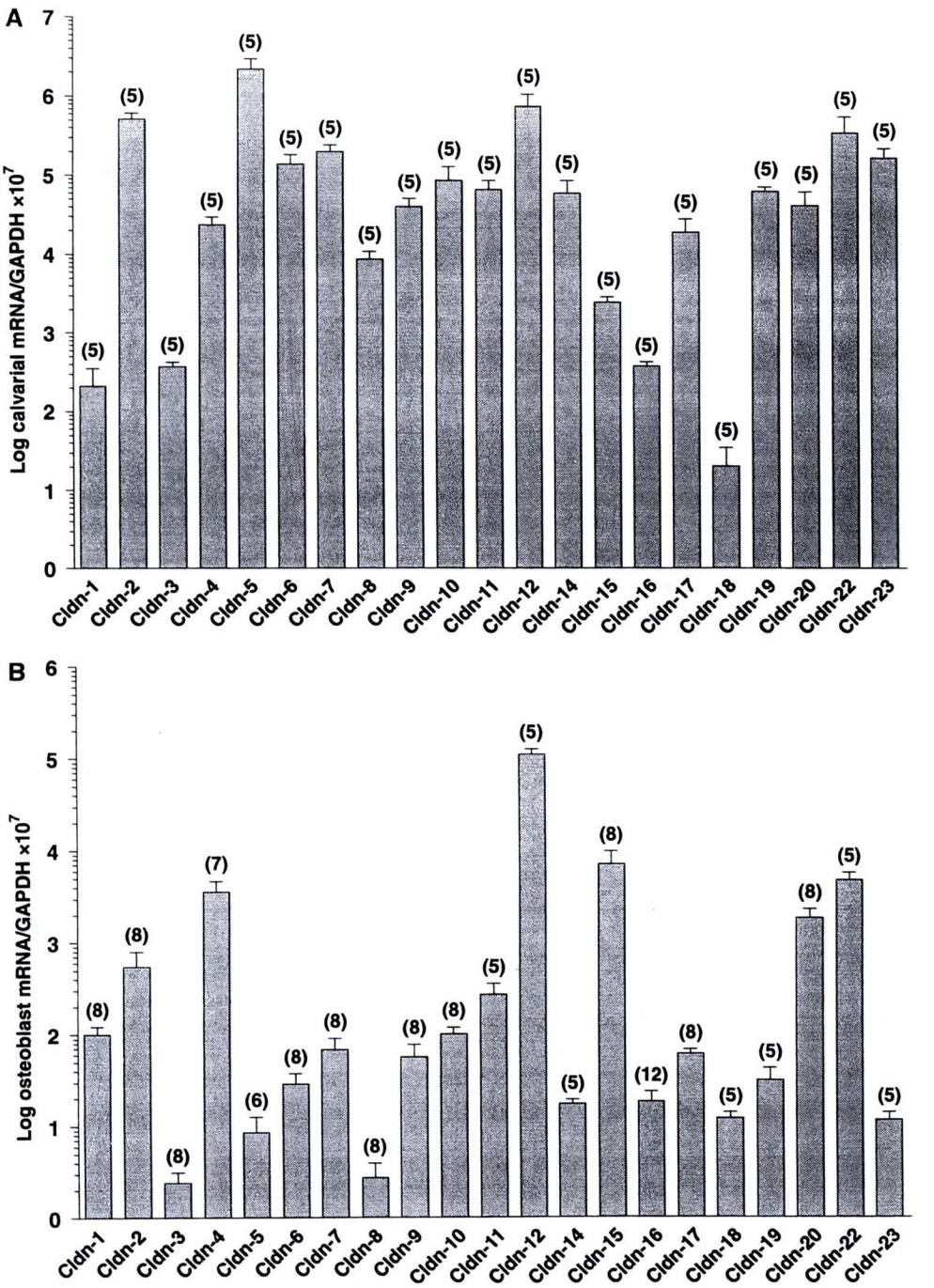

Fig. 3 Expression of claudin mRNAs in calvaria (**a**) and primary rat osteoblasts (**b**). Claudin-13, -21 and -24 were not studied, because they have never been reported in rats. GAPDH is a housekeeping gene for normalization. *Numbers* in parentheses represent the number of animals in each group

Interestingly, the expression of claudin-16 proteins in osteoblasts and kidneys were comparable (Fig. 4b).

Furthermore, protein expression of claudin-5, -11, -14, -15 and -16, but not claudin-3, were demonstrated in the primary rat osteoblasts by western blot analysis (Fig. 4c, d) and confocal immunofluorescent technique (Fig. 5a). In the methyl methacrylate-embedded tibial sections, claudin-16 localization was confined to the metaphyseal trabecular surfaces, where osteoblasts and bone-lining cells were present, but not in the cortical parts or the marrow cavities (Fig. 5b). By using immunohistochemical localization in the decalcified tibial sections, expression of claudin-5, -11, -14, -15 and -16, but not claudin-3, were visualized in bone-lining cells (arrows; Fig. 6), which are inactive osteoblasts lining the bone matrix.

After being cultured in Snapwell for 19, 21, 23 or 26 days, the tibia-derived cells formed a homogeneous monolayer that strongly expressed osteocalcin, osteopontin, Runx2, osterix, Dlx5, Msx2, AJ18, OPG and RANKL (data not shown) similar to osteoblasts cultured

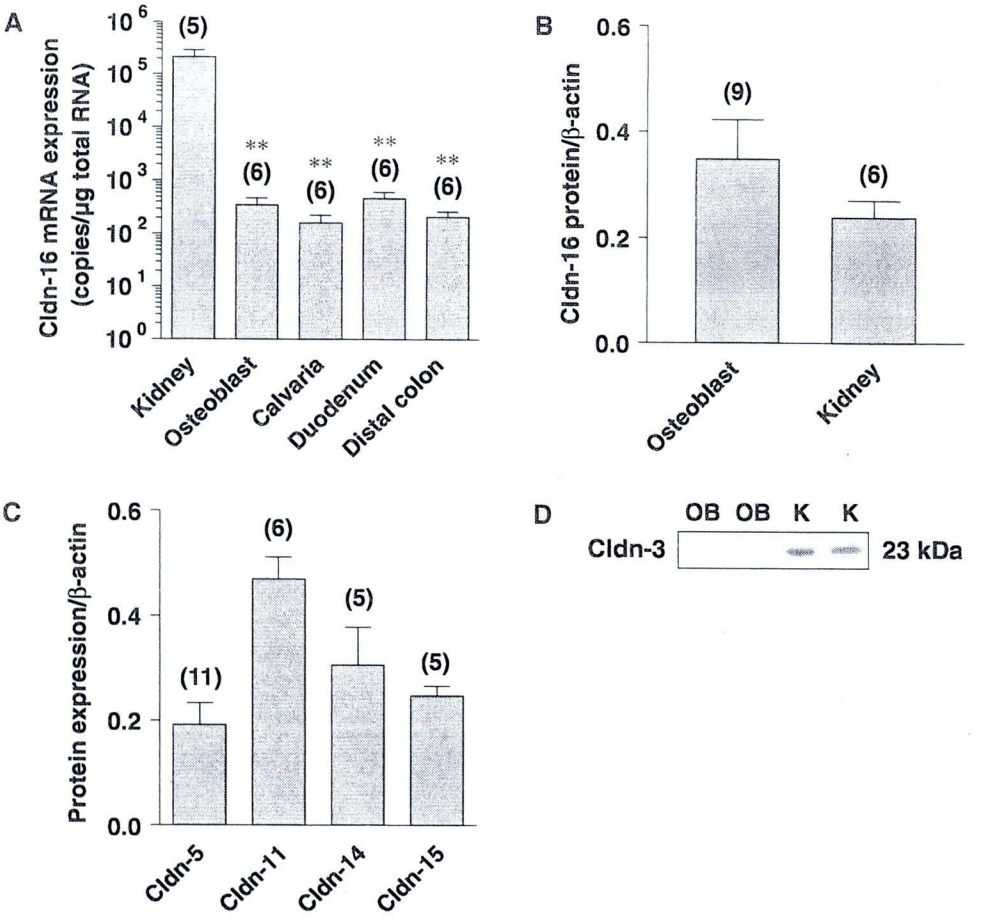

Fig. 4 **a** Absolute qRT-PCR analysis of claudin-16 expression in kidney (positive control), primary osteoblasts, calvaria, duodenum and distal colon. $^{**}P < 0.01$ compared with kidney. **b** Western blot analysis of claudin-16 expression in the kidney and primary rat osteoblasts. **c** Protein expression of claudin-5, -11, -14 and -15 in primary rat osteoblasts. β-actin is a housekeeping protein for normalization. *Numbers* in parentheses represent the number of animals in each group. **d** Representative electrophoretic bands of the western blot analysis of claudin-3 expression ($n = 5$). Claudin-3 protein was not expressed in the osteoblasts (*OB*), but was strongly expressed in the kidney (*K*). Experiments were performed in duplicate

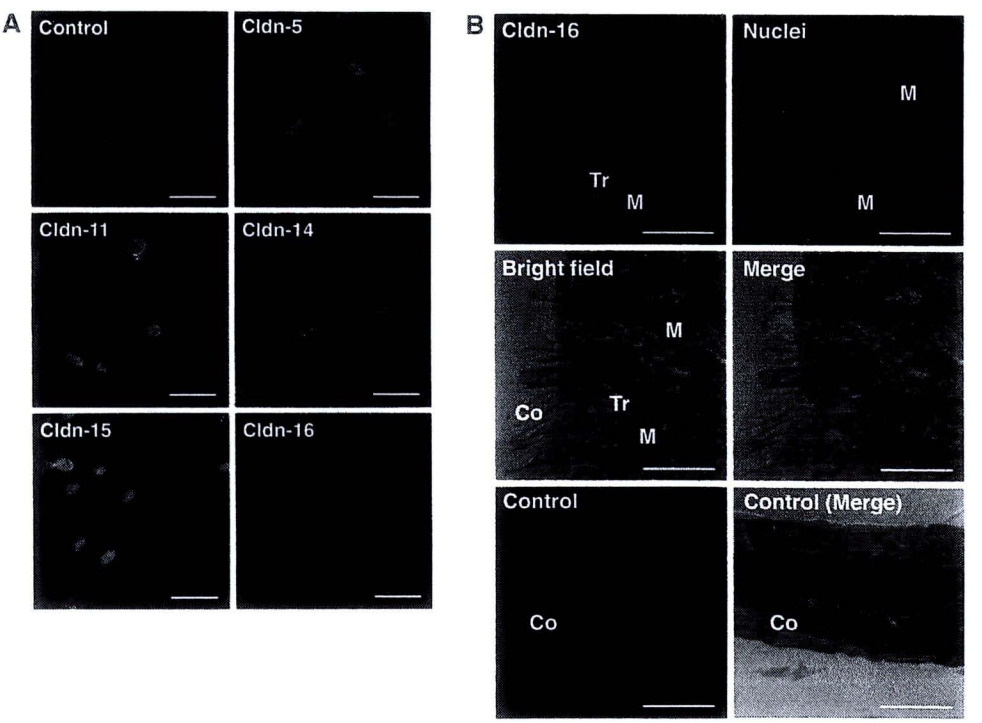

Fig. 5 **a** Expression of claudin-5, -11, -14, -15 and -16 (*green signals*) in primary rat osteoblasts ($n = 5$) as demonstrated by the confocal immunofluorescent technique. Nuclei are stained in *red*. Control image was obtained by incubating osteoblasts in the absence of anti-claudin antibodies. *Bars* 10 µm. **b** Representative confocal immunofluorescent images of claudin-16 localization in a methyl methacrylate-embedded section of the tibial metaphysis ($n = 3$). Positive signals (*green*) are visible on the surfaces of the trabeculae (*Tr*), but not on the cortical regions (*Co*) or marrow cavities (*M*). Nuclei are labeled in *red*. Control images were obtained by incubating tissue sections in the absence of anti-claudin-16 antibody. *Bars* 400 µm

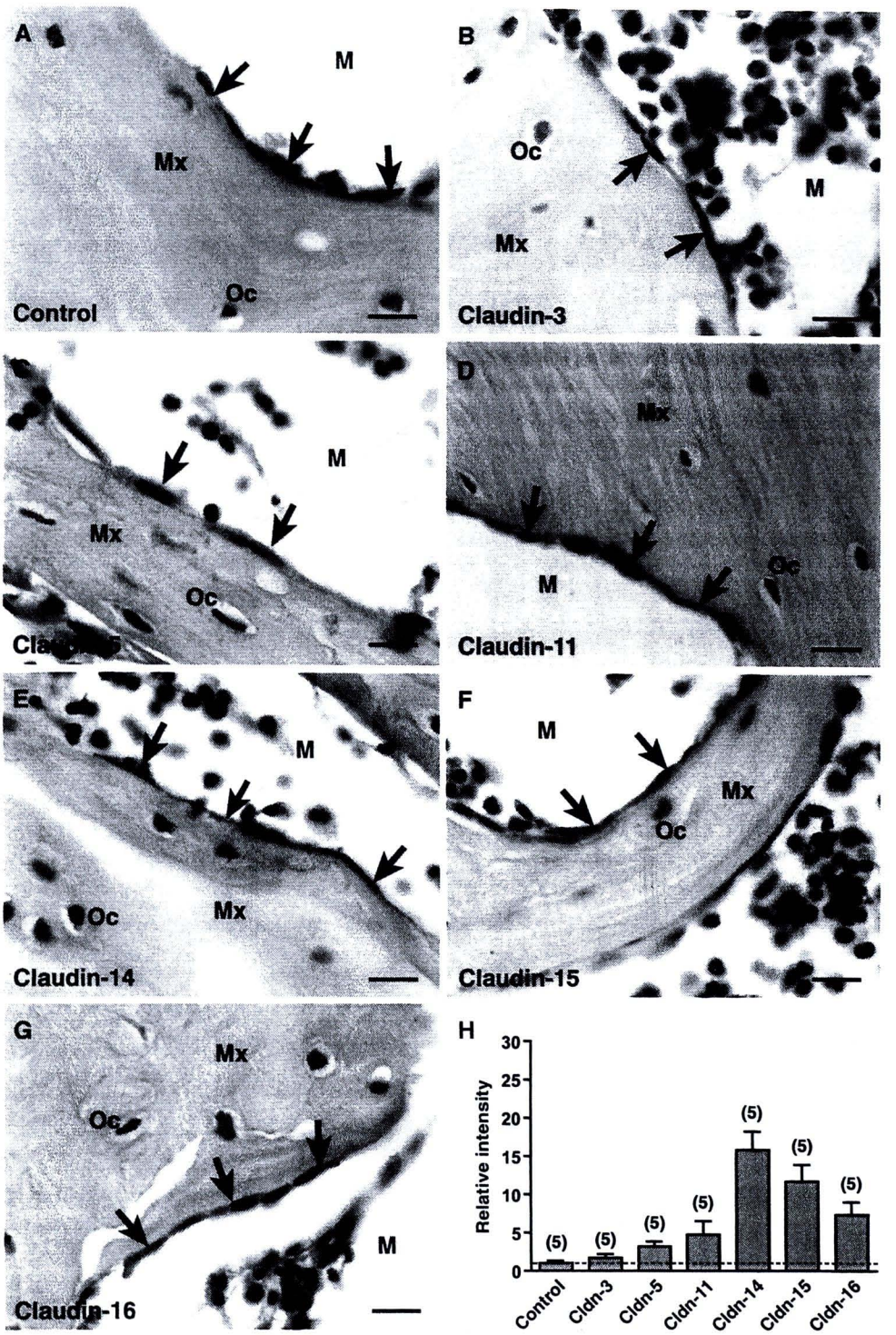

Fig. 6 **a–g** Immunohistochemical localization of claudin-5, -11, -14, -15 and -16 in decalcified tibiae ($n = 5$). Claudin-3 was not detected, whereas the positive signals for other claudins were seen in bone-lining cells (inactive flat osteoblasts; *arrows*), which covered the bone matrix (*Mx*). No signal was found in osteocytes (*Oc*) or marrow (*M*). Images of negative controls (without anti-claudin antibody) did not show immunoreactive signal. *Bars* 10 μm. **h** Relative signal intensity of claudin expression in decalcified tibial sections. The intensities of controls were normalized to 1. *Numbers* in parentheses represent the number of animals

in flasks, indicating that these cells were differentiated osteoblasts. SEM showed cells with well-developed pseudopodia firmly attached to the Snapwell forming a monolayer (Fig. 7). Electrical parameters, i.e., PD, Isc and TER, of the monolayer were measurable on day 19–26 after seeding (Table 2). The presence of TER suggested that these osteoblasts could form the tight junction in Snapwell.

Discussion

In the present study, we reported, for the first time, that osteoblasts and bone tissues of rats expressed claudins and other tight junction-associated proteins at the transcriptional and translational levels. Moreover, osteoblasts could form epithelial-like monolayers when grown on the compartmentalized permeable supports.

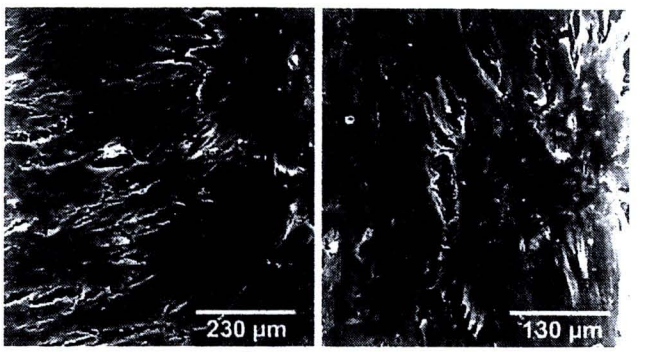

Fig. 7 Scanning electron micrographs of primary osteoblasts at day 21 of culture ($n = 6$). Cells firmly attached to Snapwell and formed a monolayer

Since the tight junction is the most important barrier which restricts ion and water from passing freely through the paracellular space, the expression of tight junction proteins in osteoblasts supports the previous hypothesis that osteoblasts and bone-lining cells, which cover 90% of bone surface, form an epithelial-like bone membrane to regulate ion transport and maintain differential ion compositions between the plasma and BECF (Bushinsky et al. 1989; Marenzana et al. 2005; Peterson et al. 1985; Trumbore et al. 1980). Normally, concentrations of Ca^{2+}, Mg^{2+} and K^+ in BECF are approximately 0.5, 0.4 and 25 mM, whereas those in plasma are 1.25, 0.7 and 4.5 mM, respectively (Armstrong and Singer 1965; Trumbore et al. 1980). These ionic gradients were thought to be actively maintained by bone membrane, and were dissipated in dead tissue or in the presence of inhibitors of ATP production (Marenzana et al. 2005; Rubinacci et al. 2002). By using the three-dimensional scanning Ca^{2+}-selective electrode technique, Marenzana et al. (2005) demonstrated Ca^{2+} efflux from bone surface through the paracellular route. Although our techniques could not show the localization of claudin expression at the tight junction, the evidence of the intensely expressed claudin-16, which is known to control the paracellular Ca^{2+} transport (Ikari et al. 2004), along the trabecular surface of the tibia suggested the transport function of the tight junctions in bone membrane. Moreover, we showed that several markers of the epithelial cells, e.g., ZO-3, cingulin and claudins, which are highly specific to the tight junction formation (Citi et al. 1991; Inoko et al. 2003) were also expressed in osteoblasts. Therefore, our findings corroborated the formation of tight junctions in osteoblasts and an existence of an epithelial-like bone membrane.

Herein, we studied the mRNA expression of the cytoplasmic tight junction proteins, ZO-1, -2, -3 and cingulin, and the transmembrane proteins, occludin and claudin-1 to -23, in calvaria and osteoblasts. Although calvarial homogenate contained mRNAs from many cell types, such as osteoblasts, osteoclasts and osteocytes, our results provided suggestive evidence that bone expressed tight junction genes. In normal epithelia, ZO-1, a member of the membrane-associated guanylate kinase-like homologues (MAGUK), directly binds to occludin, claudin-1 to -8 and -16 to modulate the assembly of the tight junction (Inoko et al. 2003; McNeil et al. 2006). Cingulin, on the other hand, is not required for the tight junction assembly, but is important for the signaling pathways that control the expression of several claudins, such as claudin-2, -6 and -7 (Guillemot and Citi 2006). Since cingulin was previously detected only in epithelial tissues, the presence of cingulin in the osteoblasts strongly suggested that osteoblasts and/or their lineages, e.g., bone-lining cells, possess epithelial characteristics.

Regarding the transmembrane protein occludin, despite being one of the tight junction-associated proteins, it may not be essential for the tight junction assembly or the paracellular ion transport, since enterocytes of the occludin-knockout mice exhibited normal morphology of the tight junction and normal epithelial barrier function (Saitou et al. 2000). The exact function of occludin, therefore, remains controversial. Among other transmembrane proteins, claudins have been widely accepted as the key proteins for the regulation of the paracellular transport of ions, water-soluble nutrients and drugs in a size- and charge-specific fashion in the gastrointestinal tract, renal tubule, respiratory tract and blood–brain barrier (Furuse and Tsukita 2006; Van Itallie and Anderson 2006). Each claudin consists of four transmembrane domains and two extracellular loops, which contain charged amino acids and also interact with those of the adjacent cells to form a paracellular barrier (Van Itallie et al. 2003). Some claudins, e.g., claudin-8, -10, -14, -16 and -19, were suggested to form arrays of tight junctional pores or channel-like structures which, in turn,

Table 2 Electrical parameters of the osteoblast monolayers grown on Snapwells for 19, 21, 23 and 26 days

Conditions	n	Electrical parameters		
		PD (mV)	Isc ($\mu A\ cm^{-2}$)	TER ($\Omega\ cm^2$)
19-Day-monolayer	6	0.59 ± 0.21	8.61 ± 1.87	114.77 ± 8.58
21-Day-monolayer	12	0.76 ± 0.25	3.47 ± 0.70	150.67 ± 26.48
23-Day-monolayer	6	1.11 ± 0.47	3.89 ± 1.29	161.63 ± 13.59
26-Day-monolayer	4	0.66 ± 0.18	3.82 ± 0.87	184.43 ± 47.55

Values are means ± SE

regulated the paracellular ion transport and were responsible for the size- and/or charge-selective properties of the tight junction (Angelow et al. 2007; Ben-Yosef et al. 2003; Ikari et al. 2004; Van Itallie et al. 2006; Yu et al. 2003). Since different types of cells expressed different fingerprints of claudin patterns, and co-localization and co-polymerization of different claudins could affect the paracellular ion movement (Furuse and Tsukita 2006), the unique transport property of each epithelium could have resulted from its distinctive pattern of claudins. Therefore, to further explore the possible epithelial-like functions of osteoblasts, information on claudin profile, as provided by the present study, was indispensable. We speculate that bone membrane may use a specific set of claudins to regulate ion transport across the paracellular channel.

Primary osteoblasts and calvaria were shown to express mRNAs of claudin-1 to -12, -14 to -20, -22 and -23. Due to a limited availability of commercial claudin antibodies suitable for bone staining, we studied protein expression of only some selected claudins, namely claudin-3, -5, -11, -14, -15 and -16, all known to be important for the charge selectivity of the renal tubular and intestinal epithelia (Ben-Yosef et al. 2003; Ikari et al. 2004; Van Itallie and Anderson 2006). As shown in the results, only claudin-3 protein was not detected in primary osteoblasts, possibly due to its low mRNA levels. Claudin-5, -11, -14, -15 and -16 were identified in primary osteoblasts and bone-lining cells by confocal microscopy and immunohistochemistry, respectively. However, we were not able to demonstrate claudin expression in the osteoblast monolayer cultured on Snapwell due to a technical limitation caused by the shape and opaqueness of Snapwell. As for the primary osteoblasts cultured on coverslips, claudins were dispersed over the plasma membrane instead of localizing around the tight junctions.

Interestingly, primary osteoblasts, calvaria and tibiae of rats expressed mRNA and protein of claudin-16, which was important for the paracellular Ca^{2+} and Mg^{2+} reabsorption in the thick ascending limb (TAL) of the loop of Henle (Simon et al. 1999). Several investigators previously suggested that claudin-16 was strongly expressed only in the TAL and distal convoluted tubules of the kidneys (Simon et al. 1999). However, our results as well as reports of claudin-16 expression in lung (Hirano et al. 2000), mammary glands (Markov et al. 2006) and salivary glands (Kriegs et al. 2007) confirmed the presence of claudin-16 in the extrarenal tissues. Moreover, as demonstrated by the present absolute qRT-PCR, mucosal cells of duodenum and distal colon, both being Ca^{2+}-transporting epithelia, also expressed claudin-16 mRNAs, but the levels were not as high as those in the kidneys.

The functions of claudin-1, -2, -4, -8, -15, and -19 have been well characterized in MDCK cells. Expression of claudin-1, -8 and -19 increased TER, while claudin-2, -4 and -15 regulated the paracellular permeability to ions (Angelow et al. 2007; McCarthy et al. 2000; Van Itallie et al. 2001, 2003; Yu et al. 2003). Because of the fact that the barrier functions of claudins (or tight junction) could be evaluated by measurement of TER, the osteoblast monolayer was grown on a compartmentalized permeable support, i.e., Snapwell. The compartmentalized culture environment is known to induce formation of the monolayer by other cell types, such as rat monoclonal bone marrow stem cells (Shu et al. 2006). As shown in Fig. 7, the primary rat osteoblasts that formed a monolayer in Snapwell did retain the osteoblast phenotypes. The presence of TER of $\sim$110–180 Ωcm^2, which is comparable to the TER reported in the duodenum (Charoenphandhu et al. 2006), confirmed that the primary rat osteoblasts were able to form a functional epithelial-like membrane in vitro with the barrier property of tight junctions. In addition, other electrical parameters, i.e., PD and Isc, implicated ion fluxes across the monolayer (Shu et al. 2006; Trumbore et al. 1980). Besides the barrier function, tight junctions of osteoblasts could play an important role in the vesicular trafficking of bone matrix proteins to the surface of bone and in maintaining the polarity of matrix-secreting osteoblasts, thereby resulting in an organized matrix deposition in bone tissue (Prêle et al. 2003).

Finally, it could be concluded that the primary osteoblasts and bone tissues expressed several tight junction proteins, thus supporting the existence of a functional epithelial-like bone membrane, its regulation of the paracellular ion transport, and the maintenance of BECF ion compositions. The osteoblast monolayer cultured on Snapwell, similar to normal epithelia, exhibited electrical parameters, i.e., PD and TER, which are indicative of the ion transport activity and barrier function of the tight junction, respectively. These novel findings are fundamental and provide the basis for further investigation to explain how osteoblasts form bone membrane in vivo, and how bone membranes regulate the ionic compositions of BECF and the paracellular transport of ions.

Acknowledgments This research was supported by grants from the Strategic Consortia for Capacity Building of University Faculties and Staff, Commission on Higher Education, Thailand (to K.W.), and the Thailand Research Fund (to N.C. and N.K.).

References

Angelow S, El-Husseini R, Kanzawa SA, Yu AS (2007) Renal localization and function of the tight junction protein, claudin-19. Am J Physiol Renal Physiol 293:F166–F177

Armstrong WD, Singer L (1965) Composition and constitution of the mineral phase of bone. Clin Orthop Relat Res 38:179–190

Bakker A, Klein-Nulend J (2003) Osteoblast isolation from murine calvariae and long bones. In: Helfrich MH, Ralston SH (eds)

Methods in molecular medicine: bone research protocols. Humana Press, New Jersey, pp 19–28

Ben-Yosef T, Belyantseva IA, Saunders TL, Hughes ED, Kawamoto K, Van Itallie CM, Beyer LA, Halsey K, Gardner DJ, Wilcox ER, Rasmussen J, Anderson JM, Dolan DF, Forge A, Raphael Y, Camper SA, Friedman TB (2003) Claudin 14 knockout mice, a model for autosomal recessive deafness DFNB29, are deaf due to cochlear hair cell degeneration. Hum Mol Genet 12:2049–2061

Bushinsky DA, Chabala JM, Levi-Setti R (1989) Ion microprobe analysis of mouse calvariae in vitro: evidence for a "bone membrane". Am J Physiol 256:E152–E158

Bushinsky DA, Riordon DR, Chan JS, Krieger NS (1997) Decreased potassium stimulates bone resorption. Am J Physiol 272:F774–F780

Charoenphandhu N, Tudpor K, Pulsook N, Krishnamra N (2006) Chronic metabolic acidosis stimulated transcellular and solvent drag-induced calcium transport in the duodenum of female rats. Am J Physiol Gastrointest Liver Physiol 291:G446–G455

Charoenphandhu N, Wongdee K, Tudpor K, Pandaranandaka J, Krishnamra N (2007) Chronic metabolic acidosis upregulated claudin mRNA expression in the duodenal enterocytes of female rats. Life Sci 80:1729–1737

Citi S, Amorosi A, Franconi F, Giotti A, Zampi G (1991) Cingulin, a specific protein component of tight junctions, is expressed in normal and neoplastic human epithelial tissues. Am J Pathol 138:781–789

Furuse M, Tsukita S (2006) Claudins in occluding junctions of humans and flies. Trends Cell Biol 16:181–188

Greger R (1996) Epithelial transport. In: Greger R, Windhorst U (eds) Comprehensive human physiology: from cellular mechanisms to integration. Springer, Berlin, pp 1217–1232

Guillemot L, Citi S (2006) Cingulin regulates claudin-2 expression and cell proliferation through the small GTPase RhoA. Mol Biol Cell 17:3569–3577

Hirano T, Kobayashi N, Itoh T, Takasuga A, Nakamaru T, Hirotsune S, Sugimoto Y (2000) Null mutation of PCLN-1/Claudin-16 results in bovine chronic interstitial nephritis. Genome Res 10:659–663

Ikari A, Hirai N, Shiroma M, Harada H, Sakai H, Hayashi H, Suzuki Y, Degawa M, Takagi K (2004) Association of paracellin-1 with ZO-1 augments the reabsorption of divalent cations in renal epithelial cells. J Biol Chem 279:54826–54832

Inoko A, Itoh M, Tamura A, Matsuda M, Furuse M, Tsukita S (2003) Expression and distribution of ZO-3, a tight junction MAGUK protein, in mouse tissues. Genes Cells 8:837–845

Jantarajit W, Thongon N, Pandaranandaka J, Teerapornpuntakit J, Krishnamra N, Charoenphandhu N (2007) Prolactin-stimulated transepithelial calcium transport in duodenum and Caco-2 monolayer are mediated by the phosphoinositide 3-kinase pathway. Am J Physiol Endocrinol Metab 293:E372–E384

Kostenuik PJ (2005) Osteoprotegerin and RANKL regulate bone resorption, density, geometry and strength. Curr Opin Pharmacol 5:618–625

Kriegs JO, Homann V, Kinne-Saffran E, Kinne RK (2007) Identification and subcellular localization of paracellin-1 (claudin-16) in human salivary glands. Histochem Cell Biol 128:45–53

Lehr HA, van der Loos CM, Teeling P, Gown AM (1999) Complete chromogen separation and analysis in double immunohistochemical stains using Photoshop-based image analysis. J Histochem Cytochem 47:119–126

Marenzana M, Shipley AM, Squitiero P, Kunkel JG, Rubinacci A (2005) Bone as an ion exchange organ: evidence for instantaneous cell-dependent calcium efflux from bone not due to resorption. Bone 37:545–554

Markov AG, Shadrin LV, Veshnyakova AU, Amasheh S, Fromm M (2006) The tight junction proteins claudin-2 and -16 expression in mammary epithelium of mice. Ross Fiziol Zh Im I M Sechenova 92:1382–1386

McCarthy KM, Francis SA, McCormack JM, Lai J, Rogers RA, Skare IB, Lynch RD, Schneeberger EE (2000) Inducible expression of claudin-1-myc but not occludin-VSV-G results in aberrant tight junction strand formation in MDCK cells. J Cell Sci 113:3387–3398

McNeil E, Capaldo CT, Macara IG (2006) Zonula occludens-1 function in the assembly of tight junctions in Madin–Darby canine kidney epithelial cells. Mol Biol Cell 17:1922–1932

Owen TA, Aronow M, Shalhoub V, Barone LM, Wilming L, Tassinari MS, Kennedy MB, Pockwinse S, Lian JB, Stein GS (1990) Progressive development of the rat osteoblast phenotype in vitro: reciprocal relationships in expression of genes associated with osteoblast proliferation and differentiation during formation of the bone extracellular matrix. J Cell Physiol 143:420–430

Peterson DR, Heideger WJ, Beach KW (1985) Calcium homeostasis: the effect of parathyroid hormone on bone membrane electrical potential difference. Calcif Tissue Int 37:307–311

Prêle CM, Horton MA, Caterina P, Stenbeck G (2003) Identification of the molecular mechanisms contributing to polarized trafficking in osteoblasts. Exp Cell Res 282:24–34

Rubinacci A, Benelli FD, Borgo E, Villa I (2000) Bone as an ion exchange system: evidence for a pump-leak mechanism devoted to the maintenance of high bone K^+. Am J Physiol Endocrinol Metab 278:E15–E24

Rubinacci A, Covini M, Bisogni C, Villa I, Galli M, Palumbo C, Ferretti M, Muglia MA, Marotti G (2002) Bone as an ion exchange system: evidence for a link between mechanotransduction and metabolic needs. Am J Physiol Endocrinol Metab 282:E851–E864

Saitou M, Furuse M, Sasaki H, Schulzke JD, Fromm M, Takano H, Noda T, Tsukita S (2000) Complex phenotype of mice lacking occludin, a component of tight junction strands. Mol Biol Cell 11:4131–4142

Shu C, Li TY, Tsang LL, Fok KL, Lo PS, Zhu JX, Ho LS, Chung YW, Chan HC (2006) Differentiation of adult rat bone marrow stem cells into epithelial progenitor cells in culture. Cell Biol Int 30:823–828

Simon DB, Lu Y, Choate KA, Velazquez H, Al-Sabban E, Praga M, Casari G, Bettinelli A, Colussi G, Rodriguez-Soriano J, McCredie D, Milford D, Sanjad S, Lifton RP (1999) Paracellin-1, a renal tight junction protein required for paracellular Mg^{2+} resorption. Science 285:103–106

Trumbore DC, Heideger WJ, Beach KW (1980) Electrical potential difference across bone membrane. Calcif Tissue Int 32:159–168

Van Itallie CM, Anderson JM (2006) Claudins and epithelial paracellular transport. Annu Rev Physiol 68:403–429

Van Itallie C, Rahner C, Anderson JM (2001) Regulated expression of claudin-4 decreases paracellular conductance through a selective decrease in sodium permeability. J Clin Invest 107:1319–1327

Van Itallie CM, Fanning AS, Anderson JM (2003) Reversal of charge selectivity in cation or anion-selective epithelial lines by expression of different claudins. Am J Physiol Renal Physiol 285:F1078–F1084

Van Itallie CM, Rogan S, Yu A, Vidal LS, Holmes J, Anderson JM (2006) Two splice variants of claudin-10 in the kidney create paracellular pores with different ion selectivities. Am J Physiol Renal Physiol 291:F1288–F1299

Weinger JM, Holtrop ME (1974) An ultrastructural study of bone cells: the occurrence of microtubules, microfilaments and tight junctions. Calcif Tissue Res 14:15–29

Yu AS, Enck AH, Lencer WI, Schneeberger EE (2003) Claudin-8 expression in Madin–Darby canine kidney cells augments the paracellular barrier to cation permeation. J Biol Chem 278:17350–17359

Zhang X, Yang M, Lin L, Chen P, Ma KT, Zhou CY, Ao YF (2006) Runx2 overexpression enhances osteoblastic differentiation and mineralization in adipose-derived stem cells in vitro and in vivo. Calcif Tissue Int 79:169–178

Regulation of electrolyte transport across cultured endometrial epithelial cells by prolactin

Chatsri Deachapunya, Sutthasinee Poonyachoti[1] and Nateetip Krishnamra[2,3]

Department of Physiology, Faculty of Medicine, Srinakharinwirot University, Sukhumvit 23, Wattana, Bangkok 10110, Thailand
[1]Department of Physiology, Faculty of Veterinary Science, Chulalongkorn University, Henri-Dunant Road, Bangkok 10330, Thailand
[2]Department of Physiology and [3]Consortium for Calcium and Bone Research, Faculty of Science, Mahidol University, Rama VI Road, Bangkok 10400, Thailand
(Correspondence should be addressed to C Deachapunya; Email: chatsri@swu.ac.th)

Abstract

The effect of prolactin (PRL) on ion transport across the porcine glandular endometrial epithelial cells was studied in primary cell culture using the short-circuit current technique. Addition of 1 μg/ml PRL either to the apical solution or to the basolateral solution produced a peak followed by a sustained increase in Isc, but with a lesser response when PRL was added apically. Basolateral addition of PRL increased the Isc in a concentration-dependent manner with a maximum effect at 1 μg/ml and an effective concentration value of 120 ng/ml. The PRL-stimulated Isc was significantly reduced by pretreatment with an apical addition of 5-nitro-2-(3-phenylpropylamino) benzoic acid (200 μM), diphenylamine-2-carboxylic acid (1 mM) or 4,4′-diisothiocyanatostilbene-2,2′-disulfonic acid (200 μM), Cl^- channel blockers, but not by amiloride (10 μM), a Na^+ channel blocker. In addition, pretreatment with bumetanide (200 μM), a Na^+–K^+–$2Cl^-$ cotransporter inhibitor, in the basolateral solution significantly reduced the PRL-stimulated Isc. Replacement of Cl^- or HCO_3^- in the bathing solutions also decreased the Isc response to PRL. Pretreatment of the monolayer with AG490 (50 μM), an inhibitor of JAK2 activity significantly inhibited the PRL-induced increase in Isc. Western blot analysis of the porcine endometrial epithelial cells revealed the presence of short isoform of PRL receptor (PRLR-S) that could be regulated by 17β-estradiol. The results of this investigation showed that PRL acutely stimulated anion secretion across the porcine endometrial epithelial cells possibly through PRLR-S present in both apical and basolateral membranes. The PRL response appeared to be mediated by the JAK2-dependent pathway.

Journal of Endocrinology (2008) **197,** 575–582

Introduction

Endometrial epithelial cells play an important role in the regulation of fluid and electrolyte volume and composition within the uterine cavity, providing an optimal intrauterine environment for implantation and embryo development. The transport-related activities of the surface and glandular epithelial cells have been shown to be regulated by several hormones, growth factors, cytokines, and a number of signaling molecules. Electrophysiological studies of cultured human endometrial epithelial cells (Matthews *et al.* 1993) and the intact porcine endometrial epithelium (Vetter & O'Grady 1996) have provided direct evidence for the regulation of Na^+ absorption and K^+ secretion. In the primary culture of mouse and porcine endometrial epithelial cells, prostaglandins (PGs) especially PGE2, adrenaline, ATP, and UTP were found to activate anion secretion (Chan *et al.* 1997, Fong *et al.* 1998, Deachapunya & O'Grady 1998, Palmer-Densmore *et al.* 2002). These epithelial cells also exhibited Na^+ transport that was activated by insulin and insulin-like growth factor, and inhibited by epidermal growth factor (Deachapunya *et al.* 1999, Deachapunya & O'Grady 2001).

Prolactin (PRL) is synthesized and secreted from the anterior pituitary gland, as well as the extrapituitary tissues including myometrium, deciduas, and mammary epithelial cells (Freeman *et al.* 2000). It exerts a wide variety of biological actions, such as the regulation of water and electrolyte balance, growth of mammary gland, milk production, and secretion. Recently, PRL has been reported to stimulate the intestinal Ca^{2+} absorption (Jantarajit *et al.* 2007), especially under conditions of high calcium demand such as pregnancy and lactation (Charoenphandhu & Krishnamra 2007).

In human endometrium, PRL receptors (PRL-R) and its mRNA have been identified in glandular epithelial and stromal cells (Jabbour *et al.* 1998, Tseng & Zhu 1998). PRL-R belongs to the superfamily of the cytokine class-1 receptor (Kelly *et al.* 1991). Several isoforms, i.e. short, intermediate, and long isoforms and the soluble PRL-binding protein have been identified in many tissues (Clevenger & Kline 2001). Binding of PRL to its transmembrane receptors induces receptor

DOI: 10.1677/JOE-08-0077
0022-0795/08/0197–575 Online version via http://www.endocrinology-journals.org

dimerization, tyrosine phosphorylation, and activation of the JAK, which leads to phosphorylation of other associated regulatory proteins especially the STAT proteins. The phosphorylated STAT proteins dimerize and translocate to the nucleus to bind to the PRL-responsive genes, resulting in target gene transcription and biological responses. Other signaling pathways involving mitogen-activated protein kinase (MAPK), insulin-receptor substrate (IRS-1), phosphoinositide 3 (PI-3) kinase, PLC, PKC, and intracellular Ca^{2+} have also been reported to mediate PRL actions (Bole-Feysot *et al.* 1998, Gubbay *et al.* 2002).

Although PRL is known as an important regulator of water and electrolyte transport in lower vertebrates (Bern 1975, Sakamoto & McCormick 2006), there were very few reports on its transport-related effect in the mammalian epithelial cells. Several studies using the everted intestinal sac technique have demonstrated the stimulatory effect of PRL on fluid and NaCl absorption in the rat, hamster, and guinea pig jejunum, but not in guinea pig ileum or rat colon (Mainoya *et al.* 1974). In the rabbit mammary glands, PRL decreased epithelial membrane permeability to sucrose, suggesting a decrease in the permeability of the tight junction (Linzell *et al.* 1975). From the studies using the mouse mammary epithelial cells grown on floating collagen gels, PRL treatment for 3 days was found to increase the short-circuit current (Isc) and transepithelial potential difference (PD), which indicated an increase in net active Na^+ absorption, probably with some Cl^- secretion (Bisbee *et al.* 1979). In the mouse mammary epithelial cell line HC11, PRL acutely increased Cl^- transport through the JAK–STAT system (Selvaraj *et al.* 2000). Eventhough PRL seemed to play an important role in the regulation of transepithelial ion transport in a variety of epithelia, its effect on the ion transport function of the endometrial epithelium has not been investigated. Since we have previously shown that the primary cultured porcine endometrial epithelial cells possessed the transport machinery capable of Na^+ absorption and Cl^- secretion (Deachapunya & O'Grady 1998, Deachapunya *et al.* 1999), the objectives of the present study were to investigate the regulatory mechanism of PRL on the ion transport across these epithelial cells.

Materials and Methods

Materials

PRL, insulin, amiloride, 5-nitro-2-(3-phenylpropylamino) benzoic acid (NPPB), diphenylamine-2-carboxylic acid (DPC), 4,4′-diisothiocyanatostilbene-2,2′-disulfonic acid (DIDS), bumetanide, acetazolamide, PGE2, 8-chloro-phenylthio-3′,5′-cyclicmonophosphate (8cpt-cAMP), non-essential amino acids, and high-purity grade salts were obtained from Sigma Chemical Co. Dulbecco's modified Eagle's medium (DMEM), Dulbecco's PBS (DPBS), fetal bovine serum (FBS), collagenase (type 1), kanamycin, penicillin–streptomycin, and fungizone were purchased from Gibco (Grand Island, NY).

Cell isolation and culture

Porcine uterine tissues collected from 5- to 6-month-old pig were obtained from the Metropolitan slaughterhouse, Klongtoey, Bangkok, under the supervision of the Department of Livestock Development, Ministry of Agriculture and Cooperatives, Thailand. The tissue was placed in an ice-cold porcine Ringer solution containing (mM): 130 NaCl, 6 KCl, 3 $CaCl_2$, 0·7 $MgCl_2$, 20 $NaHCO_3$, 0·3 NaH_2PO_4, and 1·3 Na_2HPO_4 (pH 7·4). After removal of the serosal muscle layer, the tissue fragments were cut into small pieces and digested overnight with collagenase. The epithelial glands were then isolated as described previously (Deachapunya & O'Grady 1998), and suspended in DMEM supplemented with 3·7 g/l $NaHCO_3$, 10% FBS, 850 nM (5 μg/ml) insulin, 1% non-essential amino acid, 5 μg/ml fungizone, 100 U/ml penicillin, 100 μg/ml streptomycin, and 100 μg/ml kanamycin (standard media). They were then plated onto the cell culture dishes and incubated at 37 °C in a humidified atmosphere of 5%CO_2 in air. Culture medium was changed after 24 h and then every 2–3 days. After 80% confluence (within 2–3 days), the epithelial cells were subcultured onto 24 mm (4·5 cm^2) transparent permeable membrane filters (Costar, Cambridge, MA, USA). Using this method of isolation, the purity of epithelial cells was greater than 90% as assessed by staining the isolated cells with cytokeratin (Deachapunya & O'Grady 1998). Cell monolayers were fed every 2 days and maintained in the standard media for about 7 days before the beginning of the experiment.

Measurement of electrical parameters

Before studying ion transport, the transepithelial resistance of the cell monolayer was measured with an epithelial voltohmmeter (EVOM) coupled to Ag/AgCl 'chopstick' electrodes (World Precision Instruments, Serasota, FL, USA). Monolayer with high resistance ($\approx$3000 Ωcm^2) was then mounted in Ussing Chamber, bathed in both sides with the standard porcine Ringer solution, which was maintained at 37 °C and bubbled with 95%O_2–5%CO_2. Transepithelial PD and Isc were measured with the use of voltage-clamp circuitry (EVC-4000, World Precision Instruments) with Ag/AgCl electrodes connected to the bathing solution via agar bridges. Tissue conductance (G) was calculated using Ohm's law (G = Isc/PD). The monolayer was continuously short circuited, except for a brief interval of open-circuited readings for PD measurement before and after adding any chemical. Data from the voltage clamp were connected to a MacLab 4S A/D converter and recorded with a 400 MHz PowerPC Macintosh. After mounting, the cell monolayer was equilibrated for at least 20 min to achieve a stable Isc before addition of chemicals. Positive Isc corresponded to the movement of anions in the serosal to mucosal direction or the movement of cations in the mucosal to serosal direction or a combination of both. In the anion replacement experiments, gluconate salts were substituted for chloride

and HEPES were substituted for bicarbonate. The experiment under HCO_3^- free condition was performed in the presence of 100 μM acetazolamide and bubbled with 100% O_2.

Western blot analysis

Porcine endometrial epithelial cells seeded in the 100 mm cell culture dish were allowed to grow in the standard medium up to 80% confluence. In some experiments, the medium was switched to the serum-free and phenol red-free DMEM alone or supplemented with 10^{-8} M 17β-estradiol for 48 h. Cells were then harvested and suspended in lysis buffer containing 50 mM Tris–HCl, 1% NP-40, 0·25% sodium deoxycholate, 150 mM NaCl, 1 mM EGTA, 1 mM phenylmethylsulfonyl fluoride, 20 μg aprotinin, and 1 mM NaF (pH 7·4). The supernatant was collected and protein concentrations were determined using the BCA protein assay kit (Pierce Biotechnology, Inc., Rockford, IL, USA). Protein samples (20 μg) were separated by 10% SDS-PAGE and electrically transferred to a polyvinylidene difluoride membrane (Hybond-P, Amersham Biosciences) in Tris–glycine buffer. Blotted membranes were washed and then blocked with 5% nonfat powdered milk in Tris-buffered saline for 4 h at room temperature with constant agitation. The membrane was incubated overnight at 4 °C with 1 μg/ml primary antibody, which is anti-rat PRL receptor monoclonal antibody generated against the extracellular domain of PRL receptor (clone U5, Affinity BioReagents). The membrane was then washed and incubated for 1 h at room temperature with a 1:10 000 horseradish peroxidase (HRP)-conjugated goat anti-mouse secondary antibody (Zymed Laboratories Inc., San Francisco, CA, USA). After washing, the immunoreactive protein bands were visualized using the enhanced chemiluminescence (ECL) detection system (Santa Cruz Biotechnology Inc., Santa Cruz, CA, USA) according to the manufacturer's instructions. The membranes were exposed to film (Hyperfilm-ECL, Amersham Biosciences) for adequate duration to visualize the chemiluminescent bands. To confirm equal loading, the membranes were stripped and reprobed with a 1:300 000 anti-β-actin monoclonal antibody (clone AC-15, Sigma Co.) followed by a 1:10 000 HRP-conjugated anti-mouse antibody. The intensity of the protein bands was determined using densiotometry analysis (Scion Image; Scion Cooperation, Frederick, MD, USA). Band intensity of the PRL-R from each treatment was normalized to the β-actin intensity and expressed as the PRL-R/β-actin ratio.

Data analyses

All values are presented as mean ± S.E.M. and n is the number of monolayers from at least three different uterine tissue cultures. The differences between control and experimental means were analyzed using a Student's t-test or ANOVA where appropriate. The difference between treatment and control means following a significant ANOVA was identified by Dunnett's test (Prism 3.0, GraphPad Software, Inc., San Diego, CA, USA). A value of $P<0·05$ was considered statistically significant. The effective concentration (EC_{50}) value was determined using a four-parameter logistic function to fit the data (Prism 3.0; GraphPad Software Inc.).

Results

Effect of PRL on Isc

Under basal condition, after an equilibrating period of 30 min, the porcine endometrial epithelial monolayer exhibited average Isc, PD (lumen negative), and tissue conductance of 30·68 ± 2·49 μA, −27·22 ± 3·89 mV, and 1·47 ± 0·25 mS ($n=17$) respectively. Addition of 1 μg/ml PRL to the apical or basolateral solution produced an increase in Isc that reached a peak within 2–3 min before decreasing slightly and was maintained at a level above baseline (Fig. 1A). In some experiments, the PRL-stimulated Isc gradually decreased to the baseline level. The peak Isc response to apical addition of 1 μg/ml PRL was 3·45 ± 0·94 μA ($n=4$), while the subsequent basolateral addition of 1 and 5 μg/ml PRL led

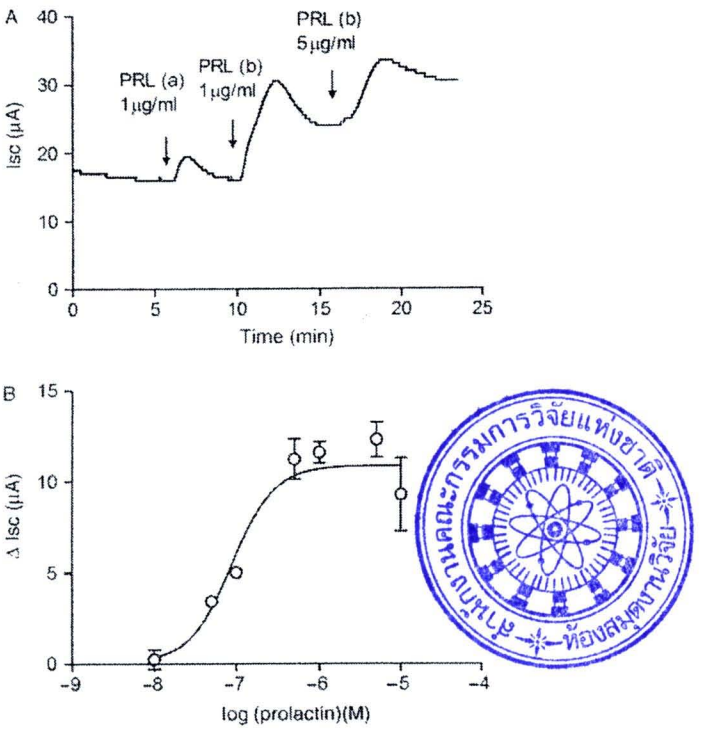

Figure 1 Effect of PRL on the basal Isc in the endometrial epithelial monolayers. (A) A representative Isc tracing responded to an addition of 1 μg/ml PRL to (a) the apical solution followed by 1 and 5 μg/ml PRL added to (b) the basolateral solution. (B) Concentration–response relationships showing the increase in Isc following basolateral treatment with various concentrations of PRL. The EC_{50} value was 120 ng/ml ($n=6$).

to a peak Isc of 11·00±0·98 μA (n=17) and 14·36±1·37 μA (n=12) respectively. Basolateral addition of PRL increased the Isc in a concentration-dependent manner with a maximum response with 1 μg/ml PRL and a half maximum EC_{50} value of 120 ng/ml (n=6, Fig 1B).

Ionic basis of the PRL-stimulated Isc

To determine the ionic basis of the Isc response induced by PRL, we examined the effect of PRL in the presence of pharmacological ion channel blockers and ion substitution solutions. An apical application of the Na^+ channel blocker amiloride at 10 μM inhibited the basal Isc by 35% (Fig. 2A). However, it did not affect the Isc response induced by PRL (1 μg/ml), which was 12·21±1·39 μA (n=5), when compared with the control value of 11·44±1·22 μA (n=12) (Fig. 2E). By contrast, the PRL-stimulated Isc was significantly decreased in the presence of Cl^- channel blockers, NPPB, DPC, and DIDS in the apical solution. NPPB and DPC have been widely used to block CFTR,

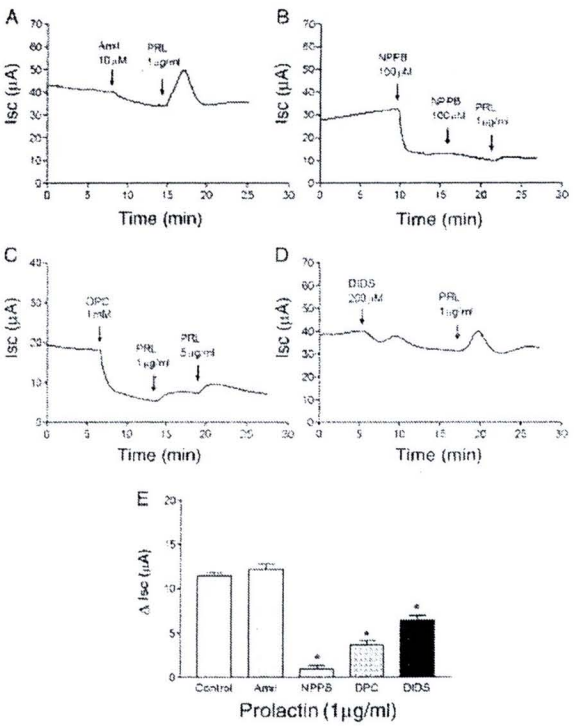

Figure 2 Effect of ion channel blockers on the PRL-stimulated Isc. (A) A representative Isc tracing showing that an apical addition of amiloride (Amil, 10 μM) produced a small decrease in basal Isc. A subsequent addition of PRL (1 μg/ml) into the basolateral solution produced an increase in Isc. (B) An apical addition of NPPB (100 μM), (C) DPC (1 mM), or (D) DIDS (200 μM) decreased the basal Isc and reduced the PRL response. (E) Bar graph illustrating the average maximal increases in Isc response produced by prolactin alone (control) and in the presence of amiloride, NPPB, DPC, or DIDS. Values represent means±S.E.M. *P<0·01 when compared with the control value by ANOVA.

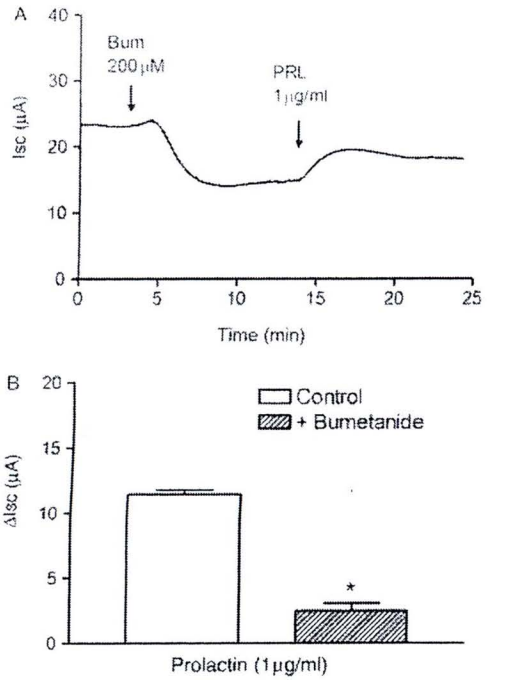

Figure 3 Effect of Na^+–K^+–$2Cl^-$ cotransporter blockers on the PRL-stimulated Isc. (A) A representative Isc tracing showing that a basolateral addition of bumetanide (200 μM) produced a decrease in basal Isc. A subsequent addition of PRL (1 μg/ml) into the basolateral solution produced a slightly increase in Isc. (B) Bar graph illustrating the average maximal increases in Isc response produced by prolactin alone (control) and in the presence of bumetanide. Values represent means±S.E.M. *P<0·01 when compared with the control value by Student's t-test.

whereas DIDS blocks the Ca^{2+}-activated Cl^- channels with no effect on the activity and conductance of CFTR (Anderson *et al.* 1992). As shown in Fig. 2B and C, pretreatment with 100 μM NPPB or 1 mM DPC reduced the basal Isc by 60 and 75% and decreased the Isc response to PRL to 1·00±0·71 μA (n=4) and 3·65±0·95 μA (n=5) respectively. An apical addition of 200 μM DIDS reduced the basal Isc by 17% and reduced the Isc response to PRL to 6·43±1·20 μA (n=4) (Fig. 2D). In addition, pretreatment with 200 μM bumetanide, a Na^+–K^+–$2Cl^-$ cotransporter inhibitor, in the basolateral solution abolished most of the PRL-induced increase in Isc from 11·44±1·22 μA (n=12) to 2·48±1·17 μA (P<0·01, n=4) (Fig. 3). Replacement of Cl^- or HCO_3^- in both the apical and the basolateral solutions markedly reduced the maximal Isc response to 1 μg/ml PRL to 1·63±1·06 μA (n=5) and 0·9±0·3 μA (n=3) respectively (Fig. 4).

Intracellular signaling pathways of PRL-induced increase in Isc

The major signaling pathway involved in PRL action is the JAK–STAT pathway which was shown to mediate Cl^-

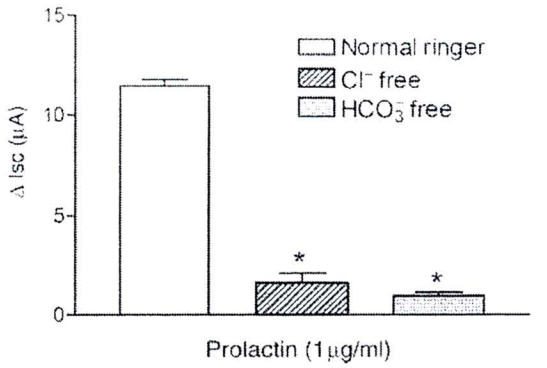

Figure 4 Effects of anion substitution on the maximal Isc response to PRL. In standard Ringer's solution, PRL (1 μg/ml) produced a mean increase in Isc of 11·44±1·22 μA (n=12). Replacement of Cl^- and HCO_3^- in both the apical and basolateral solutions significantly inhibited the maximal Isc response to PRL by 86% (n=4) and 92% (n=4) respectively. *P<0·01 when compared with the control value by ANOVA.

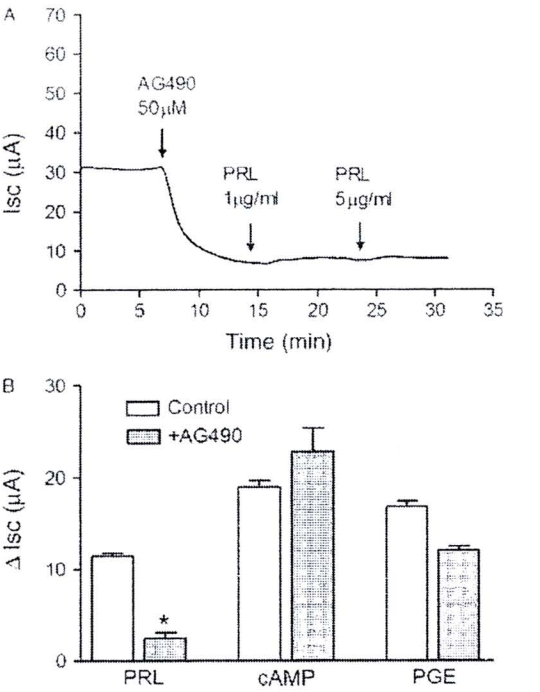

Figure 5 Effect of JAK2 activity inhibitor on the PRL-stimulated Isc. (A) A representative Isc tracing showing that an addition of AG490 (50 μM), an inhibitor of JAK2 activity, to both apical and basolateral solutions completely inhibited both basal and PRL-induced increase in Isc. (B) Bar graph illustrating the average maximal increases in Isc response produced by PRL (1 μg/ml), 8cpt-cAMP (cAMP, 100 μM), or prostaglandin E_2 (PGE, 3 μM) in the absence and presence of AG490 (50 μM). Values represent means ±S.E.M. *P<0·01 when compared with the corresponding control value by Student's t-test.

secretion in the mammary cell line, HC11 (Selvaraj *et al.* 2000). Phosphorylations of JAK2, STAT1, and STAT5 have been demonstrated in response to PRL stimulation (200 ng/ml) in human endometrium (Jabbour *et al.* 1998). To determine whether JAK2 was involved in the PRL-induced increase in Isc, we examined the effect of AG490, an inhibitor of JAK2 activity, on PRL action. As shown in Fig 5A, pretreatment with 50 μM AG490, added to both the basolateral and apical solutions, reduced the basal Isc by 55% from 26·21±4·99 to 11·75±4·01 μA (P<0·01, n=5). Sequential additions of 1 and 5 μg/ml PRL slightly increased the Isc response by 3·70±3·09 and 0·80±0·66 μA (n=5) respectively. However, the presence of AG490 did not affect the Isc response to 100 μM 8cpt-cAMP, which was 22·80±2·14 μA (n=4) when compared with the control value of 18·99±1·59 μA (n=5), but slightly decreased the Isc response to 3 μM PGE2 to 12·08±0·87 μA (n=4), which was not statistically significant from that of control (16·84±1·55 μA, n=7, Fig. 5B).

Expression of PRL receptor

To confirm the functional significance of PRL in the regulation of ion transport, the expression of PRL-R was determined using western blot analysis. A representative western blot as presented in Fig. 6A demonstrated the presence of proteins with an approximate molecular mass of 36 kDa in porcine endometrial epithelial cells as well as in the human mammary gland cancer cell MCF-7 and human endometrial cancer cell RL-95. The 36 kDa protein band corresponded to the short form of PRL-R. Replacement of the standard medium of the endometrial epithelial cells with the serum-free and phenol red-free medium reduced the expression of the protein, whereas addition of 17β-estradiol (10^{-8} M) in the serum-free medium up-regulated the PRL protein expression. Based on the densitometry analysis, the PRL-R/β-actin ratio was significantly decreased from 5·67±0·79 in the standard medium to 1·15±0·09 (P<0·05, n=4) in the serum-free medium. Treatment with 17β-estradiol increased the PRL-R/β-actin ratio by twofold to 2·35±0·12.

Discussion

A previous study in mouse mammary epithelial cells demonstrated that the PRL-induced increase in Isc was predominately mediated by Na^+ absorption (Mainoya *et al.* 1974). However, in another study in the mouse mammary epithelial cell line HC11, it was Cl^- transport that was acutely stimulated by PRL (Selvaraj *et al.* 2000). Using cultured porcine endometrial epithelial cells that possessed the machinery for Na^+ and Cl^- transports, we showed that PRL acutely stimulated anion secretion without affecting Na^+ absorption. This was further supported by the findings that the PRL-induced increase in Isc was blocked by Cl^- channel

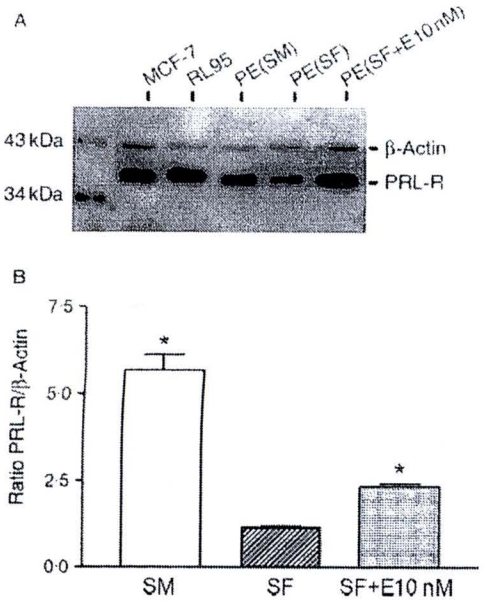

Figure 6 Expression of PRL receptor protein in porcine endometrial epithelial cells. (A) Western blot analysis of PRL receptor (PRL-R). A 36 kDa band of PRL-R was detected in human mammary gland cancer cell MCF-7, human endometrial cancer cell RL-95, and porcine endometrial epithelial cells (PE) under standard medium (SM), serum-free medium (SF) alone, or supplemented with 10^{-8} M 17β-estradiol (SF+E 10 nM). The internal control of 43 kDa band of β-actin was also detected in all samples. (B) Bar graph illustrating the ratio of PRL-R to β-actin protein expression in the endometrial epithelial cells, based on the densitometry of immunoblots obtained from SM, SF, and SF+E10 nM ($n=4$). Values represent means ± S.E.M. *$P<0{\cdot}05$ when compared with the serum-free medium condition by Student's *t*-test.

blockers, NPPB, DPC, and DIDS, but not by Na^+ channel blocker, amiloride. In addition, the basolateral pretreatment with bumetanide, a blocker of Na^+–K^+–$2Cl^-$ cotransporter, or replacement of Cl^- or HCO_3^- significantly inhibited the PRL-stimulated Isc. PRL added to the basolateral solution of the high-resistance monolayer produced a greater increase in the Isc response than when added to the apical solution, suggesting that PRL receptors were predominately located at the basolateral membrane. Western blot analysis revealed the expression of a 36 kDa protein band, which corresponded to the short form of PRL-R, indicating the role of this PRL receptor isoform in the mediation of transepithelial anion secretion in the porcine endometrial epithelium.

The basal electrical properties of cultured epithelial cells used in the present study have been described previously (Deachapunya & O'Grady 1998). Under the basal condition, these cells exhibited substantial Isc that was due to a greater Cl^- secretion than Na^+ absorption. Application of PRL produced a concentration-dependent increase in the anion transport with a maximal effect seen at 1 μg/ml PRL and an EC_{50} value of 120 ng/ml. In addition, the maximal PRL response observed within 3–5 min after application, implied a non-genomic action. At PRL concentration of 1 μg/ml, which could be considered a hyperprolactinemic level, PRL was also found to maximally stimulate Cl^- transport in the mammary epithelial HC11 cells (Selvaraj *et al.* 2000). This effective concentration of PRL was comparable with the circulating levels during pregnancy and lactation in the human and the rat (Handwerger & Freemark 1987, Arbogast & Voogt 1998). Like in many other epithelia, Cl^- secretion across the endometrial epithelial cells requires activation of the apical membrane Cl^- channels and the basolateral membrane K^+ channels with the basolateral Na^+–K^+–$2Cl^-$ cotransporters serving as the Cl^- loading step. Since two types of Cl^- channels, cAMP-activated cystic fibrosis transmembrane conductance regulator (CFTR) and Ca^{2+}-activated Cl^- channels have been identified in a variety of epithelia including endometrial epithelial cells (Deachapunya & O'Grady 1998, Palmer-Densmore *et al.* 2002), NPPB and DPC, inhibitors of anion channels including CFTR, and DIDS, an inhibitor of Ca^{2+}-activated Cl^- channels, were used to elucidate PRL action. As the present results showed that the PRL-induced increase in Isc was nearly completely inhibited by DPC and NPPB, it was most likely that CFTR was the primary target of the PRL-stimulated Cl^- secretion. However, the 40% inhibition of the PRL-stimulated Isc by DIDS indicated that the Ca^{2+}-activated Cl^- channels may also be partially involved in the PRL activation of Cl^- secretion. In addition, the PRL-stimulated increase in Isc was also diminished by bumetanide, an inhibitor of Na^+–K^+–$2Cl^-$ cotransporter, which was not surprising since the bumetanide-sensitive Cl^- uptake probably served as the Cl^- loading step for PRL-stimulated Cl^- secretion. The finding that Isc response to PRL was abolished in the Cl^-free solution further confirmed the PRL activation of Cl^- secretion. Since the electronic HCO_3^- secretion used the cAMP- and Ca^{2+}-activated Cl^- channels (Illek *et al.* 1999), a marked reduction of Isc response to PRL in the HCO_3^- free solution suggested a substantial contribution of HCO_3^- to the PRL-induced increase in Isc. Altogether, the results suggest a possible involvement of Cl^- – HCO_3^- exchangers as well as Na^+ – Na^+ – HCO_3^- cotransporters in the PRL-dependent HCO_3^- secretion. However, it was noted that the replacement of HCO_3^- itself, could have produced the intracellular acidification, which could affect the transport pathways or the signaling mechanisms that regulate anion secretion. Taken together, it could be stated that PRL-induced anion secretion by stimulating the apical Cl^- efflux through CFTR as the major channel type and through some Ca^{2+}-activated Cl^- channels, concurrently with the increase in the basolateral Cl^- uptake through the bumetanide-sensitive Na^+–K^+–$2Cl^-$ cotransporter. Although not being investigated in this study, the basolateral K^+ channels that provide the driving force for Cl^- exit across the apical membrane, could also be a target of PRL action, and are subject to further investigation.

Several signaling pathways mediating the multiple actions of PRL have been demonstrated in a variety of tissues with the

JAK–STAT pathway being most extensively studied. Previous evidence of the phosphorylation of JAK2, STAT1, and STAT5 in response to PRL stimulation in the human endometrium (Jabbour *et al.* 1998) and the PRL-stimulated Cl^- transport through the JAK2 cascade pathway in mouse mammary epithelial cell line HC11 (Selvaraj *et al.* 2000) suggested that JAK2 is a likely mediator of PRL-stimulating effect on the anion transport in the porcine endometrial epithelial cells. In the present study, pretreatment with AG490, an inhibitor of JAK2 activity inhibited both the basal Isc and the PRL-induced increase in Isc. Regarding the basal Isc, since the basal Isc of the cultured porcine endometrial epithelial cells has been shown to be generated mainly by Cl^- secretion (Deachapunya & O'Grady 1998), the fact that AG490 could inhibit the basal Isc within 10 min suggested that a constitutive JAK2 activity was responsible for the basal active Cl^- secretion. Although no direct association between JAK2 activity and Cl^- transport mechanism has been reported, the fact that tyrosine-phosphorylated proteins could regulate the basal Cl^- secretion in human colonic epithelial cell line, T84 (Uribe *et al.* 1996) suggested that the JAK2 inhibitors inhibited Cl^- secretion by interfering with the tyrosine phosphorylation of the regulatory transport proteins. Furthermore, based on the findings that i) Cl^- secretion could still be activated by 8cpt-cAMP in the presence of JAK2 inhibitor, ii) the inhibition of the basal Isc did not affect the PGE2-stimulated Isc response, and iii) the PGE2-stimulated Cl^- secretion was via the cAMP-dependent pathway (Deachapunya & O'Grady 1998), it is likely that the cAMP-dependent Cl^- secretion did not involve JAK2 pathway.

In contrast to the PGE2-stimulated Cl^- secretion, the PRL-stimulated Cl^- secretion was probably mediated by the JAK2 pathway because the PRL-induced increase in Isc was significantly inhibited by AG490. These findings were consistent with a report of AG490 blocking phosphorylation of STAT5 and PRL-induced Cl^- secretion, but not the PGE1-induced Cl^- secretion in mouse mammary cell line (Selvaraj *et al.* 2000). The effect of AG490 was more specific to PRL action, since tyrosine kinase inhibitor genistein had no effect on the PRL-stimulated Isc (data not shown).

PRL-R and its mRNA have been identified in human glandular epithelial and stromal cells (Jabbour *et al.* 1998, Tseng & Zhu 1998). Two isoforms of PRL-R, short and long, have been identified in several rat tissues including liver, ovary, thymus, and spleen (Gunes & Mastro 1996, Telleria *et al.* 1997). In the present study, we examined the expression of PRL-R protein in the endometrial epithelial cells by western blot analysis. The monoclonal antibody used in the present study detected protein with molecular mass of about 36 kDa, which corresponded to the short form of the PRL-R, similar to the predominant short isoforms expressed in the rat spleen and brain (Shingo *et al.* 2003). By contrast, the long form of PRL-R is the major receptor isoforms in the rat liver and mammary gland (Jahn *et al.* 1991, Selvaraj *et al.* 2000). Although at least two isoforms of PRL-R mRNA have been found in the reproductive tissues (Telleria *et al.* 1997), the present data indicated that the short form PRL-R was the functional PRL-R in the porcine endometrial epithelial cells, and that the PRL-stimulated Cl^- secretion in the porcine endometrial epithelial cells was mediated through the short form of PRL receptors located predominately at the basolateral membrane.

Generally, PRL is synthesized by the decidualized endometrial stromal cells during the late secretory phase of the menstrual cycle and throughout pregnancy. The level of PRL is apparently much higher in the blood and amniotic fluid during pregnancy (Golander *et al.* 1978, Daly *et al.* 1983). After conception, a continuous increase in PRL production in the decidual cells leads to an accumulation of PRL in the amniotic fluid up to 2–3 μg/ml (Golander *et al.* 1978, Daly *et al.* 1983). Concomitantly, the PRL receptor expression and its mRNA are up-regulated toward the secretory phase of the menstrual cycle (Jabbour *et al.* 1998, Jones *et al.* 1998) and maintained throughout pregnancy (Maaskant *et al.* 1996). The level of PRL receptor mRNA is much higher in the glandular cells than in the stromal cells (Jabbour *et al.* 1998, Jones *et al.* 1998). Although the exact role of PRL in the human endometrium remains to be clarified, the pattern of secretion and expression supports a role of PRL in implantation and placentation. In agreement with those reports, the presence of PRL-R protein that was up-regulated by 17β-estradiol (Fig. 6) in the cultured porcine endometrial epithelial cells strongly suggested the physiological role of PRL in pregnancy. This speculation was consistent with the report that the blastocyst implantation and the maintenance of pregnancy were impaired in the PRL and PRL-R knockout mice (Jikihara *et al.* 1996). The next question is what is the exact role of PRL in the pregnant uterus. It is known that specific concentrations of electrolytes and pH within the uterine lumen are important for implantation and embryo development. In the rhesus monkey, PRL has been shown to regulate the amniotic and fetal extracellular fluid and electrolyte balance by decreasing the water flux from the amniotic side of the fetal membrane (Josimovich *et al.* 1977). Concomitant with the present finding of PRL role in the stimulation of anion secretion across the endometrial epithelial cells, and that active secretion of Cl^- and HCO_3^- provides the driving force for fluid secretion and the regulation of luminal fluid pH, it is likely that PRL exerts endocrine and paracrine actions to regulate the volume and composition of the fluid within the uterine cavity, thus providing an optimal condition for implantation and development of the embryo.

In conclusion, this study shows for the first time the regulation of the transepithelial anion secretion by PRL in the endometrium. The results showed that PRL acutely stimulated anion secretion across the porcine endometrial epithelial cells through the short isoform of PRL receptor and the JAK–STAT-dependent pathway. The PRL-stimulated anion secretion was mostly a result of the activation of DPC- and NPPB-sensitive Cl^- channels, and bumetanide-sensitive Na^+–K^+–$2Cl^-$ cotransport. Further investigation is required to define the physiological and pharmacological significance of PRL action in the endometrium. In addition, the PRL-signaling mechanisms, i.e. intracellular Ca^{2+}, cAMP, or other signaling molecules remain to be elucidated.

Acknowledgements

The authors wish to thank Miss Norathee Buathong for her help with primary cell preparation and some of the experiments, and Dr Narattaphol Charoenphandhu for his valuable comments of the manuscript. This work was fully supported by the Thailand Research Fund (Contract grant number: TRA4780008) awarded to N M. The authors declare that there is no conflict of interest that would prejudice the impartiality of this scientific work.

References

Anderson MP, Sheppard DN, Berger HA & Welsh MJ 1992 Chloride channels in the apical membrane of normal and cystic fibrosis airway and intestinal epithelia. *American Journal of Physiology* **263** L1–L14.

Arbogast LA & Voogt JL 1998 Endogenous opioid peptides contribute to suckling-induced prolactin release by suppressing tyrosine hydroxylase activity and messenger ribonucleic acid levels in tuberoinfundibular dopaminergic neurons. *Endocrinology* **139** 2857–2862.

Bern HA 1975 Prolactin and osmoregulation. *American Zoologists* **15** 937–949.

Bisbee CA, Machen TE & Bern HA 1979 Mouse mammary epithelial cells on floating collagen gels: transepithelial ion transport and effects of PRL. *PNAS* **76** 536–540.

Bole-Feysot C, Goffin V, Edery M, Binart N & Kelly PA 1998 Prolactin (PRL) and its receptor: actions, signal transduction pathways and phenotypes observed in PRL receptor knockout mice. *Endocrine Reviews* **19** 225–268.

Chan HC, Liu CQ, Fong SK, Law SH, Wu LJ, So E, Chung YW, Ko WH & Wong PYD 1997 Regulation of Cl^- secretion by extracellular ATP in cultured mouse endometrial epithelium. *Journal of Membrane Biology* **156** 45–52.

Charoenphandhu N & Krishnamra N 2007 Prolactin is an important regulator of intestinal calcium transport. *Canadian Journal of Physiology and Pharmacology* **85** 569–581.

Clevenger CV & Kline JB 2001 Prolactin receptor signal transduction. *Lupus* **10** 706–718.

Daly DC, Maslar IA & Riddick DH 1983 Prolactin production during *in vitro* decidualization of proliferative endometrium. *American Journal of Obstetrics and Gynecology* **145** 672–678.

Deachapunya C & O'Grady SM 1998 Regulation of chloride secretion across porcine endometrial epithelial cells by prostaglandin E_2. *Journal of Physiology* **508** 31–47.

Deachapunya C & O'Grady SM 2001 EGF regulates the transition from basal sodium absorption to anion secretion in cultured endometrial epithelial cells. *Journal of Cell Physiology* **186** 243–250.

Deachapunya C, Palmer-Densmore M & O'Grady SM 1999 Insulin stimulates transepithelial sodium transport by activation of a protein phosphatase that increases Na-K ATPase activity in endometrial epithelial cells. *Journal of General Physiology* **114** 561–574.

Fong SK, Liu CQ & Chan HC 1998 Cellular mechanisms of adrenaline-stimulated anion secretion by the mouse endometrium epithelium. *Biology of Reproduction* **59** 1342–1348.

Freeman ME, Kanyicsky B, Lerant A & Nagy G 2000 Prolactin: structure, function, and regulation of secretion. *Physiological Reviews* **80** 1523–1631.

Golander A, Hurley T, Barrett J, Hizi A & Handwerger S 1978 Prolactin synthesis by human chorion decidual tissue: a possible source of prolactin in the amniotic fluid. *Science* **202** 311–313.

Gubbay O, Critchley HOD, Bowen JM, King A & Jabbour HN 2002 Prolactin induces ERK phosphorylation in epithelial and CD56+ natural killer cells of the human endometrium. *Journal of Clinical Endocrinology and Metabolism* **87** 2329–2335.

Gunes H & Mastro AM 1996 Prolectin receptor gene expression in rat splenocytes and thymocytes from birth to adulthood. *Molecular and Cellular Endocrinology* **117** 41–52.

Handwerger S & Freemark M 1987 Role of placental lactogen and prolactin in human pregnancy. *Advances in Experimental Medicine and Biology* **219** 399–420.

Illek B, Tam AW, Fischer H & Machen TE 1999 Anion selectivity of apical membrane conductance of Calu 3 human airway epithelium. *Pflügers Archiv* **437** 812–822.

Jabbour HN, Critchley HO & Boddy SC 1998 Expression of functional prolactin receptors in nonpregnant human endometrium: janus kinase-2, signal transducer and activator of transcription-1 (STAT1), and STAT5 proteins are phosphorylated after stimulation with prolactin. *Journal of Clinical Endocrinology and Metabolism* **83** 2545–2553.

Jahn GA, Edery M, Belair L, Kelly PA & Djiane J 1991 Prolactin receptor gene expression in rat mammary gland and liver during pregnancy and lactation. *Endocrinology* **128** 2976–2984.

Jantarajit W, Thongon N, Pandaranandaka J, Teerapornpuntakit J, Krishnamra N & Charoenphandhu N 2007 Prolactin-stimulated transepithelial calcium transport in duodenum and Caco-2 monolayer are mediated by the phosphoinositide 3-kinase pathway. *American Journal of Physiology. Endocrinology and Metabolism* **293** 372–384.

Jikihara H, Kessler CA, Cedars MI & Bra AK 1996 Up-regulation of the human prolactin receptor in the endometrium. *Journal of Endocrinology* **5** 157–162.

Jones RL, Critchley HO, Brooks J, Jabbour HN & McNeilly AS 1998 Localization and temporal expression of prolactin recptor in human endometrium. *Journal of Clinical Endocrinology and Metabolism* **83** 258–262.

Josimovich JB, Merisko K & Boccella L 1977 Amniotic prolactin control over amniotic and fetal extracellular fluid water and electrolytes in the rhesus monkey. *Endocrinology* **100** 564–570.

Kelly PA, Djiane J, Postel-Vinay MC & Edery M 1991 The prolactin/growth hormone receptor family. *Endocrine Reviews* **12** 235–251.

Linzell JL, Peaker M & Taylor JC 1975 The effects of prolactin and oxytocin on milk secretion and on the permeability of the mammary epithelium in the rabbit. *Journal of Physiology* **253** 547–563.

Maaskant RA, Bogic LV, Gilger S, Kelly PA & Bryant-Greenwood GD 1996 The human prolactin receptor in the fetal membranes, decidua, and placenta. *Journal of Clinical Endocrinology Metabolism* **81** 396–405.

Mainoya JR, Bern HA & Regan JW 1974 Influence of ovine prolactin on transport of fluid and sodium chloride by the mammalian intestine and gall bladder. *Journal of Endocrinology* **63** 311–317.

Matthews CJ, Thomas EJ, Redfern CPF & Hirst BH 1993 Ion transport by human endometrium *in vitro*. *Human Reproduction* **8** 1510–1575.

Palmer-Densmore M, Deachapunya C & O'Grady SM 2002 UTP-dependent inhibition of Na absorption requires activation of PKC in endometrial epithelial cells. *Journal of General Physiology* **120** 897–906.

Sakamoto T & McCormick SD 2006 Prolactin and growth hormone in fish osmoregulation. *General and Comparative Endocrinology* **147** 24–30.

Selvaraj NG, Omi E, Gibori G & Rao MC 2000 Janus kinase 2 (JAK2) regulates prolactin-mediated chloride transport in mouse mammary epithelial cells through tyrosine phosphorylation of Na^+–K^+–$2Cl^-$ cotransporter. *Molecular Endocrinology* **14** 2054–2065.

Shingo T, Gregg C, Enwere E, Fujikawa H, Hassam R, Geary C, Cross JC & Weiss S 2003 Pregnancy-stimulated neurogenesis in the adult female forebrain mediated by prolactin. *Science* **299** 117–120.

Telleria CM, Parmer TG, Zhong L, Clarke DL, Albarracin CT, Duan WR, Linzer DI & Gibori G 1997 The different forms of the prolactin receptor in the rat corpus luteum: developmental expression and hormonal regulation in pregnancy. *Endocrinology* **138** 4812–4820.

Tseng L & Zhu HH 1998 Progestin induces prolactin receptor in human endometrial stromal cells. *Journal of the Society for Gynecologic Investigation* **5** 149–155.

Uribe JM, Keely SJ, Traynor-Kaplan AE & Barrett KE 1996 Phosphatidyl-inositol 3-kinase mediates the inhibitory effect of epidermal growth factor on calcium-dependent chloride secretion. *Journal of Biological Chemistry* **271** 26588–26595.

Vetter AE & O'Grady SM 1996 Mechanisms of electrolyte transport across the endometrium I. Regulation by PGF2 and cAMP. *American Journal of Physiology. Cell Physiology* **270** 663–672.

Received in final form 29 March 2008
Accepted 4 April 2008
Made available online as an Accepted Preprint
4 April 2008

Am J Physiol Cell Physiol 294: C1158–C1168, 2008.
First published March 19, 2008; doi:10.1152/ajpcell.00020.2008.

Prolactin stimulates transepithelial calcium transport and modulates paracellular permselectivity in Caco-2 monolayer: mediation by PKC and ROCK pathways

Narongrit Thongon,[1] La-iad Nakkrasae,[2] Jirawan Thongbunchoo,[2] Nateetip Krishnamra,[1,2] and Narattaphol Charoenphandhu[1,2]

[1]*Department of Physiology and* [2]*Consortium for Calcium and Bone Research, Faculty of Science, Mahidol University, Bangkok, Thailand*

Submitted 15 January 2008; accepted in final form 18 March 2008

Thongon N, Nakkrasae L-I, Thongbunchoo J, Krishnamra N, Charoenphandhu N. Prolactin stimulates transepithelial calcium transport and modulates paracellular permselectivity in Caco-2 monolayer: mediation by PKC and ROCK pathways. *Am J Physiol Cell Physiol* 294: C1158–C1168, 2008. First published March 19, 2008; doi:10.1152/ajpcell.00020.2008.—Prolactin (PRL) was previously demonstrated to rapidly enhance calcium absorption in rat duodenum and the intestine-like Caco-2 monolayer. However, its mechanism was not completely understood. Here, we investigated nongenomic effects of PRL on the transepithelial calcium transport and paracellular permselectivity in the Caco-2 monolayer by Ussing chamber technique. PRL increased the transcellular and paracellular calcium fluxes and paracellular calcium permeability within 60 min after exposure but decreased the transepithelial resistance of the monolayer. The effects of PRL could not be inhibited by RNA polymerase II inhibitor (5,6-dichloro-1-β-D-ribobenzimidazole), confirming that PRL actions were nongenomic. Exposure to protein kinase C (PKC) or RhoA-associated coiled-coil forming kinase (ROCK) inhibitors (GF-109203X and Y-27632, respectively) abolished the stimulatory effect of PRL on transcellular calcium transport, whereas ROCK inhibitor, but not PKC inhibitor, diminished the PRL effect on paracellular calcium transport. Knockdown of the long isoform of PRL receptor (PRLR-L) also prevented the enhancement of calcium transport by PRL. In addition, PRL markedly increased paracellular sodium permeability and the permeability ratio of sodium to chloride, which are indicators of the paracellular charge-selective property and are known to be associated with the enhanced paracellular calcium transport. The permeability of other cations in the alkali metal series was also increased by PRL, and such increases were abolished by ROCK inhibitor. It could be concluded that PRL stimulated transepithelial calcium transport through PRLR-L and increased paracellular permeability to cations in the Caco-2 monolayer. These nongenomic actions of PRL were mediated by the PKC and ROCK signaling pathways.

charge selectivity; dilution potential; paracellular transport; phosphoinositide 3-kinase; protein kinase C; long form of prolactin receptor; RhoA; short interference RNA; transcellular transport

DURING PREGNANCY and lactation, prolactin (PRL) is a calcium-regulating hormone that mitigates negative calcium balance by increasing intestinal calcium absorption (10). In vivo studies in normal rats suggested that PRL stimulated both transcellular active and paracellular passive calcium transport in the duodenum and proximal jejunum (10, 33). Exposure to high physiological levels of PRL of 400–600 ng/ml, which are comparable to the levels attained during lactation and suckling (2), rapidly enhanced transepithelial calcium transport in isolated duodenal epithelium and intestine-like Caco-2 monolayer in a dose-dependent manner (25). However, the signaling pathways of PRL in the intestinal absorptive cells and the detailed mechanisms of the PRL-enhanced calcium transport were not completely understood.

Calcium traverses the intestinal epithelium via both transcellular and paracellular pathways (22). Transcellular active calcium transport is a metabolically energized process, consisting of apical calcium entry via the transient receptor potential vanilloid family Ca^{2+} channel 6 (TRPV6), cytoplasmic calcium translocation in a calbindin-D_{9K}-bound form, and basolateral calcium extrusion via the plasma membrane Ca^{2+}-ATPase (PMCA) (22). On the other hand, paracellular passive calcium transport is dependent on the transepithelial calcium gradient and transepithelial resistance (TER) and is absent when both sides of the epithelium contain equal calcium concentration (12, 29). In normal intestinal epithelia, movement of ions and nutrients across the paracellular pathway is generally regulated by the size- and charge-selective properties of the tight junction, which contains several charge-selective claudin proteins arranged in arrays of channellike barriers (32, 49, 54). Several mediators, e.g., phosphoinositide 3-kinase (PI3K), protein kinase C (PKC), and RhoA-associated coiled-coil forming kinase (ROCK), can modulate permselectivity of the paracellular pathway (5, 15, 25, 47).

Our recent investigation (25) demonstrated that the Caco-2 monolayer, which strongly expressed short and long isoforms of the PRL receptor (PRLR-S and -L, respectively), responded to PRL by increasing both transcellular and paracellular calcium transport. However, little was known regarding the effect of PRL on the paracellular permselectivity and electrical properties of the epithelium. Moreover, it was not known whether PRLR-S or PRLR-L was responsible for PRL signaling in the intestinal absorptive cells, but there was a report that in mammary epithelia PRL augmented galactopoiesis and electrolyte transport through PRLR-L, whereas PRLR-S silenced those actions (3, 6, 24, 42). The signaling pathway of PRL in Caco-2 cells, in contrast to mammary epithelial cells, may be nongenomic since the actions were observed very rapidly within 60 min after PRL exposure (25). Interestingly, in Caco-2 cells and duodenal epithelium, the nongenomic actions

Address for reprint requests and other correspondence: N. Charoenphandhu, Dept. of Physiology, Faculty of Science, Mahidol Univ., Rama VI Road, Bangkok 10400, Thailand (e-mail: naratt@narattsys.com).

The costs of publication of this article were defrayed in part by the payment of page charges. The article must therefore be hereby marked "*advertisement*" in accordance with 18 U.S.C. Section 1734 solely to indicate this fact.

of PRL were mediated by the PI3K pathway, but not the putative Janus kinase (JAK)2 or mitogen-activated protein kinase (MAPK) pathways (25). PI3K is the ultimate upstream kinase to several downstream targets, including PKC and ROCK, which are known to modulate transepithelial calcium transport and increase paracellular permeability, respectively (4, 21, 28, 36, 47). Thus PKC and ROCK pathways may mediate the actions of PRL.

In the present study, we used Caco-2 cells to demonstrate PRL-enhanced calcium absorption. Despite being human colorectal adenocarcinoma cells, confluent Caco-2 monolayers have been used widely in the studies of calcium and drug absorption because they have functional similarity to the small intestine, including the presence of brush border, expression of sucrase-isomaltase enzymes, and expression of the transcellular calcium transporters and charge-selective paracellular proteins, e.g., TRPV6, calbindin-D_{9K}, PMCA, and claudin-1, -2, -3, and -5 (37–39, 57, 58). The Caco-2 monolayer also responds to PRL in a dose-dependent manner, with a maximal effective concentration of 600 ng/ml, similar to that seen in duodenal epithelium (25). However, the normal paracellular passive calcium transport and cationic permselectivity of the Caco-2 monolayer as well as its response to PRL by altering paracellular calcium transport have not been fully characterized.

Therefore, the objectives of this study were *1*) to demonstrate that the rapid stimulatory effects of PRL on transepithelial calcium transport in the Caco-2 monolayer are nongenomic, *2*) to show that PRL signaling involves the PKC and ROCK pathways, *3*) to elucidate the normal characteristics of the paracellular calcium transport and cationic permselectivity of the Caco-2 monolayer, as well as the effects of PRL on these parameters, and *4*) to demonstrate that PRLR-L is required for the PRL-enhanced calcium absorption.

MATERIALS AND METHODS

Cell culture. Caco-2 cells [American Type Culture Collection (ATCC) no. HTB-37] were grown in Dulbecco's modified Eagle's medium (DMEM; Sigma, St. Louis, MO) supplemented with 15% fetal bovine serum (FBS; GIBCO, Grand Island, NY), 1% L-glutamine (GIBCO), 1% nonessential amino acid (Sigma), and 100 U/ml penicillin-streptomycin. Cells were propagated in 75-cm^2 T flasks (Corning) under a humidified atmosphere containing 5% CO_2 at 37°C and subcultured as described in the ATCC protocol. Confluent Caco-2 monolayers were prepared by seeding cells on polyester Snapwell inserts with 12-mm diameter and 0.4-μm pore size (catalog no. 3801; Corning) at 5×10^5 cells/well. Culture medium was changed daily after 48 h of seeding. Monolayers were incubated at 37°C for 14 days in a humidified atmosphere containing 5% CO_2.

On the experimental day, the Snapwell was mounted in a modified Ussing chamber with an exposed surface area of 1.13 cm^2 to measure electrical parameters, calcium fluxes, and/or ion permeability, as previously described (25). The monolayer was incubated for 20 min in the chamber before the 60-min experiment was carried out.

Bathing solution. The bathing solution for the Ussing chamber experiments contained (in mmol/l) 118 NaCl, 4.7 KCl, 1.1 $MgCl_2$, 1.25 $CaCl_2$, 23 $NaHCO_3$, 12 D-glucose, and 2 mannitol (all purchased from Sigma). The solution, continuously gassed with humidified 5% CO_2 in 95% O_2, was maintained at 37°C and pH 7.4 and had an osmolality of 290–293 mosmol/kgH_2O as measured by a freezing point-based osmometer (model 3320; Advanced Instruments, Norwood, MA). Water used in the present work had a resistance >18.3 MΩ·cm and a free ionized calcium concentration <2.5 nmol/l.

Short interference RNA transfection. Two short interference RNA (siRNA) sequences targeted for human PRLR-L, i.e., 5′-GGGCUAUAGCAUGGUGACCTT-3′ and 5′-GGUCACCAUGCUAUAGCCCTT-3′, scrambled siRNAs, and the transfection reagent kit were supplied by Ambion (Austin, TX). Caco-2 cells were seeded in Snapwells at 5×10^5 cells/well for 12 days. Thereafter, in vitro transfection was performed with the 1:400 siPORT amine transfection reagent (Ambion) according to the manufacturer's instruction. The siRNAs were added in the culture medium to obtain a final concentration of 1 nmol/l. Control cells were treated with siPORT without siRNA. After a 48-h transfection, the PRL-stimulated calcium transport across the PRLR-L knockdown monolayer was measured. The siRNA efficiency was determined by quantitative real-time PCR (qRT-PCR). This PRLR-L knockdown study was approved by the Institutional Biosafety Committee (IBC) of the Faculty of Science, Mahidol University.

mRNA isolation, qRT-PCR, and sequencing. With the use of TRIzol reagent (Invitrogen, Carlsbad, CA), total RNA was prepared from the PRLR-L knockdown Caco-2 cells as previously described (13). One microgram of the total RNA was reverse-transcribed with the iScript kit (Bio-Rad, Hercules, CA). Glyceraldehyde-3-phosphate dehydrogenase (GAPDH), a housekeeping gene, served as a control gene to check the consistency of reverse transcription (% coefficient of variation <1%; $n = 20$). Sense and antisense primers of PRLRs and GAPDH were designed by OLIGO 6 (Molecular Biology Insights, Cascade, CO) and Primer Validator 1.4 (Naratt Software, Bangkok, Thailand), as shown in Table 1. The amplification reaction using real-time PCR (model MiniOpticon; Bio-Rad) was performed with the iQ SYBR Green SuperMix (Bio-Rad). Relative expression of PRLR over GAPDH was calculated from the threshold cycle (C_t) values by the $2^{\Delta C_t}$ method. After qRT-PCR, the PCR products were also visualized on a 1.5% agarose gel stained with 1.0 μg/ml ethidium bromide. Thereafter, all PCR products were extracted with the HiYield Gel/PCR DNA Extraction kit (Real Biotech, Taipei, Taiwan) and were sequenced with the ABI Prism 3100 Genetic Analyzer (Applied Biosystems, Foster City, CA).

Measurement of electrical parameters. Three electrical parameters, i.e., potential difference (PD), short-circuit current (I_{sc}), and TER, were determined as previously described (12). In brief, a pair of Ag/AgCl electrodes connected to agar bridges (3.0 mol/l KCl per 4 g% agar) was located near each surface of the mounted Snapwell for measurement of PD. The other ends of the PD-sensing electrodes were connected to a preamplifier (model EVC-4000; World Precision Instruments, Sarasota, FL). Another pair of Ag/AgCl electrodes connected in series to the EVC-4000 current-generating unit was placed at the end of each hemichamber to supply I_{sc}. TER and conductance (G; $G = 1/\text{TER}$) were calculated from Ohm's equation.

Measurement of calcium, mannitol, and polyethylene glycol fluxes. Calcium transport across Caco-2 monolayer was determined by the method of Charoenphandhu et al. (12). After 20-min incubation, the Ussing chamber was filled with fresh bathing solution containing

Table 1. *Homo sapiens oligonucleotide sequences used in qRT-PCR experiments*

Name	Accession No.	Primer (forward/reverse)	Product Length, bp
PRLR-S	AF416619	5′-GGTGACCCCTTGATGTTG-3′ 5′-TTCTGGTATATGCTCTTCAGC-3′	145
PRLR-L	NM_000949	5′-ACTTGCCTCTTTCTCCAG-3′ 5′-TCCCTCAAGAATACTAAGCAG-3′	100
GAPDH	NM_002046	5′-CTGGTAAAGTGGATATTGTTG-3′ 5′-GAGGCTGTTGTCATACTTCTC-3′	359

qRT-PCR, quantitative RT-PCR; PRLR-S, short isoform of prolactin receptor; PRLR-L, long isoform of prolactin receptor; GAPDH, glyceraldehyde-3-phosphate dehydrogenase.

$^{45}CaCl_2$ (final specific activity of 500 mCi/mol; Amersham, Little Chalfont, UK). Radioactivity of ^{45}Ca was analyzed with a liquid scintillation spectrophotometer (model Tri-Carb 3100 TR; Perkin-Elmer, Shelton, CT). Total calcium concentration was analyzed by atomic absorption spectroscopy (model SpectrAA-300; Varian Techtron, Victoria, Australia). Unidirectional flux ($J_{H\rightarrow C}$, nmol·h^{-1}·cm^{-2}) of calcium from the hot side (H) to the cold side (C) was calculated with *Eqs. 1* and *2*.

$$J_{H\rightarrow C} = R_{H\rightarrow C}/(S_H \times A) \quad (1)$$

$$S_H = C_H/C_T \quad (2)$$

where $R_{H\rightarrow C}$ is the rate of tracer appearance in the cold side (cpm/h); S_H is the specific activity in the hot side (cpm/nmol); A is the surface area of the Snapwell (cm^2); C_H is the mean radioactivity in the hot side (cpm); and C_T is the total calcium in the hot side (nmol).

Calcium fluxes in the absence of calcium concentration gradient (i.e., bathing solution in both hemichambers contained equal calcium concentration) represented the transcellular active calcium transport (12). The calcium gradient-dependent paracellular passive transport was studied by determining calcium fluxes in the presence of varying apical calcium concentrations (12), i.e., 1.25, 2.5, 5, 10, 20, 40, and 80 mmol/l.

In some experiments, the Caco-2 monolayer was bathed on both sides with solution containing 1 mmol/l mannitol and 1 mmol/l polyethylene glycol (PEG). Paracellular markers [^{3}H]mannitol (Amersham; molecular weight 180; molecular radius ~350 pm) and [^{14}C]PEG (Amersham; molecular weight 4,000; molecular radius ~2.5 nm) were added in the bathing solution to obtain final specific activities of 750 and 500 mCi/mol, respectively. Transepithelial mannitol flux and PEG flux were then measured.

In an Ussing chamber, the Caco-2 monolayer was directly exposed on the basolateral side for 60 min to 600 ng/ml recombinant human PRL (rhPRL) (purity >97%; catalog no. 682-PL; R&D Systems, Minneapolis, MN), which is the maximal effective concentration reported by Jantarajit et al. (25), or rhPRL plus inhibitors, which were an RNA polymerase II inhibitor [50 μmol/l 5,6-dichloro-1-β-D-ribobenzimidazole (DRB); Calbiochem, La Jolla, CA], a panspecific PKC inhibitor (0.8 or 1 μmol/l GF-109203X; A. G. Scientific, San Diego, CA), and a selective ROCK inhibitor (1 μmol/l Y-27632; Calbiochem).

Permeability measurement. Permeability of sodium (P_{Na}) and chloride (P_{Cl}) were determined by the dilution potential technique, modified from the methods of Kahle et al. (26) and Hou et al. (23). In brief, Caco-2 monolayer was equilibrated for 20 min in normal bathing solution containing 145 mmol/l NaCl before the apical solution was replaced with 72.5 mmol/l NaCl-containing solution. Osmolality was maintained by an equivalent amount of mannitol. Changes in the electrical parameters before and after solution replacement were recorded until stable. The ion permeability ratio (P_{Na}/P_{Cl}) was calculated from the dilution potential (V_δ) with *Eq. 3* (45)

$$V_\delta = \frac{RT}{F} \ln \frac{P_{Na} C_a + P_{Cl} C_b}{P_{Na} C_b + P_{Cl} C_a} \quad (3)$$

where P_{Na} is the absolute permeability of sodium; P_{Cl} is the absolute permeability of chloride; C_a is the apical NaCl concentration; C_b is the basolateral NaCl concentration; and R, T, and F are the gas constant, temperature, and the Faraday constant.

When given $\rho = P_{Na}/P_{Cl}$, $\phi = C_b/C_a$, and $\nu = FV_\delta/RT$, *Eq. 3* is rewritten as

$$\rho = (\phi - e^{\nu})/(\phi e^{\nu} - 1) \quad (4)$$

According to the Kimizuka-Koketsu equation (31),

$$G = \frac{F^2}{RT}(P_{Na} C_b + P_{Cl} C_a) \quad (5)$$

where G is the transepithelial conductance and P_{Na} and P_{Cl} are calculated from G and ρ by using *Eqs. 6* and *7*, respectively.

$$P_{Na} = \frac{GRT}{C_a F^2} \times \frac{\rho}{1+\rho} \quad (6)$$

$$P_{Cl} = P_{Na}/\rho \quad (7)$$

To study the permeability ratios of metal ions in the Group 1 series (alkali metals), i.e., P_X/P_{Cl} (X^+ is Li^+, Na^+, K^+, Rb^+, or Cs^+ in the form of chloride salt; all purchased from Sigma), Na^+ as the primary conductor in the bathing solution was substituted with X^+, while pH was maintained with 10 mmol/l HEPES (Sigma). The solution used was titrated with 1 mol/l mannitol until the osmolality of 290 mosmol/kgH_2O was obtained. During the experimental period, the Caco-2 monolayer was equilibrated for 20 min in normal bathing solution containing 145 mmol/l NaCl before the apical solution was replaced with 100 mmol/l X^+-containing solution. Thereafter, the concentration of X^+ was diluted to 50 mmol/l to create diffusion (dilution) potential. P_X/P_{Cl} was calculated as described previously (45).

Calcium permeability (P_{Ca}) of the Caco-2 monolayer via the paracellular pathway was calculated from *Eq. 8* (12)

$$P_{Ca} = J_{Ca}/\Delta C \quad (8)$$

where J_{Ca} is the paracellular passive calcium flux and ΔC is the difference between the apical and basolateral calcium concentrations.

In some experiments, the monolayer was exposed to 1 μmol/l GF-109203X, 1 μmol/l Y-27632, or 75 μmol/l LY-294002 (PI3K inhibitor; Tocris Bioscience, Bristol, UK).

Statistical analyses. Results are expressed as means ± SE. Two sets of data were compared with the unpaired Student's *t*-test. Multiple comparisons were performed by one-way analysis of variance (ANOVA) with Dunnett's posttest. Linear regression with slope analysis was performed to obtain the apical calcium concentration-calcium flux and TER relationships. Nonlinear regression was performed with the one-phase exponential decay equation to demonstrate the Δcalcium-calcium permeability relationship as previously described (12). The level of significance for all statistical tests was $P < 0.05$. Data were analyzed by GraphPad Prism 4.0 for Mac OS X (GraphPad Software, San Diego, CA).

RESULTS

Nongenomic action of PRL on transcellular active calcium transport involves PKC and ROCK pathways. As shown in Fig. 1, 600 ng/ml rhPRL significantly stimulated the transcellular active calcium transport in Caco-2 monolayer from the control value of 9.22 ± 0.48 ($n = 10$) to 18.04 ± 0.51 nmol·h^{-1}·cm^{-2} ($n = 12$, $P < 0.01$). PRL concurrently decreased the TER of the monolayer by ~30% (Table 2). Here, 50 μmol/l DRB, a classic RNA polymerase II inhibitor, was used to inhibit gene transcription. DRB has been used to demonstrate nongenomic effects of several hormones, including vitamin D (43). Since the effect of PRL occurred within 60 min and was not inhibited by DRB, PRL exerted its rapid action via nongenomic signaling pathway(s).

In the presence of 0.8 μmol/l GF-109203X (PKC inhibitor) and 1 μmol/l Y-27632 (ROCK inhibitor), the effect of PRL on the transcellular active calcium transport was diminished (Fig. 1), while only Y-27632 inhibited the action of PRL on the TER (Table 2), suggesting that both PKC and ROCK pathways were involved in the signal transduction of PRL. A higher concentration of GF-109203X, i.e., 1 μmol/l, was used to confirm that

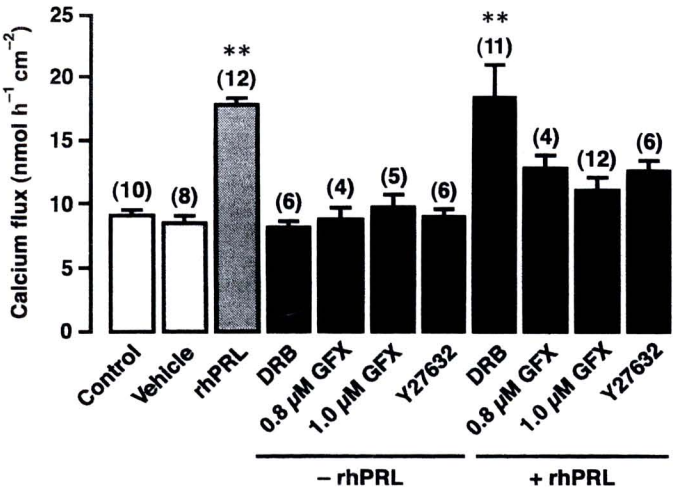

Fig. 1. Transcellular active calcium fluxes in Caco-2 monolayer exposed to RNA polymerase II inhibitor (50 μmol/l 5,6-dichloro-1-β-D-ribobenzimidazole; DRB), protein kinase C (PKC) inhibitor (0.8 and 1 μmol/l GF-109203X; GFX), or RhoA-associated coiled-coil forming kinase (ROCK) inhibitor (1 μmol/l Y-27632) in the presence (+rhPRL) or absence (−rhPRL) of 600 ng/ml recombinant human prolactin (rhPRL). DMSO 0.3% (vol/vol) was used as vehicle for preparation of inhibitors. $^{**}P < 0.01$ compared with control group. Numbers in parentheses represent the number of independent Snapwells.

inhibition of PKC completely abolished the effect of PRL on the transcellular calcium transport. Neither inhibitor alone nor 0.3% (vol/vol) DMSO, a vehicle for the preparation of inhibitors, had an effect on the transcellular active calcium flux or TER (Fig. 1).

PRL stimulates paracellular passive calcium transport via ROCK pathway. The relationship between apical calcium concentrations (C_{Ca}), which created the transepithelial calcium gradient (Δcalcium), and calcium flux (J_{Ca}) in Caco-2 monolayer shows linearity ($r^2 = 0.964$, Fig. 2, *A* and *B*). J_{Ca} under this condition represents the Δcalcium gradient-dependent paracellular passive transport. After exposure to rhPRL, J_{Ca} at all C_{Ca} (1.25–80 mmol/l) were significantly increased compared with their respective controls ($r^2 = 0.956$, $P < 0.01$). The slope, but not the *y*-intercept, of the PRL-exposed graph is higher than that of the control, i.e., 3.76 ± 0.13 vs. 6.41 ± 0.24 × 10^{-3} cm/h ($P < 0.001$). Interestingly, incubation of Caco-2 monolayer with rhPRL plus 1 μmol/l GF-109203X did not affect the paracellular passive calcium transport (Fig. 2*A*), whereas Y-27632 completely abolished the effect of PRL on this mode of calcium transport (Fig. 2*B*). In addition, rhPRL increased the paracellular P_{Ca}, and this effect was abolished by Y-27632 but not 1 μmol/l GF-109203X (Fig. 2, *C* and *D*).

Since tight junctions of several epithelia, as an array of channellike structures, show a conductance block after exposure to divalent cations, including calcium (49), we measured the TER of the monolayer in the presence of transepithelial calcium gradient. As depicted in Fig. 3, increases in apical C_{Ca} led to an increase in TER with linear correlation ($r^2 = 0.882$). Exposure to rhPRL, on the other hand, decreased the TER of the monolayer ($P < 0.01$) compared with the corresponding control values at the respective C_{Ca}. However, the TER of the PRL-exposed monolayer was still increased with the apical C_{Ca} ($r^2 = 0.842$). The slopes of both regression lines are significantly different, i.e., 6.71 ± 0.43 vs. 3.67 ± 0.28 Ω·cm^2·l·mmol^{-1} ($P < 0.001$). A reduction in TER after PRL exposure explained the PRL-stimulated paracellular passive calcium transport.

The ROCK inhibitor (Fig. 3*B*), but not the PKC inhibitor (Fig. 3*A*), abolished the effect of PRL on the apical calcium-induced alteration in TER. Since we recently reported (25) that PI3K inhibitor (75 μmol/l LY-294002) also compromised the paracellular passive calcium transport in Caco-2 monolayer, the effect of this inhibitor on the apical calcium-induced alteration in TER was also examined. Figure 3*C* shows that PI3K inhibitor, similar to ROCK inhibitor, totally abolished the effect of PRL on TER. Inhibitor alone or 0.3% (vol/vol) DMSO had no effect on the paracellular passive calcium transport and did not alter TER (data not shown).

PRL alters charge-selective property of paracellular pathway via ROCK pathway. Increased paracellular transport of calcium is usually associated with alterations in the size- and charge-selective properties of the tight junction, which is the principal barrier for paracellular ion transport (53, 54). However, in the present study, transepithelial fluxes of mannitol and PEG-4000, which are indicators of the widening of the tight junction or change in size selectivity (50), were not affected by PRL (Table 3), suggesting that charge selectivity rather than size selectivity was the determinant of the paracellular transport in the presence of PRL.

The paracellular charge selectivity is determined by P_{Na}, P_{Cl}, and P_{Na}/P_{Cl}. By using the dilution potential technique, we found that rhPRL increased P_{Na} (Fig. 4*A*), but not P_{Cl} (Fig. 4*B*), of Caco-2 monolayer from the control value of 7.81 ± 0.32 ($n = 8$) to 10.96 ± 0.42 × 10^{-6} cm/s ($n = 8$, $P < 0.01$), thereby increasing P_{Na}/P_{Cl} from 3.73 ± 0.23 ($n = 8$) to 8.07 ± 0.82 ($n = 8$, $P < 0.01$) (Fig. 4*C*). The effects of PRL on P_{Na} and P_{Na}/P_{Cl} were completely abolished by Y-27632, but not by 1 μmol/l GF-109203X. Inhibitor alone or vehicle had no effect on the charge selectivity.

Furthermore, we investigated permselectivity of the paracellular pathway to other cations in the alkali metal series with

Table 2. *Epithelial electrical parameters for Caco-2 monolayer*

Condition	*n*	PD, mV	I_{sc}, μA/cm^2	TER, Ω·cm^2
Control	15	0.89±0.12	2.53±0.40	368.17±11.44
Vehicle	10	0.95±0.12	2.40±0.31	381.67±9.11
600 ng/ml rhPRL	15	0.94±0.06	3.67±0.27	255.67±7.10*
Inhibitors				
50 μmol/l DRB	12	0.81±0.11	2.17±0.27	371.53±23.49
1 μmol/l GF-109203X	13	0.95±0.18	2.62±0.47	348.97±19.80
1 μmol/l Y-27632	14	0.63±0.08	2.00±0.30	373.81±18.55
600 ng/ml rhPRL+				
50 μmol/l DRB	14	0.96±0.14	3.71±0.53	261.71±11.52*
1 μmol/l GF-109203X	15	0.79±0.15	3.07±0.51	249.44±13.64*
1 μmol/l Y-27632	14	0.85±0.10	2.29±0.28	377.38±18.54

Values are means ± SE for transepithelial potential difference (PD), short-circuit current (I_{sc}), and transepithelial resistance (TER) in Caco-2 monolayer directly exposed to recombinant human prolactin (rhPRL), RNA polymerase II inhibitor [5,6-dichloro-1-β-D-ribobenzimidazole (DRB)], protein kinase C (PKC) inhibitor (GF-109203X), RhoA-associated coiled-coil forming kinase (ROCK) inhibitor (Y-27632), or rhPRL plus inhibitors. DMSO 0.3% (vol/vol) was used as vehicle for preparation of inhibitors. The monolayer was bathed on both sides with 1.25 mmol/l calcium-containing solution. The apical side was negative with respect to the basolateral side. $^{*}P < 0.01$ vs. control group.

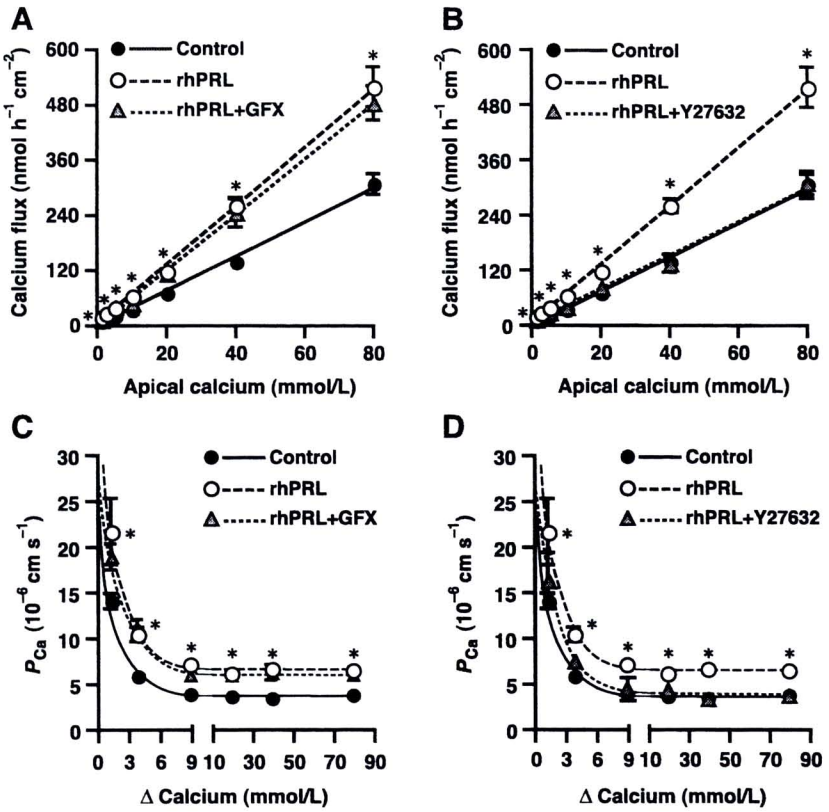

Fig. 2. Gradient-dependent paracellular passive calcium fluxes (*A* and *B*) and calcium permeability (P_{Ca}; *C* and *D*) in Caco-2 monolayer directly exposed to 600 ng/ml rhPRL, PKC inhibitor (1 μmol/l GFX), or ROCK inhibitor (1 μmol/l Y-27632). The apical bathing solution contained a calcium concentration of 1.25, 2.5, 5, 10, 20, 40, or 80 mmol/l. Inhibitors alone or vehicle (DMSO) had no effect on either calcium flux or permeability (data not shown). This experiment was performed on 210 independent Snapwell setups (n = 5 per value of apical calcium concentration). Control and rhPRL data in *A* and *C* were reused in panels *B* and *D*, respectively, for better presentation. *$P < 0.01$, control vs. rhPRL.

ionic radii ranging from 90 to 181 pm (ionic radii of Na^+ and Ca^{2+} are 114 and 116 pm, respectively). Under normal conditions, the Caco-2 monolayer showed relative permeability to alkali metal ions as follows: $P_{Na} > P_K > P_{Rb} > P_{Cs} > P_{Li}$ (Fig. 5*A*). rhPRL also increased P_X/P_{Cl} (where X^+ is Li^+, K^+, Rb^+, or Cs^+) of all other alkali metal ions (Fig. 5, *B*, *D–F*), i.e., P_{Li}/P_{Cl} from 1.09 ± 0.02 to 1.86 ± 0.09 (n = 6, $P < 0.01$), P_K/P_{Cl} from 2.14 ± 0.07 to 3.41 ± 0.17 (n = 6, $P < 0.01$), P_{Rb}/P_{Cl} from 1.75 ± 0.07 to 2.18 ± 0.15 (n = 6, $P < 0.01$), and P_{Cs}/P_{Cl} from 1.70 ± 0.03 to 1.91 ± 0.08 (n = 6, $P < 0.05$). The effect of PRL on P_X/P_{Cl} was diminished by Y-27632 and LY-294002, but not by 1 μmol/l GF-109203X. Therefore, the PRL-induced alteration in the cationic permselectivity in Caco-2 monolayer involved the ROCK pathway as well as the PI3K pathway.

In another series of experiments, we investigated whether the TER-reducing action of PRL could be applied to other cations of variable sizes. The monolayer was bathed on both sides with solution containing the alkali metal ion of interest, while TER was measured simultaneously. Under control conditions, the TER-ionic radius graph showed a V-shaped relationship, with the lowest TER (or the highest conductance) when Na^+ was used as the primary conductor (Fig. 6). Exposure to PRL significantly decreased TER (or increased ion conductance) no matter which alkali ion was used as the primary conductor. Similar to the permeability studies, this

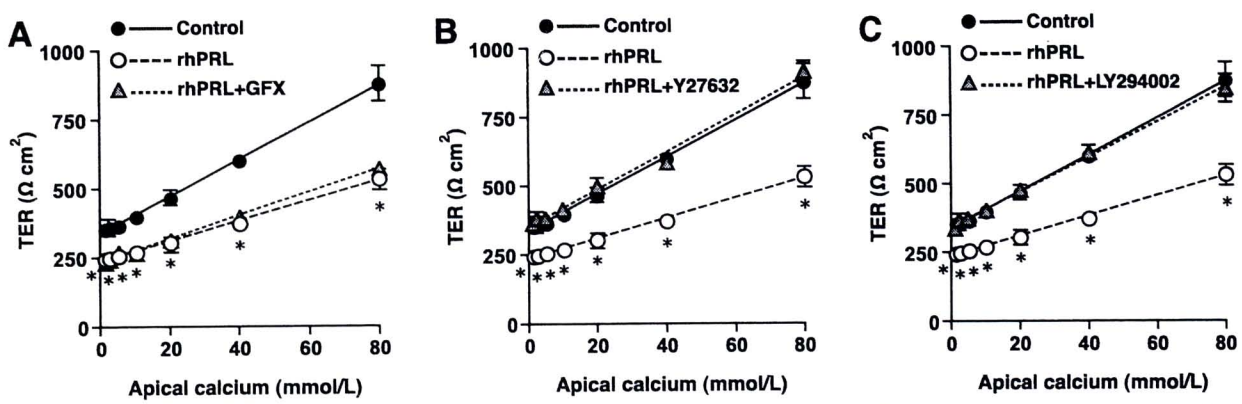

Fig. 3. Effect of 600 ng/ml rhPRL on the relationship between apical calcium concentration and transepithelial resistance (TER) in Caco-2 monolayer (n = 5 per value of apical calcium concentration) incubated with PKC inhibitor (1 μmol/l GFX; *A*), ROCK inhibitor (1 μmol/l Y-27632; *B*), or phosphoinositide 3-kinase (PI3K) inhibitor (75 μmol/l LY-294002; *C*). Inhibitors alone or vehicle (DMSO) had no effect on TER (data not shown). Control and rhPRL data in *A* were reused in *B* and *C* for better comparison. *$P < 0.01$, control vs. rhPRL.

Table 3. *Transepithelial mannitol and PEG-4000 fluxes*

Condition	n	Mannitol, nmol·h^{-1}·cm^{-2}	PEG-4000, nmol·h^{-1}·cm^{-2}
Control	7	5.60±0.27	3.89±0.58
600 ng/ml rhPRL	7	5.36±0.34	3.96±0.28

Values are mean ± SE transepithelial fluxes. Caco-2 monolayer was bathed with ^{3}H-labeled mannitol- and ^{14}C-labeled polyethylene glycol (PEG)-containing solution, with or without 600 ng/ml rhPRL. Both mannitol and PEG-4000 are exclusively transported via the paracellular channel and can be used to demonstrate the widening of the tight junction or change in size selectivity.

effect of PRL was abolished by Y-27632 (Fig. 6*B*) and LY-294002 (Fig. 6*C*), but not by 1 μmol/l GF-109203X (Fig. 6*A*).

PRL exerts its stimulatory action on transepithelial calcium transport via PRLR-L. Since PRL normally uses PRLR-L to exert its actions, especially on the mammary gland epithelia (3), we investigated whether PRLR-L is required for the action of PRL in Caco-2 cells with a PRLR-L siRNA knockdown technique. After 48-h incubation with PRLR-L siRNA, expression of PRLR-L mRNA in Caco-2 cells was abolished (n = 5, $P < 0.01$) (Fig. 7, *A* and *C*), while the expression of PRLR-S was unaltered (Fig. 7, *A* and *B*). The siPORT used as a transfection reagent had no effect on the expression of PRLR-L or PRLR-S. Amplicon sequencing confirmed the results of qRT-PCR.

In the Ussing chamber experiments (Fig. 8), the PRLR-L knockdown monolayer (siPORT+, siRNA+) exhibited transcellular active calcium flux and electrical properties comparable to those of the control (siPORT−, siRNA−) or siPORT-treated (siPORT+, siRNA−) monolayers (Fig. 8 and Table 4). Similar to the effect of PRL on the normal Caco-2 monolayer in Fig. 1, rhPRL enhanced the transcellular active calcium flux of the siPORT-treated monolayer (siPORT+, siRNA−, rhPRL−) from 9.25 ± 1.08 (n = 5) to 17.05 ± 0.65 nmol·h^{-1}·cm^{-2} (siPORT+, siRNA−, rhPRL+) (n = 5, $P <$ 0.01). The TER of the siPORT-treated monolayer was also decreased by PRL (Table 4). After incubation with PRLR-L siRNA, the PRL-enhanced calcium transport and the PRL-altered TER in Caco-2 monolayer were completely reverted to basal levels. These findings indicated that PRL exerted its stimulatory action on calcium transport in the Caco-2 monolayer via PRLR-L.

DISCUSSION

PRL has been shown to exert both genomic and nongenomic actions on duodenum and proximal jejunum (25, 50, 51). In the present study, the effect of PRL on transepithelial calcium transport in Caco-2 monolayer was nongenomic, since the responses to PRL could be observed within 60 min and were not diminished by 50 μmol/l DRB, which is an inhibitor of gene transcription (43). We also demonstrated that the nongenomic action of PRL was mediated by the PKC and ROCK pathways.

The Caco-2 monolayer is a suitable model for investigating PRL action on transcellular active calcium transport because Caco-2 cells possess functional PRLR and transcellular calcium transporters (19, 25). In the absence of transepithelial calcium gradient, electrogenic transcellular active calcium transport involves the functions of TRPV6, calbindin-D_{9K}, and PMCA (22). We previously showed (11) that PRL stimulated both apical calcium uptake and activity of the basolateral PMCA of purified duodenal membrane vesicles. The present results confirmed that transcellular calcium transport was increased by twofold after exposure to rhPRL, consistent with findings in the duodenal epithelium (25).

Interestingly, the TER of Caco-2 monolayer was decreased by PRL, similar to that observed after exposure to vitamin D, which is an important regulator of calcium absorption (14). Since the PD of the PRL-treated monolayer was not changed, it was conceivable that PRL did not interfere with the electrogenic transcellular sodium transport via Na^+-K^+-ATPases, which, in the absence of chemical gradient and diffusion

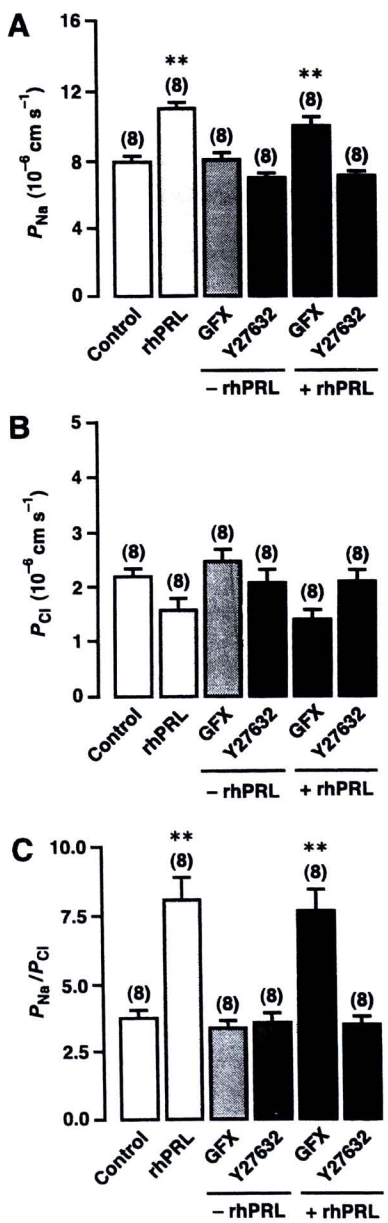

Fig. 4. Effects of rhPRL on sodium permeability (P_{Na}; *A*), chloride permeability (P_{Cl}; *B*), and P_{Na}/P_{Cl} (*C*), which indicate charge-selective property of Caco-2 monolayer. Cells were incubated with PKC inhibitor (1 μmol/l GFX) or ROCK inhibitor (1 μmol/l Y-27632) in the presence (+rhPRL) or absence (−rhPRL) of 600 ng/ml rhPRL. DMSO 0.3% (vol/vol) used as vehicle had no effect on these parameters (data not shown). **$P < 0.01$ compared with control group. Numbers in parentheses represent the number of independent Snapwells.

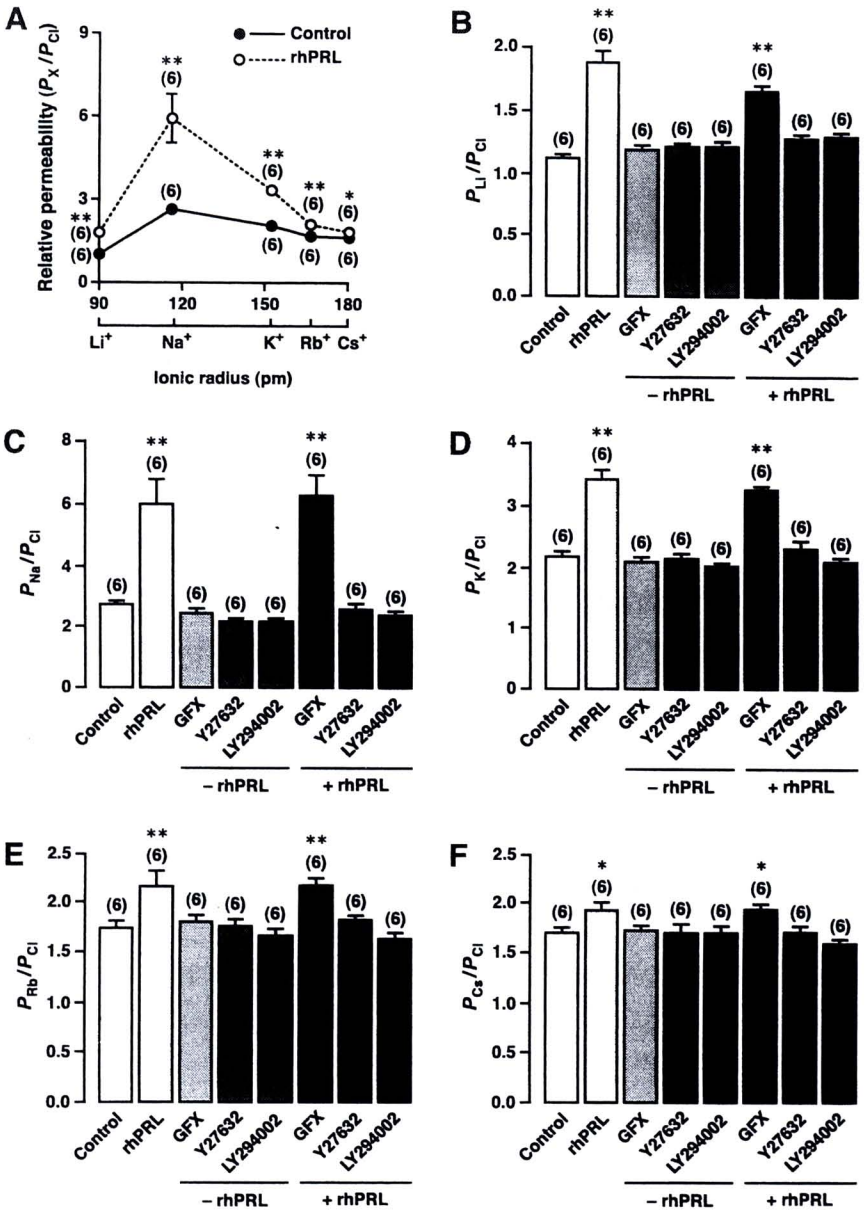

Fig. 5. *A*: effect of 600 ng/ml rhPRL on the relative paracellular permeability of the alkali metal ions over chloride (P_X/P_{Cl}; X = Li^+, Na^+, K^+, Rb^+, or Cs^+) plotted against their ionic radii. *B–F*: P_X/P_{Cl} of Caco-2 monolayer incubated with PKC inhibitor (1 μmol/l GFX), ROCK inhibitor (1 μmol/l Y-27632), or PI3K inhibitor (75 μmol/l LY-294002) in the presence (+rhPRL) or absence (−rhPRL) of 600 ng/ml rhPRL. DMSO 0.3% (vol/vol) used as vehicle had no effect on P_X/P_{Cl} (data not shown). $^*P < 0.05$, $^{**}P < 0.01$ compared with control group. Numbers in parentheses represent the number of independent Snapwells.

potential, contributed up to 95% of the PD (46). Although PRL increased the electrogenic transcellular calcium transport, changes in the PD should be very small and not detectable by the Ussing technique. The PD change ($V_{\Delta,Ca}$) due to the PRL-enhanced transcellular calcium transport, if present, could be estimated from the TER and the difference ($J_{\Delta,Ca}$) between the control (9.22 nmol·h^{-1}·cm^{-2}) and PRL-exposed (18.04 nmol·h^{-1}·cm^{-2}) fluxes, i.e., $V_{\Delta,Ca} = J_{\Delta,Ca}zF \times$ TER (z = +2, F = 96,485.34 C/mol, TER = 255.67 Ω·cm^2). Hence $V_{\Delta,Ca}$ was 120.88 μV, which could be considered negligible. When the monolayer was short-circuited, the external current (I_{sc}) moved across the monolayer via the low-resistance pathway, i.e., the paracellular pathway (20). Therefore, a decrease in TER that was calculated from PD and I_{sc} in the presence of PRL must have resulted from the PRL-induced increase in paracellular permeability, and thus enhanced paracellular calcium transport was anticipated.

Little is currently known regarding the paracellular calcium transport in Caco-2 monolayers. Generally, the paracellular passive calcium transport is more physiologically important since it is achieved at a small cost of energy and is nonsaturable (i.e., a graph of apical calcium vs. calcium flux shows linearity) (29). This transport mechanism, which occurs along the entire length of the small intestine, becomes significant when luminal calcium concentration exceeds 5 mmol/l, which is an average luminal calcium concentration in the rat duodenum (12, 55). When the apical calcium concentration was 20 mmol/l, the transcellular calcium flux contributed <10% of the total flux (Fig. 2). Nevertheless, transcellular calcium transport is still important during increased calcium demand, e.g., during pregnancy, lactation, and low calcium intake (8, 10). Here we found that PRL enhanced both transcellular and paracellular calcium transport as well as calcium permeability. The PRL-stimulated paracellular calcium flux at 5 mmol/l apical calcium was

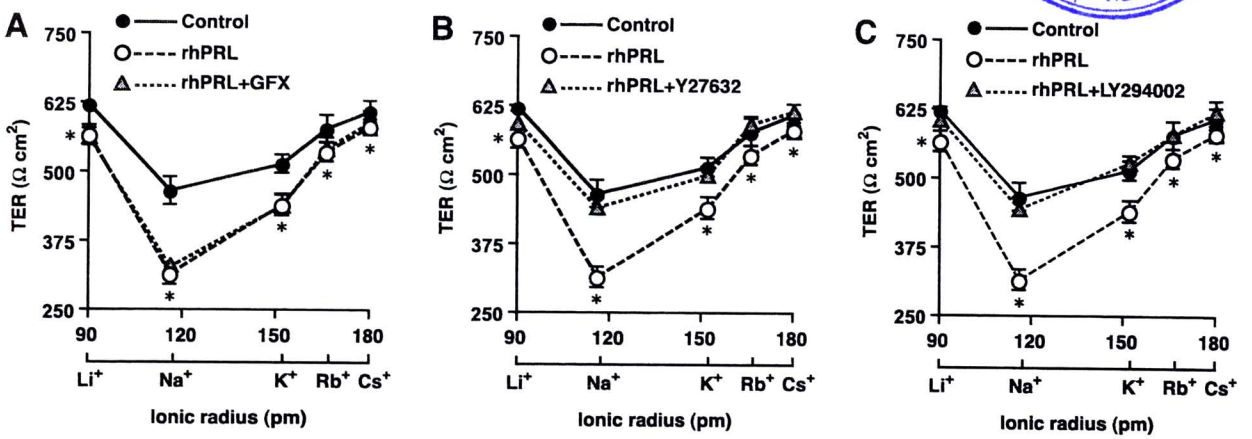

Fig. 6. Alterations of TER after apical Na^+ being substituted with other alkali metal ions. Caco-2 monolayers (n = 6 per studied ion) were directly incubated with 600 ng/ml rhPRL with or without PKC inhibitor (1 μmol/l GFX; *A*), ROCK inhibitor (1 μmol/l Y-27632; *B*), or PI3K inhibitor (75 μmol/l LY-294002; *C*). TER values of the monolayer exposed to inhibitors alone or vehicle (DMSO) are comparable to those of control (data not shown). Control and rhPRL data in *A* were reused in *B* and *C*. *$P < 0.01$, control vs. rhPRL.

~2.1-fold higher than that at 1.25 mmol/l calcium in the transcellular study, implicating the physiological significance of the paracellular transport. Moreover, as seen in Fig. 3, an increase in the apical calcium concentration also led to a divalent ion-induced conductance block, i.e., a linear increase in TER, as seen with many conventional ion channels (30, 40). Conductance block is probably caused by binding of calcium to the fixed negative charges of the paracellular proteins (49). A similar effect of high apical calcium has been reported in other epithelia, e.g., MDCK-II monolayer (49). After exposure to PRL, the increase in TER was attenuated, i.e., the paracellular conductance was increased, thus explaining increases in the paracellular calcium flux, calcium permeability, and slope of the apical calcium vs. paracellular calcium flux relationship.

Paracellular conductance and transport of ions can be regulated by changing the size- and/or charge-selective property of the paracellular pathway (32, 54). These properties are determined by different mechanisms (32). Paracellular size restriction, which is between 350 and 540 pm in the Caco-2 monolayer (9), is compromised by the myosin light chain kinase-mediated contraction of the perijunctional actomyosin ring complex and cytoskeletal arrangement (52). However, previous investigation using cytochalasin E, which widens the tight junction by disrupting actin polymerization, suggested that PRL-induced increase in duodenal calcium flux did not involve size selectivity of the paracellular pathway (50). This was confirmed by the present finding of no change in mannitol and PEG fluxes after exposure to PRL. Therefore, it appeared that

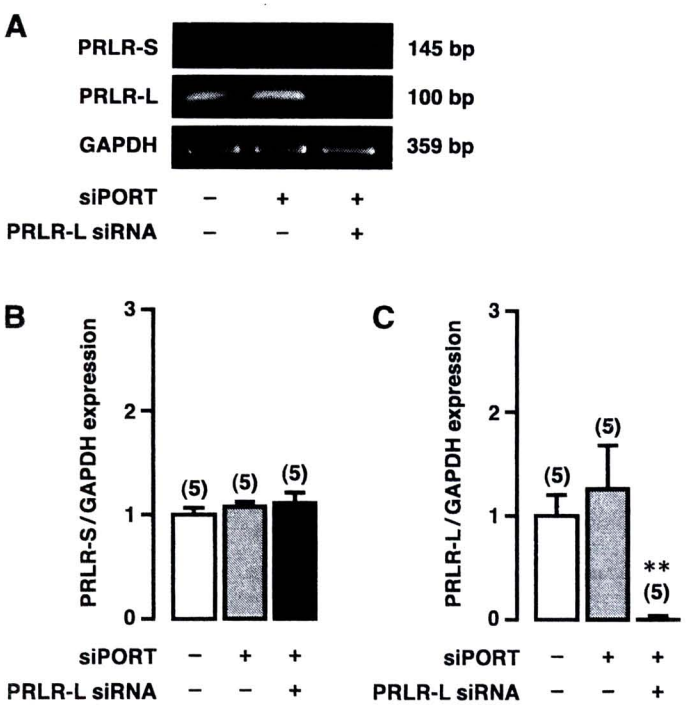

Fig. 7. Representative electrophoretic image (*A*) and quantitative real-time PCR (*B* and *C*) demonstrate expression of short (PRLR-S) and long (PRLR-L) forms of PRL receptor in Caco-2 monolayer incubated for 48 h with siPORT (transfection agent) or siPORT + 1 nmol/l PRLR-L short interference RNA (siRNA). The absence of PRLR-L expression confirms the success of PRLR-L knockdown. **$P < 0.01$ compared with control group (−siPORT/−siRNA). Numbers in parentheses represent the number of independent Snapwells.

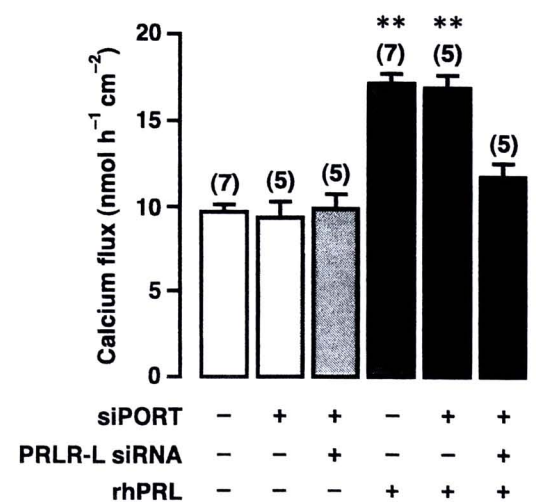

Fig. 8. Transcellular active calcium fluxes in Caco-2 monolayer exposed to 600 ng/ml rhPRL, siPORT (transfection agent), and/or 1 nmol/l siRNA targeting PRLR-L. **$P < 0.01$ compared with control group (−siPORT, −siRNA, −rhPRL). Numbers in parentheses represent the number of independent Snapwells.

Table 4. *Epithelial electrical parameters for PRLR-L knockdown experiment*

Condition	n	PD, mV	I_{sc}, μA/cm^2	TER, Ω·cm^2
Control	7	0.74±0.10	2.00±0.31	395.24±11.90
siPORT	5	0.64±0.12	2.00±0.32	390.00±29.15
siPORT+siRNA	5	0.80±0.13	2.00±0.32	400.00±15.81
rhPRL	7	0.83±0.06	3.14±0.26	258.10±12.12*
rhPRL+siPORT	5	0.72±0.19	3.40±0.68	206.67±22.11*
rhPRL+siPORT+siRNA	5	0.88±0.13	2.40±0.40	376.67±24.49

Values are means ± SE for transepithelial PD, I_{sc}, and TER in Caco-2 monolayer exposed to 600 ng/ml rhPRL, siPORT (transfection agent), and/or 1 nmol/l short interference RNA (siRNA) targeting PRLR-L. The monolayer was bathed on both sides with 1.25 mmol/l calcium-containing solution. The apical side was negative with respect to the basolateral side. *$P < 0.01$ vs. control group.

the epithelial charge selectivity, but not the size selectivity, regulated the intestinal paracellular calcium transport. Generally, charge selectivity is defined by fixed negative or positive charges on the extracellular loops of tight junction proteins of the claudin family, which provide a hindrance for the permeation of ions with the opposite charge (32). Expressions of some claudins are associated with increased calcium permeability. For example, claudin-16 is widely recognized to be important for paracellular calcium and magnesium reabsorption in the thick ascending limb of the loop of Henle (17). Expression of claudin-3 in the duodenum is under the regulation of vitamin D (34), a hormone that also stimulates paracellular calcium transport (14). However, it is not known whether PRL alters the functions or localization of claudins in the Caco-2 monolayer and intestinal epithelia.

To access the charge-selective property of the Caco-2 monolayer, we used P_{Na}/P_{Cl} as an indicator. Under control conditions, a P_{Na}/P_{Cl} of 3.73 is comparable to those previously reported in Caco-2 monolayer (9) and small intestine (12, 41), indicating that these epithelia are more permeable to cations than anions. In contrast, normal colonic epithelium is more permeable to anions (16). It is noteworthy that the paracellular selectivity causes sodium and chloride movement to deviate from the mobility ratio of ~0.6 in free solution (20, 41). In addition, permeabilities of other cations in the alkali metal series, i.e., Li^+, K^+, Rb^+, and Cs^+, are also greater than that of Cl^-, and comply with Eisenman sequence VII (i.e., $P_{Na} > P_K > P_{Rb} > P_{Cs} > P_{Li}$) (for review, see Ref. 18). Similar to that reported in other epithelia (49), the conductance (reciprocal of TER) of the paracellular pathway was greatest when NaCl was used as the primary conductor, as seen in the ionic radius vs. TER curve, which showed a V-shaped relationship (Fig. 6). Such patterns were not altered by PRL. Although the paracellular pathway of the Caco-2 monolayer manifests a selective property similar to that of typical ion channels, whereby an ion current is not simply determined by the ionic or hydrated size of the ion, PRL enhanced the paracellular permeability of both sodium and calcium, which are of comparable ionic sizes. Our findings that PRL increased P_{Na} and permeability to other alkali metal ions, but not P_{Cl}, suggested that PRL could increase the activity of the paracellular proteins with fixed negative charges by an unknown mechanism, thereby enhancing paracellular conductance, calcium permeability, and paracellular calcium transport.

PRL exerts its functions by binding to the membrane-bound PRLRs with a ratio of PRL to PRLRs of 1:2 (3). Two isoforms of PRLRs, i.e., PRLR-S and -L, have been identified in intestinal absorptive cells and Caco-2 cells (25). Investigations in mammary epithelia demonstrated that signal transduction of PRL was transferred by PRLR-L, whereas PRLR-S silenced PRL actions because it lacks the cytoplasmic tails required to activate downstream pathways (3, 6, 24, 42). On the other hand, PRLR-S may transmit PRL signals in the liver and endothelial cells (24, 44). In the PRLR-L knockdown Caco-2 monolayer, which expressed a normal level of PRLR-S, the effects of PRL on transcellular calcium transport and TER were totally abolished, indicating that actions of PRL are primarily mediated by PRLR-L.

Despite strong evidence pertaining to PRL-stimulated intestinal calcium absorption (10), little is known regarding PRL signal transduction in the intestinal epithelia and the Caco-2 monolayer. In mammary epithelia, PRL binding to PRLRs triggers dimerization of PRLRs, leading to activation of the putative JAK2 signaling (3). However, our recent investigation (25) elucidated that the PI3K pathway, but not the JAK2 pathway, is involved in the PRL-enhanced transcellular and paracellular calcium transport. The present data clearly showed that the PI3K pathway was involved in the rapid effects of PRL on the paracellular permeability to alkali metal ions and TER. Signal transduction of PRL via PI3K has also been reported in liver, pancreas, and T-lymphoma Nb2 cells (1, 7, 56). The PI3K pathway covers a large number of downstream targets, including PKC and ROCK (21). The Rho-related pathway was found to be associated with PRL signaling in endothelial cells (35), while the PKC pathway mediated PRL actions in cholangiocytes (48), adrenocortical cells (27), and the intestine, in which PKC enhanced intestinal calcium transport (4). Activation of the ROCK pathway increased paracellular permeability in several epithelia, such as brain endothelium and renal proximal tubule (28, 47). PKC-ROCK cross talk could also affect paracellular permeability in endothelial cells (47). Therefore, in the present study we focused on the PKC- and ROCK-mediated PRL actions in Caco-2 cells and were able to demonstrate that the ROCK pathway mediated PRL actions on transcellular and paracellular calcium transport, calcium permeability, charge selectivity, and TER. On the other hand, inhibition of the PKC pathway could only diminish transcellular calcium transport. Nevertheless, further investigations are required to demonstrate the detailed molecular mechanisms of PKC- and ROCK-mediated PRL actions in Caco-2 monolayer.

In conclusion, we provide evidence, for the first time, that PRL exerts its nongenomic stimulatory action on transcellular active calcium transport in the Caco-2 monolayer via the PKC and ROCK pathways. PRL also increased paracellular permeability and decreased TER via the ROCK pathway, thereby enhancing paracellular passive calcium transport. Moreover, PRL-induced increase in paracellular transport was by altering epithelial charge selectivity rather than size selectivity. The actions of PRL were mediated by the long isoform of PRLR. Our findings elaborate possible mechanisms of the PRL-stimulated intestinal calcium transport, which has long been reported in the rat (10).

GRANTS

This research was supported by grants from the Royal Golden Jubilee Program (PHD48K0063 to N. Thongon), the Mahidol University Postdoctoral Fellowship Program (to L-I. Nakkrasae), the Commission on Higher Education, and the Thailand Research Fund (RSA5180001 to N. Charoenphandhu and RTA5080008 to N. Krishnamra).

REFERENCES

1. **Amaral ME, Cunha DA, Anhê GF, Ueno M, Carneiro EM, Velloso LA, Bordin S, Boschero AC.** Participation of prolactin receptors and phosphatidylinositol 3-kinase and MAP kinase pathways in the increase in pancreatic islet mass and sensitivity to glucose during pregnancy. *J Endocrinol* 183: 469–476, 2004.
2. **Arbogast LA, Voogt JL.** Endogenous opioid peptides contribute to suckling-induced prolactin release by suppressing tyrosine hydroxylase activity and messenger ribonucleic acid levels in tuberoinfundibular dopaminergic neurons. *Endocrinology* 139: 2857–2862, 1998.
3. **Bachelot A, Binart N.** Reproductive role of prolactin. *Reproduction* 133: 361–369, 2007.
4. **Balogh G, de Boland AR, Boland R.** Influence of age on $1,25(OH)_2$-vitamin D_3 activation of protein kinase C in rat duodenum. *Mol Cell Endocrinol* 129: 127–133, 1997.
5. **Banan A, Zhang LJ, Shaikh M, Fields JZ, Choudhary S, Forsyth CB, Farhadi A, Keshavarzian A.** θ Isoform of protein kinase C alters barrier function in intestinal epithelium through modulation of distinct claudin isotypes: a novel mechanism for regulation of permeability. *J Pharmacol Exp Ther* 313: 962–982, 2005.
6. **Berlanga JJ, Garcia-Ruiz JP, Perrot-Applanat M, Kelly PA, Edery M.** The short form of the prolactin (PRL) receptor silences PRL induction of the β-casein gene promoter. *Mol Endocrinol* 11: 1449–1457, 1997.
7. **Bishop JD, Nien WL, Dauphinee SM, Too CK.** Prolactin activates mammalian target-of-rapamycin through phosphatidylinositol 3-kinase and stimulates phosphorylation of p70S6K and 4E-binding protein-1 in lymphoma cells. *J Endocrinol* 190: 307–312, 2006.
8. **Boass A, Lovdal JA, Toverud SU.** Pregnancy- and lactation-induced changes in active intestinal calcium transport in rats. *Am J Physiol Gastrointest Liver Physiol* 263: G127–G134, 1992.
9. **Carr G, Haslam IS, Simmons NL.** Voltage dependence of transepithelial guanidine permeation across Caco-2 epithelia allows determination of the paracellular flux component. *Pharm Res* 23: 540–548, 2006.
10. **Charoenphandhu N, Krishnamra N.** Prolactin is an important regulator of intestinal calcium transport. *Can J Physiol Pharmacol* 85: 569–581, 2007.
11. **Charoenphandhu N, Limlomwongse L, Krishnamra N.** Prolactin directly enhanced Na^+/K^+- and Ca^{2+}-ATPase activities in the duodenum of female rats. *Can J Physiol Pharmacol* 84: 555–563, 2006.
12. **Charoenphandhu N, Tudpor K, Pulsook N, Krishnamra N.** Chronic metabolic acidosis stimulated transcellular and solvent drag-induced calcium transport in the duodenum of female rats. *Am J Physiol Gastrointest Liver Physiol* 291: G446–G455, 2006.
13. **Charoenphandhu N, Wongdee K, Tudpor K, Pandaranandaka J, Krishnamra N.** Chronic metabolic acidosis upregulated claudin mRNA expression in the duodenal enterocytes of female rats. *Life Sci* 80: 1729–1737, 2007.
14. **Chirayath MV, Gajdzik L, Hulla W, Graf J, Cross HS, Peterlik M.** Vitamin D increases tight-junction conductance and paracellular Ca^{2+} transport in Caco-2 cell cultures. *Am J Physiol Gastrointest Liver Physiol* 274: G389–G396, 1998.
15. **D'Souza T, Indig FE, Morin PJ.** Phosphorylation of claudin-4 by PKCε regulates tight junction barrier function in ovarian cancer cells. *Exp Cell Res* 313: 3364–3375, 2007.
16. **Davis GR, Santa Ana CA, Morawski SG, Fordtran JS.** Permeability characteristics of human jejunum, ileum, proximal colon and distal colon: results of potential difference measurements and unidirectional fluxes. *Gastroenterology* 83: 844–850, 1982.
17. **Efrati E, Arsentiev-Rozenfeld J, Zelikovic I.** The human paracellin-1 gene (*hPCLN-1*): renal epithelial cell-specific expression and regulation. *Am J Physiol Renal Physiol* 288: F272–F283, 2005.
18. **Eisenman G, Horn R.** Ionic selectivity revisited: the role of kinetic and equilibrium processes in ion permeation through channels. *J Membr Biol* 76: 197–225, 1983.
19. **Fleet JC, Eksir F, Hance KW, Wood RJ.** Vitamin D-inducible calcium transport and gene expression in three Caco-2 cell lines. *Am J Physiol Gastrointest Liver Physiol* 283: G618–G625, 2002.
20. **Greger R.** Epithelial transport. In: *Comprehensive Human Physiology: From Cellular Mechanisms to Integration*, edited by Greger R, Windhorst U. Berlin: Springer, 1996.
21. **Hirsch E, Costa C, Ciraolo E.** Phosphoinositide 3-kinases as a common platform for multi-hormone signaling. *J Endocrinol* 194: 243–256, 2007.
22. **Hoenderop JG, Nilius B, Bindels RJ.** Calcium absorption across epithelia. *Physiol Rev* 85: 373–422, 2005.
23. **Hou J, Paul DL, Goodenough DA.** Paracellin-1 and the modulation of ion selectivity of tight junctions. *J Cell Sci* 118: 5109–5118, 2005.
24. **Jahn GA, Daniel N, Jolivet G, Belair L, Bole-Feysot C, Kelly PA, Djiane J.** In vivo study of prolactin (PRL) intracellular signalling during lactogenesis in the rat: JAK/STAT pathway is activated by PRL in the mammary gland but not in the liver. *Biol Reprod* 57: 894–900, 1997.
25. **Jantarajit W, Thongon N, Pandaranandaka J, Teerapornpuntakit J, Krishnamra N, Charoenphandhu N.** Prolactin-stimulated transepithelial calcium transport in duodenum and Caco-2 monolayer are mediated by the phosphoinositide 3-kinase pathway. *Am J Physiol Endocrinol Metab* 293: E372–E384, 2007.
26. **Kahle KT, Macgregor GG, Wilson FH, Van Hoek AN, Brown D, Ardito T, Kashgarian M, Giebisch G, Hebert SC, Boulpaep EL, Lifton RP.** Paracellular Cl^- permeability is regulated by WNK4 kinase: insight into normal physiology and hypertension. *Proc Natl Acad Sci USA* 101: 14877–14882, 2004.
27. **Kaminska B, Ciereszko RE, Opalka M, Dusza L.** Prolactin signaling in porcine adrenocortical cells: involvement of protein kinases. *Domest Anim Endocrinol* 23: 475–491, 2002.
28. **Kapus A, Szászi K.** Coupling between apical and paracellular transport processes. *Biochem Cell Biol* 84: 870–880, 2006.
29. **Karbach U.** Paracellular calcium transport across the small intestine. *J Nutr* 122: 672–677, 1992.
30. **Kerschbaum HH, Cahalan MD.** Monovalent permeability, rectification, and ionic block of store-operated calcium channels in Jurkat T lymphocytes. *J Gen Physiol* 111: 521–537, 1998.
31. **Kimizuka H, Koketsu K.** Ion transport through cell membrane. *J Theor Biol* 6: 290–305, 1964.
32. **Krause G, Winkler L, Mueller SL, Haseloff RF, Piontek J, Blasig IE.** Structure and function of claudins. *Biochim Biophys Acta* 1778: 631–645, 2008.
33. **Krishnamra N, Wirunrattanakij Y, Limlomwongse L.** Acute effects of prolactin on passive calcium absorption in the small intestine by in vivo perfusion technique. *Can J Physiol Pharmacol* 76: 161–168, 1998.
34. **Kutuzova GD, DeLuca HF.** Gene expression profiles in rat intestine identify pathways for 1,25-dihydroxyvitamin D_3 stimulated calcium absorption and clarify its immunomodulatory properties. *Arch Biochem Biophys* 432: 152–166, 2004.
35. **Lee SH, Kunz J, Lin SH, Yu-Lee LY.** 16-kDa prolactin inhibits endothelial cell migration by down-regulating the Ras-Tiam1-Rac1-Pak1 signaling pathway. *Cancer Res* 67: 11045–11053, 2007.
36. **Little D, Dean RA, Young KM, McKane SA, Martin LD, Jones SL, Blikslager AT.** PI3K signaling is required for prostaglandin-induced mucosal recovery in ischemia-injured porcine ileum. *Am J Physiol Gastrointest Liver Physiol* 284: G46–G56, 2003.
37. **McLaughlin J, Padfield PJ, Burt JP, O'Neill CA.** Ochratoxin A increases permeability through tight junctions by removal of specific claudin isoforms. *Am J Physiol Cell Physiol* 287: C1412–C1417, 2004.
38. **Murphy EF, Hooiveld GJ, Muller M, Calogero RA, Cashman KD.** Conjugated linoleic acid alters global gene expression in human intestinal-like Caco-2 cells in an isomer-specific manner. *J Nutr* 137: 2359–2365, 2007.
39. **Nakane M, Ma J, Rose AE, Osinski MA, Wu-Wong JR.** Differential effects of vitamin D analogs on calcium transport. *J Steroid Biochem Mol Biol* 103: 84–89, 2007.
40. **Nasi E, del Pilar Gomez M.** Divalent cation interactions with light-dependent K channels. Kinetics of voltage-dependent block and requirement for an open pore. *J Gen Physiol* 114: 653–672, 1999.
41. **Powell DW.** Barrier function of epithelia. *Am J Physiol Gastrointest Liver Physiol* 241: G275–G288, 1981.
42. **Qazi AM, Tsai-Morris CH, Dufau ML.** Ligand-independent homo- and heterodimerization of human prolactin receptor variants: inhibitory action of the short forms by heterodimerization. *Mol Endocrinol* 20: 1912–1923, 2006.

43. **Rebsamen MC, Sun J, Norman AW, Liao JK.** 1α,25-Dihydroxyvitamin D_3 induces vascular smooth muscle cell migration via activation of phosphatidylinositol 3-kinase. *Circ Res* 91: 17–24, 2002.
44. **Ricken AM, Traenkner A, Merkwitz C, Hummitzsch K, Grosche J, Spanel-Borowski K.** The short prolactin receptor predominates in endothelial cells of micro- and macrovascular origin. *J Vasc Res* 44: 19–30, 2007.
45. **Salas PJ, López EM.** Validity of the Goldman-Hodgkin-Katz equation in paracellular ionic pathways of gallbladder epithelium. *Biochim Biophys Acta* 691: 178–182, 1982.
46. **Schultz SG, Zalusky R.** Ion transport in isolated rabbit ileum. I. Short-circuit current and Na fluxes. *J Gen Physiol* 47: 567–584, 1964.
47. **Stamatovic SM, Dimitrijevic OB, Keep RF, Andjelkovic AV.** Protein kinase Cα-RhoA cross-talk in CCL2-induced alterations in brain endothelial permeability. *J Biol Chem* 281: 8379–8388, 2006.
48. **Taffetani S, Glaser S, Francis H, DeMorrow S, Ueno Y, Alvaro D, Marucci L, Marzioni M, Fava G, Venter J, Vaculin S, Vaculin B, Lam IP, Lee VH, Gaudio E, Carpino G, Benedetti A, Alpini G.** Prolactin stimulates the proliferation of normal female cholangiocytes by differential regulation of Ca^{2+}-dependent PKC isoforms. *BMC Physiol* 7: 6, 2007.
49. **Tang VW, Goodenough DA.** Paracellular ion channel at the tight junction. *Biophys J* 84: 1660–1673, 2003.
50. **Tanrattana C, Charoenphandhu N, Limlomwongse L, Krishnamra N.** Prolactin directly stimulated the solvent drag-induced calcium transport in the duodenum of female rats. *Biochim Biophys Acta* 1665: 81–91, 2004.
51. **Tudpor K, Charoenphandhu N, Saengamnart W, Krishnamra N.** Long-term prolactin exposure differentially stimulated the transcellular and solvent drag-induced calcium transport in the duodenum of ovariectomized rats. *Exp Biol Med (Maywood)* 230: 836–844, 2005.
52. **Turner JR.** "Putting the squeeze" on the tight junction: understanding cytoskeletal regulation. *Semin Cell Dev Biol* 11: 301–308, 2000.
53. **Van Itallie CM, Anderson JM.** The role of claudins in determining paracellular charge selectivity. *Proc Am Thorac Soc* 1: 38–41, 2004.
54. **Van Itallie CM, Anderson JM.** Claudins and epithelial paracellular transport. *Annu Rev Physiol* 68: 403–429, 2006.
55. **Wasserman RH.** Vitamin D and the dual processes of intestinal calcium absorption. *J Nutr* 134: 3137–3139, 2004.
56. **Yamauchi T, Kaburagi Y, Ueki K, Tsuji Y, Stark GR, Kerr IM, Tsushima T, Akanuma Y, Komuro I, Tobe K, Yazaki Y, Kadowaki T.** Growth hormone and prolactin stimulate tyrosine phosphorylation of insulin receptor substrate-1, -2, and -3, their association with p85 phosphatidylinositol 3-kinase (PI3-kinase), and concomitantly PI3-kinase activation via JAK2 kinase. *J Biol Chem* 273: 15719–15726, 1998.
57. **Yee S.** In vitro permeability across Caco-2 cells (colonic) can predict in vivo (small intestinal) absorption in man—fact or myth. *Pharm Res* 14: 763–766, 1997.
58. **Zweibaum A, Triadou N, Kedinger M, Augeron C, Robine-Leon S, Pinto M, Rousset M, Haffen K.** Sucrase-isomaltase: a marker of foetal and malignant epithelial cells of the human colon. *Int J Cancer* 32: 407–412, 1983.

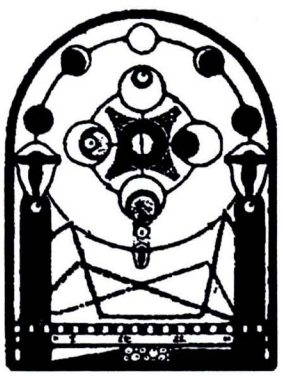

Prolactin decreases expression of Runx2, osteoprotegerin, and RANKL in primary osteoblasts derived from tibiae of adult female rats

Narattaphol Charoenphandhu, Jarinthorn Teerapornpuntakit, Methajit Methawasin, Kannikar Wongdee, Kanogwun Thongchote, and Nateetip Krishnamra

Abstract: Hyperprolactinemia caused by physiological or pathological conditions, such as those occurring during lactation and prolactinoma, respectively, results in progressive osteopenia. The underlying mechanisms, however, are controversial. Prolactin (PRL) may directly attenuate the functions of osteoblasts, since these bone cells express PRL receptors. The present study therefore aimed to investigate the effects of PRL on the expression of genes related to the osteoblast functions by using quantitative real-time PCR technique. Herein, we used primary osteoblasts that were derived from the tibiae of adult rats and displayed characteristics of differentiated osteoblasts, including in vitro mineralization. Osteoblasts exposed for 48 h to 1000 ng/mL PRL, but not to 10 or 100 ng/mL PRL, showed decreases in the mRNA expression of Runx2, osteoprotegerin (OPG), and receptor activator of nuclear factor κB ligand (RANKL) by 60.49%, 72.74%, and 87.51%, respectively. Nevertheless, PRL did not change the RANKL/OPG ratio, since expression of OPG and RANKL were proportionally decreased. These concentrations of PRL had no effect on the mRNA expression of osteocalcin and osteopontin, nor on mineralization. High pathologic concentrations of PRL (1000 ng/mL) may downregulate expression of genes that are essential for osteoblast differentiation and functions. The present results explained the clinical findings of hyperprolactinemia-induced bone loss.

Key words: hyperprolactinemia, mineralization, osteocalcin, osteopontin, real-time PCR.

Résumé : L'hyperprolactinémie d'origine physiologique ou pathologique, comme celle associée à la lactation et au prolactinome, entraîne une ostéopénie progressive. Toutefois, les mécanismes sous-jacents font l'objet de controverse. La prolactine (PRL) pourrait atténuer directement les fonctions des ostéoblastes, puisque ces cellules osseuses expriment les récepteurs de la PRL. Ainsi, la présente étude a eu pour but d'évaluer, par PCR quantitative en temps réel, les effets de la PRL sur l'expression des gènes associés aux fonctions des ostéoblastes. Nous avons utilisé des ostéoblastes primaires provenant de tibias de rats adultes, et présenté les caractéristiques des ostéoblastes différenciés, y compris la minéralisation in vitro. Les ostéoblastes exposés à 1000 ng/mL de PRL, mais pas à 10 ni à 100 ng/mL, pendant 48 h, ont montré des diminutions de l'expression des ARNm de Runx2, de l'ostéoprotégérine (OPG) et de l'activateur du récepteur du ligand du facteur nucléaire κB (RANKL) de 60,49 %, 72,74 % et de 87,51 % respectivement. Toutefois, la PRL n'a pas modifié le rapport RANKL/OPG, puisque l'expression de l'OPG et celle de RANKL ont diminué de manière proportionnelle. Ces concentrations de PRL n'ont pas eu d'effet sur l'expression des ARNm de l'ostéocalcine et de l'ostéopontine, ni sur la minéralisation. On a pu conclure que la forte concentration pathologique de PRL (1000 ng/mL) a diminué l'expression des gènes qui étaient essentiels aux fonctions et à la différenciation des ostéoblastes. Ces résultats ont expliqué les découvertes cliniques de la perte osseuse induite par l'hyperprolactinémie.

Mots-clés : hyperprolactinémie, minéralisation, ostéocalcine, ostéopontine, PCR temps réel.

[Traduit par la Rédaction]

Received 10 November 2007. Published on the NRC Research Press Web site at cjpp.nrc.ca on 17 April 2008.

N. Charoenphandhu[1] and N. Krishnamra. Department of Physiology, Faculty of Science, Mahidol University, Rama VI Road, Bangkok 10400, Thailand; Consortium for Calcium and Bone Research, Faculty of Science, Mahidol University, Bangkok, Thailand.
J. Teerapornpuntakit. Department of Physiology, Faculty of Science, Mahidol University, Rama VI Road, Bangkok 10400, Thailand.
M. Methawasin and K. Thongchote. Consortium for Calcium and Bone Research, Faculty of Science, Mahidol University, Bangkok, Thailand.
K. Wongdee. Consortium for Calcium and Bone Research, Faculty of Science, Mahidol University, Bangkok, Thailand; Department of Pathobiology, Faculty of Science, Mahidol University, Bangkok, Thailand.

[1]Corresponding author (e-mail: naratt@narattsys.com).

 doi:10.1139/Y08-037

Introduction

A growing body of evidence suggests a connection between high serum prolactin (PRL) levels, calcium metabolism, and bone disorders (Biller et al. 1992; Charoenphandhu and Krishnamra 2007; Lotinun et al. 2003). Pathologic hyperprolactinemia can lead to bone loss and progressive osteopenia in adult rats and humans (Biller et al. 1992; Haddad and Wieck 2004; Jung et al. 2006), whereas physiologic hyperprolactinemia, such as that during pregnancy (75–100 ng/mL) and lactation (200–300 ng/mL), enhances bone turnover with decreased bone mineral density (Lotinun et al. 2003; Ritchie et al. 1998; Sengupta et al. 2005; Ulrich et al. 2003). Although lactation-induced osteopenia is usually reversible after weaning, severe osteoporosis and higher risk of fracture have been reported (Bezerra et al. 2004; Honjo and Mizunuma 2001). Osteopenia and osteoporosis are common in pathologic conditions with chronic hyperprolactinemia (up to 1000 ng/mL), for example, prolactinoma and prolonged antipsychotic drug uses (Biller et al. 1992; Haddad and Wieck 2004).

Suppression of ovarian estrogen synthesis has long been accepted as a mechanism of hyperprolactinemia-induced bone loss (Wang and Chan 1982; Wang et al. 1980). A possible direct action of PRL on bone cells, however, is suggested by the findings that osteosarcoma cell lines MG-63 and Saos-2, as well as primary osteoblasts, expressed transcripts of PRL receptors (PRLR) (Bataille-Simoneau et al. 1996). Coss and co-workers (2000) by using immunohistochemical technique confirmed the presence of PRLRs in the osteoblasts of intact calvaria. Since reduction in bone mass can result from a decrease in bone formation and (or) an increase in bone resorption, and since little is known regarding the direct action of PRL on osteoblasts, it is hypothesized that, besides PRL-induced hypoestrogenemic bone loss, PRL may decrease the bone-forming functions of osteoblasts, thus leading to osteopenia.

Bone formation commences after osteoblast differentiation. A transcription factor named *runt*-related transcription factor (Runx) 2, previously known as the core binding factor a1 (Cbfa1), is essential for osteoblast differentiation and maturation (Komori et al. 1997; Xiao et al. 2005). *Runx2*$^{-/-}$ mice are not viable and completely lack bone formation due to the absence of osteoblast differentiation (Komori et al. 1997). Once differentiated, osteoblasts express several key proteins, such as osteocalcin, osteopontin, receptor activator of nuclear factor κB ligand (RANKL), and osteoprotegerin (OPG). Osteocalcin and osteopontin are required for matrix mineralization, while the balance between RANKL and OPG determines bone remodeling (Addison et al. 2007; Hoang et al. 2003; Kostenuik 2005). Both soluble and membrane-bound forms of RANKL activate osteoclastogenesis through their receptors on the plasma membrane of osteoclasts, whereas their soluble decoy receptors, OPG, reduce osteoclast number and bone resorption (Kostenuik 2005). Thus, PRL may decrease the expression of these genes and thus, in turn, reduce the rate of bone formation in adult animals.

Therefore, the objective of this study was to investigate the effect of PRL on the expression of Runx2, osteocalcin, osteopontin, OPG, and RANKL, all of which represent osteoblast functions. Primary osteoblasts derived from the tibiae of sexually mature adult rats were used in the present study, since the osteopenic effect of hyperprolactinemia on bone was trivial in weaning and adolescent rats (Bole-Feysot et al. 1998).

Materials and methods

Animals

Eight-week-old female Sprague–Dawley rats weighing 180–200 g were obtained from the National Laboratory Animal Centre, Thailand. They were placed in hanging stainless steel cages, fed standard pellets containing 1% *w/w* calcium and 4000 IU/kg vitamin D (Perfect Companion, Bangkok, Thailand), and distilled water ad libitum under a 12 h light : 12 h dark cycle. Room temperature was controlled at 23–25 °C, and the relative humidity was about 50%–60%. Body weight and food intake were daily recorded. Animals were cared for in accordance with the *Guide to the Care and Use of Experimental Animals* of the Canadian Council on Animal Care. This study has been approved by the institutional animal care and use committee of the Faculty of Science, Mahidol University, Thailand.

Primary osteoblast culture

The culture technique was modified from the method of Bakker and Klein-Nulend (2003). Under 50 mg/kg sodium pentobarbitone (Abbott, North Chicago, Ill.) i.p. anesthesia, tibiae were dissected from a rat by sterile surgical technique. After removing the connective tissues and marrow cells, bones were cut into small dice and incubated on a shaker (60 cycles/min) for 2 h at 37 °C in a 25 cm^2 T-flask (Corning, N.Y.) containing DMEM supplemented with 100 U/mL penicillin/streptomycin and 2 mg/mL collagenase (all purchased from Sigma, St. Louis, Mo.). Thereafter, bone dice were washed with DMEM and then cultured in DMEM supplemented with 15% FBS, 100 U/mL penicillin/streptomycin, 100 μg/mL ascorbate-2-phosphate, and 0.5 mmol/L sodium pyruvate (Sigma) at 37 °C with 5% CO_2. Osteoblasts proliferated and migrated from bone dice into the media within 3 days. Media were changed daily until day 14 or 20 for expression study or mineralization assay, respectively. After 14 or 20 days of culture, primary osteoblasts were sampled from culture flasks, evaluated for morphology with a light microscope, and investigated for the expression of markers of osteoblast differentiation, that is, mRNA expression of important transcription factors AJ18, Runx2, osterix, distal-less homeobox 5 (Dlx5), and *msh* homeobox homolog 2 (Msx2) (Koga et al. 2005; Takagi et al. 2004; Takayama et al. 2007). Cultures were discarded if the percentage coefficient of variation of the marker gene between each culture was more than 5%. Since morphology and viability of the tibia-derived primary osteoblasts, in contrast to that of the primary osteoblasts from neonatal rat calvaria, became variable after the fourth passage (Charoenphandhu and Krishnamra 2007; unpublished observation), we used only confluent cells from the second passage in this study.

Mineralization assay

In vitro mineralization, an important characteristic of pri-

Table 1. *Rattus norvegicus* oligonucleotide sequences used in PCR experiments.

Gene	Accession No.	Primer, forward/reverse	Product length, bp
PRLR-S	NM_012630	5′-CCTCGGAACCTGACATTAGA-3′	492
		5′-CTTGTATTTGCTTGGAGAACC-3′	
PRLR-L	NM_001034111	5′-CCTCGGAACCTGACATTAGA-3′	660
		5′-AGAGTCACTGTCGGGATCTAG-3′	
PRL	NM_012629	5′-CAAACCTTCTGTTCTGCC-3′	171
		5′-CACGATCTTGGACATACTG-3′	
AJ18	AF321874	5′-GTCCCTGGTATGTATCAC-3′	133
		5′-GAAGACTTTGGCTAAAAC-3′	
Osterix	AY177399	5′-GCCTACTTACCCGTCTGA-3′	139
		5′-CTCCAGTTGCCCACTATT-3′	
Dlx5	NM_012943	5′-CTCTCTAGGACTGACGCAAAC-3′	135
		5′-GAGTTACACGCCATAGGGTC-3′	
Msx2	NM_012982	5′-TAGACCTGTGCTTCCCAT-3′	114
		5′-ACAAACATCCATCCTAGAGTG-3′	
Runx2	XM_001066909	5′-TAACGGTCTTCACAAATCCTC-3′	145
		5′-GGCGGTCAGAGAACAAACTA-3′	
Osteocalcin	J04500	5′-CACAGGGAGGTGTGTGAG-3′	203
		5′-TGTGCCGTCCATACTTTC-3′	
Osteopontin	NM_012881	5′-TTCACTGCCAGCACACAA-3′	101
		5′-TTTGACCTCAGTCCGTAAGC-3′	
OPG	NM_012870	5′-ATTGGCTGAGTGTTCTGGT-3′	140
		5′-CTGGTCTCTGTTTTGATGC-3′	
RANKL	NM_057149	5′-TCGCTCTGTTCCTGTACT-3′	145
		5′-AGTGCTTCTGTGTCTTCG-3′	
GAPDH	NM_017008	5′-AGTCTACTGGCGTCTTCAC-3′	133
		5′-TCATATTTCTCGTGGTTCAC-3′	

Note: PRLR-S, short isoform of prolactin receptor; PRLR-L, long isoform of prolactin receptor; PRL, prolactin; Dlx5, distal-less homeobox 5; Msx2, *msh* homeobox homolog 2; Runx2, *runt*-related transcription factor 2; OPG, osteoprotegerin; RANKL, receptor activator of nuclear factor κB ligand; GAPDH, glyceraldehyde-3-phosphate dehydrogenase.

mary osteoblasts, was determined by the alizarin red-S staining technique. Cells were washed with PBS pH 7.4, and fixed at 25 °C with 4% paraformaldehyde in PBS. After washing with distilled water, cells were stained at room temperature with 2% *w/v* alizarin red-S (Fluka, Seelze, Germany) dissolved in water (pH 4.1) for 5 min. After a final wash with distilled water, the stained mineralizing nodules were visualized under a light microscope.

Total RNA preparation

Total RNA was prepared from primary rat osteoblasts and pituitary glands using Trizol reagent (Invitrogen, Carlsbad, Calif.), and purified with RNeasy Mini kit (Qiagen, Valencia, Calif.). Purity of the total RNA was determined by the ratio of absorbance readings at 260 and 280 nm, the ratio of which fell in the range of 1.8–2.0. Integrity of RNA was analyzed by denaturing agarose gel electrophoresis with the 28S rRNA band appearing approximately twice as intense as the 18S rRNA band. 1 μg of the total RNA was reverse-transcribed with the oligo-dT_{15} primer and the iScript kit (Bio-Rad, Hercules, Calif.). Glyceraldehyde-3-phosphate dehydrogenase (GAPDH), a housekeeping gene, served as a control gene to check the consistency of the reverse transcription (coefficient of variation was less than 1%, $n = 20$).

qRT-PCR and sequencing

Primers used in the present study were designed by Oligo 6 (Molecular Biology Insights, Cascade, Co.) and Primer Validator 1.4 (Naratt Software, Bangkok, Thailand), as shown in Table 1. Quantitative real-time (qRT)-PCR and melting curve analysis were performed by Bio-Rad Mini-Opticon with the iQ SYBR Green Supermix (Bio-Rad). Conventional PCR was performed with the GoTaq Green Master Mix (Promega, Madison, Wis.) and Bio-Rad MyCycler. The PCR products were also visualized on a 1.5% agarose gel stained with 1.0 μg/mL ethidium bromide under a UV transilluminator (Alpha Innotech, San Leandro, Calif.). After electrophoresis, all PCR products were purified by the HiYield Gel/PCR DNA Extraction kit (Real Biotech Corporation, Taipei, Taiwan) and were sequenced by the ABI Prism 3100 Genetic Analyzer (Applied Biosystems, Foster City, Calif.).

Experimental design

Primary osteoblasts were subcultured in petri dishes. At day 14, cells were incubated in media containing 10, 100, or 1000 ng/mL PRL (Sigma) for 48 h. Confluent cells from the same rat in 6 petri dishes were pooled together for the total RNA preparation. Expression of Runx2, osterix, AJ18, osteocalcin, osteopontin, OPG, and RANKL was investigated by qRT-PCR. The PCR experiments were performed in triplicate. As for the mineralization study, confluent cells (day 14) were continuously incubated for 5 days with normal media (control) or 1000 ng/mL PRL-containing media. In some experiments, 14-day untreated osteoblasts were de-

Fig. 1. (A) Expression of mRNAs encoding transcription factors AJ18, Runx2, osterix, Dlx5, and Msx2 used as markers of cell differentiation in primary osteoblasts derived from tibiae of adult female rats (n = 3). (B) Expression of short (PRLR-S) and long (PRLR-L) isoforms of prolactin receptors (PRLRs) in primary osteoblasts (n = 3). (C) Prolactin (PRL) mRNA was not expressed in primary osteoblasts (OB, n = 3). The pituitary glands (PG) were used as positive controls (n = 3). GAPDH is a housekeeping gene. (D) A representative micrograph of the alizarin-stained mineralizing nodule (arrow), magnification × 60. Primary rat osteoblasts were cultured in DMEM containing 100 μg/mL ascorbate-2-phosphate for 20 days before staining (n = 5). (E) Expression of GAPDH in primary osteoblasts incubated for 48 h with 10, 100, or 1000 ng/mL PRL. Numbers in parentheses are the number of animals in each group.

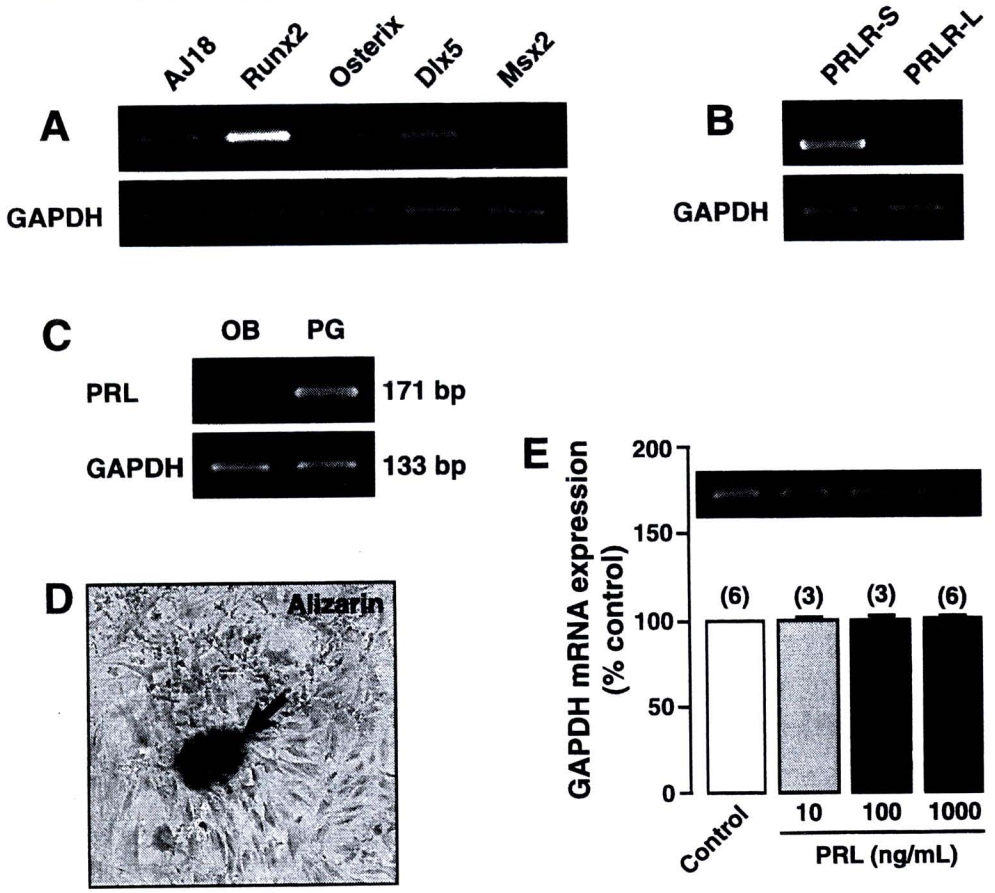

termined for the expression of PRLRs and PRL by using conventional PCR, while 20-day osteoblasts were used for mineralization assay. The total RNA of pituitary glands was used as a positive control for the PRL expression study.

Statistical analysis

Results were expressed as means ± SE. Multiple comparisons were performed by Kruskal–Wallis nonparametric test with Dunn's multiple comparison method, that is, the Gaussian distributions were not assumed. The level of significance for all statistical tests was $p < 0.05$. Data were analyzed by GraphPad Prism 4.0 for Mac OS X (GraphPad Software, San Diego, Calif.).

Results

After 14 days of culture, cells derived from rat tibiae were confluent, adhered to the surface of petri dish, and displayed typical osteoblast morphology with numerous filopodia. They strongly expressed several markers of differentiation, including AJ18, Runx2, osterix, Dlx5, and Msx2 (Fig. 1A), indicating that these cells were differentiated osteoblasts. In addition, they were found to express PRLRs, but not PRL (Figs. 1B and 1C). At day 20 of culture, alizarin red-S staining revealed the formation of mineralizing nodules that were important characteristics of differentiated osteoblasts (Fig. 1D). The mineralizing nodules were found in all cultures. In the gene expression study, we used GAPDH for normalization because expression of GAPDH was not changed after PRL incubation (Fig. 1E).

After 48-hour exposure to high concentrations of PRL, functions of the primary osteoblasts were compromised. High pathologic PRL of 1000 ng/mL, but not normal concentration of 10 ng/mL or high physiologic concentration of 100 ng/mL, decreased the expression of a salient transcription factor Runx2 to 39.51% (–2.53 fold change, $p < 0.01$) of the control level (Fig. 2A). The same concentrations, however, had no effect on the mRNA expression of osterix (Fig. 2B), AJ18 (Fig. 2C), osteocalcin (Fig. 3A), or osteopontin (Fig. 3B). Interestingly, only 1000 ng/mL PRL significantly downregulated the expression of OPG (Fig. 4A) and RANKL (Fig. 4B) by 72.74% (–3.67 fold change, $p < 0.05$) and 87.51% (–8.01 fold change, $p < 0.01$), respectively. As OPG and RANKL expression were decreased, the expres-

sion ratios of RANKL/OPG of PRL-treated osteoblasts were comparable to that of the control (Fig. 4C). Moreover, 1000 ng/mL PRL did not affect mineralizing capacity of primary osteoblasts (Fig. 5).

Discussion

Direct actions of PRL on rat bone cannot be investigated in vivo because it is not possible to induce hyperprolactinemia without changing serum concentrations of other hormones, for example, estrogen and gonadotropins. It is also not technically possible to purify sufficient numbers of living osteoblasts from bone tissues for in vitro experiment. Therefore, we used the tibia-derived primary osteoblasts, which manifested typical osteoblast morphology and characteristics including the ability to form mineralizing nodules (Aronow et al. 1990), as an in vitro experimental model to illustrate the direct effect of PRL on osteoblasts. In the present study, we demonstrate, for the first time, that high PRL decreased the expression of the osteoblast genes, that is, Runx2, OPG, and RANKL, which are important for osteoblast differentiation and bone remodeling (Kostenuik 2005; Lambertini et al. 2007; Xiao et al. 2005). Since extrapituitary PRL produced in several tissues (for example, lymphoid cells in bone marrow and mammary epithelial cells (Bole-Feysot et al. 1998)) may interfere with data interpretation, the expression of PRL was first investigated to show that primary rat osteoblasts did not synthesize PRL and that the observed PRL action was due to the exogenous PRL added to the media.

Both physiologic and pathologic hyperprolactinemia can lead to trabecular bone loss and osteoporosis in adult rats and humans (Biller et al. 1992; Liu-Seifert et al. 2004; Lotinun et al. 2003). Our previous in vivo study in lactating rats showed that PRL enhanced bone turnover, which was accompanied by a significant increase in the excretion of bone formation marker deoxypyridinoline (Lotinun et al. 2003). On the other hand, administration of bromocriptine, as an inhibitor of the pituitary PRL secretion, to lactating rats decreased the calcium resorption rate in the femora, tibiae, L5–6 vertebrae, and sternum by 20%–42% (Lotinun et al. 2003). Furthermore administration of PRL to unmated adult female rats increased bone turnover similar to that in lactating rats (Krishnamra and Seemoung 1996; Krishnamra et al. 1997). In hyperprolactinemic premenopausal patients, progressive trabecular osteopenia with low spinal bone density was also observed at the end of the 1.7-year study (Biller et al. 1992).

Although it is widely accepted that bone loss is a common finding in hyperprolactinemia, the mechanism of PRL action on bone remains controversial. PRL is believed to induce bone loss by suppressing ovarian estrogen production (Wang and Chan 1982; Wang et al. 1980). This was confirmed by an in vitro study on cultured ovarian granulosa cells that showed 1000 ng/mL PRL suppressed estrogen production by 80% (Wang and Chan 1982). The expression of PRLRs in osteoblasts, however, strongly suggested bone as a direct target of PRL (Bataille-Simoneau et al. 1996; Coss et al. 2000; Clément-Lacroix et al. 1999). In contrast, osteoclasts did not express PRLRs (Coss et al. 2000). Therefore, in addition to hypoestrogenemia, the PRL-induced osteopenia may be partly due to a decrease in the osteoblast function. In other words, PRL may exert its direct action on osteoblasts concurrently with the indirect action via suppression of the ovarian estrogen secretion, thereby leading to osteopenia.

Regarding a direct action of PRL on osteoblasts, Coss and

Fig. 2. Expression of the transcription factor (A) Runx2, (B) osterix, and (C) AJ18 in primary osteoblasts incubated for 48 h with 10, 100, or 1000 ng/mL prolactin (PRL). GAPDH is a housekeeping gene for normalization. Significant at **, $p < 0.01$ compared with the control group. Numbers in parentheses are the number of animals in each group.

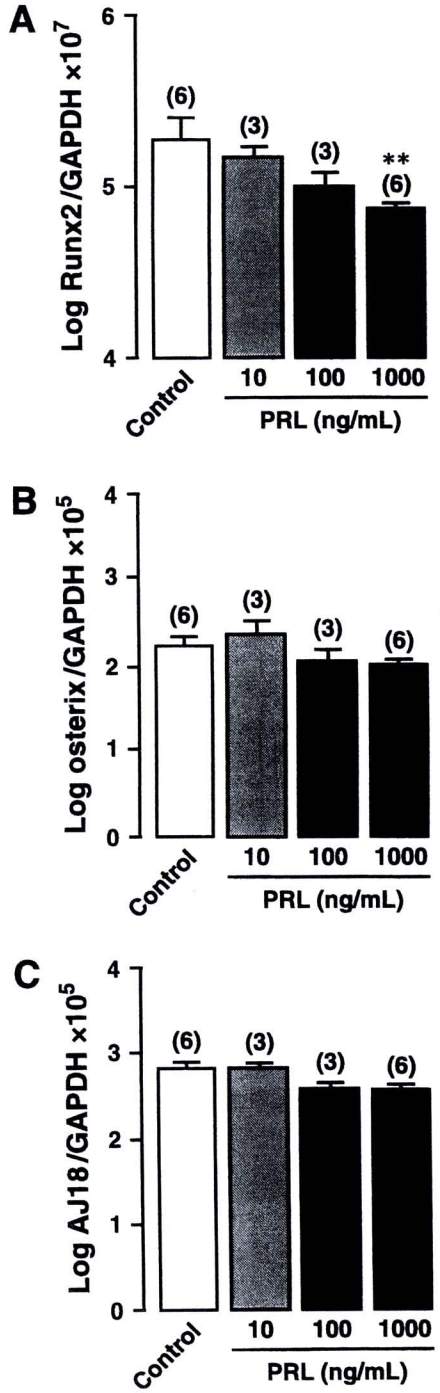

Fig. 3. Expression of (A) osteocalcin and (B) osteopontin in primary osteoblasts incubated for 48 h with 10, 100, or 1000 ng/mL prolactin (PRL). GAPDH is a housekeeping gene for normalization. Numbers in parentheses are the number of animals in each group.

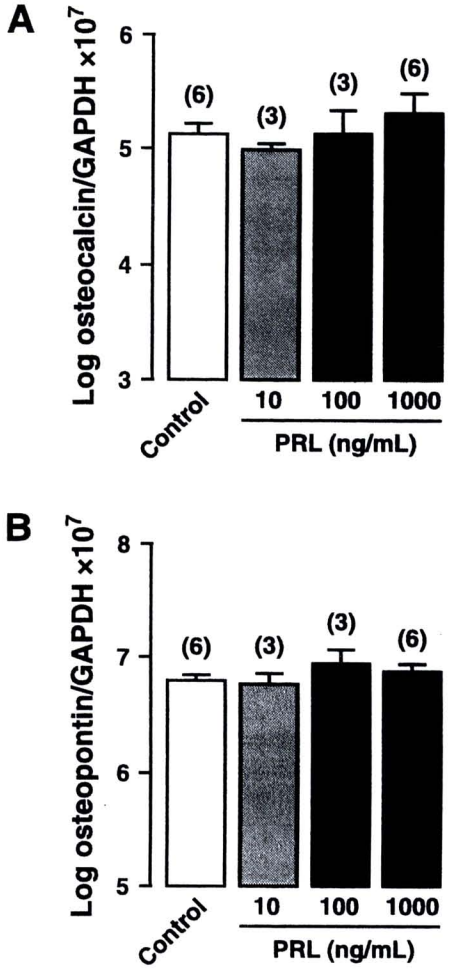

co-workers reported that in vitro proliferation of primary osteoblasts from neonatal rats was not altered after exposure to 1000 ng/mL PRL (Coss et al. 2000); however, 100 and 1000 ng/mL PRL, but not 10 ng/mL PRL, suppressed the osteoblast alkaline phosphatase activity by 10% and 25%, respectively (Coss et al. 2000). Therefore, PRL may predominantly affect osteoblast functions rather than osteoblast number. Osteoblast functions such as matrix protein synthesis and mineralization generally start after cells become fully differentiated (Aronow et al. 1990). Extensive investigations have demonstrated that Runx2 is an essential transcription factor for the differentiation of osteoblasts. After binding to the specific promoters, Runx2 regulates transcription of a number of osteoblast-expressed genes, for example, bone morphogenetic proteins, alkaline phosphatase, and bone sialoprotein (Bertaux et al. 2005; Lambertini et al. 2007; Young et al. 2005). Komori and colleagues (1997) showed that *Runx2* knockout was lethal and that mouse embryos exhibited a complete lack of bone formation. Our findings, which show downregulation of Runx2, confirm the hypothesis that PRL interferes with osteoblast differentiation, thus, in turn, contributing to bone loss.

Bone remodeling can be altered by a minor change in the

Fig. 4. Expression of (A) OPG, (B) RANKL, and (C) ratio of RANKL/OPG in primary osteoblasts incubated for 48 h with 10, 100, or 1000 ng/mL prolactin (PRL). Significant at *, $p < 0.05$ and **, $p < 0.01$ compared with respective control group. Numbers in parentheses are the number of animals in each group.

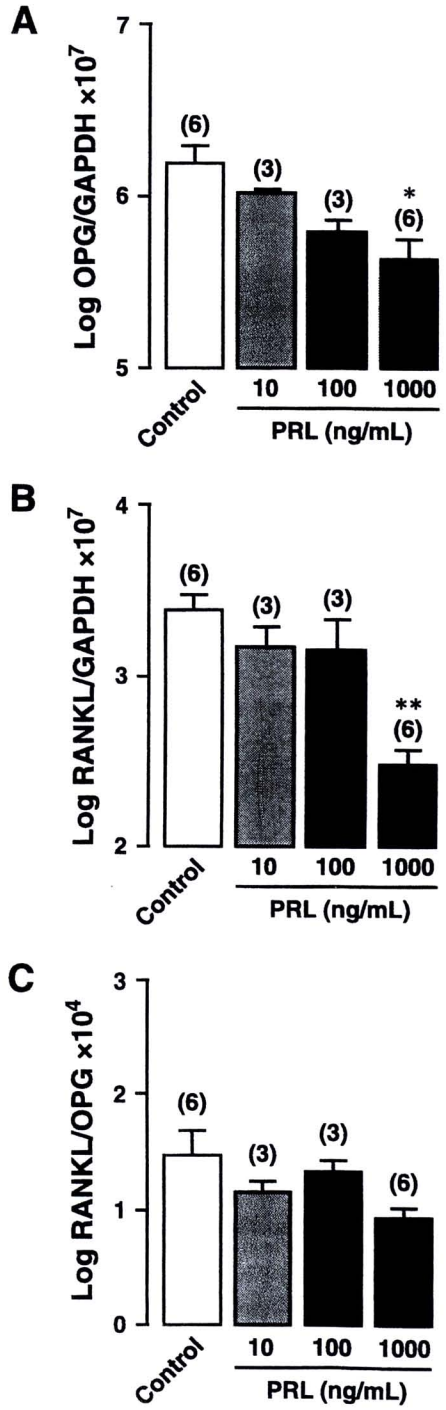

RANKL/OPG ratio (Kostenuik 2005). Increases in the RANKL/OPG ratio are positively correlated with eroded bone surface, hip fracture, and osteoporosis (Abdallah et al. 2005; Fazzalari et al. 2001; Grimaud et al. 2003; Kostenuik 2005). Thus, a slight decrease in the RANKL/OPG ratio especially in the 1000 ng/mL-treated group, despite being insignificant, could have changed the rate of bone remodeling

Fig. 5. Representative images of mineralization of confluent osteoblasts incubated for 5 days with normal media (control, n = 3 rats) or media containing 1000 ng/mL prolactin (PRL) (n = 3 rats). Mineralization was visualized by alizarin red-S staining.

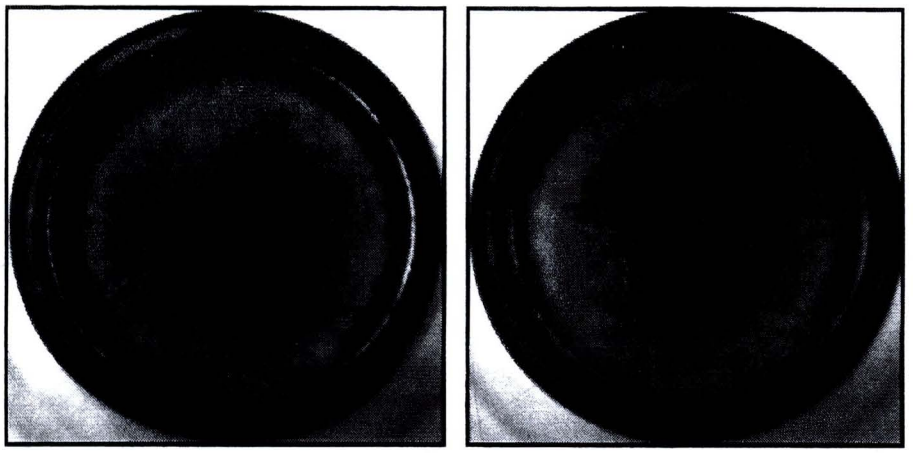

Control **1000 ng/mL PRL**

in vivo. Nevertheless, the concurrent downregulation of both OPG and RANKL expression by 1000 ng/mL in the present study indicates that PRL could directly modulate the osteoblast function, which, in turn, regulates bone remodeling.

Osteocalcin is the most abundant noncollagenous calcium-binding protein in bone, while osteopontin, a phosphorylated glycoprotein, comprises approximately 2% of the noncollagenous protein in bone (Haylock and Nilsson 2006). These two proteins are synthesized by differentiated osteoblasts, especially at the initiation of mineralization, and are required for bone calcium acquisition and mineralization (Addison et al. 2007; Hoang et al. 2003). The present data show, however, that 10–1000 ng/mL PRL did not alter the expression of osteocalcin or osteopontin (Fig. 3) as well as mineralization (Fig. 5). It appears that PRL via its direct action selectively affects certain functions of osteoblasts, such as expression of genes involved in cell differentiation and bone remodeling, rather than the gene transcription of noncollagenous matrix proteins or mineralization. Further study is required to demonstrate the effect of PRL on osteoblast differentiation.

Interestingly, the effective concentration of PRL on primary osteoblasts was 1000 ng/mL, which can be found in certain pathologic conditions, such as prolactinoma. Effects of the lower concentrations of PRL (10 and 100 ng/mL) on primary osteoblasts were not observed here, although both concentrations showed a tendency to decrease the mRNA expression of Runx2 and OPG (Figs. 2 and 4). These results agreed with the reported findings that pregnancy, which is accompanied by high physiologic PRL levels of 75–100 ng/mL, causes a minimal change in bone mineral density and mineral content (Ritchie et al. 1998). Nevertheless, a 3-fold further increase in PRL levels during lactation (200–300 ng/mL) can result in transient osteopenia, or even osteoporosis (Lotinun et al. 2003; Ritchie et al. 1998). Because normal concentrations of PRL of approximately 7–10 ng/mL are also essential for normal maintenance of the basal rate of bone remodeling, suppression of endogenous PRL secretion by 15 days of bromocriptine administration in unmated female rats led to uncoupling of bone resorption and bone formation, resulting in a significant increase in calcium deposition in the sternum and L5–6 vertebrae (Puntheeranurak et al. 2006). Since the effect of 10 ng/mL was not observed in this study, the action of basal levels of PRL on bone may be acting indirectly through an unidentified mechanism.

In conclusion, besides the indirect osteopenic effects through suppression of estrogen production, PRL appears to have direct actions on osteoblasts. High pathologic PRL, but not normal (basal) or high physiologic concentrations, suppresses osteoblast functions by decreasing the mRNA expression of Runx2, OPG, and RANKL. Although the present study was performed only at the transcriptional level, the results could partly explain hyperprolactinemia-induced progressive osteopenia in rats and humans.

Acknowledgements

We thank Jirawan Thongbunchoo for excellent technical assistance. This research was supported by grants from the Thailand Research Fund (TRF) and the Commission on Higher Education (CHE). The authors declare no conflicts of interest.

References

Abdallah, B.M., Stilgren, L.S., Nissen, N., Kassem, M., Jorgensen, H.R., and Abrahamsen, B. 2005. Increased RANKL/OPG mRNA ratio in iliac bone biopsies from women with hip fractures. Calcif. Tissue Int. **76**: 90–97. doi:10.1007/s00223-004-0074-4. PMID:15570403.

Addison, W.N., Azari, F., Sørensen, E.S., Kaartinen, M.T., and McKee, M.D. 2007. Pyrophosphate inhibits mineralization of osteoblast cultures by binding to mineral, up-regulating osteopontin, and inhibiting alkaline phosphatase activity. J. Biol. Chem. **282**: 15872–15883. doi:10.1074/jbc.M701116200. PMID: 17383965.

Aronow, M.A., Gerstenfeld, L.C., Owen, T.A., Tassinari, M.S., Stein, G.S., and Lian, J.B. 1990. Factors that promote progressive development of the osteoblast phenotype in cultured fetal rat calvaria cells. J. Cell. Physiol. **143**: 213–221. doi:10.1002/jcp.1041430203. PMID:2332447.

Bakker, A., and Klein-Nulend, J. 2003. Osteoblast isolation from

murine calvariae and long bones. *In* Methods in Molecular Medicine: Bone Research Protocols. *Edited by* M.H. Helfrich and S.H. Ralston. Humana Press, New Jersey. pp. 19–28.

Bataille-Simoneau, N., Gerland, K., Chappard, D., Basle, M.F., and Mercier, L. 1996. Expression of prolactin receptors in human osteosarcoma cells. Biochem. Biophys. Res. Commun. **229**: 323–328. doi:10.1006/bbrc.1996.1800. PMID:8954126.

Bertaux, K., Broux, O., Chauveau, C., Jeanfils, J., and Devedjian, J.C. 2005. Identification of CBFA1-regulated genes on SaOs-2 cells. J. Bone Miner. Metab. **23**: 114–122. doi:10.1007/s00774-004-0549-4. PMID:15750689.

Bezerra, F.F., Mendonca, L.M., Lobato, E.C., O'Brien, K.O., and Donangelo, C.M. 2004. Bone mass is recovered from lactation to postweaning in adolescent mothers with low calcium intakes. Am. J. Clin. Nutr. **80**: 1322–1326. PMID:15531682.

Biller, B.M., Baum, H.B., Rosenthal, D.I., Saxe, V.C., Charpie, P.M., and Klibanski, A. 1992. Progressive trabecular osteopenia in women with hyperprolactinemic amenorrhea. J. Clin. Endocrinol. Metab. **75**: 692–697. doi:10.1210/jc.75.3.692. PMID: 1517356.

Bole-Feysot, C., Goffin, V., Edery, M., Binart, N., and Kelly, P.A. 1998. Prolactin (PRL) and its receptor: actions, signal transduction pathways and phenotypes observed in PRL receptor knockout mice. Endocr. Rev. **19**: 225–268. doi:10.1210/er.19.3.225. PMID:9626554.

Charoenphandhu, N., and Krishnamra, N. 2007. Prolactin is an important regulator of intestinal calcium transport. Can. J. Physiol. Pharmacol. **85**: 569–581. doi:10.1139/Y07-041. PMID: 17823618.

Clément-Lacroix, P., Ormandy, C., Lepescheux, L., Ammann, P., Damotte, D., Goffin, V., et al. 1999. Osteoblasts are a new target for prolactin: analysis of bone formation in prolactin receptor knockout mice. Endocrinology, **140**: 96–105. doi:10.1210/en.140.1.96. PMID:9886812.

Coss, D., Yang, L., Kuo, C.B., Xu, X., Luben, R.A., and Walker, A.M. 2000. Effects of prolactin on osteoblast alkaline phosphatase and bone formation in the developing rat. Am. J. Physiol. Endocrinol. Metab. **279**: E1216–E1225. PMID:11093907.

Fazzalari, N.L., Kuliwaba, J.S., Atkins, G.J., Forwood, M.R., and Findlay, D.M. 2001. The ratio of messenger RNA levels of receptor activator of nuclear factor κB ligand to osteoprotegerin correlates with bone remodeling indices in normal human cancellous bone but not in osteoarthritis. J. Bone Miner. Res. **16**: 1015–1027. doi:10.1359/jbmr.2001.16.6.1015. PMID:11393778.

Grimaud, E., Soubigou, L., Couillaud, S., Coipeau, P., Moreau, A., Passuti, N., et al. 2003. Receptor activator of nuclear factor κB ligand (RANKL)/ osteoprotegerin (OPG) ratio is increased in severe osteolysis. Am. J. Pathol. **163**: 2021–2031. PMID: 14578201.

Haddad, P.M., and Wieck, A. 2004. Antipsychotic-induced hyperprolactinaemia: mechanisms, clinical features and management. Drugs, **64**: 2291–2314. doi:10.2165/00003495-200464200-00003. PMID:15456328.

Haylock, D.N., and Nilsson, S.K. 2006. Osteopontin: a bridge between bone and blood. Br. J. Haematol. **134**: 467–474. doi:10.1111/j.1365-2141.2006.06218.x. PMID:16848793.

Hoang, Q.Q., Sicheri, F., Howard, A.J., and Yang, D.S. 2003. Bone recognition mechanism of porcine osteocalcin from crystal structure. Nature, **425**: 977–980. doi:10.1038/nature02079. PMID:14586470.

Honjo, S., and Mizunuma, H. 2001. Changes in biochemical parameters of bone turnover and bone mineral density in postpregnancy osteoporosis. Am. J. Obstet. Gynecol. **185**: 246–247. doi:10.1067/mob.2001.113910. PMID:11483939.

Jung, D.U., Conley, R.R., Kelly, D.L., Kim, D.W., Yoon, S.H., Jang, J.H., et al. 2006. Prevalence of bone mineral density loss in Korean patients with schizophrenia: a cross-sectional study. J. Clin. Psychiatry, **67**: 1391–1396. PMID:17017825.

Koga, T., Matsui, Y., Asagiri, M., Kodama, T., de Crombrugghe, B., Nakashima, K., and Takayanagi, H. 2005. NFAT and osterix cooperatively regulate bone formation. Nat. Med. **11**: 880–885. doi:10.1038/nm1270. PMID:16041384.

Komori, T., Yagi, H., Nomura, S., Yamaguchi, A., Sasaki, K., Deguchi, K., et al. 1997. Targeted disruption of Cbfa1 results in a complete lack of bone formation owing to maturational arrest of osteoblasts. Cell, **89**: 755–764. doi:10.1016/S0092-8674(00)80258-5. PMID:9182763.

Kostenuik, P.J. 2005. Osteoprotegerin and RANKL regulate bone resorption, density, geometry and strength. Curr. Opin. Pharmacol. **5**: 618–625. doi:10.1016/j.coph.2005.06.005. PMID: 16188502.

Krishnamra, N., and Seemoung, J. 1996. Effects of acute and long-term administration of prolactin on bone ^{45}Ca uptake, calcium deposit, and calcium resorption in weaned, young, and mature rats. Can. J. Physiol. Pharmacol. **74**: 1157–1165. doi:10.1139/cjpp-74-10-1157. PMID:9022836.

Krishnamra, N., Seemoung, J., and Limlomwongse, L. 1997. Acute effect of prolactin on bone ^{45}Ca accumulation in rats. Endocr. J. **44**: 257–264. doi:10.1507/endocrj.44.257. PMID:9228461.

Lambertini, E., Penolazzi, L., Tavanti, E., Schincaglia, G.P., Zennaro, M., Gambari, R., and Piva, R. 2007. Human estrogen receptor α gene is a target of Runx2 transcription factor in osteoblasts. Exp. Cell Res. **313**: 1548–1560. doi:10.1016/j.yexcr.2007.02.002. PMID:17350616.

Liu-Seifert, H., Kinon, B.J., Ahl, J., and Lamberson, S. 2004. Osteopenia associated with increased prolactin and aging in psychiatric patients treated with prolactin-elevating antipsychotics. Ann. N. Y. Acad. Sci. **1032**: 297–298. doi:10.1196/annals.1314.044. PMID:15677434.

Lotinun, S., Limlomwongse, L., Sirikulchayanonta, V., and Krishnamra, N. 2003. Bone calcium turnover, formation, and resorption in bromocriptine- and prolactin-treated lactating rats. Endocrine, **20**: 163–170. doi:10.1385/ENDO:20:1-2:163. PMID: 12668882.

Puntheeranurak, S., Charoenphandhu, N., and Krishnamra, N. 2006. Enhanced trabecular-bone calcium deposition in female rats with a high physiological dose of prolactin diminishes after ovariectomy. Can. J. Physiol. Pharmacol. **84**: 993–1002. doi:10.1139/Y06-047. PMID:17218965.

Ritchie, L.D., Fung, E.B., Halloran, B.P., Turnlund, J.R., Van Loan, M.D., Cann, C.E., and King, J.C. 1998. A longitudinal study of calcium homeostasis during human pregnancy and lactation and after resumption of menses. Am. J. Clin. Nutr. **67**: 693–701. PMID:9537616.

Sengupta, S., Arshad, M., Sharma, S., Dubey, M., and Singh, M.M. 2005. Attainment of peak bone mass and bone turnover rate in relation to estrous cycle, pregnancy and lactation in colony-bred Sprague-Dawley rats: suitability for studies on pathophysiology of bone and therapeutic measures for its management. J. Steroid Biochem. Mol. Biol. **94**: 421–429. doi:10.1016/j.jsbmb.2004.12.039. PMID:15876407.

Takagi, M., Kamiya, N., Takahashi, T., Ito, S., Hasegawa, M., Suzuki, N., and Nakanishi, K. 2004. Effects of bone morphogenetic protein-2 and transforming growth factor β1 on gene expression of transcription factors, AJ18 and Runx2 in cultured osteoblastic cells. J. Mol. Histol. **35**: 81–90. doi:10.1023/B:HIJO.0000021151.31118.e3. PMID:15323353.

Takayama, T., Suzuki, N., Ikeda, K., Shimada, T., Suzuki, A.,

Maeno, M., et al. 2007. Low-intensity pulsed ultrasound stimulates osteogenic differentiation in ROS 17/2.8 cells. Life Sci. **80**: 965–971. doi:10.1016/j.lfs.2006.11.037. PMID:17174343.

Ulrich, U., Miller, P.B., Eyre, D.R., Chesnut, C.H., 3rd, Schlebusch, H., and Soules, M.R. 2003. Bone remodeling and bone mineral density during pregnancy. Arch. Gynecol. Obstet. **268**: 309–316. doi:10.1007/s00404-002-0410-8. PMID: 14504876.

Wang, C., and Chan, V. 1982. Divergent effects of prolactin on estrogen and progesterone production by granulosa cells of rat Graafian follicles. Endocrinology, **110**: 1085–1093. PMID: 6800769.

Wang, C., Hsueh, A.J., and Erickson, G.F. 1980. Prolactin inhibition of estrogen production by cultured rat granulosa cells. Mol. Cell. Endocrinol. **20**: 135–144. doi:10.1016/0303-7207(80) 90077-5. PMID:6777214.

Xiao, G., Jiang, D., Ge, C., Zhao, Z., Lai, Y., Boules, H., et al. 2005. Cooperative interactions between activating transcription factor 4 and Runx2/Cbfa1 stimulate osteoblast-specific osteocalcin gene expression. J. Biol. Chem. **280**: 30689–30696. doi:10. 1074/jbc.M500750200. PMID:16000305.

Young, D.W., Pratap, J., Javed, A., Weiner, B., Ohkawa, Y., van Wijnen, A., et al. 2005. SWI/SNF chromatin remodeling complex is obligatory for BMP2-induced, Runx2-dependent skeletal gene expression that controls osteoblast differentiation. J. Cell. Biochem. **94**: 720–730. doi:10.1002/jcb.20332. PMID:15565649.

J. Physiol. Sci. Vol. 58, No. 1; Feb. 2008; pp. 39–45
Online Jan. 17, 2008; **doi:10.2170/physiolsci.RP015007**

High Physiological Prolactin Induced by Pituitary Transplantation Decreases BMD and BMC in the Femoral Metaphysis, but Not in the Diaphysis of Adult Female Rats

Kanogwun THONGCHOTE[1], Narattaphol CHAROENPHANDHU[1,2], and Nateetip KRISHNAMRA[1,2]

[1]Department of Physiology and [2]Consortium for Calcium and Bone Research, Faculty of Science, Mahidol University, Rama VI Road, Bangkok 10400, Thailand

Abstract: High physiological prolactin (PRL) stimulated intestinal calcium absorption and renal calcium uptake in mammals. Previous histomorphometric study revealed a significant increase in bone turnover in the trabecular part of the PRL-exposed long (cortical) bone; however, whole-bone densitometric analysis was unable to demonstrate such effect. We therefore studied differential changes in bone mineral density (BMD) and contents (BMC) of the femoral diaphysis and metaphysis in adult female rats exposed to high PRL induced by anterior pituitary (AP) transplantation. The estrogen-dependent effects of PRL on the femur were also investigated. We found that chronic exposure to PRL had no effect on BMD or BMC of the femoral diaphysis, which represented the cortical part of the long bone. It is interesting that 7 weeks after an AP transplantation, BMD and BMC of the femoral metaphysis were significantly decreased by 8% and 14%, respectively. Ovariectomy (Ovx) for 2, 5, and 7 weeks also decreased BMD and BMC in the femoral metaphysis, but not in the diaphysis. However, the AP transplantation plus Ovx (AP+Ovx) produced no additive effects. Nevertheless, 2.5 μg/kg 17β-estradiol (E2) supplementation abolished the osteopenic effects of both Ovx and AP+Ovx on the femur. As for the L5–6 vertebrae, BMD and BMC were not affected by PRL exposure, but were significantly decreased by Ovx and AP+Ovx, and such decreases were completely prevented by E2 supplementation. It could be concluded that high physiological PRL induced a significant osteopenia in the trabecular part, i.e., the metaphysis, of the femora of adult female rats in an estrogen-dependent manner. Since PRL had no detectable effect on the vertebrae, the effects of PRL on bone appeared to be site-specific.

Key words: diaphysis, femur, metaphysis, prolactin, vertebrae.

Prolactin (PRL), as a calcium-regulating hormone, has been reported to stimulate intestinal calcium absorption, enhance renal calcium reabsorption, and induce high bone turnover in nonmated female rats [1–3]. By regulating calcium mobilization in these target organs during pregnancy and lactation, the high physiological PRL of 75–300 ng/ml increases calcium availability for fetal growth and milk production [4]. Moreover, the basal PRL level of 7–10 ng/ml was required for the maintenance of normal bone turnover and duodenal calcium absorption in rats [5, 6].

It has been shown that PRL acted directly on the intestinal absorptive cells to enhance calcium absorption [3]. In bone, osteoblasts but not osteoclasts strongly expressed functional PRL receptors (PRLR), indicating that bone was also a target of PRL [7]. However, the direct effect of PRL on osteoblasts to enhance bone turnover was complicated by its indirect actions through hyperprolactinemia-induced hypogonadism, which in turn induced chronic estrogen deficiency [8, 9]. Moreover, the PRL-enhanced calcium absorption may indirectly contribute to the increase in bone calcium deposition, as previously suggested by the ^{45}Ca kinetic and histomorphometric techniques [10–12]. Nevertheless, the effects of PRL on bone were mostly confined to the trabecular sites [13], e.g., sternum, vertebrae, and trochanter, because a 2-week exposure to high physiological PRL altered calcium deposition or the total calcium content in these bones, but not in the tibia and femur of adult rats [6, 14]. By using bone histomorphometry, we found that the trabecular microarchitecture of long bone was indeed markedly changed by long-term exposure to PRL, i.e., increased trabecular separation and decreased trabecular number [12]. Such changes were not detectable by the whole-bone densitometric study [12, 14]. We therefore hypothesized that in vivo exposure to high physiological PRL, despite showing no effect on the whole femur, may in fact alter bone mineral density

Received on Dec 13, 2007; accepted on Jan 12, 2008; released online on Jan 17, 2008; doi:10.2170/physiolsci.RP015007
Correspondence should be addressed to: N. Charoenphandhu or N. Krishnamra, Department of Physiology, Faculty of Science, Mahidol University, Rama VI Road, Bangkok 10400, Thailand. Tel/Fax: +66-2-354-7154, E-mail: naratt@narattsys.com or scnks@mahidol.ac.th

(BMD) and content (BMC) of the femoral metaphysis, the trabecular part of the long bone. Furthermore, a comparative study of PRL action on the femoral metaphysis and other primarily trabecular sites, such as vertebrae, was necessary to show whether the observed action of high physiological PRL was site-specific and confined to the trabecular part of the long bone.

In the present study, the anterior pituitary (AP) transplantation technique was used to induce the sustained high physiological PRL levels of 90–100 ng/ml [15–17], which were comparable to the levels during pregnancy in humans and rats [1]. Within 15 days after two extra AP glands were transplanted from donors under the renal capsule of a recipient (i.e., distant from the hypothalamus), a continuous secretion of PRL from the AP allografts in the absence of the hypothalamic dopaminergic inhibition resulted in a sustained physiological hyperprolactinemia [16, 18]. Other pituitary hormones were not secreted from the grafts because of the absence of their respective hypothalamic trophic factors. Moreover, by using this technique we did not subject the PRL-exposed rats to chronic stress from daily handling and PRL injection.

The objectives of the present study were to investigate changes in BMD and BMC in the femoral diaphysis, femoral metaphysis, and vertebrae of PRL-exposed female rats. Since PRL may exert its estrogen-dependent actions through hypogonadism, we also studied the effects of PRL on bone in ovariectomized (Ovx) rats with or without estrogen supplementation.

MATERIALS AND METHODS

Animals. Female Sprague-Dawley rats (10 weeks old, weighing 200–220 g), were obtained from the Animal Centre of Thailand, Salaya, Thailand. They were placed in hanging stainless steel cages, fed standard pellets containing 1% w/w calcium and 4,000 IU/kg vitamin D (Perfect Companion Co., Ltd., Bangkok, Thailand), and distilled water ad libitum under a 12 h:12 h light:dark cycle. Room temperature was controlled at 23°–25°C, and the relative humidity was about 50%–60%. Body weight and food intake were recorded daily. The animals were cared for in accordance with the "Guiding Principles for the Care and Use of Animals in the Field of Physiological Sciences." This study has been approved by the Institutional Animal Care and Use Committee of the Faculty of Science, Mahidol University, Thailand. After a 7-day acclimatization, bone mineral density (BMD) and content (BMC) were measured before surgery (considered as week 0).

Anterior pituitary (AP) transplantation. The procedure was modified from the methods of Adler *et al.* [15] and Charoenphandhu *et al.* [14]. After diethylether anesthesia, a 1.0 cm paracostal incision was made to expose the left renal capsule of the recipient rat. Two anesthetized 10-week-old donors were then decapitated, enabling us to collect the pituitary glands, which were immediately inserted into the prepared renal capsule of the recipient rat (i.e., 2 glands/rat). Both transplanted pituitary glands were covered with the renal fascia. Muscle and skin were sutured with sterile silk 3/0 and cleaned with 70% ethanol and povidone-iodine. A wound dressing was performed daily. The sham operation consisted of the exposure of the left kidney and a gentle touch of the renal fascia with forceps. The visual examination of a well-vascularized hypophyseal graft was performed at the end of the experiments to assure successful AP transplantation.

To confirm that PRL was synthesized in the transplanted glands, we dissected the hypophyseal grafts from the perirenal tissues for an immunohistochemical analysis of PRL production, as previously described [14]. In brief, formalin-fixed, paraffin-embedded 4.0 μm sections of grafts were incubated for 60 min with 1:300 PRL polyclonal primary antibody (Dako, Carpinteria, CA, USA), and they were later incubated for 10 min with 1:3,000 biotin-conjugated antirabbit secondary antibody and peroxidase-conjugated streptavidin (Dako). The chromogenic reaction was carried out with 3′,3′-diaminobenzidine to produce a brownish product. Digital images were acquired from a light microscope (model BX51 TRF, Olympus, Tokyo, Japan). All AP grafts were positive for PRL immunoreactivity (Fig. 1). This technique has also been known to raise plasma PRL to 90–100 ng/ml (comparable to the levels during pregnancy) [16] and to suppress plasma estrogen below 50 pg/ml [17].

Bilateral ovariectomy. Bilateral ovariectomy (Ovx) has been a widely accepted surgical procedure to induce chronic estrogen deficiency [17]. In brief, the rat was anesthetized with diethylether before two 1.5-cm paralumbar incisions were made. The distal parts of both fallopian tubes were ligated prior to the removal of the ovaries. The

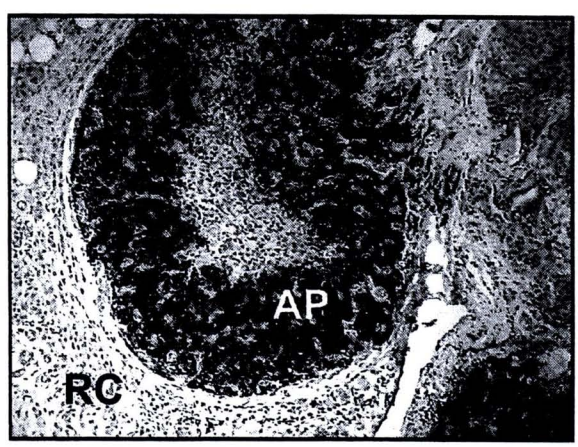

Fig. 1. Representative image of a hypophyseal allograft excised from a 7-week AP rat; magnification ×40 (n = 6). The slide was stained with anti-PRL antibody. The anterior pituitary gland (AP) is strongly labeled with brownish products of peroxidase, whereas the surrounding renal capsule (RC) is negative.

skin was finally sutured with sterile silk 3/0 and cleaned with 70% ethanol and povidone-iodine. Vital signs were carefully monitored until the rat recovered from anesthesia. The sham operation was similar to the bilateral ovariectomy, except that both ovaries were gently touched with forceps and left in place. Uterine weight and vaginal cytology confirmed the success of the surgery.

BMD and BMC measurements. BMD and BMC were determined by the modified method of Binkley *et al.* [19]. Under 50 mg/kg sodium pentobarbitone i.p. (Abbott Laboratories, North Chicago, IL, USA) anesthesia, BMD and BMC of the femora were assessed by dual-energy X-ray absorptiometry (DXA; model Lunar PIXImus2, GE Medical Systems, Madison, WI, USA), operated with a software version 2.10. The dual-energy supply was 80/35 kVp at 500 μA. The animals were laid prone on a supporting board with reproducible positioning. Both femora were placed parallel to the scan direction with knees flexed at 90°. The regions of interest (ROI) for femoral metaphysis included the distal 8 mm of the femur, whereas the ROI of femoral diaphysis included the middle part of femur between its 8-mm ends.

As for the vertebral BMD and BMC, L5–6 vertebrae were dissected and cleaned of adhering tissues. Fat-containing tissues were eluted by a 1:1 mixture of 100% ethanol and diethylether. Thereafter the bones were dried at 80°C for 48 h to obtain a constant dry weight. Ex vivo BMD and BMC were then determined. The ROI of vertebrae included the L5–6 segments.

Experimental design. To study the effect of high physiological PRL on the cortical and trabecular sites in the presence and absence of chronic estrogen deficiency, we divided the rats into 6 groups, i.e., sham-operated (Sham), ovariectomized (Ovx), Ovx supplemented with 2.5 μg/kg 17β-estradiol s.c. (Sigma) 3 times a week (Ovx+E2), AP-grafted (AP), AP+Ovx, and AP+Ovx+E2. Both AP transplantation and ovariectomy were performed on the same day (week 0). Intact BMD and BMC of the femoral diaphysis and metaphysis were measured at 2, 5, and 7 weeks postsurgery. At week 7, all rats were sacrificed for ex vivo BMD and BMC measurements in the L5–6 vertebrae.

Statistical analysis. The results are expressed as mean ± SE. Multiple comparisons were performed by one-way analysis of variance (ANOVA) with a Newman-Keuls posttest. The level of significance for all statistical tests was $P < 0.05$. The data were analyzed by GraphPad Prism 4.0 for Mac OS X (GraphPad Software, San Diego, CA, USA).

RESULTS

High PRL did not affect body weight of AP rats

At 7 weeks postsurgery, the body weights of Ovx ($n = 10$, $P < 0.001$) and AP+Ovx rats ($n = 6$, $P < 0.05$) were significantly increased (Fig. 2) and could be completely normalized by 17β-estradiol (E2) supplementation. The body weights of AP rats were comparable to those of Sham rats.

PRL decreased BMD and BMC in the femoral metaphysis in an estrogen-dependent manner

It has been known that exposure to high physiological PRL for 4–7 weeks did not change the BMD and BMC of the whole cortical bones, including the femur [12]. In the present study, we found that AP transplantation for 2, 5, and 7 weeks had no effect on BMD and BMC of the femoral diaphysis (Fig. 3). We found it interesting that a 7-week AP transplantation significantly decreased the metaphyseal BMD (Fig. 4) by 8%, i.e., from 0.229 ± 0.002 ($n = 6$) to 0.210 ± 0.003 g/cm^2 ($n = 10$, $P < 0.01$), and the metaphyseal BMC by 14%, i.e., from 0.169 ± 0.003 ($n = 6$) to 0.146 ± 0.002 g ($n = 10$, $P < 0.01$).

Similar to AP rats, the Ovx rats manifested a decrease in BMD in the metaphysis, but not in the diaphysis (Figs. 3 and 4), i.e., from 0.209 ± 0.002 ($n = 7$) to 0.186 ± 0.001 g/cm^2 ($n = 10$, $P < 0.001$) at 2 weeks, from 0.225 ± 0.003 ($n = 6$) to 0.205 ± 0.003 g/cm^2 ($n = 10$, $P < 0.01$) at 5 weeks, and from 0.229 ± 0.003 ($n = 6$) to 0.210 ± 0.004 g/cm^2 ($n = 10$, $P < 0.05$) at 7 weeks, post-Ovx. The metaphyseal BMC in Ovx rats was also consistently decreased with BMD, i.e., from 0.143 ± 0.004 ($n = 7$) to 0.125 ± 0.003 g ($n = 10$, $P < 0.05$) at 2 weeks, from 0.160 ± 0.004 ($n = 6$) to 0.139 ± 0.002 g ($n = 10$, $P < 0.01$) at 5 weeks, and from 0.169 ± 0.003 ($n = 6$) to 0.144 ± 0.003 g ($n = 10$, $P < 0.01$) at 7 weeks, post-Ovx. In rats with AP transplantation plus Ovx (AP+Ovx), their decreased metaphyseal BMD and BMC at 2, 5, and 7 weeks postsurgery were comparable to those in Ovx rats, suggesting that high physiological PRL had no additional osteopenic effect on the femoral metaphysis in Ovx rats.

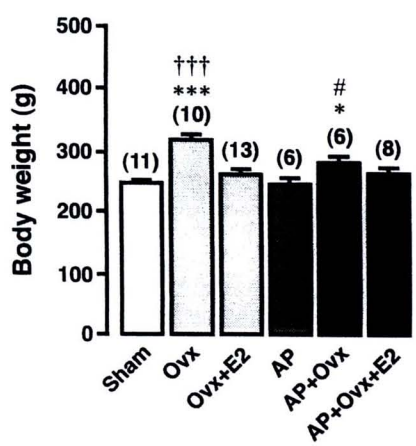

Fig. 2. Body weight of Sham, Ovx, Ovx+E2, AP, AP+Ovx, and AP+Ovx+E2 rats at 7 weeks postsurgery. $^*P < 0.05$, $^{***}P < 0.001$ compared with Sham. $^{\dagger\dagger\dagger}P < 0.001$ compared with Ovx+E2. $^{\#}P < 0.05$ compared with AP. Numbers in parentheses are the numbers of experimental animals.

The E2 supplementation of 2.5 μg/kg s.c. 3 times a week completely abolished the osteopenic effect of Ovx on the femoral metaphysis (Figs. 3 and 4), indicating that the supplement regimen was sufficient to provide circulating estrogen for the maintenance of normal bone mass. We noticed with interest that E2 supplementation also re-

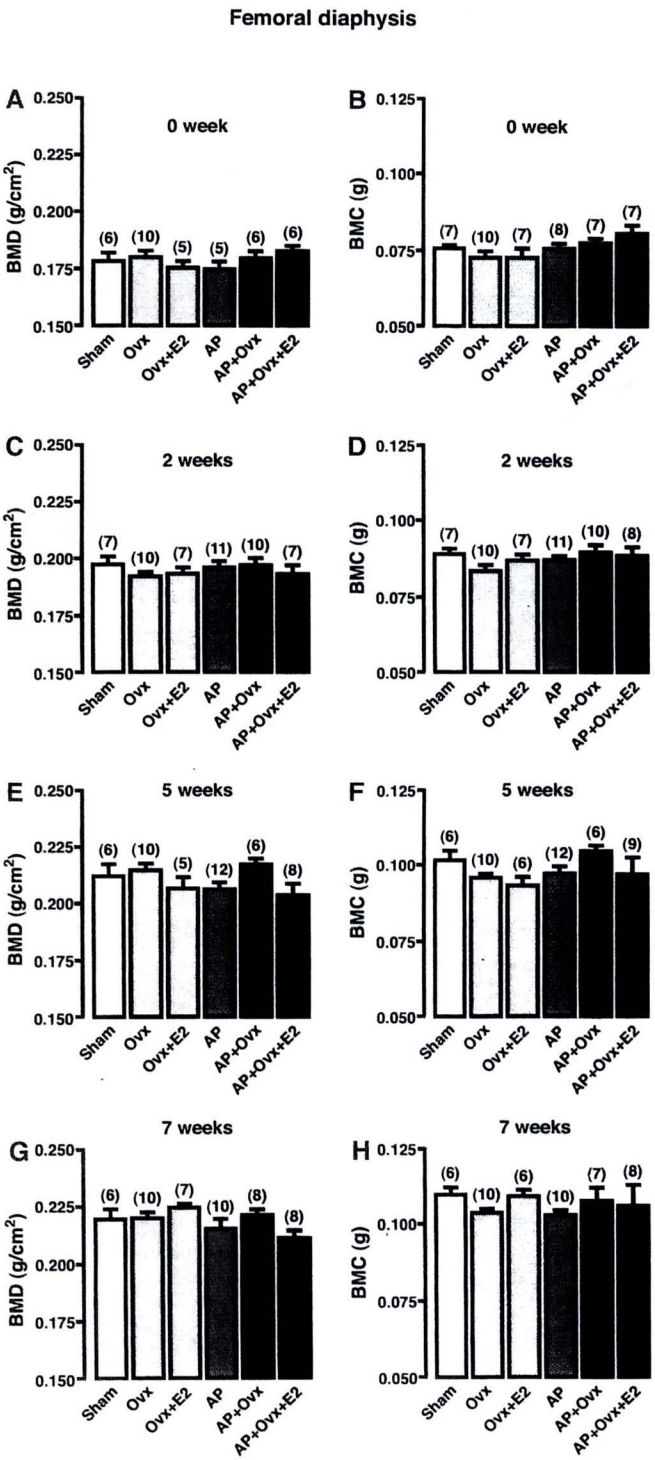

Fig. 3. In situ BMD and BMC of the femoral diaphysis of Sham, Ovx, Ovx+E2, AP, AP+Ovx, and AP+Ovx+E2 rats at 0, 2, 5, and 7 weeks postsurgery. The ROI of the femoral diaphysis was the area between the 8-mm ends of the left femur. Numbers in parentheses are the numbers of experimental animals.

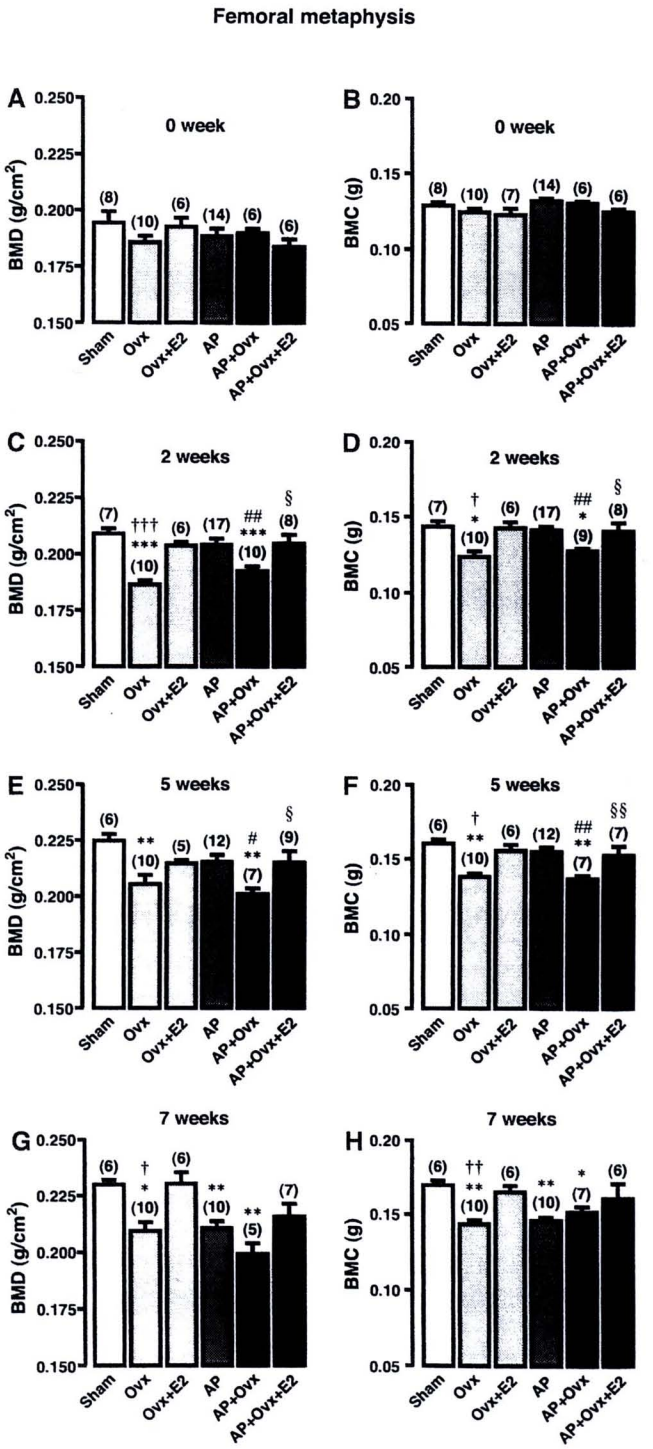

Fig. 4. In situ BMD and BMC of the femoral metaphysis of Sham, Ovx, Ovx+E2, AP, AP+Ovx, and AP+Ovx+E2 rats at 0, 2, 5, and 7 weeks postsurgery. The ROI of the femoral metaphysis was the area in the 8-mm distal end of the left femur. $^{*}P < 0.05$, $^{**}P < 0.01$, $^{***}P < 0.001$ compared with Sham. $^{\dagger}P < 0.05$, $^{\dagger\dagger}P < 0.01$, $^{\dagger\dagger\dagger}P < 0.001$ compared with Ovx+E2. $^{\#}P < 0.05$, $^{\#\#}P < 0.01$ compared with AP. $^{\S}P < 0.05$, $^{\S\S}P < 0.01$ compared with AP+Ovx. Numbers in parentheses are the numbers of experimental animals.

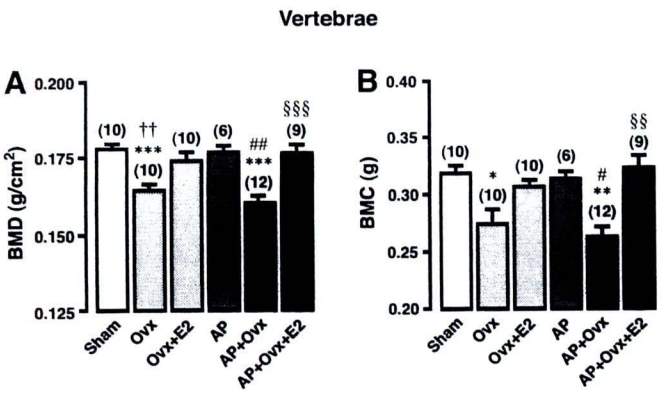

Fig. 5. Ex vivo BMD and BMC of the vertebrae of Sham, Ovx, Ovx+E2, AP, AP+Ovx, and AP+Ovx+E2 rats at 7 weeks post-surgery. The ROI covered the area of L5–6 vertebrae. $^{*}P < 0.05$, $^{**}P < 0.01$, $^{***}P < 0.001$ compared with Sham. $^{\dagger\dagger}P < 0.01$ compared with Ovx+E2. $^{\#}P < 0.05$, $^{\#\#}P < 0.01$ compared with AP. $^{\S\S}P < 0.01$, $^{\S\S\S}P < 0.001$ compared with AP+Ovx. Numbers in parentheses are the numbers of experimental animals.

versed BMD and BMC in AP+Ovx rats to the normal levels. Since osteopenia in AP+Ovx rats could be restored by E2 supplement, our results suggested that high physiological PRL induced a significant bone loss in the femoral metaphysis in an estrogen-dependent manner.

High physiological PRL did not change vertebral BMD and BMC

To demonstrate a site-specific action of PRL, we investigated whether high PRL induced by AP transplantation affected BMD and BMC of the L5–6 vertebrae in normal and Ovx rats (Fig. 5). Seven weeks after an Ovx, the vertebral BMD and BMC were decreased by 7% and 14%, i.e., from 0.178 ± 0.002 ($n = 10$) to 0.166 ± 0.001 g/cm^2 ($n = 10$, $P < 0.001$), and from 0.318 ± 0.007 ($n = 10$) to 0.275 ± 0.014 g ($n = 10$, $P < 0.05$), respectively. AP transplantation did not affect BMD and BMC of the vertebrae, and both parameters in AP+Ovx rats were comparable to those in the Ovx rats. E2 supplementation restored BMD and BMC in the Ovx and AP+Ovx rats to the Sham levels. The results indicated that in contrast to the trabecular part of the femur, the L5–6 vertebrae showed no decreases in the densitometric parameters after chronic exposure to high physiological PRL, implying a site-specific action of PRL on bone.

DISCUSSION

In the present study, we provide evidence that high physiological PRL of 90–100 ng/ml (comparable to the levels during pregnancy) could induce bone loss in the femoral metaphysis as demonstrated by DXA. In contrast, BMD and BMC of the L5–6 vertebrae, which were primarily trabecular bones, were not changed by PRL, suggesting a site-specific action of PRL. Our findings could be physiologically relevant, since chronic exposure to high physiological PRL for a few months, similar to that occurring during pregnancy, does not usually induce overt osteopenia in rats and humans [12, 20, 21]. On the other hand, long-term exposure to pathological hyperprolactinemia (up to ~1,000 ng/ml), such as in prolactinoma or prolonged antipsychotic drug uses, leads to massive bone loss and increased risk of osteoporosis [22–24].

High plasma PRL level, especially under pathological conditions, has been known to be associated with gonadal dysfunction [8]. In schizophrenic patients treated with antipsychotic drugs that induced hyperprolactinemia, peak serum E2 in periovulatory phase was suppressed below 100 pg/ml by PRL [25]. AP rats, similar to Ovx rats, also manifested a decrease in the plasma estrogen concentration to less than 50 pg/ml [17]. PRL was therefore thought to indirectly cause bone loss by inducing estrogen deficiency. However, our recent histomorphometric study in the tibial metaphysis of AP rats showed that besides the Ovx-liked effects on bone, such as decreases in bone volume and trabecular number, high PRL also exerted an estrogen-independent action by increasing bone formation rate [12]. The presence of PRLR in osteoblasts confirmed a direct action of PRL on bone [7]. By using RT-PCR and Southern blot technique, Bataille-Simoneau and co-workers [26] demonstrated the expression of PRLR in two human osteoblast-like cell lines, MG-63 and Saos-2. Neonatal rat osteoblasts and primary osteoblasts derived from the tibia of adult rats also expressed functional PRLR [7, 12], implicating rat osteoblasts as targets of PRL. Recently, we reported that MG-63 osteoblast-like cells, when directly exposed to recombinant human PRL for 48 h, exhibited significant decreases in osteocalcin mRNA expression, osteoprotegerin protein expression, and alkaline phosphatase activity [12]. Thus PRL was able to exert both direct and indirect actions on bone, though their relative contributions were not known. In the present study with PRL-stimulated bone loss in the femoral metaphysis, because the AP+Ovx rats produced no more severe osteopenia than that seen in Ovx or AP alone suggested that the estrogen-dependent (indirect) action of PRL was predominant. This was confirmed by the finding that E2 supplementation completely restored BMD and BMC in AP+Ovx rats to the Sham levels. Although high-dose E2 supplementation of 50 μg/week may increase serum PRL concentration by enhancing pituitary PRL secretion [17], a lower dose of ~2.2 μg/week used in the present study was unlikely to induce significant PRL secretion, either from the intracranial gland or implanted glands. An indirect action of PRL on bone through other calciotropic hormones, e.g., parathyroid hormone, has never been reported.

Besides the estrogen-dependent action, the effect of PRL on bone was also dependent on the circulating levels

of PRL and duration of exposure [6, 16]. We previously showed that the basal levels of PRL of ~7–10 ng/ml were necessary for the maintenance of the normal rate of bone turnover in nonmated adult female rats [6]. This was consistent with reports of less developed and poorly ossified calvariae of 18.5-day PRLR-knockout ($PRLR^{-/-}$) murine fetuses and a 60% decrease in the bone formation rate of 8-week-old adult $PRLR^{-/-}$ mice [27]. During pregnancy with higher physiological PRL concentrations in the range of 75–100 ng/ml, PRL was found to increase both the rates of bone formation and the resorption, i.e., inducing a state of high bone turnover, thus resulting in minimal or undetectable changes in the densitometric parameters [13, 21]. In long-term lactation with an increased loss of calcium in milk, higher PRL levels in the range of 200–300 ng/ml could induce significant bone loss, which was totally reversible after the cessation of lactation [20, 28, 29]. Prolonged pathological hyperprolactinemia, on the other hand, was accompanied by persistent bone loss with low BMD and BMC and increased risks of osteoporosis and fracture [22–24]. The present AP rats with the plasma PRL levels in the same range as that of pregnant rats could provide a model of PRL-induced bone loss during pregnancy with regional trabecular osteopenia.

Apparently the site-specific trabecular bone loss was also observed during lactation [13]. Generally, the effects of high physiological PRL are not substantial enough to be detectable by the macroscopic techniques, such as the total body or whole-bone DXA. Only when the more sensitive ^{45}Ca kinetic technique and bone histomorphometry were used were the effects demonstrated of high physiological PRL, which accelerated bone turnover to mobilize calcium to satisfy the increased calcium demand [4, 20]. However, when the trabecular region of cortical bone was examined separately as femoral metaphysis, significant decreases in BMD and BMC after exposure to high PRL could be detected by DXA, implying that the trabecular part of cortical bones was more responsive or susceptible to PRL than the primarily trabecular bone, i.e., vertebrae. Meanwhile, the unaffected BMD and BMC of the femoral diaphysis confirmed the absence of the effects of high PRL and estrogen deficiency on the cortical sites [12, 14].

At the histological level, PRL-enhanced bone turnover in the trabecular microarchitecture was associated with concurrent increases in the eroded surface, osteoblast surface, and osteoclast surface [12]. Moreover, bone mineral apposition rate was also elevated together with an increase in trabecular bone calcium deposition [6], suggesting that new calcium was supplied to bone to overcome bone loss, possibly through the parallel stimulation of the intestinal calcium absorption by PRL [2, 30]. Nevertheless, these compensatory mechanisms were inadequate for the maintenance of the femoral metaphysis, whereas they may successfully prevent an overt bone loss in the vertebrae. Although other mechanisms, such as different regional distribution of PRLR, might also explain the absence of PRL effect on the vertebrae, the present results clearly demonstrated the heterogeneity of bones in their responses to high physiological PRL. Since the metaphyseal bone loss weakens the whole bone, further investigations are required to demonstrate whether the biomechanical properties of the femoral metaphysis and fracture risk are also changed by long-term exposure to high physiological PRL.

In conclusion, we provided evidence that high physiological PRL induced bone loss in the trabecular part of the cortical bones, i.e., the femoral metaphysis, in estrogen-dependent and site-specific manners. The effects of high PRL and estrogen deficiency on the femoral diaphysis were undetectable by the DXA technique. Since decreases in BMD and BMC were found in the femoral metaphysis but not in the vertebrae, these changes in the femur may have some physiological significance or clinical relevance that needs to be further investigated.

We are grateful to Professor Vorachai Sirikulchayanonta and Professor Somnuek Domrongkitchaiporn, members of the Faculty of Medicine, Ramathibodi Hospital, Mahidol University, for their technical guidance and helpful comments. This research was supported by grants from the King Prajadhipok and Queen Rambhai Barni Memorial Foundation (to K.T.), the Thailand Research Fund (TRF), and the National Center for Genetic Engineering and Biotechnology (BIOTEC).

REFERENCES

1. Boass A, Lovdal JA, Toverud SU. Pregnancy- and lactation-induced changes in active intestinal calcium transport in rat. Am J Physiol. 1992;263:G127-34.
2. Charoenphandhu N, Krishnamra N. Prolactin is an important regulator of intestinal calcium transport. Can J Physiol Pharmacol. 2007;85:569-81.
3. Jantarajit W, Thongon N, Pandaranandaka J, Teerapornpuntakit J, Krishnamra N, Charoenphandhu N. Prolactin-stimulated transepithelial calcium transport in duodenum and Caco-2 monolayer are mediated by the phosphoinositide 3-kinase pathway. Am J Physiol Endocrinol Metab. 2007;293:E372-84.
4. Lotinun S, Limlomwongse L, Krishnamra N. The study of a physiological significance of prolactin in the regulation of calcium metabolism during pregnancy and lactation in rats. Can J Physiol Pharmacol. 1998;76:218-28.
5. Amnattanakul S, Charoenphandhu N, Limlomwongse L, Krishnamra N. Endogenous prolactin modulated the calcium absorption in the jejunum of suckling rats. Can J Physiol Pharmacol. 2005;83:595-604.
6. Puntheeranurak S, Charoenphandhu N, Krishnamra N. Enhanced trabecular-bone calcium deposition in female rats with a high physiological dose of prolactin diminishes after ovariectomy. Can J Physiol Pharmacol. 2006;84:993-1002.
7. Coss D, Yang L, Kuo CB, Xu X, Luben RA, Walker AM. Effects of prolactin on osteoblast alkaline phosphatase and bone formation in the developing rat. Am J Physiol Endocrinol Metab. 2000;279:E1216-25.
8. Wang C, Chan V. Divergent effects of prolactin on estrogen and progesterone production by granulosa cells of rat Graafian follicles. Endocrinology. 1982;110:1085-93.
9. Wang C, Hsueh AJ, Erickson GF. Prolactin inhibition of estrogen production by cultured rat granulosa cells. Mol Cell Endocrinol. 1980;20:135-44.
10. Krishnamra N, Seemoung J. Effects of acute and long-term administration of prolactin on bone ^{45}Ca uptake, calcium deposit, and calcium resorption in weaned, young, and mature rats. Can J Physiol Pharmacol. 1996;74:1157-65.
11. Krishnamra N, Seemoung J, Limlomwongse L. Acute effect of prolactin on bone ^{45}Ca accumulation in rats. Endocr J. 1997;44:257-64.
12. Seriwatanachai D, Thongchote K, Charoenphandhu N, Pandaranandaka J, Tudpor K, Teerapornpuntakit J, Suthiphongchai T, Krishnamra N. Prolactin directly enhances bone turnover by raising osteoblast-expressed receptor activator of nuclear factor κB ligand/osteoprotegerin ratio. Bone. 2008 (in press).
13. Ulrich U, Miller PB, Eyre DR, Chesnut CH, 3rd, Schlebusch H, Soules MR. Bone remodeling and bone mineral density during pregnancy. Arch Gynecol Obstet.

2003;268:309-16.
14. Charoenphandhu N, Tudpor K, Thongchote K, Saengamnart W, Puntheeranurak S, Krishnamra N. High-calcium diet modulates effects of long-term prolactin exposure on the cortical bone calcium content in ovariectomized rats. Am J Physiol Endocrinol Metab. 2007;292:E443-52.
15. Adler RA, Farrell ME, Krieg RJ, Deiss WP. Hypogonadism does not mediate urinary calcium loss in pituitary-grafted rats. Metabolism. 1989;38:805-9.
16. Piyabhan P, Krishnamra N, Limlomwongse L. Changes in the regulation of calcium metabolism and bone calcium content during growth in the absence of endogenous prolactin and during hyperprolactinemia: a longitudinal study in male and female Wistar rats. Can J Physiol Pharmacol. 2000;78:757-65.
17. Ribeiro MF, Ferigolo M, Reis FM, Barros HM, Spritzer PM. Paradoxical effect of imipramine in hyperprolactinemic female rats exposed to the forced swimming test. Physiol Behav. 2000;68:619-23.
18. Ishibashi T, Shiino M. Ultrastructural and immunocytochemical changes of prolactin cells of grafted pituitary after the injection of dopamine in the albino rat. Acta Anat. 1988;131:66-72.
19. Binkley N, Dahl DB, Engelke J, Kawahara-Baccus T, Krueger D, Colman RJ. Bone loss detection in rats using a mouse densitometer. J Bone Miner Res. 2003;18:370-5.
20. Prentice A. Calcium in pregnancy and lactation. Annu Rev Nutr. 2000;20:249-72.
21. Ritchie LD, Fung EB, Halloran BP, Turnlund JR, Van Loan MD, Cann CE, King JC. A longitudinal study of calcium homeostasis during human pregnancy and lactation and after resumption of menses. Am J Clin Nutr. 1998;67:693-701.
22. Biller BM, Baum HB, Rosenthal DI, Saxe VC, Charpie PM, Klibanski A. Progressive trabecular osteopenia in women with hyperprolactinemic amenorrhea. J Clin Endocrinol Metab. 1992;75:692-7.
23. Haddad PM, Wieck A. Antipsychotic-induced hyperprolactinaemia: mechanisms, clinical features and management. Drugs. 2004;64:2291-314.
24. Jung DU, Conley RR, Kelly DL, Kim DW, Yoon SH, Jang JH, Shin JG, Shim JC. Prevalence of bone mineral density loss in Korean patients with schizophrenia: a cross-sectional study. J Clin Psychiatry. 2006;67:1391-6.
25. Bergemann N, Mundt C, Parzer P, Jannakos I, Nagl I, Salbach B, Klinga K, Runnebaum B, Resch F. Plasma concentrations of estradiol in women suffering from schizophrenia treated with conventional versus atypical antipsychotics. Schizophr Res. 2005;73:357-66.
26. Bataille-Simoneau N, Gerland K, Chappard D, Basle MF, Mercier L. Expression of prolactin receptors in human osteosarcoma cells. Biochem Biophys Res Commun. 1996;229:323-8.
27. Clément-Lacroix P, Ormandy C, Lepescheux L, Ammann P, Damotte D, Goffin V, Bouchard B, Amling M, Gaillard-Kelly M, Binart N, Baron R, Kelly PA. Osteoblasts are a new target for prolactin: analysis of bone formation in prolactin receptor knockout mice. Endocrinology. 1999;140:96-105.
28. Bezerra FF, Mendonca LM, Lobato EC, O'Brien KO, Donangelo CM. Bone mass is recovered from lactation to postweaning in adolescent mothers with low calcium intakes. Am J Clin Nutr. 2004;80:1322-6.
29. Lotinun S, Limlomwongse L, Sirikulchayanonta V, Krishnamra N. Bone calcium turnover, formation, and resorption in bromocriptine- and prolactin-treated lactating rats. Endocrine. 2003;20:163-70.
30. Tudpor K, Charoenphandhu N, Saengamnart W, Krishnamra N. Long-term prolactin exposure differentially stimulated the transcellular and solvent drag-induced calcium transport in the duodenum of ovariectomized rats. Exp Biol Med. 2005;230:836-44.

ELSEVIER

Bone 42 (2008) 535 – 546

BONE

www.elsevier.com/locate/bone

Prolactin directly enhances bone turnover by raising osteoblast-expressed receptor activator of nuclear factor κB ligand/osteoprotegerin ratio

Dutmanee Seriwatanachai [a,1], Kanogwun Thongchote [a,1], Narattaphol Charoenphandhu [a,b,*], Jantarima Pandaranandaka [b,d], Kukiat Tudpor [b], Jarinthorn Teerapornpuntakit [a], Tuangporn Suthiphongchai [b,c], Nateetip Krishnamra [a,b,*]

[a] *Department of Physiology, Faculty of Science, Mahidol University, Rama VI Road, Bangkok 10400, Thailand*
[b] *Consortium for Calcium and Bone Research (COCAB), Mahidol University, Rama VI Road, Bangkok 10400, Thailand*
[c] *Department of Biochemistry, Faculty of Science, Mahidol University, Rama VI Road, Bangkok 10400, Thailand*
[d] *Faculty of Medicine, Thammasat University, Pathumthani 12120, Thailand*

Received 1 June 2007; revised 2 November 2007; accepted 15 November 2007
Available online 31 December 2007

Abstract

Hyperprolactinemia leads to high bone turnover as a result of enhanced bone formation and resorption. Although its osteopenic effect has long been explained as hyperprolactinemia-induced hypogonadism, identified prolactin (PRL) receptors in osteoblasts suggested a possible direct action of PRL on bone. In the present study, we found that hyperprolactinemia induced by anterior pituitary transplantation (AP), with or without ovariectomy (Ovx), had no detectable effect on bone mineral density and content measured by dual-energy X-ray absorptiometry (DXA). However, histomorphometric studies revealed increases in the osteoblast and osteoclast surfaces in the AP rats, but a decrease in the osteoblast surface in the AP+Ovx rats. The resorptive activity was predominant since bone volume and trabecular number were decreased, and the trabecular separation was increased in both groups. Estrogen supplement (E2) fully reversed the effect of estrogen depletion in the Ovx but not in the AP+Ovx rats. In contrast to the typical Ovx rats, bone formation and resorption became uncoupled in the AP+Ovx rats. Therefore, hyperprolactinemia was likely to have some estrogen-independent and/or direct actions on bone turnover. Osteoblast-expressed PRL receptor transcripts and proteins shown in the present study confirmed our hypothesis. Furthermore, we demonstrated that the osteoblast-like cells, MG-63, directly exposed to PRL exhibited lower expression of alkaline phosphatase and osteocalcin mRNA, and a decrease in alkaline phosphatase activity. The ratios of receptor activator of nuclear factor κB ligand (RANKL) and osteoprotegerin (OPG) proteins were increased, indicating an increase in the osteoclastic bone resorption. The present data thus demonstrated that hyperprolactinemia could act directly on bone to stimulate bone turnover, with more influence on bone resorption than formation. PRL enhanced bone resorption in part by increasing RANKL and decreasing OPG expressions by osteoblasts.

Keywords: Alkaline phosphatase; Bone histomorphometry; Bone mineral density; Hyperprolactinemia; Pituitary transplantation

Introduction

Hyperprolactinemia is associated with a number of physiological and pathological conditions, such as pregnancy, lactation, prolactinoma and chronic uses of dopamine-related antipsychotic drugs [1,2]. High physiological levels of prolactin (PRL) of ~200–350 ng/mL in prolonged lactation led to transient osteopenia and reversible negative calcium balance [3]. On the other hand, sustained pathological PRL exposure (up to ~1000 ng/mL) not only stimulated bone turnover but also produced a massive calcium loss, overt osteopenia, and osteoporosis [2,4,5]. Further studies using the ^{45}Ca kinetic technique showed the impact of hyperprolactinemia on trabecular sites, but not on cortical sites [6,7]; however, it was not known

* Corresponding authors. Department of Physiology, Faculty of Science, Mahidol University, Rama VI Road, Bangkok 10400, Thailand. Fax: +66 2 354 7154.
E-mail addresses: naratt@narattsys.com (N. Charoenphandhu), scnks@mahidol.ac.th (N. Krishnamra).
[1] D.S. and K.Th. contributed equally to this study.

8756-3282/$ - see front matter © 2007 Elsevier Inc. All rights reserved.
doi:10.1016/j.bone.2007.11.008

whether the microstructures of cortical and trabecular bones were altered in chronic hyperprolactinemia.

Accelerated bone turnover is a common feature of physiological and pathological hyperprolactinemia [8]. During pregnancy and lactation, high bone turnover was a mechanism to rapidly supply calcium for fetal growth and milk production [9]. Our histomorphometric study in lactating rats showed that suppression of endogenous PRL by bromocriptine induced a decrease in maternal bone turnover [10]. From the studies of pathological hyperprolactinemia, several investigators suggested that PRL-accelerated bone turnover was likely due to estrogen deficiency, since hyperprolactinemia suppressed estrogen production [4,5,11]. However, we recently demonstrated the expressions of both short and long isoforms of PRL receptors (PRLR) in tibiae, femora and vertebrae of adult female rats [6]. Therefore, we hypothesized that PRL could directly exert its effects on bone to stimulate bone turnover.

It is known that osteoblasts expressed the receptor activator of nuclear factor κB ligand (RANKL) and osteoprotegerin (OPG) [12]. Binding of RANKL to its receptors on the osteoclast progenitor cells induces bone resorption, whereas binding of RANKL to its decoy receptor OPG inhibits bone resorption. Thus, the ratio of RANKL/OPG expression by osteoblasts was an important determinant of osteoclastogenesis and osteoclast activity as well as bone turnover [12]. Osteoblasts also expressed alkaline phosphatase and osteocalcin, both of which were used as indicators of the osteoblast activity [13,14]. Since high bone turnover resulted from enhanced bone formation and resorption, we hypothesized that the osteoblast activity as well as the expression ratio of RANKL and OPG would be increased by hyperprolactinemia.

Studies of chronic hyperprolactinemia in rats require an induction of highly sustained plasma PRL without the stress-induced PRL release. To achieve this, we used the anterior pituitary (AP) transplantation instead of the more stressful daily PRL injections [6,15]. Within 15 days, after transplanting two extra AP glands from donors under the renal capsule of the recipient, continuous PRL secretion from the AP allografts in the absence of hypothalamic dopaminergic inhibition resulted in a physiological hyperprolactinemia of 90–100 ng/mL, comparable to the levels reported during pregnancy [6,15,16]. Other pituitary hormones were not secreted from the grafts due to the absence of the stimulatory hypothalamic hormones.

Therefore, the objectives of the present investigation were (*i*) to demonstrate that bone was a direct target of PRL by PRLR expression studies; (*ii*) to evaluate changes in the microscopic osseous structures after chronic hyperprolactinemia; (*iii*) to demonstrate the estrogen-independent effects of PRL on bone; and (*iv*) to confirm the direct effect of hyperprolactinemia on bone by showing changes in the osteoblast activity at the molecular level.

Materials and methods

Animals

Female Sprague–Dawley rats (10-week-old, weighing 200–220 g), were obtained from the Animal Centre of Thailand, Salaya, Thailand. They were placed in hanging stainless steel cages, fed standard pellets containing 1% w/w calcium (Perfect Companion Co., Ltd., Bangkok, Thailand) and distilled water ad libitum under 12 h:12 h light:dark cycle. Room temperature was controlled at 23–25 °C, and the relative humidity was about 50–60%. This study was approved in accordance with the principles and guidelines of the Laboratory Animal Ethics Committee of Mahidol University, Bangkok, Thailand. After acclimatization, bone mineral density (BMD) and content (BMC) were measured before surgery (0 week).

Cell culture

Osteoblast-like MG-63 cell line (ATCC No. CRL-1427; a kind gift from Dr. Suttatip Kamolmatyakul, Prince of Songkla University, Thailand) or human fetal osteoblast 1.19 (hFOB) cells (ATCC No. CRL-11372) were cultured in 75-cm^2 T flasks with α-MEM (for MG-63) or DMEM/F-12 (for hFOB) supplemented with 10% fetal bovine serum (FBS), 100 U/mL penicillin/streptomycin, and 0.25 μL/mL amphotericin B (Sigma, St. Louis, MO, USA). 1 μM dexamethasone and 0.1 μM 1,25-$(OH)_2D_3$ (Sigma) were also added to the medium to induce maximal expression of PRLR as previously described [17]. Cells were incubated at 37 °C with 5% CO_2, and subcultured according to the ATCC's protocol.

As for the primary osteoblast culture, two tibiae were removed from a 10-week-old rat by sterile surgical technique. After removing the connective tissues and marrow cells, bones were cut into small dice, and cultured in DMEM supplemented with 15% FBS, 100 U/mL penicillin/streptomycin and 100 μg/mL ascorbate-2-phosphate (Sigma). Cells were incubated at 37 °C with 5% CO_2, and subcultured every 3 days.

Anterior pituitary (AP) transplantation

The procedure was modified from the methods of Adler et al. [15] and Charoenphandhu et al. [6]. In brief, during diethylether anesthesia, a 1.0-cm paracostal incision was made to expose the left kidney of the recipient rat. Two anesthetized donors were then decapitated to remove the pituitary glands which were immediately inserted into the prepared left renal capsule of the recipient. Renal fascia, muscle and skin were sutured, and cleaned with 70% ethanol and povidone–iodine. Sham operation consisted of exposure of the left kidney and a gentle touch of the renal fascia with forceps. Visual examination of the well-vascularized hypophyseal graft and immunohistochemical staining for PRL production were performed at the end of the experiments to confirm successful AP transplantation. Animals with unsuccessful transplantation were excluded from data analyses.

Bilateral ovariectomy

Bilateral ovariectomy (Ovx) has been an accepted surgical procedure for inducing estrogen deficiency [18]. In brief, the rat was anesthetized with diethylether before two 1.5-cm paralumbar incisions were made. The fallopian tubes were then ligated prior to the removal of both ovaries. The skin was finally sutured and cleaned with 70% ethanol and povidone–iodine. Sham operation was similar to the bilateral ovariectomy except that both ovaries were gently touched with forceps and left in place. Uterine weight and vaginal cytology confirmed the success of the surgery.

BMD and BMC measurements

Both parameters were determined as previously described [6]. Under 50 mg/kg sodium pentobarbitone i.p. (Abbott, North Chicago, IL, USA) anesthesia, BMD and BMC of the right femur were assessed by dual-energy X-ray absorptiometry (DXA) (model Lunar PIXImus2; GE Medical Systems, Madison, WI, USA), operated with a software version 2.10. The dual-energy supply was 80/35 kVp at 500 μA. Animals were laid prone on a supporting board with reproducible positioning. To confirm that the surrounding connective tissue and fat did not interfere with the in situ BMD and BMC measurement, femur was dissected for ex vivo BMD and BMC determination at the end of the 7-week experiment.

Bone preparation

After sacrifice, the right femur was dissected and cleaned of adhering tissues. Fats and marrow tissues were eluted by 1:1 mixture of 100% ethanol and diethylether. Thereafter, bones were dried at 80 °C for 48 h to obtain a constant dry weight. BMD and BMC of the ex vivo femur were determined. For bone

Table 1
Homo sapiens and *Rattus norvegicus* oligonucleotide sequences used in the PCR experiments (Protocol 2)

Gene	Ref. or accession no.	Primer (forward/reverse)	Product length (bps)	Cycle
Homo sapiens				
hPRLR	[17]	5′–AAATGTGGCATCTGCAACCGTTTTCAC–3′ 5′–GCACTTGCTTGATGTTGCAGTGAAGTT–3′	1790	30
hOC	[22]	5′–GGCCAGGCAGGTGCGAAGC–3′ 5′–GCCAGGCCAGCAGAGCGACAC–3′	271	30
hALP	[23]	5′–ACGTGGCTAAGAATGTCATC–3′ 5′–CTGGTAGGCGATGTCCTTA–3′	475	32
RANKL	[24]	5′–GCCAGTGGGAGATGTTAG–3′ 5′–TTAGCTGCAAGTTTTCCC–3′	486	33
hOPG	[24]	5′–GCTAACCTCACCTTCGAG–3′ 5′–TGATTGGACCTGGTTACC–3′	324	22
hGAPDH *	NM_002046	5′–CACCCACTCCTCCACCTTTG–3′ 5′–CCACCACCCTGTTGCTGTAG–3′	110	20
Rattus norvegicus				
rPRLR-S *	NM_012630	5′–TTCTACCACCATCGCAAC–3′ 5′–CTGATCTCGTTTGTCATTGAG–3′	120	–
rPRLR-L *	NM_001034111	5′–TCAAGCAACCGCAGACTC–3′ 5′–CAGTTTAGCCAATCGTTCCA–3′	107	–
rOC *	J04500	5′–CACAGGGAGGTGTGTGAG–3′ 5′–TGTGCCGTCCATACTTTC–3′	203	–
rOPG *	NM_012870	5′–ATTGGCTGAGTGTTCTGGT–3′ 5′–CTGGTCTCTGTTTTGATGC–3′	140	–
rGAPDH *	NM_017008	5′–AGTCTACTGGCGTCTTCAC–3′ 5′–TCATATTTCTCGTGGTTCAC–3′	133	–

PRLR, prolactin receptor; rPRLR-S, short-form rPRLR; rPRLR-L, long-form rPRLR; OC, osteocalcin; ALP, alkaline phosphatase; RANKL, receptor activator of nuclear factor κB ligand; OPG, osteoprotegerin; GAPDH, glyceraldehyde-3-phosphate dehydrogenase.
* Custom-design primers.

histomorphometry, the right tibia was removed, dehydrated with sequential concentrations of ethanol (70%, 95%, and 100%), and embedded in methyl methacrylate resin. The embedded tibia was cut longitudinally at the thickness of 7 and 12 μm with a RM2255 microtome (Leica, Nussloch, Germany). The 12-μm section was used for determination of dynamic histomorphometric parameters under fluorescent microscope, while the 7-μm section was stained with Goldner-trichrome for determination of the static parameters under light microscope.

Bone histomorphometry

Bone histomorphometric analysis was modified from the methods of Li et al. and Lotinun et al. [10,19] with the Osteomeasure system (Osteomeasure Inc., Atlanta, GA, USA), operated with software version 4.1. The images of specimens were observed under a real-time video-assisted BX51 TRF fluorescent/light microscope (Olympus, Tokyo, Japan), and processed using a plotter. Primary static parameters obtained from stained sections included trabecular bone volume (BV/TV, %), trabecular number (Tb.N, mm^{-1}), trabecular separation (Tb.Sp, μm), trabecular thickness (Tb.Th, μm), osteoclast surface (Oc.S/BS, %), osteoblast surface (Ob.S/BS, %), and eroded surface (ES/BS, %). Dynamic parameters obtained from unstained sections were double-labelled surface (dLS/BS, %), mineral apposition rate (MAR, μm/day), and bone formation rate (BFR/BS, 10^{-2} $\mu m^3/\mu m^2$/day). The nomenclature, symbols, and units complied with the report of the American Society for Bone and Mineral Research Nomenclature Committee [20].

Immunohistochemistry

At the end of the experiment, the hypophyseal graft was dissected from the perirenal tissues. Paraffin-embedded 4.0-μm sections were used to detect PRL production in the transplanted gland. After blocking endogenous peroxidase activity with 3.0% H_2O_2 and 3.0% horse serum (Sigma), the sections were incubated with 1:300 PRL polyclonal primary antibody (Dako, Carpinteria, CA, USA) for 60 min prior to incubation for 10 min with biotin-conjugated anti-rabbit secondary antibody and peroxidase-conjugated streptavidin (Dako). The chromogenic reaction was carried out with 3′,3′-diaminobenzidine (Dako) to produce a brownish product. The slides were finally counterstained with hematoxylin (Sigma) for 5 min. The normal pituitary gland and perirenal fat pad were used as positive and negative controls, respectively. Hematoxylin-eosin (H&E) staining was also performed to identify structures of the graft. Images were acquired under light microscope (model BX51 TRF; Olympus, Tokyo, Japan).

Immunofluorescent analysis

MG-63 cells or primary rat osteoblasts cultured on a glass cover slip were fixed with a fixative containing 3% paraformaldehyde and 2% sucrose for 10 min at 25 °C. Cells were permeabilized with 0.5% Triton-X 100 in PBS for 5 min, and blocked with 10% FBS for 20 min at room temperature. Samples were then incubated with 1:300 PRLR polyclonal primary antibody (Santa Cruz Biotechnology, Santa Cruz, CA, USA) overnight at 4 °C, and later with FITC-conjugated goat anti-rabbit secondary antibody (Stratech, Cambridge, UK). Images were captured by an inverted fluorescent microscope (model Eclipse TE2000-U; Nikon, Tokyo, Japan) or a confocal laser-scanning microscope (model FV1000; Olympus, Tokyo, Japan).

Cell proliferation assay

MG-63 cells were inoculated in a 96-well culture plate (5000 cells/well). After 48-h PRL incubation, the culture medium was replaced by medium containing 10% 3-(4,5-dimethylthiazol-2-yl)-2,5-diphenyltetrazolium bromide (MTT) (Sigma). After a 3-h incubation with MTT at 37 °C, the absorbance of each well was determined at 540 nm by a microplate reader (model Multiscan EX; Thermo Labsystems, Cergy-Pontoise, France), as described previously [21]. Experiments were performed in 6 replications, and the relative proliferation of each n was averaged from three independent experiments.

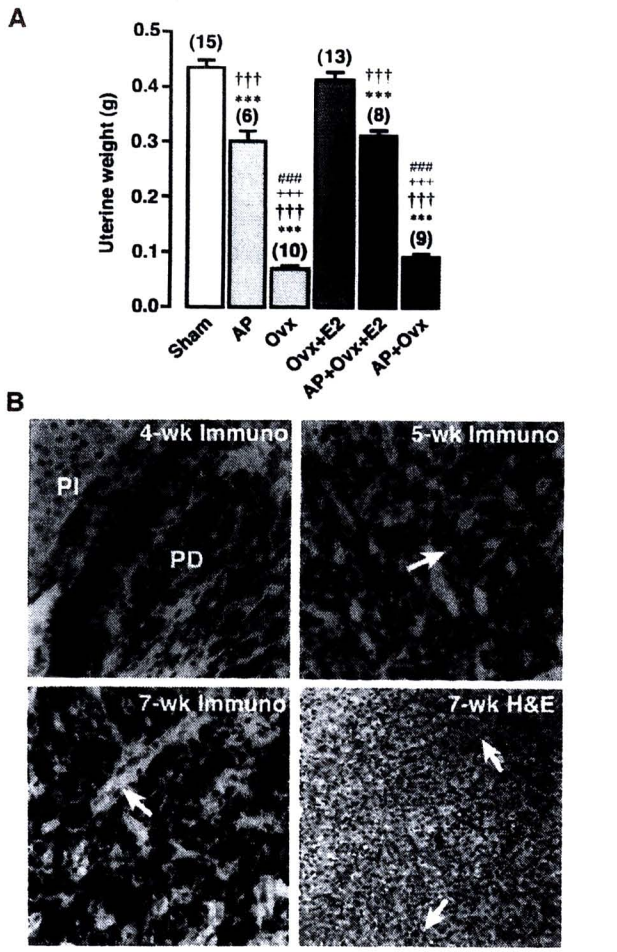

Fig. 1. (A) Uterine weight of experimental rats at 7 weeks post-surgery. ***$P<0.001$ compared with Sham. $^{\dagger\dagger\dagger}P<0.001$ compared with Ovx+E2. $^{+++}P<0.001$ compared with AP. $^{\#\#\#}P<0.001$ compared with AP+Ovx+E2. Numbers in parentheses are numbers of experimental animals. (B) Representative data of the immunohistochemical analyses (Immuno) of PRL production in the hypophyseal allografts at 4, 5 and 7 weeks post-surgery ($n=15$), magnification ×400. Corresponding 7-week graft section stained with H&E is also shown, magnification ×100. The arrows indicate sinusoids filled with numerous red blood cells. The pars distalis (PD) is strongly positive with the brownish products of peroxidase, indicating the PRL synthesis, whereas pars intermedia (PI) is negative.

Alkaline phosphatase activity assay

MG-63 cells were cultured in a 6-well culture plate (100,000 cells/well). Alkaline phosphatase activity was determined by the conversion of *p*-nitrophenyl phosphate to *p*-nitrophenol, as previously described [13]. In brief, cells were washed twice with PBS, and incubated for 1 h with 2 mL solution containing (in mM) 100 Na_2CO_3, 10 $MgCl_2$, 20 *p*-nitrophenyl phosphate (Sigma), pH 10.3. Thereafter, 1 mL of 5 M NaOH was added. Absorbance was read at 410 nm.

Osteoblast mRNA isolation, PCR, and sequencing

The total RNA of MG-63 cells or primary rat osteoblasts were prepared by using the RNeasy mini kit (Qiagen, Valencia, CA, USA). 2.0 μg of the total RNA was reverse-transcribed with the SuperScript III (Invitrogen, Carlsbad, CA, USA) to cDNA by a thermal cycler (model Minicycler; MJ Research, Watertown, MA, USA). Sense and antisense primers for PRLR, osteocalcin, alkaline phosphatase, RANKL, OPG, and glyceraldehyde-3-phosphate dehydrogenase (GAPDH) were shown in Table 1. GAPDH served as a control gene to check the consistency of the reverse transcription and to normalize values

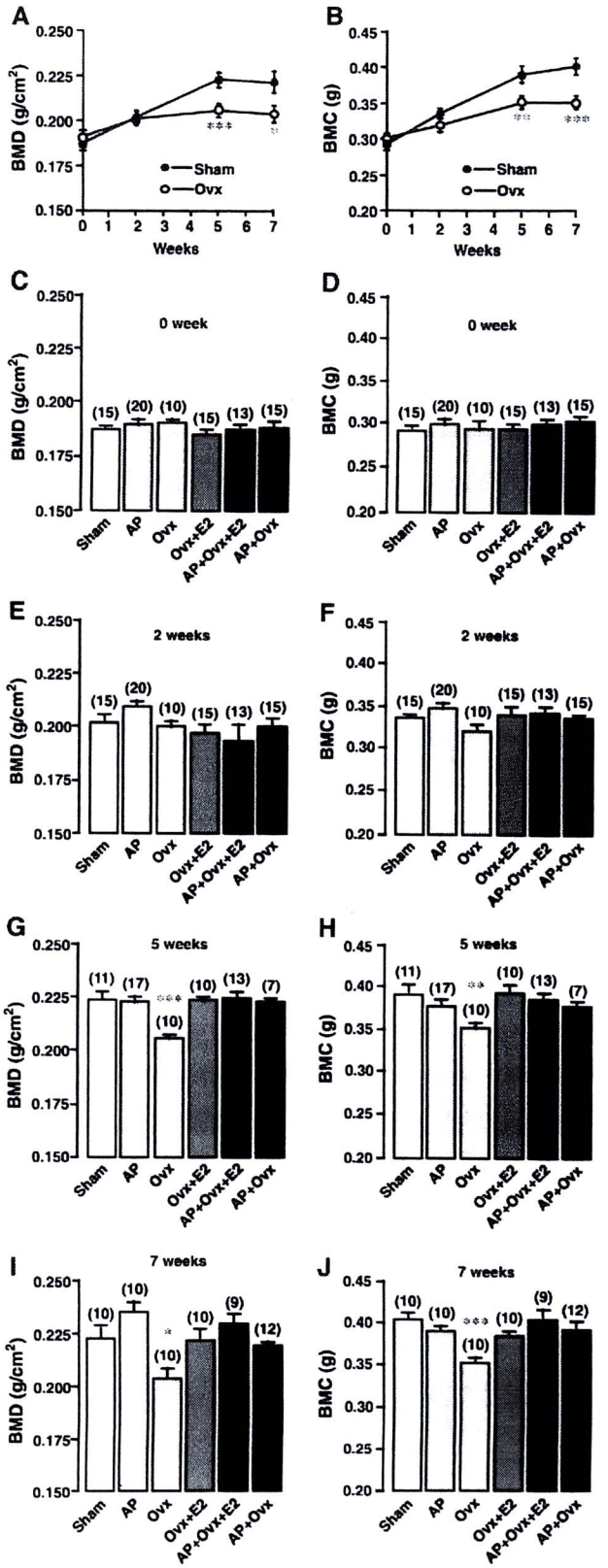

Fig. 2. (A) BMD and (B) BMC measurements of the right femur of anesthetized Sham ($n=10$–15) and Ovx ($n=10$) rats. (C–J) Femoral BMD and BMC of anesthetized Sham, AP, Ovx, Ovx+E2, AP+Ovx+E2, and AP+Ovx rats at 0, 2, 5, and 7 weeks post-surgery. *$P<0.05$, **$P<0.01$, ***$P<0.001$ compared with their respective values of Sham rats. Numbers in parentheses are numbers of experimental animals.

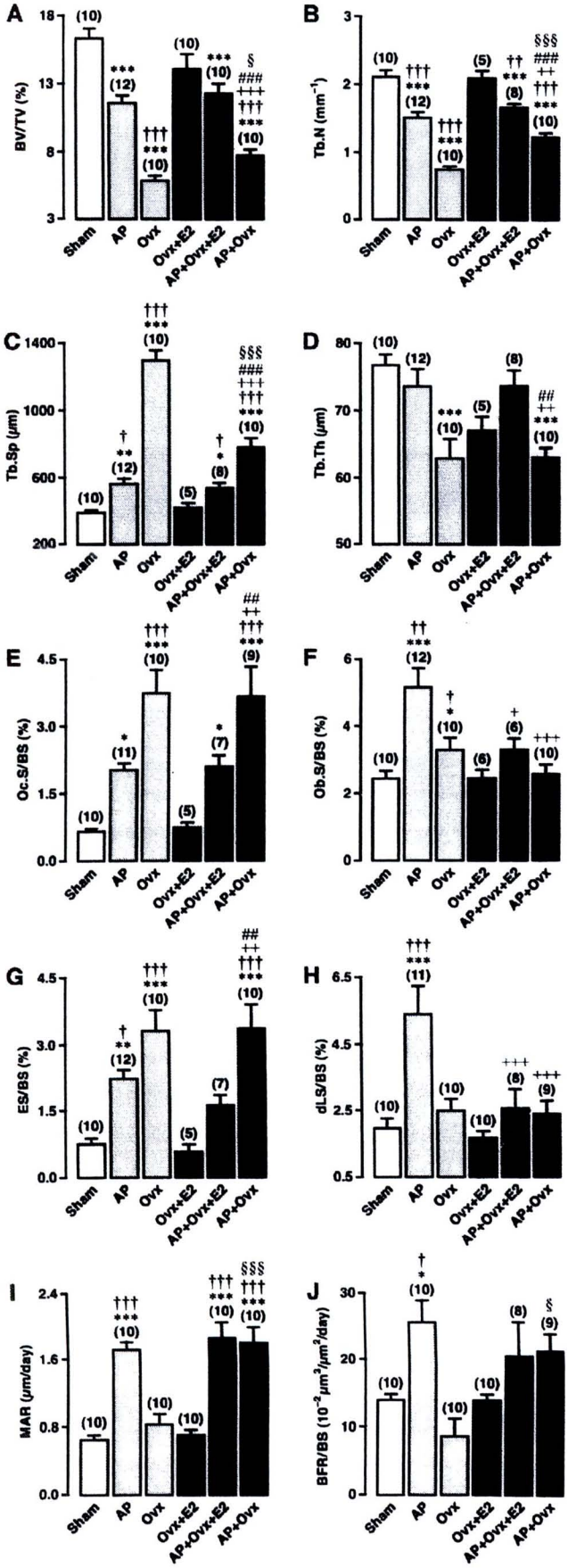

between samples. After amplification with Taq polymerase (Qiagen), the PCR products were visualized on a 2% agarose gel stained with 1.0 μg/mL ethidium bromide under a trans-UV system (model Quantity One 2000; Bio-Rad, Hercules, CA, USA). The cycle–band intensity curve was plotted for each gene to obtain an optimal PCR cycle which fell in the exponential phase. For a semi-quantitative analysis (semi-qRT-PCR), the expression of a studied gene in the control group was considered to be 100%, while that in the experimental group was calculated as a percent change relative to the value of the control group. Expressions of rat PRLR (rPRLR), osteocalcin and OPG mRNAs were quantitatively determined by a real-time PCR (model MiniOpticon; Bio-Rad) with iQ SYBR Green Supermix kit (Bio-Rad). Amplicon sequencing was performed by the ABI Prism 3100 Genetic Analyzer (Applied Biosystems, Foster City, CA, USA), as described previously [25].

Western blot analysis

MG-63 cells or primary rat osteoblasts were lysed in the lysis buffer (150 mM Tris at pH 7.4, 150 mM NaCl, 2 mM EGTA, 2 mM EDTA, 1 mM DTT, 1 mM NaF, 0.5 mM Na_3VO_4, 1 mM β-glycerophosphate, 0.1% SDS, 1% DOC, 1% NP-40, and protease inhibitor cocktail) (Sigma). After a 30-min incubation at 4 °C, lysates were sonicated and centrifuged at 12,000 × g for 10 min at 4 °C, and then heated for 5 min at 95 °C before being loaded on a gel. Proteins were separated by sodium dodecylsulfate polyacrylamide gel electrophoresis (SDS-PAGE), and subsequently transferred to a nitrocellulose membrane (Amersham, Buckinghamshire, UK) by electroblotting. Membranes were probed overnight at 4 °C with 1:500 rabbit anti-rPRLR (for primary rat osteoblasts), 1:1000 rabbit anti-human RANKL or OPG antibodies (Santa Cruz), and re-probed with 1:5000 mouse anti-β-actin antibody (Santa Cruz). After 1-h incubation at 25 °C with 1:2000 goat anti-rabbit or anti-mouse secondary antibodies (Santa Cruz), blots were visualized using the enhanced chemiluminescence kit (Amersham).

Experimental protocols

Protocol 1

The objectives of this protocol were to demonstrate changes in bone remodeling during chronic hyperprolactinemia, and to elucidate whether hyperprolactinemia had an estrogen-independent effect on bones of adult female rats. Hyperprolactinemia and estrogen deficiency were induced by AP transplantation and Ovx, respectively. Rats were randomly divided into 5 groups, i.e., sham-operated (Sham), AP-grafted (AP), Ovx supplemented with 2.5 μg/kg 17β-estradiol s.c. (Sigma) 3 times a week (Ovx+E2), AP+Ovx+E2, and AP+Ovx. Sham operation was performed in all rats which were not subject to AP transplantation or Ovx. An equivalent volume of purified corn oil was administered s.c. to all non-Ovx rats. Intact BMD and BMC of all rats were measured prior to surgery, and at 2, 5 and 7 weeks post-surgery. BMD and BMC of Ovx rats served as a positive control to demonstrate the efficiency of the densitometric technique. Then, 25 mg/kg tetracycline i.p. (Sigma) was administered twice to label bone for the histomorphometric analysis of dynamic parameters 6 days and 1 day before the animals were killed. After the rats were sacrificed (7 weeks), uterine weight measurement, PRL immunohistochemistry, ex vivo BMD and BMC measurements, and bone histomorphometry were

Fig. 3. Bone histomorphometry performed on the right tibia of Sham, AP, Ovx, Ovx+E2, AP+Ovx+E2, and AP+Ovx rats at 7 weeks post-surgery. Primary static parameters were obtained from the Goldner-trichrome-stained sections under a light microscope, including trabecular bone volume (BV/TV, A), trabecular number (Tb.N, B), trabecular separation (Tb.Sp, C), trabecular thickness (Tb.Th, D), osteoclast surface (Oc.S/BS, E), osteoblast surface (Ob.S/BS, F), and eroded surface (ES/BS, G). Dynamic parameters obtained from unstained tetracycline-labelled bone sections under a fluorescent microscope included double-labelled surface (dLS/BS, H), mineral apposition rate (MAR, I), and bone formation rate (BFR/BS, J). $^{*}P<0.05$, $^{**}P<0.01$, $^{***}P<0.001$ compared with Sham. $^{\dagger}P<0.05$, $^{\dagger\dagger}P<0.01$, $^{\dagger\dagger\dagger}P<0.001$ compared with Ovx+E2. $^{+}P<0.05$, $^{++}P<0.01$, $^{+++}P<0.001$ compared with AP. $^{\#\#}P<0.01$, $^{\#\#\#}P<0.001$ compared with AP+Ovx+E2. $^{\S}P<0.05$, $^{\S\S\S}P<0.001$ compared with Ovx. Numbers in parentheses are numbers of experimental animals.

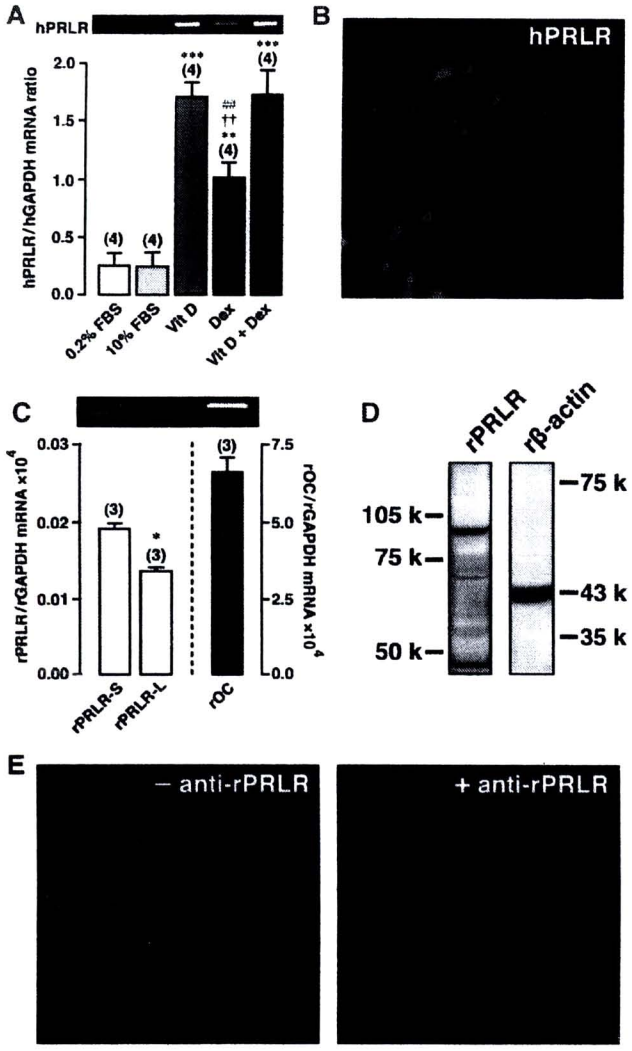

Fig. 4. (A) Expression of hPRLR mRNA (semi-qRT-PCR) in the osteoblast-like MG-63 cells exposed for 48 h to 0.2% and 10% fetal bovine serum (FBS, control), 0.1 μM 1,25-$(OH)_2D_3$ (Vit D), 1 μM dexamethasone (DEX), or a combination of Vit D and DEX (Vit D+DEX). $^{**}P<0.01$, $^{***}P<0.001$ compared with 0.2% FBS group. $^{\dagger\dagger}P<0.01$ compared with Vit D group. $^{\#\#}P<0.01$ compared with DEX group. Numbers in parentheses are numbers of independent flasks. (B) Immunofluorescent analysis of hPRLR protein expression in MG-63 cells exposed for 48 h to Vit D+DEX ($n=5$), magnification ×400. (C) Quantitative real-time PCR study of short (rPRLR-S) and long (rPRLR-L) isoforms of rPRLR and osteocalcin (rOC) in cultured osteoblasts derived from rat tibiae. $^{*}P<0.05$ compared with rPRLR-S. Numbers in parentheses are numbers of experimental animals. All experiments were performed in triplicate. (D) Western blot analysis of rPRLR protein expressions in primary rat osteoblasts ($n=5$). rβ-actin was a housekeeping protein. (E) Representative confocal immunofluorescent images of primary rat osteoblasts ($n=5$), magnification ×60. Cells were incubated in the presence (+anti-rPRLR) and absence (−anti-rPRLR) of primary antibody against rPRLR proteins. rPRLRs and nuclei were labelled in green and red, respectively.

performed. Immunohistochemical analysis of PRL production was also performed separately in 4-, 5-and 6-week AP-grafted rats. Serum OPG levels of Sham and AP-grafted rats were measured by a sandwich ELISA kit (Biomedica, Vienna, Austria), according to the manufacturer's instruction.

Protocol 2

The objective of this protocol was to elucidate the direct effects of hyperprolactinemia on osteoblast functions. To show that PRL could exert a direct action on bone, expression of rPRLR in rat cultured osteoblasts was demonstrated. Expression of human PRLR (hPRLR) in MG-63 cells was determined in the presence of 0.2% and 10% fetal bovine serum (FBS; controls), 0.1 μM 1,25-$(OH)_2D_3$ (Vit D) (Sigma), 1 μM dexamethasone (DEX) (Sigma), and a combination of Vit D and DEX by using RT-PCR and immunofluorescent analysis. Since both Vit D and DEX enhanced expression of hPRLR without effect on the studied parameters (Fig. 4), both chemicals were added to the culture medium. Thereafter, MG-63 or hFOB cells were incubated with normal medium (Control) or medium containing various concentrations of recombinant human PRL (rhPRL) (purity>97% as determined by SDS-PAGE; R&D Systems, Minneapolis, MN, USA) of 1, 10, 100, 1000 ng/mL at 37 °C for 0.5, 3, 6, 12, 24 and 48 h prior to determination of osteoblast functions. Parameters of bone formation included osteoblast proliferation, osteocalcin and alkaline phosphatase mRNA expressions, and alkaline phosphatase activity, while those of bone resorption were the ratios of RANKL/OPG mRNA and protein expressions. In some experiments, OPG mRNA expression was determined in primary rat osteoblasts incubated for 48 h with 1000 ng/mL PRL (Sigma). Expressions of mRNAs and proteins were analyzed in triplicate by RT-PCR and Western blot analysis, respectively.

Statistical analyses

Results were expressed as mean±SE. Two sets of data were compared using the unpaired Student's *t*-test. Multiple comparisons were performed by one-way analysis of variance (ANOVA) with Newman–Keuls post-test. The difference between expressions of short and long isoforms of rPRLRs was compared by Mann–Whitney test. The level of significance for all statistical tests was $P<0.05$. Data were analyzed by GraphPad Prism 4.0 for Mac OS X (GraphPad Software Inc., San Diego, CA, USA).

Results

Uterine weight and PRL immunohistochemistry confirmed successful Ovx and AP transplantation

In the present study, estrogen deficiency and hyperprolactinemia were induced by Ovx and AP transplantation, respectively. After a 7-week period of Ovx, the uterine weight was markedly decreased as expected, and 2.5 μg/kg 17β-estradiol supplementation (E2) completely reversed the effect of Ovx (Fig. 1A). Both AP and AP+Ovx+E2 rats showed similar decreases in the uterine weight, which was greater than those of Ovx rats, suggesting an anti-estrogen-like effect of hyperprolactinemia on the uteri. Uterine weights of AP+Ovx rats were not different from that of Ovx rats.

To examine the viability and function of the AP allografts, the grafts were dissected from the perirenal tissues of 4-, 5-, 6- and 7-week AP rats, and analyzed histologically and immunohistochemically. They were highly vascularized reddish tissue with a diameter of ~2 mm. H&E staining showed typical cells of varying sizes, arranged in irregular cords and clusters, consistent with normal pituitary glands (Fig. 1B). Numerous sinusoidal networks were seen between the clusters of cells (arrows in Fig. 1B). Immunohistochemistry revealed active PRL production in the pars distalis, but not in the pars intermedia or surrounding connective tissues (Fig. 1B). As microvascular endothelial damage and lymphoid infiltration were not seen, there was neither graft rejection nor allograft vasculopathy. The AP rats thus possessed two healthy ectopic pituitary glands which, unlike the normal pituitary gland under the hypothalamic dopaminergic control, actively and continuously produced PRL. Sustained plasma PRL levels induced by this procedure

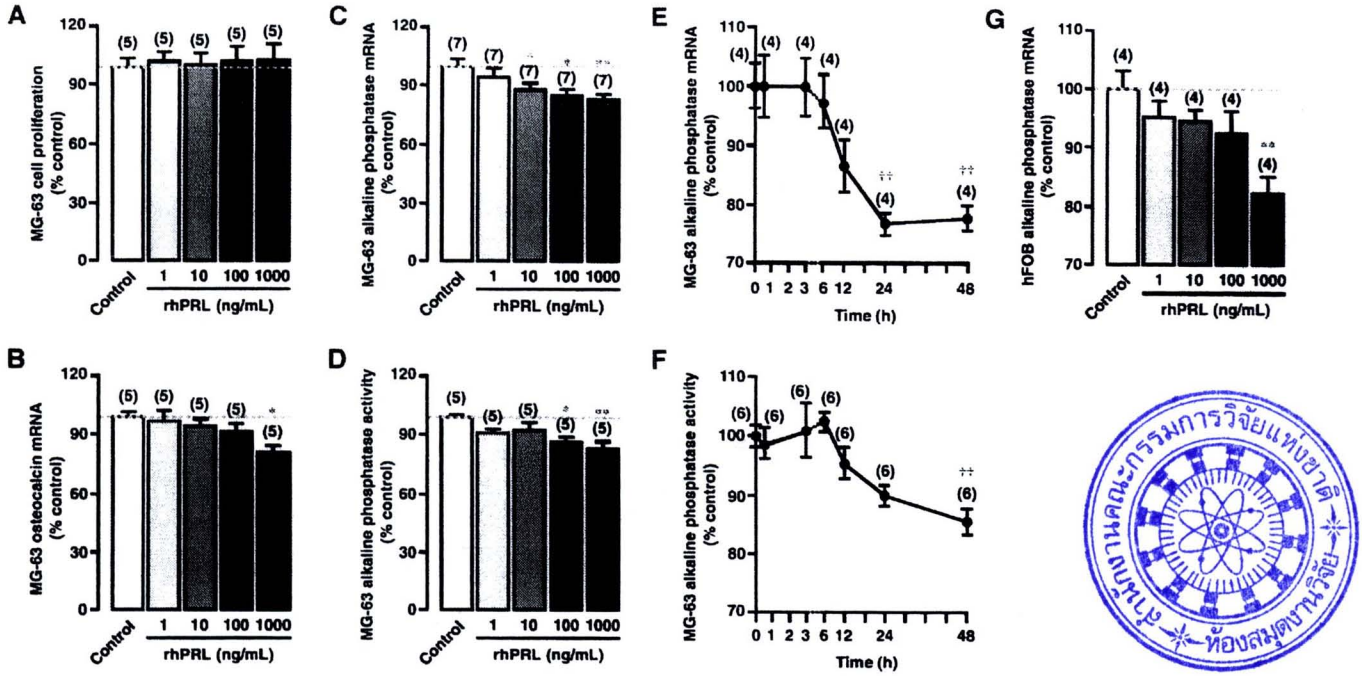

Fig. 5. Dose-dependent changes in bone formation parameters which are osteoblastic cell proliferation (A), osteocalcin mRNA expression (B), alkaline phosphatase mRNA expression (C), and alkaline phosphatase activity (D) in MG-63 cells incubated for 48 h with 1, 10, 100 or 1000 ng/mL rhPRL. (E) and (F) present time-dependent changes in alkaline phosphatase mRNA expression and activity, respectively, in MG-63 cells directly exposed to 1000 ng/mL rhPRL. (G) dose-dependent changes in alkaline phosphatase mRNA expression in hFOB cells incubated for 48 h with 1, 10, 100 or 1000 ng/mL rhPRL. mRNA expressions were demonstrated by semi-qRT-PCR. $^{*}P<0.05$, $^{**}P<0.01$ compared with the control group. $^{\dagger\dagger}P<0.01$ compared with the values at 0 h. Numbers in parentheses are numbers of independent flasks. Experiments were performed in triplicate.

averaged about 91 ng/mL [16] which was comparable to the levels in pregnant rats [26], and much higher than ~7–10 ng/mL in normal non-pregnant adult female rats [16,26].

Hyperprolactinemia did not change femoral bone mineral density (BMD) or content (BMC)

In situ femoral BMD and BMC were determined at 0-, 2-, 5- and 7-week post-surgery to evaluate the effect of Ovx and hyperprolactinemia. In all groups, BMD and BMC gradually increased with age. Ovx rats characteristically showed BMD and BMC that were lower at weeks 5 and 7 (Figs. 2A and B), but were fully restored to the Sham values by estrogen supplementation. BMD and BMC of ex vivo femurs also exhibited consistent results (data not shown). Hyperprolactinemia did not affect BMD or BMC in AP and AP+Ovx+E2 groups (Figs. 2C–J). Interestingly, BMD and BMC of AP+Ovx rats were comparable to those of the age-matched Sham rats (Figs. 2C–J). Our results suggested that hyperprolactinemia may have an estrogen-independent action on bone since it maintained, instead of reduced, bone mass in AP+Ovx rats.

Histomorphometric analyses revealed complex patterns of microscopic changes in AP rats, and suggested a direct action of PRL on bone

Although densitometric analyses did not show any change in BMD or BMC of AP rats, histomorphometric analyses revealed high bone turnover in AP rats, as shown in Fig. 3. Our data indicated enhanced bone resorption with decreases in bone volume (BV/TV) and trabecular number (Tb.N) in AP rats, whereas trabecular separation (Tb.Sp), osteoclast surface (Oc.S/BS), and eroded surface (ES/BS) were increased with no change in the trabecular thickness (Tb.Th). Meanwhile, increases in the osteoblast surface (Ob.S/BS), double-labelled surface (dLS/BS), mineral apposition rate (MAR), and bone formation rate (BFR/BS) indicated enhanced bone formation. However, it was likely that changes in the resorptive parameters were predominant as BV/TV was decreased.

In the Ovx rats, most histomorphometric parameters including BV/TV, Tb.N, Tb.Sp, Tb.Th, Oc.S/BS and ES/BS showed explicit bone resorption, whereas a bone formation parameter, Ob.S/BS, was also increased. Effects of Ovx on bone were completely prevented by estrogen supplementation as indicated by all histomorphometric parameters in the Ovx+E2 group being comparable with those of the Sham group. AP+Ovx+E2 rats, similar to the AP rats, manifested high bone turnover although some parameters were not significantly different from those in the Sham or Ovx+E2 rats, i.e., Ob.S/BS, ES/BS, dLS/BS, and BFR/BS. In the AP+Ovx group, BV/TV, Tb.N and Tb.Th were much lower than those in the Sham or AP groups, whereas Tb.Sp, Oc.S/BS and ES/BS were greater, consistent with those in estrogen-deficient animals. However, BV/TV, Tb.N and BFR/BS in AP+Ovx rats were greater, while Tb.Sp was less than those in Ovx rats. Of interest, in contrast to the Ovx rats, Ob.S/BS in the AP+Ovx rats were not increased, and MAR was significantly higher than that in Sham and Ovx rats. We therefore postulated that the effects of hyperprolactinemia on bone were

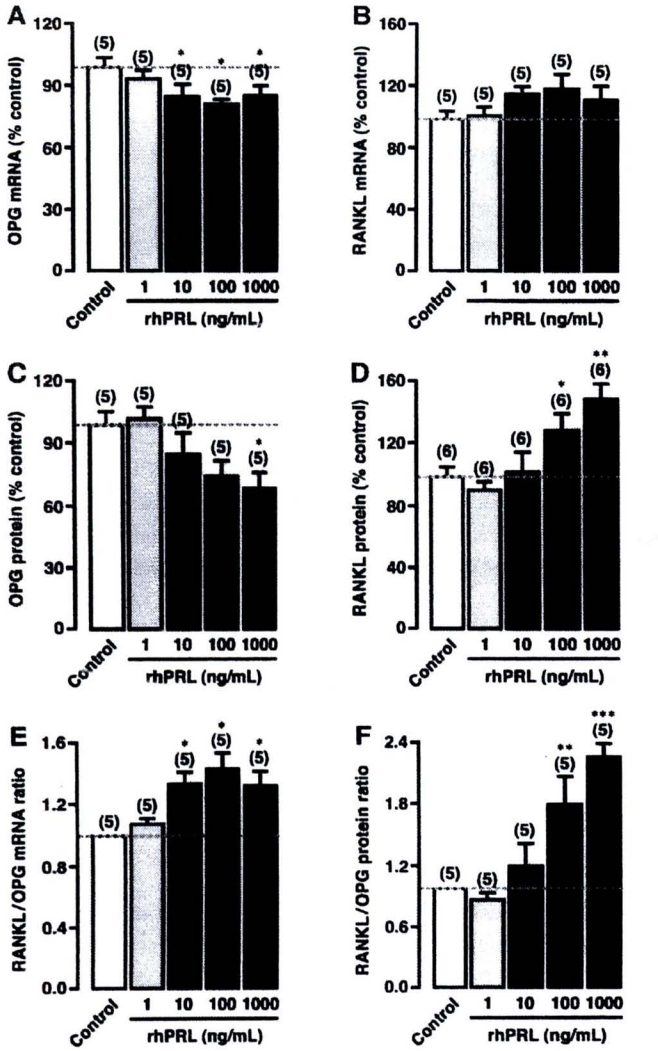

Fig. 6. Dose-dependent changes in the bone resorption-associated parameters which are mRNA expressions of OPG (A) and RANKL (B), protein expressions of OPG (C) and RANKL (D), and the ratios of RANKL/OPG mRNA (E) and protein (F) expressions in MG-63 cells incubated for 48 h with 1, 10, 100 or 1000 ng/mL rhPRL. mRNA expressions were demonstrated by semi-qRT-PCR, while protein expressions were studied by Western blot analysis. $^{*}P<0.05$, $^{**}P<0.01$, $^{***}P<0.001$ compared with the control group. Numbers in parentheses are numbers of independent flasks. Experiments were performed in triplicate.

different from those of estrogen depletion, and PRL possibly exerted a direct action on bone partly in an estrogen-independent manner.

The osteoblast-like cells MG-63 and rat cultured osteoblasts expressed PRLR

To investigate if PRL had a direct action on bone, we studied bone formation and resorption parameters in human osteoblast-like cells (MG-63). As shown in Fig. 4A, the expression of human PRLR (hPRLR) mRNA, which was considerably weak in 0.2% and 10% fetal bovine serum (FBS)-treated groups (controls), was strongly enhanced by 0.1 μM 1,25-$(OH)_2D_3$ (Vit D), 1 μM dexamethasone (DEX), and the combination of both. The effect of DEX on hPRLR mRNA expression was lower than that of Vit D. Since Vit D and DEX affected neither studied parameters nor cell proliferation (data not shown), both agents were added in the culture media in the following experiments. Vit D+DEX not only upregulated hPRLR mRNA but also stimulated hPRLR protein expression in MG-63 cells (Fig. 4B).

Moreover, by using the quantitative real-time PCR, cultured osteoblasts derived from the rat tibiae were shown to express mRNAs of short and long isoforms of rat PRLR (rPRLR) with a predominant short isoform, as well as bone-specific marker, osteocalcin (Fig. 4C). Several isoforms of rPRLR proteins migrated as multiple bands in the molecular weight range of 40 to 100 kDa (Fig. 4D). Confocal fluorescent imaging also demonstrated expressions of rPRLR proteins in primary rat osteoblasts (Fig. 4E). These results confirmed that osteoblasts were targets of PRL.

Expressions of bone formation markers in MG-63 were decreased by recombinant human PRL (rhPRL)

Fig. 5 shows the effects of 48-h rhPRL (1, 10, 100 and 1000 ng/mL) on the osteoblastic markers of bone formation. While none of the concentrations used changed the rate of MG-63 proliferation (Fig. 5A), rhPRL of 1000 ng/mL significantly downregulated osteocalcin mRNA expression to 81.65±3.40% of control ($P<0.05$) (Fig. 5B). Alkaline phosphatase mRNA expression was decreased by 10, 100 and 1000 ng/mL rhPRL to 88.62±3.02 ($P<0.05$), 85.43±2.57 ($P<0.05$), 83.11±2.57 ($P<0.01$) % of control (Fig. 5C), respectively, while 100 and 1000 ng/mL rhPRL reduced the activities of alkaline phosphatase to 87.46±2.89 and 84.19±2.77% of control (Fig. 5D). In the time–response studies, 1000 ng/mL rhPRL significantly decreased mRNA expression (Fig. 5E) and activity of alkaline phosphatase (Fig. 5F) at 24 h and 48 h after exposure, respectively. A decrease in the mRNA expression of alkaline phosphatase was also observed in hFOB cells (Fig. 5G). Therefore, our findings indicated that the direct effects of PRL on osteoblasts were on the osteoblastic functions rather than on cell proliferation.

High PRL exposure increased the ratios of MG-63-expressed RANKL/OPG mRNAs and proteins

Effects of rhPRL exposure on the markers of bone resorption are presented in Fig. 6. The ratio of RANKL and OPG, both of

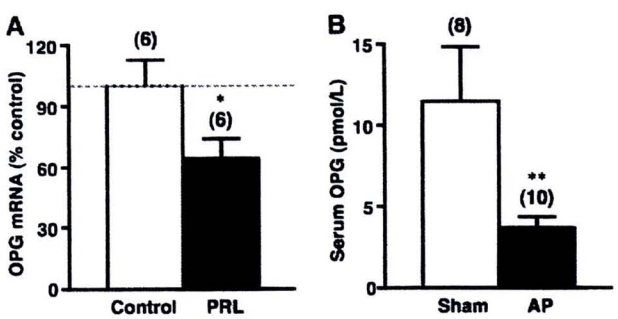

Fig. 7. (A) Expression of OPG mRNA (real-time PCR) in primary rat osteoblasts incubated for 48 h with 1000 ng/mL PRL. (B) Serum OPG levels in Sham and AP rats. $^{*}P<0.05$ compared with control. $^{**}P<0.01$ compared with Sham rats. Numbers in parentheses are numbers of experimental animals.

which were synthesized by osteoblasts, represented bone resorption [12]. In the present investigation, 48-h exposure to 10, 100 or 1000 ng/mL rhPRL decreased OPG mRNA expression in MG-63 cells to 85.83±4.49 ($P<0.05$), 82.68±1.05 ($P<0.05$), and 85.37±4.37 ($P<0.05$) % of control (Fig. 6A), respectively, while the same concentrations had no effect on RANKL mRNA expression (Fig. 6B). At the translational level, 48-h 1000 ng/mL rhPRL exposure downregulated OPG protein expression to 69.23±7.58% of control ($P<0.05$) (Fig. 6C), whereas 100 and 1000 ng/mL rhPRL increased RANKL protein expression to 127.73±10.07 ($P<0.05$) and 147.30±9.22 ($P<0.01$) % of control (Fig. 6D), respectively. The RANKL/OPG mRNA ratios were therefore increased by 10, 100 and 1000 ng/mL rhPRL to 1.35±0.08 ($P<0.05$), 1.43±0.11 ($P<0.05$) and 1.32±0.12 ($P<0.05$), respectively (Fig. 6E). Similarly, the ratios of RANKL/OPG protein were increased by 100 and 1000 ng/mL rhPRL to 1.81±0.25 ($P<0.01$) and 2.27±0.19 ($P<0.001$) (Fig. 6F). rhPRL of 10 ng/mL tended to increase the ratio of RANKL/OPG protein; however, the change was statistically insignificant (Fig. 6F).

In primary rat osteoblasts, 1000 ng/mL PRL decreased OPG mRNA expression to 64.21±10.12% of control ($P<0.05$) (Fig. 7A). Moreover, high PRL in AP-grafted rats showed a decrease in serum OPG level (Fig. 7B), i.e., from 11.47±3.35 to 3.63±0.71 pmol/L ($P<0.01$). Our results suggested that PRL enhanced bone resorption by increasing RANKL expression and decreasing OPG expression, thereby raising the RANKL/OPG ratio.

Discussion

Physiological hyperprolactinemia occurs during pregnancy and lactation, while pathological hyperprolactinemia is a common presentation in clinical practice. Effects of hyperprolactinemia on bone have been documented in patients and experimental animals [2,6,9], but it was not known whether PRL exerted its actions on bone directly or via PRL-induced hypogonadism. Therein, we provided supportive evidence that high physiological levels of PRL (~90–100 ng/mL) could directly regulate the osteoblast functions with a consequent increase in bone turnover, that involved a complex microscopic change leading to bone loss in an estrogen-independent manner.

In the present investigation, we used Ovx and AP transplantation to induce estrogen deficiency and hyperprolactinemia, respectively, and the differential bone responses in these conditions were evaluated. AP transplantation has two advantages over PRL injection in that, (*i*) it does not induce chronic stress in animals, and (*ii*) it produces sustained PRL levels of ~90–100 ng/mL, comparable to the levels during pregnancy in humans and rats [16,26]. Consequently, our results represent changes in bone calcium metabolism under the physiological hyperprolactinemia. The present data show that, during the 7-week AP transplantation, there was no sign of graft rejection or atrophy, and the AP allografts continued to synthesize PRL. Regarding the uterine weight which is normally used to indicate estrogenic status in rats, no change in the uterine weights of Ovx+E2 rats from those of Sham indicated that 2.5 μg/kg 17β-estradiol supplementation was sufficient to replace the circulating estrogen in Ovx rats. Since the serum estrogen concentrations in both AP and Ovx rats were reported to be comparable and less than 50 pg/mL [27], the estrogen levels in the AP group after estrogen supplementation (AP+Ovx+E2) should be close to normal. However, the uterine weights in AP+Ovx+E2 rats were still significantly lower than those in Ovx+E2 rats. Hence, PRL may have some direct antiestrogenic actions on the uterus independently of circulating estrogen. In other words, if the effect of PRL on the uterus is solely due to the PRL-suppressed serum estrogen level, this dose of estrogen supplement should be sufficient to restore the uterine weight. Such antiestrogenic action of PRL has been reported before in the mouse uterus, in which PRL prevented the formation of atypical hyperplasia [28].

Although several investigators suggested that the effects of hyperprolactinemia on bone were produced by prolactin-induced estrogen deficiency [5,11], the presence of PRLRs in osteoblasts, but not in osteoclasts, implicated osteoblasts as a direct target of PRL [6,13,17]. PRLRs were identified in the dexamethasone-stimulated osteoblast-like cells MG-63 and Saos-2 human osteosarcoma cell lines [17], as well as in the primary osteoblasts obtained from neonatal calvaria [29]. MG-63 cells normally express a very low amount of hPRLR mRNA. However, consistent with the previous report [17], hPRLR expression could be upregulated by dexamethasone and the physiological concentration of 1,25-$(OH)_2D_3$. Moreover, we recently demonstrated that tibia, femur, calvaria and L5-6 vertebrae of adult female rats expressed both short and long isoforms of rPRLR, suggesting that both cortical and trabecular sites were targets of PRL [6]. Expressions of rPRLR transcripts and proteins in rat cultured osteoblasts, as seen in the present study, further confirmed this hypothesis. In addition, decreases in BMD, MAR and BFR in $PRLR^{-/-}$ mice strongly suggested a direct action of PRL on bone [29]. We therefore performed a series of in vivo experiments to demonstrate mechanisms underlying changes in bone remodeling induced by hyperprolactinemia and estrogen deficiency.

An absence of change in the femoral BMD, BMC and bone calcium content during hyperprolactinemia has been reported before [6]. In the present study, unaltered BMD and BMC in the 2-, 5-and 7-week AP rats could be interpreted as PRL having no effect on bone, bone formation and resorption being equally affected, or changes being too small to be detected by DXA. However, the fact that high PRL could restore BMD and BMC in the AP+Ovx rats to Sham level suggested differential responses of bone to Ovx-induced estrogen deficiency and hyperprolactinemia. If hyperprolactinemia reduced bone mass solely through hypogonadism, AP+Ovx rats should have exhibited osteopenia as in the Ovx rats. Therefore, it was likely that PRL had an estrogen-independent action on bone.

By using bone histomorphometry, it was found that hyperprolactinemia in AP and AP+Ovx rats differentially stimulated tibial bone turnover, possibly in an estrogen-independent fashion. In the Ovx rats, most parameters, i.e., BV/TV, Tb.N, Tb.Sp, Tb.Th, Oc.S/BS and ES/BS, implicated severe bone resorption, whereas increased Ob.S/BS indicated enhanced bone formation. These data confirmed accelerated bone turnover with

bone formation coupled to bone resorption, as previously reported in Ovx rats [30,31]. This osteopenic state could be detectable by DXA as early as 5 weeks post-Ovx. However, despite having changes in parameters such as Tb.N, Tb.Sp, Oc.S/BS and ES/BS indicative of enhanced bone resorption as in the Ovx rats, the small decrease in BV/TV in the AP rats which was not large enough to be detected by DXA was probably a result of the concurrent increase in bone formation as indicated by two-fold increase in Ob.S/BS, MAR, and BFR/BS. Increases in Ob.S/BS and Oc.S/BS further suggested the coupled activation of osteoblastic and osteoclastic activities, and/or proliferation of both cell types in the AP rats. Thus, unlike in Ovx, bones exposed to high physiological PRL were in a high bone turnover state, and not in an overt osteopenic state.

Estrogen-independent action of PRL was further demonstrated in the AP+Ovx rats. Unchanged Ob.S/BS, dLS/BS, and BFR/BS in AP+Ovx rats not only indicated bone formation being uncoupled from bone resorption, but also demonstrated the differential responses of in vivo bone to hyperprolactinemia and estrogen deficiency. Increases in MAR and BFR/BS in AP rats were also in agreement with the report of Clément-Lacroix et al., which showed decreases in both parameters in $PRLR^{-/-}$ mice [29]. Interestingly, the AP+Ovx group, despite having a high osteoclastic activity, also exhibited a high MAR similar to the AP rats. Therefore, under the hyperprolactinemic condition, there was a PRL-mediated increase in the mineralization process which, in turn, helped prevent a further decrease in BMD. Incidentally, we have recently demonstrated a ~64% increase in the transcellular active calcium transport in the duodenum of the 4-week AP+Ovx rats [32]. In the presence of a high physiological PRL (~90–100 ng/mL), the extra calcium from the enhanced intestinal calcium absorption probably contributed to the increased mineralization, and in doing so, alleviated bone loss during estrogen deficiency. Increased bone calcium deposition also partly explained the undetectable change in BMD in the AP+Ovx rats.

Our densitometric and histomorphometric findings corroborated the estrogen-independent effects of PRL, and strengthened the hypothesis of a direct PRL action on bone. However, since the serum estrogen and PRL concentrations were not measured, the presents results provided only a suggestive evidence for the estrogen-independent effects of PRL. Indeed, direct actions of PRL could not be concluded solely from the in vivo findings, since effects of other factors, e.g., changes in the gonadotrophin levels, extraovarian estrogen and dietary calcium, could not be excluded. To show that PRL had a direct action on bone, we studied the in vitro effects of rhPRL on the synthesis of bone formation and bone resorption markers by the osteoblast-like MG-63 and hFOB cells.

Even though PRL was known to stimulate cell proliferation and tumorigenesis in mammary epithelial and Nb2 cells [33,34], a previous study by Coss et al. [13] and the present study found no effect of PRL on osteoblast proliferation. Nevertheless, the mRNA expression of osteocalcin and alkaline phosphatase, markers of osteoblast functions, were attenuated by rhPRL. The PRL-induced decrease in alkaline phosphatase activity in MG-63 cells was consistent with the findings in primary neonatal rat osteoblasts [13] and human fetal osteoblast (hFOB) 1.19 cells (Fig. 5G). These in vitro findings were contrary to the histomorphometric data of the AP rats that indicated an enhanced mineral apposition and bone formation. Increased bone formation seen in vivo could be due to the coupling of bone formation to bone resorption, which was absent in vitro. Alternatively, an increase in bone formation could have resulted from the increased calcium supply from the PRL-stimulated intestinal calcium absorption [16,32]. As bone formation is a complex process consisting of osteoid formation and mineralization, availability of calcium in the plasma is crucial for mineralization, thereby increasing the rate of bone formation even in the vitamin D-deficient rats [35]. Further investigations are required to demonstrate the effects of PRL on the intricate interactions between bone and intestine.

Regarding markers of bone resorption, we determined the change in the RANKL/OPG expression ratio in MG-63 cells. A number of studies reported that the age-related osteopenia, eroded bone surface, and high incidence of hip fracture in humans were positively correlated with an increase in RANKL/OPG ratio [12,36–38]. So far, there has been no report on the effect of PRL on the osteoblast expression of RANKL and OPG. Expression of PRLR exclusively in osteoblasts, but not in osteoclasts [13,39], evinced the osteoblast as the modulator of PRL-induced bone resorption. Herein, we demonstrated, for the first time, that rhPRL upregulated the expression of RANKL but downregulated that of OPG, thus leading to an increase in the RANKL/OPG ratio both at the transcriptional and translational levels. Downregulation of OPG mRNA expression in primary rat osteoblasts and a decrease in serum OPG levels in AP rats were consistent with the findings in MG-63 cells.

The concentration of PRL may be a salient determinant of bone loss, because PRL regulated the expression of bone markers, including osteocalcin, alkaline phosphatase, RANKL and OPG, in a dose-response manner. A pathological level of rhPRL (1000 ng/mL) markedly changed all measured parameters of bone turnover, whereas 100 ng/mL rhPRL had less effect on the osteoblastic function. It was also apparent from our previous report that decreases in bone formation and bone mass may be prevented by the concurrent stimulation of the intestinal calcium absorption with ~100 ng/mL PRL [32,40]. Our postulation corroborated findings that pregnancy did not induce significant osteopenia, whereas long-term lactation with ~200–400 ng/mL plasma PRL led to reversible bone loss [3]. Since PRLR knockout impaired ossification in neonatal mice and decreased BMD in adult mice [29], the basal circulating PRL (~7–10 ng/mL) must also be essential for the maintenance of normal bone growth and remodeling. In the present study, 10 ng/mL PRL maintained a slightly elevated expression ratio of RANKL/OPG mRNA which was apparently appropriate for normal bone functions. On the other hand, pathological levels of PRL often resulted in overt osteopenia similar to estrogen deficiency [1,2]. Our findings confirmed that 1000 ng/mL PRL could increase bone resorption, as indicated by a marked increase in the RANKL/OPG ratio. Of note was our previous finding that 1000 ng/mL PRL exerted a typical biphasic action on the small intestine, i.e., the enhanced calcium absorption was diminished

to the basal level [41,42], thereby aggravating a negative calcium balance. Thus, the massive bone loss in pathological hyperprolactinemia could result from the PRL-enhanced bone resorption without matching increase in the intestinal calcium absorption.

In conclusion, hyperprolactinemia in adult rats resulted in a high bone turnover and bone loss, but its effects on bone resorption were not as prominent as in Ovx rats. High physiological PRL and estrogen deficiency each rendered distinct patterns of bone remodeling, supporting our hypothesis that PRL had some estrogen-independent actions in bone. Further investigation in MG-63 cells confirmed the direct actions of PRL on osteoblasts in which PRL suppressed the osteocalcin expression and alkaline phosphatase activity while increasing the RANKL/OPG ratio. Our results were able to explain the clinical findings of the hyperprolactinemia-induced high bone turnover and osteopenia.

Conflict of interest statement

The authors declare no conflict of interest.

Acknowledgments

We thank Prof. Vorachai Sirikulchayanonta, Prof. Somnuek Domrongkitchaiporn, and Dr. Sinee Disthabanchong from the Faculty of Medicine, Ramathibodi Hospital, Mahidol University for their technical guidance and helpful comments. We thank Jirawan Thongbunchoo for her excellent technical assistance. This research was supported by grants from the Royal Golden Jubilee Program (to D.S.), the King Prajadhipok and Queen Rambhai Barni Memorial Foundation (to K.Th.), the Thailand Research Fund (TRF) and the National Center for Genetic Engineering and Biotechnology (BIOTEC).

References

[1] Jung DU, Conley RR, Kelly DL, Kim DW, Yoon SH, Jang JH, et al. Prevalence of bone mineral density loss in Korean patients with schizophrenia: a cross-sectional study. J Clin Psychiatry 2006;67:1391–6.

[2] Haddad PM, Wieck A. Antipsychotic-induced hyperprolactinaemia: mechanisms, clinical features and management. Drugs 2004;64:2291–314.

[3] Ritchie LD, Fung EB, Halloran BP, Turnlund JR, Van Loan MD, Cann CE, et al. A longitudinal study of calcium homeostasis during human pregnancy and lactation and after resumption of menses. Am J Clin Nutr 1998;67:693–701.

[4] Biller BM, Baum HB, Rosenthal DI, Saxe VC, Charpie PM, Klibanski A. Progressive trabecular osteopenia in women with hyperprolactinemic amenorrhea. J Clin Endocrinol Metab 1992;75:692–7.

[5] Naliato EC, Farias ML, Braucks GR, Costa FS, Zylberberg D, Violante AH. Prevalence of osteopenia in men with prolactinoma. J Endocrinol Invest 2005;28:12–7.

[6] Charoenphandhu N, Tudpor K, Thongchote K, Saengamnart W, Puntheeranurak S, Krishnamra N. High-calcium diet modulates effects of long-term prolactin exposure on the cortical bone calcium content in ovariectomized rats. Am J Physiol Endocrinol Metab 2007;292: E443–52.

[7] Puntheeranurak S, Charoenphandhu N, Krishnamra N. Enhanced trabecular-bone calcium deposition in female rats with a high physiological dose of prolactin diminishes after ovariectomy. Can J Physiol Pharmacol 2006;84:993–1002.

[8] Naylor KE, Iqbal P, Fledelius C, Fraser RB, Eastell R. The effect of pregnancy on bone density and bone turnover. J Bone Miner Res 2000;15:129–37.

[9] Kovacs CS. Calcium and bone metabolism during pregnancy and lactation. J Mammary Gland Biol Neoplasia 2005;10:105–18.

[10] Lotinun S, Limlomwongse L, Sirikulchayanonta V, Krishnamra N. Bone calcium turnover, formation, and resorption in bromocriptine- and prolactin-treated lactating rats. Endocrine 2003;20:163–70.

[11] Schlechte JA. Clinical impact of hyperprolactinaemia. Baillières Clin Endocrinol Metab 1995;9:359–66.

[12] Kostenuik PJ. Osteoprotegerin and RANKL regulate bone resorption, density, geometry and strength. Curr Opin Pharmacol 2005;5:618–25.

[13] Coss D, Yang L, Kuo CB, Xu X, Luben RA, Walker AM. Effects of prolactin on osteoblast alkaline phosphatase and bone formation in the developing rat. Am J Physiol Endocrinol Metab 2000;279:E1216–25.

[14] Ducy P, Schinke T, Karsenty G. The osteoblast: a sophisticated fibroblast under central surveillance. Science 2000;289:1501–4.

[15] Adler RA, Farrell ME, Krieg RJ, Deiss WP. Hypogonadism does not mediate urinary calcium loss in pituitary-grafted rats. Metabolism 1989;38: 805–9.

[16] Piyabhan P, Krishnamra N, Limlomwongse L. Changes in the regulation of calcium metabolism and bone calcium content during growth in the absence of endogenous prolactin and during hyperprolactinemia: a longitudinal study in male and female Wistar rats. Can J Physiol Pharmacol 2000;78: 757–65.

[17] Bataille-Simoneau N, Gerland K, Chappard D, Basle MF, Mercier L. Expression of prolactin receptors in human osteosarcoma cells. Biochem Biophys Res Commun 1996;229:323–8.

[18] Colin EM, Van Den Bemd GJ, Van Aken M, Christakos S, De Jonge HR, DeLuca HF, et al. Evidence for involvement of 17β-estradiol in intestinal calcium absorption independent of 1,25-dihydroxyvitamin D_3 level in the rat. J Bone Miner Res 1999;14:57–64.

[19] Li CY, Jee WS, Chen JL, Mo A, Setterberg RB, Su M, et al. Estrogen and "exercise" have a synergistic effect in preventing bone loss in the lumbar vertebra and femoral neck of the ovariectomized rat. Calcif Tissue Int 2003;72:42–9.

[20] Parfitt AM, Drezner MK, Glorieux FH, Kanis JA, Malluche H, Meunier PJ, et al. Bone histomorphometry: standardization of nomenclature, symbols, and units. Report of the ASBMR Histomorphometry Nomenclature Committee. J Bone Miner Res 1987;2:595–610.

[21] Mosmann T. Rapid colorimetric assay for cellular growth and survival: application to proliferation and cytotoxicity assays. J Immunol Methods 1983;65:55–63.

[22] Robbins JR, Thomas B, Tan L, Choy B, Arbiser JL, Berenbaum F, et al. Immortalized human adult articular chondrocytes maintain cartilage-specific phenotype and responses to interleukin-1β. Arthritis Rheum 2000;43:2189–201.

[23] Rickard DJ, Kassem M, Hefferan TE, Sarkar G, Spelsberg TC, Riggs BL. Isolation and characterization of osteoblast precursor cells from human bone marrow. J Bone Miner Res 1996;11:312–24.

[24] Granchi D, Cenni E, Savarino L, Ciapetti G, Forbicini G, Vancini M, Maini C, Baldini N, Giunti A. Bone cement extracts modulate the osteoprotegerin/osteoprotegerin–ligand expression in MG63 osteoblast-like cells. Biomaterials 2002;23:2359–65.

[25] Charoenphandhu N, Wongdee K, Tudpor K, Pandaranandaka J, Krishnamra N. Chronic metabolic acidosis upregulated claudin mRNA expression in the duodenal enterocytes of female rats. Life Sci 2007;80:1729–37.

[26] Boass A, Lovdal JA, Toverud SU. Pregnancy- and lactation-induced changes in active intestinal calcium transport in rats. Am J Physiol 1992;263:G127–34.

[27] Ribeiro MF, Ferigolo M, Reis FM, Barros HM, Spritzer PM. Paradoxical effect of imipramine in hyperprolactinemic female rats exposed to the forced swimming test. Physiol Behav 2000;68:619–23.

[28] Gunin AG, Emelianov V, Tolmachev AS, Tolmacheva A. Effect of prolactin and dopaminergic drugs on uterine response to chronic estrogen exposure. J Endocrinol 2002;172:61–9.

[29] Clément-Lacroix P, Ormandy C, Lepescheux L, Ammann P, Damotte D, Goffin V, et al. Osteoblasts are a new target for prolactin: analysis of bone

formation in prolactin receptor knockout mice. Endocrinology 1999;140: 96–105.
[30] Ke HZ, Simmons HA, Pirie CM, Crawford DT, Thompson DD. Droloxifene, a new estrogen antagonist/agonist, prevents bone loss in ovariectomized rats. Endocrinology 1995;136:2435–41.
[31] Turner RT, Evans GL, Sluka JP, Adrian MD, Bryant HU, Turner CH, et al. Differential responses of estrogen target tissues in rats including bone to clomiphene, enclomiphene, and zuclomiphene. Endocrinology 1998;139:3712–20.
[32] Tudpor K, Charoenphandhu N, Saengamnart W, Krishnamra N. Long-term prolactin exposure differentially stimulated the transcellular and solvent drag-induced calcium transport in the duodenum of ovariectomized rats. Exp Biol Med 2005;230:836–44.
[33] Harvey PW. Human relevance of rodent prolactin-induced non-genotoxic mammary carcinogenesis: prolactin involvement in human breast cancer and significance for toxicology risk assessments. J Appl Toxicol 2005;25: 179–83.
[34] Wang YF, Walker AM. Dephosphorylation of standard prolactin produces a more biologically active molecule: evidence for antagonism between nonphosphorylated and phosphorylated prolactin in the stimulation of Nb2 cell proliferation. Endocrinology 1993;133:2156–60.
[35] Weinstein RS, Underwood JL, Hutson MS, DeLuca HF. Bone histomorphometry in vitamin D-deficient rats infused with calcium and phosphorus. Am J Physiol 1984;246:E499–505.
[36] Abdallah BM, Stilgren LS, Nissen N, Kassem M, Jorgensen HR, Abrahamsen B. Increased RANKL/OPG mRNA ratio in iliac bone biopsies from women with hip fractures. Calcif Tissue Int 2005;76:90–7.
[37] Grimaud E, Soubigou L, Couillaud S, Coipeau P, Moreau A, Passuti N, et al. Receptor activator of nuclear factor κB ligand (RANKL)/osteoprotegerin (OPG) ratio is increased in severe osteolysis. Am J Pathol 2003;163:2021–31.
[38] Fazzalari NL, Kuliwaba JS, Atkins GJ, Forwood MR, Findlay DM. The ratio of messenger RNA levels of receptor activator of nuclear factor κB ligand to osteoprotegerin correlates with bone remodeling indices in normal human cancellous bone but not in osteoarthritis. J Bone Miner Res 2001;16:1015–27.
[39] Kelly PA, Binart N, Freemark M, Lucas B, Goffin V, Bouchard B. Prolactin receptor signal transduction pathways and actions determined in prolactin receptor knockout mice. Biochem Soc Trans 2001;29:48–52.
[40] Charoenphandhu N, Krishnamra N. Prolactin is an important regulator of intestinal calcium transport. Can J Physiol Pharmacol 2007;85:569–81.
[41] Tanrattana C, Charoenphandhu N, Limlomwongse L, Krishnamra N. Prolactin directly stimulated the solvent drag-induced calcium transport in the duodenum of female rats. Biochim Biophys Acta 2004;1665:81–91.
[42] Jantarajit W, Thongon N, Pandaranandaka J, Teerapornpuntakit J, Krishnamra N, Charoenphandhu N. Prolactin-stimulated transepithelial calcium transport in duodenum and Caco-2 monolayer are mediated by the phosphoinositide 3-kinase pathway. Am J Physiol Endocrinol Metab 2007;293:E372–84.

8. บทความสำหรับเผยแพร่

ความรู้ทางด้านวิทยาศาสตร์และเทคโนโลยีในปัจจุบันทำให้มีความก้าวหน้าทางการแพทย์และการสาธารณสุขอย่างรวดเร็ว มีผลให้ประเทศพัฒนาและกำลังพัฒนา เช่น ประเทศไทยมีประชากรสูงอายุเพิ่มขึ้นอย่างรวดเร็วเช่นกัน ประชากรสูงอายุของประเทศไทยมีอัตราเพิ่มขึ้นปีละประมาณ 4.5 % เปรียบเทียบกับอัตราการเพิ่มของประชากรทั่วไปไม่ถึง 1 % คาดการณ์ได้ว่าโรคของผู้สูงอายุเช่น โรคกระดูกจะมีอุบัติการณ์เพิ่มขึ้นและจะเป็นปัญหาด้านสาธารณสุขเศรษฐกิจและสังคมอย่างแน่นอน การป้องกันและลดอุบัติการณ์ของโรคกระดูกในผู้สูงอายุจะต้องดำเนินการตั้งแต่ในเด็ก เราต้องหาวิธีการที่จะทำให้เด็กมีการเจริญเติบโตของกระดูกที่ดีจนมีค่ามวลกระดูกสูงที่สุดเท่าที่จะเป็นไปได้ในช่วงอายุ 25-30 ปี และหาวิธีชะลอการสูญเสียกระดูกในสตรีวัยหมดประจำเดือน และการสูญเสียมวลกระดูกในวัยผู้สูงอายุ ดังนั้นกลุ่มวิจัยของเราจึงมีวัตถุประสงค์ที่จะศึกษาวิจัยเพื่อให้ได้องค์ความรู้ที่เป็นองค์รวมเกี่ยวกับกลไกการดูดซึมแคลเซียมและวัฏจักรสร้าง-สลายกระดูก (Bone turnover) และปัจจัยควบคุมต่างๆ ตลอดจนสาเหตุของพยาธิสภาพ ความรู้เหล่านี้สามารถใช้เป็นฐานต่อยอดความรู้ทางการแพทย์เพื่อพัฒนาไปสู่วิธีการป้องกัน การวินิจฉัยความผิดปกติ และการรักษาได้

กลุ่มวิจัยของเรา คือ **เครือข่ายวิจัยด้านแคลเซียมและกระดูก (Consortium for Calcium and Bone Research หรือ COCAB)** ได้ใช้สัตว์ทดลองศึกษาวิจัยกลไกการดูดซึมแคลเซียมและวัฏจักรการสร้าง-สลายกระดูกทั้งในแนวราบหรือในสภาวะต่างๆ เช่น วัยเจริญเติบโต วัยเจริญพันธุ์ ภาวะท้องและให้นมลูก และในพยาธิสภาพ เช่น ภาวะเลือดเป็นกรดและภาวะขาดฮอร์โมนเพศ และศึกษาในแนวลึกคือ กลไกในระดับร่างกาย อวัยวะ เนื้อเยื่อ เซลล์ โปรตีนไปจนถึงระดับโมเลกุล การศึกษาโดยใช้เทคนิควิจัยหลากหลายสาขา (Multidisciplinary) เช่น สรีรวิทยา ชีวเคมี จุลกายวิภาค ชีวโมเลกุล และพยาธิชีววิทยาทำให้เราสามารถตอบโจทย์วิจัยได้เป็นภาพรวมและสามารถอธิบายการเปลี่ยนแปลงที่เกิดขึ้นในระดับต่างๆของร่างกาย

การวิจัยในส่วนแรกเกี่ยวกับ**บทบาทใหม่ของโพรแลคตินในฐานะฮอร์โมนควบคุมสมดุลแคลเซียมและกระดูก**โดยเฉพาะในภาวะท้องและให้นมบุตร โพรแลคตินเป็นฮอร์โมนที่หลั่งจากต่อมใต้สมอง ปกติจะมีในระดับเลือดต่ำมาก แต่มีระดับสูงขึ้นหลายเท่าตัวในช่วงท้องและให้นม โดยมีหน้าที่หลักคือ กระตุ้นการสังเคราะห์น้ำนมในเต้านม งานวิจัยในหลายๆ ปีที่ผ่านมาของเราได้นำไปสู่องค์ความรู้ใหม่เกี่ยวกับโพรแลคติน เราพบว่าโพรแลคตินมีหน้าที่จัดการให้ร่างกายของแม่มีแคลเซียมในเลือดในระดับที่เพียงพอสำหรับส่งผ่านรกเพื่อใช้ในการเจริญเติบโตของลูกในท้อง และเพียงพอสำหรับเซลล์เต้านมใช้ในการผลิตน้ำนมเลี้ยงลูกหลังคลอด โดยโพรแลคตินออกฤทธิ์กระตุ้นลำไส้ส่วนต้นทำให้ดูดซึมแคลเซียมได้มากขึ้น และยังกระตุ้นการสลายแคลเซียมจากกระดูกอีกด้วย ขณะเดียวกันก็ลดการขับถ่ายแคลเซียมทิ้งทางปัสสาวะ เป็นที่น่าสนใจมากว่าผลของโพรแลคตินต่อการดูดซึมแคลเซียมเกิดขึ้นเป็น 2 ขั้นตอน ทั้งนี้ขึ้นอยู่กับระดับฮอร์โมนในเลือด กล่าวคือโพรแลตตินที่มีระดับในเลือดสูงเป็นระยะเวลานาน เช่น 75 -100

นาโนกรัม/มิลลิลิตรระหว่างตั้งท้องและ 200-300 นาโนกรัม/มิลลิลิตร ในช่วงให้นมหลังคลอดมีผลกระตุ้นการแสดงออกของยีนส์ที่เกี่ยวข้องกับการขนส่งแคลเซียมในโพรงลำไส้มีผลให้การดูดซึมแคลเซียมเพิ่มจากภาวะไม่ท้องถึง 2 เท่า เราเรียกการเปลี่ยนแปลงนี้ว่า ขั้นที่ 1 ในช่วงหลังคลอดเมื่อลูกดูดนมโพรแลคตินของแม่จะพุ่งสูงขึ้นอีกถึง 600-800 นาโนกรัม/มิลลิลิตร การดูดซึมแคลเซียมก็พุ่งสูงตามเป็นขั้น -2 การดูดซึมแคลเซียมในขั้น 2 นี้มีความสัมพันธ์กับปริมาณน้ำนมที่หลั่งและเป็นการตอบสนองอย่างเฉียบพลันโดยใช้กลไกกระตุ้นให้โปรตีนขนส่งแคลเซียมทำงานดีขึ้น งานวิจัยนี้แสดงว่าแม่จะได้ประโยชน์จากการดูดซึมแคลเซียมมากขึ้น ถ้าดื่มนมหรือรับประทานแคลเซียมเสริมประมาณครึ่งชั่วโมงก่อนให้นมลูก ระดับโพรแลคตินในเลือดที่พุ่งสูงขึ้นตอนลูกดูดนมและช่วยกระตุ้นการดูดซึมแคลเซียมของแม่ ทำให้แม่มีแคลเซียมเพียงพอในการผลิตน้ำนม โดยไม่ต้องดึงแคลเซียมออกมาจากกระดูก ซึ่งจะเป็นประโยชน์ต่อสุขภาพของแม่ในระยะยาว

ผลของโพรแลคตินที่กระดูกก็น่าสนใจมาก เราพบว่าโพรแลคตินร่วมกับฮอร์โมนอีกบางชนิดกระตุ้นให้แม่สะสมแคลเซียมในกระดูกในช่วงตั้งท้อง แต่พอหลังคลอดโพรแลคตินก็จะมีผลให้มีการสลายกระดูกปล่อยแคลเซียมมาเพื่อใช้ผลิตน้ำนม บางครั้งแม่อาจมีความหนาแน่นของกระดูกลดลงถึง 30 % แต่ก่อนเชื่อว่าโพรแลคตินมีผลสลายกระดูกผ่านทางการยับยั้งการหลั่งฮอร์โมนเพศหญิงเอสโตรเจนเท่านั้น แต่เราได้พิสูจน์แล้วว่าโพรแลคตินสามารถออกฤทธิ์โดยตรงที่เซลล์กระดูกออสติโอบลาสท์ ซึ่งจะหลั่งสารเช่น RANKL เพิ่มขึ้นและหลั่ง osteoprotegerin ลดลง ทำให้เกิดการสลายกระดูกโดยเซลล์ออสติโอคลาสท์มากขึ้น จึงจะเห็นได้ว่าโพรแลคตินเป็นฮอร์โมนสำคัญที่มีบทบาทควบคุมการเคลื่อนย้ายหรือขนส่งแคลเซียมระหว่างอวัยวะต่าง ๆ ทั้งนี้เพื่อให้แม่มีแคลเซียมเพียงพอเพื่อการเจริญเติบโตของลูกในท้อง และการผลิตน้ำนมเพื่อลูกอ่อน

การวิจัยอีกส่วนหนึ่งเกี่ยวกับ**กลไกการควบคุมวัฏจักรการสร้าง-สลายกระดูกโดยระบบประสาท** ระบบประสาทเป็นระบบควบคุมหลักของร่างกาย แต่ความรู้เกี่ยวกับการควบคุมกระดูกโดยระบบประสาทมีน้อยมาก มีรายงานว่าระบบประสาทซิมพาเตติกสามารถควบคุมเซลล์กระดูกออสติโอบลาสท์ผ่านตัวรับ β_2-AR ทำให้มีการหลั่งRANKL มากขึ้นและหลั่ง osteoprotegerin ลดลง ซึ่งมีผลเพิ่มจำนวนเซลล์ออสติโอคลาสท์ให้ไปสลายกระดูกมากขึ้น จากงานวิจัยเราได้พบตัวรับอีกชนิดหนึ่งที่เซลล์ออสติโอบลาสท์ ได้แก่ β_3-AR ซึ่งเราพบว่ามีหน้าที่ป้องกันการสลายกระดูกและยังช่วยให้มีการสร้างกระดูกมากขึ้น ในปัจจุบันมียาหลายชนิดที่ใช้ลดการสลายกระดูกเพื่อป้องกันการสูญเสียมวลกระดูก โดยเฉพาะในสตรีวัยหมดประจำเดือนหรือผู้ป่วยโรคกระดูกพรุน แต่ยาที่ใช้กระตุ้นการสร้างกระดูกมีเพียงฮอร์โมนพาราไทรอยด์ที่ใช้ฉีดให้ผู้ป่วย ดังนั้นองค์ความรู้ใหม่นี้น่าจะนำไปสู่การวิจัยต่อยอดเพื่อพัฒนายากระตุ้น β_3-AR เพื่อเพิ่มการสร้างกระดูกและลดการสูญเสียมวลกระดูก

ดังนั้นงานวิจัยองค์ความรู้ใหม่ของเรา ไม่ว่าจะเป็นเรื่องบทบาทใหม่ของโพรแลคตินในฐานะฮอร์โมนควบคุมสมดุลแคลเซียมและวัฏจักรการสลายกระดูก หรือเกี่ยวกับบทบาทของระบบประสาทซิมพาเตติกในการควบคุมกระบวนการสร้าง/สลายกระดูก ทำให้เราเข้าใจว่าการดูด

ซึมแคลเซียมที่ลำไส้ และกระบวนการสร้าง-สลายกระดูกที่เกิดขึ้นตลอดเวลานี้มีกลไกอย่างไร มีการควบคุมอย่างไร และสามารถใช้ข้อมูลเหล่านี้เป็นฐานให้ค้นคว้าวิธีการที่จะทำให้จะใช้บทบาทของฮอร์โมนในร่างกายเองให้เกิดประโยชน์สูงสุด และเป็นฐานให้พัฒนาวิธีการให้คนไทยมีกระดูกที่แข็งแรงและสุขภาพดีจนวัยสูงอายุ

Mol Cell Biochem
DOI 10.1007/s11010-010-0674-4

Prolactin alters the mRNA expression of osteoblast-derived osteoclastogenic factors in osteoblast-like UMR106 cells

Kannikar Wongdee · Warut Tulalamba · Jirawan Thongbunchoo · Nateetip Krishnamra · Narattaphol Charoenphandhu

Received: 29 August 2010 / Accepted: 15 November 2010

Abstract Prolactin (PRL) is known to participate in the lactation-induced maternal bone loss, presumably by inducing the release of receptor activator of nuclear factor-κB ligand (RANKL), a potent osteoclastogenic factor from osteoblasts. Since maternal bone resorption was too massive to be solely explained by RANKL and osteoclasts did not express PRL receptors (PRLR), the involvement of some other osteoblast-derived osteoclastogenic modulators was anticipated. Herein, the authors used quantitative real-time PCR to investigate the mRNA expressions of various osteoclastogenic factors in osteoblast-like UMR106 cells directly exposed to PRL for 48 h. These cells were found to express PRLR and respond to 300 ng/ml PRL by increasing RANKL mRNA expression. This PRL concentration (comparable to plasma PRL levels in lactation) also induced the upregulation of monocyte chemoattractant protein (MCP)-1, cyclooxygenase (Cox)-2, and ephrin-B1, whereas a higher concentration (500 ng/ml) was required to upregulate tumor necrosis factor (TNF)-α and interleukin (IL)-1. However, 100–500 ng/ml PRL affected neither the cell proliferation, the cell viability nor the mRNA expressions of macrophage colony-stimulating factor, IL-6, ephrin type-B receptor 4 and ephrin-B2. In conclusion, besides RANKL overexpression, PRL upregulated the expressions of other osteoclastogenic modulators, i.e., MCP-1, Cox-2, TNF-α, IL-1, and ephrin-B1, thus, further explaining how PRL induced bone loss in lactating mothers.

Keywords Hyperprolactinemia · Osteoblast-derived factors · Osteoclastogenesis · Prolactin receptor · RANKL · Real-time PCR

K. Wongdee · W. Tulalamba · J. Thongbunchoo · N. Krishnamra · N. Charoenphandhu
Consortium for Calcium and Bone Research (COCAB), Faculty of Science, Mahidol University, Bangkok, Thailand

K. Wongdee
Faculty of Allied Health Sciences, Burapha University, Chonburi, Thailand

W. Tulalamba
Molecular Medicine Graduate Program, Faculty of Science, Mahidol University, Bangkok, Thailand

N. Krishnamra · N. Charoenphandhu (✉)
Department of Physiology, Faculty of Science, Mahidol University, Rama VI Road, Bangkok 10400, Thailand
e-mail: naratt@narattsys.com

Introduction

With the clearly observed link between hyperprolactinemia and the lactation-induced maternal bone loss [1], prolactin (PRL) has been postulated to be an important regulator of maternal bone metabolism during lactation [2], in which the average plasma PRL levels are markedly elevated by ~30-fold (i.e., ~7–10 ng/ml in non-mated rats vs. ~200–300 ng/ml in lactating rats). The authors' recent investigation in lactating rats showed that PRL markedly stimulated osteoclastic bone resorption, particularly in the trabecular areas [1]. The resorptive effects of PRL on bone were accomplished by its direct actions on osteoblasts, but not osteoclasts, since only osteoblasts were found to express functional PRL receptors (PRLR) [3, 4]. At the molecular level, the PRL-induced bone resorption was partially explained by an overexpression of the receptor activator of nuclear factor-κB (RANK) ligand (RANKL) [5], an osteoblast-derived factor that increased osteoclast differentiation and survival [6].

Since progressive bone loss in lactating rats was too massive to be explained solely by the RANKL

Published online: 30 November 2010